

AD-A087 594

ADVISORY GROUP FOR AEROSPACE RESEARCH AND DEVELOPMENT--ETC F/6 11/2
CERAMICS FOR TURBINE ENGINE APPLICATIONS.(U)
MAR 80 H M BURTE, J ACURIO, W HANSEN

UNCLASSIFIED AGARD-CP-276

NL

1 of 4

AD-A087 594



AGARD-CP-276

AGARD-CP-276

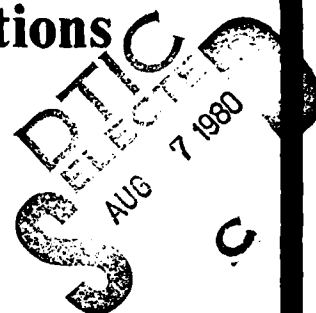
AGARD

ADVISORY GROUP FOR AEROSPACE RESEARCH & DEVELOPMENT

7 RUE ANCELLE 92200 NEUILLY SUR SEINE FRANCE

AGARD CONFERENCE PROCEEDINGS No. 276

Ceramics for Turbine Engine Applications



NORTH ATLANTIC TREATY ORGANIZATION



DISTRIBUTION AND AVAILABILITY
ON BACK COVER

This document has been approved
for public release and sale; its
distribution is unlimited.

80 8 6 040

ADA 087594

DDC FILE COPY

①

NORTH ATLANTIC TREATY ORGANIZATION
ADVISORY GROUP FOR AEROSPACE RESEARCH AND DEVELOPMENT
(ORGANISATION DU TRAITE DE L'ATLANTIQUE NORD)

⑩ Harnisch / Harnisch
Schröder / Harnisch
Harnisch / Harnisch
Harnisch / Harnisch
Harnisch / Harnisch

AGARD Conference Proceedings, No. 276

CERAMICS FOR TURBINE ENGINE APPLICATIONS.

11 Mar 1979
⑩ 366

REC-100

Papers presented at the 49th Meeting of the AGARD Structures and Materials Panel
held in Porz-Wahn, Köln, Germany on 8-10 October 1979.

This document has been approved
for use by the AGARD member states
and is available to the public.

THE MISSION OF AGARD

The mission of AGARD is to bring together the leading personalities of the NATO nations in the fields of science and technology relating to aerospace for the following purposes:

- Exchanging of scientific and technical information;
- Continuously stimulating advances in the aerospace sciences relevant to strengthening the common defence posture;
- Improving the co-operation among member nations in aerospace research and development;
- Providing scientific and technical advice and assistance to the North Atlantic Military Committee in the field of aerospace research and development;
- Rendering scientific and technical assistance, as requested, to other NATO bodies and to member nations in connection with research and development problems in the aerospace field;
- Providing assistance to member nations for the purpose of increasing their scientific and technical potential;
- Recommending effective ways for the member nations to use their research and development capabilities for the common benefit of the NATO community.

The highest authority within AGARD is the National Delegates Board consisting of officially appointed senior representatives from each member nation. The mission of AGARD is carried out through the Panels which are composed of experts appointed by the National Delegates, the Consultant and Exchange Programme and the Aerospace Applications Studies Programme. The results of AGARD work are reported to the member nations and the NATO Authorities through the AGARD series of publications of which this is one.

Participation in AGARD activities is by invitation only and is normally limited to citizens of the NATO nations.

The content of this publication has been reproduced
directly from material supplied by AGARD or the authors.

Published March 1980

Copyright © AGARD 1980
All Rights Reserved

ISBN 92-835-0261-2



*Printed by Technical Editing and Reproduction Ltd
Harford House, 7 9 Charlotte St, London, W1P 1HD*

PREFACE

The importance of advances in high temperature materials technology to progress in aerospace is well recognized. For example, improved materials and/or the design and fabrication approaches to use them provide broad opportunities to increase the performance or durability, or to reduce the cost of turbine engines. One specific approach being investigated in several NATO nations involves high temperature ceramics and the associated design technology for using brittle materials. Ceramics are also being actively explored for turbines for other uses such as in automobile engines and electric power generators. Many of these have progressed into first generation attempts to design, fabricate and test actual components, and it is appropriate to try to "take stock" of the results, to evaluate the implications for aerospace applications, and to identify deficiencies in the "state-of-the-art" and directions for future emphasis. Since the effective use of ceramics will require an extremely close interaction between materials and design, it is particularly important to provide forums which promote close cooperation between the engine community and the materials community. A Specialists Meeting on "Ceramics for Turbine Engine Applications", to accomplish the above objectives, was thus organized by a subcommittee of the Structures and Materials Panel with the extensive cooperation and participation of the Propulsion and Energetics Panel.

AGARD interest in this area has deep roots. A 1955 meeting in Rome considered "cermets", an early approach to the problem of brittleness. In 1971 a "Handbook of Brittle Materials Design Technology" was published as AGARDograph No. 152. Recent activity in the High Temperature Materials Sub-Committee of the Structures and Materials Panel yielded AGARD Report 634 "Mechanical Property Testing of High Temperature Materials" (1975) and AGARD Report 651 "Mechanical Properties of Ceramics for High Temperature Applications" (1976), and led to formation of a daughter subcommittee on Ceramics for Turbine Engine Applications. The specialists meeting which resulted was held in Cologne, Germany on October 8-10, 1979. Participation was broad and multinational. Attendance approached 200 and often caused "standing room only" in the meeting hall. Question and discussion periods were very active, and were limited by the demands of the schedule rather than by a lack of contributions or interest. Interaction between materials scientists, materials engineers, manufacturing engineers, and engine designers did occur, and sometimes led to constructive conflict. All of these were indicators of a successful meeting in an evolving, complex and promising area of materials and propulsion technology.

On behalf of the Structures and Materials Panel I would like to express our thanks to all authors, recorders, round table participants and session chairmen. In particular, the contributions of Dr Norman M. Tallan former Chairman, High Temperature Materials Sub-Committee, Mr George C. Deutsch, my predecessor as Chairman, Ceramics for Turbine Engine Applications Sub-Committee, and Mr John Acurio from our co-sponsor the Propulsion and Energetics Panel must be recognized. The activity that they and others initiated was well underway when I accepted the responsibility of leading its final phases.

HARRIS M. BURTE
Chairman
Sub-Committee on
Ceramics for Turbine Engine Applications

Accession For	
NTIS	GRA&I
DDC	TAB
Unannounced	
Justification	
By	
Date	
Initials	
Signature	
A	

CONTENTS

	Page
PREFACE by Harris M. Burte	iii
TECHNICAL EVALUATION REPORT by H.M. Burte and J. Acurio	vi
	Reference
<u>KEYNOTE ADDRESS</u>	
ENGINE TECHNOLOGY IN THE PROCESS OF CHANGE by W. Hansen	K
<u>SESSION I: REQUIREMENTS AND CRITERIA FOR GAS TURBINE ENGINES</u>	
BENEFITS OF CERAMICS TO GAS TURBINES by A. Brooks and A.I. Bellin	1
CERAMICS FOR SMALL AIRBORNE ENGINE APPLICATIONS by R.N. Katz and E.M. Lenoe	2
REQUIREMENTS FOR MATERIALS FOR LAND VEHICLE GAS TURBINES by D.F. Moss	3
TECHNOLOGIES CONCUES POUR L'UTILISATION DES CERAMIQUES DANS LES TURBOREACTEURS par S. Boudigues et G. Fratacci	4
DISCUSSION SUMMARY: Session I by E.M. Lenoe	D1
<u>SESSION II: ROTATING CERAMIC COMPONENTS</u>	
SILICON NITRIDE TURBINE BLADE DEVELOPMENT by F.B. Wallace, J.E. Harper, C.R. Dins, D.W. Richerson and H.L. Kington	5
DUO-DENSITY CERAMIC TURBINE ROTOR -- CONCEPTS, MATERIALS PROCESSES AND TEST RESULTS by R.R. Baker and A.F. McLean	6
DEVELOPMENT OF AN INTEGRAL CERAMIC BLADE-METAL DISK WITH CIRCUMFERENTIAL BLADE ATTACHMENT by S.A. McLeod, B.H. Walker and M.I. Mendelson	7
INVESTIGATIONS OF A HOT-PRESSED SILICON NITRIDE TURBINE ROTOR by E. Tiefenbacher	8
CERAMICS IN ROLLING ELEMENT BEARINGS by C.F. Bersch	9
THE FABRICATION AND PROPERTIES OF REFEL SILICON CARBIDE IN RELATION TO GAS TURBINE COMPONENTS by P. Kennedy	10
DISCUSSION SUMMARY: Session II by A.F. McLean	D2

SESSION III: NON-ROTATING CERAMIC COMPONENTS

STATIONARY CERAMIC COMPONENT CONSIDERATIONS FOR LARGE INDUSTRIAL COMBUSTION TURBINES by R.J.Bratton and K.L.Rieke	11
DEVELOPMENT OF CERAMIC NOZZLE SECTION FOR SMALL RADIAL GAS TURBINE by J.C.Napier and J.P.Arnold	12
DEVELOPMENT OF A CERAMIC TURBINE NOZZLE RING by H.Burfeindt, M.Langer and P.M.Stuart	13
DEVELOPMENT OF COMBUSTORS OF CERAMIC MATERIALS by G.Kappler, G.Langel and L.Schindhelm	14
SOME EXPERIENCE IN THE DESIGN AND EVALUATION OF CERAMIC COMBUSTION CHAMBERS by G.Sedgwick	15
DISCUSSION SUMMARY: Session III by K.Trappman	D3

SESSION IV: EMERGING DEVELOPMENTS

STATE-OF-THE-ART OF SiAlON MATERIALS by S.Dutta	16
PRESSURELESS SINTERING OF SILICON CARBIDE by E.Gugel and G.Leimer	17
HIP SILICON NITRIDE by H.T.Larker	18
NONDESTRUCTIVE FAILURE PREDICTION IN CERAMICS by A.G.Evans	19
FRACTURE STATISTICS IN DESIGN AND APPLICATION by C.A.Johnson	20
REACTION-BONDED, SiAlON AND CVD Si_3N_4 CERAMICS FOR ENGINEERING APPLICATIONS by D.J.Godfrey	21
COMPRESSION LOADED CERAMIC TURBINE ROTOR by R.Kochendörfer	22
OXIDATION AND HOT CORROSION BEHAVIOUR OF SINTERED NITROGEN CERAMICS by P.L.Cavallotti, U.Ducati and P.C.Martinengo	23
DEVELOPMENT IN SINTERED SILICON NITRIDE by E.Campo and P.C.Martinengo	24
DISCUSSION SUMMARY: Session IV by W.Wallace	D4

SESSION V: ROUND TABLE DISCUSSION

Prospects and Obstacles to Application Design and Materials Viewpoints

(Discussion not reproduced See Half Title Page for details of Chairmen and Participants	RTD
DISCUSSION SUMMARY: Session V by H.B.Probst	D5

THE POTENTIAL FOR CERAMICS IN AEROSPACE TURBINE ENGINES

A Technical Evaluation Report

By

Harris M. Burte
Director, Metals & Ceramics Division
Air Force Materials Laboratory
Wright-Patterson AFB, OH USA

and

John Acurio
Director, Propulsion Laboratory
U.S. Army Aviation R&D Command
Lewis Research Center, Cleveland, OH USA

OVERVIEW

The development of both materials and design technology to permit wider use of high temperature but brittle materials has been a goal of the aerospace community for many years. It has led to considerable success in demonstrating the potential of ceramics and graphites to perform as nose caps and leading edges of re-entry and other hypersonic vehicles. During the last decade there has also been growing effort in several countries to explore the application of ceramics to turbine engines. The motivation for much of the latter has been towards uses other than aerospace, such as in automobile engines and electric generators. Several programs have reached the stage of first generation attempts to design, fabricate and test actual components and it is timely to compile and assess the overall results, to identify deficiencies in the "state-of-the-art" and directions for future emphasis, and from the viewpoint of AGARD to evaluate the implications for aerospace applications. This Technical Evaluation Report provides such an evaluation from the dual and combined viewpoints of materials and engine technologies. It concludes that ceramics offer significant profitable potential for use in aerospace turbine engines and that the NATO/AGARD community should vigorously pursue the necessary technologies. Since this will involve expensive iterations of materials and design development, fabrication, and test, it is desirable to focus much of the effort towards a single goal and to stimulate more cooperative activity. A small, limited life, non man-rated turbine engine for missile applications is proposed as such a target.

INTRODUCTION

To provide a basis from which an evaluation of the "state-of-the-art" could be derived, and a forum to stimulate future progress, the Structures and Materials Panel and the Propulsion and Energetics Panel of AGARD cooperated to organize and conduct a multinational, multidisciplinary Specialists Meeting on "Ceramics for Turbine Engine Applications" which was held in Cologne, Germany on October 8 - 10, 1979. Twenty three papers during two very full days presented progress in materials, design and production technologies, the results of component test programs, and analyses of potentially profitable applications for ceramics and the requirements that these generate. They were supplemented by extensive discussion and a half-day round table designed to stimulate interaction between materials scientists, materials engineers, manufacturing engineers and engine designers, and to illuminate important issues.

ISSUES

Throughout the meeting, the participants were challenged to evaluate the status of the science and technology against a framework such as that as shown in Figure 1,

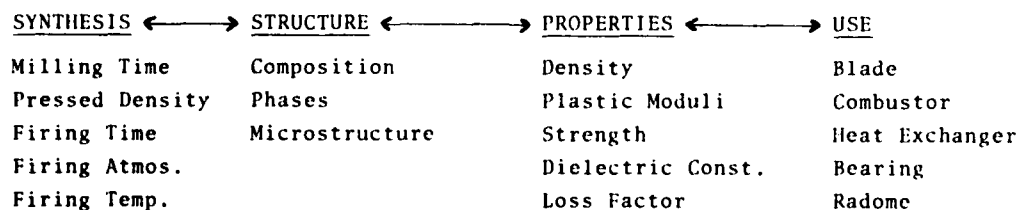


Figure 1. - An Approach to Organizing and Describing Ceramic Science and Technology

and to answer questions such as:

Are properties such as creep strength or oxidation resistance adequate for the intended applications?

Is the reproducibility or uniformity of properties adequate for the intended applications?

Is the understanding of structure \leftrightarrow property relationships in the materials being considered adequate to provide a guide to improved properties? Does it explain the sources of scatter in properties?

Is there enough knowledge of how to synthesize/process these materials to attain the desired microstructures (and thus properties) in components with desired geometries? Can this be done at affordably low cost?

Is the science base for ceramic processing adequate to support the scale up and productionizing of new approaches without encountering serious problems in uniformity or reproducibility?

Do the properties now measured in the laboratory really correlate with behavior in use?

Can the operating environment and the demands it places the materials - e.g. in terms of stress and temperature - be adequately analyzed and described?

Are design approaches being developed which take adequate cognizance of the brittle nature of ceramics? Are the materials parameters appropriate for such design approaches understood, and methods for measuring them available?

Is component testing carried to failure, and does it occur when and where materials properties and design analysis predict it will?

Are adequate inspection or other quality assurance approaches available?

For these and related questions, if the knowledge or capability necessary for the intended applications is not sufficient, the extent of current effort to remedy the situation, particularly in the NATO community, was discussed. Since more current effort is directed towards non-aerospace applications for turbines than for aerospace uses, the transferability of the technology from the former to the latter was considered.

Another set of questions considered by invited papers and during discussion focussed attention on projected uses and competition with other materials:

Based upon current knowledge and reasonable projections into the future, in what kinds of engines for what applications are ceramics good contenders?

What property, cost, uniformity etc. requirements must ceramics meet if they are to compete with other approaches such as improved/cooled superalloys or coated refractory metals?

What benefits must be possible to overcome the inertia of doing nothing (considering the risk and cost of the R&D involved)? What "windows" into first generation use are credible from the viewpoints of both technological possibility and attractive payoff?

The authors, representing both the Structures and Materials Panel and the Propulsion and Energetics Panel developed a set of broad conclusions and recommendations as a result of considering the questions and issues indicated above. These were tested during a concluding presentation to the meeting participants and with other appropriate members of the AGARD panels. There was no significant disagreement, and they are therefore offered for guidance within the NATO community.

CONCLUSIONS

1. The military value of higher operating temperatures for gas turbines is well established and was reaffirmed. Ceramics offer a very competitive route towards cost-affordable (using readily available raw materials) attainment of such higher temperatures.

2. Significant progress has been made in the last five years, but the technology required for highly profitable use of ceramics in turbine engines has not yet matured or been adequately demonstrated.

3. Three areas of technology have not received adequate attention. If ceramics are to compete with other approaches and/or fulfill their anticipated potential, much more emphasis than heretofore must be placed on:

a) Low cost processing, and the science base underlying the ability to synthesize ceramic components to a desired size, shape, microstructure and properties (including desired gradients or within necessary tolerances of geometry and properties).

b) Reduced cost approaches to quality assurance, and finding an optimum between process control and data generation, nondestructive inspection and proof testing.

c) The development of innovative design approaches-not only for the ceramic components but for the overall gas turbine - that adequately take account of the brittle and thus unforgiving nature of ceramics, and the cost of providing additional increments in materials reproducibility and uniformity.

Many other areas of the science and technology base such as resistance to slow crack growth at high temperature) warrant continued effort but relative to the three areas mentioned above they are already receiving significant attention under aerospace or non-aerospace projects.

4. Deficiencies in current ability to define detailed operating conditions or to analyze and predict the response of components or engine subsystems dictate that a combination of analytical and empirical approaches to the development of ceramic components and their use in engines must be pursued. Emphasis on the three areas of technology listed above must be closely coupled to continuous expensive efforts to fully characterize the materials being used, to design, fabricate and test (to eventual failure) realistic components, and to be prepared to reiterate this process. More involvement of ceramic materials suppliers in the mainstream of these efforts is required. At this time, hardware testing must be considered to be a necessary, albeit expensive part of learning and development, not as a go - no go demonstration.

5. The application of ceramics to critical gas-path components of small, limited life, non man-rated turbine engines appears to have high payoff for aerospace applications. No fundamental barriers inhibiting the use of ceramics for such an application have been defined. In the opinion of the authors, the prognosis for success is "good." It is credible in that it offers a worthwhile return on investment in a time which will not exhaust the patience or resources of the sources of support, or the enthusiasm of the research and development people.

RECOMMENDATIONS

1. The NATO community should vigorously explore and develop the potential of ceramics for use in turbine engines for aerospace. Increased effort is needed in the three areas of the science and technology base described above.

2. The expense and time (involving iterations) of the R&D task suggest that much of the limited resources available be focussed into developing and demonstrating the necessary technology for a single aerospace goal. Increased cooperative effort within and between the NATO nations is an obvious corollary.

3. The use of ceramics in a small, limited life, non man-rated turbine engine for aerospace uses such as in missiles is a credible goal towards which available resources should be focussed.

ENGINE TECHNOLOGY IN THE PROCESS OF CHANGE

by

Dr.-Ing. Wolfgang Hansen
Vice President of MTU Motoren- und
Turbinen-Union München GmbH

We engineers are said to be insufficiently interested in historical and economic circumstances. There may indeed be good reasons for this. Overcoming of obstacles which nature places in our path and the creative process of shaping new technical products leave us little time to look back. Yet we should not overlook that, without the achievements of engineers of genius in earlier generations and the achievements of notable companies both large and small, some of which no longer exist, we could not have been where we are today in technology.

So I should like to invite you to accompany me on an, admittedly, fragmentary excursion into the history of German aero engine construction. In the process, we shall have to span an era starting with the first flying machine of Clement A d e r (picture 1) and bringing us up to one of the world's most advanced supersonic aircraft, the Tornado combat aircraft (picture 2). About 100 years lie between these designs at the two extremes. It is a short period measured in terms of the history of mankind.

Flying was always a dream of man. Accounts of his unavailing attempts to emulate the birds crop up throughout the centuries. Two vital problems had to be solved, one that of aerodynamic lift and the other how to supply motive power. While the detailed sketches (picture 3) of a Leonardo da Vinci never took on real form, indeed were not even known to his contemporaries, Otto Lilienthal was able to prove to an astonished world that, at least, it is possible to glide (picture 4).

Endeavours by man to use his muscular power to get a flying apparatus to climb into the air, usually greeted with smiles, have never led to success, if we leave aside the recent crossing of the English channel, and it was conceded that more strength was needed by man than he could muster.

Before we concern ourselves further with technical development, I should like to sketch in briefly the general background against which major development in the field of engines took place.

Let us, for a moment, imagine ourselves back in the nineteenth century. Particularly the second half of that century is marked by the effect of the advancing industrial revolution and the spirit of enlightenment. Spreading out from England, a wave of industrialisation sweeps away the centuries-old social order based on the mediaeval estates. Crafts and craftsmen had certainly played throughout the centuries a subordinate role beside the important scholarly classes. Overnight, as it were, an industrial society arises which progressively becomes the dominating factor in the life of the peoples.

The population of Europe (picture 5) goes up by leaps and bounds. Around the year 1800, it was only more than 187 million, whereas at the end of the 19th century the European countries had already reached a population of 447 million, that is to say, an increase of approx 2 1/2 times. James W a t t devises his epoch-making inventions to improve the steam engine (picture 6). The steam engine thus becomes the first engine which can be used in a wide variety of industries. A new type of workshops emerges, in which items are "produced" in growing quantities. At the beginning, mechanical means had to be used to distribute energy, but soon the electric motor replaces belt drives. Electricity indeed transformed the daily scene.

Regular steamship lines come into existence; a changeover to steel construction for all warships is possible. George S t e p h e n s o n invents the steam locomotive and there follows a rapid succession of railways which provide links between the countries. Despite the protective tariffs and other trade barriers which are set up in a state of alarm, there is a rapid and irresistible growth of traffic routes between the European countries.

The morse telegraph and wireless telegraphy are introduced. International congresses come into fashion. A blossoming trade press disseminates scientific findings far faster than in previous centuries.

Now back to the aeroplane!

An engine-driven flying machine (picture 8) flies for the first time in 1901. In 1903, the Wright brothers (picture 9) build their first engine-driven flying machine and name it "Flyer 1". They had themselves to develop and build the water-cooled 4-cylinder engine with its modest output of 12 horsepower expressly for the purpose (picture 10).

Their flight should have attracted a lot of notice throughout the world.

However, the use of piston engines for land-bound vehicles had already progressed much further at this point in time, as is shown, for instance, by a glimpse at what two important pioneers of the aero-engine, Gottlieb D a i m l e r and Carl B e n z had

developed (picture 11), and the majority of the Wright brothers contemporaries doubtless gave better chances to a flying machine which separated the "lift" and "motive power" functions and did this very successfully, namely the airship with its gas-filled hull.

But let us go back a few decades again.

In 1860, the Belgian L e n o i r had invented a gas engine which differed but little from a horizontal steam engine. It was, however, the engineer Nikolaus August O t t o who, in 1867 (picture 12), together with Eugen L a n g e n , invented the four-stroke piston engine which still bears his name. As an engine which was operated with gas was involved, it could only be used as a stationary engine at the beginning. As soon as the new principle became known, inventors and engineers throughout the world, including Gottlieb D a i m l e r (picture 13) among others, set about developing an engine. The production version of the engine created by his chief designer, Wilhelm M a y b a c h , can be considered to have set a standard typical for all Daimler engines which were to follow.

Development proceeded apace. The first Daimler patent was granted in 1833. By 1893, Daimler had already brought out the taxicab (picture 14). By mid-1885, some 5,000 Otto engines had been manufactured in Cologne-Deutz alone. Quite an acceptable solution had been found to one of the most difficult technical problems, that of ignition in the combustion chamber. Rudolf D i e s e l evades it, when in 1892 he files his application for a patent on a self-ignition engine. In the year 1896 (picture 15), the first functioning Diesel engine is built.

The work of these and many other men set an example to enthusiastic aviation pioneers for their amateur engine constructions. Scarcely known are the names of many who emulated the example of the Wright brothers. Between the years 1903 and 1914, fervent and resourceful engineers developed countless variants of engines for use in flying machines (pictures 16 and 17). It is clear that low weight and a relatively high performance were always the most salient features of the first aero engines.

As an incentive, prizes were offered by various organizations and individuals for flights over specific distances or for engine performance. In this way, for instance, a Daimler engine was in 1911 awarded the prize of the "Automobiltechnische Gesellschaft". In 1912, a Benz engine won the famous "Emperor's Prize" (pictures 18 and 19), which had been offered personally by the reigning Emperor Wilhelm. For the prize, the best of 24 competing aero engines had been selected.

In this period up to the outbreak of World War I, numerous companies were set up. Here I can name only just a few.

In 1909, Karl M a y b a c h (picture 20) founds his company "Luftfahrzeug-Motoren GmbH", which in 1912 is turned into "Maybach-Motoren GmbH Friedrichshafen".

Gustav O t t o , the son of the inventor of the Otto engine, sets up in 1910 in Munich an aeroplane factory in which, at the beginning, not only aeroplanes but also the engines for them were manufactured. The list of newly set-up companies (picture 21) from this time includes familiar names which later emerge in companies whose products have nothing more whatsoever to do with aviation.

Now let us look also at the major technical developments, apart from the engine types. It is a surprise for us to find that most features of modern piston aero engines had already been developed in the years up to 1914:

- manufacturing techniques for lightweight construction
 - multi-stage carburetors and fuel injection
 - air-cooled cylinders
 - sodium-cooled valves
 - precompression of air, inter alia for turbo-superchargers
- and so on.

Nevertheless, some of the engine designs were exotic by today's standards. Four- and six-cylinder in-line engines were tried out, but also Vee engines and radial engine with rotating cylinders or rotating crankshafts.

Eventually, by 1914 German aero engine development had caught up with foreign designs. Then came World War I. The military command recognized the importance of the aeroplane (picture 22). The variety of models had to be drastically cut down. Only a few of the still young companies survived. For the first time, aero engines are manufactured in considerable quantities. After the war, aero engine manufacture was not allowed in Germany at first, and so the companies looked for other uses for them, for instance to power motor vehicles or ships.

Thus it was that Karl M a y b a c h came to build, in the twenties, those now famous deluxe automobiles (picture 23) whose fortunate owners nowadays still gather together once a year in Friedrichshafen.

In 1924, M a y b a c h built the first Diesel-powered railbound vehicle (picture 24) in the world, thereby founding a tradition which is upheld by the present-day Friedrichshafen company of Motoren- und Turbinen-Union.

Let us take a brief look at the family tree of the Munich branch of MTU, which at the time was in competition with M a y b a c h (picture 25). In 1923, B M W (Bayerische Motorenwerke) is set up in Munich, being built up, as can be seen, from the earlier aeroplane and aero engine development activity. At that time, air traffic was already a permanent albeit more luxurious part of the general volume of traffic. Ultimately, in 1926, Deutsche Lufthansa AG was founded. Aero engines, as the motive power for regular scheduled traffic in the air, had adequately proved themselves.

Now let us turn to another, less conspicuous problem area, which rapidly gained in importance when aviation began on a regular basis: that of "reliability".

To start with, designers were satisfied if their engines lasted 10 - 50 hours. By then, it was in any case time to strip them, to salvage serviceable parts, to repair them or to scrap them. Then came the requirement that regular civil air passengers had at all cost to arrive at their destinations unharmed. Data on the reliability of engines in those days is now very difficult to come across. Let one example serve for many.

The famous BMW 132 radial engine (picture 26 and picture 27) achieved by 1940 a TBO of about, 1,000 hours. By the way, several Ju 52 aircraft are still flying nowadays, for example in Switzerland, with these engines.

Here it becomes clear what effort was needed, comparatively, to make progress in improving design and quality. Three major factors played a role:

- materials
- calculation of safety factors
- and quality control of components.

Now that we have seen that the main features of aero engine design had been developed by the twenties, let us turn briefly to the question of what the situation was on materials.

A story of the development of materials in the 20th century would rapidly convince the reader that most of the crucial discoveries nowadays in materials technology date from the century in which we are living. Let us single out one typical aviation material, aluminium (picture 28), a material which now seems almost antiquated. Nevertheless, so-called Duralumin, an AlMgMn alloy, was not discovered until 1906 by W i l m . It is one of the first high-strength, corrosion-resistant and, at the same time, fine-grained aluminium alloys.

However, not only the materials themselves but also knowledge about them at the turn of the century was, by present-day standards, still in its infancy. As an example, one of the classic authorities among German materials scientists C. B a c h wrote in 1905, in what was for a long time a standard work:

that he declined "to determine the safe working stresses from strength under the various types of loading by dividing with a safety factor, as the gap which exists, for instance, between tensile strength and safe working stress under static load seemed to him to be too big".

Not until the years after 1945 did knowledge about the effect of multi-axial states of stress, elevated temperatures and incipient crack formation lead to an exact design of engine components.

That non-destructive testing was also still in infancy, can be seen from the example of X-ray inspection. In 1917, a start was made in England at Woolwich Arsenal with radiological examination of solid bodies.

In 1929, in Germany, the German Society for Technical Radiology was founded.

Just from these dates it can be inferred that it was a long time after aero engines had started in service in civil aviation that X-raying for non-destructive testing of materials could become a means of quality inspection. By the way, magnetic particle testing, too, was not patented until 1919 by W. E. H o k e . So it is not surprising that the pioneers of aero engine technology suffered countless setbacks before they could build sturdy engines. All the more remarkable is the high standard of performance, as development of all crucial components for modern piston aero engines went on until the years after 1945. So there was considerably more technological basic knowledge available for an entry into the gas-turbine era than there had been when the piston engine was started.

The fascination of a new dimension to shape the world in which we live spurred on engineers at the beginning of the 20th century to a headlong development of aero engines. Sporting ambition was coupled with dogged engineering toil and led, via countless failures, even without the adequate backing of theoretical fundamentals, to technical solutions of genius. The application of the engine for locomotion on land, on water and in the air, has transformed the world since the end of the 19th and the beginning of the 20th century.

In the thirties of this century, it became ever clearer that the piston engine with propeller to power aircraft scarcely allowed a further increase in the flying speeds already achieved. This applied particularly to high altitudes. It was then that a start was made with development work on mobile gas turbines and rocket motors.

The principle of gas turbines had long been known. Franz S t o l z e (picture 29) had a gas turbine machine patented in 1897 and conducted tests with the first such machine in the next years. To start with, he had no great success. The materials available at the time could not withstand the high stresses and basic knowledge of aerodynamics was inadequate or still unavailable to design a gas turbine in the best possible way.

Incidentally, the first design for a sort of "gas turbine with extremely slow speeds" also dates back to Leonardo da V i n c i (picture 30). Around the year 1500, he designed a simple auxiliary device to turn meat which was being roasted, for installation in a fireplace or, as one might put it, "complete with ceramic combustion chamber".

In the year 1910, the K ö r t i n g brothers' (picture 31) in Hanover built the first explosion gas turbine to H o l z w a r t h ' s specifications, with an output of 200 horsepower. Other gas turbines, exclusively to drive generators, were to follow.

A start was made in Germany on developing the gas turbine as a jet engine (picture 32) around 1935, first of all at the H e i n k e l company and later at B M W as well (picture 33 and picture 34). In August 1939, the first successful flight by a jet-propelled aircraft was made. The aircraft had been built by the H e i n k e l company. Designated the He 178, it was powered by a jet engine which developed a thrust of 380 kp.

During this period, there were already four companies in Germany occupied with the development of aero gas turbines, namely J u n k e r s , B M W and D a i m l e r - B e n z in addition to H e i n k e l . Important features of the gas turbines developed by B M W , even in those days, were the axial compressor and the annular combustion chamber.

The scientific work carried out by the Aerodynamics Research Institute at Göttingen was an aid in designing and testing compressors. The first B M W experimental engine reached the test bed in 1941 and achieved a modest thrust of 150 kp (picture 35).

Of interest is the design of its turbine wheel, which was divided into two parts. Between two turbine discs, blades formed from sheet metal were welded in, and cooling air flowed inside through the blades.

The welding work created great difficulties, as one can readily imagine. At the beginning, the blades broke away at 8,000 r.p.m. In addition, the combustion chamber produced a non-uniform temperature profile, which led to local overheating of the turbine blades. As one sees, some of these basic problems in turbine construction have still not been completely solved.

In 1943, the first prototypes of the BMW 003 engine were built and a start was made on series production virtually at the same time. Several 700 of these engines were manufactured but only a few reached practical service. If a closer look is taken at a table of leading data on the gas turbines developed in Germany at that time (picture 36), it is amazing what performance those engines already had, despite the inadequate materials then available. Another handicap was that, for obvious reasons, these very latest power units had to be developed in the greatest secrecy.

If reports are read on the early years of gas turbine development, the following thought persists: the crucial aspects of technical problems have changed little right up to the objectives for further development remain the same. What is a decisive change, on the other hand, is the demand for a longer service life of such power systems.

I come now to the latest period of aero engine development in Germany, for which I want to take only the gas turbines into consideration and not to deal any further with piston engines. In the fifties, it was possible, also in Germany, to gradually resume and continue development work. German engineers and - not least important - the manufacturing and testing facilities as well, lagged almost hopelessly behind those in the U.S.A. and England. It could be said, jumping ahead to the position nowadays, that German research and industry caught up in this field, too, only through participation in international programmes such as the one, for instance, on the RB 199 engine.

Scarcely noticed by the general public, six German companies, at first largely independently of one another, had since about 1958 been doing fundamental work on experimental turbines and had started to manufacture under licence. The companies involved were Heinkel, Junkers, BMW, KHD, Daimler-Benz and M.A.N. There is not time here to even attempt to describe the stages of development which the companies had reached. The high costs involved in products demanding high standards in development and manufacture compelled concentration in the German aero engine industry. Nowadays, only the KHD and MTU companies still have a stake, with items they developed themselves, in important international programmes.

At this point, let me show the complete family tree of MTU (picture 37). It can be seen that, in this company, the aero engine developments of BMW, MAN and Daimler-Benz have been combined through merger of the respective capacities. In the field of aero engine construction, MTU thus carries on the tradition associated with the names of Otto-Daimler-Maybach and Benz from the very beginnings of engine technology. At the same time, MTU is nowadays the biggest company which develops, manufactures and provides support for aero gas turbines. Let us not fail to recognize, however, that the total European volume is still comparatively modest (picture 38 and picture 39).

A start was made by us at MTU with the manufacture under licence of engines from 1958 onwards. In this context, the J 79-11 A (picture 40) for the Starfighter and the J 79-17 for the Phantom combat aircraft must be mentioned. This engine, built in great numbers all over the world, constituted the foundation on which production was built up on modern lines.

Later on, there followed the T 64 engine (picture 41) - also under licence from GE - as well as the TYNE MK 21 and TYNE MK 22 as a turboprop engine under licence from R.R. (picture 42). Finally, there is the Larzac engine (picture 43) which MTU is nowadays manufacturing for the Alpha Jet in cooperation with one German and two French companies.

Engines and components for military use make up more than 80 % of MTU's turnover. An objective of the company is to increase gradually the share of engine manufacture for civil aviation. A substantial part of development capacity is also used for the latter purpose.

An important feature of all expenditure on development by companies which are developing gas turbines is nowadays the significance which material technology has acquired in this framework. For this reason, MTU is also dealing with specific crucial aspects of this specialized field. Among other things, these include

(picture 44)

- investigation of mechanical strengths of metallic alloys under actual service stress

(picture 45)

- investigation of the effect of hot-gas corrosion on the service life of turbines and components and the development of appropriate protective coatings

(picture 46)

- optimisation of processes for joining components

(picture 47)

- further development of processes to make extremely small cooling-air holes in turbine blades

- further development of special methods for measuring the dimensions of components and for non-destructive testing of them

(picture 48 and picture 49)

- and finally - last not least - the design, testing and entire further development of ceramic components.

This brings us to the subject for this meeting.

In this paper with its largely historical bent, permit me one last glance backward at historical development, again only in outline.

In the year 1943, a member of the staff of M.A.N., Augsburg, Dr. A. Schütte, took out a patent on (picture 50) a turbine rotor which had interesting features. It involved a ceramic turbine wheel held between two shafts with disc-shaped attachments of steel. From 1940 onwards until 1959, experiments were made at M.A.N. with all sorts of ceramic blades (picture 51). The records show that in those days silicon carbide, nitride, boride, silicon oxide and many mixtures such as steatite were already familiar. Intensive cooperation with ceramics manufacturers had also been started.

In the same period, but apparently without people at the one company knowing what people at the other were doing, the people at J u n k e r s working on the development of aero gas turbines were trying out ceramic blades for the gas turbines which were just coming into existence. On all sides, difficulties were being encountered with the problems of high brittleness, of big fluctuations in properties, inadequate strength and of processing as well. Even in those days, the considerable possibility of saving costs on materials had been recognized. This happened, in Germany, particularly under the harassment of the inadequacy of available supplies of chromium and nickel.

From this period, the most varied vaporizing methods in fixing ceramic blades in metal discs are known: vapour-deposited or brazed-on metal discs, embedded foils or also wire gauze. Even abradable coatings or abradable rings made of ceramics, which were intended to be run in when contact was made with them, were tried out so long ago. These are also design features which, nowadays, play an important role in the RB 199 (picture 52) engine. No publications from those days are available, as such work had to be kept secret.

Somewhere around 1959, this development work was discontinued at M.A.N. I suspect that, up to that time, publications from the America literature, for instance those of B o b r o w s k y from the year 1949, were not known at all. At any rate, ceramic components today, forty years after those initial beginnings, are still largely at the stage of component or prototype trials. Maybe your reports at this meeting will give us another picture.

One is mindful of the fact that the development of materials until they are actually used in technical products obviously takes much longer than does, for example, the development of new types of engines. Let me remind you: nine years after the invention of the four-stroke gas engine, this engine was already being produced in considerable numbers. As against this, let us compare the application of the material titanium. In 1795, it was discovered by Messrs. G r e g o r and K l a p r o t h in oxide form. Only 170 years later was it possible for titanium to be used as a structural metal in industrial products.

Or let us take another example, nickel. In the middle ages, Saxon miners tried to extract copper from reddish-brown niccolite, which they mistakenly considered to be copper. As they were not successful in doing so, they felt somehow that "demons" had hoaxed them ("old Nick"!). Another expression used for demon in the language at that time was "nickel" and that is how the metal acquired its name. In 1751, C r o n s t e d t finally discovered the metal, which has been produced since 1905. By 1928, world production was only some 45,000 tonnes.

It can be said that, up to the present time, the properties of metal alloys are far from being fully explored, and already the spectre of reserves becoming scarce is making its rounds. It is reported that chromium and nickel will not even last for 100 years.

I do not wish to, and cannot here, go into the degree of probability behind such predictions and whether, perhaps by way of recycling, there may be possibilities of holding up this demise.

At all events, mankind is summoned to bid farewell to the thought that the materials used so far are available in unlimited quantity.

One possible path to escape coming bottlenecks is certainly by way of new materials, or had I better say "old" materials? Only recently, it was disclosed in the press that the estimated age of stone tools of quartz found during excavations near Ptolemais in northern Greece was some three million years. Stone and wood are certainly the oldest materials which man has made use of. If the runaway pace of the technical world, in which new developments succeed each other at ever shorter intervals, allows it at all, it might be suspected that the 21st century will nevertheless see a return - admittedly with more refined ceramics - to a sort of "stone age".

It is true, of course, that there are some technical problems to be solved in the meantime, and the papers to come will deal with them. It seems to me - I want to conclude this excursion into the past with a thought for the future - that there are also some psychological problems to solve. These include, for instance, a better understanding, by those concerned with ceramics, of the objectives and the realities. Better understanding must come

- between materials specialist and designer
- between materials practitioner and stress theoretician
- between materials user and ceramics manufacturer
- and, finally, between industry and research.

K-7

Ceramics will lose the stigma of an exotic material. The gas turbine of ceramics - as one of the possible applications - is nevertheless not an objective like that of the landing of the first man on the moon. This was goal and fulfilment at the same time, the beginning and end of a mighty effort by mankind. The journey of technical ceramics towards extensive application, though beset by inevitable setbacks, was to be marked by a continuous struggle for step-by-step solutions.

Munich, 8th October 1979

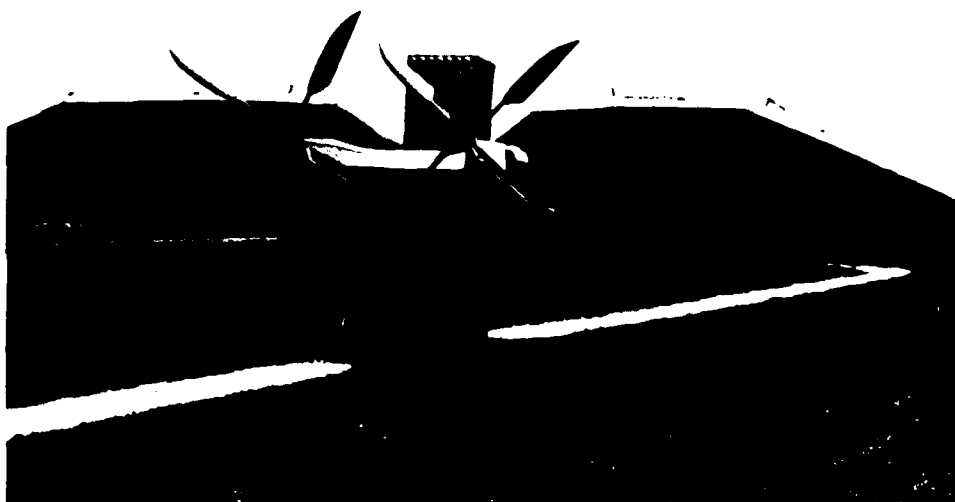


Fig. 1
Clement Ader's
aeroplane of 1878



Fig. 2
Tornado MRCA,
1978

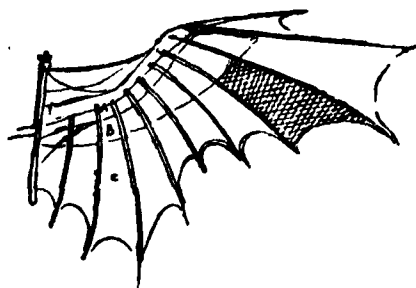


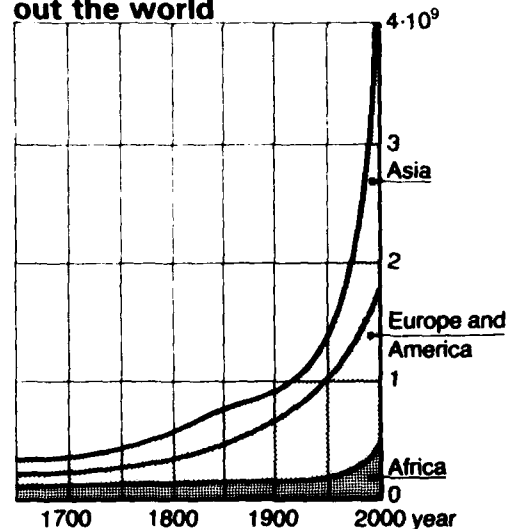
Fig. 3
Leonardo da Vinci (15.4.1452 - 2.5.1519)



Fig. 4

Otto Lillenthal
(23.5.1848 – 10.8.1896)

**Population growth through
out the world**



Population growth in Europe

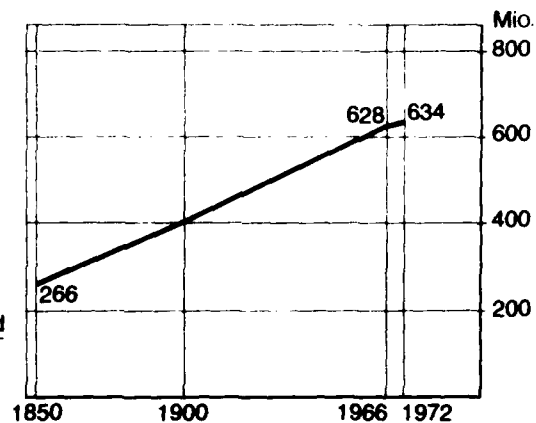


Fig. 5

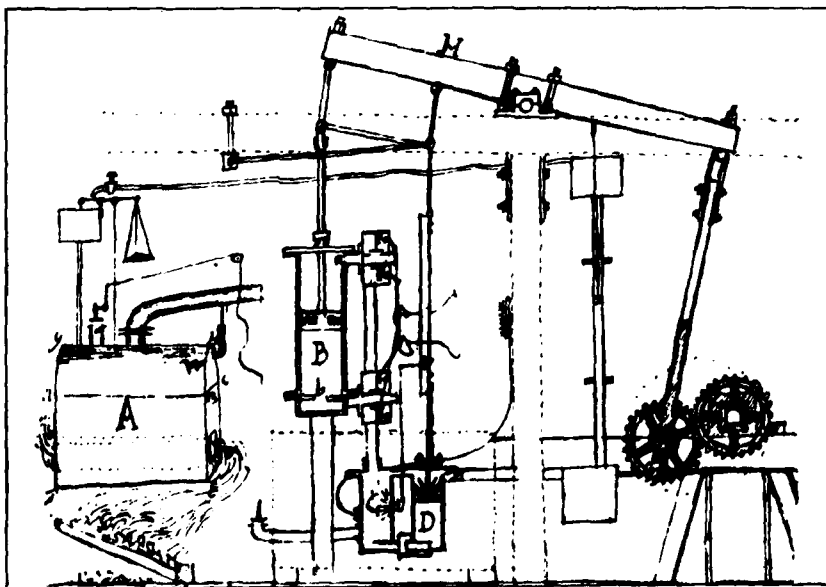


Fig. 6

James Watt's steam engine,
1784



Fig. 7
View of mechanical
workshop of the
Deutsche Elektrizitätswerke
showing the
belt-drive system

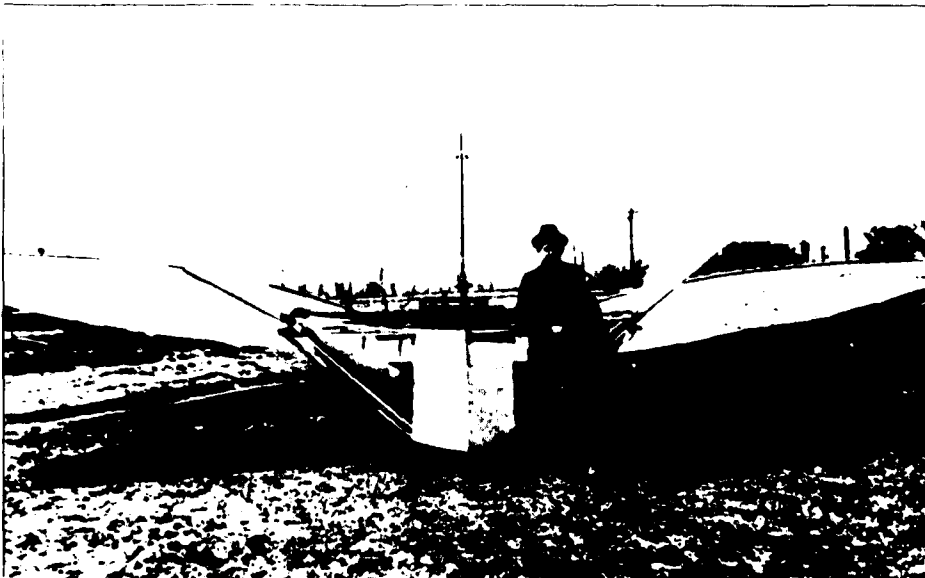


Fig. 8
First flight by
Gustav Weisskopf
in 1901

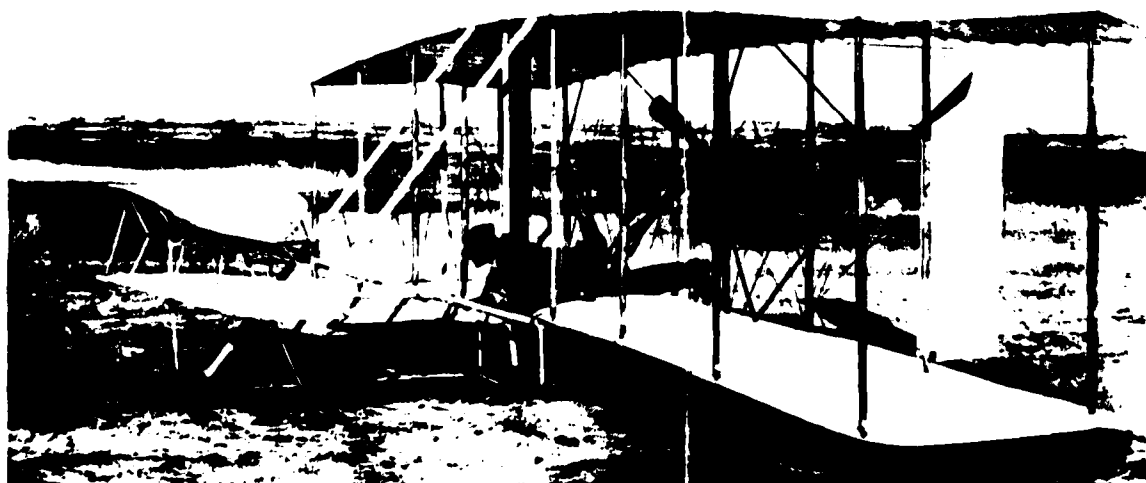


Fig. 9
„Flyer I“, 1903



▲ Fig. 14.1

Benz-omnibus, 1895
(5 HP, 8 - seater)

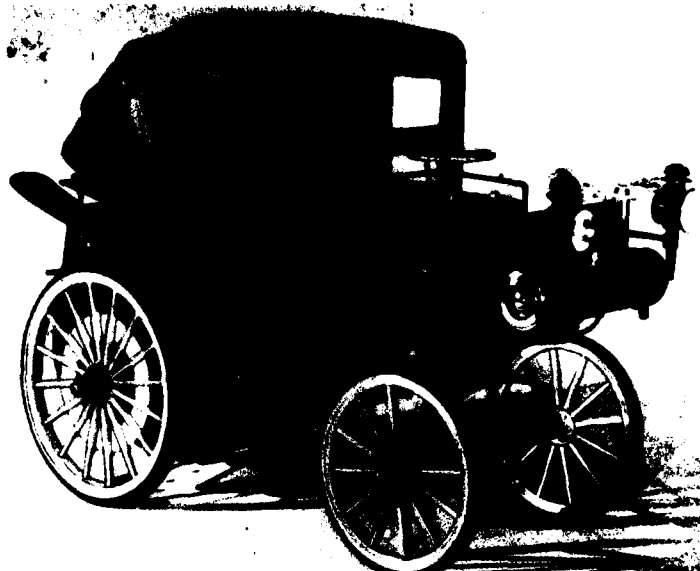


Fig. 14.2 ►

First DB-taxi, 1897
(4 HP, 25 km/h)

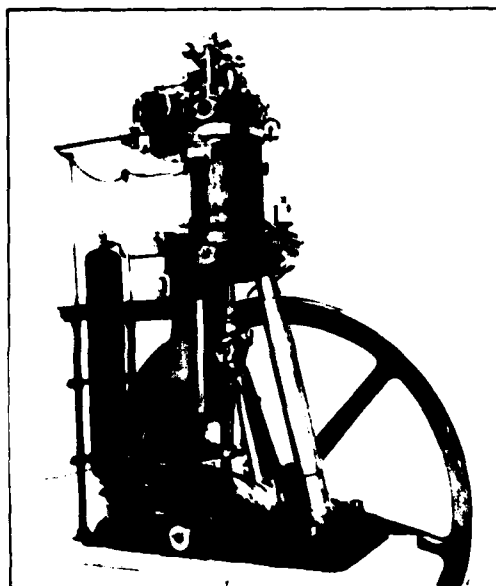


Fig. 15

First operational Diesel engine, 1896

In-line engines for aircraft built up to 1922 (selection)

Year (approx)	Make	No.of Cylinders	Hp	Country
1903	Original Wright	4	15	USA
1909	Adler	6	50	Germany
1909	Mercedes-Daimler	4	80	Germany
1912	Austro-Daimler	6	120	Austria
1915	Benz	6	160	Germany
1915	Rolls-Royce	6	100	Great Britain
1915	Maybach	6	180	Germany
1916	Mercedes	6	180	Germany
1917	BMW	6	185	Germany
1917	Siddeley-Puma	6	250	Great Britain
1920	Maybach	6	260	Germany

Fig. 16

V-engines for aircraft built up to 1923				
Year (approx)	Make	No. of Cylind.	Hp	Country
1905–1907	Antoinette	8	50	France
1907	Körting (airship engine)	8	75	Germany
1909	H. Grade (2-cycle)	4	30	Germany
1910	Wolseley	8	60	Great Britain
1913	Renault	8	80	France
1915	Rolls-Royce "Falcon"	12	250	Great Britain
1916	Hispano-Suiza	8	200	France
1917	Rapp	8	200	Germany
1917	Rolls-Royce "Eagle" VIII	12	360	Great Britain
1918	Sunbeam "Manitou"	12	300	Great Britain
1923	Fiat	12	700	Italy

Fig. 17

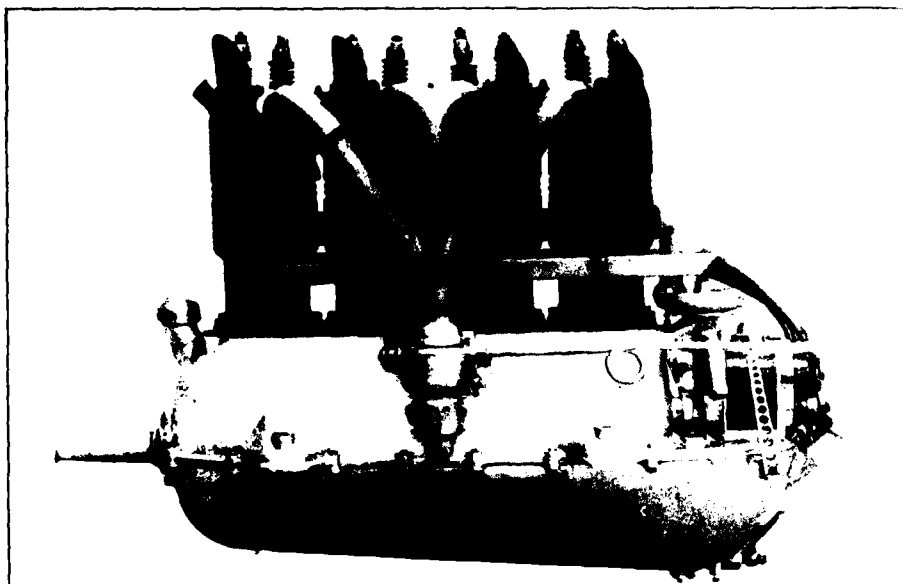


Fig. 18

Benz "Kaiserpreis"
engine, 1913

Characteristics of Benz "Kaiserpreis" engine

Water cooled, 4-cylinder in-line aero engine

100/90 HP at 1350/1280 rpm

Individual vertical cast-iron cylinders with
welded sheet-steel cooling jackets

Two overhead valves per cylinder
actuated by push-rods

Mixture preheating by cooling
water-heated intake pipe

Fuel consumption 210 gr/HP/h

Power to weight-ratio: 1,5 kg/HP

Fig. 19

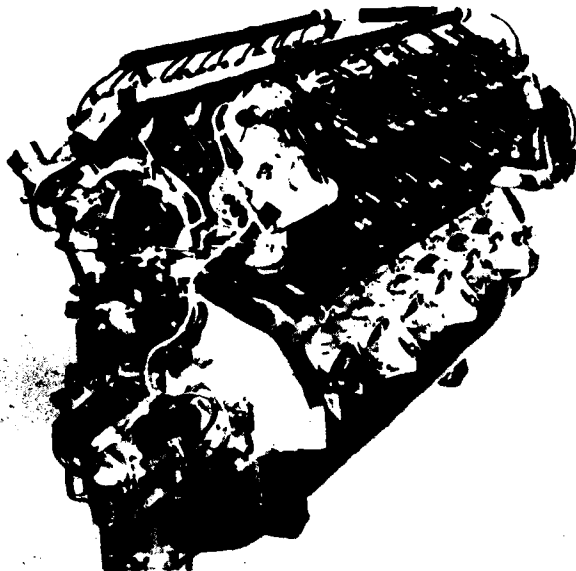


Fig. 20
Maybach aero engine (VL2)

German aero engine manufacturers up to 1918

Year	Company	Location
1906 - 1910	Argus-Motorenengesellschaft mbH NAG Neue Automobilgesellschaft mbH Hermann Haake, Motorenbau	Berlin-Reinickendorf Berlin-Oberschönweide Berlin-Johannisthal
1910	Adler Motorenwerke, vorm. Heinrich Kleyer Daimler-Motorenengesellschaft August Arthur Delfosse, Motorenwerk	Frankfurt am Main Stuttgart-Untertürkheim Köln-Riehl
1911	Rheinische Aerowerke GmbH Hilz-Motorenfabrik GmbH Paleus und Beuse Luftfahrzeugmotorenfabrik J. Schneeweis Motorenfabrik Steffen H.W. Schulz Aeolus-Flugmotor-GmbH	Düsseldorf-Oberkassel Düsseldorf Berlin-Neukölln Chemnitz Kiel Karlsruhe Berlin
1912	Benz u. Cie Nürnberg Motoren- und Maschinenfabrik Carl Wunderlich, Motorenfabrik Oskar Kersten, Spezialmotoren für Flug- und Luftschiffe Gebr. Körting AG Opel-Werke AG Rotor-Werke, Georg Hoffmann Dixi, Luftfahrt- u. Bootsmotor-Verkaufsgesellschaft mbH Riedl-Motorenengesellschaft mbH	Mannheim Nürnberg Berlin Berlin Körtingsdorf b. Hannover Russelsheim am Main Frankfurt a. Main Oberursel Berlin Chemnitz
1913	Motorenfabrik Oberursel AG (zunächst Lizenz Gnome) Rapp-Motorenwerke GmbH Otto Schwade u. Co., Motorenfabrik Flugmotorenfabrik Deutschland GmbH (Rapp) Motorenfabrik Sirius GmbH Basse u. Selve	Oberursel b. Frankfurt/Main München Erfurt München-Milbertshofen Nürnberg Altena i. Westfalen
1914 - 1918	Bayerische Motorenwerke Gasmotorenfabrik Deutz Güldner-Motorenengesellschaft Maschinenfabrik Augsburg-Nürnberg Maschinenfabrik L.A. Riedinger Maybach-Motorenbau GmbH Stoewer-Werke AG Maschinenfabrik Georg Goebel Rhema-Rhenania, Motorenfabrik Siemens u. Halske AG	München Köln-Deutz Aschaffenburg Augsburg Augsburg Friedrichshafen a.B. Stettin Darmstadt Mannheim Berlin-Siemensstadt

Fig. 21

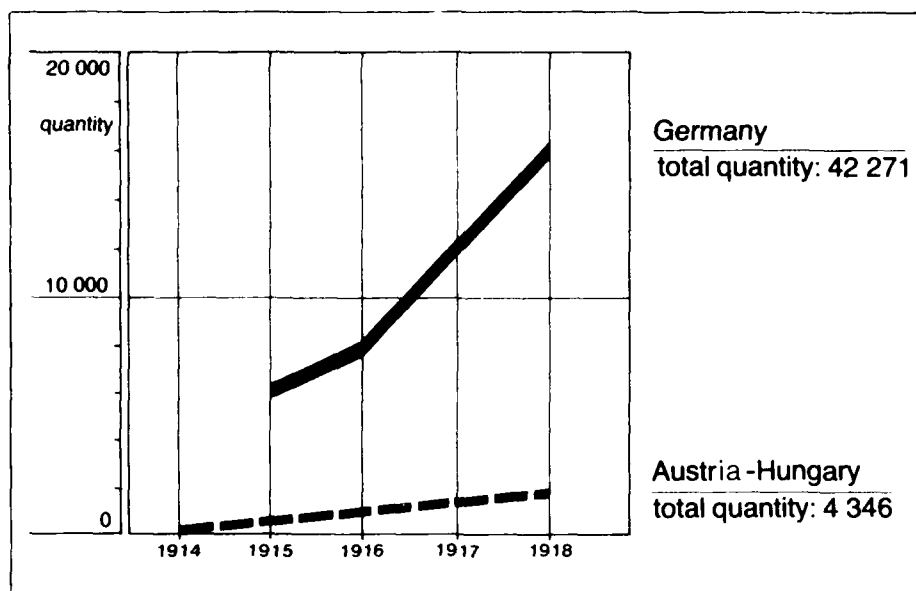


Fig. 22

Aero engine
production figures
1914-1918
(Germany and
Austria-Hungary)

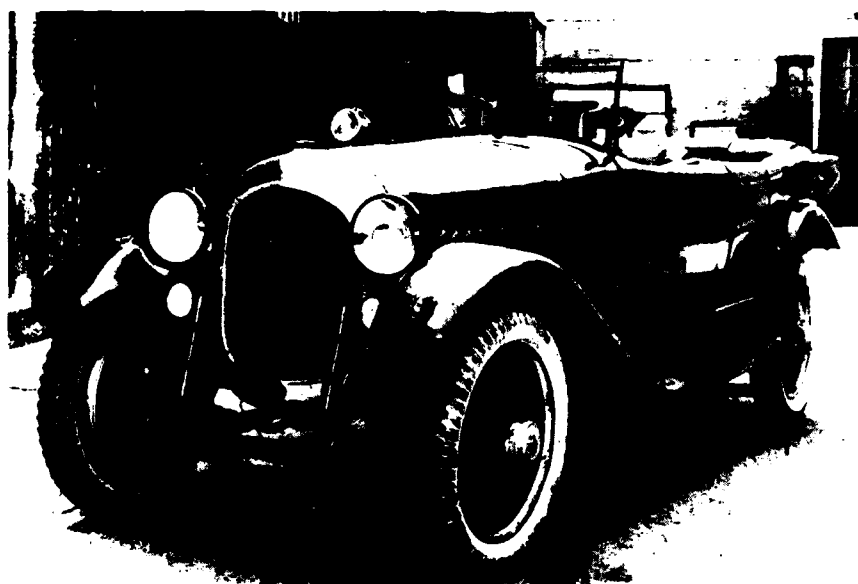


Fig. 23

Maybach car
built after 1920



Fig. 24

Diesel railway traction
unit Maybach
"Seddinger Triebwagen"

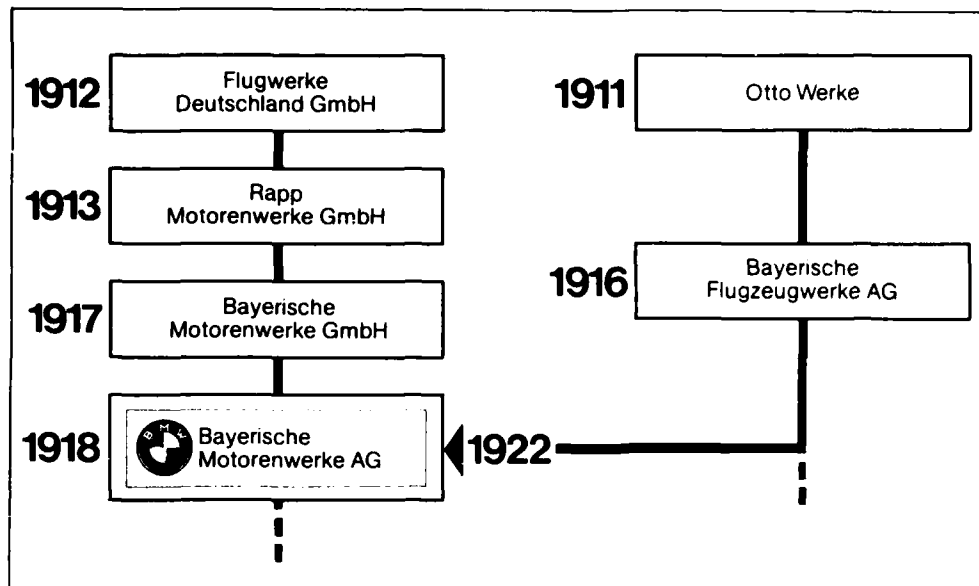


Fig. 25

Section of MTU's
genealogical tree
(1912-1922)

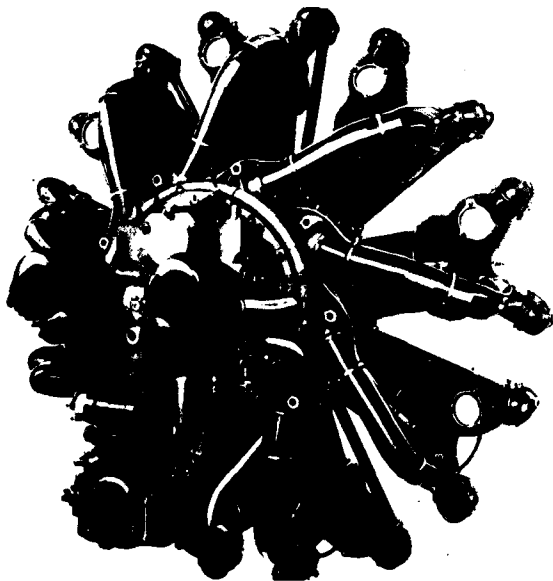


Fig. 26

BMW 132 radial engine

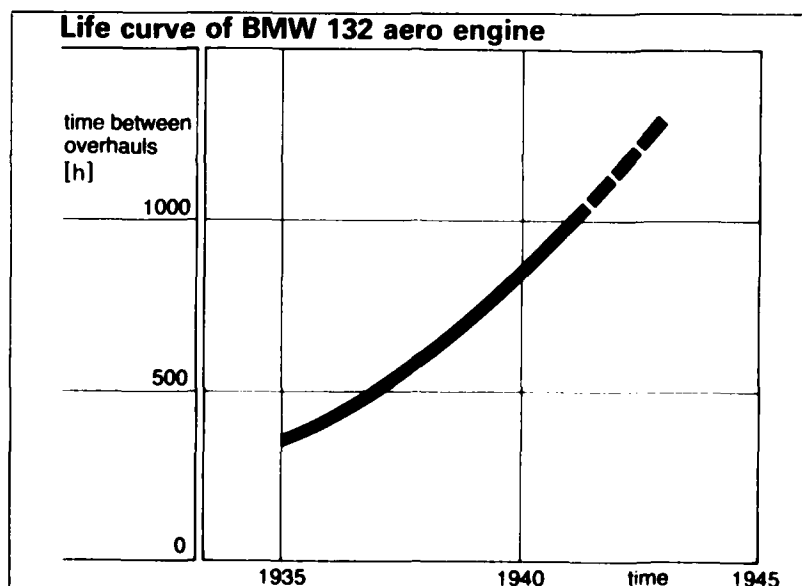


Fig. 27

Production figures for aluminium alloys 1920-1955

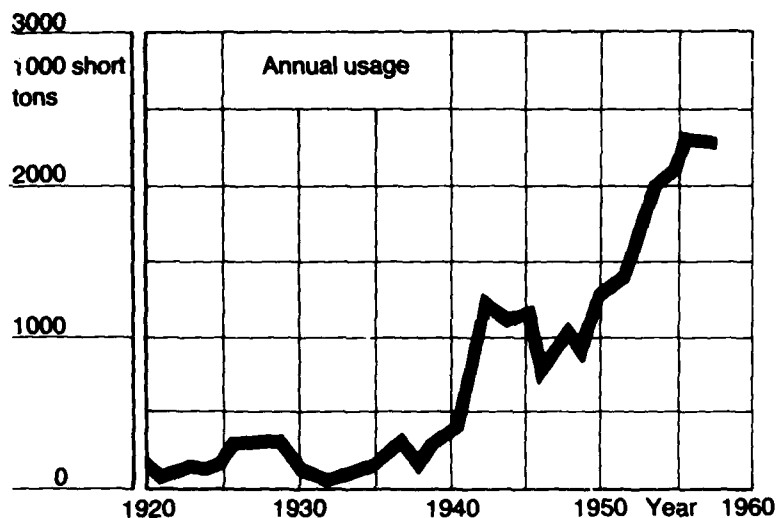
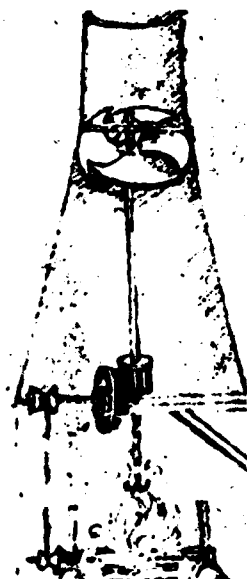
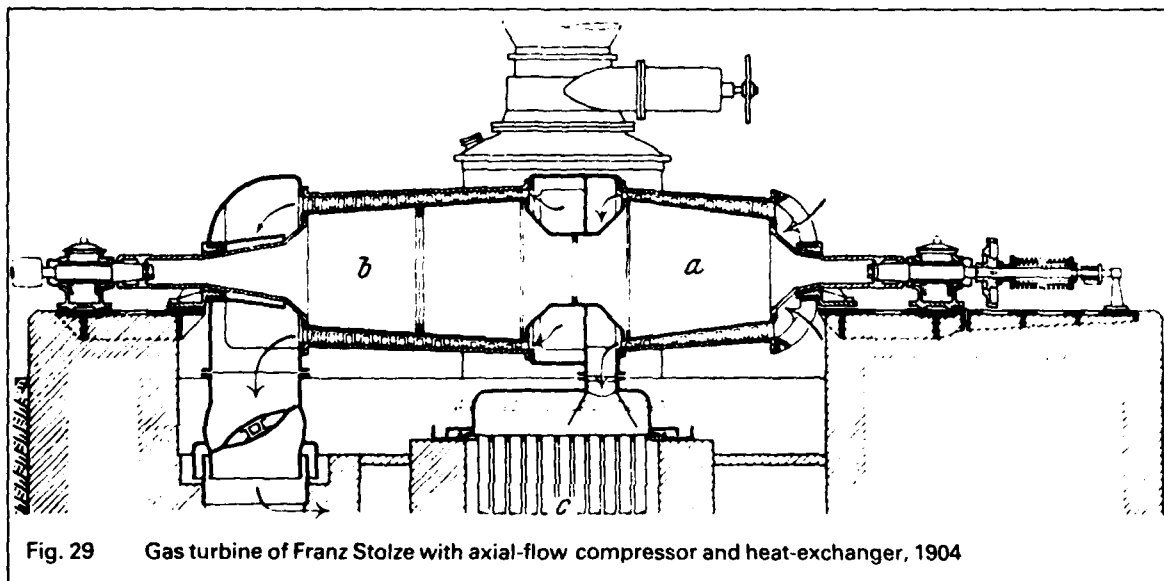
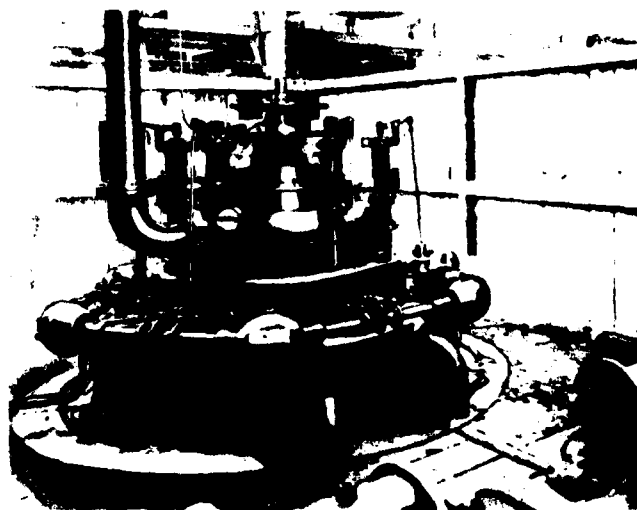


Fig. 28



◀ Fig. 30
Spit by
Leonardo da Vinci



▲ Fig. 31 Gasturbine by H. Holzwarth
built by Gebr. Körting AG, Hannover, 1909

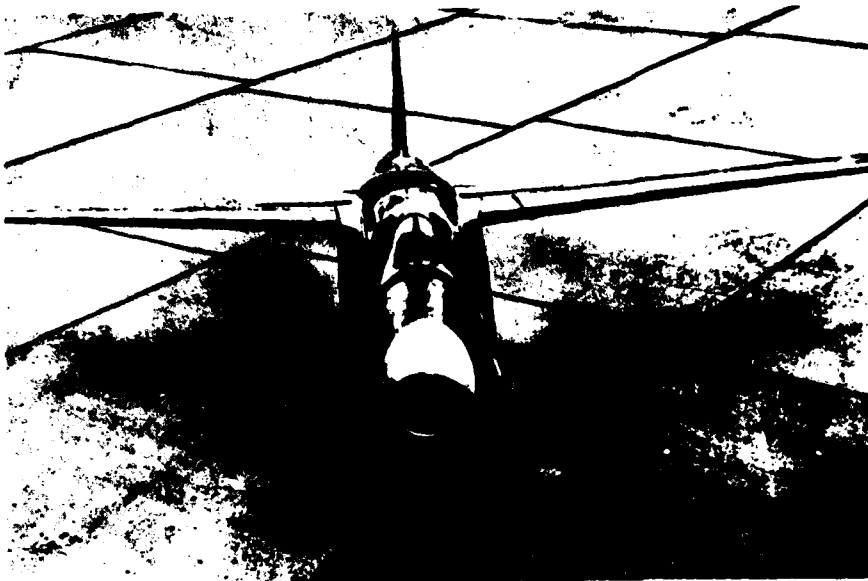


Fig. 32
Heinkel He 178 powered
by HeS-3-B jet engine

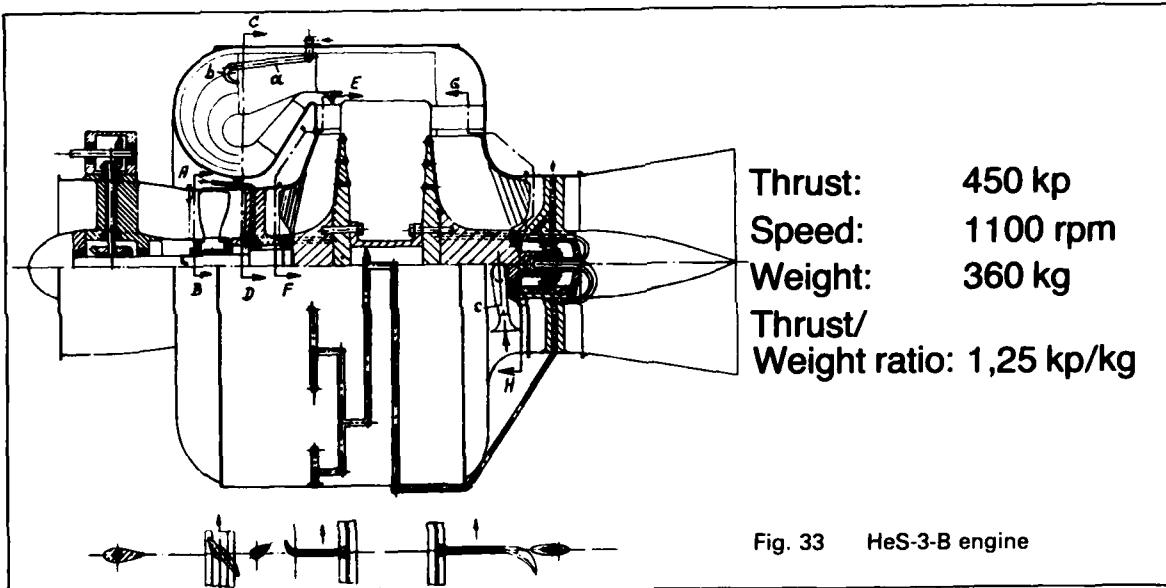


Fig. 33 HeS-3-B engine



Fig. 34
He 162 "Volksjäger"

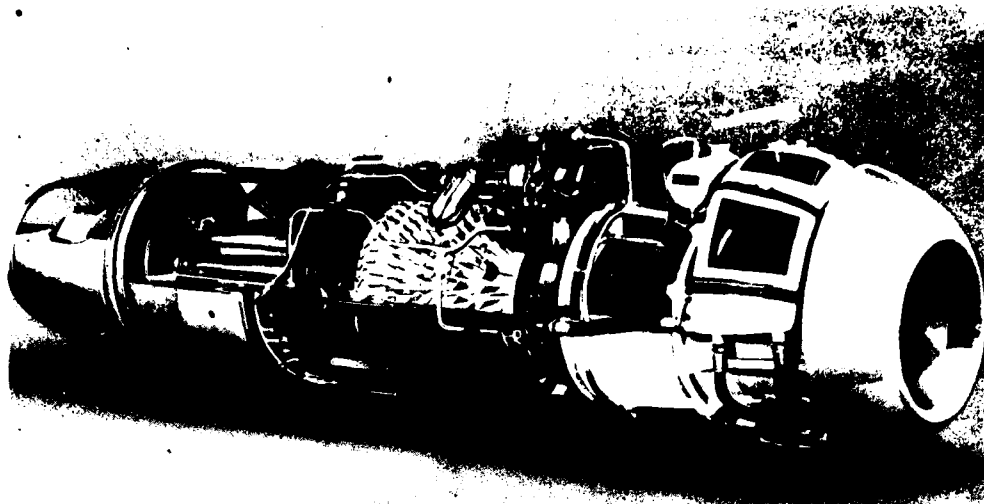


Fig. 35
BMW-03
single-shaft
jet engine,
power to weight
ratio 1.4 kp/kg

Make	Type	Power/ Thruster	spec. fuel cons.	Temp.	Speed.	Weight	Length	Diameter	Compressor	Comb. chamber	Turbine	Remarks
Junkers	TL 109004 B	900 kp	1.4 kg/h/kp	800° C	8700 rpm	750 kg	3820 mm	762 mm	8-stage axial-flow 3.5:1	6 comb. chambers with counterflow injection	Single-stage with hollow blades	Improved production aircraft, several 1000 built
BMW	TL 109003 A	800 kp	1.4 kg/h/kp	770° C	9500 rpm	606 kg	3500 mm	712 mm	7-stage axial-flow 3.1:1	Annular uniflow injection	Single-stage hollow air- cooled blades	He 162 „Volkstiger” production aircraft
Heinkel- Muth	He. S. 3	500 kp	—	—	13000 rpm	360 kg	1220 mm	965 mm	axial-flow compressor radial blower	Annular reverse-flow	Radial turbine	experimental machine World's first jet to fly. He 176

Fig. 36 German aero engines

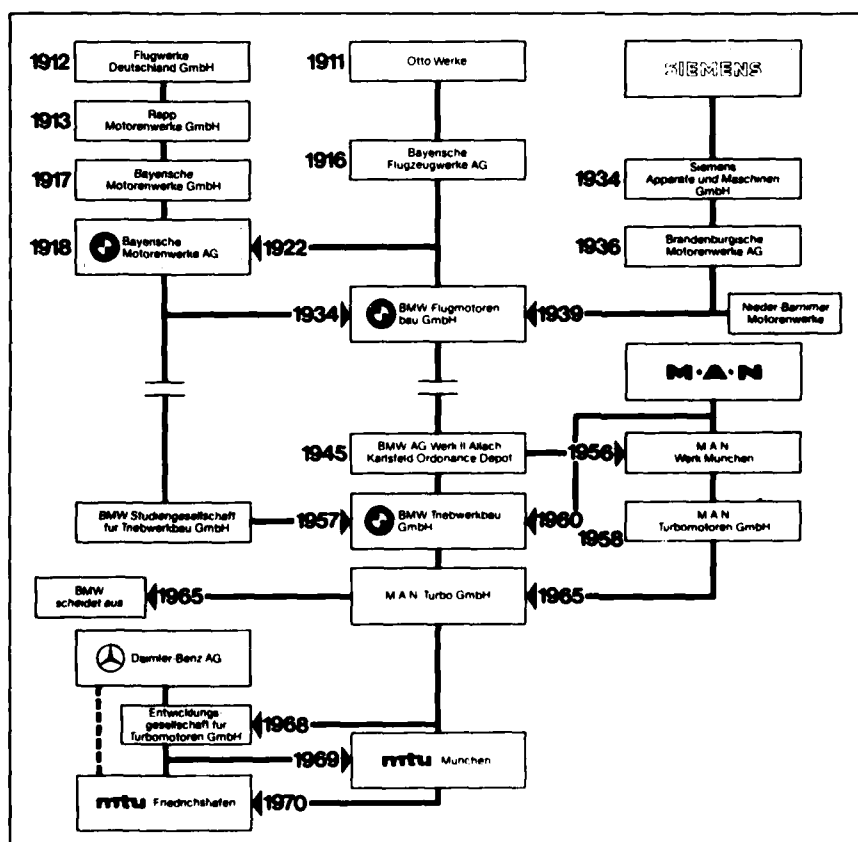


Fig. 37
History of MTU Motoren- und Turbinen-Union München GmbH

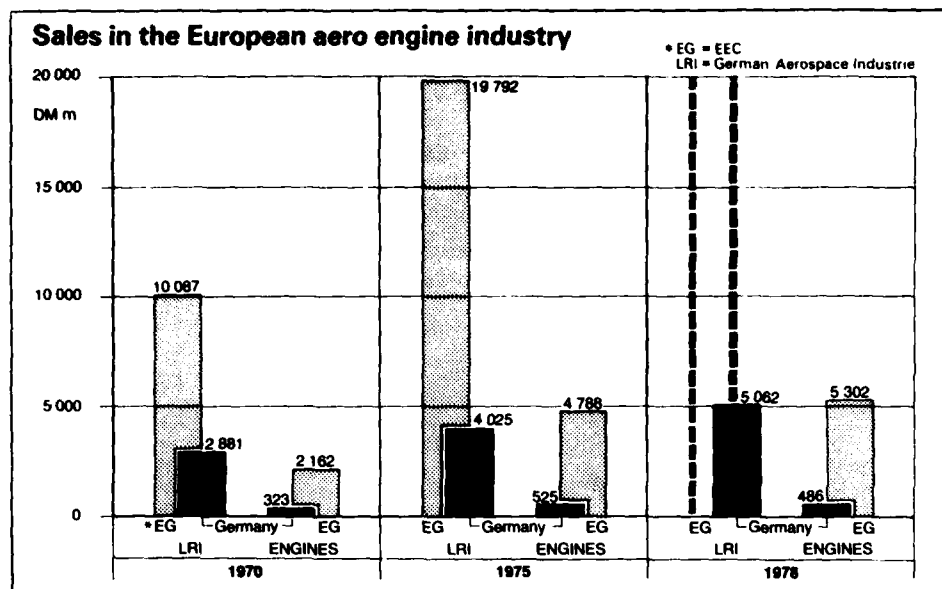


Fig. 38

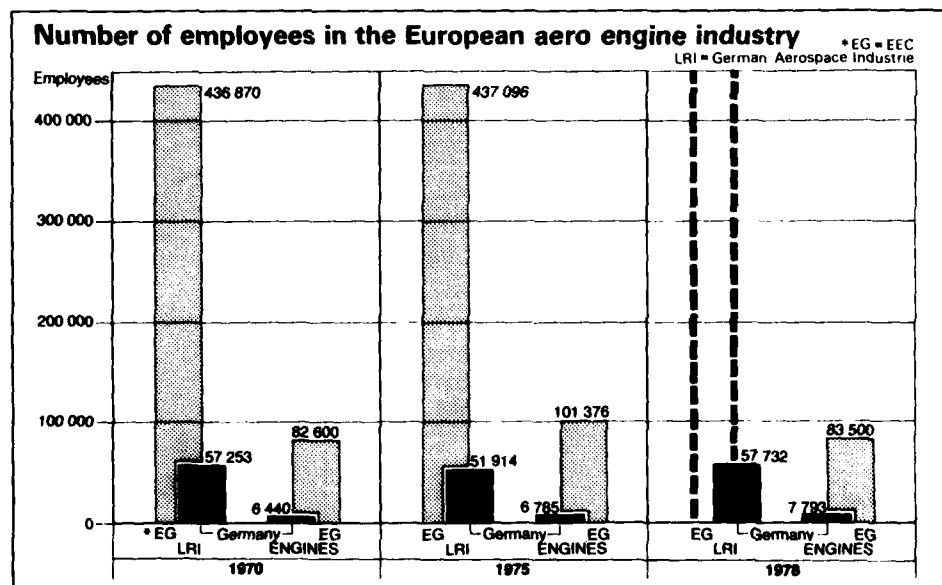


Fig. 39

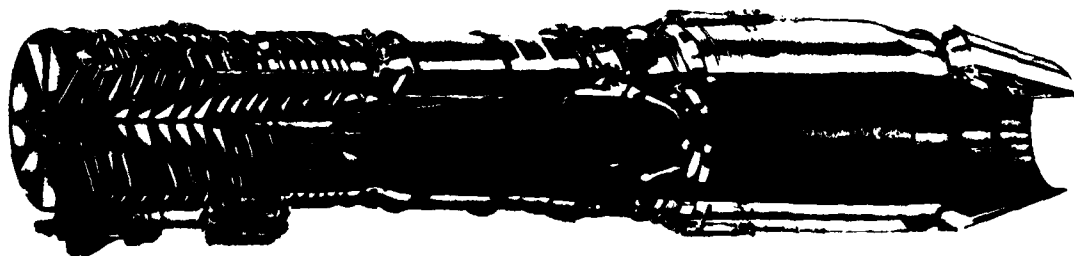


Fig. 40 J79-MTU-J1K engine

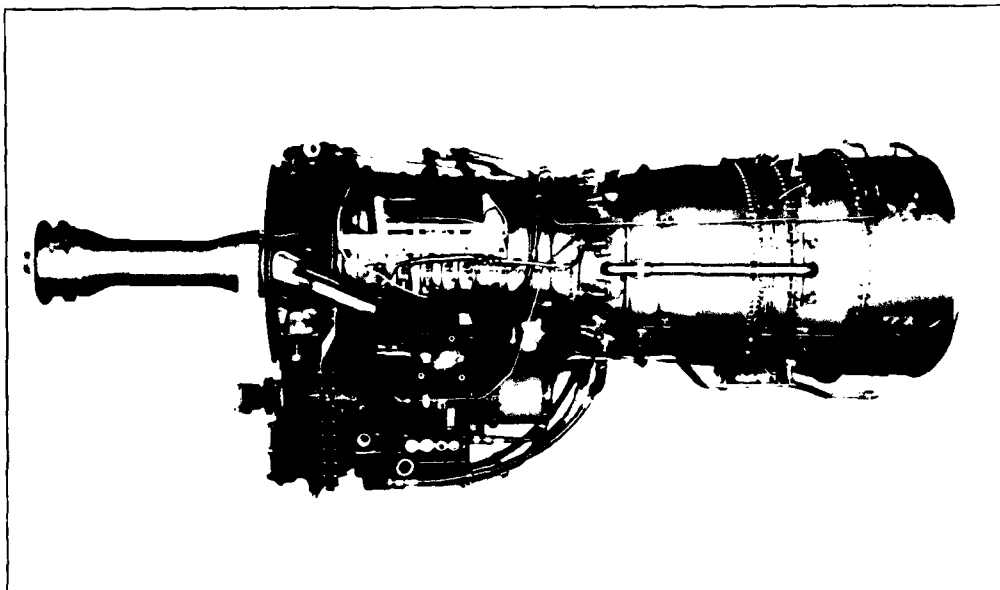


Fig. 41
T64-MTU-7
turboshaft
engine

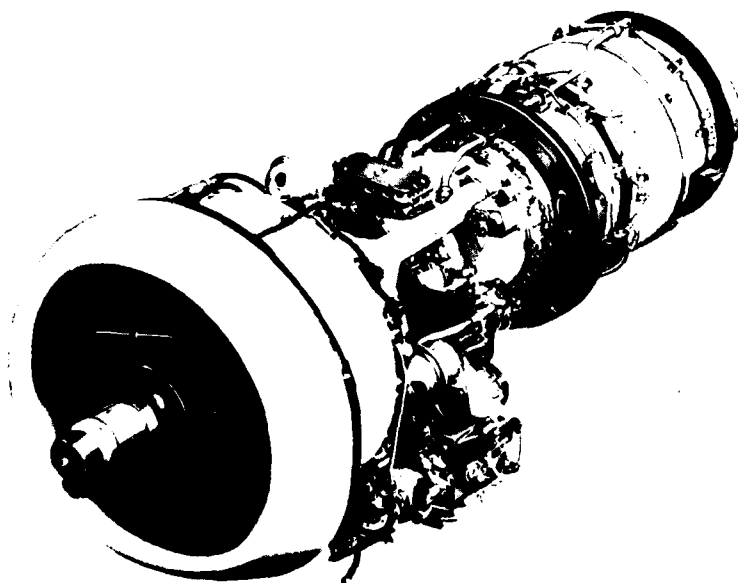


Fig. 42
MTU Tyne R.Ty20Mk22

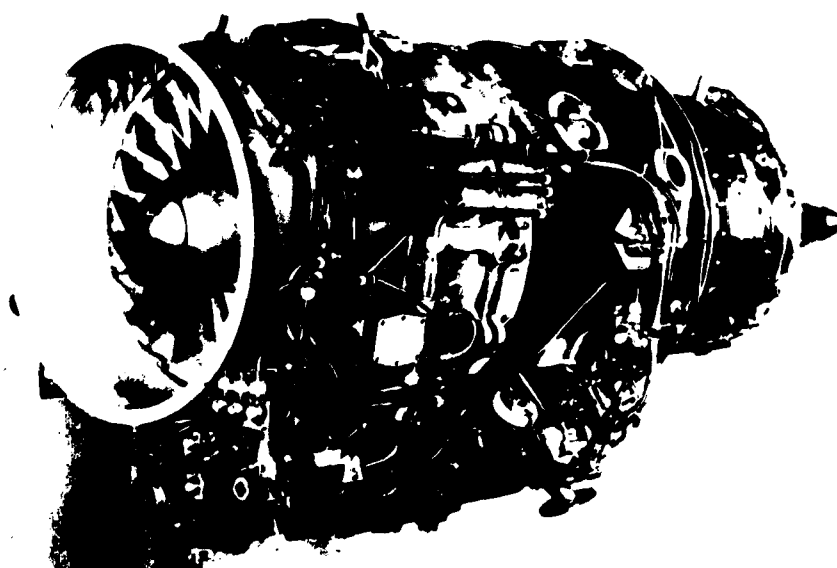


Fig. 43
Larzac 04

LCF strength of turbine and compressor disc materials

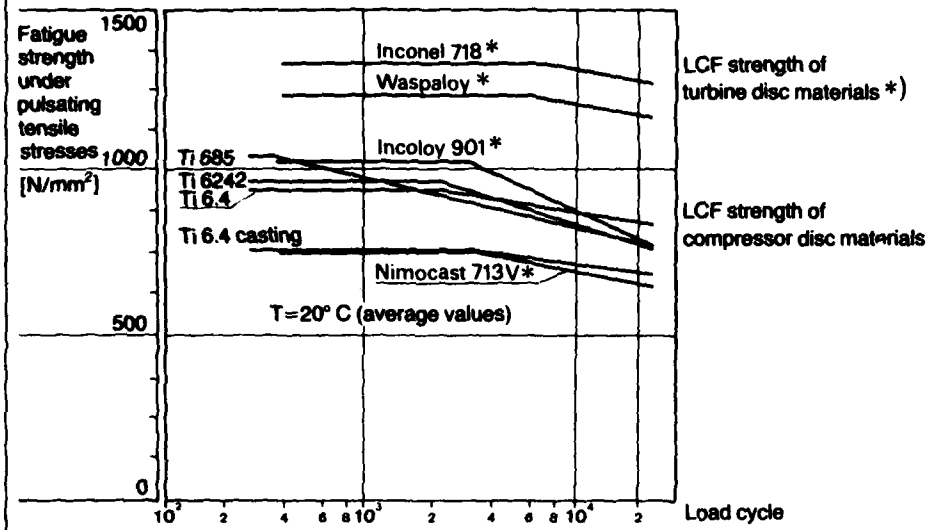


Fig. 44

Influence of Hot Gas Corrosion on Creep Rupture Life of Uncoated and Coated Turbine Blade Alloy: IN 100 (950°C)

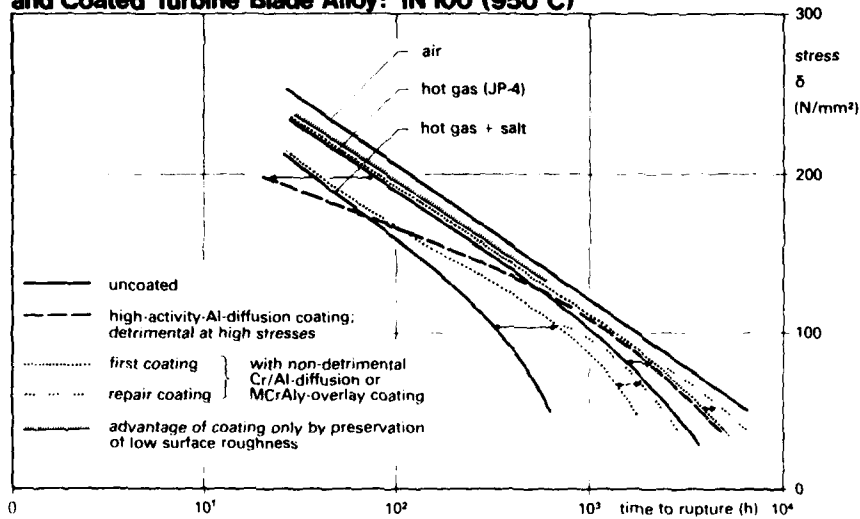


Fig. 45

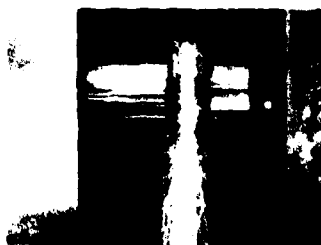
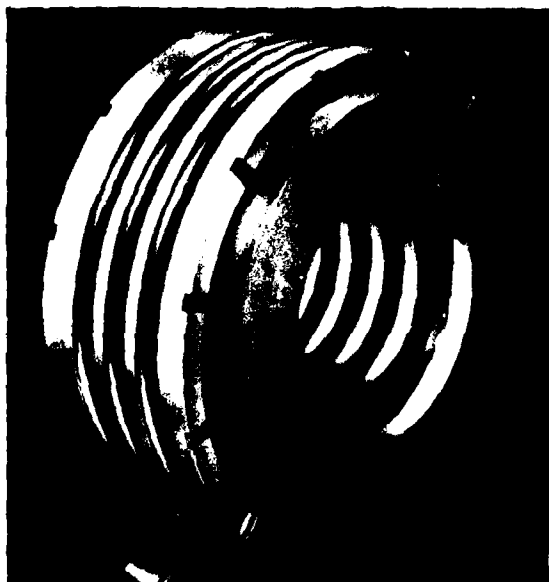


Fig. 46

Inertia-welded joint
on RB 199 HPC rotor
with connecting flange



Material: Inconel 718
Dia.: ≈ 328 mm
Welding heat: 255.000 Nm
Upsetting force: 1100.000 N

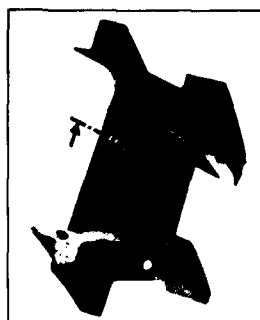
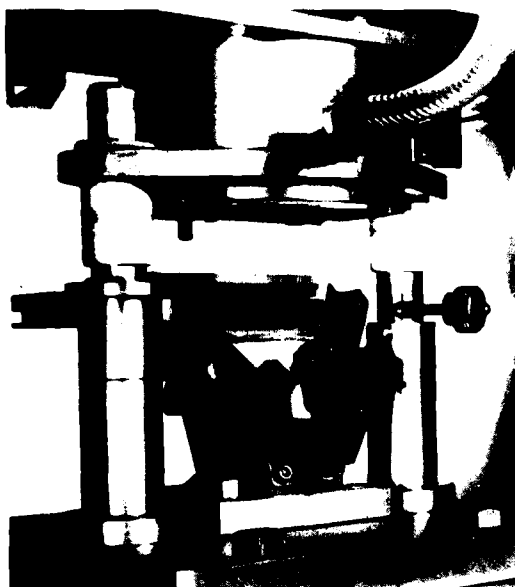


Fig. 47
Electrochemical fine boring

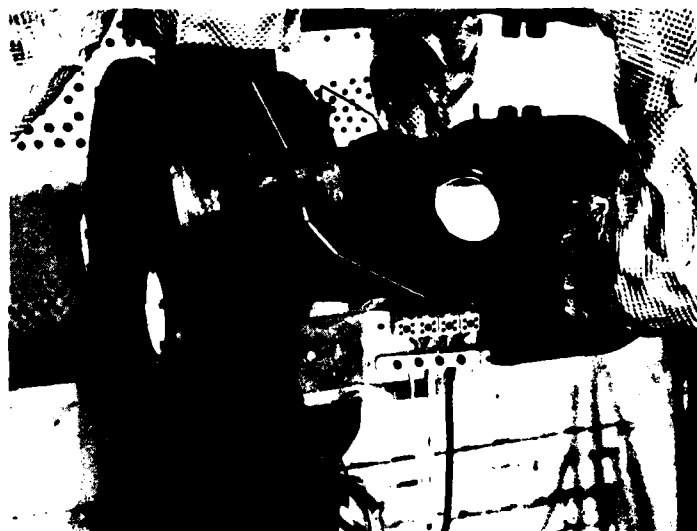
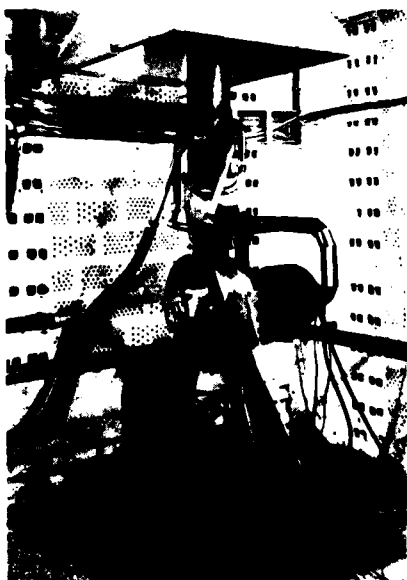
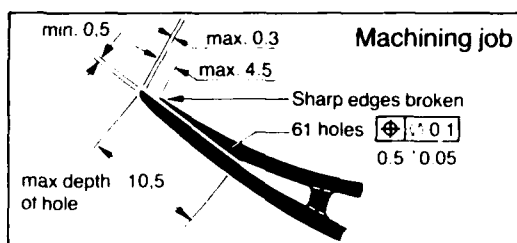


Fig. 48 Ceramic combustion chamber test stand

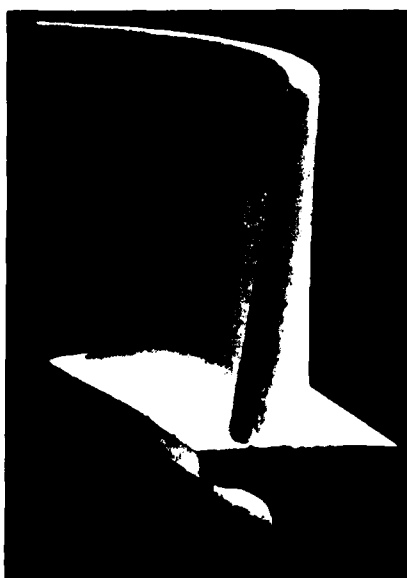


Fig. 49 Ceramic blades

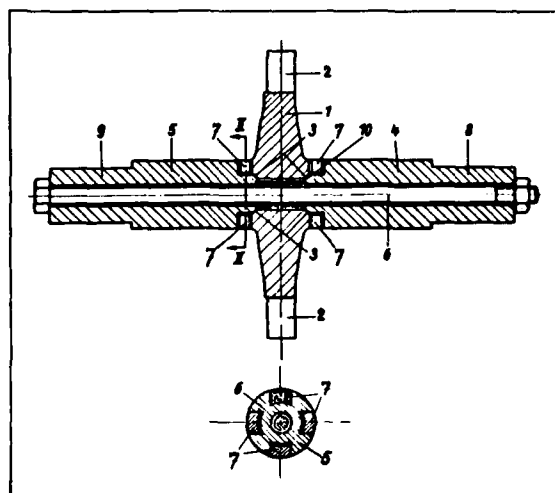
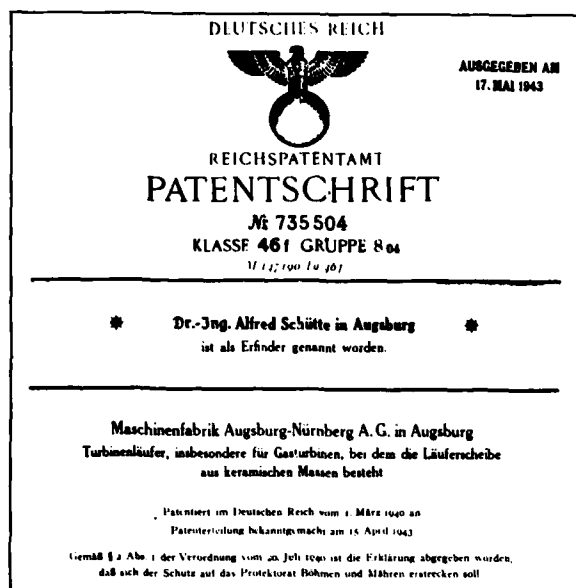
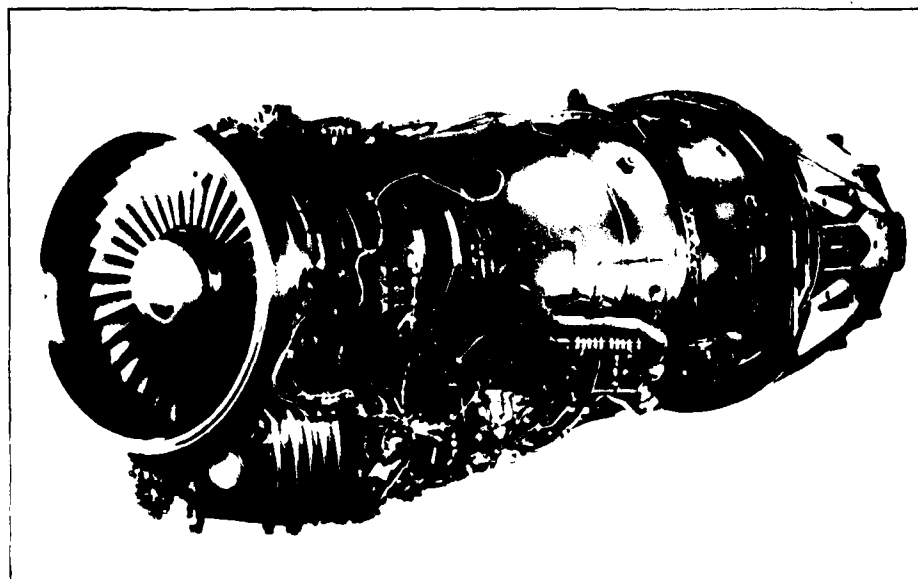


Fig. 50 MAN-AG, Letter of patent, 1940

Fig. 51
Various stages
of blade developmentFig. 52
Turbo Union
RB 199 engine

BENEFITS OF CERAMICS TO GAS TURBINES

by

Arnold Brooks and Albert I. Bellin
Aircraft Engine Group
General Electric Company
1000 Western Avenue
Lynn MA 01910 USA

SUMMARY

Technology advances for aircraft propulsion engines are extending engine operating conditions to higher temperatures, stresses, and to more stringent oxidation and corrosion requirements. At the same time, approaches are being sought for lower cost fabrication techniques. Such diverse needs have focused interest on the selective use of ceramics to replace conventional metal parts. This paper addresses to the potential areas of benefit of structural ceramics in advanced propulsion engines for manned and short-life, unmanned aircraft applications.

Ceramic characteristics such as rupture strength, creep, oxidation and corrosion are viewed in the perspective of advanced metal alloys. For various engine elements, operating regimes are indicated in which ceramics are anticipated to have benefits over metal parts. Considerations of cooling requirements, contours and tolerances, clearances and contacts, inspection and proof tests are discussed and their impact on engine performance, durability and cost are assessed. For parts such as turbine blades and vanes, bearings, combustors and flame-holders, establishment of benefit for ceramics is dependent upon the engine size.

An example is presented for a ceramic turbine blade which shows that for conventional scaling, the probability of part survival decreases as engine size increases due to the brittle, statistical, volume dependent characteristics of the material. In general, as engine size increases, the design approaches and the degree of benefit for various ceramic parts will be modified and/or a size limit will be reached. Within the ceramic payoff regime, low cost relative to metal parts is anticipated to be a significant benefit.

INTRODUCTION

There has been a burgeoning of research and development effort in structural ceramics for gas turbine power plants. The preponderant share of this effort has been expended on automotive and stationary gas turbine engines. Comparatively little effort has been devoted specifically to aircraft gas turbine applications, but to a great extent, the experience gained in automotive and stationary power plants is transferable to aircraft engines. This presentation takes up the issue of ceramics for aircraft engines specifically and considers ceramics within the historical context of aircraft engine materials development. Also considered are the specific characteristics of ceramic materials significant for aircraft engine component designs as well as the requirements to which the components must be designed; stress, temperature, and life. Finally, a view of the future of ceramics in aircraft gas turbine engines is presented, indicating the interacting influences and anticipating the areas of application.

CONTEXT

DESIGN. In the forty or so years since the initiation of intensive development of the aircraft gas turbine we have seen the virtually complete change-over from reciprocating engine to gas turbine in military and commercial aviation. Starting with the pioneering efforts in England and Germany and continuing to the present, the way has been marked by continual and aggressive development resulting in contemporary power plants which are impressive syntheses of the metallurgical, aerodynamic and design sciences. We see in today's aircraft gas turbines:

- Cycle temperatures commonly in the mid 2000°F [1093°C] regime
- Compressor and fans with highly supersonic relative Mach numbers
- Stress levels in turbines and compressors of the order of 120 kpsi [827 MPa].

We see all of the above in engines which function for thousands of hours and require a minimum of maintenance attention.

In the last decade, as part of the normal sweep of development in the gas turbine, much attention has been paid to ceramics as a material with possible application to the gas turbine. The effort has been significant in scope. In the U.S. alone, the commitment to-date has been of the order of \$100 million, and allocated by agencies as shown in Figure 1 which indicates the total of U.S. Government expenditures to-date plus announced firm plans. The lure of ceramics is easy to understand and is based on:

- Its high temperature capability
- Its potential for low cost manufacture
- The great availability of raw materials.

The virtues of ceramics are balanced, however, by the well known problem areas:

- Brittleness
- Mechanical interface matching problems.

The problems notwithstanding, the attractiveness of ceramics has impelled Government and industry to continue research and application investigations in gas turbines. The great preponderance of program funding shown in Figure 1 has been devoted to programs concerned with automotive and stationary gas turbines, while aircraft gas turbine effort has been at a much lower funding level. This paper will stress the application of ceramics to aircraft engines.

It is helpful to consider ceramics against the background of main stream developments which have occurred and are occurring in the realm of aircraft gas turbine design and development. For the aircraft gas turbine designer, the motivations which have driven him to seek improvements are:

- Performance
- Size
- Weight
- Cost
- Reliability
- Durability
- Maintainability
- Safety.

The items listed are not given in any ranking of desirability or priority, but the top three - performance, size, and weight - are coupled directly to thermodynamic design choices. In fact, pressure ratio and turbine temperature, particularly, will strongly influence these factors. The relatively strong dependence of specific fuel consumption on both turbine temperature and pressure ratio is shown in Figure 2 which demonstrates that increases of turbine temperature have a beneficial, though varying, impact on specific fuel consumption. Figure 3 shows the particularly strong influence, at all temperature levels, of turbine temperature on specific output, hence on size and weight. For engines with heat exchangers for waste heat recovery, that is recuperators/regenerators, the dependence of fuel consumption on turbine temperature would be even more marked than shown in Figure 2.

HISTORICAL PERSPECTIVE

CYCLES. D.M. Dix's paper on Small Aircraft Engine Technology (Reference 1) furnishes, in convenient form, a summary of historical progress in turboshaft, turbojet and turbofan engines design progress. Figure 4 shows for turboshaft engines the progress in sfc and power to weight ratio. For turbojets and turbofans, Figure 5 shows historical trend data for cruise specific fuel consumption and shows the impact of high bypass ratio on attainable cruise fuel consumption. Figure 6 shows the thrust to weight ratio trends. The variations in cycle temperature for both shaft and jet engines are given in Figure 7 which shows:

- A steady monotonic rise in cycle temperature with time
- Turboshaft engines lagging turbofan engines by at least five years in the attainment of specific levels of turbine temperature
- The strong impact of turbine cooling.

MATERIALS. The turbine temperature increases have occurred as a result of improvement in:

- Material properties
- Heat transfer cooling concepts.

The progress in turbine blade materials is shown in Figure 8 which indicates that for superalloys the progression through air melting, vacuum melting and directional solidification has given an increase in material capability of 500°-600°F [260°-316°C] in the past forty years.

Figure 9 illustrates the corresponding trends in turbine vane (or stator blade) material showing contemporary metal vane capability at approximately 2200°F [1204°C]. In vanes, the progression has been from investment cast alloys to dispersion strengthened alloys. Ceramics are a potential for the future. Finally Figure 10 depicts, over the same interval in time, the progress in turbine wheel (or disc) materials. Here the progress is shown in terms of yield strength improvement as a constant (1000°F) [538°C] temperature. In the past forty or so years, a five fold increase in strength has been achieved.

COOLING CONCEPTS. In parallel with the steady improvement of materials properties, the design sophistication and complexity of blade air cooling systems has evolved as shown in Figure 11, which schematically delineates cooling concepts from the original single pass radial convection configuration to the configuration shown on the right featuring:

- Turbulence promoters
- Impingement cooling
- Film cooling
- Multiple pass convection.

DESIGN STRESS LEVELS. The great progress in materials and cooling techniques has been accompanied by increases in turbine stage loading and wheel speeds. The increase in tip speed has resulted from the desire to minimize the number of stages required by the turbine. This increase in tip speed and its effects on centrifugal stress is shown in Figure 12 which delineates an approximate two-fold increase in turbine tip speed within a period from 1955 to the present and a 1.7 increase in blade root stress factor - annulus area multiplied by square of rotational speed - in the same time period.

ROLE OF CERAMICS

In the previous section the historical perspectives for modern aircraft gas turbines have been described. Through four decades of development, gas turbines, whether shaft, turbojet or turbofan have been refined and improved to an impressive level of capability. At the heart of this evolution has been the development of air cooled turbines capable of reliable operation over long periods of time at elevated temperature and through many thermal cycles.

The characteristics of metal engine components, either uncooled or cooled, are well understood. Their strong and weak points are well documented and are part of the lore carried by all engine component designers. For ceramics to be adopted in favor of metals, some significant advantages must exist. The advantages must in turn, devolve from ceramic materials' intrinsic properties. The following paper in these proceedings by Katz and Lencoe, Reference 2, presents a more complete discussion of ceramics' properties and discusses the application of ceramics to small airborne engines primarily from a materials laboratory perspective.

In comparing properties of ceramics relative to metals, one must consider:

- Rupture
- Creep
- Oxidation
- Corrosion.

RUPTURE. Figure 13 from Reference 3 shows a comparison of several ceramic materials applicable to gas turbine components; sintered silicon carbide and reaction bonded silicon nitride, and a representative modern directionally solidified superalloy (see Reference 4). The rupture properties of the ceramics demonstrate an advantage over the metal at elevated temperatures, notwithstanding the statistical property variations (low Weibull modulus). An uncooled ceramic blade, from a rupture point of view, can be designed to a moderate design stress even at the minus 3σ level.

CREEP. Figure 14 defines the generally favorable creep behavior of ceramics compared to superalloys. For a stress level of 10 kpsi, the ceramics have an increased temperature capability of approximately 200°F [93°C] to 500°F [260°C] (Reference 5).

OXIDATION RESISTANCE. The relative resistance to oxidation of ceramics and superalloys is illustrated in Figure 15 with ceramics demonstrating a 3 to 4 order of magnitude edge in oxidation resistance as measured by weight gain per unit area (Reference 3).

CORROSION RESISTANCE. Ceramic benefits in resistance to hot corrosion are anticipated. Figure 16 (Reference 6) presents recent data comparing the resistance of two ceramic materials with that of a nickel based alloy, bare and coated. The corrosion penetrations for the ceramics are comparable to that of the coated metal and are significantly less than for the uncoated metal. It is anticipated that the strength characteristics of the corrosion exposed materials will compare correspondingly. The ability of ceramics to operate without a coating, which may erode or otherwise lose its integrity, is an attractive benefit.

PERFORMANCE. The major incentive, according to conventional wisdom for ceramic blading is the ability to operate at higher cycle temperatures than would be capable with metal blading. Implicitly, the comparison is made with uncooled metal blading. These comparisons which have shown large increments in engine output with the use of ceramics are naive if not misleading since air-cooled metal blading should be the datum against which ceramics are measured. The intrinsic benefit in performance of ceramics vis-a-vis air cooled metal blading is the performance gain associated with reduction in required cooling flow. Figure 17 shows schematically typical cooling flow ranges and distribution. It should be noted that elimination of the need for blade cooling does not reduce to zero the required quantity of cooling air; some air will be required to cool the wheel or wheels, some will be required to cool the static structure. Figure 18 illustrates the magnitude of performance gain estimated for a hypothetical case of reduction of blade cooling flow to zero with cycle temperature as a parameter. The case shown applies to subsonic cruise specific fuel consumption for a subsonic turbofan of modest bypass ratio.

COST. In addition to performance benefits, the other fundamental parameter likely to be affected favorably by the use of ceramics is cost. The fabrication of ceramic blading to final net shape without the need for extensive machining or grinding processes will result in a cost reduction relative to air-cooled metal blading. Figure 19 is a graphical representation of the estimated relative costs of manufacture of injection molded ceramic blading and air-cooled metal blading. The metal and ceramic blades are assumed to be comparable in function; that is, size and cycle temperature. The total cost of the ceramic blade was estimated to be approximately 40% of the metal blade and the major savings were assessed to be associated with:

- Reduction of the cost of the casting/molding
- Reduction of machining cost.

Note, however, an increase is estimated in the cost of inspection and quality assurance.

CERAMIC PROBLEM AREAS

The ceramics characteristic most often discussed and the one most difficult to accommodate in design is the brittleness of the material. Overall, this characteristic requires design approaches significantly different from those normally used for metallic engine parts. Problem areas related to the material's brittleness include:

- High localized stresses at points of contact where surface irregularities do not yield to accommodate imperfect surface fits

- "Unforgiving" high stress concentrations due to material flaws and design or damage discontinuities
- A complex failure mechanism involving propagation of material flaws with a resultant statistical strength relationship that includes such parameters as part size, stress distribution and type of loading
- Wide variability in part strength due to the probabilistic nature of the material failure mechanism
- Inability to classify part strength by practical non-destructive tests to measure material flaw size and distribution.

Each of these problem areas must be understood and addressed before the benefits of ceramics can be realized in engine designs.

The problem of contact stresses is common to all structural ceramic parts and is a major design challenge for rotating and static parts. For parts such as in turbines, high thermal gradients, high loads, mismatch in coefficients of expansion between metal structure and ceramic parts and small tolerance requirements to establish part location - all contribute to the difficulty of this problem. The objective is to minimize the stresses at ceramic-metal and ceramic-ceramic interfaces while accommodating other competing requirements, including the following:

- Minimizing gas leakage between parts such as turbine vanes
- Maintaining tolerably low temperatures of metal supporting structure without imposing high thermal gradients in the ceramic parts
- Accommodating capability for relative expansion between ceramic parts and structure without imposing significant loads and without allowing loose part impacts.

A number of approaches are available for dealing with these opposing requirements. Generally the designs should assure determinate reactions so that, at least, the configuration can be analyzed with more certainty. There may be a choice between combining several parts, such as vanes, into a single ceramic element thereby eliminating several interfaces. The benefit relative to contact stresses must then be compared with potentially higher thermal stresses in the combined part and the more difficult task of fabricating a larger part to a high quality standard. Additionally, compliant layers or ductile metal foils can be added at interfaces to reduce peak contact stresses. Soft spring elements can be used within space and position tolerance limitations, for ceramic part support. All of these approaches have been used without complete success; more must be done in order to solve this basic problem.

Sensitivity to geometric stress concentrations can be accommodated in the design process even though parts may have an appearance somewhat different from metal parts due to larger fillet radii and more gradual transitions. A consequence of this solution may be a small impact on performance for ceramic parts that are in the engine gas path.

The problems of strength variability, size effects, loading effects, time dependent effects and uninspectability are fundamental to the ceramics materials and require specialized analytic and test approaches as well as design ingenuity. Figure 13 which compares rupture properties for typical structural ceramics with that of a superalloy, shows the average and average minus 3 standard deviations (σ) strengths. These data highlight the broad range of strength variation for the ceramics in contrast to metal. The Weibull modulus, m , indicated for the ceramic materials in Figure 13 is a measure of the spread of the strength distribution; the larger the m , the narrower the spread (see Reference 7).

The consequence of the material variability for engine parts is indicated in Figure 20 from Reference 7. For scaled parts with similar loading, the ordinate in Figure 20 is proportional to part volume. The abscissa is proportional to the reciprocal of the part's maximum stress. The radial lines represent conditions for 0.5 probability of failure as a function of the material's Weibull modulus. With a Weibull modulus of 7, this figure shows that a part such as a turbine blade or vane for a large engine could sustain a maximum stress of only one half that of a similar small engine part. This situation, where the allowable design stress is strongly dependent upon part size is in contrast to the design approach generally used for metal parts, where for many critical engine components, performance parameters such as tip speed are held constant while maintaining geometric and aerodynamic similarity between a small and large engine. In so doing, maximum stresses of the similar rotating parts will be the same, independent of scale. This ability to scale directly, however, cannot be used for ceramic parts if the probability of failure is to be fixed, due to the ceramics' size-strength effect.

For the specific, similar small and large engine parts that were analyzed in Reference 7, Figure 21 indicates how the probability of failure changes with design stress level and with scale. As seen for a given probability of failure, the difference in allowable design stress between large and small parts depends upon the material strength variability, m ; the larger the Weibull modulus for the ceramic, the smaller the difference in allowable stress. For example, with an m equal to 7, to obtain a ten fold reduction in the probability of failure for that engine part, the maximum stress must be reduced by about 30%. On the other hand, for the same stress level, the larger part with a volume 100 times that of the smaller one will have a probability of failure of approximately 100 times greater than for the small part.

The combined effects of part size and type of loading upon fracture strength are shown in Figure 22 from Reference 8 and are described in Reference 9. The data in Figure 22 are for self-bonded silicon carbide; from left to right, for small bend bars, large bend bars, spin test bars and spin test disks. The separate effects of type of loading upon strength of components are discussed in References 7 and 10. The former applies a statistical design methodology that incorporates ceramic strength degradation due to material flaw crack growth under various loading conditions and analyzes several configurations applicable to turbine parts. The latter presents test and analytic data on the strength and life of hot pressed silicon nitride for constant stress rate, linear cycle stress and constant-stress loading. Reference 2 presents results and discusses the degradation of properties resulting from exposure of ceramics to the complex environmental/loading/time factors.

The interaction of property variability, size effects, loading effects and time dependent effects, coupled with the practical inability to sort and reject the low end of the statistical distribution by non-destructive testing leads to the consideration of proof tests for ceramic engine parts. If a proof test can be designed that is indicative of the part loading, then exposure to a given test severity would fail those parts having strength below a designated level. This approach, presumably, would eliminate the statistical failure of parts during normal usage. By raising the severity level of the proof test, fewer but stronger parts would survive, which could, in turn, be applied for correspondingly more severe engine operating conditions. As an example, for the small engine part with an m of 7 analyzed in Figure 21, a proof test that fails one out of ten parts would qualify those parts to a stress level about 40% higher than if the same parts were proof tested with a failure rate of one out of a hundred.

In addition to the strength variability due to inherent material properties, scale and loading, there may be an additional process effect related to fabricating a complex shape rather than a simple test specimen shape. Use of a proof test would also account for this additional cause for uncertainty in part strength and would serve as the prime quality assurance check for the part. The challenge in the use of proof tests for ceramic parts is two-fold:

- (1) Achieving a valid proof test
- (2) Achieving economic pay off for the combined cost of testing and of rejected parts as compared with the alternative of using metal parts in place of ceramics.

Progress has been made toward solving the above formidable problems.

APPLICATION REALMS

The high temperature strength/weight, low oxidation, low corrosion characteristics of the various ceramic materials provide potential for applying ceramics in a number of aircraft engine components. Table 1 lists some engine design requirements that are considered representative for such components. For the turbine, combustor and exhaust components, uncooled ceramics have the potential for meeting these requirements and replacing more complex, more expensive, air cooled metal parts. The benefits for ceramic bearings are corrosion resistance and potential to operate unlubricated. The values shown in the table could differ from those of a particular design and application depending upon such specifics as engine transient times, use of monolithic parts versus segmented or assembled parts, self-supporting structures versus coverings for metal skeleton structures, etc.

The two sets of temperature/stress values shown for the turbine blade represent the dovetail area (high er stress) and the airfoil (higher temperature). To meet the dovetail requirement necessitates a properly distributed contact load with the wheel, by use of a coating or an intermediate ductile material. The two sets of data for the turbine vane represent the simultaneous combinations for the extremes in each parameter. For the wheel, as well as for most of the other items listed, a major requirement is capability to tolerate the imposed interface loads. The stationary turbine shroud over the blade tips, as listed, is a non-structural element relying upon a metal support. In addition to fulfilling the requirements shown, the shrouds must maintain dimensional stability, be resistant to erosion and withstand severe thermal cycling.

Depending upon the configuration, the stresses (and the probability of failure for the combustor) may vary considerably from the values given in Table 1, as shown in Reference 11. The afterburner concept considered in Table 1 provides a ceramic temperature resistant configuration with little load carrying requirement. Exhaust components referred to in Table 1 include such elements as centerbodies, struts, rings, flaps and exit guide vanes. Thermal barrier coatings applied to stationary or rotating metal surfaces provide a thermal resistance between the hot gas and the base metal structure. The adherence integrity requirements for the thermal barrier coatings apply to conditions of thermal cycling and centrifugal force, if the base structure rotates. In addition, the coating must have strain compatibility with the base structure under mechanical loads as well as resistance to erosion and oxidation.

Ceramic bearings may have the potential for operating unlubricated with the temperature environment of about 1000°F. For a lubricated bearing, the temperature requirement would be substantially lower, as limited by the lubricant. The challenging requirements are achieving interface compatibility with the metal shaft and structure and operating the bearing at high values of DN (inner race diameter x RPM).

Among the design requirements not listed are vibratory strength requirements, fuel and gas compatibility, dimensional stability and erosion resistance. All of the above requirements are important for the successful application of ceramics in engines. It appears to be within the potential of ceramics, with the use of creative design techniques, to satisfy these requirements with functional and cost advantages over metal parts. In general, basic design approaches are now available (References 7, 11, 12, 13).

The most challenging of the applications are turbine blades and vanes with their high steady state and transient stresses, high contact loads and complex shapes with small tolerances. Of particular interest for these parts are the comparisons with air-cooled metal parts as related to engine performance. Table 2 assesses the major factors that affect turbine and engine performance. A number of factors in this comparison contribute toward lowering performance when utilizing ceramics:

- Thicker trailing edge - required of injection molded parts for the necessary part integrity
- Blade taper - to achieve stress-strength compatibility
- Clearance - to avoid the possibility of transient rubs.

With experience and development, these factors could change and possibly achieve parity with the cooled metal parts relative to performance. The factors that contribute to improved turbine performance include:

- Elimination of internal cooling flow for the blade and vane
- More favorable overall aerodynamic contour for the blade and an improved leading edge contour.

DESIGN APPROACH - EXAMPLE

As indicated above, with conventional scaling where peak stresses are held fixed, the probability of failure increases with part sizes. Degrees of freedom can be introduced, however, and the design approaches can be modified so that failure probabilities can be tailored while still satisfying component aerodynamic requirements. The following example treats a parametric design study for a turbine blade to assess the resulting changes in probability of failure for one blade in the entire stage of blades. The design analysis is based on the methodology described in Reference 7.

A 3-D analysis including thermal and centrifugal loading of a base configuration silicon carbide blade (Figure 23) rotating at 45,000 RPM was performed (Reference 14), and defined the peak stress to occur in the blade dovetail fillet. For the base configuration with 24 blades in the stage the maximum stress is computed to be 40 kpsi [276 MPa]. The design approach used for the parametric study considered a family of designs with:

- Fixed rotational speed, consistent with the engine compressor speed
- Fixed airfoil solidity (ratio of blade chord to blade spacing) with geometrically similar cross-sections
- Fixed inner and outer flowpaths
- Geometrically scaled dovetails.

With these considerations, the following proportionalities exist for the parametric designs:

Airfoil chord	proportional to	$1/n$
Airfoil cross-sectional area	proportional to	$1/n^2$
Airfoil load	proportional to	$1/n^2$
Dovetail linear dimension	proportional to	$1/n$
Dovetail load	proportional to	$1/n^3$

where n is the number of blades in the stage. Since the dovetail cross-sectional area is proportional to $1/n^2$, the dovetail stress due to the airfoil load is constant as the number of blades is varied while the dovetail stress due to the dovetail load is proportional to $1/n$. Hence, the total dovetail stress equals a constant plus a term proportional to the inverse of the number of blades. By this approach of pseudo-scaling, designs for the same turbine situation can be defined with the peak stress decreasing as the number of blades in the stage are increased. These results (Reference 15) are given in Figure 24 for the range in number of blades between 24 and 42.

Making use of the statistical analytic approach of Reference 7 for a Weibull modulus of 12, the probability of failure of one blade in a stage for each of the designs is given in Figure 25. It is seen that increasing the number of blades per stage from 24 to 34 decreases the probability of failure from approximately .01 to .001. In this case, the lower failure rate is achieved by an increase of parts cost of $34/24 - 1$, or 42%.

The above example is indicative of approaches that may be used to balance performance, design stress, probability of failure and parts cost.

PROGNOSTICATIONS

The case for ceramics applications in aircraft engines can be made on the basis of cost advantages over metal and performance advantages. There is a spirit of conservatism concerning the early application of structural ceramic components to aircraft propulsion power plants, particularly, in manned applications. It is possible to differentiate among the application regimes insofar as either the probability of use of ceramics or the earliness of use of ceramics is concerned. The demarcations are:

- Unmanned vs. manned applications
- Primary gas path components (such as blades, vanes, combustors, etc.) versus non-critical components which are either outside of gas path (such as turbine shrouds) or down stream of rotating machinery (such as exhaust components).

In the consideration of unmanned vs. manned applications, one is inclined to be more optimistic about early application for unmanned uses because of no need for personnel safety concern and because of the short life requirement for unmanned applications. Even for manned vehicle uses, the case can be made for early use of ceramics for those portions of the engine that are not highly stressed and are generally outside of the primary gas path or, for those components which would exhibit benign failure modes. Early applications of ceramics are quite possible in exhaust system components such as flameholders, exhaust nozzle elements, centerbodies and outlet guide vanes. Table 3 summarizes the anticipated degree of immediacy for incorporating various ceramic elements into engine use.

A summary of probable areas of application of ceramics to aircraft gas turbines both manned and unmanned is given in Figures 26 and 27 in terms of stress and temperature requirements. Except for the information in italics and the \oplus symbols, Figures 26 and 27 are from the Katz-Lenoe paper (Reference 2) showing turbine blade and vane design requirements versus strength data for various silicon carbides and silicon nitrides. The added symbols \oplus reflect requirements for other components from Table 1 of this paper and show overall consistency of requirements and strength properties. As noted in Reference 2, additional comparisons of requirements versus properties must be made for all other characteristics (creep, rupture, oxidation, etc.) that must be considered in the design of an engine part.

To conclude, an attempt has been made here to provide a general view of the development history of engines and a presentation of the context within which material developments occur. Ceramics will find their way into future engines on the basis of their objective merits. Some ceramic end item applications are seen more clearly for the immediate future than others. In any event, much work remains to be done.

REFERENCES

1. D.M. Dix, "Small Aircraft Engine Technology: An Assessment of Future Benefits", Institute for Defense Analyses Paper P-1077, January 1975.
2. R.N. Katz and E.N. Lenoe, "Ceramics for Small Airborne Engine Applications", Conference Proceedings - AGARD Ceramics for Turbine Engine Applications, Cologne, Germany, October 8 - 10, 1979.
3. R.J. Charles, Private Communication, June 1979.
4. R.J. Charles, "Stress Rupture Evaluations of High Temperature Structural Materials", Fracture Mechanics of Ceramics, Ed. R.C. Bradt et al, Vol. 4, Plenum Press, N.Y. 1978, pp. 623-639.
5. R.J. Charles and J.A. Palm, Private Communication, June 1979.
6. J.A. Palm and C.T. Sims, Private Communication, June 1979.
7. G.G. Trantina and H.G. deLorenzi, "Design Methodology for Ceramic Structures", Trans. of ASME - Journal of Engineering for Power, Vol. 99, No. 4, October 1977, pp. 559-566.
8. G.G. Trantina and C.A. Johnson, "Spin Testing of Ceramic Materials", General Electric Co. Report 77CRD200, September 1977.
9. G.G. Trantina and C.A. Johnson, "Spin Testing of Ceramic Materials", Fracture Mechanics of Ceramics, Ed. R.C. Bradt et al, Vol. 3, Plenum Press, N.Y. 1978, pp. 177-188.
10. G.G. Trantina, "Strength and Life Prediction for Hot-Pressed Silicon Nitride", Journal American Ceramic Society, Vol. 62, No. 7-8, 1979, pp. 377-380.
11. G. Trantina and C. Grondahl, "Demonstration of Ceramic Design Methodology for a Ceramic Combustor Liner", Trans. of ASME - Journal of Engineering for Power, Vol. 101, July 1979, pp. 320-325.
12. R.N. Katz, "Some Aspects of Materials and Structures Engineering with Ceramics for Engine Applications", Third International Conference on Mechanical Behavior of Materials, University of Cambridge, U.K., August 20, 1979.
13. R.J. Charles and S. Prochazka, "Failure Prediction of a Ceramic Component at Very High Temperature", Submitted to Journal American Ceramic Society.
14. G.G. Trantina and J.A. Palladino, "Design Methodology for Ceramic Vanes and Blades", General Electric Co., Report 78CRD016, February 1978.
15. D.R. Abbott, Private Communication, June 1979.

ACKNOWLEDGEMENTS

The writers thank R.J. Charles, G.G. Trantina, D.R. Abbott and B.J. Ferrari of the General Electric Company for their useful contributions. Particular thanks are expressed to R.N. Katz of the U.S. Army Materials and Mechanics Research Center for his most helpful discussions and constructive suggestions.

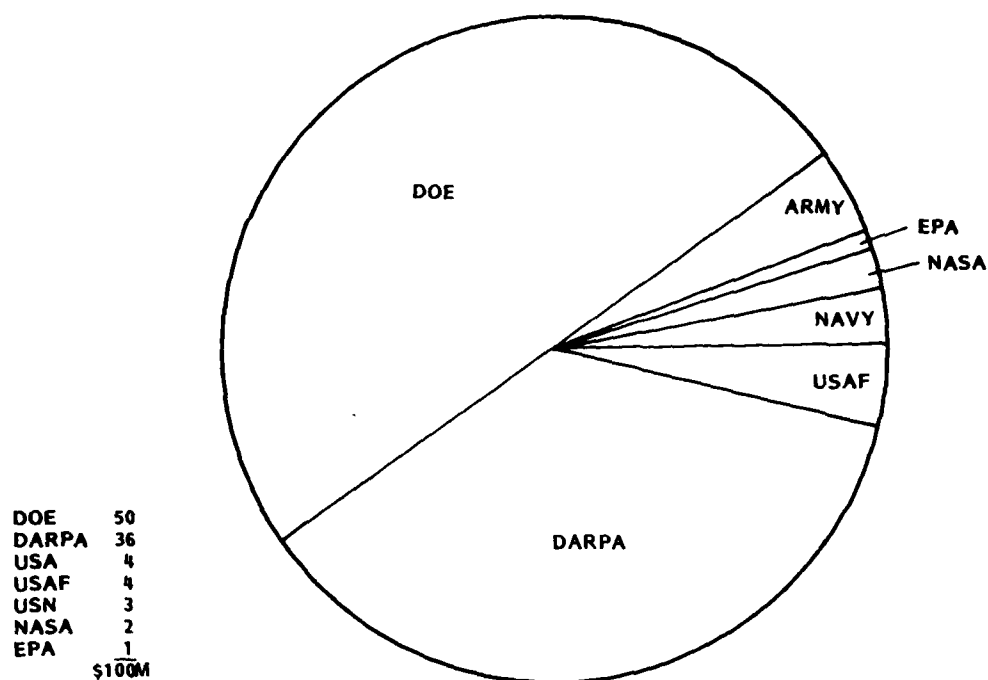


Figure 1. Sponsoring U.S. Agencies Funding Ceramic Developments

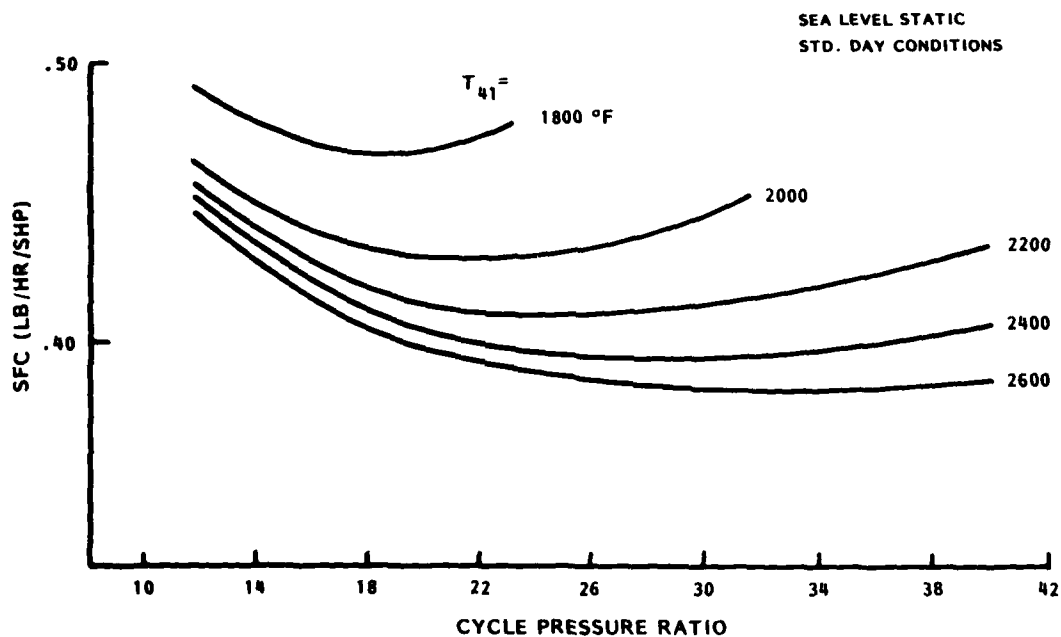


Figure 2. Cycle Trends - SFC vs. Cycle Pressure Ratio

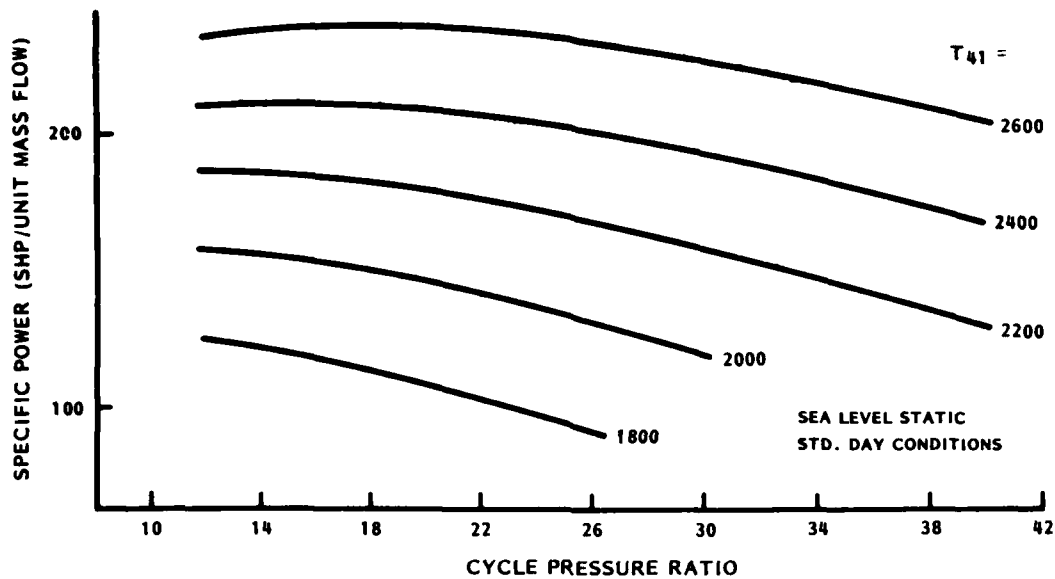


Figure 3. Cycle Trends - SHP/w vs. Cycle Pressure Ratio

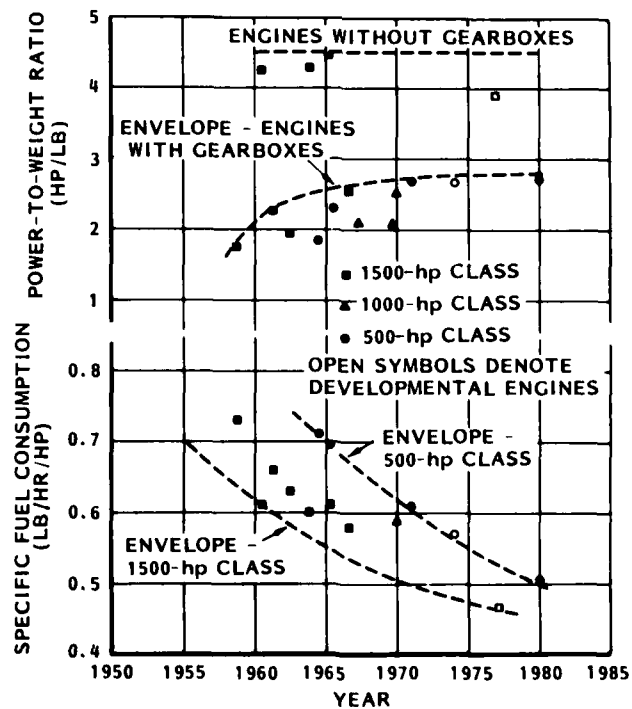


Figure 4. Trends in Specific Fuel Consumption and Power-to-Weight Ratio for Turbo shaft Engines

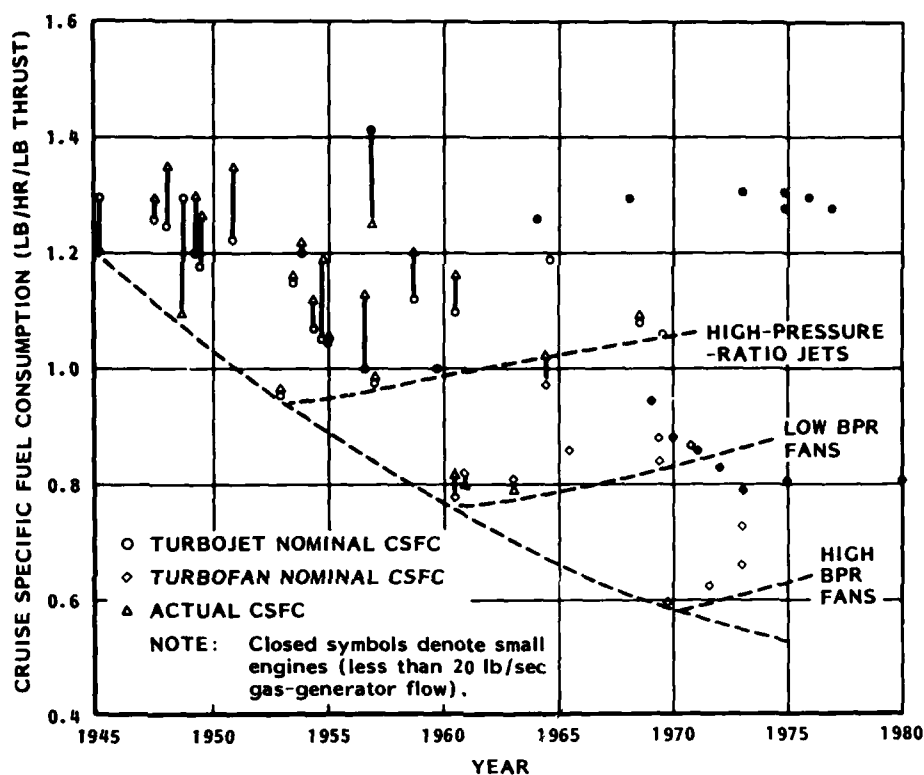


Figure 5. Trends in Cruise Specific Fuel Consumption for Turbojet and Turbofan Engines

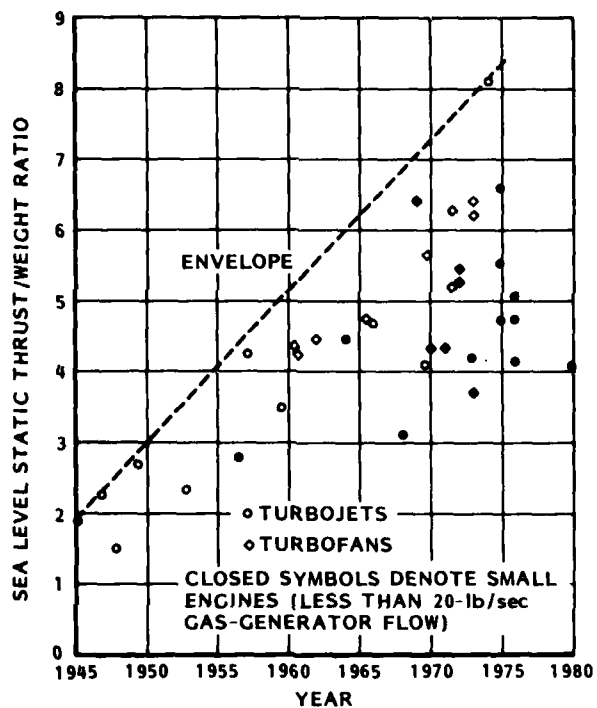


Figure 6. Trends in Thrust/Weight Ratio for Turbojet and Turbofan Engines

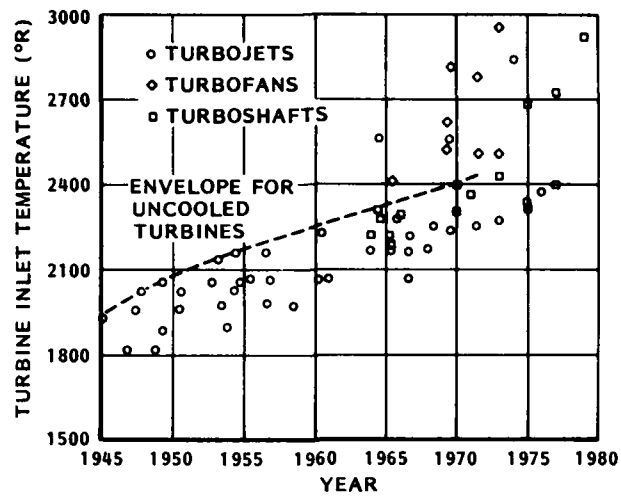


Figure 7. Trends in Turbine Inlet Temperature for all Engine Types

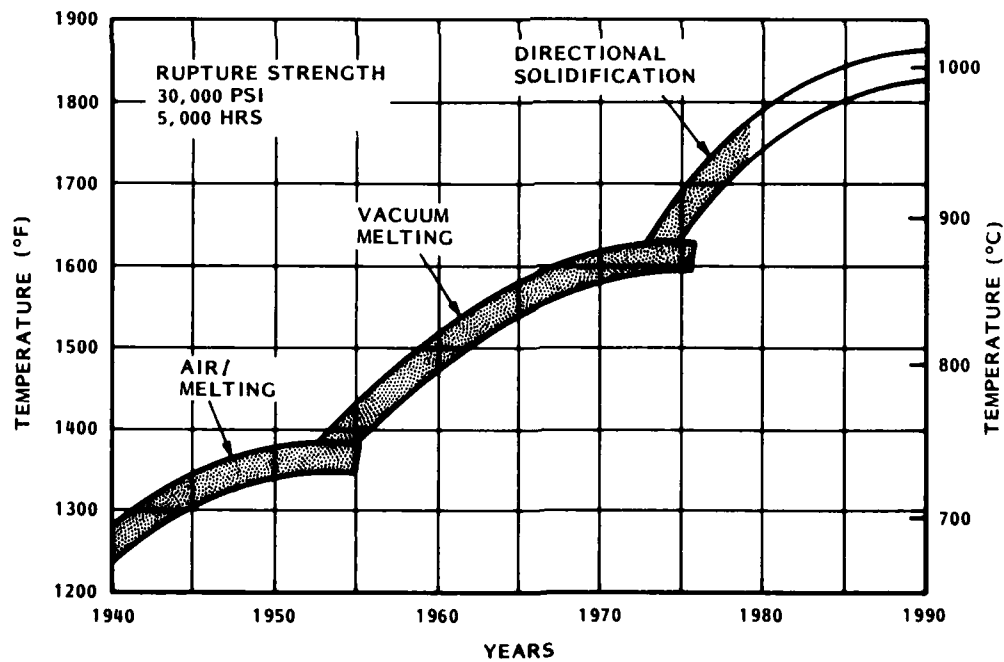


Figure 8. Progress in Turbine Blade Materials

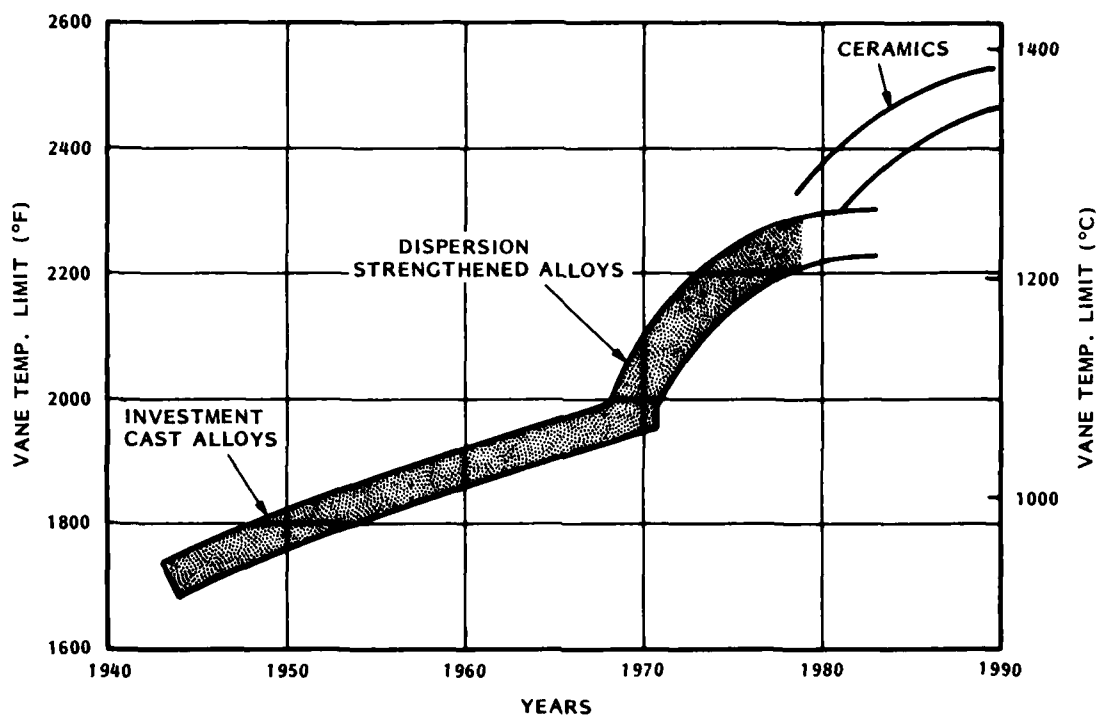


Figure 9. Progress in Turbine Vane Materials

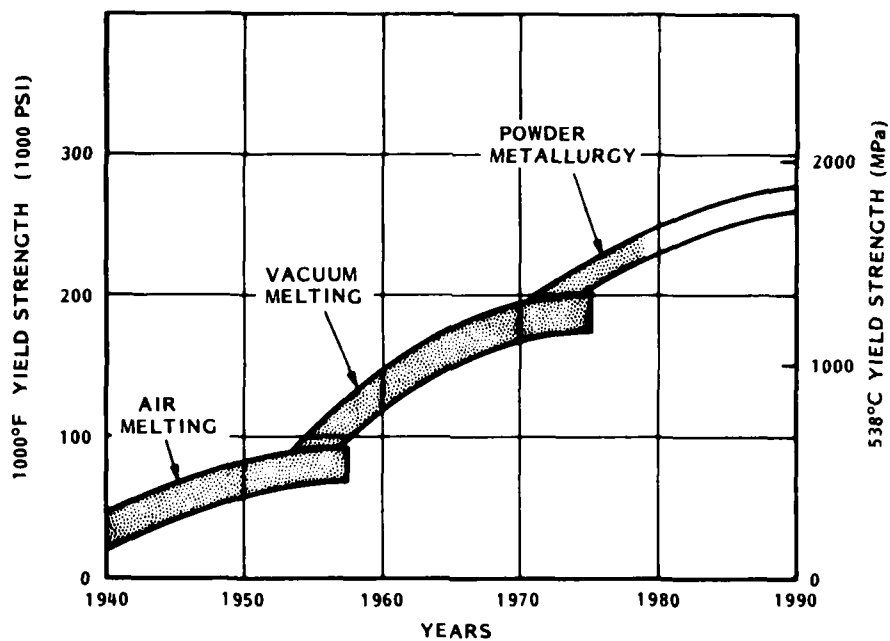


Figure 10. Progress in Turbine Wheel Materials

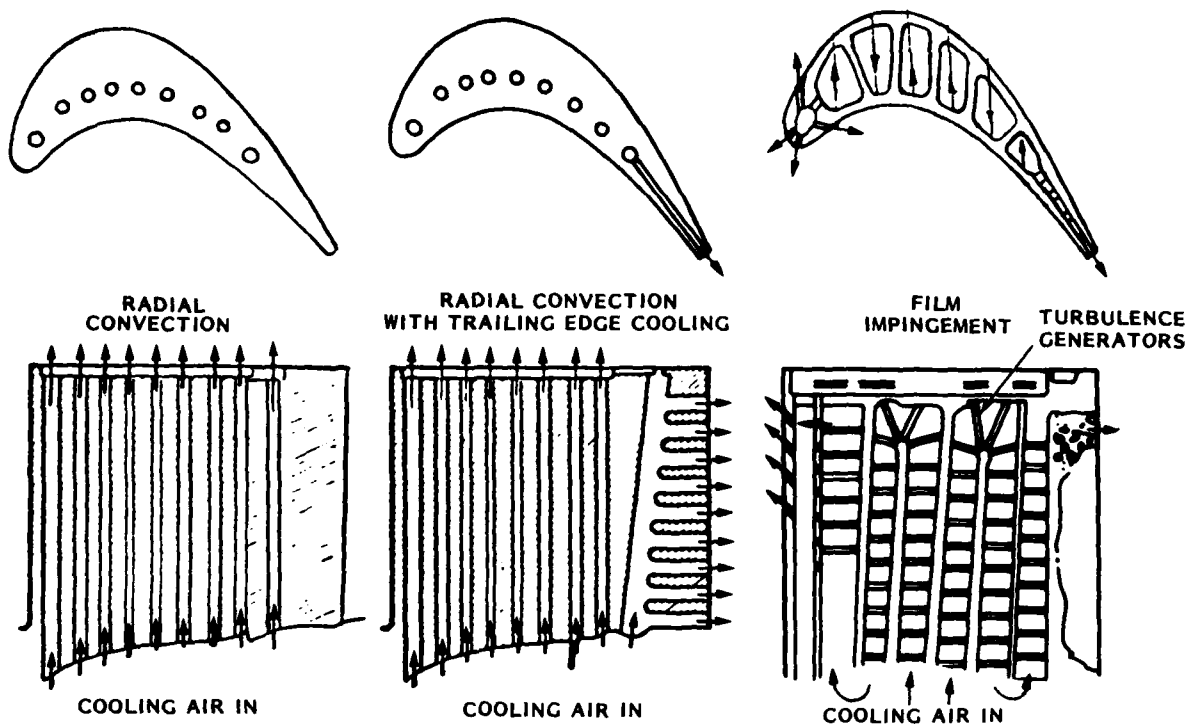


Figure 11. Evolution of Turbine Blade Cooling Concepts

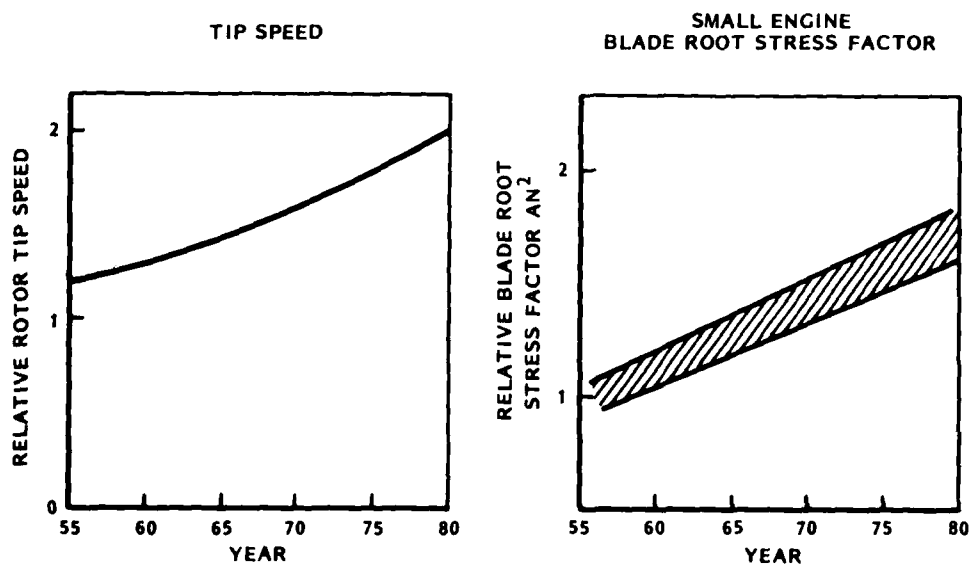


Figure 12. Progress in Turbine Blade Tip Speed and Root Stress

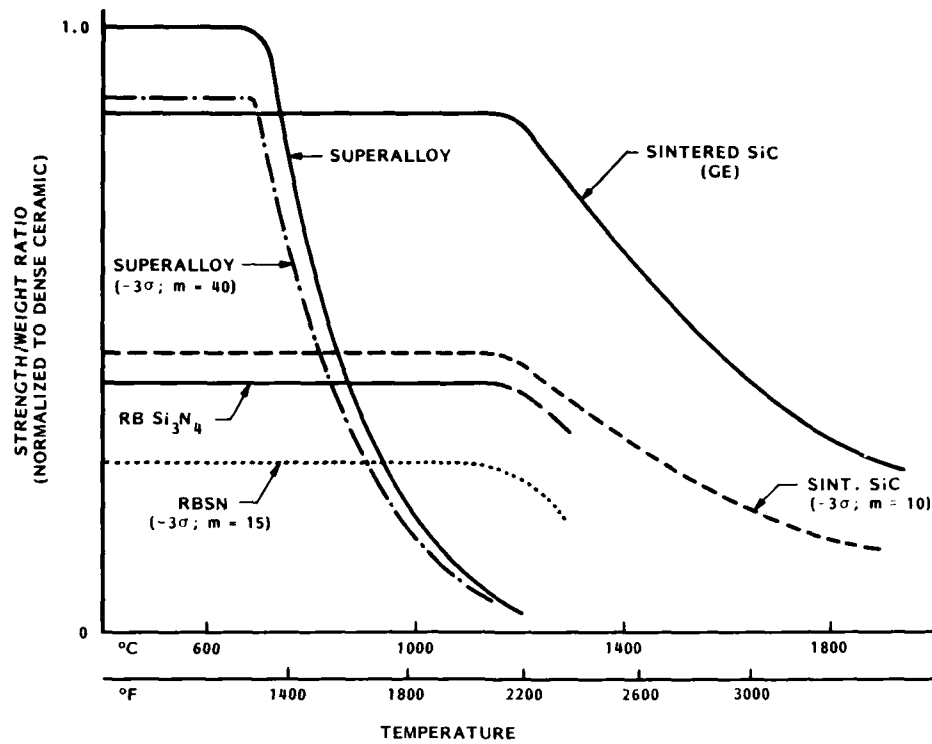


Figure 13. Estimated 100 Hour Rupture Curves for Ceramics and Superalloy (Average and -3σ)

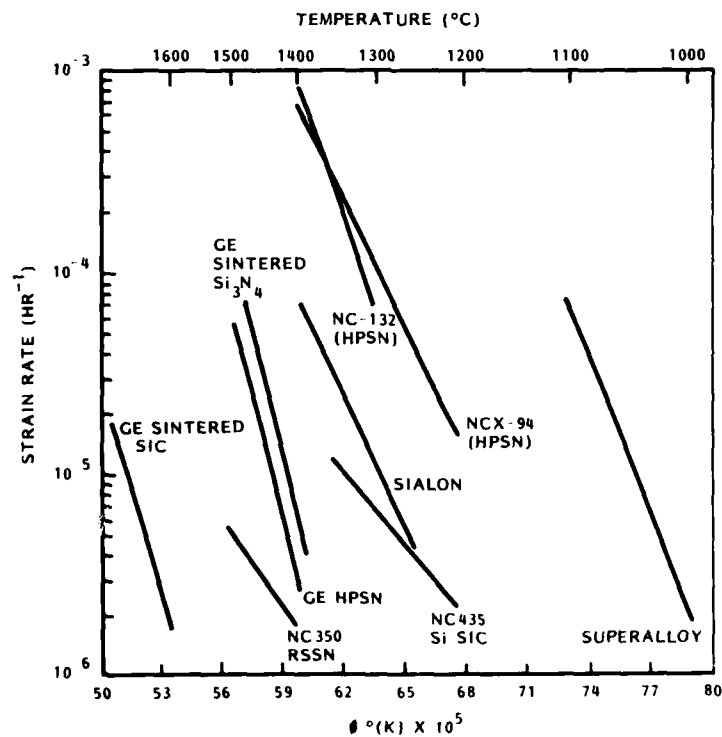


Figure 14. Creep Resistant Silicon Ceramics (10 KPSI)

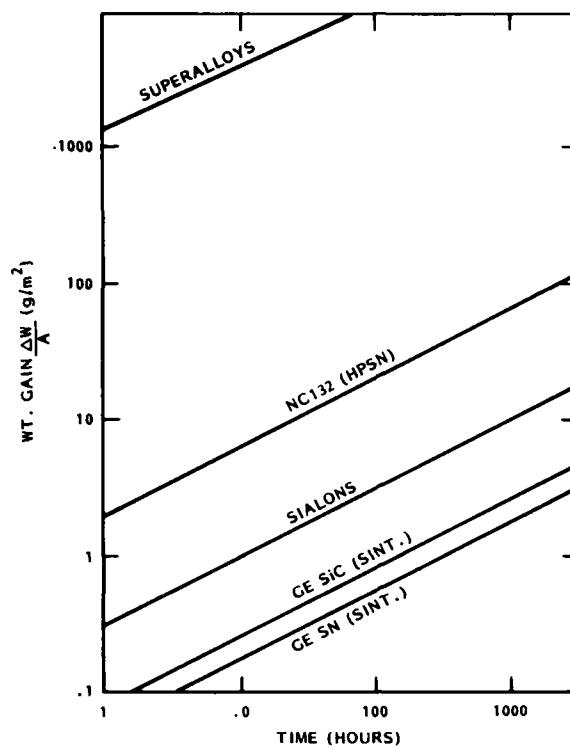


Figure 15. Oxidation Resistance of Ceramics & Alloys (1400°C Air)

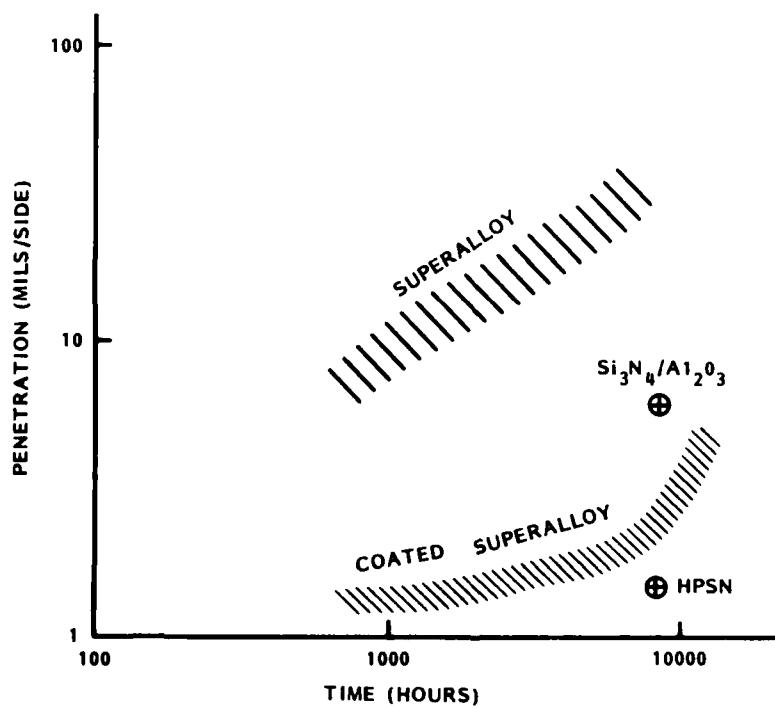
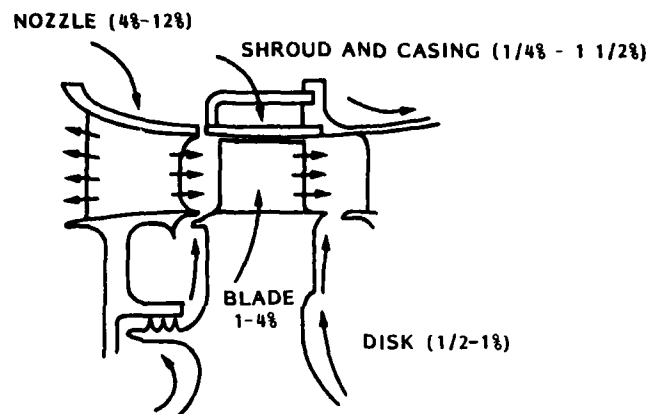
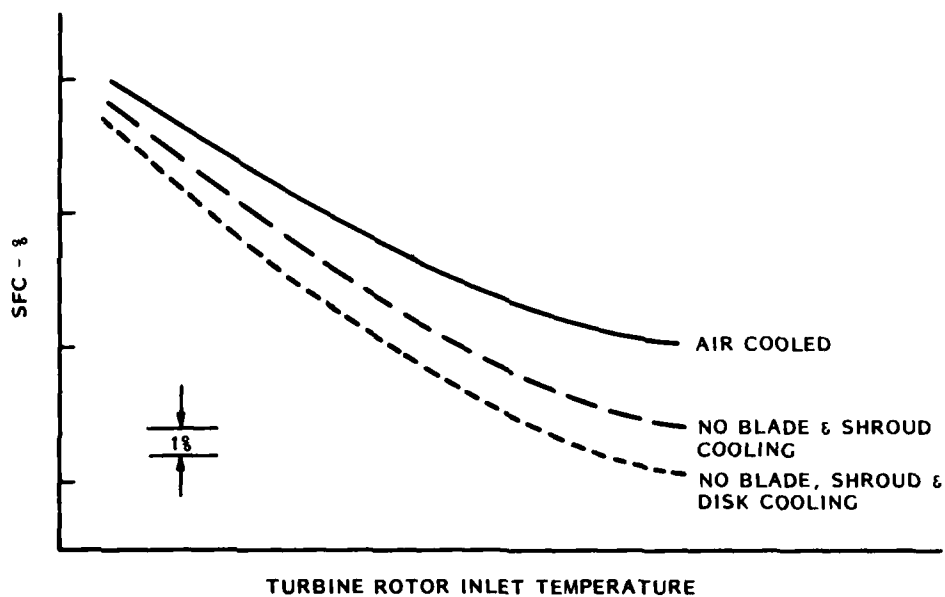


Figure 16. Hot Corrosion of Ceramics and Superalloy (Bare and Coated)



$$\dot{W}_c = f \left(\begin{array}{l} \text{COMPRESSOR DISCHARGE TEMPERATURE,} \\ \text{TURBINE TEMPERATURE,} \\ \text{SURFACE HEAT TRANSFER.} \end{array} \right)$$

Figure 17. Turbine Cooling Flow Distribution

Figure 18. SFC Gain With Reduced Turbine Cooling
(Installed Thrust, Fan P/P, Cycle P/P Constant)

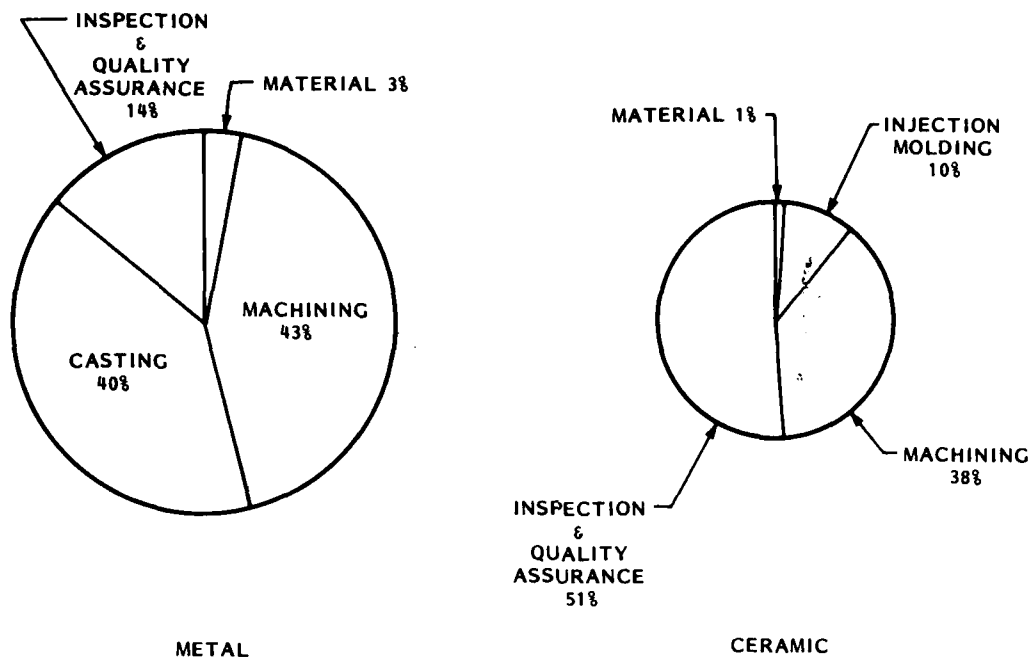


Figure 19. Turbine Blade Cost Comparisons: Aircooled Metal vs. Uncooled Ceramic

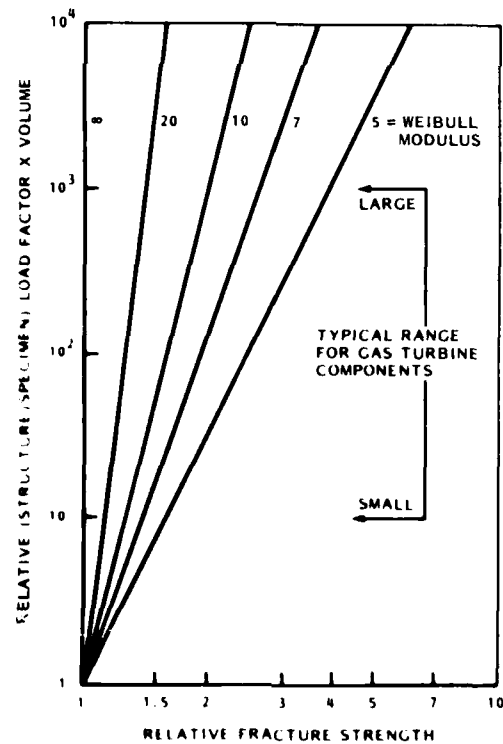


Figure 20. Relative Stressed Volume vs. Relative Fracture Strength

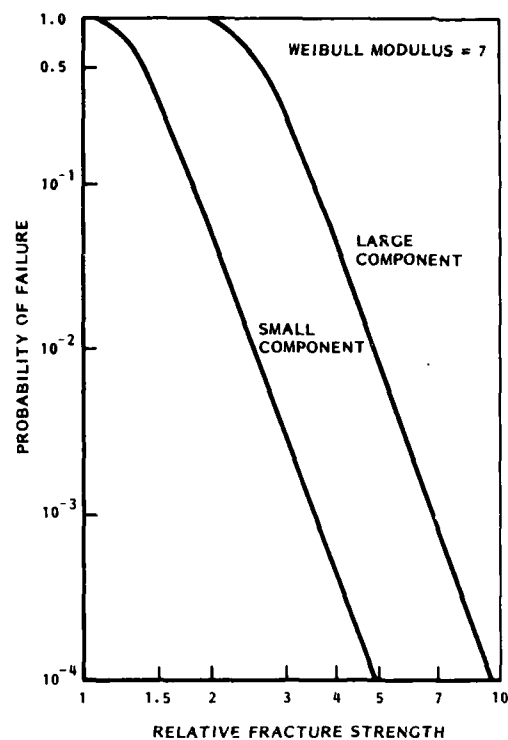


Figure 21. Probability of Failure vs. Relative Fracture Strength

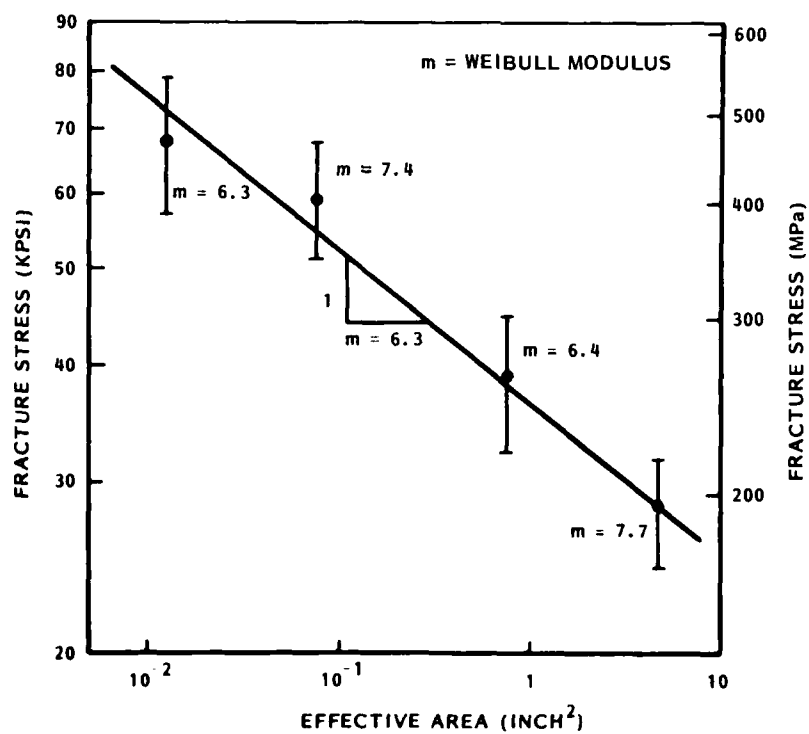


Figure 22. Size Effect for Self-Bonded SiC - Small Bend Bars, Large Bend Bars, Spin Bars, and Spin Disks (Left to Right)

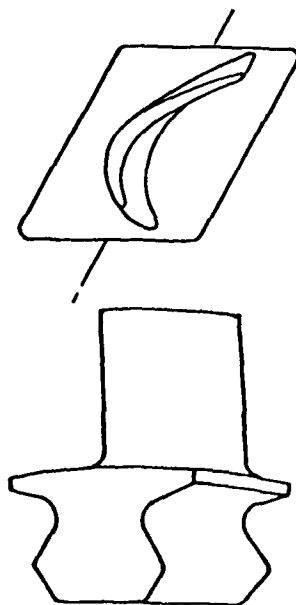


Figure 23. Ceramic Turbine Blade Study Configuration

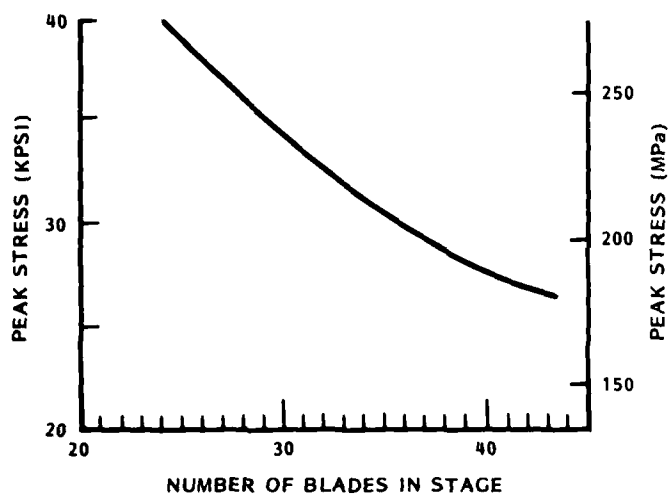


Figure 24. Peak Dovetail Stress vs. Number of Blades in Stage

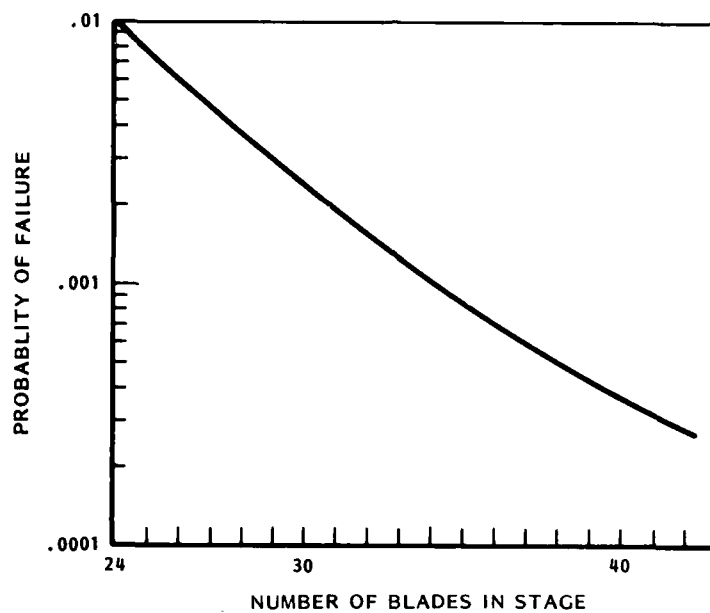


Figure 25. Probability of Failure vs. Number of Blades in Stage

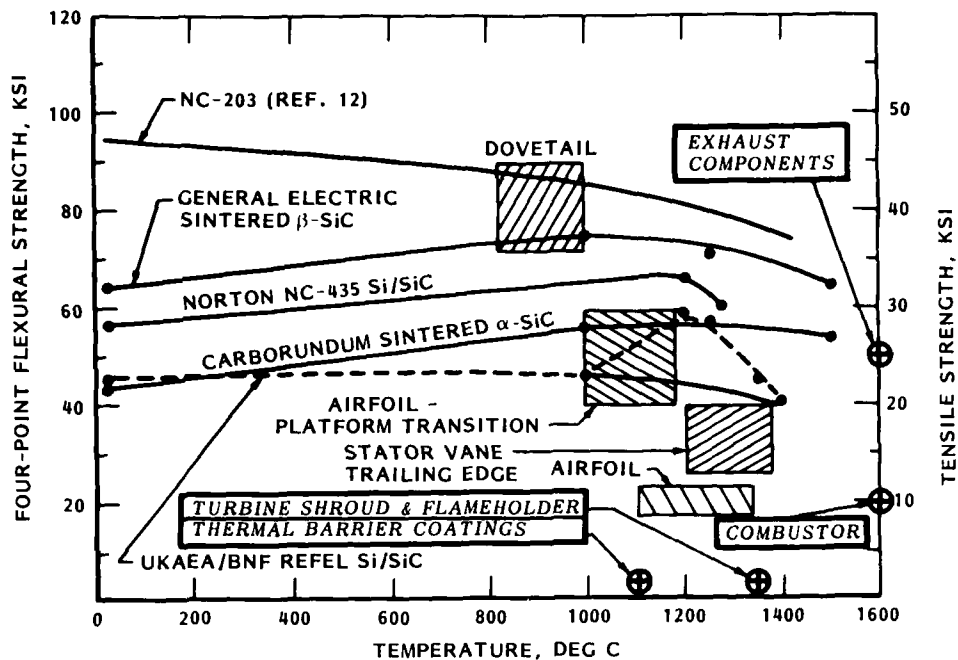


Figure 26. Strength of Silicon Carbide Materials vs. Required Strengths for Engine Components *

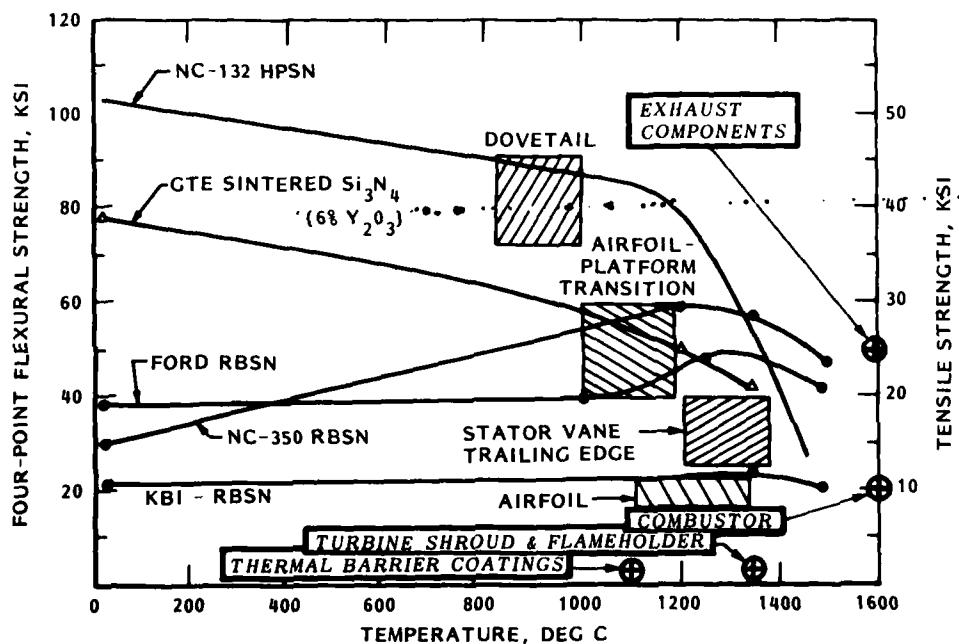


Figure 27. Strength of Silicon Nitride Materials vs. Required Strengths for Engine Components *

*(WITH \oplus REQUIREMENTS FOR ADDITIONAL COMPONENTS SUPERIMPOSED UPON THE BASIC FIGURE FROM REFERENCE 2)

TABLE 1
REPRESENTATIVE ENGINE DESIGN REQUIREMENTS FOR CERAMICS APPLICATIONS

ITEM	TEMP °F	TEMP [°C]	STRESS KPSI [MPa]	ADDITIONAL CONSIDERATIONS	HOURS(a)	CYCLES(a)
TURBINE BLADE	1400	[760]	40 [276]	• HIGH CONTACT LOADS BETWEEN BLADE AND DISK		
	2000	[1093]	25 [172]	• CONTOUR TOLERANCE TO ±.001 IN. FOR SMALL ENGINE AIRFOILS		
TURBINE VANE	2000	[1093]	20 [138]	• INTERFACE LOAD CAPABILITY		
	3000	[1649]	10 [69]	• CONTOUR TOLERANCE SAME AS FOR BLADE		
TURBINE DISK	1000	[538]	65 [448]	• TEMPERATURE, EXPANSION AND LOAD COMPATIBILITY AT INTER-FACE WITH METAL SHAFT	5000 (25)	25000 (50)
TURBINE SHROUD	2500	[1371]	(b)	• RESISTANCE TO OXIDATION AND SPALLING UNDER RUB CONDITIONS		
COMBUSTOR	3000	[1649]	10	• HIGH THERMAL TRANSIENT CAPABILITY		
				• COMPATIBILITY WITH FUEL		
AFTERBURNER FLAMEHOLDER	2500	[1371]	(b)	• HIGH THERMAL TRANSIENT CAPABILITY		
				• COMPATIBILITY WITH FUEL		
EXHAUST COMPONENTS	3000	[1649]	25 [172]		1000	2000
THERMAL BARRIER COATINGS	2000	[1093]	(b)	• ADHERENCE INTEGRITY		
BEARINGS	400 lub. 1000 unlub.	[204] [538]	(c)	• DN CAPABILITY 2.5 x 10 ⁶ mm-RPM	(25)	

(a) Hours and cycles shown in () are for unmanned applications. Other values are for manned applications.

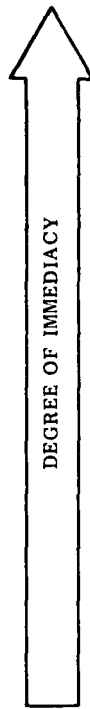
(b) Stress requirements are low for these items.

(c) Stresses are highly localized, Hertzian in character.

TABLE 2
IMPACT OF CERAMICS ON TURBINE PERFORMANCE

FACTOR	UNCOOLED CERAMIC PARTS RELATIVE TO COOLED METAL PARTS	EFFECT ON PERFORMANCE RELATIVE TO COOLED METAL PARTS
COOLING FLOW	NOT REQUIRED FOR BLADE AND VANE. REQUIRED FOR RELATED METAL STRUCTURE	+
CONTOUR	NO COMPROMISE REQUIRED FOR BLADE TO ACCOMMODATE COOLING SYSTEM AS IN METAL BLADE. NO DIFFERENCE IN CONTOUR OF VANE	+
TOLERANCE	SAME	0
CLEARANCE	LARGER, TO AVOID RUBS	-
FINISH	SAME OR BETTER	0
FILLET RADII	LARGER, TO REDUCE STRESS CONCENTRATIONS. EFFECT CAN BE COMPENSATED FOR IN THE AERODYNAMIC DESIGN.	0
BLADE LEADING EDGE	THINNER	+
BLADE TRAILING EDGE	THICKER	-
BLADE TAPER RATIO	GREATER FOR STRENGTH REQUIREMENTS	-

TABLE 3
ANTICIPATED INCORPORATION OF CERAMICS INTO AIRCRAFT ENGINES



THERMAL BARRIER COATING	TURBINE SHROUDS	EXHAUST COMPONENTS	COMBUSTORS	BEARINGS	TURBINE BLADES & VANES
●					
	●				
		●	●	●	
					●

CERAMICS FOR SMALL AIRBORNE ENGINE APPLICATIONS

R. Nathan Katz and Edward M. Lenoe

Army Materials and Mechanics Research Center
Watertown, MA 02172

ABSTRACT

An increasing number of successful demonstrations of ceramics as significant structural components in small land based heat engines, especially gas turbines, has drawn the attention of small aircraft and missile engine designers to this class of materials. The question which is being asked with increasing frequency is: "Do ceramics measure up to the criteria and requirements of airborne engines?" This question obviously does not have a simple answer, mainly because of the wide range of systems requirements and duty cycles which exist amongst airborne engines themselves. In this paper the authors assess the likelihood for successful application of ceramics to several classes of airborne engines with different duty cycles. The general design criteria and associated key materials and requirements for generic engines for limited life, APU, and man-rated helicopter use will be addressed. Materials, processes, design approaches, and reliability considerations appropriate to each generic engine category will be briefly discussed. A scenario for a least risk strategy for the introduction of ceramics into airborne engines will be presented. Key issues in materials research and development will be identified.

1. Introduction

The energy crisis, environmental concerns, and critical materials supply considerations are the driving force behind the current emphasis on ceramic materials technology for gas turbine (GT) engines. Since the early 1970's the focus of this emphasis on ceramic technology exploitation has been for vehicular engines (1-5). As a consequence, an increasing number of successful demonstrations of ceramics as significant structural components in small terrestrially based heat engines, has drawn the attention of aircraft and missile engine designers to this class of materials. For example, a study by Blankenship (6) has shown that for conventional take off and landing type of aircraft, the cost savings which can accrue by using ceramic vanes, would be ~\$110 million for 100 aircraft over 15 years of operation. The \$110 million saving would require an investment of an ~\$12 million for a cost/benefit ratio of about 10 (6). Table I lists the current experience on four terrestrially based, ceramic configured gas turbines (or components in G.T. test rigs). Given the fact that ceramics have now demonstrated feasibility for further development in terrestrially based applications it becomes appropriate to ask the question; "Do ceramics measure up to the requirements of small airborne engines?" This question obviously does not have a simple answer, mainly because of the wide range of systems requirements and duty cycles which exist amongst airborne engines themselves.

Table I.
SIGNIFICANT ACHIEVEMENTS IN CURRENT TERRESTRIALLY BASED CERAMIC-GT PROGRAMS

Program (Reference)	Type of Engine	Major Achievements
DARPA/Ford (1) (7)	~200 hp Regenerated, Axial Single Shaft, 2500 F TIT	<ul style="list-style-type: none"> All Stationary Ceramic Components in Reaction-Bonded Si₃N₄ Demonstrated 200 hours life in Engine Rig to 2500 F Duo Density Si₃N₄ Rotor Demonstrated 200 hours at ~2200 F TIT, 50,000 RPM First Stage Ceramic Hardware Run in an Engine 36.5 hours 2100-2500 F, 40,000-50,000 RPM
MERADCOM/Solar (8)	~10 kw Turbogenerator, Radial, ~1700 F TIT	<ul style="list-style-type: none"> Run ~50 hours with Ceramic Vanes, Producing ~10 kw Run ~40 hours with all Ceramic Nozzle Stage, Producing ~10 kw Demonstration of Ceramic Bearing
DARPA/AirResearch (9)	~1000 hp Simple Cycle 3-Stage 2200 F TIT	<ul style="list-style-type: none"> Integration of Over 100 Separate Ceramic Components in a High Performance Engine. Run at Full Speed and Temperature in Excess of 2 hours, Includes 2 Shutdowns and Starts. Ceramics Demonstrated 200 + hp Increase Over Base Engine
DDA/DOE (10)	~350 hp Regenerated 2 Shaft, 2265 F TIT	<ul style="list-style-type: none"> Ceramic Stators Run in Excess of 1000 hours at 1900 F TIT. Ceramic Vanes in Vehicle on the Road for Over 25 hours

In this paper we will attempt to assess the likelihood for successful application of ceramics to several classes of airborne engines with different duty cycles. The general design criteria and associated key materials properties and requirements for generic engines of the APU, limited life, and man-rated helicopter type will be addressed. The major focus of this paper will be on the materials and processes appropriate to the generic man-rated helicopter engine, as this represents the most rigorous duty cycle of the three classes of engines considered. Key issues in materials research and development will be discussed. A scenario for a least risk strategy for the introduction of ceramics into airborne engines will be presented. However, it is appropriate to first, briefly, review some aspects of the brittle materials design process.

II. Brittle Materials Design Process

Design with brittle materials requires a very precise definition of the state of stress at every point in the component. Brittle materials can, in fact, be quite strong, but generally manifest a wide scatter in strength and do not have the ability to redistribute high local stress concentration by yielding as in the case in metals. This in turn means that ceramics are extremely sensitive to high localized

stress gradients due to notches or other sources. In this regard, Dukes (11) has pointed out that the most difficult aspect of high temperature design with brittle materials is the definition of, and subsequent minimization of thermal stresses. Thus, a realistic expectation of exploiting the potential of ceramics in heat engines requires the availability of two technologies. These are: an analytic design capability to predict the thermal and stress environments from point to point in a component, and high temperature engineering materials with low thermal expansions in order to minimize thermal stresses. Advances in 2 and 3-D computerized finite element thermal and stress analysis techniques have provided the former, and the development to silicon nitrides and improved silicon carbides have provided the latter. Both of these developments reached a sufficient level of maturity in the late 1960's for various research programs for demonstration of ceramics in gas turbines to be initiated (1-3).

While a low thermal expansion is necessary for a ceramic engine material, other properties must be considered. All of the materials properties and requirements listed in Table II must be adequate. In particular, the time, temperature, stress and environmental dependencies of the mechanical properties must be known (or predictable) for the entire engine duty cycle. As will be discussed later in this paper the "virgin" materials properties are unlikely to be retained late in the engine's projected life time. Thus it is important to acquire design data on materials exposed to service environments for realistic times. One must also know the effects of processing method on these properties. Of particular importance in brittle material design, where probabilistic versus deterministic design procedures are used (11, 12) is the trade-off between strength and Weibull Modulus with respect to calculated component probability of success. As shown in Fig. 1 an increase in Weibull Modulus "m" is "worth more" than an increase in average strength (provided of course that the strength is at an acceptable level) in attaining a given level of component reliability. This point will be referred to later when key issues for future materials R&D are discussed. Having the information just described, the designer is in a position to perform trade-off studies as in Fig. 2 and specify an optimum design/material/processing combination for a given component in the system under consideration. Once the design/material/process for a given component has been selected, validation by rig and/or engine tests usually requires several passes through.

Table II.

GENERAL PROPERTIES REQUIRED OF A CERAMIC HEAT ENGINE COMPONENT

LEVEL I. TECHNICAL FEASIBILITY DEMONSTRATION

- THERMAL SHOCK/THERMAL FATIGUE RESISTANCE
- NECESSARY TEMPERATURE CAPABILITY
- ADEQUATE STRENGTH AND CREEP BEHAVIOR AS A FUNCTION OF TEMPERATURE
- NECESSARY LONGIVITY IN THE ENGINE ENVIRONMENT

LEVEL II ENGINEERING FEASIBILITY DEMONSTRATION

- CONSISTANCY OF ADEQUATE PROPERTIES IN AS-FABRICATED COMPONENTS
- ADEQUATE LEVELS OF RELIABILITY ATTAINED
- ADEQUATE COST EFFECTIVE FABRICATION POTENTIAL

LEVEL III TECHNOLOGY IMPLEMENTATION

- DEMONSTRATED BENEFIT/COST FOR THE TECHNOLOGY MUST BE SUFFICIENTLY HIGH TO WARRANT IMPLEMENTATION VERSUS EXISTING OR OTHER ALTERNATE TECHNOLOGIES

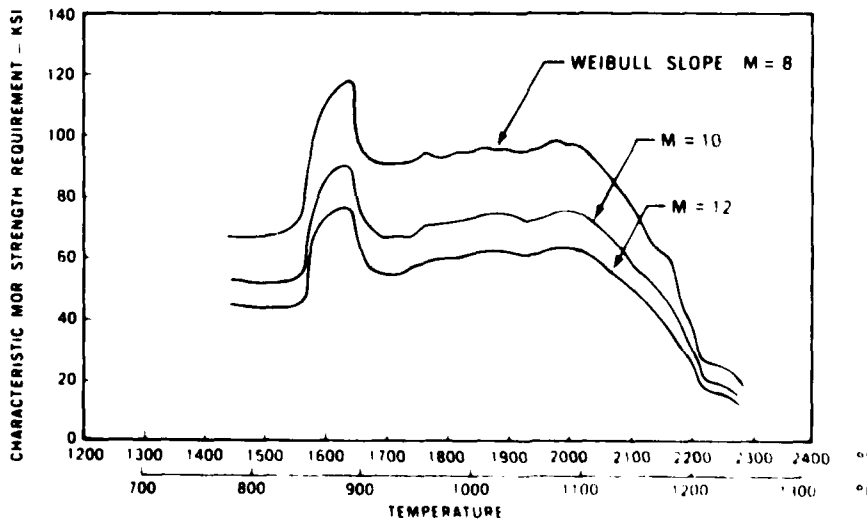


Figure 1. TRADE-OFF BETWEEN MOR AND WEIBULL MODULUS IN BRITTLE MATERIAL DESIGN (Ref. 13)

the iterative design scheme shown in Fig. 3. It is important to note that there is unlikely to be one optimum material/process that will satisfy a wide variety of systems requirements. Thus, the successful development of ceramic engine technology will require the existence of many materials and processing options. Similarly, a wide variety of innovative design concepts (particularly for attachment areas) will be required in order to develop compliant structures. This is essential, since brittle materials do not possess the capacity to redistribute over-stresses without failure, the structure must itself provide the means to redistribute stress (i.e., compliant structures). While the focus of this paper is on materials, the authors wish to point out their view that the development of compliant structures is currently a major pacing problem in high performance structural utilization of brittle materials.

III. Systems Requirements

As is clear from Fig. 2, the first step in defining materials requirements is an appropriate specification of systems requirements. The preceeding paper by Brooks & Bellin, (14) has provided these for both limited life (LL) and man-rated generic engines. Similarly the paper of Napier & Arnold (15) will partially provide this input for an APU type engine. However, it is worth while to reiterate in the broadest terms the systems requirements or goals for all these classes of engines, with special emphasis on Army goals. These are presented in Tables III thru V. Obviously, these general goals will take on appropriate numerical values and trade-off weights when a specific engine design study is initiated.

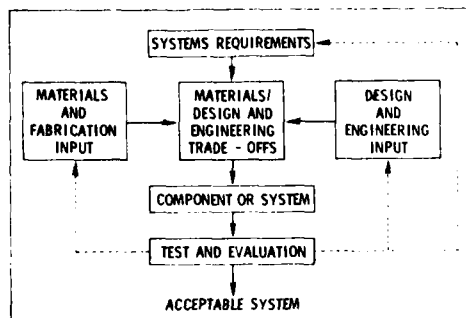


Figure 2. THE ENGINEERING TRADE-OFF LOGIC FOR INTRODUCING A NEW MATERIAL OR DESIGN INTO A SYSTEM

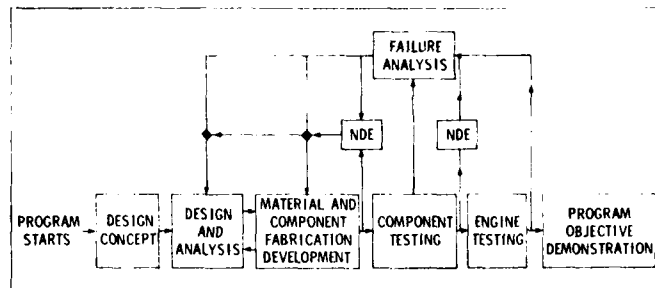


Figure 3. "BRITTLE MATERIALS DESIGN" ITERATIVE DESIGN SCHEME

Table III.
REQUIREMENTS FOR ARMY AVIATION APU'S

- LONGER TBO/LESS MAINTENANCE
- HIGHER SPECIFIC POWER FROM CONSTANT VOLUME PACKAGE
- LOWER SFC
- HIGH RELIABILITY (BUT LOWER THAN MAN-RATED IS PERMISSIBLE)
- DUTY CYCLE - MODERATE WITH LOTS OF STARTS, RELATIVELY FEW HOURS
- LOW COST (ACQUISITION AND LIFE CYCLE)

Table IV.
REQUIREMENTS FOR ARMY AVIATION LIMITED LIFE ENGINES

- 50 HOURS - 50 STARTS AND/OR CYCLES
- NONCORRODING/NONBRINNELING BEARINGS
- HIGHER THRUST/WEIGHT
- LOWER SFC
- HIGH RELIABILITY (BUT LOWER THAN MAN-RATED IS PERMISSIBLE)
- MODERATE SEVERITY DUTY CYCLE
- LOW ACQUISITION COST

Table V.
GENERAL REQUIREMENTS FOR MAN-RATED ENGINES FOR ARMY HELICOPTERS

- 4000-HR COMPONENT LIFE
- HIGHER SPECIFIC POWER (HP/WT)
- LOWER SFC
- LUBRICATION STARVATION TOLERANT BEARINGS
- VERY SEVERE DUTY CYCLE (LOTS OF ACCEL/DECEL)
- VERY HIGH RELIABILITY
- LOW LIFE CYCLE COSTS

IV. Requirements on Ceramics for Airborne Engine Applications

To discuss the requirements on ceramic materials for the three classes of airborne engines in detail would require a major monograph rather than a brief paper. Therefore, the authors have elected to focus on the strength requirements for vanes and rotor blades for man-rated engines, since these represent the most demanding application. As shown in the previous paper (14) the design stresses in the vanes and blades in limited life and man-rated engines fall in the same range. Also despite differences in thermal and physical properties, the predicted stresses in vanes and blades of the various candidate ceramic materials will be similar due to design practices.

Using the data of Brooks & Bellin (14) as well as data from the literature (16-19) it is possible to identify the key stress-temperature combinations for the principal design points of vanes and blades for a generic helicopter or limited life engine with a TIT range of 2200-2500°F. These are presented in Fig. 4.

While vanes and blades are the most demanding of the high temperature applications, there is one important low temperature application, namely, bearings. Ceramic bearings offer important advantages in potential for lubrication starvation tolerance, high DN, and cooler running bearings. This subject will be reviewed in detail by Bersch (20) in these proceedings. Therefore, we will not deal with the materials or requirements for ceramic airborne bearings. However, we will return to bearings in our recommendation for exploitation of ceramics in airborne engines.

Before proceeding to match the available ceramic properties with the generic design requirements, we will introduce the various families of engineering nitride and carbide together with their fabrication processes.

V. Families of Candidate Airborne GT Ceramics, Processing Routes and Some Properties

Materials which are considered candidates for airborne G.T. application include state-of-the-art and developing materials, principally from two broad materials/process families; the silicon nitrides and the silicon carbides.* Typical properties of members of these two families of engineering ceramics are presented in Table VI. A brief description of each family of materials follows.

Silicon Nitride Based Ceramics

The silicon nitride families of ceramic materials include:

- Hot Pressed Silicon Nitride (HPSN)
- Reaction Bonded Silicon Nitride (RBSN)

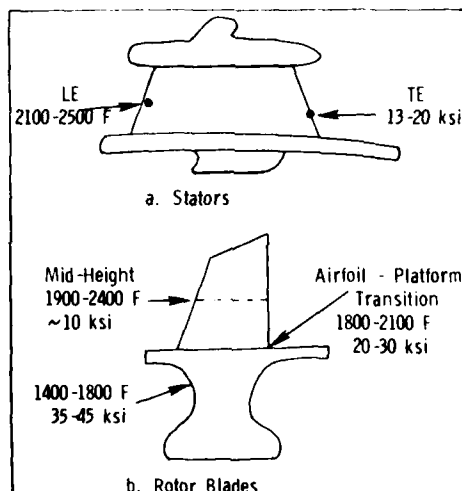


Figure 4. STRESS-TEMPERATURE RANGES AT DESIGN POINTS FOR GENERIC LIMITED LIFE AND HELICOPTER GAS TURBINE ENGINES - 2100-2500 F TIT FIRST STAGE COMPONENTS

		MOR (RT, psi)	MOR (1000 C, psi)	MOR (1375 C, psi)	RT - α ($\text{psix}10^{-6}$)	α (10^{-6} deg C ⁻¹)	K (Wm ⁻¹ deg C ⁻¹)
SILICON NITRIDE	HOT-PRESSED (MgO ADDITIVE)	100,000	90,000	48,000	46	3.0	30-15
	SINTERED (Y ₂ O ₃ ADDITIVE)	95,000	85,000	40,000	40	3.2	28-12
	REACTION-BONDED (2.45 g/cc)	30,000	50,000	55,000	24	2.8	6-3
SILICON CARBIDES	HOT-PRESSED (Al ₂ O ₃ ADDITIVE)	95,000	85,000	75,000	65	4.5	85-35
	SINTERED (a PHASE)	45,000	45,000	45,000	59	4.8	100-50
	REACTION-SINTERED (20 vol Free Si)	55,000	60,000	40,000	50	4.4	100-50
	CVD (Lower Values)	60,000	80,000	80,000	60	-	-

*Zirconia based thermal barrier coatings might also be appropriately included, however, this paper as well as these Proceedings, deals with monolithic ceramics.

Sintered Silicon Nitride (SSN)

β' SiAlON's (SiMON)

Chemically Vapor Deposited Silicon Nitride (CVD-SN)

Hot Pressed Silicon Nitride can be produced by either conventional uniaxial (21) or hot isostatic (22, 23) routes. One generally starts with α - Si_3N_4 powder and adds a densification aid such as; MgO , Y_2O_3 , ZrO_2 , CeO_2 , or SiBeN_2 . Depending on the purity and phase composition of the starting Si_3N_4 powder, the percentage and type of additive, milling and mixing procedures, and hot pressing parameters (T,t) one can obtain a very wide range of strength, strength vs. temperature, creep, fracture toughness, or oxidation behaviors. Illustrative of such variety of behavior, the strength vs. temperature curves of HPSN's as a function of some of the foregoing processing variables, are shown in Fig. 5. To make an important point, one cannot look at the data in Fig. 5 and make an arbitrary judgement that one material is "better" than another. The concept of "better" depends on the application requirement. The lower curve in Fig. 5 may be "better" for a given application than one of the higher curves, (i.e., it may have adequate strength, Weibull "m", creep, etc, and be cheaper and easier to fabricate).

Almost all HPSN's exhibit MOR values of 100,000 psi (690 MPa) or greater at RT and retain these values to 1000-1100°C (dependent on amount and type of additive), have high K_{IC} ($\sim 5-8 \text{ MN/m}^{3/2}$), high thermal shock resistance, and excellent erosion resistance.

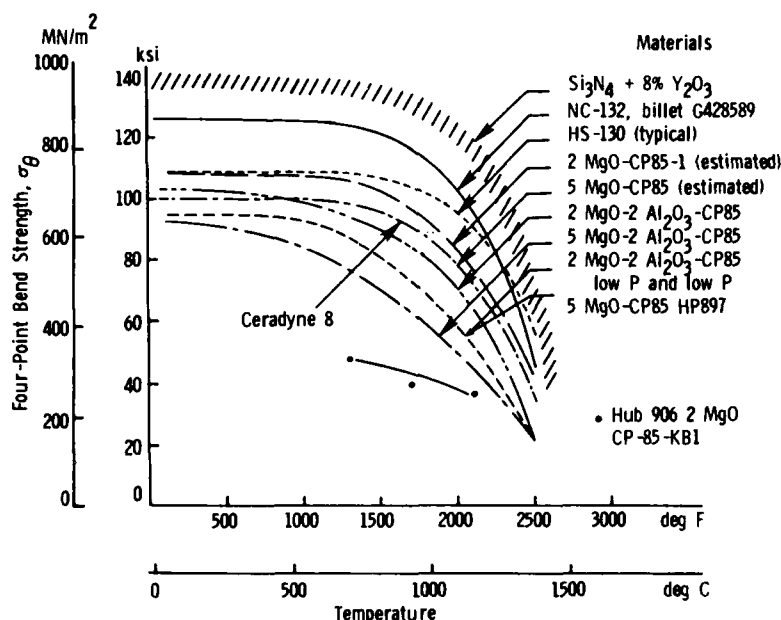


Figure 5. FLEXURAL STRENGTH OF VARIOUS TYPES OF HPSN

Hot pressed silicon nitride with MgO as an additive, typified by NC-132 material, most nearly approaches a mature engineering material. HPSN with Y_2O_3 additives typically have higher strengths at both room and elevated temperatures (see Fig. 5), as well as, better oxidation resistance and K_{IC} and less slow crack growth than MgO containing HPSN. However, this material has been plagued with an intermediate temperature ($\sim 1000^\circ\text{C}$) oxidation problem. While it appears that the post-fabrication nitridation treatment demonstrated by Gazza, Knoch, and Quinn (25) can overcome this problem, more work needs to be carried out before HPSN with Y_2O_3 is as developed as the MgO containing varieties. Very high strengths have been attained by Tsuge, et al, in Japan (26) with $\text{Y}_2\text{O}_3 + \text{Al}_2\text{O}_3$ additive using the grain boundary crystallization approach. The high cost associated with diamond machining of HPSN from simple billets to complex geometry components, has led to research in near net shape hot pressing, in several laboratories. Significant progress in hot pressing Si_3N_4 to near net shape has been demonstrated by Ford (27), AMMRC (28) and Annawerk (29). Such work has demonstrated the utility of hot pressing in engine development programs, and the costs may be acceptable for some airborne engine application.

Reaction Bonded Silicon Nitride, has been developed, largely to obtain a readily formable (little machining required), low cost material. In contrast to HPSN, RBSN maintains its strength to temperatures beyond 1400°C . RBSN can be made with creep rates significantly below HPSN (30). As a consequence of the reaction bonding process, RBSN is of necessity at least 10% porous which makes it less oxidation resistant than HPSN at intermediate temperatures (31), and limits its strength to less than 60 KSI (415 MPa) or more typically to about 35 KSI (245 MPa).

The fabrication of RBSN components begins with a silicon metal preform made by slip casting, dry pressing, flame spraying, injection molding or various other techniques. The preform is then nitrided in an atmosphere of pure N_2 or $\text{N}_2 + \text{H}_2$, at either a preselected temperature schedule (32) or now more usually using a nitrogen demand control cycle (33). The nitridation process of such a Si preform is a remarkable, if still somewhat imperfectly understood event. For $3\text{Si(s)} + 2\text{N}_2(\text{g}) \rightarrow \text{Si}_3\text{N}_4(\text{s})$ there is a 23% expansion in the solid volume compared to Si; yet, when this reaction is carried out on a preform there is essentially no change in dimensions ($\sim 0.1\%$). The reason for this appears to be that the first Si_3N_4 to form, does so by a complex solid-liquid-vapor whisker growth into the void space of the Si preform. The net result is that what appears to be a rather complex series of processing steps, and

what is a complex series of chemical reactions, yields a product of great technological import-- an engineering ceramic which can be mass produced to tight dimensional tolerances with little or no machining and at low cost.

Reaction bonded silicon nitride has improved considerably over the past few years, as shown in Fig. 6. Nevertheless, where high strength, more oxidation resistant material is required, it would be desirable to have a readily fabricable, fully dense silicon nitride. This has been the impetus for the development of sintered silicon nitride.

Sintered Silicon Nitrides are a rather recent development. Although, Si_3N_4 was sintered prior to 1976 (34), the balance between dissociation of the Si_3N_4 and densification was such that densities of only 90% were obtainable. Indeed, the possibility of sintering fully dense silicon nitride at reasonable pressures was still an open question as late as 1976. Since then several groups have succeeded in producing sintered Si_3N_4 of at least 95% density, and a few groups have obtained greater than 99% density. Gazza (35) has reviewed the status of SSN. Table VI shows a SSN material with strengths between HPSN and RBSN. Some more recent experimental SSN materials have approached the properties of HPSN. SSN has been formed by injection molding, and provided isotropic shrinkage can be obtained components will require little machining. Recently, Giachello and Popper (36) have demonstrated that it is possible to post sinter a RBSN preform to ~98% density, with increased strength and oxidation resistance. With this development one could start with a sintering preform that would yield only 6-8% shrinkage as opposed to 18-20% shrinkage for sintering with a powder preform. It is also possible that sintered Si_3N_4 bodies of over 95% T.D. may be used as preforms for cladless hiping. Such a development would be a major breakthrough towards attaining high reliability, affordable, high performance components such as rotors.

SiAlON's represent an important new class of ceramic materials which are solid solutions of metal oxides in the $\beta\text{-Si}_3\text{N}_4$ lattice. These solid solutions distort the lattice to $\beta'\text{-Si}_3\text{N}_4$ lattice (hence, β' , SiAlON's). SiAlON's were originally developed from Al_2O_3 solid solution, but MgO , BeO , Y_2O_3 , etc have all been found to yield β' solid solutions, as well as a variety of other phases. SiMON's have been developed with a view toward application in heat engines (37, 38). However, these materials are still in early development and have not been used in engine demonstration programs to date. It is likely that they will play a role in future engine programs. SiMON phases are of major importance in determining the controlling the grain boundary phases which in turn control the behavior of HPSN and SSN. Therefore, understanding phase relationships in these systems is of major importance. These phase relationships are discussed in the papers of Prof. K.H. Jack and his students at Newcastle-Upon-Tyne (39-41).

CVD-SN in very thin layer form is currently an important electronic material. Building on this thin film technology some research in the use of CVD-SN coatings and optical windows is in progress, but bulk CVD-SN has yet to be demonstrated as a structural material.

Silicon Carbide Based Ceramics

The silicon carbide based families of ceramic materials include:

- Hot Pressed SiC (HP-SiC)
- Reaction Sintered (or bonded) SiC's (RS-SiC)
- Sintered SiC's (S-SiC)
- Silicon Carbide/Silicon Composites (Si/Comp)
- Chemically Vapor Deposited Silicon Carbide (CVD-SiC)

REACTION-BONDED SILICON NITRIDES		
RECENT ADVANCES:		
• INCREASING COMPONENT DENSITIES		
2.2 g/cc → 2.7 g/cc		
• RATE-CONTROLLED REACTION BONDING		
→ IMPROVED MATERIALS UNIFORMITY		
Property	1972	1978
ρ (g/cc)	2.2	2.7
4-PT MOR-RT (ksi)	~17	~36
Stress Rupture at 2200 F, 30 ksi	Failure	>300 Hour Suspension
Oxidation - Weight Gain in 200 Hours at 1900 F (Worst Case)	~6%	~0.75%

Figure 6. REACTION-BONDED SILICON NITRIDES

Hot Pressed SiC can be formed with various densification aids, but only HP-SiC utilizing Al_2O_3 additions has been considered for high performance engine applications (42). Properties of NC-203, the most mature example of this material are shown in Table VI, while HP-SiC is not as strong as HPSN at low temperatures, it retains useful strength out to ~1400°C. Thus, it might be an attractive material where high strength is required at 1400°C or beyond. The major drawback of this material is the need to diamond machine parts from a hot pressed billet.

27

Reaction Sintered (or bonded) Silicon Carbides, cover a wide range of compositions and manufacturing processes (43). Typical examples of these materials include; BNF Refel, KI, NC-430, NC-435, and Ford Siliconized Silicon Carbide. While each material is formed by its own proprietary process, in general, a plastic body is formed of SiC powder, graphite, and plasticizer. In some variants of the process SiC powder plus a char forming plastic binder are used (44). The plastic body is pressed, extruded, injection molded or otherwise formed into a green body. Plasticizers are burned off or converted to a porous char by pyrolysis. Silicon metal as a liquid or vapor is intruded into the body and reacts with the graphite powder or char to form SiC in situ, which reaction sinters (or bonds) the component. Excess silicon is usually left to fill any voids, thus yielding a non-porous body. Such materials exhibit quite reasonable strengths, and hold them to the melting point of silicon ($\sim 1400^\circ\text{C}$) or beyond, dependent upon the amount of free silicon retained. A variety of successful experimental gas turbine components, such as combustors or stators have been made by this materials/process route.

Sintered Silicon Carbide is a rather recent innovation. The benefit of having a fully dense silicon carbide with no silicon, and not requiring expensive machining (as with HP-SiC), was recognized very early. However, pressureless sintering of SiC to full density was thought unattainable until Prochazka demonstrated that by using B and C additions, β -SiC could be sintered to near full density at $\sim 2000^\circ\text{C}$. Prochazka also demonstrated that sintered β -SiC could be formed into useful shapes by slip casting, die pressing and extrusion. Distribution of the carbon additive and exaggerated grain growth of α -SiC were found to interfere with densification. Coppola and McMurtry (46) developed sintered α -SiC in an effort to eliminate the problems associated with the $\beta \rightarrow \alpha$ transformation. Sintered α -SiC has been demonstrated in several engine applications. Table VI provides some additional properties for sintered α -SiC.

Reaction-Formed SiC/Si Composites, developed by Hillig (47), are the first engineered composite ceramic/ceramic materials which offers the possibility of low cost for structural components. The process consists of starting with a graphite (or carbon) cloth, tow, felt, chopped fiber array or any other possible precursor; forming a precursor preform by any one of a variety of routes; and infiltrating liquid Si into the graphite precursor. The molten Si reacts with the graphite materials to form polycrystalline SiC fibers (which may or may not have graphite fiber cores, dependent upon process parameters) in a Si matrix. The result is a fully dense oxidation resistant body with about 30 to 50 vol % Si reinforced by 50 to 70 vol % SiC. (This high percentage of Si and the fibrous SiC morphology makes this material quite different from Refel-type materials). While the material shows promise of ease and versatility of fabrication, it is not yet clear what the costs may be. The material offers the ability to design a composite component optimized for mechanical and thermal requirements. The materials strength is at the 50,000 to 60,000 psi level. Preliminary stress rupture data indicate that the strength of this material is independent of time below 1500°C , unlike most high temperature ceramics (48). Perhaps the most intriguing advantage is that damaged areas have been removed and the components repaired with improved properties. The presence of free silicon would be thought to limit a use to temperatures of $\sim 2400^\circ\text{F}$. In spite of this, the material has been used in an experimental combustion liner application at temperatures above 2600 F (47). Although the material is still in a very early stage of development, the fact that it is an "engineered" composite material makes it a very exciting new development.

CVD - Silicon Carbide in contrast to CVD- Si_3N_4 has been produced in bulk. Gas turbine component fabrication capability, including radial and axial rotors has been demonstrated (49). The strength properties shown in Table VI represent the lower end of the scatter band. The very large scatter of strength in CVD-SiC is still a major problem due to columnar grains and residual deposition resistance. Another major drawback from an application point of view is likely to be cost. The process may be useful in coating SiC ceramics formed by more conventional routes.

VI. Property - Requirements Comparison

To illustrate how available materials properties compare with design requirements, we will examine the tensile strength - component stress situation. Obviously, in a real preliminary design/materials selection study, a similar process must be gone through for creep, stress rupture, oxidation, corrosion/erosion, etc. Figures 7 and 8 show the strength vs. temperature behavior of various silicon nitrides and silicon carbides respectively. Superimposed on the same figures we have mapped the stresses expected at the major design points of vanes and blades for man-rated and limited life engines as shown in Fig. 4. It is important to note that the design stresses are maximum principle tensile stresses, whereas the strength measurements are 4 point modulus of rupture (MOR) strengths. Therefore, in order to map the stresses we have adapted the conservative convention of setting the tensile strength as half of the 4 pt. MOR strength. This underestimates the true tensile strength of the ceramic (50) but for preliminary design it is an acceptable artifice.

As can be seen in Figures 7 and 8, all materials with the exception of one variety of RBSN appear to be suitable as vane materials. However, economic considerations would rule out the hot pressed silicon nitrides and silicon carbides for this application. Similarly, the likelihood that combustor pattern factors would produce temperatures near or above the melting point of silicon rules out the materials with high ($\geq 8\%$) free Si. Thus we are left with several RBSN's SSN, S-SiC, and several reaction sintered SiC's as viable candidates for vanes from the strength point of view. It is important to re-emphasize that a similar evaluation for other properties will further reduce this list. For example, a 4000 hour requirement may eliminate RBSN materials on the basis on oxidation resistance.

A similar evaluation shows that quite a few materials appear to have adequate strength at temperature for both the blade airfoil and the airfoil platform transition requirements. (Note in this case creep considerations will very probably reduce the number of viable candidate materials). However, only HPSN or HPSiC presently appears acceptable for the dovetail. Sintered silicon carbide and sintered silicon nitride look promising if their strength can be increased by about 25-50%.

The major point to be drawn from the above is that looking only at short time strength the current level of high temperature strength (ca 1900 - 2500°F) is not the limiting problem, but intermediate temperature (ca 1400 - 1800°F) strength (which occur in areas of highest stress) is. On the otherhand, if one were to go through a similar analysis for creep or time dependent strength properties, requirements for improved high temperature behavior would most likely emerge. In the next section we will show examples of how time dependent materials behavior might be factored into the preliminary design process.

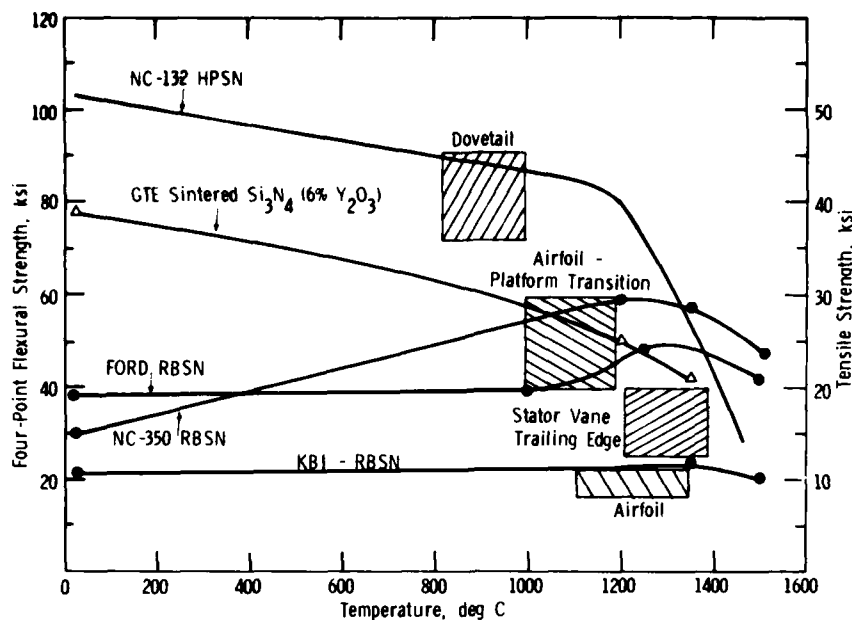


Figure 7. FLEXURAL STRENGTH OF SILICON NITRIDE MATERIALS VERSUS REQUIRED STRENGTHS FOR BLADES AND VANES

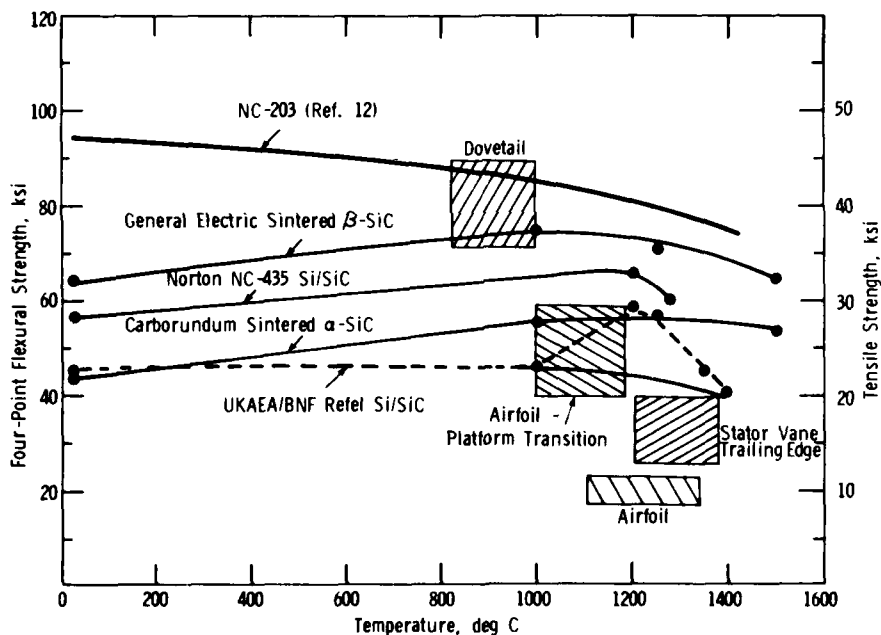


Figure 8. FLEXURAL STRENGTH OF SILICON CARBIDE MATERIALS VERSUS REQUIRED STRENGTHS FOR BLADES AND VANES

VII. Time Dependent Properties

In the gas turbine engine the ceramic material will see a very complex superposition of environmental factors. For example, high temperatures (imposing substantial radial and axial thermal gradients), varying contact and aerodynamic loads, oxidation (with the possibility of intermittent localized reduction), erosion/corrosion, vibration etc., will all be occurring and interaction in ways not yet fully understood. This complex environment will produce equally complex materials responses. Creep, slow crack growth, pitting, surface layer formation and alteration, crack healing etc. may all be proceeding simultaneously, and interacting in ways not yet observed. In spite of all of this complexity and uncertainty, there is one thing which we can state with assurance. Namely, the surface and near surface character after hundreds of hours of duty cycle exposure will not be the same as that of the "virgin" material originally put in the engine. Therefore, it is prudent to initiate laboratory scale tests to model and measure what might happen to materials properties after environmental exposure. While it is impossible in a laboratory test on MOR bars to duplicate engine environments, it is at least possible to evaluate what long time exposure combined with thermal cycling in air or combustion gas will do to the strength of candidate ceramics materials. Quinn at AMMRC (51), Richerson and Carruthers at Aircsearch (52) and Siebells at VW (53) have conducted such studies. All of them have found that there is, in

general, a significant reduction in the strength of the candidate ceramics by such exposure. Table VII gives some results from the work of Quinn for 6 such materials exposed to the oxidative exposure cycle reported in ref. 51. Also in Table VII are results from the work of Richerson and Carruthers on RBSN and sintered α -SiC tested in their combustion rig (52).

Knowing that the various classes of candidate materials may undergo strength degradation in these laboratory tests, it would be appropriate for the designer to apply a "strength reduction factor" to those parts of his design where appropriate. In this case if a RT strength of 100,000 KSI is required of a HPSN part that has spent several hundred hours cycling between 2500F and RT, that level of strength will not be available (the strength will be ~50,000 KSI).

High temperature strength or stress rupture data on samples exposed to such cycles is not available at present. Stress-rupture tests on uncycled samples do show time dependence for these materials so that one must assume that the strength available in the part will decrease with exposure time. Thus the available evidence indicates that the designer should use the lower strength values typical of exposed samples rather than MOR data from short time tests on "virgin" materials. Table VIII lists MOR-stress rupture strengths at 300 hours and 1200°C (2200F) from the data of Quinn (54). Figure 9 shows how these stress-rupture values reduce the options available to the designer. Also note that there are still materials with satisfactory properties at 2200F for the vane, blade and airfoil. Using the stress rupture data it appears that improved materials may be required for the blade airfoil/platform transition. Again increases of the order of 20-50% would seem to be required.

Table VII. COMBINED THERMAL EXPOSURE -
THERMAL CYCLING TESTS OF ENGINE CERAMICS TO 2500 F

Material	Virgin MOR (ksi)	Exposed MOR (ksi)	% Change in MOR	Laboratory and Test-Condition
NC-132 HPSN	104	50.5	-51	AMMRC - 360 hour/500 cycles in air and flame [51]
NC-203 HP SiC	99	102	+3	
NC-350 RBSN	43	35	-19	
KBI-RBSN	30	24	-20	
Silcomp - Si/SiC	47	32	-32	
Ford - RBSN	42	36	-15	Airesearch - 350 hour/1700 cycles in combustor gas [52]
ACC RBSN-101	37.4	29.4	-21	
Sintered α -SiC	45.8	45.9	0	

Table VIII. 300-HOUR STRESS
RUPTURE STRENGTHS AT 1200 C

Material	Strength	
	~ ksi	~ MPA
NC-132 (HPSN)	35	245
NC-350 (RBSN)	50	345
KBI-RBSN	28	195
Ford - RBSN	40	280
NC-203 (HP SiC)	60	410
α -Sintered SiC	40	280
NC-433 (RS-SiC)	45	315
NC-435 (RS-SiC)	45	315

Data from Quinn, 4-point flexural stress-rupture

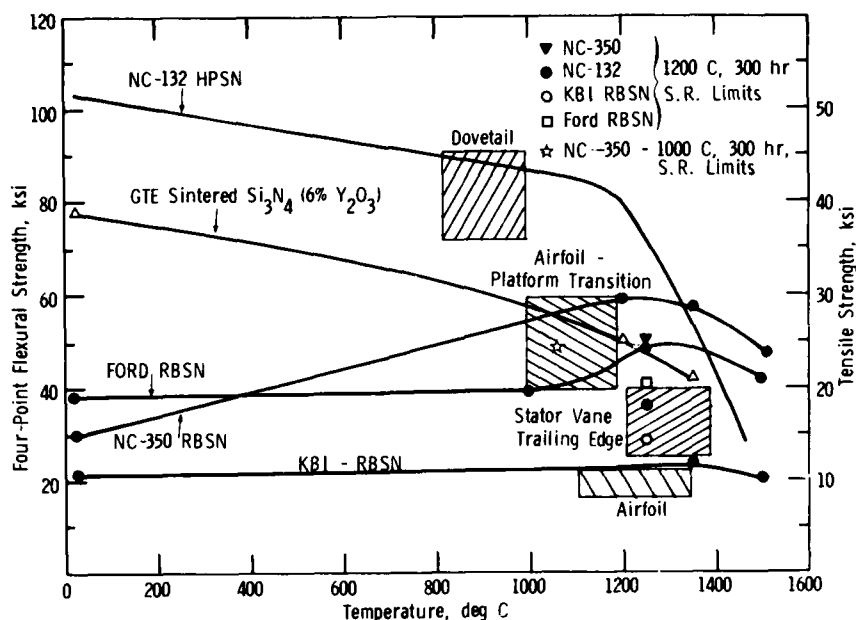


Figure 9. FLEXURAL STRENGTH OF SILICON NITRIDE MATERIALS VERSUS REQUIRED STRENGTHS FOR BLADES AND VANES

VIII. Desirable Nearterm Material Improvements

In the two foregoing sections we have shown that while adequate materials strength exists to consider the use of ceramics in some limited life airborne engine applications, due to time dependent property considerations strength improvements for both Si_3N_4 and SiC materials on the order of 20 to 50% are in some cases desirable and in other cases necessary. As discussed in section II, concurrent increases in the Weibull Modulus "m" are also desired (a higher "m" in both the as fabricated and the service exposed conditions.) What is the likelihood of attaining property increases of this order?

For the silicon nitride families of materials the outlook is quite good for achieving the above goals from RT to $\sim 1350^\circ\text{C}$. The use of the grain boundary engineering (GBE) approach (54, 55) coupled with microstructural optimization is leading to considerably improved properties. At a recent meeting, Dr. Komeya of Toshiba showed results on a sintered Si_3N_4 which on a laboratory size sample under fast fracture conditions maintained 200,000 psi strength from RT to $\sim 1000^\circ\text{C}$ and was significantly stronger than NC-132 out to 1350°C (56). As this material had a crystallized $\text{Y}_2\text{O}_3:\text{Al}_2\text{O}_3:\text{SiO}_2:\text{Si}_3\text{N}_4$ grain boundary, long term phase stability and considerably less than 50% strength fall off after environmental exposure can be anticipated. However, this anticipation needs to be verified in practice. No data on Weibull Modulus of this material was presented, but HIPPING of such near full density sintered products should considerably increase the Weibull "m".

In the area of reaction bonded silicon nitride recent work by Giachello and Popper (36) has shown that RBSN can be made significantly stronger from RT to about 1000°C - 1100°C and more oxidation resistant out to $\sim 1350^\circ\text{C}$. This significant development coupled with the relative ease of fabrication of RBSN should yield material which meet the requirements of vanes and blades shown in Figs. 7, 8 and 9.

In the area of SiC , attainment of 90,000 psi with a Weibull Modulus of 12-20 is considered a reasonable target for the near term. Phoenix, et al, have recently reported on progress towards attaining this goal (57). A sintered α - SiC with such properties would be expected to maintain them from RT to 1400°C with little time dependence of strength.

These near term materials improvements are proceeding mainly from state of the art materials processing efforts. Table IX presents some advances in processing technology which might significantly and favorably impact the homogeneity, reliability and cost of ceramic engine hardware.

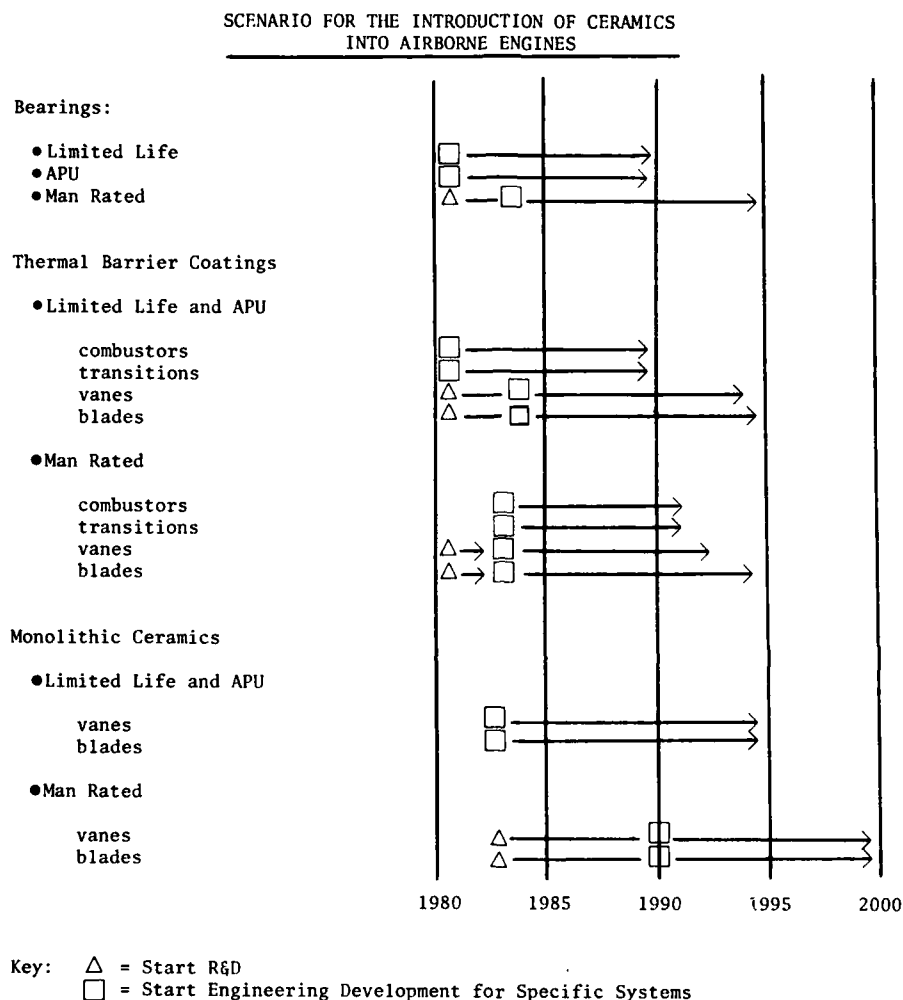
Table IX
POSSIBLE NEW DIRECTIONS FOR
ENGINE CERAMICS PROCESSING

- FLUIDIZED BED NITRIDATION
- FLUIDIZED BED ADDITION AND PREREACTION OF DENSIFICATION AIDS
- DEVELOPMENT OF SINTERING FOLLOWED BY CLADLESS HIP
- POWDER PRODUCTION FROM ORGANIC PRECURSORS
- FORMATION OF HIGH STRENGTH, LOW α CERAMIC BY DEVITRIFICATION OF N_2 OR C CONTAINING GLASS
- POST FABRICATION THERMAL TREATMENTS

The point is that many materials science and engineering approaches have yet to be exploited and the application of these approaches will result in continued improvement of the silicon nitride and silicon carbide families of materials.

IX. Scenario for Ceramic Introduction into Airborne Engines

Based on what the authors have presented above, as well as, their ongoing surveillance of the state of the art in monolithic ceramics, and thermal barrier coatings the following scenario for introduction of ceramics into Airborne Engines operating at ~2200 to 2500°F, TIT, is proposed:



X. Summary

This paper has reviewed some aspects of brittle materials design, systems requirements for small airborne engines, the requirements these impose on the ceramic materials and the ability of the existing ceramics to meet these requirements. We have seen that for some limited life and APU applications that existing ceramics have a reasonable chance of successful use as engine components. For other applications strength (also creep, and other time dependent properties) will have to be improved. Our judgment is the 20-50% increases in strength which appear to be required for long life man rated applications are attainable by extension of the current state of the art. Based on this optimistic assessment a scenario was presented which outlines, in the authors opinion, when work should be initiated to have airborne ceramics engine ready for the mid 80's to the end of the century.

REFERENCES

1. McLean, A.F., Fisher, E.S., & Harrison, D.E., "Brittle Materials Design, High Temperature Gas Turbine" Interim Report 1, AMMRC CTR 72-3 (March 1972) (AD 894-0521)
2. Ceramics for Turbines & Other High Temperature Engineering Applications, Ed. D.J. Godfrey, Proceedings of the British Ceramic Society, 22 (1973)
3. Ceramics for High Performance Applications, Eds, J.J. Burke, A.E. Gorum, and R.N. Katz, Brook Hill Publishing Co., Chestnut Hill, MA (1974)
4. Ceramics for High Performance Applications II, Eds, J.J. Burke, E.M. Lenoe, and R.N. Katz, Brook Hill Publishing Co., Chestnut Hill, MA (1978)
5. Workshop on Ceramics for Advanced Heat Engines, Conference Proceedings, ERDA Conf-77-0110, Orlando, FL (1977)
6. Blankenship, C.P., "Trends in High Temperature Materials Technology for Advanced Aircraft Turbine Engines," SAE Paper 751050, SAE, (1975)
7. McLean, A.F. & Baker, R.R., "Brittle Materials Design, High Temperature Gas Turbine", Interim Report 12, AMMRC TR-78-14, March 1978
8. Metcalfe, A.G., Chap 35 in Reference 3, PP 739-747
9. Wallace, E.B. & Harper, J.E., "Ceramic Gas Turbine Engine Demonstration Program," Interim Report #13, Air research report #76-212188(13) (May 1979)
10. Janovicz, M.A., Rockwood, F.A. & Helms, H.E., "Ceramic Applications in Turbine Engines," DDA ZDR 9722 (1979)
11. Dukes, W.H., "Handbook of Brittle Materials Design Technology," AGARDograph #152, North Atlantic Treaty Organization, Feb. 1971, P. 5
12. Nichollis, P.F. & Paluszny, A., Chap. 3 in Reference 3, PP 63-78
13. Jeryan, R.A., Reference 4, Chap. w, P 35-51
14. Brooks A. & Bellin A., "Benefits of Ceramics to Aircraft Gas Turbines," These proceedings
15. Napier, J.C. & Arnold, J.P., "Development of Ceramic Nozzle Sections for Small Radial Gas Turbines," These proceedings
16. Peschel, W.H., Siebmans, W. & Trappmann, K., Chap. 26 in Reference 4, PP 481-502
17. Wallace, E.B., Stone, A.J. & Nelson, N.R., Chap. 34 in Reference 4, PP 593-624
18. Tree, D.J. & Kington, H.C., in "Proceedings of the 1977 DARPA/NAUSEA Ceramic Gas Turbine Demonstration Engine Review," MCIC-78-36, PP 41-76
19. "Ceramic Components for Turbine Engines," 5th Interim Report, Contract F 33615-77-C-5171, Air Research, June 5, 1979
20. Bersch, C.F., "Ceramics in Rolling Element Bearings," These Proceedings
21. Vasilos, T., "Densification of Nitrides by Hot Pressing", Nitrogen Ceramics, Noordhoff, Leydon, P. 367 (1977)
22. Larker, H., Adlerborn, J., Bohman, H., "Fabricating of Dense Si_3N_4 Parts by Hot Isostatic Pressing", SAE Paper 770-35, March 1977.
23. Larker, H.T., "HIP Silicon Nitride", These Proceedings.
24. McLean, A.F., Gorum, A.E., Lenoe, E.M., and Katz, R.N., "Status of Vehicular Turbine Engine Ceramics," Proceedings of the 3rd Conference on Gas Turbines in a Marine Environment, U. Bath (1976).
25. Gazza, G.E., Knoch, H., Quinn, G.D., "Hot Pressed Si_3N_4 with Improved Thermal Stability", Am. Ceram. Soc. Bulletin 57, [11], (1978) pp. 1059-60.
26. Komsya, K., Tsuge, A., Hashimoto, H., Kubo, T., and Ochiai, T., "Silicon Nitride Ceramics for Gas Turbine Engines" Gas Turbine Society of Japan, Paper No. 65, Tokyo Joint Gas Turbine Conference, May 1977.
27. See Chapters 1, 11 and 15 in Reference 4.
28. McLean, A.F., and Fisher, E.A., "Brittle Materials Design, High Temperature Gas Turbine", AMMRC CTR 77-20, August 1977, P. 45.
29. Chapter 28 in Reference 4, pp. 515-526.
30. Larson, C., Bortz, S.A., Ruh, R. and Tallan, N.M., Chapter 36 in Reference 4, pp. 65-668.

31. McLean, A.F., Chapter 1 in Reference 4, pp. 1-34.
32. Messier, D.R., and Wong, P., Chapter 8 in Reference 3, pp. 181-194.
33. Wong, P., and Messier, D.R., "Procedure for Fabrication of Si_3N_4 by Rate Controlled Reaction Sintering", Am. Ceram. Soc. Bulletin 57 [5], 1978, p. 525-6.
34. Terwilliger, G.R., and Lange, F.F., "Pressureless Sintering of Si_3N_4 ", J. Mat. Sci. 10 [7], 1975, p. 1169-1174.
35. Gazza, G., Chapter 53 in Reference 4, pp. 1001-1010.
36. Giachello, A., Popper, P., "Post Sintering of Reaction Bonded Si_3N_4 " Proceedings of 4th CIMTEC, to be Published.
37. Arrol, W.J., Chapter 34 in Reference 3, pp. 729-738.
38. Lumby, R.J., North, B., and Taylor, A.J., Chapter 46 in Reference 4, pp. 893-906.
39. Jack, K.H., Chapter 14 in Reference 3, pp. 265-286.
40. Rea, A.W.J.M., Thompson, D.P., and Jack, K.H., Chapter 56 in Reference 4, pp. 1039-1068.
41. Jack, K.H., "SiAlONs and Related Nitrogen Ceramics", J. Mat. Sci. 11 (1976), pp. 1135-1158.
42. Lange, F.F. and Iskoe, J.L. Chapter 11 in Reference 3, pp. 223-238.
43. Alliegro, R.A., Chapter 13 in Reference 3, pp. 253-264.
44. Whalen, T.J., Noakes, J.E., Turner, L.L., Chapter 9 in Reference 4, pp. 179-193.
45. Prochazka, S., Chapter 12 in Reference 3, pp. 239-252.
46. Coppola, J.A., and McMurtry, C.H., "Substitution of Ceramics for Ductile Materials in Design", presented at National Symposium on Ceramics in the Service of Man, 7 June 1976, Carnegie Institution, Washington D.C.
47. Hillig, W.B., Chapter 52 in Reference 4, pp. 989-1000.
48. Quinn, G.D., unpublished research.
49. Engdahl, R.E., "Progress Toward Ceramic Turbine Rotors by CVD", in Reference 5.
50. Baratta, F.I., Driscoll, G.W., and Katz, R.N., "The Use of Fracture Mechanics and Fractography to Define Surface Finish Requirements for Si_3N_4 " chap. 21 in ref. 3.
51. Katz, R.N., Lenoe, E.M., and Quinn, G.D. "Durability Testing of Structural Ceramics", Proceedings of the Thirteenth Highway Vehicle Systems Contractors Coordination Meeting, DOE CONF-771037, March 1978, p. 208-223.
52. Benn, K.W., and Carruthers, W.D., "3500 Hour Durability Testing of Commercial Ceramic Materials", 5th Interim Report on Contract DEN 3-27, June 15, 1979.
53. Siebels, J.E., "Oxidation and Strength of Silicon Nitride and Silicon Carbide", Presented at the 6th Army Technology Conference: "Ceramics for High Performance Applications-III", Orcas Island, WA, July 1979 (to be published).
54. Katz, R.N., and Gazza, G.E. "Grain Boundary Engineering and Control in Nitrogen Ceramics", Nitrogen Ceramics, Noordhoff, Leyden, 1977, p. 417-431.
55. Katz, R.N., and Gazza, G.E. "Grain Boundary Engineering in Non-Oxide Ceramics" in Processing of Crystalline Ceramics, H. Palmour, R.F. Davis, and T.M. Hare, ed., Plenum Publishing Co, New York, 1978, p. 547-560.
56. Komeya, K., Presentation at the 6th Army Technology Conference: "Ceramics for High Performance Applications-III", Orcas Island, WA, July 1979 (to be published).
57. Phoenix, R., Presentation at the 6th Army Technology Conference: "Ceramics for High Performance Applications-III", Orcas Island, WA, July 1979 (to be published).

ACKNOWLEDGMENTS

The authors wish to acknowledge the helpful discussions and inputs, with and from numerous colleagues, in particular we wish to thank; Dr. John Accurio, AMRL-Lewis, Drs. A. Brooks and I. Bellin, G.I., Lynn, MA, and Dr. D. R. Messier, G. E. Gazza, and G. D. Quinn of AMMRC.

REQUIREMENTS FOR MATERIALS FOR LAND VEHICLE GAS TURBINES

D F MOSS, BA Hon Cantab
Head of Engineering Analysis
Noel Penny Turbines Ltd, Siskin Drive, Toll Bar End, Coventry CV3 4FE, England.

SUMMARY

The gas turbine has many virtues as a power plant for land-vehicles, including low maintenance cost, low noise, vibration and emissions and good "driveability". Estimates of production costs indicate that the turbine need be no more expensive in first cost than reciprocating engines. To be competitive, the gas turbine needs only to demonstrate low fuel consumption. This can be achieved by the use of high working temperatures and an effective heat exchanger. Low cost materials are therefore being developed for operation at high temperatures and which can be fabricated into the complex components used in gas turbines. After a review of the requirements and duty cycles of gas turbines for land vehicles, the material requirements for each of the major components are discussed.

1 INTRODUCTION

The gas turbine has many virtues as a power-plant for land-vehicles, including low maintenance cost, low noise, vibration and emissions and good "driveability". Estimates of production costs indicate that the turbine need be no more expensive in first cost than reciprocating engines. To be competitive, the gas turbine needs only to demonstrate low fuel consumption similar to that of the Diesel engine. By discussing the requirements for land-vehicle power-plants, it will be shown how engine concepts and working cycles are being developed, and how improvements in materials will contribute to making the gas turbine a major competitor in this field.

2 REQUIREMENTS FOR LAND-VEHICLE POWER-PLANT

The requirements for a land-vehicle power-plant are as follows, with relative importance in various applications as shown in figure 7:-

- Low fuel consumption
- Low maintenance cost
- High reliability
- Good driveability (response)
- Multi-fuel capability
- Low first cost
- Low weight
- Small bulk
- Low noise and vibration
- Compliance of emissions with legal restrictions

The main types of vehicle under consideration are cars, long distance trucks, earth-moving vehicles and fighting vehicles. The above order of importance varies slightly according to vehicle type - for trucks and earth-moving vehicles running costs are paramount, ie low fuel consumption, low maintenance cost and high reliability (minimum down-time). For fighting-vehicles, response and low overall weight are important and low fuel consumption is required to reduce fuel weight. For cars, the priorities are a more complex mixture, but low fuel consumption at part-load and idle is essential. Figures 1 to 3 show breakdowns of time spent at various power-levels for different types of vehicle and show that good part-load fuel consumption is a requirement common to all types of land-vehicle.

3 THERMODYNAMIC CYCLE

The working cycle which has been evolved to meet the above requirements is that of a low-pressure ratio with heat exchanger. The heat exchanger is necessary to give good part-load fuel consumption - gas turbines without heat exchangers can give competitive full-load specific fuel consumption (sfc) at high pressure ratios (around 20:1), but are very poor at part-load. With the heat-exchanger, the variation of sfc with load is much flatter, like that of the Diesel engine, and there is the additional advantage that the optimum is achieved at low pressure ratios - around 4 to 8.

The main performance parameters affecting the identified priorities are:-

- Combustion temperature, usually referred to as turbine entry temperature or TET.
- Cycle pressure ratio.
- Heat exchanger effectiveness, ie proportion of exhaust heat recovered.
- Compressor and turbine aerodynamic efficiencies.
- Miscellaneous losses - mechanical loss, duct pressure loss, mass flow losses both intentional (cooling flows) and unintentional (leaks).

The above parameters all affect specific fuel consumption and also specific power, the amount of power per unit mass flow of air through the engine. If specific power is increased, engine size, and hence weight, can be reduced for the same output power. Component efficiencies are influenced by the characteristics of the material used, as will be discussed later. Here it is assumed that they are maximised and losses are minimised. Figure 4 shows the effect of the major cycle parameters - TET, pressure ratio and heat exchanger effectiveness - upon specific fuel consumption and specific power. It illustrates the importance of using the highest TET and heat exchanger effectiveness possible, and also of selecting the optimum pressure ratio. Material properties are the main obstacle to raising temperatures and achieving reliable low-cost heat exchangers. The incidence of optimum pressure ratio at a value which can be attained by single stages of compressor and turbine is crucial in making the gas turbine feasible for automotive use, as the construction is greatly simplified and production cost reduced.

Current specific fuel consumption of Diesel engines is around 0.21 to 0.24 kg/kWh (0.35 to 0.40 lb/hph) and may be expected to reduce within a few years to 0.18 or 0.21 kg/kWh (0.30 to 0.35 lb/hph). In order to be competitive, the gas turbine must achieve an sfc below 0.20 kg/kWh (0.33 lb/hph) and a specific power approaching 250 kW/kg (150 hps/lb). Figure 4 shows that the gas turbine begins to be competitive at a TET of 1350K and a heat exchanger effectiveness of 0.85. This is feasible in a metal engine with current technology, but reliability must be proved. Curves are also shown for a TET of 1450K, probably the limit for a metallic engine of the simplicity required for land-vehicle use - and for the turbine entry temperatures of 1550K and 1650K likely to be achieved by first and second generation ceramic engines.

4 ENGINE CONCEPT

Within the cycle considerations outlined above, two engine concepts have evolved. Most development engines built to date have been based upon the two shaft, free power turbine engine (Figure 5). The free power turbine with variable incidence vanes is necessary to give flexibility of operation (not least the availability of high torque at low output speed). The variable vanes also allow the TET to remain high at part-load, which is necessary for good part-load fuel consumption.

The single-shaft engine (Figure 6) has currently been revived as the constantly-variable transmission has come within reach, together with the micro-processor to provide the necessary programming. This engine has fewer components in concept than the two-shaft engine and is basically simpler. However, variable compressor geometry as well as variable turbine geometry will be necessary to give good part-load fuel consumption. This together with the complicated transmission would tend to rule it out. However, a single radial turbine could be used in the place of the two turbine stages of the two-shaft engine. Detailed stress analysis by Arnold (ref 1) has indicated that this could allow a significant increase in TET without increased metal temperatures. This makes the single-shaft engine very attractive.

Table 1 lists the components of an automotive gas turbine engine and compares the two types of engine.

Looking further ahead, a futuristic concept for which Noel Penny Turbines Ltd has commissioned performance studies, is a twin-spool gas turbine of high pressure-ratio (30:1). This would have specific fuel consumption comparable to the best of the low-pressure engines presented above, and higher specific power. The concept requires a simple variable transmission and a variable-throughput heat exchanger programmed to achieve optimum economy from idle to maximum power. The engine would be a small sealed-for-life unit which would fit in a suitcase. The turbomachinery required would be very small. Noel Penny Turbines has tested a compressor of diameter 26 mm and a turbine of diameter 12 mm, although not in connection with this engine. The turbine in particular is ideal for construction in ceramic.

5 DUTY CYCLES

In selection of power-plant materials, it is very important to consider the vehicle duty cycle. For all land-vehicles, the duty cycles are very arduous, as is shown by the low-cycle fatigue and creep lives demanded of the rotating and hot components. Table 2 compares duty cycles of cars with that of trucks and earth-moving vehicles. This shows the major factors affecting the life of the main components - thermal shock, low-cycle fatigue and creep. Thermal shock is experienced at every cold start. Thermal gradients of several hundred degrees are experienced in combustor, turbine rotors and structures, and heat exchanger, leading to very high thermal stresses. This is a complex phenomenon involving aspects of creep and fatigue, and can only be evaluated by engine running.

Low-cycle fatigue results from cycling of stress with time, usually in gas turbines associated with changes in shaft speed. Table 2 indicates that the low-cycle fatigue life required for components will be of the order of 500,000 cycles, which is an order of magnitude larger than for aero-engines. Also, a much higher proportion of the time is spent at peak rating, especially in truck engines, than in aero-engines, where the peak rating is used only about 1% of the time. This means that design creep lives in automotive gas turbines must be much longer than in aircraft gas turbines.

6 GENERAL MATERIAL REQUIREMENTS

Careful material selection is one way in which the designer guards against failure in service. The objective in developing advanced materials is to allow components to operate in more arduous conditions without prejudicing reliability. Typical failure modes in engines are as follows:-

- Fracture due to gross overload.
- Yielding due to gross overload.
- Fracture due to creep.

Fracture due to low-cycle fatigue (including thermal fatigue).

Elastic instability (buckling).

Vibration - leading to engine roughness or fracture due to high-cycle fatigue.

Excessive deflection, leading to mal-function.

Fracture under impact.

Corrosion.

Abrasion.

Apart from strength and failure considerations, there are many other design considerations, of which one of the most important is the ability to form the required shape. This is important in gas turbines as high performance blading requires complex shapes with thin sections. A full list of design considerations is given in Table 3.

A further important consideration in choosing a material is the amount and consistency of data available as to its properties. A well-documented material is often chosen in preference to a material with higher strength but less documentation, in order to minimise development risk. Similarly, a reduction of scatter in, say, fatigue strength, would permit a higher design strength without changing the nominal strength of the material, as minimum properties are always used in design calculations. Stress-levels are commonly chosen to achieve a 99.9% probability of survival of the design life. In metals this usually implies a safety factor of 4 in fatigue life and 8 in creep life. A requisite of any replacement material is that it should be consistent enough to allow some practical determination of life before entry into service.

7 DETAILED REQUIREMENTS OF COMPONENTS

7.1 Compressor

The performance requirements of the compressor are to achieve the optimum pressure ratio for the chosen TET with high efficiency and a broad flow range at part-load to enable the TET to be kept high at that condition. Depending upon the chosen cycle, the required pressure ratio is likely to be in the range 1 to 8. In order to achieve high efficiency and broad range, thin blading with sweep-back must be used. As sweep-back is introduced, rim speed and hence stress is increased. The material to be used must therefore be capable of developing high specific strength in thick sections and the ability to be formed (or machined) into complex thin sections. As blade thicknesses are determined by manufacturing capability and not stress limits (although vibratory stress can lead to failure in high-cycle fatigue), there is considerable advantage in using the lightest material with sufficient strength, rather than the one with highest strength-density ratio. Although weight-saving in relation to the whole engine is small, it is vitally important to minimise the polar moment of inertia of the compressor shaft as this is the main factor governing response times. Design stresses in automotive compressors must be kept much lower than in other gas turbines because of the large number of major cycles (changes in steady stress-level) required.

Current material capability is as follows:-

Aluminium alloy	-	used up to 5.5 pressure ratio.
Steel	-	could be used to achieve pressure ratio of 7 - disadvantage is high density, hence high inertia.
Titanium alloy	-	could be used at pressure ratios up to 8 - disadvantages are cost and poor abrasion resistance leading to complex and costly shaft fixing arrangement.

7.2 Turbine Nozzle Vanes

The turbine nozzle vanes are generally the hottest part of the engine, but are not so highly-stressed as the rotor blades. The only imposed stresses are in bending due to gas loads, and these are in absolute terms low. However, there is likely to be an overall variation (maximum to minimum) in temperature around the annulus of at least 30% of the combustor temperature rise. The temperature of the hottest vane is therefore likely to be 70 - 100K higher than the nominal TET and at such temperatures the creep strength of even the best cast nickel alloys is such that gas bending stresses become significant. Another factor is that oxidation of nickel alloys starts to occur above 1350K. In order to minimise cost, it is desirable to use vanes without coatings or cooling. Such vanes are likely to be limited to a maximum temperature of 1400K, in turn limiting the engine to a TET of at most 1350K (see Figure 4 for effects of performance).

With coatings to reduce oxidation and small amounts of cooling, which can be introduced simply, turbine entry temperatures of 1450K could be achieved in a metal engine. Beyond that temperature, ceramics would be introduced. Their major virtues are good strength at high temperature, excellent oxidation resistance, low density, low raw material cost and low coefficient of expansion. Problems yet to be overcome are the development of proven designs incorporating low elasticity materials capable of reliable long-life operation over a wide range of temperature (including sub-zero), and wide scatter of properties. However, these are far less serious in the turbine nozzle vanes than in the rotor and consideration is being given to the use of ceramic vanes with metallic rotors in engines up to 1450K. Such an engine would be competitive with advanced Diesel engines, as discussed in section 3 in relation to Figure 4.

Further gains will be achieved when ceramic rotors can be introduced - figure 4 also shows engines with turbine entry temperatures of 1550K and 1650K, as are currently being proposed. This is further discussed in the next section.

7.3 Turbine Rotors

Turbine rotors are subject to conflicting requirements - high creep and oxidation resistance in the blades and high fatigue strength in the rotor. In general, creep strength is associated with large grain size and fatigue strength with very small grain size. Cast alloys have been developed to maximise the former, and in the latter case forging alloys. In large gas turbines, the solution is to use different materials for blades and disc. In small engines, the cost of root fixings is prohibitive and generally the solution has been to cast the disc integrally with the blades and restrict the rim speed of the disc so that bore stresses are not too high for the cast material. As TET is raised, restrictions from nozzle temperature being removed as discussed in section 7.2, the turbine rotor becomes the next limiting consideration. The ways around this are to:-

- a) Cool the rotor blades - too expensive for automotive engines.
- b) Use a radial turbine - this has the characteristic that the highest blade stress and the highest metal temperature do not coincide as closely as in the axial turbine and hence higher TET can be used. This effect is much more marked at the expansion ratio of 5 or 6:1 of the single-shaft engine than at the expansion ratio of 2:1 typical of each turbine stage in the two-shaft engine.
- c) Form the turbine by one of the powder-metallurgy/hot isostatic pressing methods. This appears to offer better blend of properties than the integrally-cast rotor and it is considered that in combination with (b), a TET of 1450K could be achieved with a single-shaft engine.
- d) Use a ceramic turbine. Subject to the problems noted in section 7.2, turbine entry temperatures of 1550 - 1650K are possible. Turbine blading is likely to be shorter and thicker than in metal turbines, where there is continual effort to reduce trailing-edge thickness. Ceramic blading will therefore tend to increase the aerodynamic loss.

7.4 Turbine Rotor Shroud

The gap between the tip of the rotor blade and its casing (shroud) is very difficult to control on the first stage. This leads to a large aerodynamic loss which could be eliminated if a suitable material with low coefficient of expansion could be used for the shroud. The shroud is often made integral with the nozzle set, and in any case requires high thermal shock resistance in its own right. The combination of high temperature capability with low expansion coefficient seems elusive in metallic materials and is an advantage of ceramics.

7.5 Combustor

The flame within the combustor is stabilised by the creation of a toroidal vortex around the burner. On leaving the recirculation zone, in which only a small amount of heat exchanger delivery air is used, the gas temperature is typically 1800K, so much of the air flow must be used for wall cooling. This greatly reduces the amount of air available for dilution, in which the air not used in the recirculation zone is mixed with the burnt products to ensure complete combustion and minimise the temperature variation at exit. Complete combustion is important in heat exchange engines, not only for performance reasons but also to prevent heat exchanger fouling. If the temperature variation at combustor exit is reduced so is the peak metal temperature, and a higher TET can be used. There is therefore considerable advantage in allowing combustor wall temperatures to rise, thus reducing the amount of cooling air used. The main obstacles to this are oxidation and thermal stress. The latter is caused by variations in temperature along the wall of the combustor, in which one factor is cool areas around air admission holes, and (much less important in metallic combustors), through-thickness temperature gradients. Ceramic combustors are highly likely to be used to overcome these problems and these may well use laminated construction to combat wall-cracking.

7.6 Heat Exchangers

Heat exchangers used in automotive engine development have been of two types, the ceramic rotating regenerator and the metallic counter-flow recuperator. The former has been highly favoured by virtue of its small bulk, and intensive research has been conducted to overcome its basic problems, namely leakage and lack of reliability. It consists of a rotating disc typically 60 mm deep and up to 700 mm in diameter, and composed of a honeycomb of triangular passages roughly parallel to the axis of rotation. Typical matrix dimensions are 0.5 mm (height) by 0.45 mm (base) with 0.1 mm wall thickness. The disc rotates at about 20 rev/min such that exhaust gas and compressor delivery air pass alternately through the same passage, transferring heat to and from the walls and thus from exhaust to combustor inlet air. As the two air streams pass through in opposite directions, one face of the disc is maintained at 1050K and the other at 500K (figures are given for an engine with a TET of 1350K). The rim is usually at the temperature of the cool side. The wall temperature of the passages fluctuates by 50K in each cycle of the disc. With such a complex temperature system, considerable thermal stress is set up. Stresses may be minimised by use of a low coefficient of expansion and calculations have indicated that a suitable value is about 0.5×10^{-6} per K.

Further requirements are:-

- a) Resistance to attack by sulphuric acid, which arises from sulphur in the fuel and condenses in the regenerator, and to attack from salt in the air.
- b) Low thermal conductivity to prevent heat flow through the disc thickness, which would reduce the thermal efficiency of the heat exchanger.
- c) High specific heat
- d) Low wall thicknesses - reduction to 0.05 mm would significantly benefit thermal ratio..

Recuperators are generally constructed from stainless steel. The most effective type consists of a counter-flow core composed of a stack of plates with convoluted fins, with a cross-flow entry system. As in the regenerator, there is a complex thermal stress system, particularly severe at cold start. A major problem is thermal shock at the attachment of the matrix to the leading-edge bars facing the exhaust stream - it is difficult to provide a strong location for the matrix without creating a large difference in thermal inertia between the supporting structure and the thin plates of the matrix. The matrix must also be capable of supporting the pressure difference of five atmospheres between the channels carrying the two streams of gas. Metal temperatures in the recuperator are higher at part-load than at full-load as a consequence of the need to keep TET high for good part load fuel consumption. The use of stainless steel is therefore ruled out as turbine entry temperatures go above 1350K, nickel alloy or ceramic being used instead. Ability to be formed into complex shapes with a sheet thickness of 0.1 mm or less is essential.

8 CONCLUSIONS

With its air-rich continuous combustion providing low exhaust pollution and simple silencing, coupled with the absence of reciprocating masses and vibration, the gas turbine has major virtues as a land-vehicle power plant. It needs only to demonstrate overall fuel economy comparable with advanced reciprocating engines to gain worldwide acceptance for volume production.

Two engine concepts are currently feasible, single-shaft and two-shaft (free power turbine), both with heat exchanger. Whichever is chosen, the solution will require materials capable of operating at high temperature for a very long and arduous life. Only in this way will high turbine entry temperatures and effective and reliable heat exchangers be available. As important is the ability to create complex shapes in thin sections, for high performance turbo-machinery and heat-exchangers. Competitive engines can be made by use of cast nickel super-alloys and hot isostatically-pressed nickel super-alloys offer further increase in temperature. Ceramics are likely to be considered increasingly in such engines because of their high temperature capability, as their other limitations are overcome.

REFERENCES

- 1) D J Arnold and O E Balje "High Temperature Potential of Radial Turbines" ASME 77-GT-46.
- 2) "Advanced Developments in Turbomachinery for Use in Small RPV Engines" by R W Chevis, Noel Penny Turbines Limited, International Conference on RPV's, University of Bristol, September 1979
- 3) "Future Turbine Wheel Design" by Noel Penny, SAE Panel Session on Manufacture and Durability of Turbine Blades and Wheels, January 1968
- 4) "The Development of the Glass Ceramic Regenerator for the Rover 25/170 R Engine" by Noel Penny, SAE 660301, 1966
- 5) "The Classification of Gas Turbine and Piston Engines for Competition Purposes" by Noel Penny and Peter Spear, SAE January 1965
- 6) "Regenerators for High Temperature Gas Turbine Engines" by Noel Penny, Institution of Mechanical Engineers Proc. I Mech.E, 1968-69, 183 Pt.3.N.

ACKNOWLEDGEMENT

The author wishes to thank the Directors of Noel Penny Turbines Limited for permission to publish the paper.

TABLE 1 - COMPARISON OF COMPONENTS OF SINGLE-SHAFT AND TWO-SHAFT ENGINES

COMPONENT	SINGLE-SHAFT ENGINE	TWO-SHAFT ENGINE
Compressor	Single-stage centrifugal with variable inlet vanes	Single-stage centrifugal (fixed geometry)
Combustor	Single tubular can	Single tubular can
Turbine	Single radial or two stage axial - probably variable vanes	Single stage turbine driving compressor (axial or radial). Single stage axial power turbine with variable vanes
Heat Exchanger	Regenerator or recuperator	Regenerator or recuperator
Transmission	Constantly variable	Conventional single or two-stage reduction (dependent upon shaft speeds)
Control System	Electronic: controls fuel supply, variable compressor and turbine vanes and transmission	Electronic: controls fuel supply and power turbine vanes

Other components common to both engines but having material limitations are:-

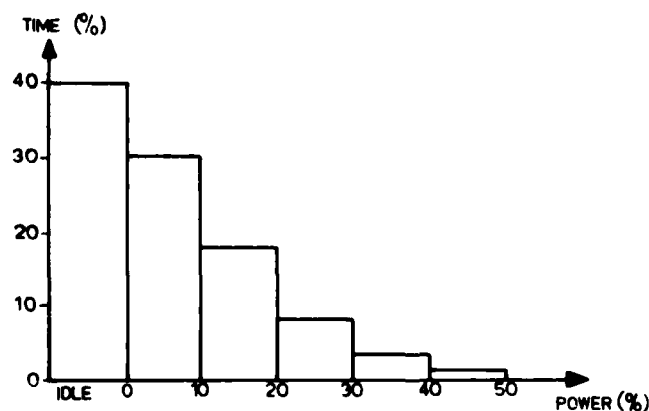
Casings and structure
 Rotor Containment Rings
 Mountings
 Gears
 Bearings - rolling element, plain (oil-lubricated) or gas
 Shafts
 Insulation
 Bolts and Fasteners.

TABLE 2 - DUTY CYCLES OF LAND VEHICLES

	CARS	TRUCKS/EARTH-MOVING VEHICLES
Design Life (hours)	3,000	10,000
Number of cold starts per hour	4	0.25
Number of cycles per hour (idle to full load)	50	50
Time spent at full load (%)	10	80
Required thermal shock life (cycles)	12,000	2,500
Required low-cycle fatigue life (cycles)	150,000	500,000
Required creep life at full-load condition (hours)	300	8,000

TABLE 3 - GENERAL CRITERIA FOR MATERIAL SELECTION

Material Characteristic	Components Affected
High tensile strength	Rotors, gears, bearings, some structures
High fatigue strength (with low notch sensitivity)	As above
High temperature capability (creep and oxidation resistance)	Combustor, turbine rotor blades and vanes, hot ducts
Low density	Important in rotors to keep inertia (response-times) low
Stiffness	Casings - to keep deflections low and maintain clearances
Expansion coefficient	Shrouds, casings, bolts, heat exchangers
Hardness and abrasion resistance	Gears, bearings - any fretting surfaces
Impact resistance	Blades (foreign object damage), rotor containment rings, transmission, mountings
Formability - low processing cost	All components, but especially bladed components with complex thin sections
Machineability	As above
Weldability	Structural components
Resistance to chemical attack & corrosion	Hot components; most components in marine environment; some materials subject to attack by oil additives, etc
Low raw material cost & plentiful non-strategic supply	Especially affects hot components and rotors
Permeability	Heat exchanger matrix
Thermal conductivity	Insulation

FIG. 1. POWER USAGE - CAR ENGINE
(U.S. URBAN DRIVING CYCLE)

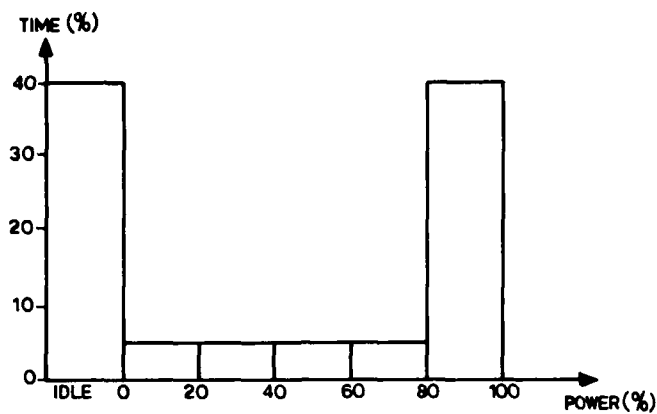


FIG. 2. POWER USAGE - EARTH MOVING VEHICLE

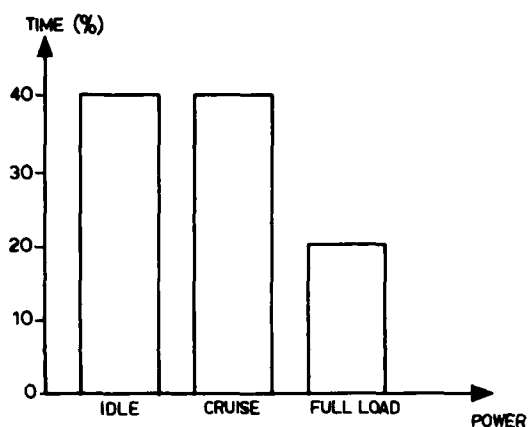
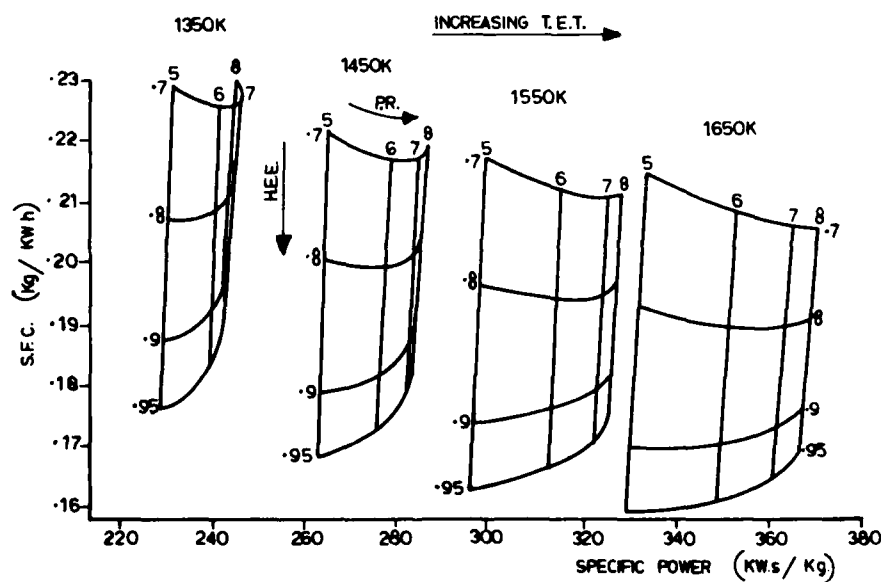


FIG. 3. POWER USAGE - FIGHTING VEHICLE.

FIG. 4. TRUCK ENGINE DESIGN POINT PERFORMANCE AGAINST
T.E.T., PRESSURE RATIO (PR), HEAT EXCHANGER EFFECTIVENESS (H.E.E.)

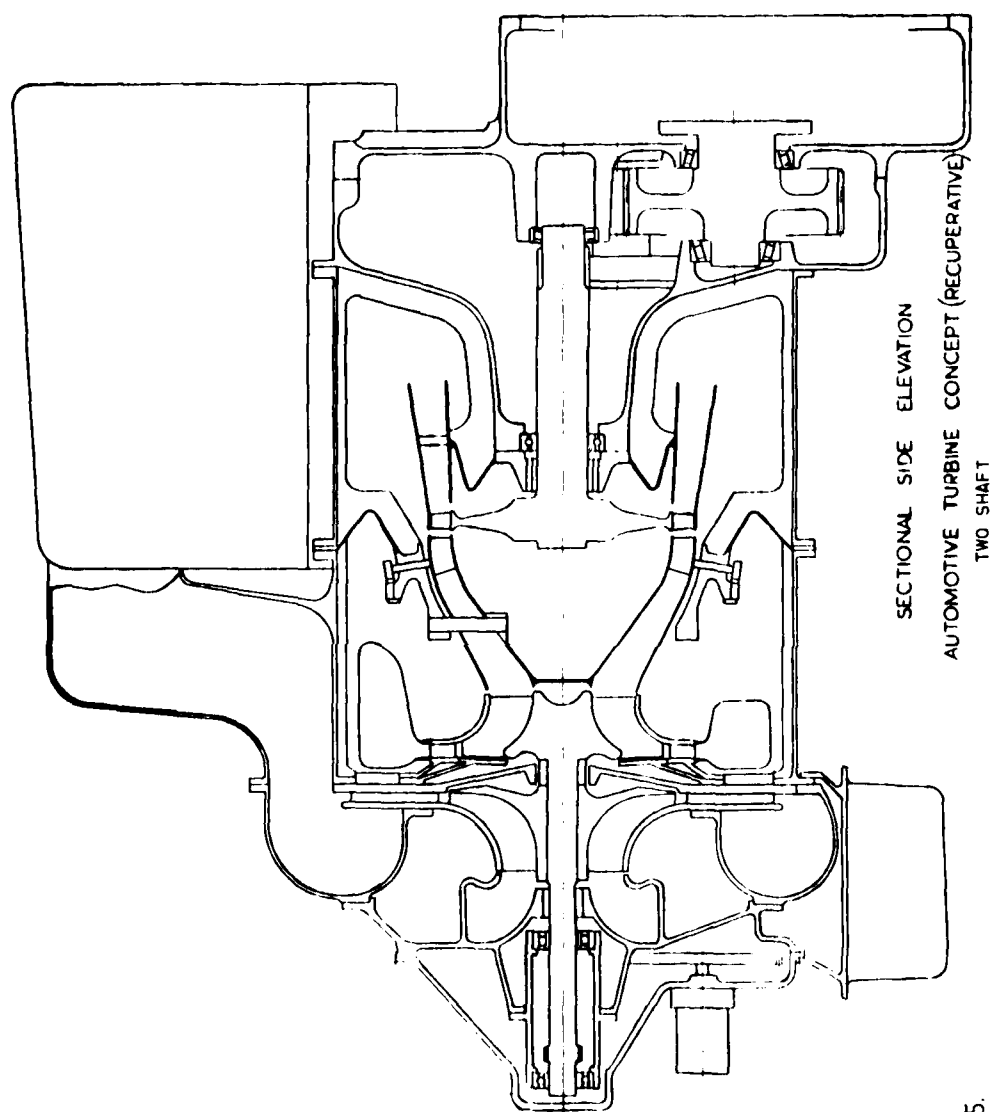
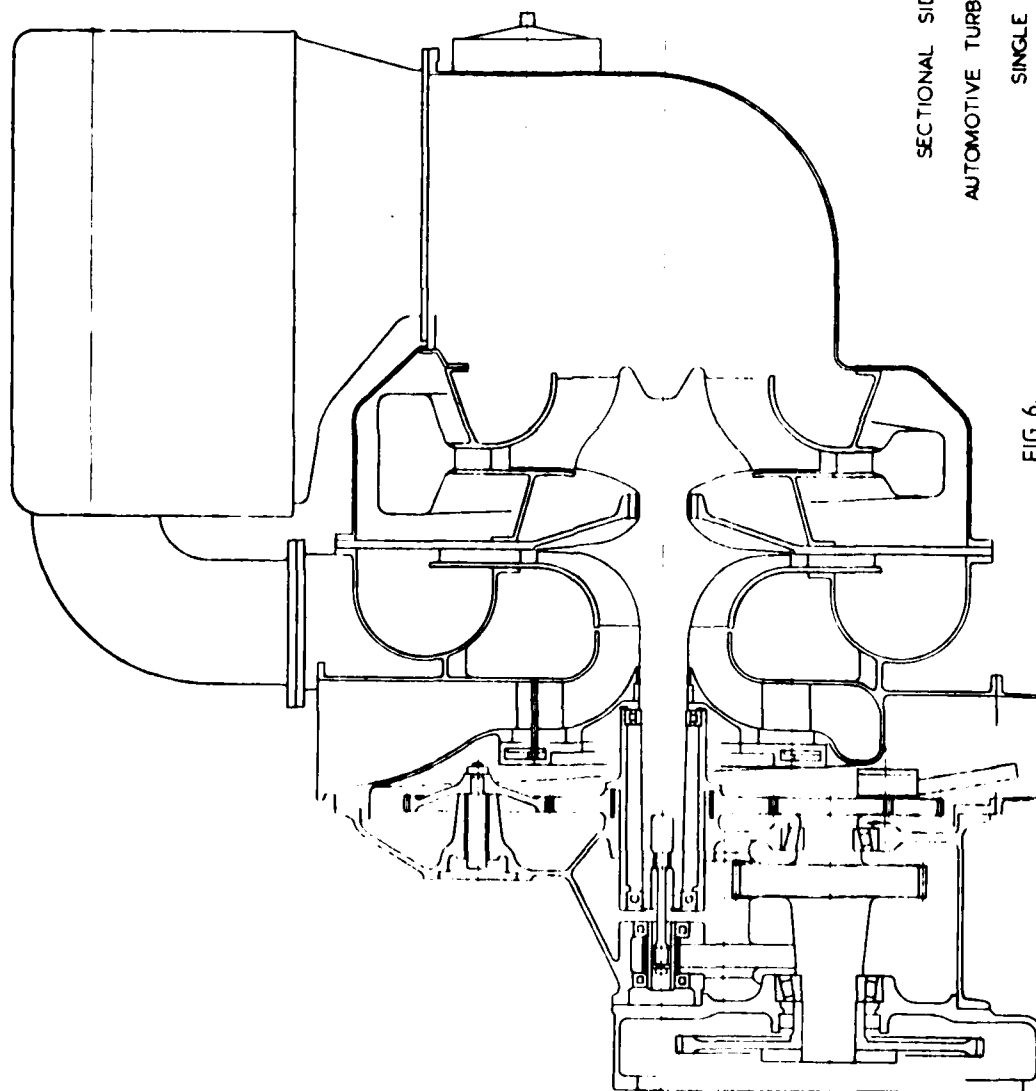


FIG 5.



SECTIONAL SIDE ELEVATION
AUTOMOTIVE TURBINE CONCEPT (RECUPERATIVE)
SINGLE SHAFT

FIG. 6.

PARAMETER APPLICATION	LOW FIRST COST	LOW MAINTENANCE COST	HIGH RELIABILITY	HIGH AVAILABILITY	LONG LIFE	FUEL ECONOMY	MULTIFUEL CAPABILITY	HIGH POWER/WT	HIGH POWER/BULK	LOW NOISE	LOW VIBRATION	CLEAN EXHAUST	INFRA-RED RADIATION
Passenger Cars	1	3	3	3	3	2	4	2	2	2	2	2	5
Trucks & Buses	2	2	2	2	3	2	4	2	2	2	2	2	5
Off-Highway	3	2	3	1	3	3	4	3	3	3	3	3	5
Military Roles	4	3	1	1	3	3	1	2	2	2	3	2	2
Rail Traction	3	2	3	1	3	3	4	4	4	2	3	3	5

KEY: 1 - EXTREME
 2 - HIGH
 3 - AVERAGE
 4 - LOW
 5 - INSIGNIFICANT

FIGURE 7: RELATIVE IMPORTANCE OF OPERATING PARAMETERS

TECHNOLOGIES CONCUES POUR L'UTILISATION DES CÉRAMIQUES DANS LES TURBORÉACTEURS

par Serge BOUDIGUES
Office National d'Etudes et de Recherches Aéronautiques (ONERA)
92320 Châtillon (France)

et Georges FRATACCI
Direction des Recherches, Etudes et Techniques (DRET)
75015 Paris (France)

Les céramiques se distinguent des matériaux réfractaires utilisés dans les parties chaudes des turboréacteurs par :

- une possibilité d'utilisation à plus haute température,
- une masse volumique trois fois plus faible,
- une meilleure tenue en compression qu'en traction.

Nous avons abordé les problèmes posés par l'introduction des céramiques dans les moteurs d'avions par deux voies :

- 1° - adaptation des formules technologiques utilisées avec les métaux,
- 2° - conception d'une aérodynamique et d'une technologie de turbine pensée en fonction du matériau céramique.

Après une justification aérothermique des formules contrarotatives adoptées, l'exposé présente diverses formules de turbines intégrées dans un moteur complet.

Pour ce cas particulier on précise, pour les aubes, les charges aérodynamiques, la température, les contraintes, la fabrication en grappes, la fixation sur l'alésage du disque... et, pour les disques, le niveau des contraintes, la possibilité de frettage par fibres et l'isolation thermique.

Quelques idées sur l'adaptation aux céramiques des formules classiques sont présentées sur des coupes de moteurs complets avec, en particulier, une technologie diminuant les pertes de charge en amont et en aval d'un échangeur en céramique.

TECHNOLOGIES FOR USE OF CERAMICS IN TURBOENGINES

Ceramics differ from refractory metallic alloys used in hot parts of turboengines by :

- a possibility of operation at a higher temperature,
- a density three times lower,
- a better resistance in compression than in tension.

We approached the problems raised by the introduction of ceramics in aeroengines from two sides :

- i) - adaptation of technological solutions used for metals,
- ii) - concept of aerodynamics and turbine technology adapted to ceramic materials.

After an aerothermics justification of the contrarotative solutions proposed, the paper presents several formulas of turbines integrated in a complete engine.

In this particular case we determine, for the blades, the aerodynamic loads, temperature, stresses, batch fabrication, fixation on the disc circumference, etc... and, for the discs, the stress level, the possibility of fretting with fibres and the thermal insulation.

A few ideas on the adaptation to ceramics of the classical formulas are presented for section of complete engines with, in particular, a technique reducing pressure losses upstream and downstream of a ceramics heat exchanger.

1 - INTRODUCTION

Le vocable céramique recouvre une très grande variété de produits. Nous avons pris pour base un nitrure de silicium Si_3N_4 pour lequel on possède les caractéristiques suivantes :

Masse volumique (kg / m^3)	$2,5 \cdot 10^3$
Résistance à la rupture (Pa)	$215 \cdot 10^6$ (à l'ambiance)
Module d'élasticité (Pa)	$110 \cdot 10^9$
Coefficient de dilatation	$2,9 \cdot 10^{-6}$
Conductibilité thermique ($\text{W/m} \cdot ^\circ\text{K}$)	$1,7 \cdot 10^{-3}$

On sait que ce matériau travaille mieux en compression qu'en traction et qu'il garde de très bonnes caractéristiques jusqu'à 1500°C .

Il est donc tout particulièrement indiqué pour les parties chaudes des turbines à gaz et plus spécialement pour les parties tournantes (du fait de sa faible densité) surtout si on lui permet de travailler en compression.

2 - LES TURBINES CONTRAROTATIVES

Connues depuis plus de 50 ans dans les turbines à vapeur (à grilles radiales) les technologies contrarotatives n'ont pas encore été utilisées dans les turbines à gaz. Elles réclament en effet quelques précautions si l'on veut qu'elles présentent un intérêt par rapport aux formules classiques.

Nous ne considérerons que les turbines axiales.

2.1 - Formules classiques

Nous rappelons les triangles de vitesses des turbines haute pression des turbines à gaz modernes (fig. 1).

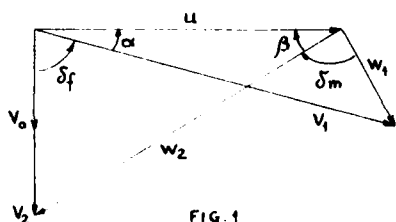


FIG. 1

- u Vitesse de rotation
- V_0 Vitesse absolue d'entrée
- V_1 Vitesse absolue de sortie
- w_1 Vitesse relative d'entrée
- w_2 Vitesse relative de sortie
- V_2 Vitesse absolue de sortie
- δ_f Déviation dans la grille fixe
- δ_m Déviation dans la grille mobile
- α Angle de sortie de la grille fixe
- β Angle de sortie de la grille mobile

Nous considérons une vitesse absolue de sortie axiale alors que, le plus souvent, il existe une faible composante tangentielle en sens inverse de la rotation. La comparaison entre les formules classiques et la formule contrarotative est plus facile quand la sortie est axiale et la faible composante tangentielle résiduelle peut être introduite dans les deux formules sans altérer la comparaison.

2.2 - Formules contrarotatives

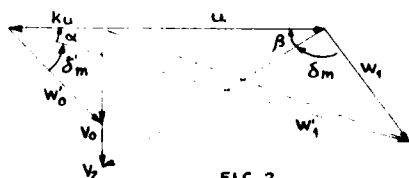


FIG. 2

2.2.1. - Formules à deux grilles mobiles

Elles consistent à faire tourner le distributeur en sens inverse de la roue mobile à la vitesse $k u$ (fig. 2).

Il n'y a pas de grille fixe ni en amont ni en aval.

- Soient :
- T la température totale en sortie de chambre
 - ΔT la chute de température totale dans les deux grilles
 - δT la différence entre T et la température totale dans la grille aval (température totale relative conditionnant le fluage de l'aube)
 - M_{w_1} nombre de Mach relatif à w_1
 - M_{V_2} nombre de Mach relatif à V_2
 - $M_u = \frac{u}{\sqrt{\gamma R T}}$
 - δ_m déviation dans la grille aval

Pour $k=0$ on retrouve la formule classique.

Nous avons tracé sur la figure 3 en fonction de M_u : (pour $\alpha = 16$, $M_{w_1} = 0,5$, $M_{v_2} = 0,5$)

$$\frac{\Delta T}{T}, \frac{\delta T}{T}, \frac{\Delta T}{\Delta T(k=0)}, \frac{\delta T}{(\delta T)_{k=0}}, \delta_m$$

On voit sur cette planche :

1°) les gains apportés sur ΔT , δT et δ_m sont sensibles déjà pour $k = 0,5$

40 % sur ΔT

55 % sur δT

10 % sur la déviation δ_m

2°) au-delà de $k = 0,5$ on gagne très peu. Il faut donc éviter de dépasser cette valeur. Pratiquement on prendra :

$$0,25 < k < 0,75$$

Pour une température de 1600°K en sortie de foyer, en faisant tourner la première grille en sens inverse et à demi vitesse on gagne $(0,22 - 0,19) 1600^\circ = 128^\circ$ sur ΔT

$$(0,158 - 0,102) 1600^\circ = 90^\circ \text{ sur } \delta T$$

Sur la figure 4 avec $\alpha = 18^\circ$ on a donc tracé pour $k = 0$ et $k = 0,5$ en fonction de M_u , $\frac{\Delta T}{T}$ pour différentes valeurs de M_{w_1} ,

On voit sur cette planche que le gain du contrarotatif n'est important que pour les valeurs de $M_{w_1} \geq 0,5$. Pour les valeurs faibles, 0,3 et 0,4 de M_{w_1} , il est même impossible de réaliser les triangles de vitesses dès que M_u dépasse 0,63 et 0,78 respectivement.

Sur la figure 5 enfin on a regardé l'influence de l'angle α .

On voit que pour $\alpha = 22$ les gains de $\frac{\Delta T}{T}$ et $\frac{\delta T}{T}$ sont très faibles quand on passe de la formule classique $k = 0$ au contrarotatif $k = 0,5$.

Au contraire le gain augmente quand α diminue ; pour $\alpha = 16^\circ$ il atteint 40 % sur ΔT

55 % sur δT

Sur cette figure nous avons fait figurer le nombre de Mach M_{w_1}' relatif à la vitesse w_1' (ou V_1 quand $k = 0$) c'est le nombre de Mach de sortie de la première grille. On voit que, pour M_{w_1} donné, (en l'occurrence 0,5) M_{w_1}' augmente quand M_u augmente et quand α diminue. Mais cette augmentation de la vitesse relative de sortie ne doit pas augmenter les pertes qui sont beaucoup plus sensibles à M_{w_1} (qui est le même pour $k = 0$ et $k = 0,5$) et à δ_m (qui est inférieur de 10° pour $k = 0,5$).

En conclusion on peut dire que le contrarotatif est très avantageux, non pas en toutes circonstances, mais dans des cas bien précisés et chiffrés sur les planches I, II et III qui expriment les formules mathématiques qu'on peut facilement établir :

$$\frac{\Delta T}{T} = (\gamma - 1)(1+k)M_u \cos \alpha \left[\frac{(1+k)M_u \cos \alpha + \sqrt{[(1+k)M_u \cos \alpha]^2 - [(1+k)^2 M_u^2 - (1 + \frac{\gamma-1}{2} k^2 M_u^2) M^2 w_1] (1 + \frac{\gamma-1}{2} M_{w_1}^2)}}{1 + \frac{\gamma-1}{2} M_{w_1}^2} - k \frac{M_u}{\cos \alpha} \right]$$

$$\frac{\delta T}{T} = \frac{\Delta T}{T} - (\gamma - 1) M_u^2$$

$$\lg \beta = \frac{M_{v_2}}{M_u} \sqrt{\frac{1 - \frac{\Delta T}{T}}{1 + \frac{\gamma-1}{2} M_{v_2}^2}}$$

$$\lg L = \lg \alpha \frac{\frac{\Delta T}{T} + (\gamma - 1) k (1+k) M_u^2}{\frac{\Delta T}{T} - (\gamma - 1)(1+k) M_u^2}$$

$$\delta = 180^\circ - (\beta + L)$$

$$M_{w_1}' = M_{w_1} \frac{\sin L}{\sin \alpha}$$

2.2.2 - Contrarotatif multigrilles

A partir de cette cellule contrarotative à deux grilles on peut généraliser la formule comme indiqué figure 6.

En prenant : $u = 400 \text{ m/s}$ ($M_u = 0,5$ pour $T = 1623^\circ\text{K}$)

$$k = 0,5$$

on donne sur cette figure les charges ΔH que l'on peut obtenir en fonction du nombre de grilles. Soulignons que le nombre de grilles influence directement la masse et le prix du moteur.

Les deux grilles de base donnent $390 \text{ K}_j/\text{kg}$

Une grille fixe placée en amont ajoute $80 \text{ K}_j/\text{kg}$

Une grille mobile placée en aval ajoute $150 \text{ K}_j/\text{kg}$

On voit qu'une troisième grille si elle est mobile est nettement plus intéressante qu'une grille fixe (et pourtant elle ne tourne qu'à 200 m/s).

Si l'on passe à 4 grilles :

par une grille fixe en amont des trois précédentes on gagne $80 \text{ K}_j/\text{kg}$

par une grille mobile en aval des trois précédentes on gagne $300 \text{ K}_j/\text{kg}$

La grille mobile, dans ce cas là, est donc beaucoup plus intéressante (car elle tourne à 400 m/s).

Si l'on passe à 5 grilles :

par rapport aux quatre grilles précédentes, on gagne $80 \text{ K}_j/\text{kg}$ par une grille fixe placée en amont,
 $150 \text{ K}_j/\text{kg}$ par une grille mobile placée en aval.

En résumé on peut obtenir :

390 K_j/kg	avec 2 grilles
540 "	avec 3 grilles
840 "	avec 4 grilles
990 "	avec 5 grilles

Or les moteurs civils les plus performants exigent aujourd'hui moins de $900 \text{ K}_j/\text{kg}$ et pour obtenir cette charge ils ont besoin de :

10 grilles pour le CFM56 (SNECMA-GE)
" pour le RB211 (R.R.) (triple corps)
12 grilles pour JT9B (PW)
" pour CF6 (GE)

Le contrarotatif divise donc par deux le nombre de grilles nécessaires.

3 - CONTRAROTATIF A TROIS GRILLES

3.1 - Aspect aérodynamique

Il est clair que les valeurs maximum des charges calculées au paragraphe 2.2.2 ne sont pas toujours utilisées, en raison du fait que la vitesse de rotation du compresseur étant la même que celle de la turbine qui l'entraîne, on est amené à des compromis.

Sur le programme $Z = 0$, $M = 0,7$ nous avons dessiné sur la figure 7 le moteur de plus simple qu'on puisse imaginer : une soufflante à un étage
 une roue centrifuge pour le compresseur HP.

Pour une ambiance $T_0 = 288^\circ\text{K}$ la température d'admission sur la soufflante est
 $T_2 = 288 \times (1 + 0,2 \cdot 0,7^2) = 316^\circ\text{K}$. Pour conserver de bons rendements on prendra dans la soufflante une variation d'enthalpie de $41 \text{ K}_j/\text{kg}$ (rapport de pression 1,44) et dans le compresseur centrifuge une variation d'enthalpie de $275 \text{ K}_j/\text{kg}$ (rapport de pression 5,55) soit un rapport global de $1,49 \times 5,55 = 8$.

Si l'on admet une température de 1500 K en sortie de foyer un taux de dilution de 4 laisse une vitesse d'éjection primaire convenable.

Avec un débit primaire de $2,9 \text{ kg/s}$ ($14,5 \text{ kg/s}$ de débit total) on obtient en croisière une poussée de 2200 Newtons avec une C_s de $0,98 \text{ kg/daN} \cdot \text{s}$

Ce propulseur très simple impose en formule classique un étage HP et deux étages BP soit au total six grilles.

Avec notre proposition trois grilles suffisent comme le démontrent les triangles de vitesses de la figure 8.

La charge de $480 \text{ K}_j/\text{kg}$ fournie par ces trois grilles est inférieure aux 540 calculés au paragraphe 2.2.2 mais la roue HP logée sous la chambre de combustion ne peut, puisqu'elle est accouplée à un compresseur centrifuge tournant à 550 m/s , dépasser au diamètre intérieur la vitesse de 305 m/s . Le rotor, lui, tourne à 200 m/s au diamètre intérieur ($k = 200/305 = 0,66$).

Notre proposition économise donc 3 grilles. Ceci entraîne un gain de masse, un gain de prix et sans doute de rendement car les nombres de Mach et les déviations sont à l'avantage du contrarotatif et de plus les surfaces portantes sont divisées par deux.

3.4 - Durée de vie

Au Laboratoire de l'Ecole des Mines de Paris, M. J. LAMON et J.P. TORRE ont développé une méthode de calcul de la durée de vie en service des pièces en céramique.

On sait que les céramiques se dégradent par croissance lente, à chaud, des principaux défauts présents dans leurs microstructures (les pores). Ce phénomène porte le nom de "fissuration sous-critique".

L'évolution des défauts entraîne une augmentation du facteur d'intensité K_I . La rupture brutale intervient lorsque K_I atteint la valeur critique K_{IC} .

La valeur initiale K_{Ii} du facteur d'intensité dépend de la dimension initiale du défaut à l'origine de la fissuration principale.

La durée de vie d'une pièce soumise, en service, à la contrainte σ_a est donc le temps t que met le facteur d'intensité pour passer de la valeur K_{Ii} à la valeur K_{IC} .

La vitesse de fissuration V peut être représentée par une loi de la forme :

$$V = A K_I^n$$

les valeurs A et n dépendent de la céramique.

J. LAMON et J.P. TORRE proposent alors la formule donnant la durée de vie en fonction de la contrainte d'utilisation σ_a :

$$t = \frac{2}{(n-2)\pi} \frac{1}{A \sigma_a^n} \left(\frac{\sigma_0}{K_{IC}} \right)^{n-2} \left[L \frac{1}{1-p} \right]^{\frac{n-2}{m}} \quad \text{en secondes}$$

σ_0 et m dépendent du matériau et prennent en compte le caractère aléatoire de la distribution des défauts.

p désigne le pourcentage de pièces qui ne survivraient pas à un essai, à la température ambiante, sous une contrainte $\sigma > \sigma_a$.

p et K_{Ii} sont liés par l'intermédiaire de la dimension initiale du défaut qui conditionne le processus de rupture. Le terme p est plus concret que K_{Ii} et reflète mieux la qualité de fabrication.

Nous avons pris dans le commerce le nitrure de silicium consolidé par le frittage réactif (Reaction Bonded Silicon Nitride). Ce produit est commercialisé par la Société Rosenthal (R.F.A.). Il existe en laboratoire des produits ayant des caractéristiques très supérieures mais nous avons choisi un produit que l'on peut se procurer sans difficulté.

Avec notre proposition de technologie en compression pour les aubes lentes le point le plus critique est soumis à une contrainte de traction de $\sigma_a = 20$ MPa due à la flexion du talon situé au diamètre intérieur.

Pour le matériau ci-dessus référencé nous avons mesuré à 1500°K dans l'air :

$$K_{IC} = 2.10^6 \text{ N/m}^{3/2}$$

$$\sigma_0 = 54,5 \text{ (si } K_{IC} \text{ et } \sigma_0 \text{ en MPa)}$$

$$A = 1,1.10^{-8}$$

$$n = 2,5$$

$$m = 15,7$$

Si l'on est prêt à consentir un rebut $p = 10\%$ de pièces lors d'un essai de réception sous une contrainte, à la température ambiante, égale à σ_a , la formule ci-dessus donne $t = 87^h$ (Rappelons qu'il s'agit d'une céramique actuellement commercialisée).

Avec les formules classiques, la contrainte σ'_a serait de l'ordre de 80.10^6 N/m^2 . La durée de vie serait donc divisée par :

$$\left(\frac{\sigma'_a}{\sigma_a} \right)^n = \left(\frac{80}{20} \right)^{2,5} = 32 !$$

Ainsi, notre proposition multiplie par 32 la durée de vie des céramiques ! Ce fait est lié à la valeur 2,5 de l'exposant de σ_a .

Si au lieu de 10% on tolère 20 ou 30% de rebut par un essai à froid, les durées de vie sont augmentées proportionnellement à la fonction $\left(L \frac{1}{1-p} \right)^{0,032}$. Entre 10% et 30% de rebut la durée passe de 87 h à 90 h. Avec un rebut de 1% la durée tombe à 80 h. Cette relative invariance de la durée de vie à l'égard du rebut est liée à la très faible valeur (0,032) pour ce matériau du rapport $\frac{n-2}{m}$.

3.2 - Aspect thermique

Si les aubes de la première grille lente sont réalisées en céramique leur contrainte de compression est de 14 MPa pour une limite à la rupture de 215 MPa. Elles n'ont pas besoin d'être refroidies.

La température des gaz dans la grille mobile rapide qui suit est de 1307°K (1134°C). Compte tenu de la faible vitesse de rotation (305 m/s) la contrainte maximum ne dépasse pas 50 MPa ce qui permet pour un fonctionnement de courte durée de ne pas la refroidir.

Dans la formule classique il faut refroidir le distributeur s'il n'est pas en céramique. Si on le réalise en céramique il est soumis à des contraintes de flexion de 20 à 30 MPa suivant la technologie retenue. Or la céramique supporte beaucoup moins bien la flexion que la compression. Par ailleurs les inévitables hétérogénéités circonférentielles donnent $\pm 200^\circ$ par rapport à la valeur moyenne. Il est donc prudent, même pour des céramiques, de prévoir un refroidissement de la grille fixe.

La grille mobile qui suit cette grille fixe est environ 40° plus chaude qu'en formule contrarotative il faudra donc prévoir un refroidissement.

La première grille fixe BP devra impérativement être refroidie si elle n'est pas en céramique. Mais les contraintes de flexion sont de 50 à 60 MPa ce qui est peut être limite pour les céramiques en flexion et à cette température (1225°K).

En définitive la formule contrarotative économise de l'air de refroidissement. On ne peut chiffrer cette économie que sur des projets très élaborés. Mais on peut noter que sur le cycle défini en 3.1 si p est le pourcentage d'air primaire pris pour le refroidissement on trouve comme influence sur F et c_5 les valeurs suivantes :

$p \%$	$\frac{\Delta c_5}{c_5} \%$	$\frac{\Delta F}{F} \%$
2	0,65	- 2,6
4	1,4	- 5,3
6	2,3	- 8,1

L'influence est donc importante en particulier sur la poussée c'est-à-dire en fin de compte sur la masse et l'encombrement frontal.

Notons, en outre, que les valeurs du tableau ne prennent pas en compte l'inévitable détérioration aérodynamique liée à la réintroduction de l'air de refroidissement.

3.3 - Aspect technologique

Pour les aubes travaillant en compression il est prudent de les doter d'un talon pour éviter le flambage en cas de vibration. Ces talons peuvent être jointifs. D'ailleurs les procédés d'élaboration des aubes en céramique permettent de réaliser des grappes d'aubes (de 2 à 6) à l'abri de tout ennui vibratoire.

On voit sur la figure 9 un exemple de technologie de montage des grappes sur l'alésage du disque avec les circuits d'air de refroidissement des pieds d'aubes et des anneaux. Il importe en effet que le disque anneau soit thermiquement isolé.

Avec un isolement thermique suffisamment efficace on peut même prévoir un frettage par fibres enroulées à la jante permettant ainsi une vitesse de rotation plus élevée.

Dans l'exemple présenté la jante du disque ne tourne qu'à 270 m/s et la contrainte tangentielle dans l'anneau ne dépasse pas 700 MPa (valeur très acceptable pour les métaux actuels). On notera la forme trapézoïdale de la section de l'anneau : un anneau d'égale épaisseur conduirait à une contrainte de 800 MPa (et à un diamètre plus grand).

3.4 - Conclusion sur les trois grilles

Par une étude assez détaillée de cet exemple nous voulons montrer qu'on peut réaliser avec seulement trois grilles un moteur relativement performant. L'utilisation des céramiques n'est pas une nécessité mais elle économise de l'air de refroidissement et permet une vitesse de rotation plus élevée sur le rotor lent donc plus de travail de détente. Le gain de masse, de prix et de performance ne peut être chiffré que par un projet complètement étudié. On peut cependant estimer à 40 % le gain de masse obtenu sur la partie turbine. Les économies d'air de refroidissement, les améliorations des rendements de détente doivent conduire à une amélioration de 10 à 12 % de la poussée par unité de débit et de 2 à 3 % de la c_5 .

4 - AUTRES FORMULES CONTRAROTATIVES

4.1 - Grilles lentes en compression

La figure 10 montre une amélioration de la formule précédente par l'introduction d'une grille fixe en amont. Le taux de dilution peut être ainsi porté à 5 et le rapport de pression à 14. Il en résulte un gain de C_3 de 13 % pour une température de 1570°K.

La figure 11 montre comment on peut utiliser quatre grilles mobiles (deux lentes et deux rapides). Le taux de dilution est 4 et le rapport de pression 14. Le cycle est encore très performant avec un nombre d'aubes extrêmement réduit. La technologie présentée sous sa forme la plus intéressante (deux enceintes d'huile) conduit à quelques hardiesses (deux paliers interarbres, porte à faux du compresseur lent) que l'on peut éviter avec une enceinte d'huile supplémentaire.

4.2 - Grilles lentes en traction

Les figures 12, 13, 14 et 15 montrent plusieurs images de moteurs complets contrarotatifs sur la turbine et sur le compresseur. Les deux grilles mobiles obéissent aux exigences du contrarotatif avec grille amont plus lente ($K \sim 0,5$). Pour les grilles de compression on démontre, à l'inverse de la détente, que c'est la grille aval qui doit être la plus lente. Cette remarque permet de comprendre les technologies :

- a) du monoflux figure 12 (rapport de pression 9) ;
- b) du double flux à flux mélangé figure 13 (rapport de pression 18, taux de dilution 0,2) ;
- c) des double flux plus dilués figure 14 avec un distributeur fixe, figure 15 sans distributeur.

Dans toutes ces formules la grille lente conduit, pour des aubes en céramique, à des contraintes de traction de l'ordre de 20 à 30 MPa.

On peut transformer en compression ces contraintes de traction par l'un ou l'autre des dispositifs présentés sur les figures 16 et 17.

L'aube en céramique, ou en métal, est creuse. Une âme métallique présente un épaulement au diamètre extérieur. L'aube est libre au diamètre extérieur. Il est clair que dans cette technologie l'âme doit être refroidie par une circulation d'air.

5 - LES ECHANGEURS

Pour une température maximum permise les échangeurs : diminuent le rapport de pression optimum, diminuent la poussée par unité de débit.

Ces deux éléments sont favorables aux propulseurs de faible poussée car ils conduisent à des aubes de dimensions raisonnables.

En contrepartie ils sont encombrants et lourds ce qui est un double handicap.

En réalisant les échangeurs en céramique on lève le handicap de la masse dans la mesure où l'on sait réaliser en céramique des épaisseurs du même ordre qu'en métal. De gros progrès ont été réalisés dans cette voie et les gains en masse sont appréciables.

Pour une faible durée de vie on n'a pas à craindre la décohésion et l'encrassement. Il reste donc surtout le problème de l'encombrement.

Sur la figure 18 nous avons fait figurer un circuit d'accès à l'échangeur qui diminue les pertes de charge. Le propulseur présenté possède en croisière les performances des meilleurs propulseurs modernes dès que l'échangeur possède une efficacité de 0,8. Or le nombre total de grilles (compression et détente) est de 10 alors que les propulseurs classiques sans échangeurs réclament plus de quarante grilles d'aubes.

Les céramiques par leur légèreté et leur désormais bonne fiabilité trouvent donc dans les échangeurs un terrain privilégié d'utilisation.

6 - CONCLUSION

En quarante ans d'utilisation de métaux aux caractéristiques lentement améliorées, les constructeurs ont logiquement convergé vers des formules si voisines que le profane est tenté de croire à un effet d'espionnage industriel.

Les progrès des céramiques nous ont incité à un effort d'imagination pour tenter de penser la technologie en fonction du matériau au lieu d'essayer d'intégrer ce nouveau matériau dans une logique réservée aux métaux.

Nous pensons avoir clairement démontré l'intérêt de nos propositions en masse, en performance, en encombrement et en prix. Nous avons examiné les problèmes posés sous tous leurs aspects : aérodynamique, thermique, résistance, vibration, technologie.

L'état actuel des céramiques permet leur utilisation dès aujourd'hui pour une faible durée de vie.

Pour les propulseurs civils ou militaires qui réclament de longues durées les céramiques doivent encore faire des progrès.

Mais, de même que les céramiques peuvent être utilisées (avec un moindre gain) dans les formules classiques, de même nos propositions, spécialement adaptées aux céramiques, peuvent (avec un moindre gain) utiliser les métaux classiques et permettre ainsi la mise au point de tout ce qui, dans nos propositions, est une nouveauté non spécifique de la céramique.

Fig. 4 $Mv_1, \frac{\Delta T}{T}, \frac{\delta T}{T_0}, \frac{\Delta T}{\Delta T_0}, \frac{\delta T}{\delta T_0} \left\{ \begin{array}{l} Mw_1 = 0,5 \\ f(Mu, \alpha) \end{array} \right.$

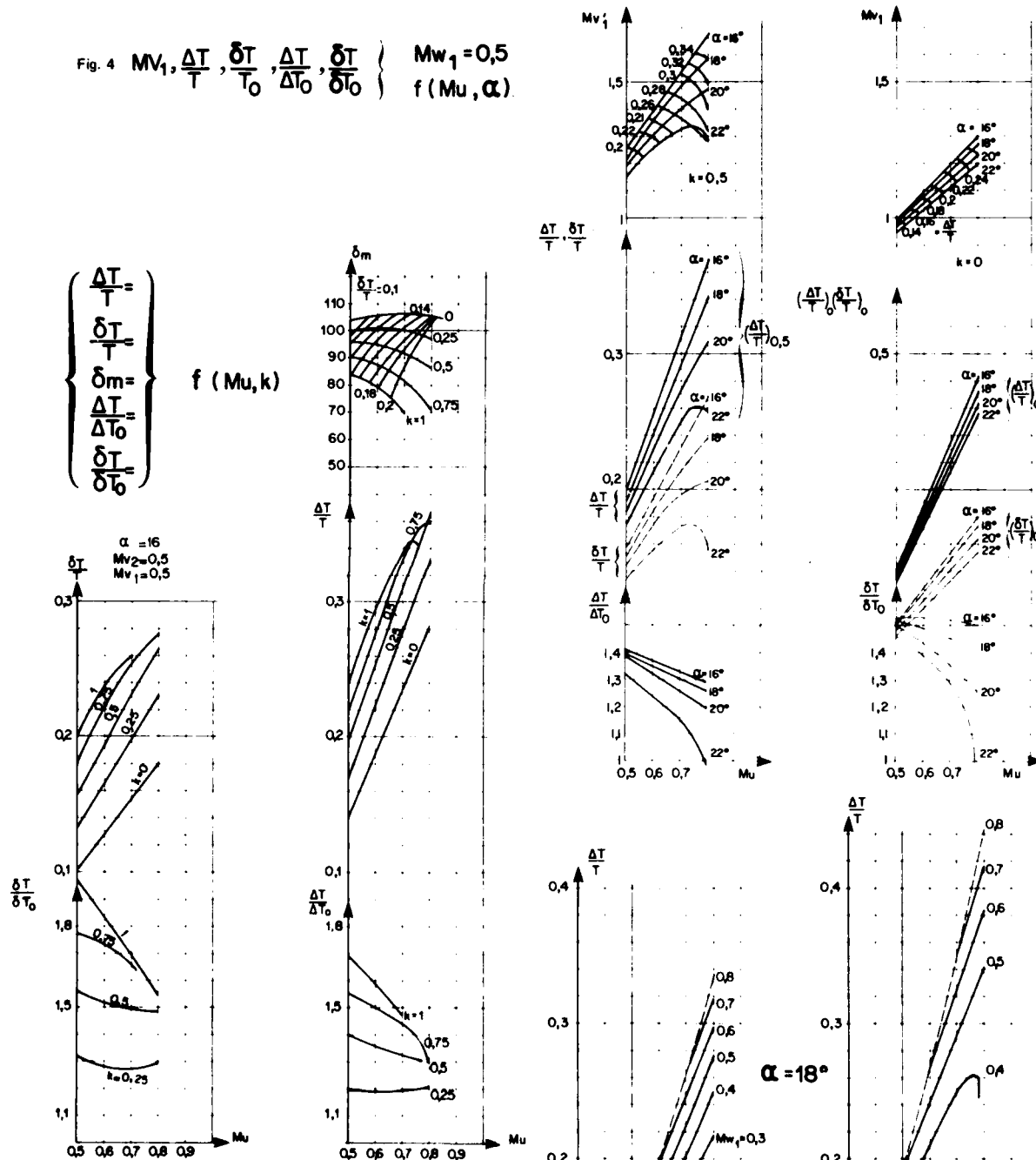
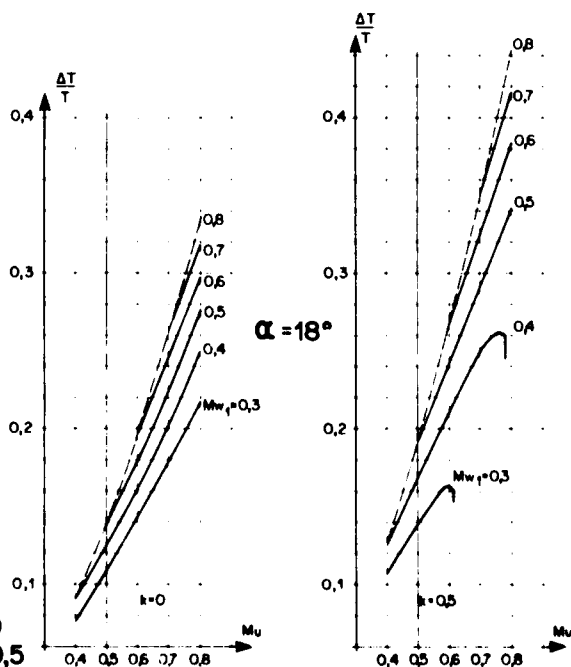


Fig. 3

Fig. 5 $\frac{\Delta T}{T} = f(Mu, Mw_1)$ POUR $k = 0, k = 0.5$



CHARGES EN FONCTION DU NOMBRE DE GRILLES

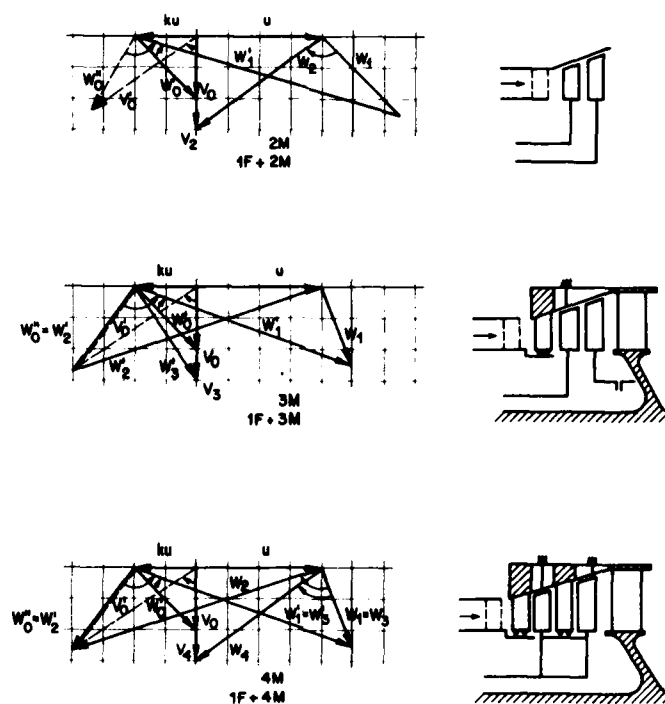


Fig. 6

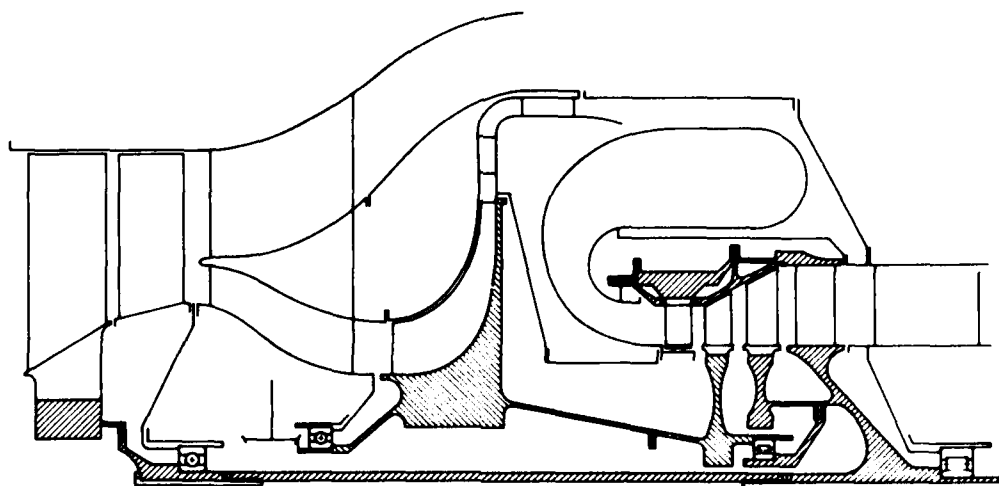
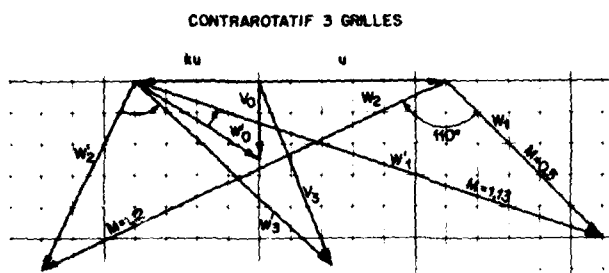


Fig. 7

TRIANGLES DE VITESSES



CLASSIQUE 6 GRILLES (2 HP + 4 BP)

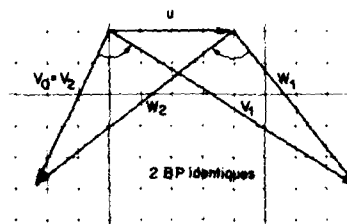
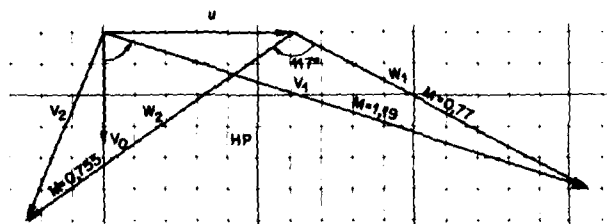


Fig. 8

TECHNOLOGIE DE TROIS GRILLES

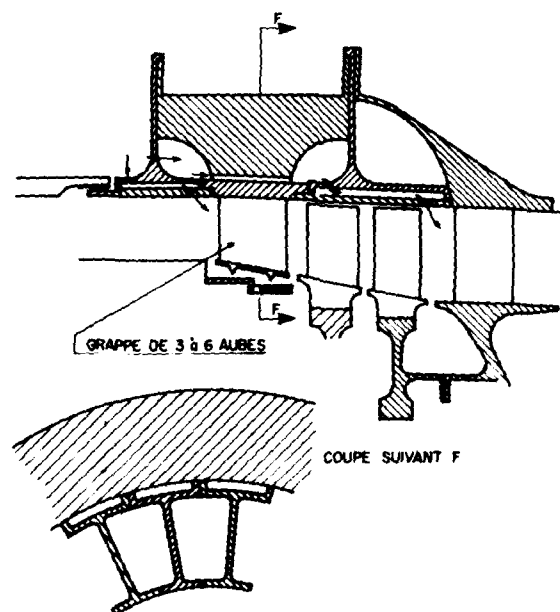


Fig 9

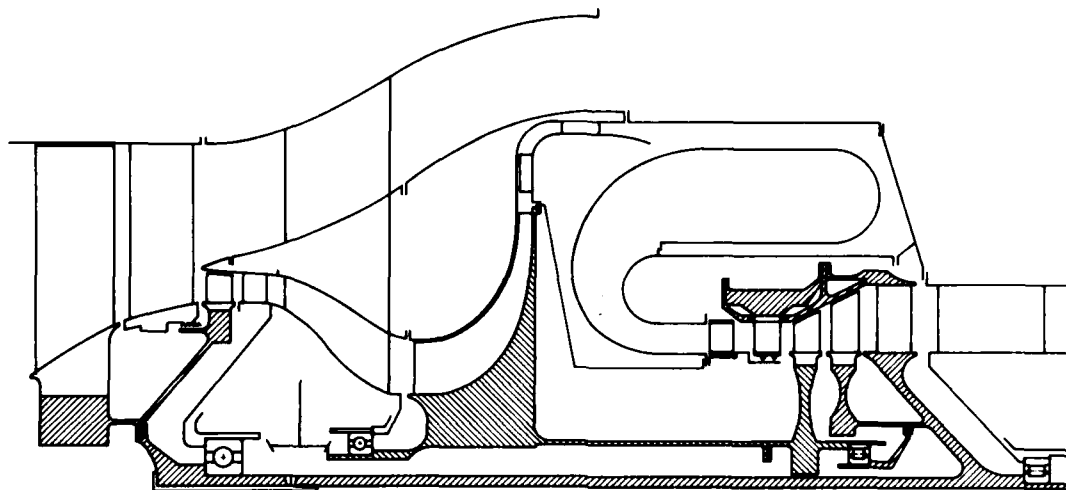


Fig. 10

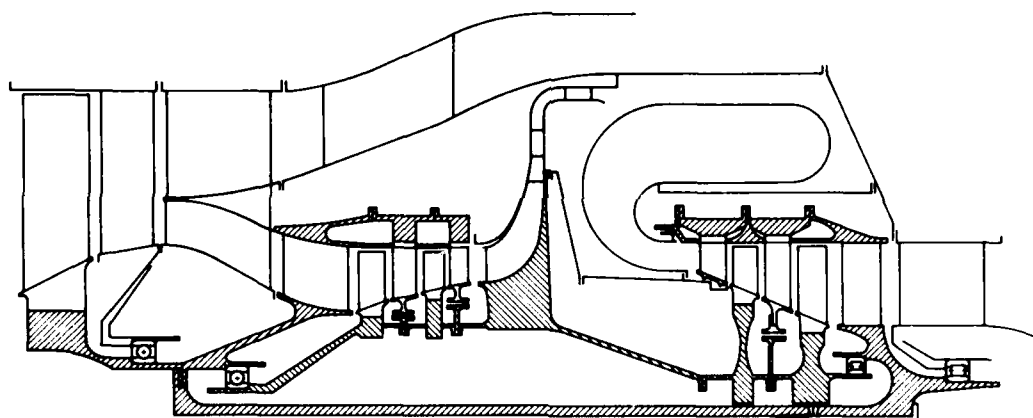


Fig. 11

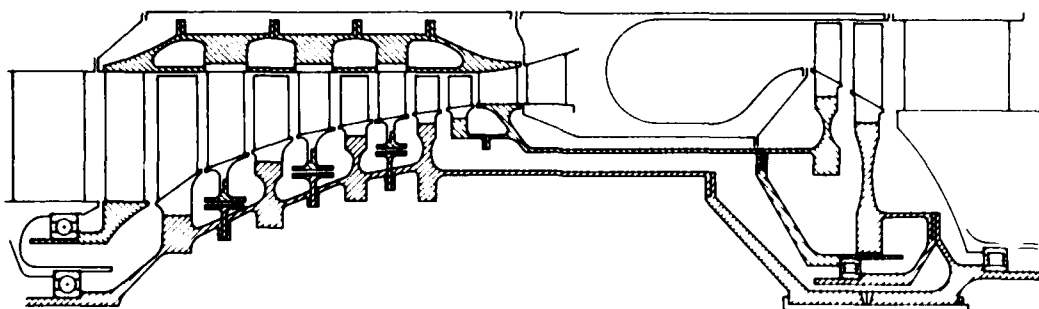


Fig. 12

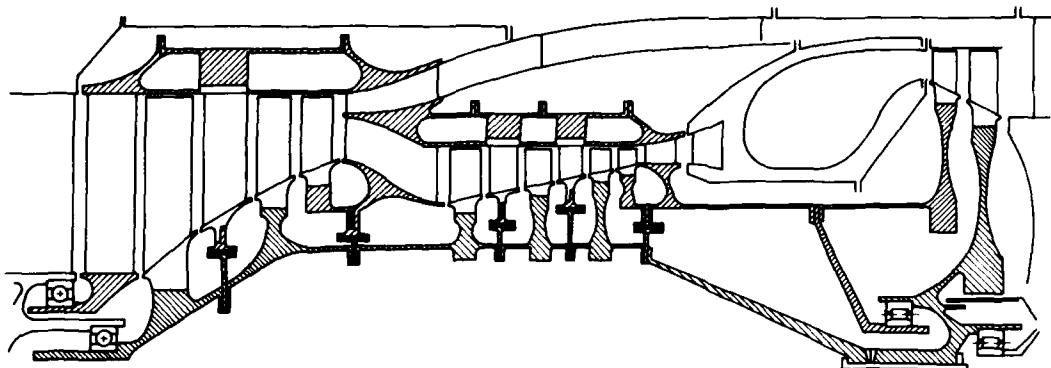


Fig. 13

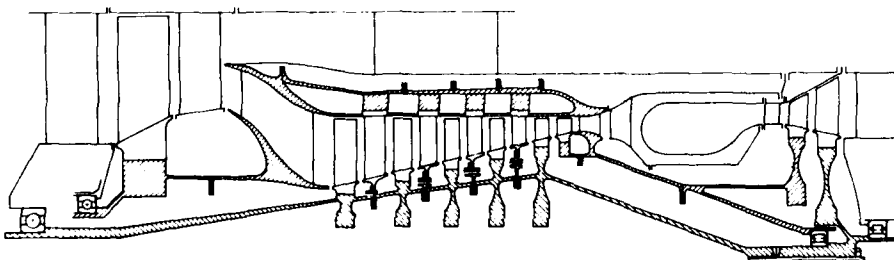


Fig. 14

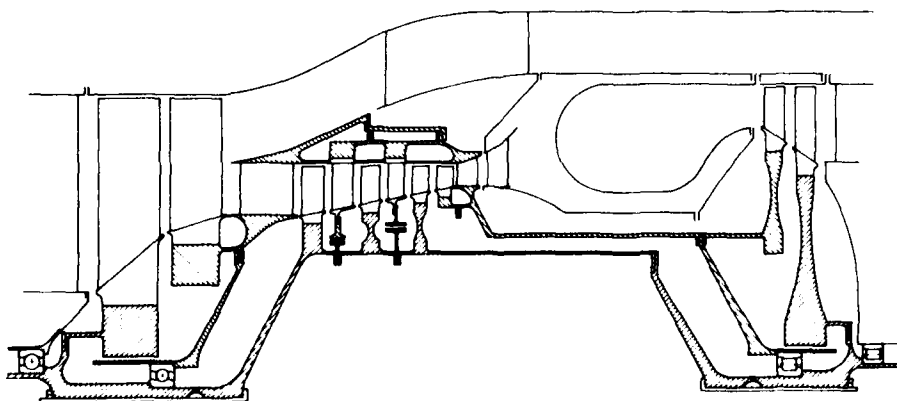


Fig. 15

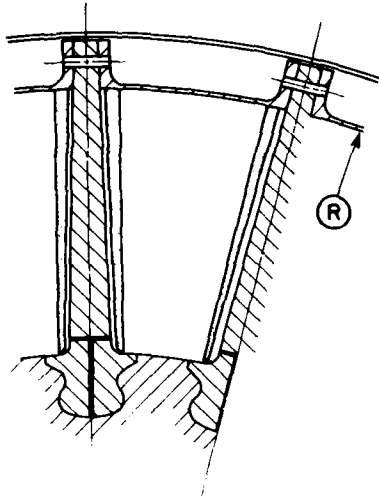
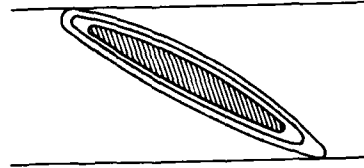
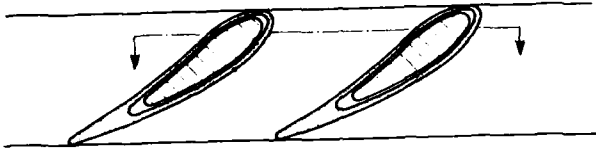


Fig. 16

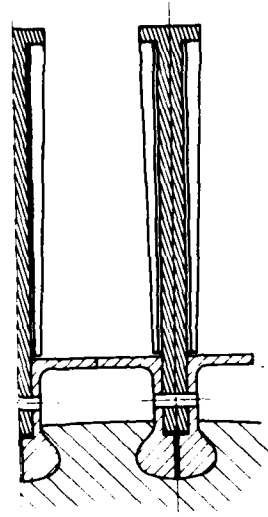


Fig. 17

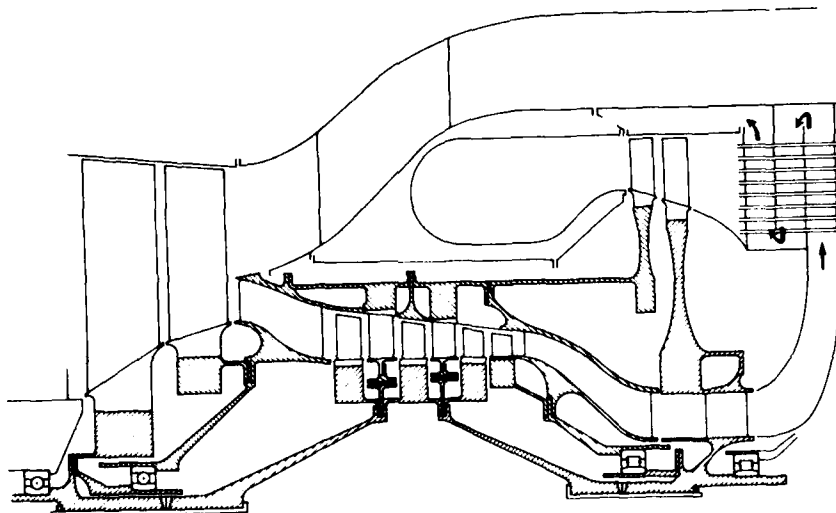


Fig. 18

DISCUSSION SUMMARY

SESSION I - REQUIREMENTS AND CRITERIA FOR GAS TURBINE ENGINES

by

E.M.Lenoe
US Army Materials and Mechanics Research Center
Watertown, Massachusetts, USA

Following is a summary of the discussions of each paper presented in Session I: Requirements and Criteria for Gas Turbine Engines.

BENEFITS OF CERAMICS TO GAS TURBINES

by A.Brooks and A.I.Bellin

E.C. van Reuth, US

Thank you for the very nice overview. However, there was one development, particularly in superalloys, that I think should be mentioned as an addendum to an overview paper of this sort and that is the rapid solidification technology which has recently emerged and is demonstrating rather remarkable temperature improvements on the order of 100°C and very exciting oxidation resistant properties, to mention only a few.

Author's Reply

Right, not to mention single crystals as well. But just one word, if I may, and I'd like to stress this. The propulsion industry is a very hard headed thing and I'd like to restate the point made at the very outset, and that is, there are competing developments coming along and it will be a question of the best material winning, it's a very unemotional business.

F.Blake Wallace, US

With respect to your study of the number of blades and the decreasing root stresses as you went to a larger number of shorter chord blades, do you put a limit on that in terms of either the physical size of the attachment or the vibration characteristics of the blades?

Author's Reply

The particular analysis did not recognize the vibrational problem. We considered, for the purpose of this very simple preliminary design study, only the steady state ramifications. We think there are a number of reasons why you would want to put a limit on the number of blades. One of them is the thing that you were alluding to, the other is cost. A point to make, is that one of our motivations for ceramic materials work is primarily the issue of cost. The issue of performance is not as strong a motivation to us because high temperature capability is possible through other means. One of the things that is very attractive about ceramics is the low cost. Now, to get back to the question you asked, we did not consider the vibration aspects as a limiting factor in this particular study.

H.Liebowitz, US

Could you characterize the fracture problem a little more, as to what you expect in fracture; as a comparison to superalloys? What sort of fracture toughnesses do you get, what sort of problems do you encounter?

Author's reply

There is a fracture discussion in the paper that I did not get to. I think I would like to let that discussion wait to a later time, particularly with someone who is a bit more capable of discussing the scientific aspects.

CERAMICS FOR SMALL AIRBORNE ENGINE APPLICATIONS

by R.N.Katz and E.M.Lenoe

J.C.Napier, US

You did not include Norton NC430, the siliconized silicon carbide in your experiments showing degradation strength with time and stress. Would you say that there is a difference in behaviour of this material?

AD-A087 594

ADVISORY GROUP FOR AEROSPACE RESEARCH AND DEVELOPMENT--ETC F/6 11/2
CERAMICS FOR TURBINE ENGINE APPLICATIONS.(U)
MAR 80 H M BURTE, J ACURIO, W HANSEN

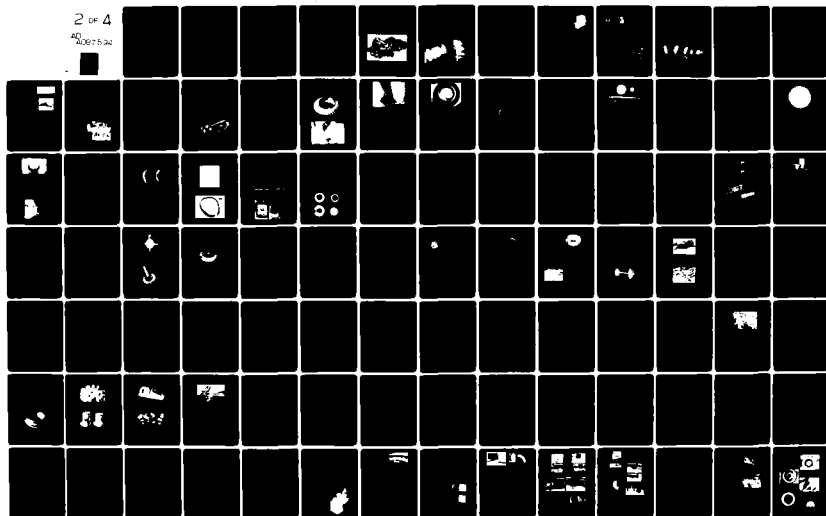
UNCLASSIFIED

AGARD-CP-276

NL

2 OF 4

40
3097532



Author's Reply

There is quite a bit more data available, actually this had to be a rather brief manuscript. We did disservice to approximately a dozen ceramics.

J.C.Napier, US

Okay, in regard to that, what did you find specifically with reference to NC430 material, over time of exposure at temperature. Was it similar to other materials? For instance, you showed the NC435.

Author's Reply

Yes, it was similar, although, in most of these materials, particularly the lower density materials, there has been quite a bit of variation in the time dependent properties. So it's difficult, let's say on the basis of five batches of a given material, to make a conclusive statement that one ceramic is better than the other.

K.L.Rieke, US

You showed stresses classified on airfoil sections. Were those steady state stresses or did they account for the transient start up and shut down mode of operation also?

Author's Reply

What we tried to do, to define regime of design stresses, was to visit engine designers, particularly with regard to helicopter engines, APU's and other limited life engines. So we are talking about rather small engines in general and stresses that are considered are the critical design points. It's a superposition, actually, in a number of cases of steady state and transient stresses. It's not a very clear way to do it, but was expedient for simple comparisons.

N.L.Parr, UK

In some of the very earliest experiments on Si_3N_4 , in the late 1950's, by myself and other workers, we demonstrated that silicon nitride/silicon carbide alloys (or textures), had very interesting properties, in particular creep strength. One could increase the creep strength of the reaction bonded by two orders of magnitude by 5 and 10% additions of SiC. I see no reference to that in this area these days. Have those materials been bypassed?

Author's Reply

There are laboratory scale data in that area. However, in my paper I tried to use only those materials that were more or less commercially available.

N.L.Parr, UK

There is work in progress do you say?

Author's Reply

Yes.

P.Popper, UK

Do you see the $\text{Si}_3\text{N}_4/\text{SiC}$ as an *and*, or as an *or*? And if you see it as an *and* situation, in other words, both materials to be used, do you see silicon component applications more in one field as in another?

Author's Reply

Personally I feel that we should nurture all classes of structural ceramics for what ever application that they can be used. I don't see one ceramic dominating all others, for example, for vanes, or blades, right now. It's just a matter of availability so it's an either/or situation to me.

E.Tiefenbacher, Ge

In your paper there is a strong reduction of the strength of the NC132 after this exposure to air and flame. Have you any explanation for that effect?

Author's Reply

Depending on the trace element impurities in the particular lot of NC132 and also depending on the environmental exposure, the effects on strength can be predominantly surface or predominantly throughout the volume. On the other hand, in some instances, this reduction is actually related to the rather severe surface erosion or the pitting one observes. In principle if that surface were removed periodically, this would be a way to work around that apparent strength reduction. Of course you would have to sacrifice tolerances. What I'm saying is the way that strength degradation results are presented, and the way most people present the strength reduction, as measured in the flexural test, does not necessarily reflect an inherent interior strength reduction. If you were to go ahead and clean up the components, in my opinion in many cases they would still be servicable. On the other hand, if trace level

impurities exceed certain limits, extensive microstructural and physical/chemical changes occur upon severe environmental exposure and properties degradation does indeed occur throughout the volume of the hot pressed silicon nitride.

A. McLean, US

Could you tell us what your plans are on this long term testing of various materials, not only in terms of evaluating properties but in terms of evaluating chemistry, microstructure, and what is really going on with these materials over periods of say 1000 hours or greater?

Author's Reply

As you know, there's quite a bit to be learned about these materials, in spite of the fact that we've been laboring with them intensely and other nations have labored before us. We still do not thoroughly understand many of the mechanisms of failure, particularly the time dependent aspects.

Unfortunately, the work going on in this area is rather disjointed. There is no current intense or concentrated effort. In the USA the Department of Energy has a program underway but in my opinion the resources are not sufficient to do the required basic work. In other words, to improve the basic material and simultaneously document the effects of long term exposure. There are plans for demonstrations in engines, as you are well aware of, at Detroit Diesel Allison and elsewhere. These efforts generally do not get at the aspects of fundamental behavior. I'd say there's of the order of one half million dollars worth of basic research work related to documenting time and environmental effects and to begin to understand how to design and analyze with these materials, over the next few years. Basically to me it's a race against attempts at accomplishments in engines and in vehicles while proceeding with limited understanding of what we are doing.

REQUIREMENTS FOR MATERIALS FOR LAND VEHICLE GAS TURBINES

by D.F. Moss

A. McLean, US

I have a few comments, but first we must update that slide of the Ford stator. That's an early Design A concept and current designs are much improved. I'd like to make a comment about ceramics for combustors. We've found in studying combustion for very low emissions, in terms of oxides of nitrogen, that we've had to go to extremely dilute combustion when we prevaporize fuel and premix with air before combustion, so then it really burns without a diffusion flame. It's just a completely even combustion, which of course, tremendously helps the hot spot problems and I'd say that we really must have ceramics in order to do that. The other comments are really questions. One is in your futuristic ceramic engine that you showed at the end, is that with or without heat exchanger and my other question is that you mentioned the single shaft engine can now be a reality because of recent transmission developments. Can you tell us a little more about that?

Author's Reply

In answer to your first question, yes, it does involve a heat exchanger because you need the heat exchanger to get part load fuel consumption, and you also need a mechanism for switching it in and out and that's why it's futuristic. A point on the transmission was that I don't think that the type of transmissions that are available have quite made it. But there is work that's going on and you know as much about the funding that's going on in the States as probably I do. But, for low power vehicles, it's very likely to become a possibility and it's much more difficult for the truck engine, at 450 horsepower.

Question: (questioner unidentified)

I noticed that you talked something on the limitation on metals and that this could be extended by use of radial turbines. We quite agree with you because we are perhaps making more radial turbines that anybody, certainly in the industrial field. I don't quite remember the numbers you had, but we are contemplating a turbine inlet temperature in a metal turbine rotor of 1350°C, in an uncooled turbine. Of course, we are using a very high tip speed and this doesn't give us more than 1050°C maximum temperature, which is well in hand. We are actually converting temperature into hub stresses by using the new developments in metal, ISR, gatorizing, etc. as was mentioned. I wasn't sure that your temperatures were at this level, but I think that you should be aware of the possibilities with metals and not get all excited about the ceramics but look at this ISR process which was also mentioned by Dr van Reuth. We are looking at 1335°C nozzle inlet temperature. What are you looking at?

Author's Reply

I was saying about 1235°C.

G.Deutsch, US

In one of your earlier slides you had a lifetime requirement of 10,000 hours. Isn't that asking more from the ceramic gas turbine engine that you're currently getting from the conventional automobile reciprocating engine?

Author's Reply

All I'm saying is there is, I think that if an automotive vehicle is going to be a reality, that's the sort of design life you've got to aim for. I'm not saying actual ceramics have demonstrated that yet. That's one of the problems of the automotive gas turbine.

G.Deutsch, US

I guess I'm thoroughly confused because it seems to me that I recently bought an automobile that has a design life-time in the engine of something between 3 and 4,000 hours. Why do you feel that for the automotive gas turbine to be successful the design requirements has to go to 10,000 hours.

Author's Reply

Well, I'm not going to argue whether it's 5,000 hours or 10,000 hours. I think for those sort of lives and for those sort of reliabilities, you can put into calculation and predictions. Then (for trucks), I think 10,000 hours is not out of the way.

C.Johnson, US

Along a similar line on that same graph, you had listed 1,000 hours at maximum power; and it's my understanding that there's no auto engine made today that can operate for more than 100 hours at maximum power, so let's not ask more of ceramics than we already get out of the present metallic engines.

Author's Reply

Yes, that's very nice, but I think a point against this is that we shall have to make much better use of materials in the future anyway and less rapidly throw away vehicles. I mean it would not be a bad thing, certainly.

E.M.Lenoe, US

I just wanted to interject that confusion was generated by the use of hours without associated design requirements, that's really the thrust of the problem.

Author's Reply

What I'm saying is that you know we have been associated with various firms in the States and these are the sort of levels they have been asking, at the design stage.

**TECHNOLOGIES CONÇUES POUR L'UTILISATION DES CERAMIQUES DANS
LES TURBOREACTEURS
par S.Boudigues et G.Fratacci**

P.F.Pucci, US

Thank you, Mr Boudigues. I see you have presented us with quite a challenge. In the propulsion and energetics panel we have a working group dealing with through flow considerations and I'm sure this would present a challenge for them.

K.Trappman, Ge

That was a very interesting proposal. I would like to ask you, have you investigated the past load performance of such an engine with controllers taking turbines and compressors and the handling characteristics of such engines?

P.Kochendorfer, Ge

Do you have any test results about your compression loaded ceramic wheel? Or is this a study phase?

J.C.Napier, US

Could you explain your last slide or show it again so that we could understand it better?

SILICON NITRIDE TURBINE BLADE DEVELOPMENT

F. Blake Wallace
John E. Harper
Carl R. Dins
David W. Richerson
Harry L. Kington

AiResearch Manufacturing Company of Arizona
A Division of The Garrett Corporation
P.O. Box 5217
Phoenix, Arizona 85010

Summary

Hot-pressed silicon nitride (HPSN) rotor blades have been developed as part of a two-stage turbine. Program activities are described including design optimization to minimize steady-state and vibratory stress, material characterization, attachment tests, manufacturing process development, inspection, proof tests, turbine-rig development, and engine tests. This successful program demonstrates for the first time that ceramics can withstand the severe environment imposed on gas turbine rotating components, and that the potential for engines with increased efficiency and decreased use of strategic materials can be realized.

INTRODUCTION

The ARPA Ceramic Gas Turbine Engine Demonstration Program was initiated in February 1976, based on the belief that sufficient progress had been made in ceramic materials and advanced analysis techniques that a successful engine demonstration could be achieved. Such a demonstration was needed to establish designer confidence, thus, leading to expanded use of ceramics in a broad range of applications. As summarized in Figure 1, the program was established to demonstrate ceramic components in an engine environment of 2200°F (1477°K) average turbine inlet temperature -- 2500°F peak (1644°K).

The program was structured with four major phases of activity.

- o Design Phase. Detail analysis and design optimization
- o Materials-Characterization Phase. Material selection, design data, process development, and NDE requirements
- o Component-Development Phase. Rig testing
- o Engine Development. Full-scale engine tests.

The program was to use state-of-the-art ceramic materials (minimum materials development), and to design, develop, and demonstrate ceramic components with minimum risk, and maximum chance of success.

The vehicle selected for this demonstration was the AiResearch Model T76 Turboprop Engine, a 715 (533 KW) horsepower engine whose various derivatives are used for military and civil aircraft propulsion, helicopter turboshaft applications, and for industrial/marine power (Figure 2). The gearbox and compressor sections were used without change; however, the turbine sections were redesigned to use ceramic gas-path components. An increase of 350°F (194°K) in the turbine temperature allowed by the ceramic components increases power to 1000 (746 KW) horsepower and decreases SFC by 10 percent.

The ceramic engine hot-end cross section is shown in Figure 3. The ceramic turbine blades of stages 1 and 2 are made of HPSN (NC-132); the static ceramic components are made of reaction-bonded silicon nitride (RBSN). This paper will address only the rotor design and development aspects of the ceramic engine program.

DISCUSSION

The rotating group is a single spool consisting of a two-stage centrifugal compressor and a three-stage turbine. Figure 4 shows the rotor turbine wheels and the second-stage compressor impeller. Note that the HPSN ceramic blades are inserted into a Waspaloy disk. The blade attachment is a single-tang dovetail with a platinum compliant layer between the ceramic blade and Waspaloy disk. The blades are held in position by metal coverplates on the forward and the aft side of the disk. Cooling air to purge the disk dovetail slot is brought up through the rotor and under the forward coverplate.

Design

Design studies were made on the third-stage rotor to determine the feasibility of either a ceramic integral blade/wheel or a ceramic inserted blade design. The gas temperatures are down in the third stage, and a metal wheel performs adequately in this environment. The studies indicated that with current ceramics and manufacturing techniques, a

PROGRAM OBJECTIVE

- DEMONSTRATE CERAMIC COMPONENTS IN AN ENGINE ENVIRONMENT

PROGRAM GOAL

- 2200°F (1477°K) AVERAGE TURBINE INLET TEMPERATURE --
2500°F PEAK (1644°K)

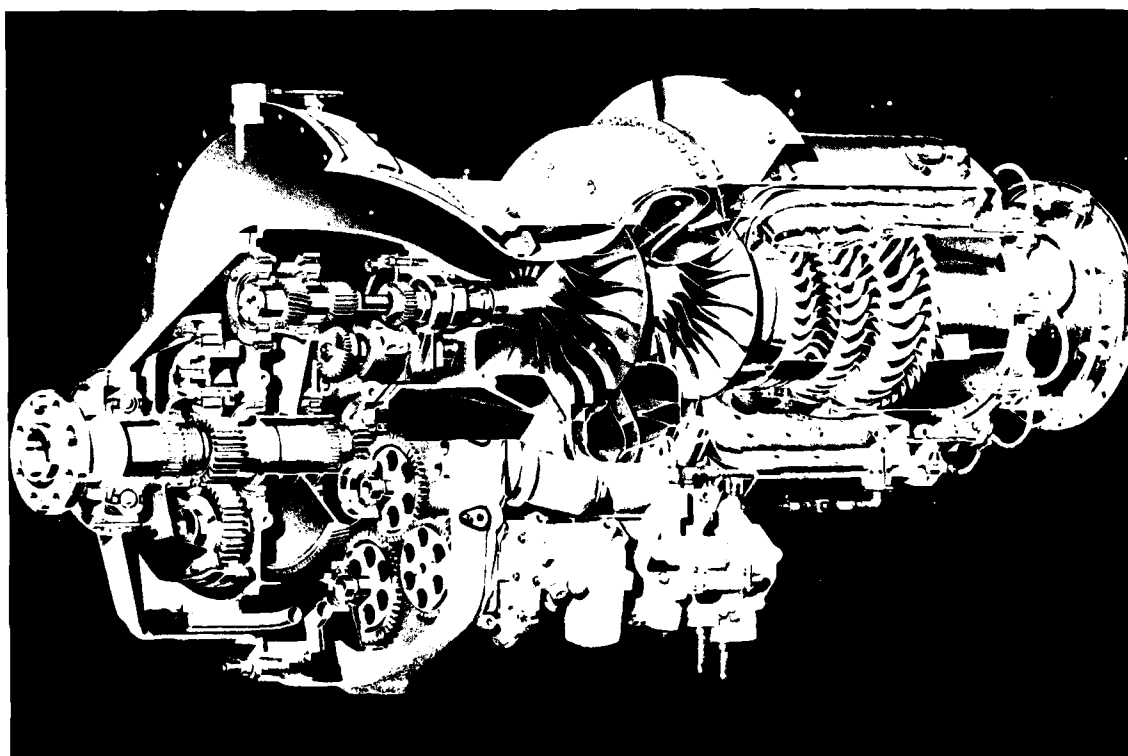
PROGRAM STRUCTURE

- 4 PHASES
 - DESIGN
 - MATERIALS CHARACTERIZATION
 - COMPONENT DEVELOPMENT
 - ENGINE DEVELOPMENT

MATERIALS

- 1977 STATE-OF-THE-ART

Figure 1. ARPA/Navy Ceramic Turbine Engine Demonstration Program.



	T76 ENGINE	CERAMIC ENGINE GOALS
POWER OUTPUT	715 SHP (533 KW)	1000 SHP (746 KW)
SPECIFIC FUEL CONSUMPTION	0.60 LB/HP-HR (0.365 KG/KW-HR)	0.54 LB/HP-HR (0.328 KG/KW-HR)

Figure 2. Demonstration Engine.

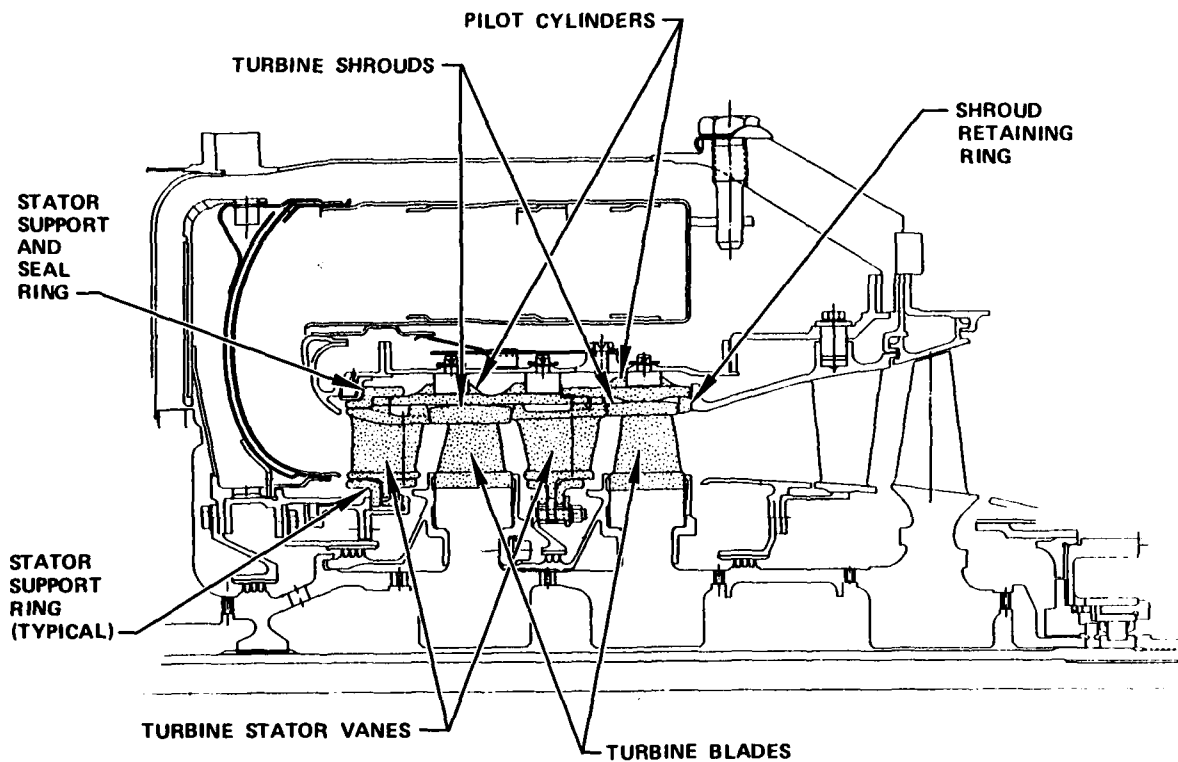
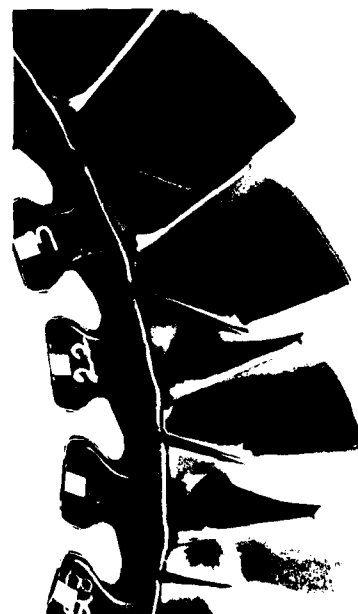
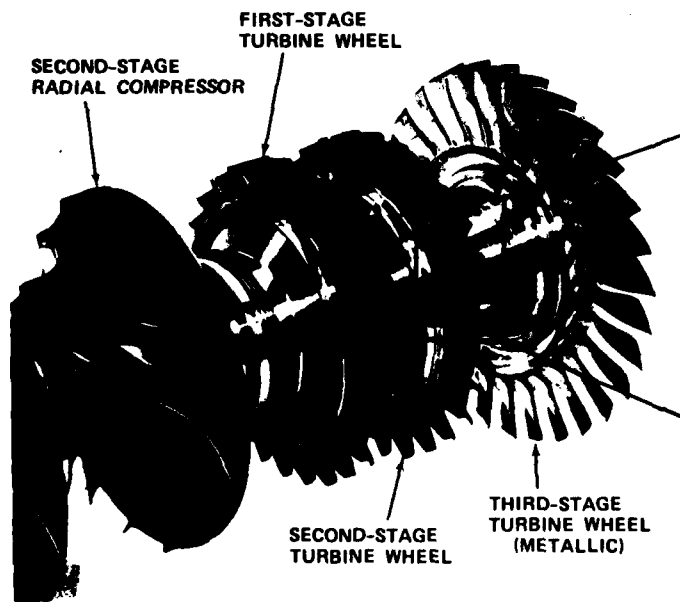


Figure 3. TSE331C-1 Turbine Section.



SECOND-STAGE CERAMIC BLADES
(FORWARD COVERPLATE REMOVED)

BLADE MATERIAL, NC-132
DISK MATERIAL, WASPALOY
COMPLIANT LAYER, PLATINUM

Figure 4. Ceramic Engine Turbine Rotor.

ceramic third-stage rotor would have an unacceptably low probability of success, and/or high performance penalties relative to a typical metallic wheel. Hence, the third stage is metallic, and only the high-temperature first and second stages are ceramic.

To meet the design goal (Figure 5) of 41,730 rpm (4370 rad/s) [1420 ft/sec (433 m/s) and 1464 ft/sec (446 m/s) tip-speed, first and second stages, respectively] and 2200°F (1477°K) average turbine inlet temperature with ceramic blades, the design requires analysis with extensive three-dimensional finite-element techniques, and evaluation of the design relative to the Weibull probabilistic failure criteria. The design objective was to meet a minimum of 95-percent probability of success per stage, with 50-hour/25-cycle life, and no blade resonance within the operating range.

Because of the lack of ductility in the ceramic material systems, the ceramic components are vulnerable to very localized stress concentration. To quantify these local peak stresses, an elaborate fine-grid, three-dimensional, finite-element stress model is essential. However, to design a part to peak stress alone would severely limit the use of ceramics. It is the combination of the flaw distribution and stress distribution (including the magnitudes of each) that determines the survivability of a component. With the Weibull analysis, both the flaw and stress distribution throughout a component can be evaluated and related to a probability of success, thus, utilizing the full potential of the material.

The flaw distribution is a characteristic of the particular material that was determined under the material characterization effort of the program. Ceramic specimens of HPSN (NC-132) were tested to fracture in 4-point bend, thus yielding the fracture rate as shown in Figure 6. Once these material parameters (such as characteristic strength and Weibull modulus) were determined, they were then applied to the blade stress model. Integrating the combined flaw and stress distribution through each element of the model, a probability of success can be calculated, and the acceptability of the design can be assessed.

To verify this design approach (the probabilistic, fast-fracture analysis), test specimens of the blade attachment, Figure 7, were analyzed and tested to failure in the whirlpit. The correlation of a group of five of the six fractured attachments with the analytical prediction was excellent. The work not only verified the blade attachment concept, but also gave credibility to this technique of design and analysis of ceramic components.

Even though state-of-the-art materials were to be used in this program, little materials design data relative to turbine components was readily available. A large amount of effort was directed toward characterization of HPSN for the ceramic turbine blade. To obtain design data, it was first required to define the blade fabrication process that would allow full utilization of the strength of HPSN.

Machining studies of HPSN indicated that specimens ground in the stressed direction were 50-percent stronger than specimens ground transverse to the stressed direction, Figure 8. Also, oxidation studies indicated that the effect of some surface defects could be reduced by exposure to an oxidizing environment. Hence, the selected surface oxidation treatment of 1800°F (1255°K) for 50 hours improved transverse grind strength, and reduced data scatter with a slight sacrifice in maximum strength. This oxidation treatment greatly increased machining flexibility, and improved predictability of the final design.

Additional materials testing was accomplished to determine HPSN rupture, creep, and cyclic-fatigue characteristics relative to the blade stresses and temperature occurring in the 50-hour demonstration tests. Since the higher stress levels (of the attachment) are well below the temperature where slow-crack growth becomes significant (Figure 9), fast fracture is the failure mode of primary concern.

Fabrication

Blade manufacturing starts with the 1.5-inch (3.8-cm) thick HPSN billet, Figure 10. These billets are sliced into rectangular blocks on which the attachment is ground by precision diamond-form-wheel grinding. The excess stock around the airfoil is separated by an ultrasonic trepanning and diamond-cutting wheel. Positioned by the attachment, the airfoil and platform are finish ground by pantography. With the corners radiused by hand, the blade is geometrically complete. Since transverse grinding was done on both the attachment and the airfoil, the blade was given the surface oxidation treatment, thus completing the manufacturing steps.

To ensure that the ceramic blades are of the highest possible quality, inspections and rigid controls are incorporated throughout the fabrication process. In addition to material and process specifications for the HPSN billet, certification of the billet strength is required through 4-point bend specimens taken from the center and edge locations of the billet in both the transverse and longitudinal directions. This certification provides both assurance of strength and data for design predictions. Because of the homogeneity and the full density of the HPSN, X-ray and Zyglo-NDE techniques yield reliable indications of material and part integrity. Visual inspection, under magnification, is an essential step in judging surface condition relative to the quality of grinding, and completeness of surface oxidation.

DESIGN CONDITIONS

- ROTOR SPEED 41,730 RPM (4370 RAD/S)
- TIP SPEED 1420 FPS (433 M/S) FIRST STAGE
1464 FPS (446 M/S) SECOND STAGE
- TEMPERATURE 2200°F (1417°K) AVERAGE T_4
2500°F (1644°K) PEAK T_4

DESIGN OBJECTIVES

- 3-D FINITE-ELEMENT ANALYSIS
 - THERMAL
 - MECHANICAL
- PROBABILISTIC EVALUATION
 - WEIBULL CRITERIA
- MINIMUM 95-PERCENT CPS PER STAGE
- 50-HOUR LIFE, 25 2-HOUR CYCLES
- NO BLADE RESONANCE IN OPERATING RANGE

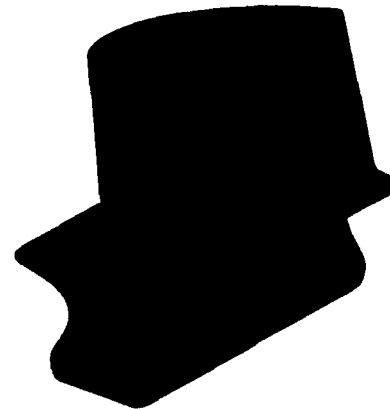


Figure 5. Ceramic Turbine Blade Design.

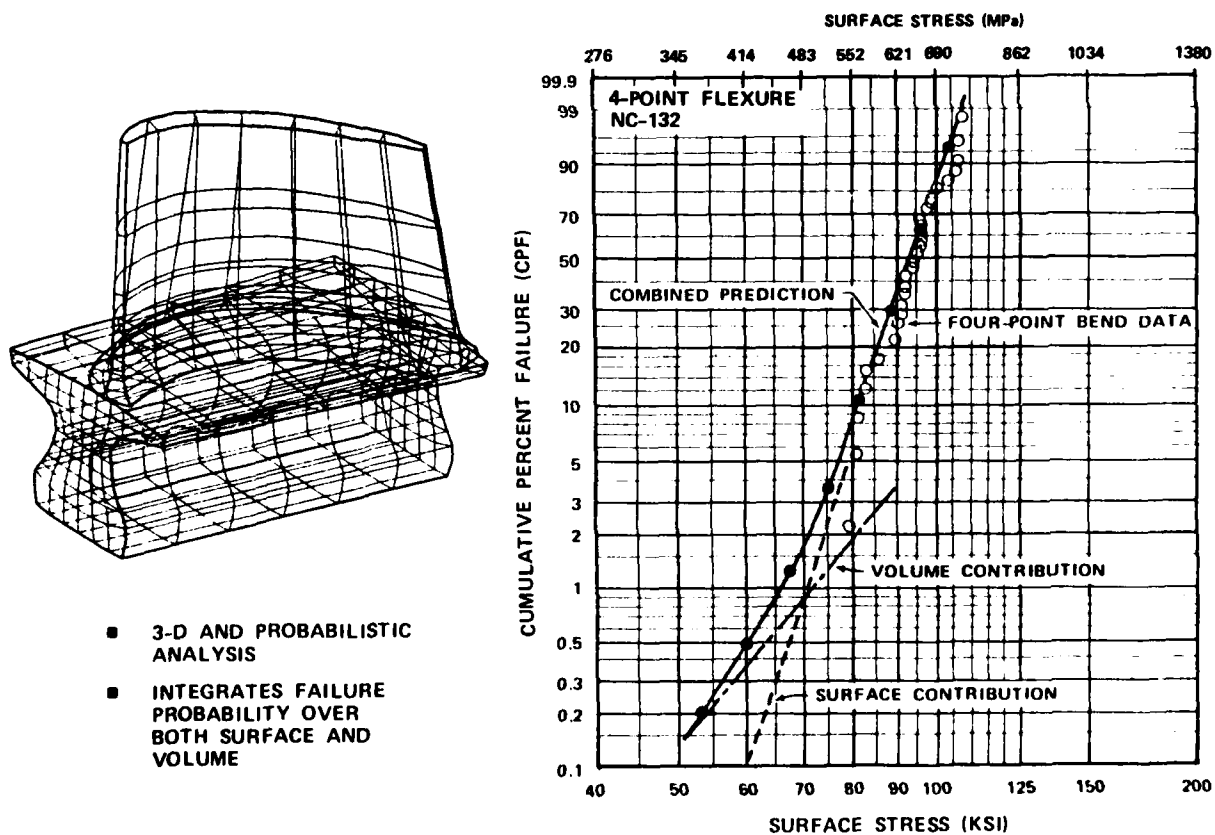
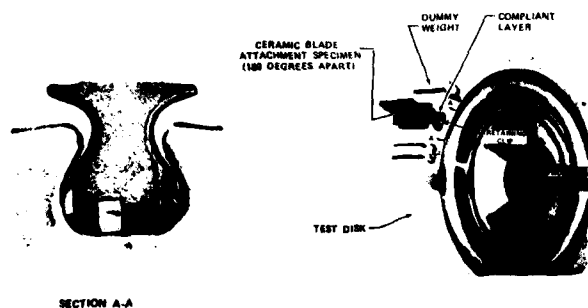
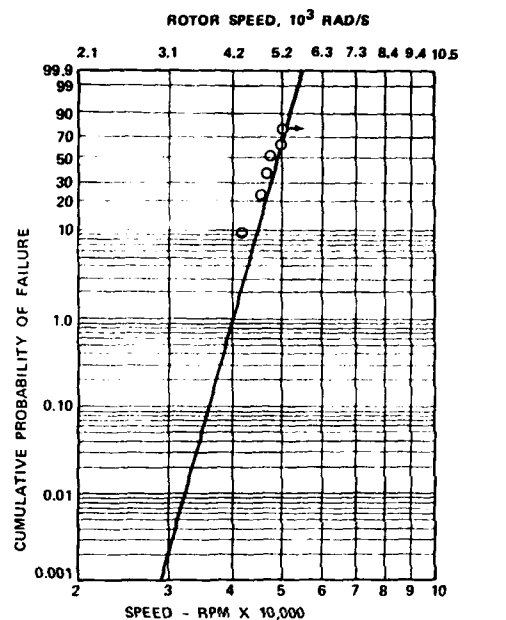


Figure 6. Design Analysis.



WHIRLPIT DISK AND ATTACHMENT CONFIGURATION



○ FAILED SPECIMENS MATERIAL STRENGTH AFTER 50 HR/1800°F (1255°K) OXIDATION TREATMENT

○➔ NO FAILURE

-2C SPECIMEN TEST RESULTS

Figure 7. Ceramic Blade Design Verification.

MATERIALS

- NC-132 HOT PRESSED Si_3N_4

PROPERTIES MEASURED

- STRENGTH VERSUS TEMPERATURE
 - TENSILE
 - 4-POINT FLEXURE
- STRENGTH/SURFACE EFFECTS
 - AS FABRICATED
 - MACHINING ORIENTATION AND TYPE
 - VENDOR QUALIFICATION
- STRENGTH/ENVIRONMENTAL INTERACTIONS
 - STATIC OXIDATION
 - CYCLIC OXIDATION
 - SEA SALT ADDITION
- STRESS RUPTURE AND CREEP
- STRENGTH CHANGE DUE TO CYCLIC FATIGUE
- THERMAL FATIGUE

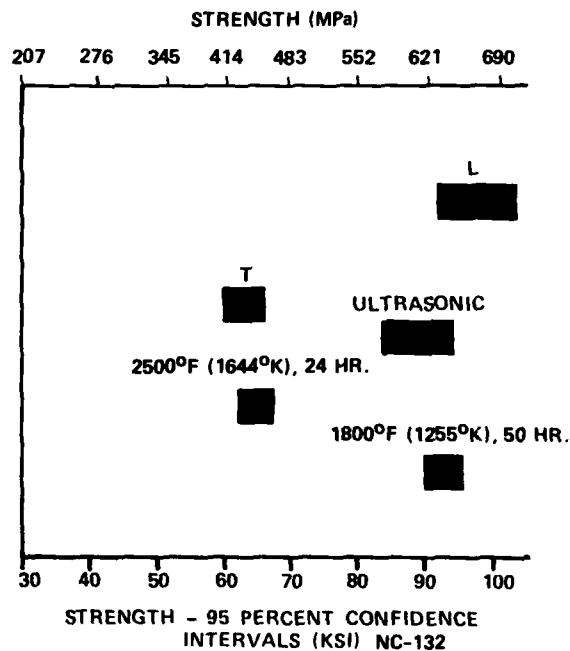


Figure 8. Material Characterization.

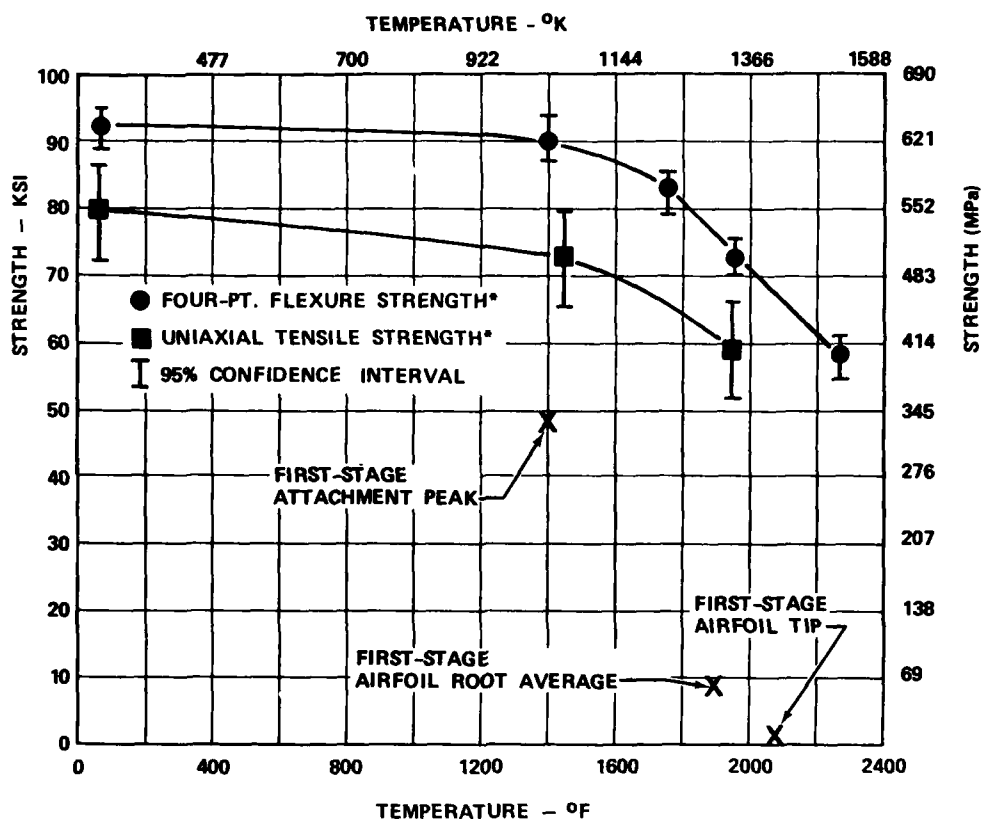


Figure 9. AiResearch Data for NC-132 Hot-Pressed Silicon Nitride and Relative Blade Stress.

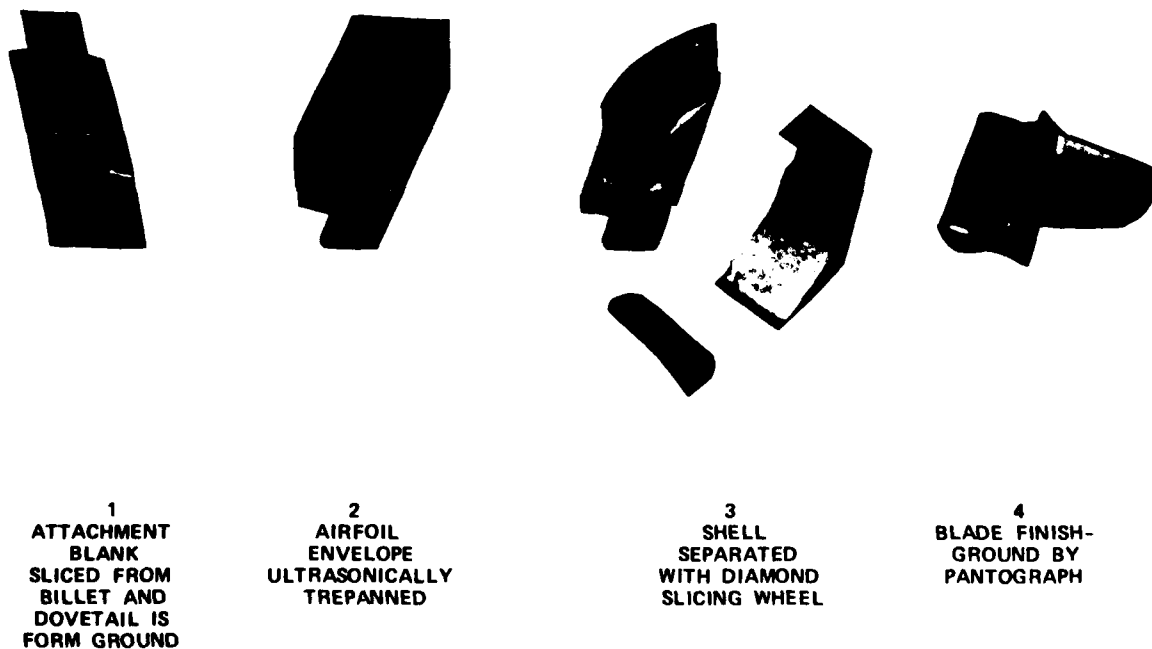


Figure 10. Blade Machining Using Ultrasonic Trepanning and Pantograph Profile Grinding.

Testing

The ultimate check on the ceramic blade integrity (particularly the critical attachment) is the proof test of the blade to 130-percent design speed. Since the principle stress component of the attachment is due to the centrifugal load, the proof test imposes a stress distribution very similar to that in the engine environment. The 30-percent overspeed provides allowances for thermal, bending, and vibratory stresses, plus margin. Since slow-crack growth is not significant at the attachment temperature, the blades can be stressed without doing damage that could cause failure on a subsequent cycle. Since new flaws are not introduced and existing critical flaws will immediately propagate to fail, only defective blades are fractured (rejected) during the proof test. All blades are proof tested prior to rig or engine use. As indicated in Figure 11, proof testing has rejected 6 of 205 blades. This excellent correlation with the analytical prediction verifies the design analysis, as well as the manufacturing process.

Prior to the engine test, the ceramic blades were rig tested to verify their integrity in the high-temperature, vibrational environment, Figure 12. The development sequence progressed from a single stage of ceramic blades with metal vanes, and increased in the number of ceramic components to ceramic blades with complete ceramic static structure. This allows an orderly development with minimum risk and loss of hardware prior to engine testing.

Seven dynamic rig tests were accomplished demonstrating both overspeed and cyclic capability, clearing the way for full-scale engine tests. During rig testing, a second-stage blade attachment failure was incurred. Fracture analysis, Figure 13, revealed the origin to be at the contact edge as opposed to the expected peak stress location. The fracture surface was a smooth, featureless surface (low-energy crack propagation) that was found to be typical of vibration fracture. Dynamic strain-gauge test in the rig indicate the blade flexural vibratory mode to be resonant with nozzle passing (21 vanes) at approximately 36,000 rpm (3770 rad/s). This resonance condition was at a lower speed than anticipated. The drop in blade resonance was the combined effect of slot waviness (due to broach flexibility), and a stiff-compliant layer, HS25, which resulted in incomplete seating of the dovetail attachment. High vibratory stresses with concentrated loading in the contact zone initiated the fracture, which was then propagated by the low-tensile stress causing a low-energy fracture surface. Using a softer-compliant layer (platinum) and lapped-flat slots, the blade flexure resonance was increased to where it correlated with the analysis, Figure 14. To further increase vibratory margin (to 12.7 percent for a minimum frequency blade), the vane count was reduced from 21 to 17. With these changes incorporated to avoid blade resonance, the ceramic blades were submitted for engine test.

Over 24 engine tests were accomplished (through April 1979) accumulating 36 hours of running time, and demonstrating conditions in excess of design to 2249°F (1505°K) average T_4 and 105-percent speed, as summarized in Figure 15. Although the development of the static structure has not been entirely without problems, the mechanical performance of the rotor blades throughout all 24 engine tests has been without incident. Furthermore, an emergency shutdown from full power was also demonstrated with no ceramic blade problems.

CONCLUSION

The ARPA Program, Figure 16, has successfully characterized the HPSN for the blade, and verified the design and fabrication capability allowing utilization of ceramics in a real turbine environment. Subsequent engine testing will be directed toward demonstrating extended life in the engine environment.

The ARPA/Navy ceramic gas turbine program has demonstrated the suitability of the ceramic rotor for limited-life applications. However, to fully exploit the potential of ceramic turbine blades, additional efforts will be required as listed in Figure 17. Current manufacturing costs are high, and reduction through reduced machining cost or net-shape casting could be important to a decision to enter production. The demonstrated long-life and high-temperature capabilities of ceramics in a turbine environment must be extended for broadening the future ceramic applications. In addition, further research into impact resistance and contact-stress tolerance is recommended, as expansion of these capabilities may be required for some applications.

MATERIAL

- POWDER QUALITY CONTROLLED
- RIGID PROCESS CONTROL
- BILLET X-RAY
- BILLET CERTIFICATION

MANUFACTURING

- X-RAY PRIOR TO AIRFOIL GRIND
- GEOMETRIC INSPECTIONS
- FINAL X-RAY AND ZYGLO
- 40X VISUAL INSPECTION BEFORE AND AFTER OXIDATION

PROOF TEST

- ALL BLADES
- OVERSPEED TO 130-PERCENT DESIGN SPEED
- 40X VISUAL INSPECTION POST TEST

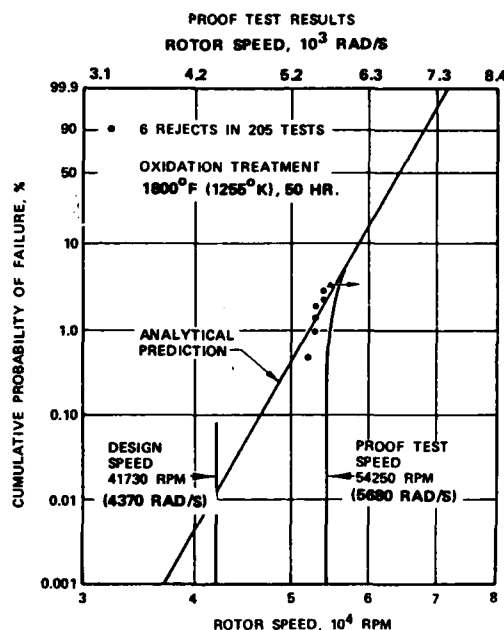
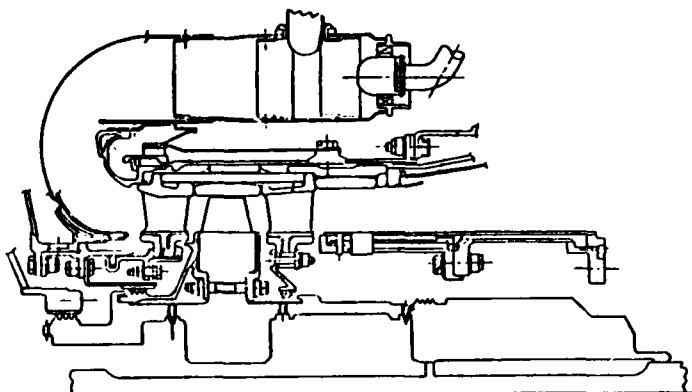


Figure 11. Ceramic Blade Quality Assurance.

ROTATING RIG**28 TO 79 CERAMIC PIECES****TEST SUMMARY**

- SEVEN RIG TESTS
- INSTRUMENTED TEST IDENTIFYING BLADE RESONANCE
- DEMONSTRATED OVERSPEED MARGIN
110 PERCENT - COLD
108 PERCENT - HOT
- DEMONSTRATED 25 CYCLES
- VERIFY CERAMIC BLADE FOR ENGINE TEST

Figure 12. Dynamic Rig Test.

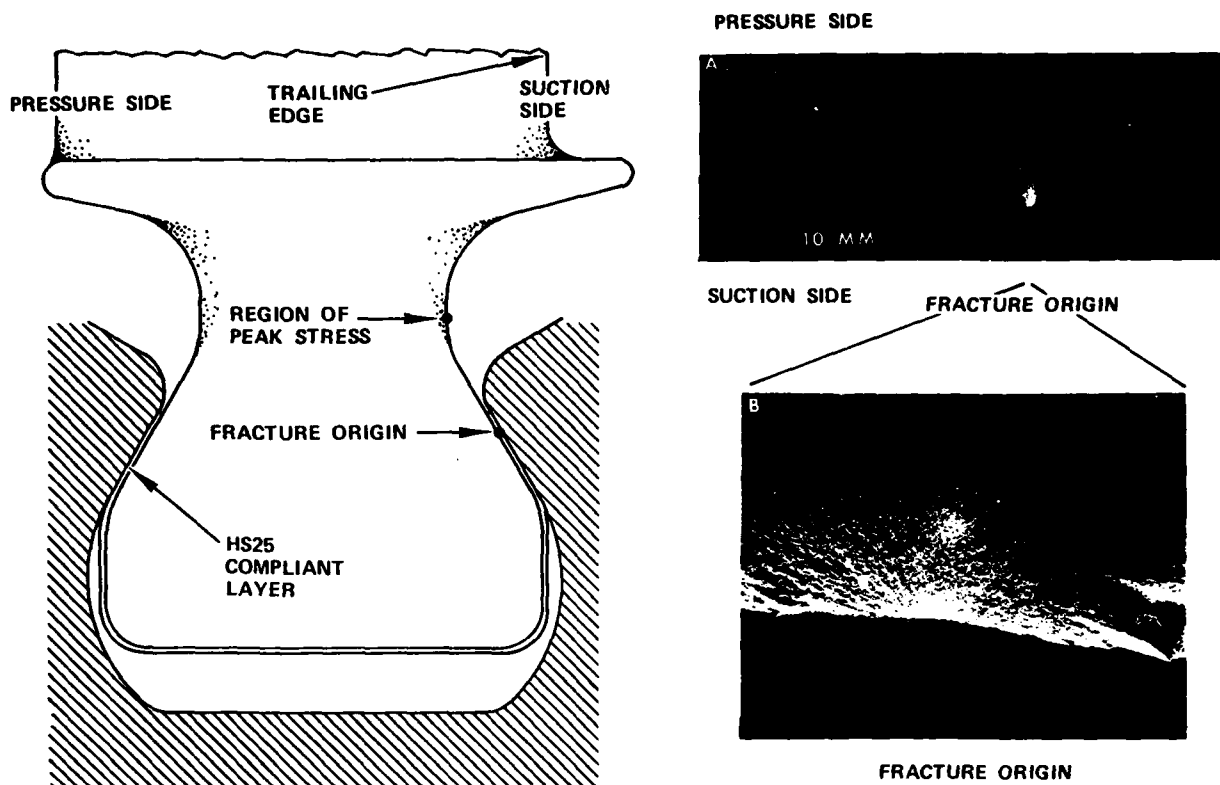


Figure 13. Vibration Investigation.

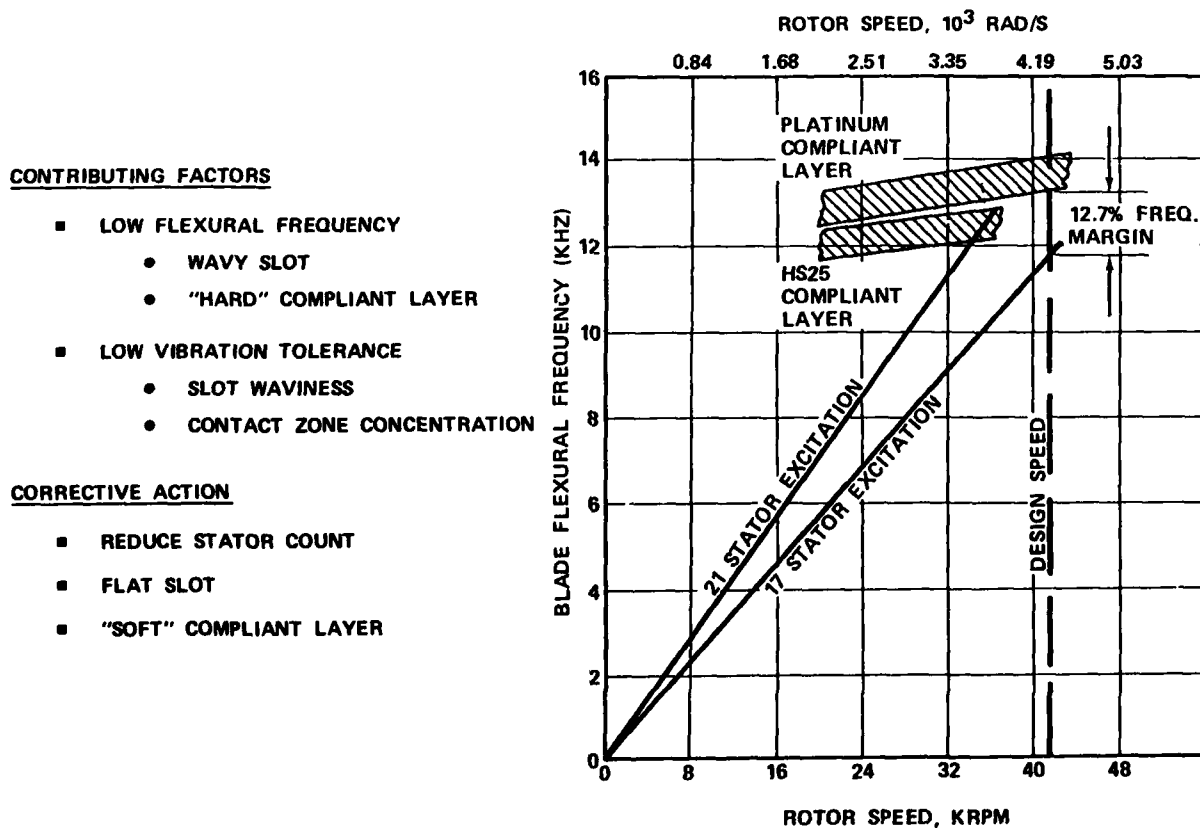
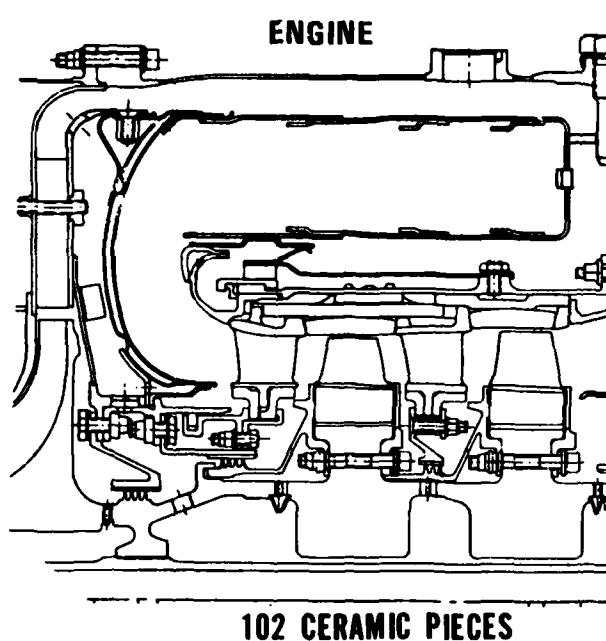


Figure 14. Vibration Investigation.



ENGINE TEST SUMMARY CERAMIC TURBINE*

- 24 ENGINE TESTS
- 36 HOURS
- FULL-DESIGN CONDITIONS
- 2249°F (1505°K) MAX T_4 RECORDED
- 105-PERCENT SPEED
- EMERGENCY SHUTDOWN FROM 2200°F (1477°K) T_4 CONDITION
- NO BLADE PROBLEMS NOTED IN ENGINE TESTS

*THROUGH APRIL 1979

Figure 15. Ceramic Engine Test.

- DESIGN CAPABILITY VERIFIED
- NC-132 HPSN CHARACTERIZED
- MANUFACTURING PROCESSES ESTABLISHED
- NDE TECHNIQUES DEVELOPED
- DEMONSTRATED CERAMIC BLADES TO FULL-DESIGN CONDITIONS
- ENGINE TEST PROGRAM EXTENDING DEMONSTRATED LIFE
- NO BLADE PRIMARY FAILURES IN ENGINES

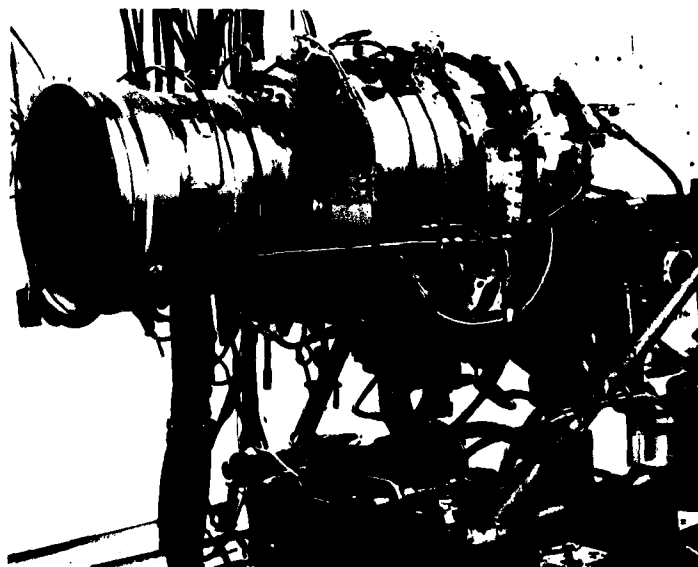


Figure 16. Ceramic Blade Accomplishments.

- LOW-COST FABRICATION TO NET SHAPE
- DEMONSTRATED LONG-LIFE/HIGH-TEMPERATURE CAPABILITY
- INCREASED IMPACT RESISTANCE
- INCREASED UNDERSTANDING OF CONTACT STRESSES

Figure 17. Future Ceramic Blade Technology Efforts.

DUO-DENSITY CERAMIC TURBINE ROTOR--CONCEPTS, MATERIALS PROCESSES AND TEST RESULTS

R. R. Baker and A. F. McLean
Engineering and Research Staff
Ford Motor Company
Dearborn, Michigan 48121

ABSTRACT

The duo-density ceramic turbine rotor concept utilizes the high strength of hot pressed silicon nitride in the simple-shaped hub and adequately high strength of reaction bonded silicon nitride for the complex-shaped blades which can be readily formed by injection molding or slip casting. Design concepts, materials and fabrication process for making duo-density rotors are presented including recent developments in Ford's hot press/press bonding process.

Background and status of the Ford/DARPA rotor testing program is presented including cold spin test and hot spin test results on duo-density rotors. Recommendations are presented for follow-on work.

INTRODUCTION

The progress of the gas turbine engine has been and continues to be closely related to the development of materials capable of withstanding the engine's environment at high operating temperature. Today's nickel-chrome superalloys are in use, without cooling, at turbine inlet temperatures of 982°C (1800°F). Ford Motor Company has been developing ceramics for gas turbine applications for over 10 years as the use of ceramics promises to make a major step in increasing turbine inlet temperatures to 1370°C (2500°F). Such engines offer significant advances in efficiency, power per unit weight, cost, exhaust emissions and materials utilization. (1)

In 1971, Ford Motor Company and the Defense Advanced Research Projects Agency (DARPA) initiated a program to develop and encourage the use of brittle materials for engineering applications, particularly demanding high temperature structural applications. The primary objective was to develop ceramic components for the entire hot flowpath of a high temperature vehicular gas turbine engine and demonstrate their survival for 200 hours over a duty cycle comprising 175 hours at an average turbine inlet temperature of 1054°C (1930°F) and 25 hours at 1370°C (2500°F). A schematic of the flowpath showing the ceramic components is shown in Figure 1.

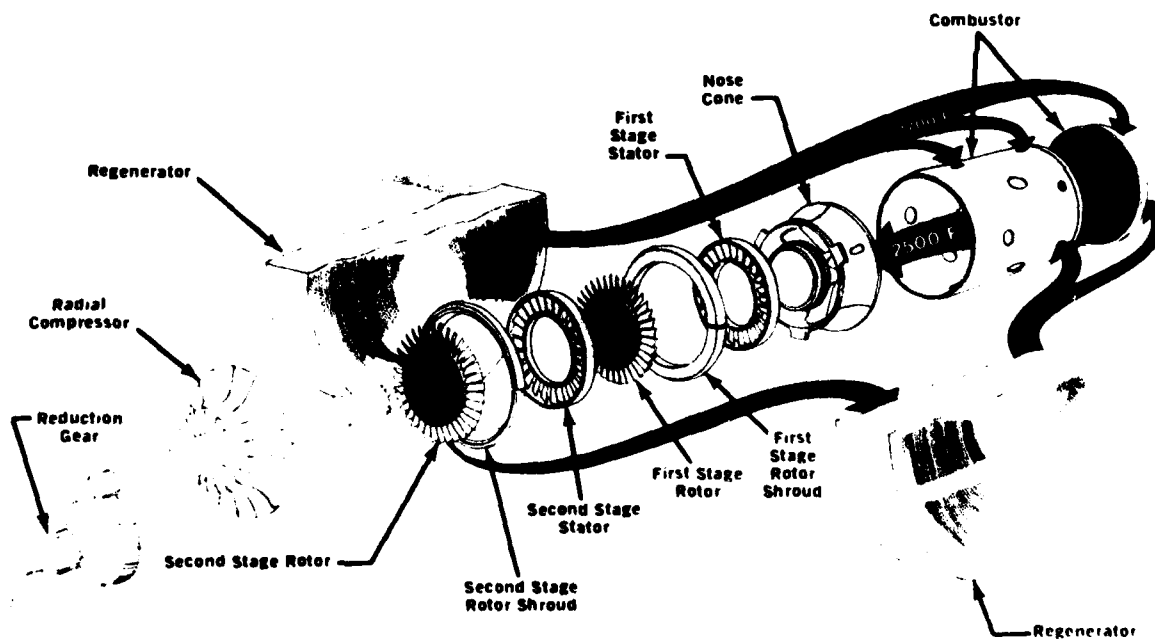


Figure 1 Schematic View of the Vehicular Gas Turbine Engine Flowpath

In 1977, the Department of Energy (DOE) joined with the Defense Advanced Research Projects Agency in partial support of Ford's work on the "Brittle Materials Design, High Temperature Gas Turbine" program (Figure 2). DARPA continued to support testing of ceramic components which subsequently met the program durability goal of 25 hours at 1370°C (2500°F) plus 175 hours at 1054°C (1930°F) Turbine Inlet Temperature.(2) DOE started to support process development to improve the quality of silicon nitride turbine rotors in addition to some work on ceramic materials characterization and development of nondestructive evaluation techniques. The Army Materials and Mechanics Research Center (AMMRC) continued to function as the technical monitor of the overall program.

The design of the vehicular turbine engine requires many complex shaped ceramic components. The most complex shaped and highly stressed components are the all-ceramic turbine rotors which have forced the development of new techniques. A major research effort was conducted on rotor fabrication. As reported at the 1977 Ceramics for High Performance Applications-II Conference, in Newport, Rhode Island,(3) all of the known major candidate approaches were investigated for making an all-ceramic rotor in silicon nitride or silicon carbide. The most advanced thus far is the duo-density rotor concept, shown in Figure 3, which was conceived to employ both hot pressed and reaction bonded silicon nitride. This concept utilizes the high strength of hot pressed silicon nitride in the simpler shaped hub where stresses are highest but temperatures are moderate and, therefore, creep and/or slow crack growth resulting from the use of a densification additive is minimized. Reaction Bonded Silicon Nitride (RBSN), which can be readily formed into complex airfoil shapes by injection molding or slip casting, is utilized for the blades. Another major advantage in using RBSN for the blades is its superior resistance to slow crack growth at the high operating temperatures encountered during service. It should also be noted that the lower density RBSN results in lower centrifugal stresses in the blades. This concept, which has undergone many iterations in design, material compositions and fabrication processes, relies on the ability to diffusion bond the two silicon nitride components (blade ring and hub) into an integral turbine rotor by employing hot-pressing technology.

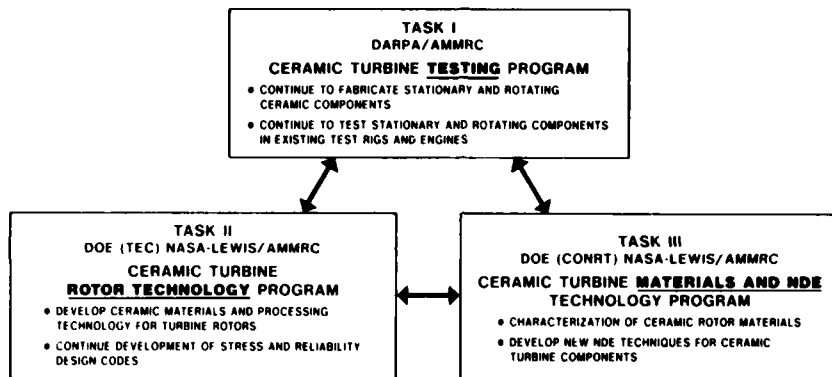


Figure 2 DARPA/DOE Supported Tasks in the "Brittle Materials Design, High Temperature Gas Turbine" Program

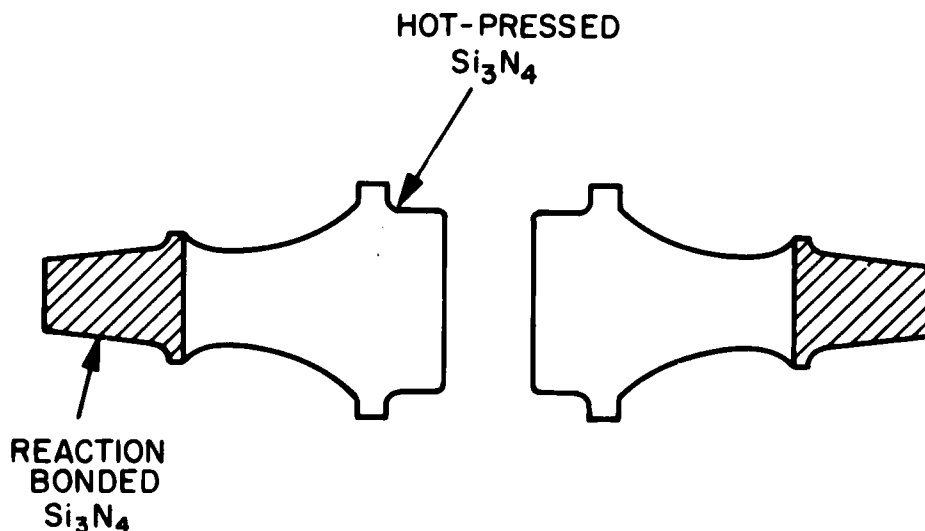


Figure 3 Duo-Density Silicon Nitride All-Ceramic Turbine Rotor

ROTOR FABRICATION

Reaction bonded silicon nitride blade rings (Figure 4) were fabricated in early 1975 using a disposable mold slip-casting technique.⁽⁴⁾ The major problems encountered were primarily due to the complex shape of the 36 tapered and twisted blades attached to the blade ring rim.

The majority of blade rings have been fabricated using the injection molding process in which the 36 complex shaped airfoils and the blade ring rim were formed as an integral part in one shot (Figure 5). The green, as-molded, blade ring was then burned out to remove the organic binders leaving a silicon metal compact, which was subsequently nitrided to 2.7 g/cc density reaction bonded silicon nitride. Many iterations of die design, molding mix composition and molding parameters were required to eliminate gross blade cracks of the type shown in Figure 6. The development of the injection molding process, including the solid state injection molding system, was covered in detail at the Newport Meeting.⁽⁵⁾ Improvements which have been made since then are presented later in this paper in the section on processing improvements.

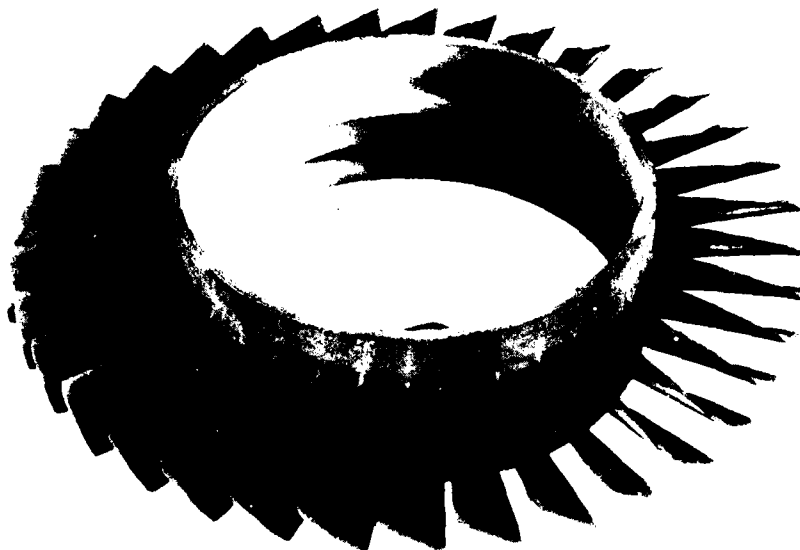


Figure 4 Slip Cast Turbine Rotor Blade Ring



Figure 5 Injection Molded Blade Ring



Figure 6 Blade Root Crack Formed During Injection Molding

During the development of the hot press bonding process, in which the hub is simultaneously densified by hot pressing and diffusion bonded to the blade ring, it became apparent that the blades and blade ring rim must be supported and also protected from the carbonaceous hot pressing environment.⁽⁶⁾ This was accomplished by slip casting a blade fill in which the first operation consisted of casting extractable inserts between the blades as shown in Figure 7. The blade ring was coated with Boron Nitride which acts as a lubricant for subsequent blade fill removal and as a barrier material to prevent blade ring to blade fill bonding during nitriding. The BN coated blade ring in the tooling is shown in Figure 8. A silicon metal slip was introduced centrifugally into the cavities between the blades through the access holes in a silastic rubber ring. This assembly was dried, again coated with boron nitride and a second blade fill cast in a rectangular shape. Controlling the thicknesses of the BN layers (Figure 9) was determined to be critical in order to prevent cracking of the blades during subsequent hot press bonding.⁽⁷⁾ If the BN was too thick in the rim region, the blade ring rim deformed and compressed the BN until the BN either supported the rim or the rim fractured. On the other hand, if the BN was too thin, the blade ring was bonded to the blade fill during the nitriding process making removal of the blade fill impossible. A thicker coating of BN was desirable on the airfoils so that small motions of the blades were accommodated without resulting in cracking of the blades.

The blade filled blade ring was then placed in graphite tooling as shown in Figure 10. The development of the tooling was covered in detail at Newport⁽³⁾ and subsequent refinements presented in reference 8. The hub was formed and simultaneously bonded to the blade ring by applying a pressure of 6895 kPa (1000 psi) for 2 1/2 hours at a temperature of 1715°C. After cooling, the blade fill was removed and the rotor machined to the contour previously shown in Figure 3.

COLD SPIN TESTING

All rotors which were to be hot tested in the hot spin rigs or engines were cold spin tested to eliminate flawed blades of the type shown in Figure 11. Two levels of cold spin qualification testing were set; 55,000 rpm for rotors to be hot tested to 50,000 rpm and 70,000 rpm for rotors to be hot tested to 64,240 rpm. Nine out of 16 rotors achieved 55,000 rpm or higher without blade failures; however, 14 out of 17 failed one or more blades while in the process of being qualified to 70,000 rpm. Figure 12 shows the Weibull distribution of 1977 vintage rotors. Also shown in this figure is the Weibull distribution representing the state-of-the-art in 1975.⁽⁹⁾ The data, while still not at desired levels, shows significant improvements in rotor processing as the 1977 vintage rotors demonstrated a cold spin reliability almost two orders of magnitude greater than the state-of-the-art in 1975.

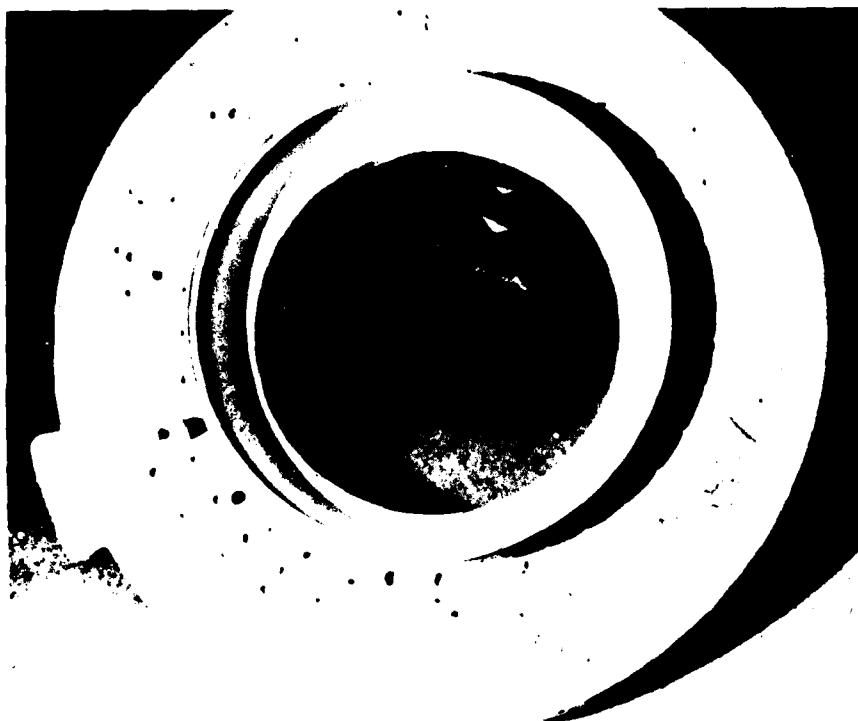


Figure 7 Rotor Blade Ring with First Blade Fill

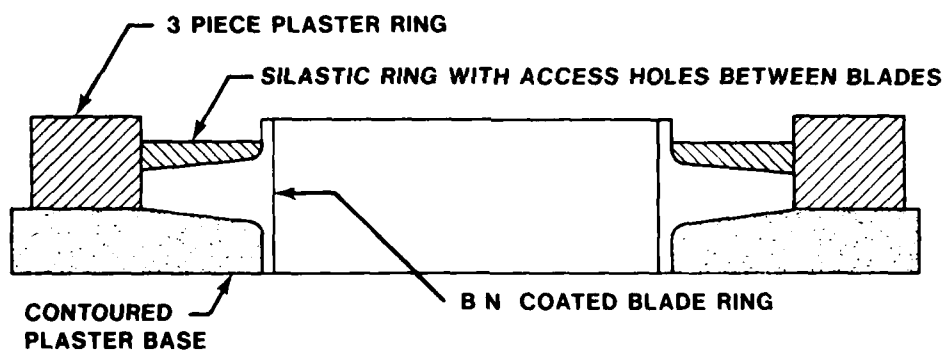


Figure 8 Schematic of First Blade Fill Operation

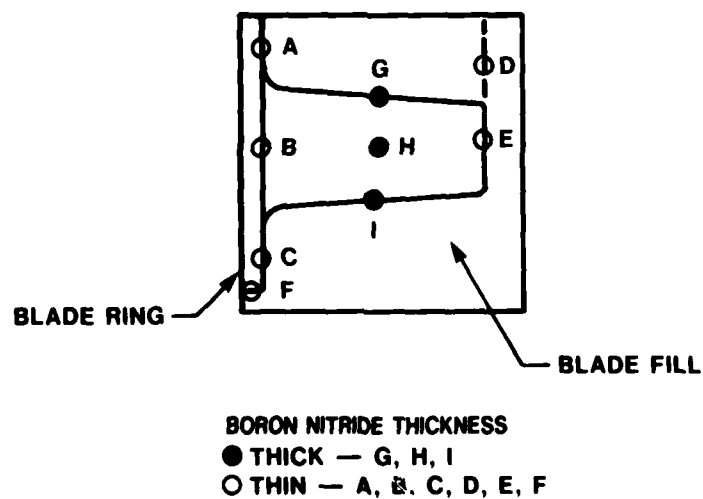


Figure 9 Blade Filled Blade Ring Showing Boron Nitride Layers

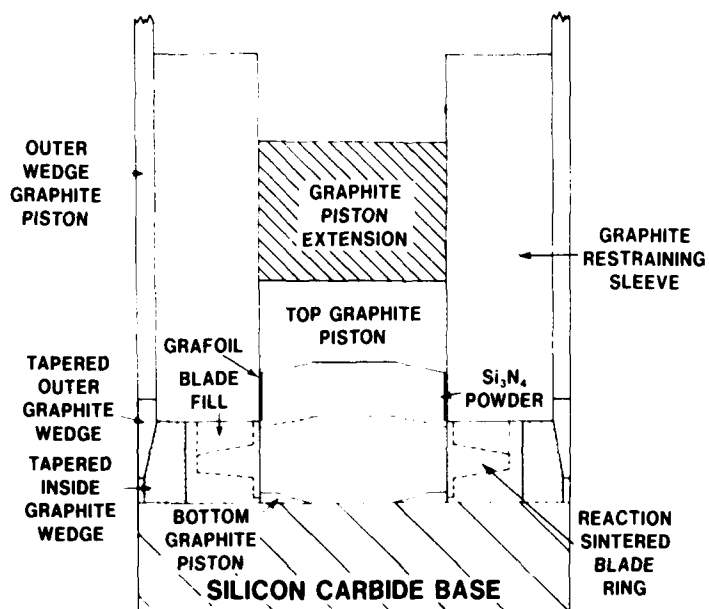


Figure 10 Simplified Two Piece Hot Press Bonding Configuration

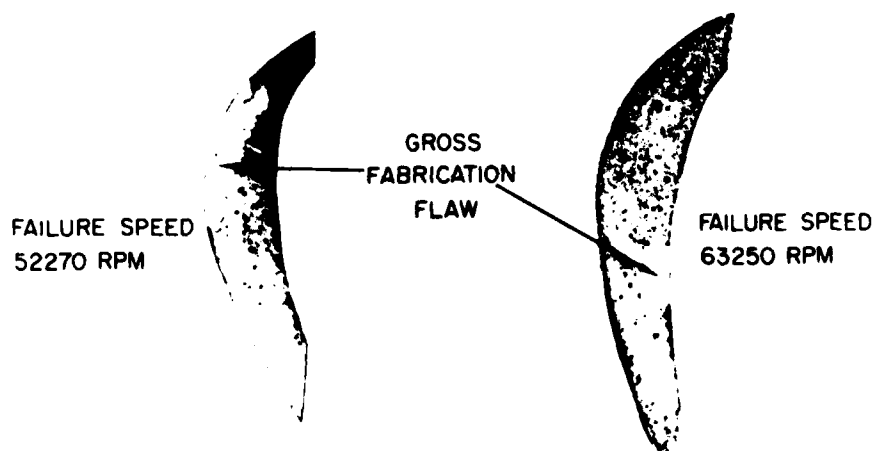


Figure 11 Typical Fracture Surfaces with Gross Fabrication Flaws

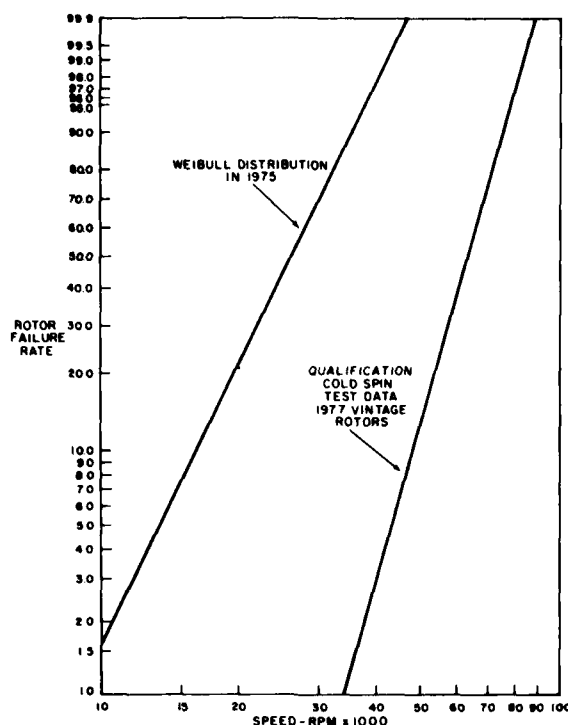


Figure 12 Weibull Distribution of Rotor Failures

ROTOR TESTING

A series of rotor tests were conducted with 1977 vintage rotors. One rotor as shown in Figure 13 with its shaft and rotating attachment hardware, was successfully tested in an engine for 10 hours at a speed of 45,000 rpm and an average turbine inlet temperature of 1232°C (2250°F). Included in the test were all the associated stationary ceramic flowpath components. Following shutdown and inspection, the same rotor and stationary ceramic components were successfully tested for 25 hours at 50,000 rpm and 1232°C (2250°F) average turbine inlet temperature and then at 1370°C (2500°F) for 1-1/2 hours. During this testing, excessive temperatures were noted, as shown in Figure 14, near the front metal curvic used in the rotor ceramic-to-metal attachment system. As a result, in terminating this successful test sequence, a failure occurred during shutdown. Post test examination revealed bits of ceramic curvic teeth embedded in the metal front curvic washer substantiating that the problem was due to the high attachment temperatures. Design modifications to redirect the attachment bolt cooling air and thereby increase cooling of the metal curvic were incorporated and a second rotor was engine tested later in the year. This test was again at 1370°C (2500°F) average turbine inlet temperature and included two shutdowns: one a normal shutdown, and the other a sudden emergency shutdown. The rotor and stationary ceramic parts survived this engine testing with no apparent damage.

A major objective was to hot spin test six duo-density silicon nitride rotors at 50,000 rpm and 982°C (1800°F) rim temperature for 25 hours or until failure. A rim temperature of 982°C (1800°F) corresponds to a turbine inlet temperature of 1149°C (2100°F). Figure 15 shows a schematic of the hot spin test rig used for these tests. A major goal during development of the hot spin test rig was to retain features of relatively inexpensive and timely parts replacement to facilitate rotor testing-to-failure. The six rotors selected for this testing were each finish machined with a wider disc throat than originally designed as a result of a lifetime reliability analysis conducted earlier in the year using the latest material and statistical time-dependent strength characteristics. Results of the test series are shown in Table 1. The first two rotors failed during acceleration to full speed and this was traced to problems in the rotor attachment system. This was a conical attachment system selected for the hot spin rig to reduce rig post-failure turn-around time and cost.

It's important to note, however, that these rotors did not fail due to centrifugal and thermal stresses. As a result of this problem, an improved design curvic attachment system which was proven successful in engine testing was utilized in the rig for testing the remaining four rotors. As can be seen from Table 1, each one successfully completed the objective 25-hour test. During some cases of disassembly of the rotor from its shaft, there was a "pinging" sound and subsequent very careful inspection revealed minute cracks in the vicinity of the ceramic curvic teeth. It also became apparent from temperature sensitive paints that the metal front curvic washer was running at a higher temperature than desired. While the stationary hardware adjacent to the rotor in the hot spin test rig is different from that used in the engine, the high metal curvic temperature was a similar problem to that experienced in the engine. Consequently a design modification was made as shown in Figure 16 and was based on the earlier engine modification to redirect the attachment bolt cooling air and thereby increase cooling of the metal curvic.

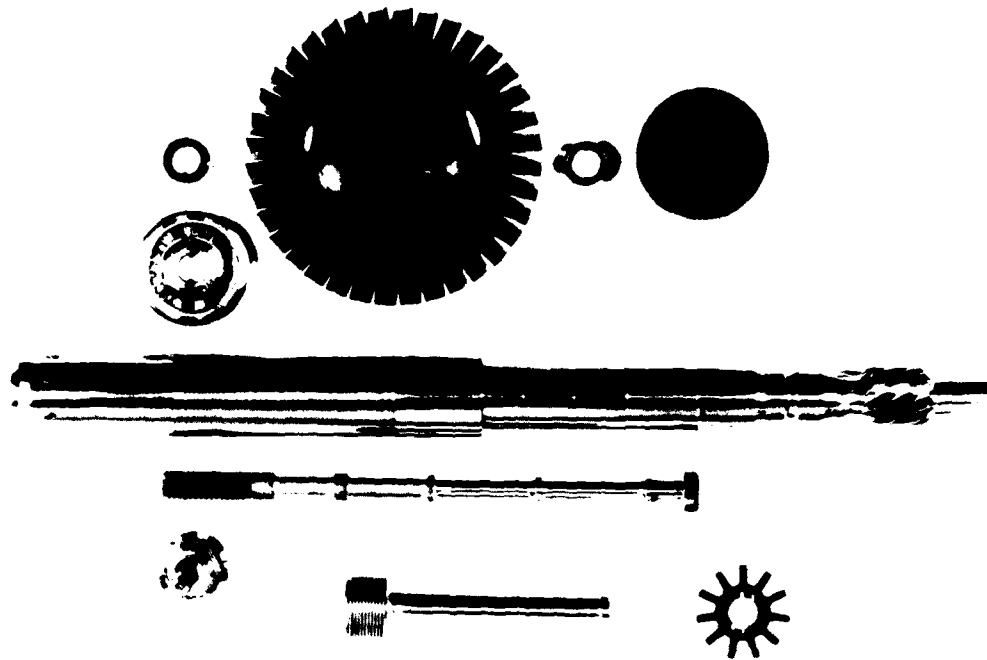


Figure 13 Ceramic Turbine Rotor 1195, Attachment Hardware and Main Shaft

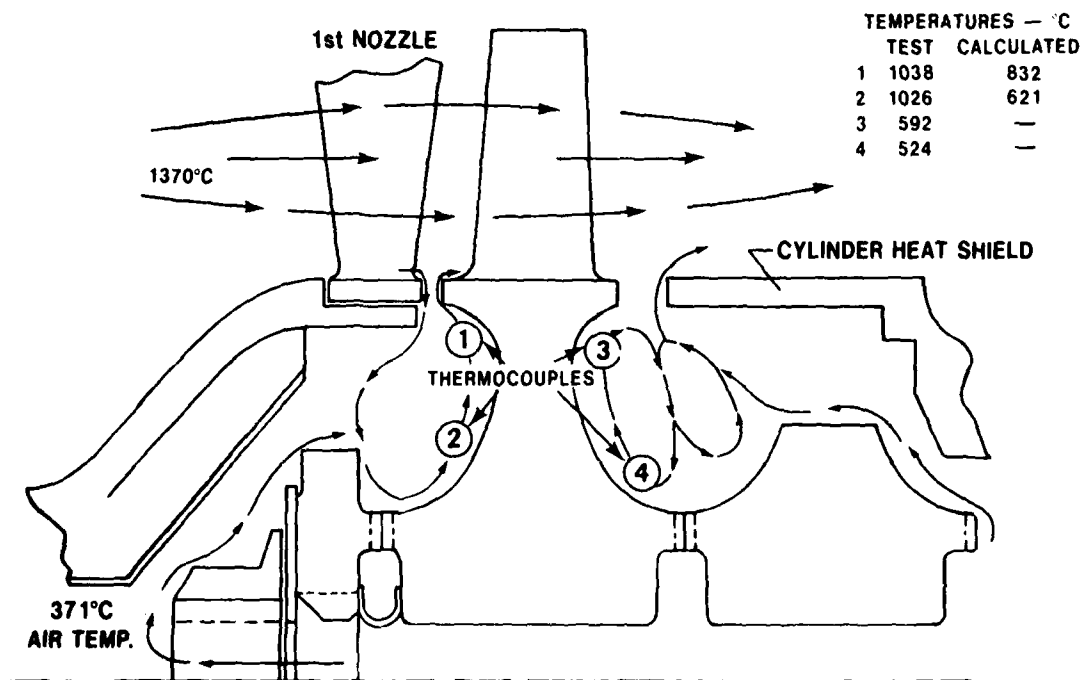


Figure 14 Cross-Sectional View Showing Rotor Front Face Cavity

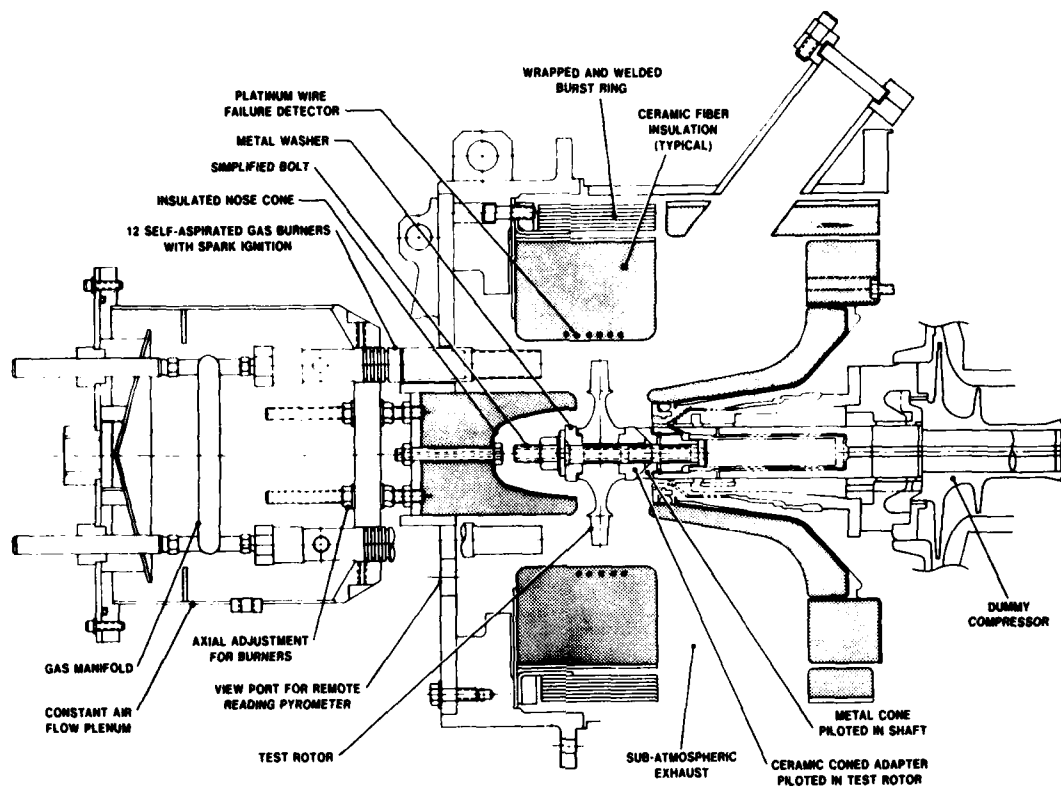


Figure 15 Early Configuration of Hot Spin Test Rig

TABLE 1 - HOT SPIN RIG TEST RESULTS

<u>ROTOR</u>	<u>ROTOR RIM TEMP., (°C)</u>	<u>RPM</u>	<u>TIME (HR.)</u>	<u>RUN</u>	<u>SURVIVED SHUTDOWN</u>	<u>DISASSEMBLY</u>	<u>PROBABLE CAUSE OF FAILURE</u>
1	982	32,000	--	NO	--	--	SIMPLIFIED BOLT AND MOUNTING
2	982	~ 24,000	--	NO	--	--	SIMPLIFIED BOLT AND MOUNTING
3	982	50,000	25	YES	YES	NO	RESIDUAL STRESS IN CURVIC ATTACHMENT
4	982	50,000	25	YES	YES	NO	RESIDUAL STRESS IN CURVIC ATTACHMENT
5	982	50,000	25	YES	YES	YES	AUDIBLE PING ON DISASSEMBLY BUT NO DETECTABLE FLAW OR CHIP
6	982	50,000	25	YES	YES	YES	NO AUDIBLE SOUNDS ON DISASSEMBLY

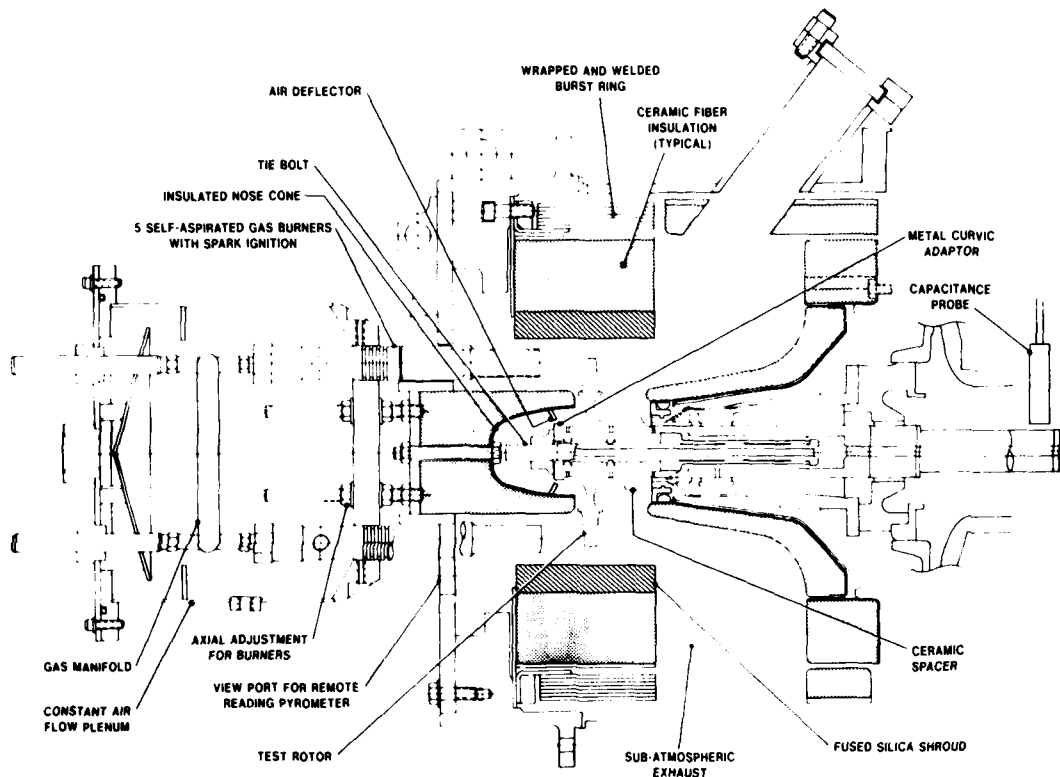


Figure 16 Hot Spin Rig Present Configuration

The curvic cooling modification was incorporated and checked out using an available bladeless rotor hub and following this duo-density rotor #1306, shown in Figure 17, was installed in the hot spin test rig. The objective was to complete the 200 hour durability test over a composite of the ARPA duty cycle as shown in Figure 18. The 100% speed condition was set at 50,000 rpm, which for the size rotor tested is representative of maximum speed for a three stage turbine. The temperature was increased from the original goal of 1054°C (1930°F) to 1149°C (2100°F) over 175 of the 200 hours. It is very encouraging that this first attempt to complete a 200-hour rotor durability test was successful. The visual appearance of the rotor after the test, Figure 19, indicated the rotor to be unaffected by the test.

The next phase of the program was to test a rotor for 25 hours at 64,240 rpm and 982°C (1800°F) rotor platform temperature. A series of tests, summarized in Table 2, have been conducted in an attempt to meet this objective. These tests have been conducted with the present rig configuration as previously shown in Figure 16. Only one of the rotors has reached 64,240 rpm, rotor 1312, and it was destroyed when a flame tube vibrated loose and worked forward striking the rotor. Four of the other rotors were completely destroyed during the acceleration from 50,000 rpm to 64,240 rpm. The three rotors which failed at low speeds, 10,000 to 23,000 rpm were different in nature as the hubs remained intact after the test while the blades and blade ring rim spalled off as shown in Figure 20.

ANALYSIS OF TEST RESULTS

A time dependent reliability analysis was conducted on the rotor configuration and operating conditions of the four rotor tests, (10) which successfully completed 25 hours of operation at 50,000 rpm and 982°C (1800°F) rim temperature (Table 1). The estimated time dependent reliability was 0.95525 at 25 hours. Although no obvious time dependent failures have been encountered in rotor testing, it is possible to estimate the demonstrated reliability using Bayes formula applied to the success run theorem. (11)

$$R_c = (1 - C)^{\frac{1}{N+1}}$$

where R_c = minimum demonstrated reliability
 C = confidence level of prediction
 N = number of successful trials with no failures

The minimum demonstrated reliability by four successes and no time dependent failures is 0.87055 at 50% confidence. It is interesting to note that in order to demonstrate a minimum reliability of 0.95525, 14 successive tests would be required without encountering any failures. (11)

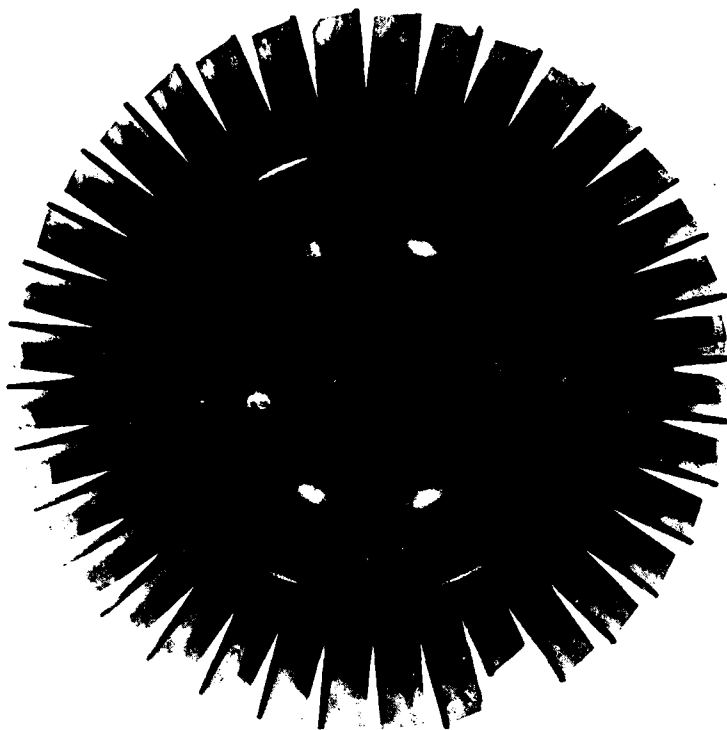


Figure 17 Duo-Density Silicon Nitride Turbine Rotor 1306 Before Test

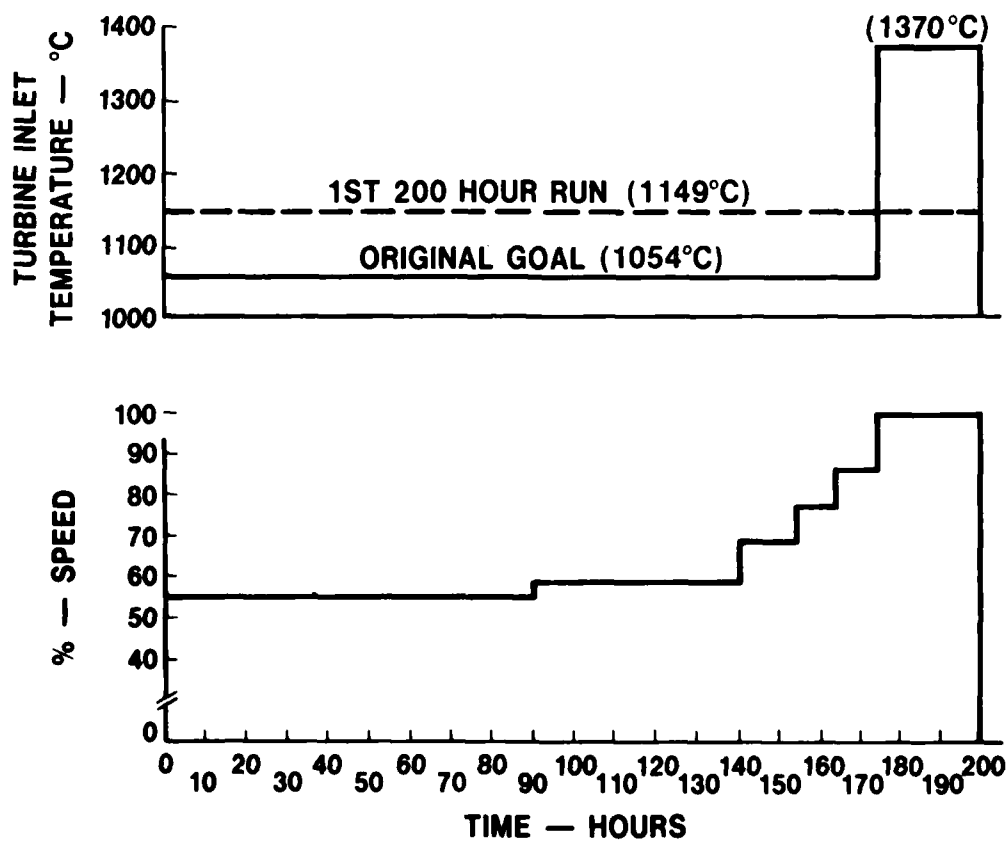


Figure 18 Duty Cycle for Ceramic Rotor Demonstration



Figure 19 Duo-Density Silicon Nitride Turbine Rotor 1306 After 200 Hours

TABLE 2 - 64240 RPM SPEED TESTS
PRESENT RIG CONFIGURATION

<u>Rotor Serial Number</u>	<u>Blade Ring Serial Number</u>	<u>Number of Blades During Hot Test</u>	<u>Rim Temperature °C</u>	<u>Speed RPM</u>	<u>Time Hours</u>	<u>Comments</u>
1312	2142	28	982	64240	1-3/4	Flame tube fell into rotor causing failure
1329	2274	24	982	52800	--	Complete rotor failure
1357	2317	19	982	57100	--	Complete rotor failure
1364	2336	24	982	55400	--	Complete rotor failure
1368	2350	36	982	10000	--	Blade/rim spalling
1382	1323	29-1/2	982	23000	--	Blade/rim spalling
1392	2371	23	982	10000	--	Blade/rim spalling
1395	2353	25	982	60600	--	Complete rotor failure



Figure 20 Blade/Rim Spalling of Rotor 1392

A correlation analysis of cold spin rotor hub failures with the calculated failure distribution was conducted in 1976.(6) Fourteen hot pressed silicon nitride rotor hubs were made under as identical conditions as possible. Five of the hubs were sectioned to provide the material strength data for the analytical prediction while the remaining nine hubs were cold spun to failure. The results are shown in Figure 21. The calculated failure distribution (characteristic speed 103,800 rpm, Weibull modulus $m = 16.8$) was within the 90 percent confidence band of the experimental data (characteristic speed 108,500 rpm, Weibull modulus $m = 14.8$). This confirmed the use of fast fracture Weibull theory in predicting cold spin failures.

The prediction of fast fracture failures at elevated temperatures is more complex due to the combined thermal and centrifugal stresses in the rotor. Speed can be controlled precisely but thermal gradients and hence thermal stresses are much more difficult to predict and control. The measurement of high temperature material properties is also more difficult; however, fast fracture reliability analyses were conducted for the rotors tested in the hot spin rig. The estimated reliability was 0.985 at 50,000 rpm(10) and 0.846 at 64,240 rpm, hence the predicted failure rates were 1.5% at 50,000 rpm and 15.4% at 64,240 rpm. The Weibull distribution of the test results previously presented in Tables 1 and 2 with the low speed blade/rim spalling failures eliminated, is shown in Figure 22. The predicted failure rates fall within the 99 percent confidence band of the experimental data indicating a reasonable correlation.

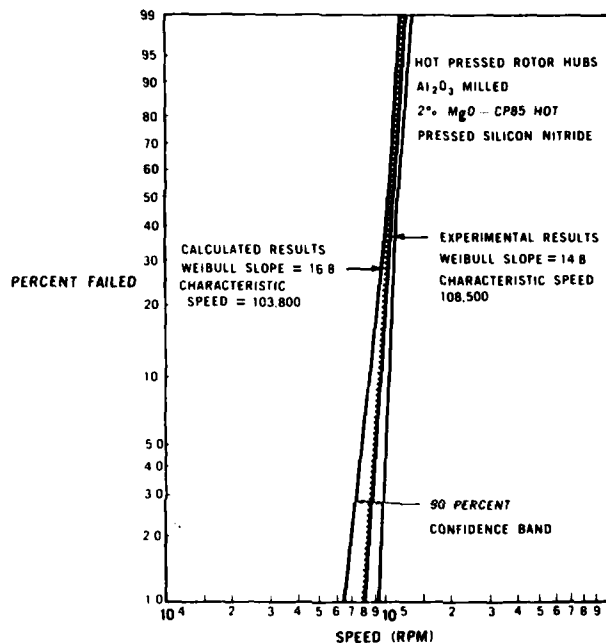


Figure 21 Predicted and Actual Weibull Distributions of Cold Burst Rotor Hubs

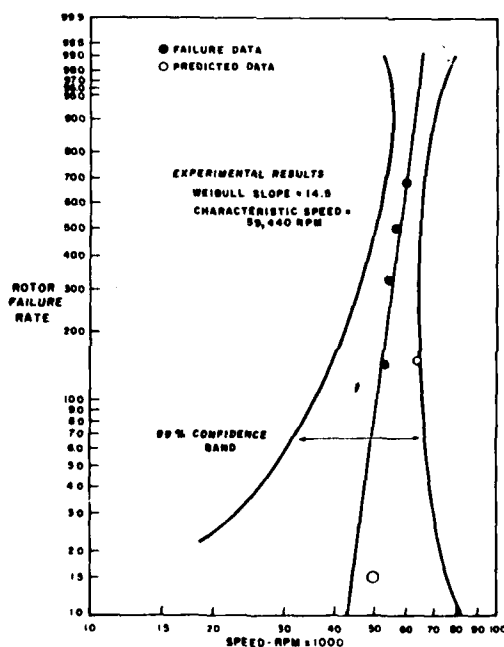


Figure 22 Predicted and Actual Weibull Distribution of Hot Burst Rotors

PROCESSING IMPROVEMENTS

Some rotors produced during the development of the simplified two-piece hot press bonding concept were cold spin tested to failure. The test results of one rotor were particularly interesting as 10 unflawed blades failed in the 87,100 to 96,900 rpm speed range. Typical fracture surfaces are shown in Figure 23. The Weibull distribution representing this data is shown in Figure 24 along with the qualification test results of 1977 vintage rotors previously shown in Figure 12. The potential for unflawed, improved process rotors is shown dramatically by comparing the failure rates at 70,000 rpm for 1977 rotors (80% failure rate) to that for unflawed, improved process rotors (8% failure rate), a ten-fold reduction in failure probability. As a result, a program was initiated to improve the rotor fabrication process by improving the injection molding and hot press bonding processes.



Figure 23 Typical Fracture Surfaces Without Gross Fabrication Flaws

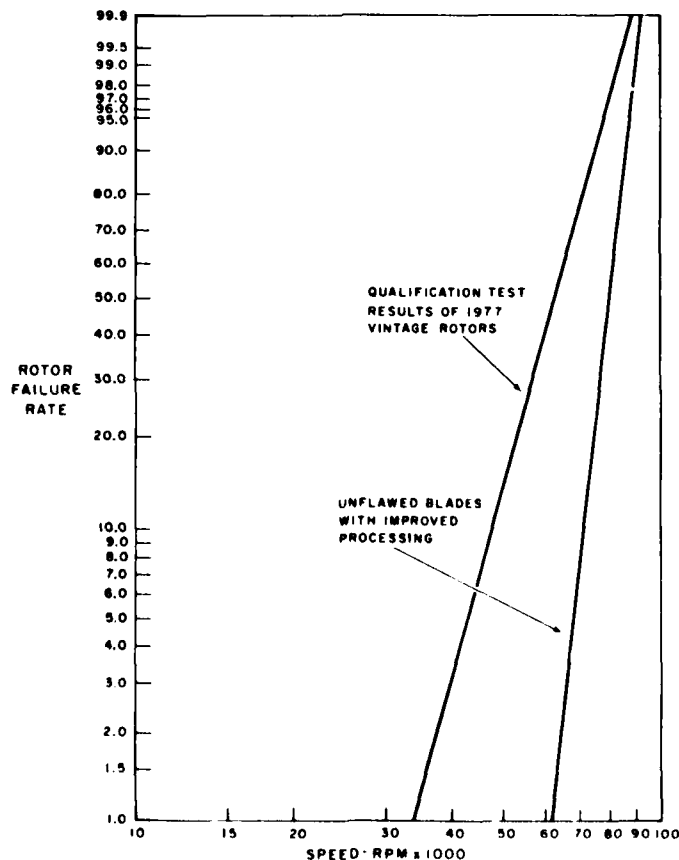


Figure 24 Weibull Distributions of Rotor Failures

Two types of blade flaws were revealed during cold spin testing to qualify rotors for further hot testing. Subsurface voids, shown in Figure 25, and planar flaws, both subsurface and surface (shown in Figure 26), were responsible for the majority of low speed cold spin failures. In the past, blade rings were injection molded, visually inspected, burned out, nitrided and visually inspected again along with conventional x-ray. Recently, conventional and microfocus x-ray techniques have been used to detect flaws in the green, as-molded, state prior to burnout and nitriding. This step was taken to eliminate the time required for burnout and nitriding, thereby providing timely feedback to the injection molding engineers who were conducting parametric experiments to eliminate molding flaws.



Figure 25 Subsurface Void Uncovered by Grinding



Figure 26 Surface Planar Flaw

A Hunkar flow control unit was coupled to the existing automated injection molding system described by Johnson at Newport.⁽⁵⁾ This new unit controls and monitors the injection velocity and die cavity pressure during the injection and hold portions of the molding cycle (Figure 27). Ten parametric molding studies were conducted with systematically varied injection profiles and hold pressures. Microfocus x-ray results indicated that high injection flow rates combined with low hold pressures in the die cavity reduced the number of subsurface void-type flaws in the outer half of the blades and completely eliminated voids in the inner, more highly stressed portion of the blades.

Conventional and microfocus x-ray techniques have been used to detect planar flaws of the type previously shown in Figure 26 in the nitrided condition. Up to 18x magnification was used with the microfocus x-ray equipment in addition to multiple orientation of the parts. Planar type flaws were only detectable after nitriding, indicating that this type of flaw may only occur after burnout and/or nitriding.

Flaws in the rim region of the blade ring were detected using the panoramic microfocus X-ray setup shown in Figure 28. The panoramic tube head fits inside the blade ring while the film strip is located outside the blade tips in one of a series of concentric grooves in the plexiglass disk. The result is a radial panoramic X-ray of the rotor blades and rim at up to 10x magnification.

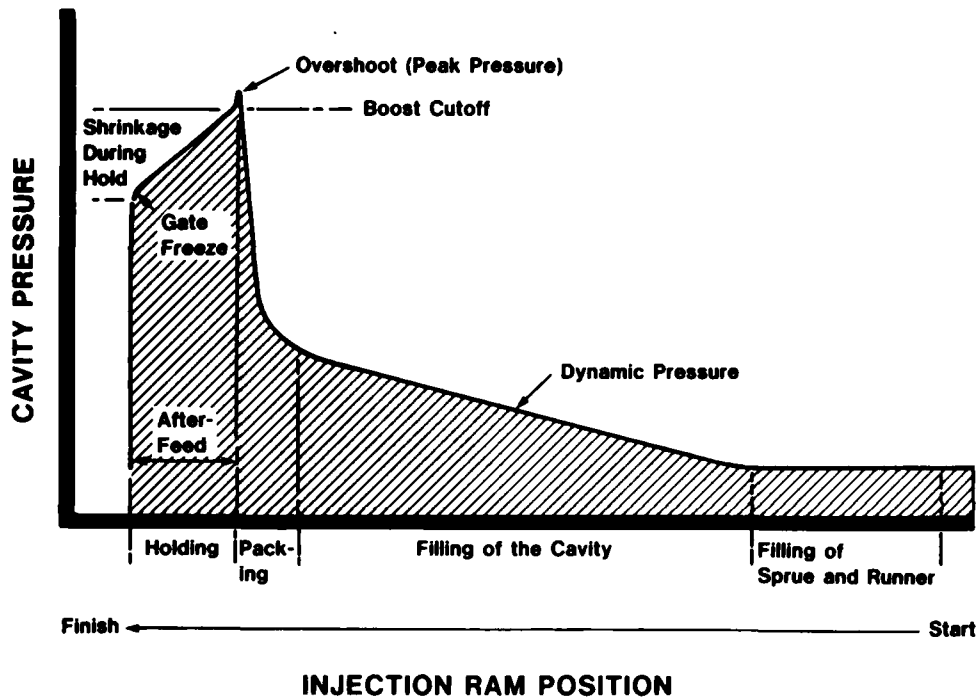


Figure 27 Schematic of Cavity Pressure versus Ram Position

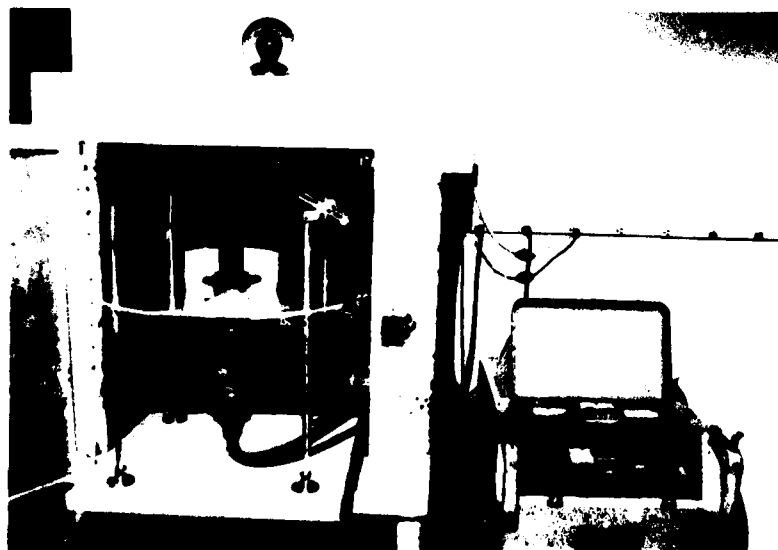


Figure 28 Panoramic Microfocus Equipment and Fixture for Radial View X-ray

Several of the 1977 vintage rotors were sectioned and examined with some interesting results with respect to the reaction bonded silicon nitride blade rings. The blade rings varied in color, from light gray to shiny black, and microstructure, from 70% to 0% alpha silicon nitride. A subsequent investigation revealed that the reaction bonded silicon nitride was dissociating, during hot press bonding, resulting in an increase in porosity, hence the gray color. A few rotors were subjected to blade bend testing to determine if blade strength was affected by hot press bonding. The results, Table 3, show the characteristic loads after press bonding were 14 to 38% lower than those for the "as-nitrided" or before hot press bonding state. As a result a degradation study was conducted, which defined the nature of the changes and identified the hot pressing parameters which could be controlled to eliminate this degradation of microstructure and strength. The processing steps in the degradation study are shown in Figure 29. Every other blade of an as-nitrided blade ring was loaded to failure (A). The blade ring was then blade filled (B) and hot press bonded. After hot press bonding (C), the remaining blades were loaded to failure. This technique provided blades from before and after hot pressing from the same blade ring, hence the same nitriding cycle, which were examined with respect to color, microstructure, hardness, and phase composition.

The ranges of hot pressing temperature and time at temperature which were investigated in this degradation study encompassed the nominal conditions of 1715°C and 150 minutes used when fabricating 1977 vintage rotors. The color changes which occurred during hot pressing are shown in Figure 30. As expected, the degree of color change, from black to light gray, increased with hot pressing time and temperature. Comparison of the microstructure before and after hot pressing, for degraded parts, showed that the "after" microstructure contained much more fine interconnected porosity, hence the gray color. This increased porosity degraded the microstructure, which resulted in a strength degradation. Figure 31 shows the relationship derived between change in strength and hot pressing time and temperature. (10) It should be noted that the expected strength degradation at the nominal hot pressing conditions (1715°C = 150 minutes) used to fabricate 1977 vintage rotors, which represent the latest rotors that have been spin tested, is 10-20%. Hence, future improved process rotors can be fabricated under hot pressing conditions, which would result in no strength degradation effectively increasing their strength 10-20% over 1977 vintage rotors.

TABLE 3 - SUMMARY OF BLADE BEND TEST RESULTS

NITRIDING NUMBER	CHARACTERISTIC LOAD (Kg)		% CHANGE
	AS-NITRIDED	AFTER HOT PRESSING	
48	40.8	34.9	-14
67	38.9	24.0	-38
78	35.9	27.9	-22

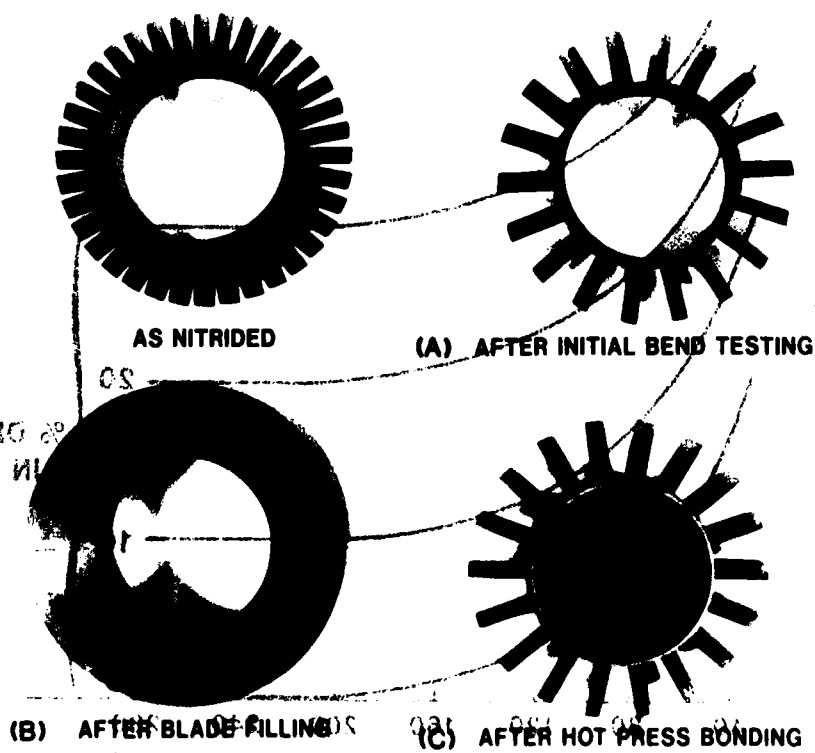


Figure 29 Processing Steps for Degradation Study

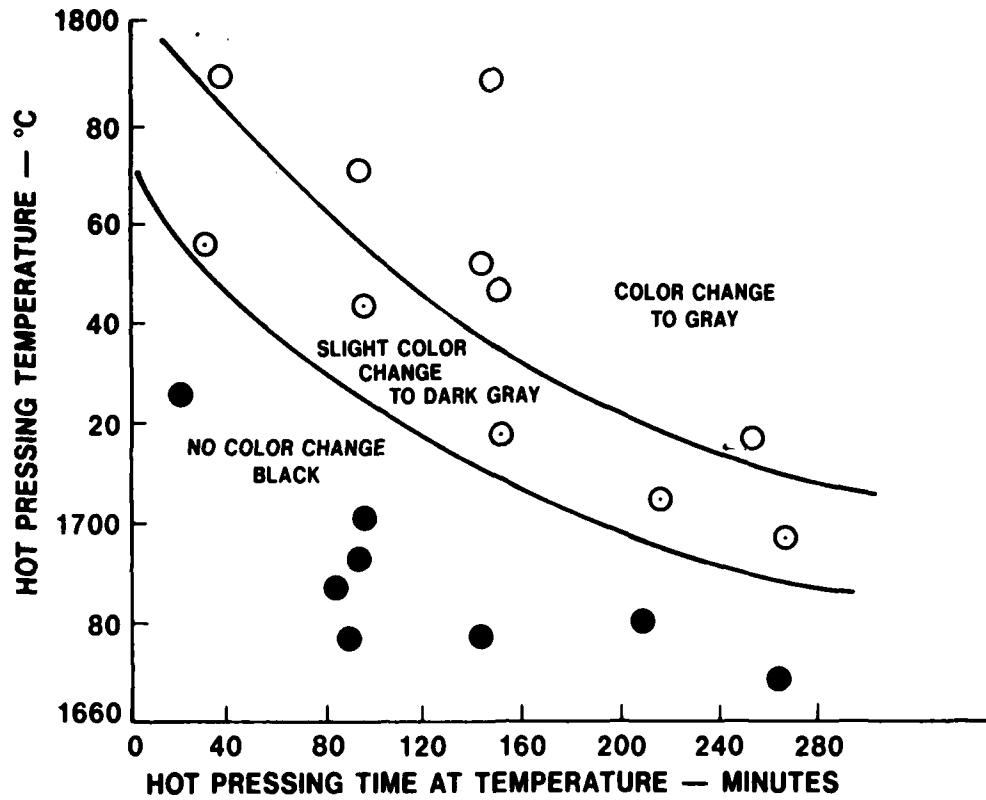


Figure 30 Color Change Versus Hot Pressing Parameters

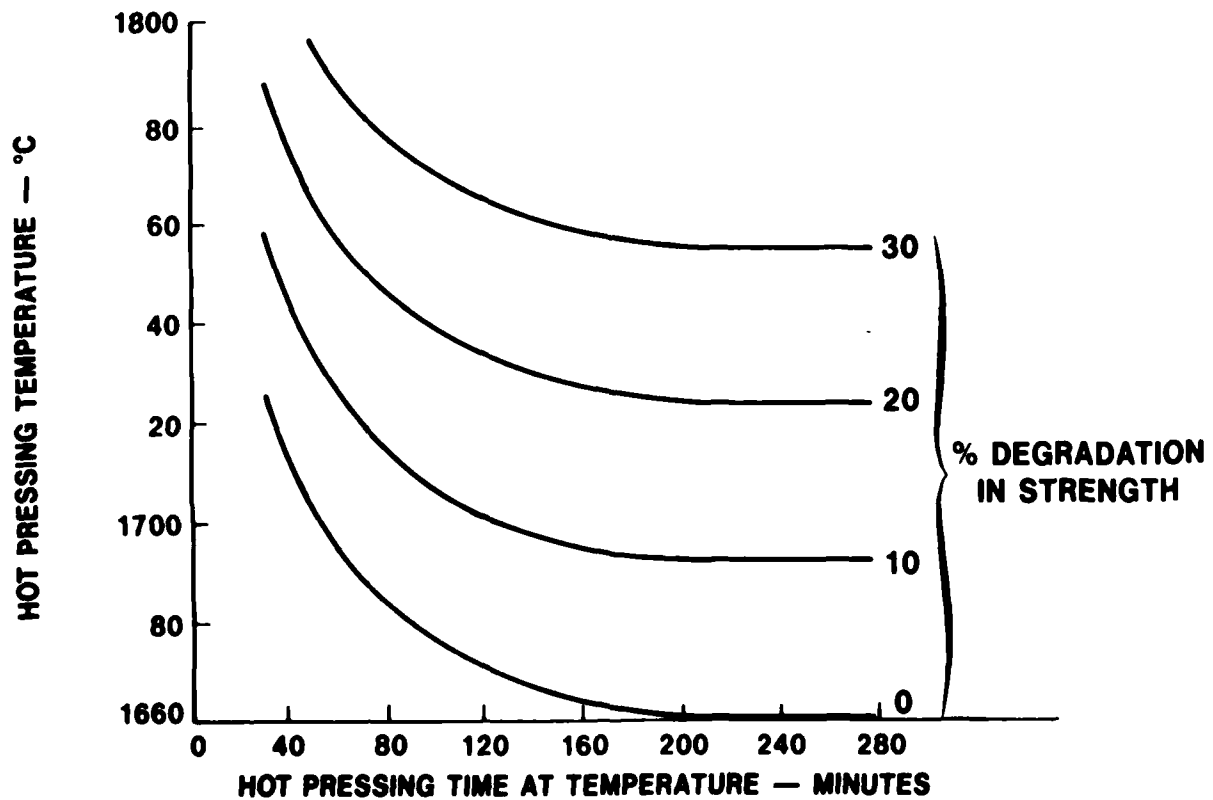


Figure 31 Percent Degradation in Strength Versus Hot Pressing Parameters

SUMMARY AND RECOMMENDATIONS

In the past few years, significant material, process and design advances have been made in attempting to realize the potential of an all-ceramic turbine rotor. The duo-density rotor was conceived and material and process developments have been underway to make the reaction bonded silicon nitride blade ring and to bond it to the hot pressed silicon nitride hub. Cold spin testing and hot spin testing were used as methods to evaluate 1975-vintage rotors and 1977-vintage rotors, resulting from material, process and design iterations.

Duo-density silicon nitride turbine rotors fabricated in 1977 demonstrated a significant improvement in cold spin reliability over state-of-the-art rotors fabricated in 1975. Hot test results (of 1977 vintage rotors) in hot spin rigs are very encouraging in that the first attempt to complete a 200-hour durability test was successful. Ceramic turbine rotors have now been run at turbine inlet temperatures of 1093-1370°C (2000-2500°F) at speeds of 27,500-64,240 rpm for periods up to 200 hours.

Reasonable correlation was demonstrated between fast fracture reliability predictions based on Weibull theory and actual test results both on cold spin disks and hot turbine rotors. Correlation between time-dependent reliability predictions and actual test results has not been confirmed nor disproved as more test results are required.

Since 1977-vintage rotors, process improvements in injection molding were identified, which eliminated subsurface voids in the inner, more highly-stressed portions of the blades. Microfocus X-ray techniques were developed to produce magnified x-rays in addition to radial view panoramic x-rays of the rotor blade ring rim. Microstructure and strength degradation of reaction bonded silicon nitride blade rings, which previously occurred during hot press bonding, was determined to be controllable. Improved process rotors can now be fabricated with no degradation utilizing the hot pressing parameters of time and temperature recently defined; this will result in a significant increase in rotor reliability. Further improvements to better detect and eliminate planar-type flaws in blades would be of added benefit.

While progress to date has shown that all-ceramic rotors "can work", at least with modest durability, additional effort is clearly required to develop all-ceramic rotors that "won't fail". Considering the relatively early stage and likely steep learning curve of developments in ceramic materials, processes, NDE, life prediction and ceramic attachment methods and considering the past investment on the duo-density rotor, a continuing strong research and development program is warranted to reach the goal of reliable all-ceramic turbine rotors.

REFERENCES

- (1) Salter, R. G., Dziter, C., Harris, E. D., Mooz, W. E., Wolf, K. A., "Strategic Defense Materials: A Case Study of High Temperature Engines", ARPA Order No. 189-1, February, 1977.
- (2) McLean, A. F., Baker, R. R., "Brittle Materials Design, High Temperature Gas Turbine, Volume 1, Ceramic Component Fabrication and Demonstration", AMMRC TR 78-14, 12th Interim Report, March, 1978.
- (3) Baker, R. R., Ezis, A., Goodyear, M. U., Hartsock, D. L., "Developments in Press Bonding of Duo-Density Rotors", Ceramics for High Performance Applications - II, J. J. Burke, E. N. Lenoe and R. N. Katz, editors, Brook Hill Publishing Company, p. 207-230.
- (4) McLean, A. F., Baker, R. R., Bratton, R. J., Miller, D. G., "Brittle Materials Design, High Temperature Gas Turbine", AMMRC CTR 76-12, 9th Interim Report, April, 1976.
- (5) Johnson, C. F., Mohr, T. G., "Injection Molding 2.7 g/cc Silicon Nitride Turbine Rotor Blade Rings Utilizing Automatic Control", Ceramics for High Performance Applications - II, J. J. Burke, E. N. Lenoe and R. N. Katz, editors, Brook Hill Publishing Company, p. 193-206.
- (6) McLean, A. F., Baker, R. R., "Brittle Materials Design, High Temperature Gas Turbine", AMMRC-CTR-76-31, 10th Interim Report, June, 1977.
- (7) Baker, R. R., "Crack Protection Method", U. S. patent 4,127,684, November 28, 1978.
- (8) McLean, A. F., Baker, R. R., "Brittle Materials Design, High Temperature Gas Turbine, Volume 2, Ceramic Turbine Rotor Technology", AMMRC-TR 78-14, 12th Interim Report, March, 1978.
- (9) McLean, A. F., Fisher, E. A., Bratton, R. J., Miller, D. G., "Brittle Materials Design, High Temperature Gas Turbine", AMMRC CTR 75-28, 8th Interim Report, October, 1975.
- (10) McLean, A. F., Baker, R. R., "Brittle Materials Design - High Temperature Gas Turbine", AMMRC TR 79-11 13th Interim Report, February, 1979.
- (11) Johnson, L. G., General Motors Research Reliability Manual, GMR 302, Chapter 2.

ACKNOWLEDGEMENTS

The authors acknowledge the partial support of the Defense Advanced Research Projects Agency, the Department of Energy and the Army Materials and Mechanics Research Center.

DEVELOPMENT OF AN INTEGRAL CERAMIC BLADE-METAL DISK WITH CIRCUMFERENTIAL BLADE ATTACHMENT

S. A. McLeod, B. H. Walker, and M. I. Mendelson*

Pratt & Whitney Aircraft Group

Government Products Division

P. O. Box 2691

West Palm Beach, Florida 33402, U. S. A.

SUMMARY

This paper summarizes the development of a hybrid turbine rotor by attaching hot-pressed Si_3N_4 airfoils to a wrought AF2-1DA superalloy disk using the GATORIZING® forging process. An approach for fabricating low cost ceramic airfoils (platformless blades) is discussed. The ceramic blade rotors were hot spin tested at 750 rev/s (45,000 rpm) and 1505°K (2250°F) blade temperature, which were representative of small gas turbine engine conditions.

INTRODUCTION

Ongoing research by the turbine engine community indicates that a satisfactory application of ceramic materials to the turbine rotor is of prime importance in achieving improved engine performance. Ceramic materials offer the advantages of higher thrust-to-weight ratio, higher turbine inlet temperatures, reduced cooling air requirements, and potentially lower cost than metal components. The Advanced Research Projects Agency has sponsored a program to demonstrate the attachment of ceramic blades to a wrought superalloy turbine disk.¹ The object of this paper is to discuss the three phases of this program which include the development and evaluation of (1) the ceramic/superalloy (hybrid) attachment concept, (2) a hybrid rotor containing ceramic pseudoblades, and (3) a hybrid rotor containing ceramic airfoil blades.

EXPERIMENTAL PROCEDURE

The rotor and ceramic blade materials used in developing the hybrid attachment concept were AF2-1DA¹, an isothermally forgeable superalloy, and NC-132, hot-pressed Si_3N_4 , from Norton Co., respectively. The hybrid attachment concept utilized the GATORIZING process to forge and diffusion bond two AF2-1DA disk halves at 1394°K (2050°F) around a circumferentially oriented ceramic blade root with a 127 μm (5 mil) thick Pt interfacial layer as shown in Figure 1. Once the attachment was bonded, the AF2-1DA was heat treated to obtain improved creep and stress rupture life.²

Machining of the first set of dummy ceramic blades in Phase I was conducted by Norton Co. with the remainder of ceramic machining conducted at P&WA/Florida, both using conventional grinding methods. The dummy blades and pseudoblades (shown in Figure 2) of Phases I and II, respectively, were machined by transverse grinding the different configurations to 10X and 20X charts using optical grind methods.¹

In Phase III the conventional airfoil design consisted of a platformed blade with airfoil twist and taper which prevented using the previous transverse grinding techniques. Therefore, a new platformless blade and machining concept was developed utilizing the above grinding techniques.¹ This concept separated the conventional turbine blade configuration into blade and platform (endwall) components, as shown in Figure 3. This enabled the components to be straight through ground (longitudinally) using a cam-follower controlled floating table as shown in Figure 4. The advantage of this machining method is a potential cost reduction over existing methods. This fabrication process also represents a practical method for high volume machining of blades from hot-pressed Si_3N_4 billets.

After machining each component, the load bearing dovetail surfaces of the blades and endwalls were longitudinally polished with 1 μm diamond paste to remove flaws. The blades were then heat treated at 1255°K (1800°F) for 180 ks (50 hr) in air prior to hybrid rotor fabrication.

Analytical evaluation of the ceramic components consisted of two-dimensional NASTRAN analyses³ of airfoil blades in Phase III to predict maximum local spin test stresses. This analysis was performed for a typical small gas turbine rotor speed of 1000 rev/s (60,000 rpm) assuming the worst possible linear blade thermal gradient, i.e., from 1505°K (2250°F) airfoil tip temperature to 1043°K (1590°F) at the airfoil base and 1063°K (1460°F) at the dovetail base.

*Person presenting paper

An experimental analysis of the Phase II hybrid rotor disk and spin tooling design shown in Figure 5, was conducted in Phases II and III to determine the maximum life, temperature, and speed capabilities. This analysis consisted of: (1) a two-dimensional photoelastic stress analysis of the disk and tooling cross sections to determine the high stress areas; (2) thermal calibrations to determine rotor temperature from the spin test temperatures of 1505°K (2250°F); (3) static thermal strain analysis using strain gages located in the high stressed locations of the disk and spin tooling, as shown in Figure 5 (locations 1, 2, and 3); (4) ambient temperature dynamic strain analysis of these high stressed locations due to the centrifugal load; and (5) stress-rupture testing⁴ of simulated disk cross sections to establish Larson-Miller life prediction curves⁵ for the rotor and attachment configuration.

Experimental evaluation of individual ceramic components in Phases I and II consisted of failure spin testing components at ambient temperature. The different attachment dovetail geometries were evaluated by determining the load-carrying capability, i.e., the blade centrifugal load (P) at failure divided by the smallest dovetail cross-sectional area (A), of each geometry. The nominal P/A data obtained was analyzed using a Weibull distribution⁶ to statistically determine the 3σ lower bound failure stress at which a 0.5% failure probability was expected. These results were then compared to determine an optimum dovetail geometry.

The configuration difference between the straight blades of Phases I and II and the airfoil blades of Phase III prevented a direct correlation of the nominal P/A stress. As a result, experimental evaluation of the airfoil blades consisted of (1) spin testing of several blades at ambient temperature to determine the ultimate stress (load/fracture area) for the failure speeds, and (2) proof spin testing of the blades prior to hybrid rotor assembly. Since the Phase II spin tooling (Figure 5) was limited to a maximum speed of 883 rev/s (53,000 rpm), the Phase III airfoil proof and failure testing were conducted using a larger diameter rotor¹ which was capable of higher airfoil centrifugal loads. These results were then recalculated to obtain "equivalent" hybrid rotor speeds.

RESULTS AND DISCUSSION

PHASE I — Attachment Concept

The first phase of this effort included the development and evaluation of the ceramic blade wrought superalloy attachment at ambient temperature. The combined GATORIZING forging process and diffusion bonding produced an attachment exhibiting both ease of fabrication and flexibility of design. This concept was optimized¹ to yield a practical attachment displaying the following characteristics: (1) a Pt compliant layer between the ceramic and wrought alloy components to eliminate ceramic/superalloy interaction during fabrication and to minimize localized stresses in the ceramic blade root; (2) intimate contact between the superalloy and ceramic blade root due to isothermally forging the attachment above the temperature it would experience in an engine.

To evaluate the integrity of this attachment, the dummy blades (Figure 2A) were individually spin tested to failure. A Weibull distribution of the blade P/A tensile stress correlated with equivalent failure speed from spin testing is shown in Figure 6. The plot reveals a 3σ lower bound stress level of 141 MPa (20.5 ksi). This exceeded the P/A stress that ceramic blades would have to withstand in a small gas turbine engine⁷. Thus, this testing demonstrated the ambient temperature feasibility of the hybrid attachment.

PHASE II — Pseudoblade Hybrid Rotor

The goal of this phase was to demonstrate the feasibility of the attachment concept for a typical small gas turbine rotor by spin testing a fully pseudobladed rotor at 750 rev/s (45,000 rpm) with a blade temperature of 1505°K (2250°F). To accomplish this objective, a small test rotor (Figure 5) was designed to use the developed attachment concept with pseudoblades (Figure 2B).

Prior to fabrication and testing rotors of this design, an experimental analysis of the high stress locations in the disk was conducted. This analysis consisted of a thermal calibration of the rotor, a two-dimensional photoelastic strain analysis of the disk dovetail slot and stress-rupture testing of flat specimens simulating the dovetail cross section to establish a disk life prediction curve. Results of the analysis confirmed that the location of primary concern was at the base of the dovetail slot where local temperature and strain were measured at 1021°K (1380°F) and 0.46%, respectively, for the desired test conditions. The resultant Larson-Miller life prediction for these test conditions showed that the expected disk life was in excess of 1.4 Ms (400 hr).

To investigate pseudoblade integrity, the nominal P/A and maximum pseudoblade dovetail stresses were calculated for comparison with the previously determined 3σ lower bound P/A stress (141 MPa). A photoelastic analysis of the pseudoblade dovetail configuration indicated that the maximum pseudoblade root stress was 45% above the nominal P/A stress. The pseudoblade P/A stress was calculated¹ to be 83 MPa (12 ksi) at 750 rev/s. Therefore, the maximum root stress was estimated at 120 MPa (17.4 ksi), which was less than the 3σ failure stress (Figure 6).

With the integrity of the blade and disk designs established, elevated temperature spin testing of single and multiple attachments was conducted. Initially, a single bladed rotor (Figure 7) was successfully tested for 238 ks (66 hr) at 750 rev/s with a blade temperature of 1505°K. During this test, the rotor was subjected to 10 thermal cycles and 97 isothermal dwell cycles, where the rotor was cycled from 0 to 750 rev/s and held at that speed for a dwell time of 300 s. Following this demonstration, several multibladed rotors were tested. A 28-bladed rotor (lacking two blades to accommodate thermocouple instrumentation) was tested successfully for 194 ks (54 hr) at 750 rev/s with a blade temperature of 1505°K. Subsequently, a full 30-bladed rotor was fabricated (Figure 8) and tested for over 317 ks (88 hr) at 750 rev/s and 1505°K with over 14 thermal cycles. The successful testing of this rotor demonstrated the integrity of the attachment concept.

PHASE III — Airfoil Hybrid Rotor

The goal of Phase III was to spin test an airfoil hybrid rotor at 1505°K (2250°F) blade temperature at rotor test speeds in excess of 750 rev/s (45,000 rpm).

To predict the integrity of the platformless blade and endwall designs, a NASTRAN two-dimensional finite element analysis of each component was conducted. The airfoil analysis predicted a maximum stress of 400 MPa (58 ksi) at 1000 rev/s (60,000 rpm) located in the concave trailing edge corner of the dovetail root (Figure 3). This is close to the reported low temperature tensile strength of NC-132⁸. In addition, the analysis predicted an airfoil failure speed range of between 1100 rev/s (66,000 rpm) and 1333 rev/s (80,000 rpm). To experimentally evaluate the airfoil design, components were individually ambient temperature spin tested to failure. The equivalent failure speeds ranged from 1142 rev/s (68,500 rpm) to 1372 rev/s (82,300 rpm) as shown in Figure 6. These test results closely agreed with the NASTRAN predicted failure range.

To screen out the low strength components prior to hybrid rotor assembly, the airfoils were proof tested at 1100 rev/s (equivalent rotor speed). Out of a total of 32 airfoils proof tested, only two failures occurred (at 863 and 1100 rev/s). The fracture origin of all failures was near the concave trailing edge surface of the dovetail (figure 9), which agreed with the maximum stress location predicted by the NASTRAN analysis. Hence, it was concluded that these proof airfoils were acceptable for hybrid rotor spin testing at speeds below the maximum spin tooling speed.

The NASTRAN analysis of the endwalls indicated a maximum stress of 117 MPa (17 ksi) at 1000 rev/s (60,000 rpm) at the overhanging leading edge (Figure 3). Six endwall components were proof tested at 1100 rev/s to verify the analysis, and no failures were observed. Hence, the endwall components were accepted without failure testing.

After substantiating airfoil and endwall component integrity, the hybrid airfoiled rotor was assembled with 24 blades for spin testing (Figure 10). A few components were omitted for thermocouple instrumentation. Next, a 180 ks (50 hr) hot spin test cycle was planned at an airfoil temperature of 1505°K (2250°F) and a rotor speed varying between 500 rev/s (30,000 rpm) and 833 rev/s (50,000 rpm). The rotor was incrementally tested at 500 rev/s for 7.2 ks, at 583 rev/s for 7.2 ks, at 667 rev/s for 3.6 ks and 750 rev/s. After 300 s at 750 rev/s a test abort occurred.

A subsequent failure analysis of the hybrid rotor and tooling assembly indicated the test abort was caused by failure of the 4.8 mm (0.188 in.) diameter metal spindle (Figure 5) supporting and connecting the assembly to the drive turbine. This caused the rotor assembly to impact against adjacent spin test structures which fractured about 70% of the airfoil and endwall components. The post-mortem fracture analysis of the ceramic airfoils indicated that blade failure was not due to centrifugal loading.

CONCLUSIONS

- The spin testing of airfoil and pseudoblade rotors was performed at 750 rev/s (45,000 rpm) and 1505°K (2250°F), which was characteristic of small gas turbine engine conditions.
- A potentially cost effective/high volume Si₃N₄ machining method was developed that separates the conventional blade configuration into platformless blade and platform (endwall) sections.
- A good correlation was obtained between analytical modeling of the platformless blade and experimental spin test results. The airfoil maximum stress and failure locations were predicted.
- Proof testing of individual blades eliminated unexpected failures prior to hybrid rotor fabrication.

ACKNOWLEDGEMENTS

The authors would like to thank the following people for their helpful contributions:

R. B. Bogard	J. F. Schratt
W. D. Carruthers	M. C. VanWanderham
W. F. Forrester	R. M. Walker
G. W. Gallops	M. D. Watson
D. G. MacNitt	G. W. Waxler
	M. L. Zaccagnino

We would also like to acknowledge the Defense Advanced Research Projects Agency represented by Dr. E. C. vanReuth for funding this development effort.

REFERENCES

1. S. A. McLeod and B. H. Walker, "Design, Fabrication, and Evaluation of GATORIZED® Ceramic-Wrought Alloy Attachment Concepts," Final Report for Contract N00019-74-C-0484, Pratt & Whitney Aircraft Group, Government Products Division, Report No. FR-9787, January 1979.
2. W. F. Simmons, "Description and Engineering Characteristics of Eleven New High-Temperature Alloys," Defense Metals Information Center, Memorandum 225, Battelle Memorial Institute, Columbus, Ohio, June 1971, p. 20.
3. MSC-NASTRAN User's Manual, Mac-Neal-Schwendler Corp. Los Angeles, CA, ed. by Caleb W. McCormick, May 1976, Revision January 1977.
4. "Conducting Creep, Creep-Rupture, and Stress-Rupture Tests of Metallic Materials," Annual Book of ASTM Standards, Part 10, Amer. Society of Testing and Materials, Philadelphia, PA. E 129-70, 1976, p. 20.
5. F. R. Larson and J. Miller, "A Time-Temperature Relationship for Rupture and Creep Stresses," Trans. Amer. Soc. of Mech. Engr., Vol. 74, 1952, 765-771.
6. W. Weibull, "A Statistical Distribution Function of Wide Applicability," J. App. Mech., Vol. 18, 1951, 293-297.
7. R. E. Wallace, "Ceramic Gas Turbine Engine Demonstration Program," Interim Report No. 2 for Contract N00024-76-C-5352, Garrett AiResearch Corp., Report No. 76-212188 (2), Sept. 1976, p. 2.5-29.
8. D. C. Larsen, S. A. Bortz, R. Ruh, N. M. Tallan, "Evaluation of Four Commercial Si_3N_4 and SiC Materials for Turbine Applications," *Ceramics for High Performance Applications — II*, ed. by J. J. Burke, E. N. Lenor, R. N. Katz, Brook Hill Publ. Co., Chestnut Hill, Mass., 1978, 651-667.

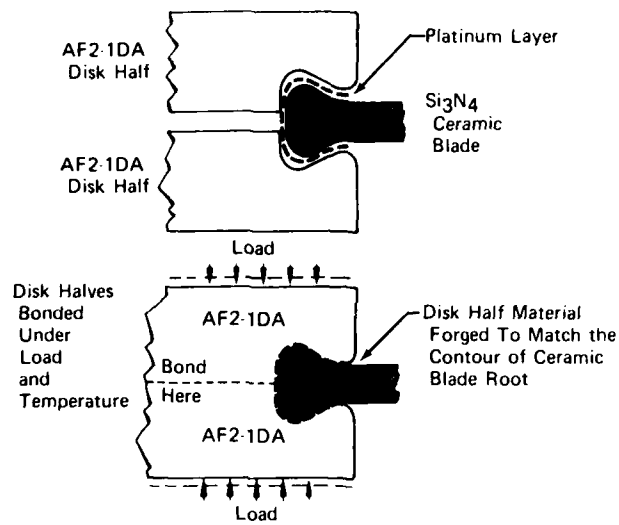


Figure 1. Fabrication Process for the Ceramic-Wrought Alloy Attachment

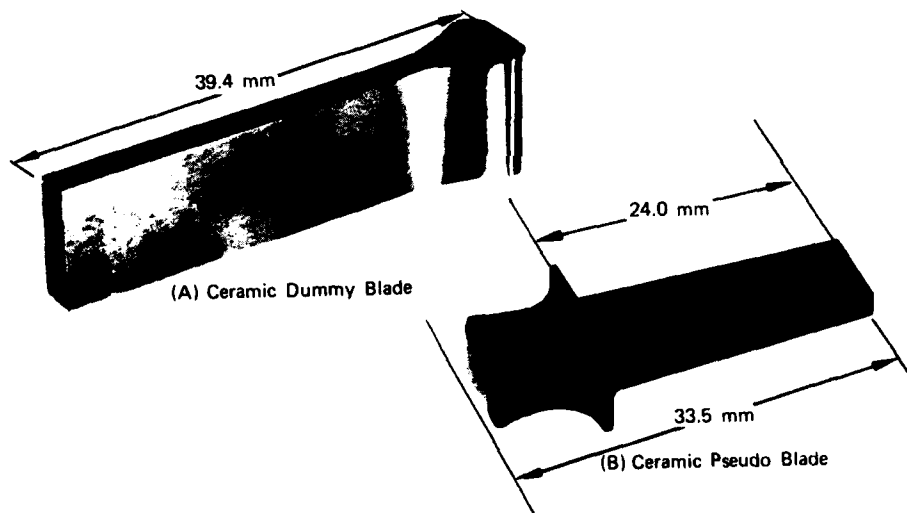


Figure 2. Ceramic Blades Used in (A) Phase I and (B) Phase II

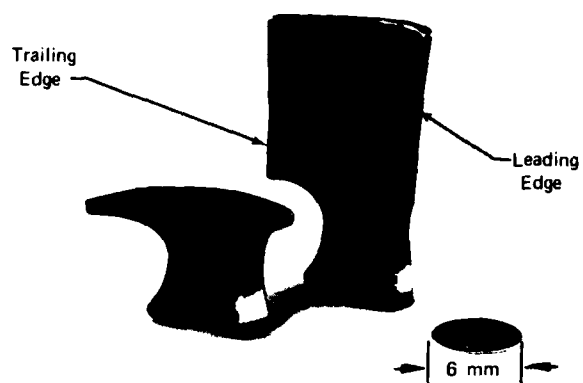


Figure 3. Exploded View of Platformless Blade and Endwall Used in Phase III

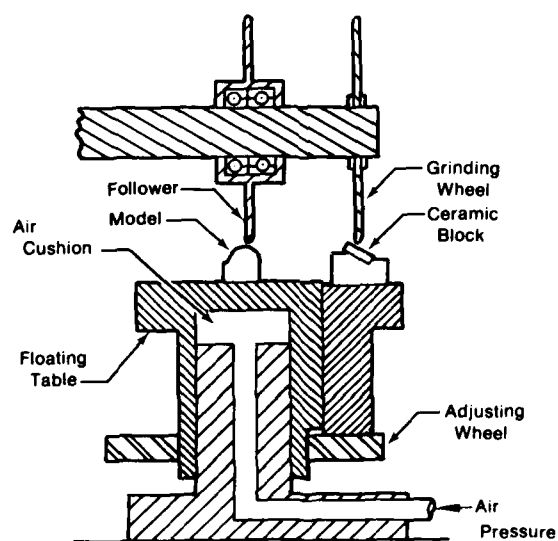


Figure 4. Air Cushion Duplicating Fixture

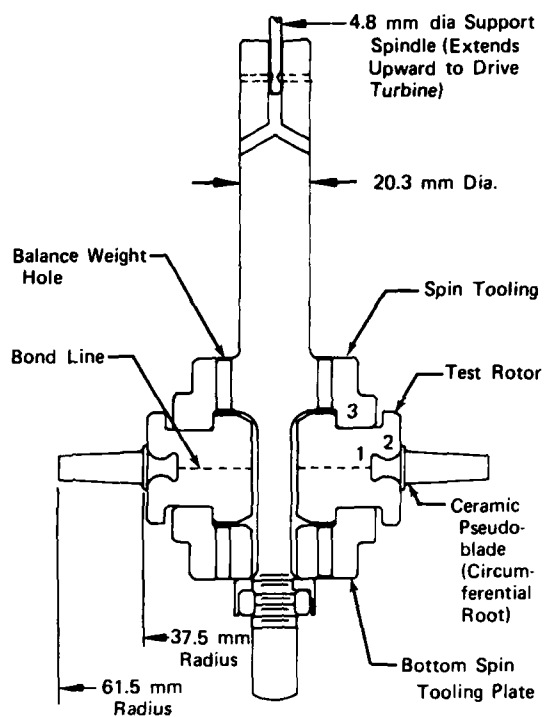


Figure 5. Spin Tooling and Rotor Assembly of Phase II

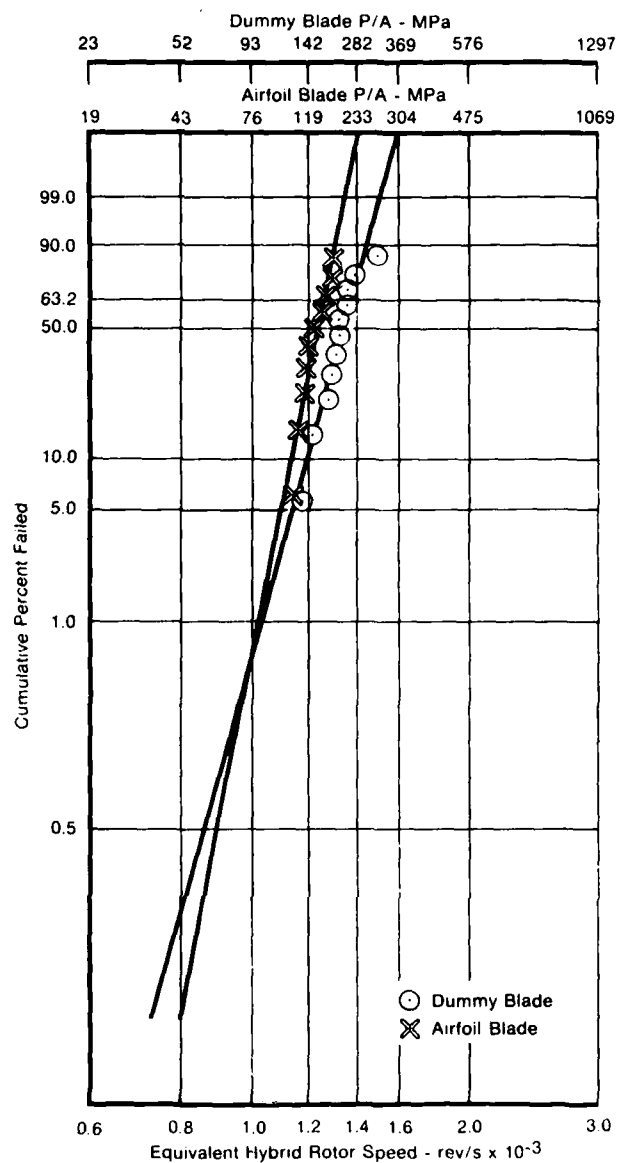


Figure 6. Weibull Analysis of Room-Temperature Dummy and Airfoil Blade Failure Speeds Correlated With Blade Root P/A Stress

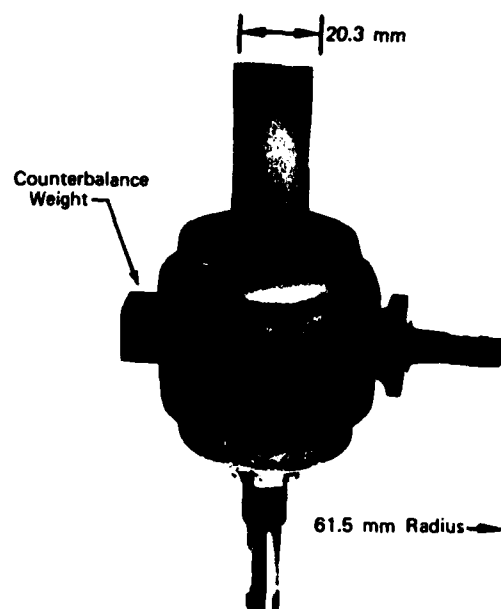


Figure 7. *Single-Bladed Rotor and Tooling After 66 hr, 10 Thermal Cycles, and 97 Isothermal Dwell Cycles*

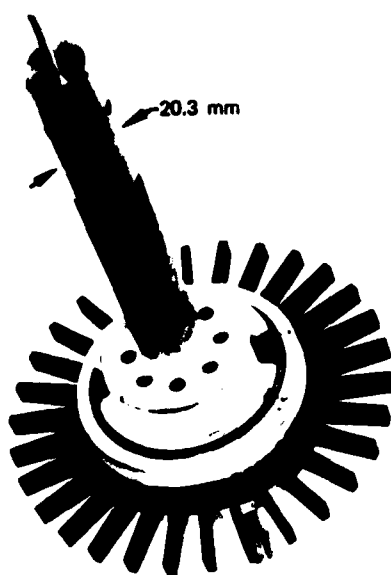


Figure 8. *The 30-Bladed Hybrid Rotor and Spin Tooling Prior to Spin Test*

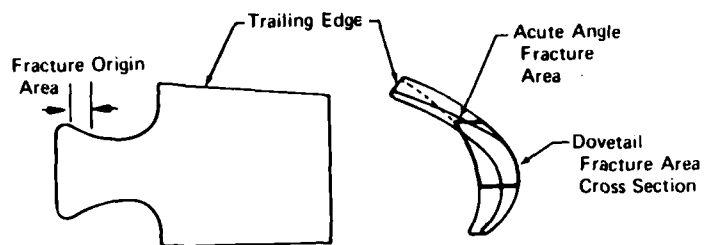


Figure 9. Fracture Origin Location on Failed Airfoil Blades

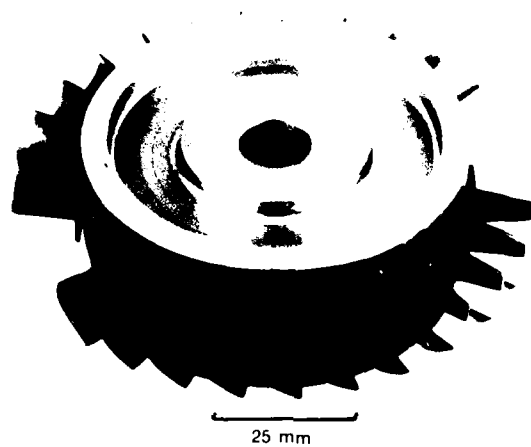


Figure 10. Hybrid Rotor Prior to Assembly With Spin Tooling

INVESTIGATIONS OF A HOT-PRESSED SILICON NITRIDE TURBINE ROTOR

by

Eberhard Tiefenbacher

Daimler-Benz Aktiengesellschaft

Postfach 202

7000 Stuttgart 60

Germany

SUMMARY

Within the context of the German Ceramics Program Daimler-Benz is working on the development of turbine wheels consisting of hot-pressed silicon nitride.

In the following, a description is given of the preliminary tests carried out to examine the thermal shock characteristics of hot-pressed silicon nitride, together with an explanation of the aerodynamic design and stress calculation of a turbine wheel. Reference is also made to turbine wheel manufacturing and the results of tests carried out so far.

1. INTRODUCTION

Since the beginning of the German Ceramics Program, Daimler-Benz has been trying together with firms from the ceramics industry to develop an axial-flow turbine wheel according to the duodensity principle, with blades of reaction-bonded silicon nitride and a hub of hot-pressed silicon nitride.

Work is still being continued in this field, however, once it became clear this development involved more difficulties than originally had been assumed, it was decided to start on another approach, this being the trial to manufacture a turbine wheel consisting only of hot-pressed silicon nitride.

2. HOT-PRESSED SILICON NITRIDE AS A MATERIAL FOR TURBINE BLADES AND TURBINE WHEELS

Hot-pressed silicon nitride has some characteristics which at first sight would cast doubt upon its suitability as a material for turbine blades.

Because of the way it is manufactured it contains a small amount of magnesium oxide, which results in creeping at high temperatures and loads. There is also evidence of slow crack growth: very small and invisible cracks present in the component enlarge under the influence of temperature and stress and can lead to premature failure. Also, not enough is known about its oxidation characteristics; for example, up to now not enough experience has been gathered to enable one to judge reliably the degree to which oxygen contained in the hot turbine gases can damage the surface of the turbine and so lead to a decrease in its resistance to stress. Finally, there is as yet no suitable manufacturing process which enables complete turbine wheels to be produced economically.

3. PRELIMINARY TESTS WITH A BLADE SEGMENT

First practical experience was gained by manufacturing a blade segment consisting of 3 axial-flow blades (see Fig. 1) and subjecting it to extensive thermal shock tests. As can be seen from the picture, a piece was removed from one of the blades to enable examination of the material once the tests had been completed.

During testing the component was exposed 3700 times at regular intervals to a stream of hot gas for 60 secs (gas temperature 1350 °C) and to an airstream of 70 °C for 60 secs. There was a continuous flow of hot gas and cold air, the segment being pushed to and fro between the two channels by means of a pneumatically operated sled. The velocity of the hot gas relative to the blade was approx. 250 m/sec, while the air and gas pressure was 1 bar.

The first important result of these tests was that no visual damage could be determined, that means that the relative high thermal stresses resulting from the large temperature gradients caused by the sharp cross-sectional variations did not lead to a destruction of the component. However, material changes were observed, in that the material became lighter in colour at the edges. Examinations using the micro-probe showed that a certain diffusion of magnesium oxide had taken place towards the blade surface. Fig. 2 shows the quantitative result: the MgO content near the edges is about 6 times the average content. At the moment it is not clear whether this might in fact lead to damage after a longer period of time.

4. AERODYNAMIC DESIGN OF THE TURBINE WHEEL

The following data were chosen as design criteria:

Flow rate	0.72	kg/sec
Gas inlet temperature	1623	K
Pressure ratio (total - total)	1.89	-
Speed	60,000	1/min

Blade design was done with standard methods, which need not to be discussed here. The circumferential speed of the wheel was limited to 400 m/sec in consideration of the strength of the available material. As opposed to the circumferential speeds being used with comparable metal turbines, this means a reduction in turbine efficiency of 1 to 1.5 %.

5. STRESS AND VIBRATIONS

The load imposed on a turbine wheel is composed basically of centrifugal force and thermal stress. In the case of thermal stress one must differentiate between steady-state and transient factors, whereby transient stresses occur especially during starting, but also during all acceleration and deceleration processes, and lead in general to an increase in load.

(a) Hub

After numerous calculations by iteration the shape of the turbine disc was defined as shown in Fig. 3.

Table 1 shows the calculated stress values at various points. The stresses caused by centrifugal force were calculated for a speed of 66,000 1/min, i. e. with an over-speed of 10 %. One sees that bore and neck are subjected to similar amounts of stress in both steady-state and transient conditions, with maximum stress occurring during the transient stage - meaning here the condition 50 secs after the cold start.

Fig. 4 shows the temperature distribution calculated for the transient phase.

(b) Turbine blades

The calculation was based on the finite element structure shown in Fig. 5. However, there is still no reliable calculation which gives the magnitude of maximum stress at the root of the blade including the stress concentration factor.

Some natural frequencies of the blade are shown in Fig. 6. Fig. 7 shows the 4th mode of natural vibration.

It can generally be said that the smaller density and the larger Young's modulus considerably increase the natural frequencies of ceramic blades as compared to metal blades.

6. TURBINE WHEEL MANUFACTURE

Once these calculations had been completed, work was started on manufacturing the first turbine wheel.

Because of experience gained with spin testing numerous discs, and as a result of knowledge gained from the examination of bending specimens, the following process was chosen:

- (1) The turbine wheel should be made out of a cylindrical disc of constant thickness, as greater homogeneity of the blank can be expected herewith.
- (2) The blank is first of all subjected to a cold spin test, where, by choosing the right speed, an initial stress of 350 N/mm^2 is produced at the edge of the bore in the centre of the disc.
- (3) As shown in Fig. 8 two discs are separated from this blank and used to make specimens for bending tests as illustrated in the specimen plan in Fig. 9. The figures 1 to 26 are the numbers of the bending specimens, and the 3-digit numbers are measured values of four-point bending tests. The bending specimens give an indication of the quality of the disc. The turbine disc in its cross-sectional form as shown in Fig. 8 was made by grinding.
- (4) The blade profiles should be made by a combined ultrasonic and diamond grinding process.

A turbine wheel manufactured according to this procedure is shown in Fig. 10.

Basically the method described here is also suitable for the manufacture of turbine wheels of other ceramic materials, for example of hot-pressed silicon carbide. Up to now, however, only hot-pressed silicon nitride appears to have the necessary strength for the given application.

The described manufacturing method is of course suitable only for prototypes and not for series production.

7. TESTING

The turbine wheels are tested on a thermal shock test rig and a hot gas turbine test rig.

The test rig depicted in Fig. 11 was constructed for the thermal shock test. Attached to an arm, the non-rotating turbine wheel is swung into a stream of hot gas and is thus subjected to a sudden thermal stress as it would occur during the ignition of a turbine. The thermal shock which occurs when a turbine is decelerated or stopped is relatively small because of the large heat capacity of the heat exchanger, and so in this rig the turbine wheel is not exposed to a stream of cold air when it is swung out of the gas stream, but just cools down in the static ambient air.

At the same time attempts are made with the help of this test rig to measure the temperature distribution by using infrared photography when the turbine wheel has been swung out. This is in order to gain information which will allow the calculation of the thermal stress. Fig. 12 shows a temperature distribution graph determined in this way.

The rig in Fig. 13 was built in order to test the wheel under original conditions.

The ceramic turbine wheel is mounted on a shaft together with a radial compressor. In order to avoid any constrictions in regard of air flow, pressure and speed, the hot gas is not produced by the air from the radial compressor, but by air from a stationary source. The air provided by the radial compressor is used to cool the rig casing after expansion in a throttle. The rig is suitable for a flow rate of up to approx. 1 kg/s, a pressure ratio of up to 3, a temperature of up to 1670 K and a speed of up to 85,000 1/min. Fig. 14 shows a turbine wheel together with the radial compressor. This arrangement is similar to the gas generator of a two-shaft turbine.

The first turbine wheel, made of an older hot-pressed silicon nitride of relatively poor quality, suffered damage at a speed of 13,000 1/min and a temperature of 1523 K. Examination revealed that previous minor damage to the wheel had apparently produced a crack which, in conjunction with the high thermal stress occurring during the last spin test, had probably caused the fracture. That the material was of inferior quality is shown by the photos in Figs. 15 and 16 which were taken while the broken pieces of the wheel were being inspected.

With the second wheel, several test runs were carried out at various temperatures and speeds. Total running time was 3 h 20 min. The wheel was destroyed at a temperature of 1343 K. The probable cause seems to be excessive thermal stresses near the hub. No faults in the material could be found in this case.

A third wheel is still being tested. It is being used mainly to determine the temperature distribution in the hub with the aid of thermal colours. However, it turned out that relatively large variations occur in the test values, such that it is not yet possible to give a sufficiently precise temperature distribution curve for a precise thermal stress calculation. Up to now, tests have been carried out on this wheel at speeds of up to 60,000 1/min at temperatures of 1170 K, and up to 50,000 1/min at temperatures of up to 1350 K. Total running time is 12 hours.

Table 2 shows the speeds and temperatures achieved up to this time.

8. OUTLOOK

It still remains to test turbine wheels at higher speeds and stresses, particularly as they occur under transient conditions. Further improvements in the material are necessary for this purpose. Finally, a certain long-term test should be carried out in order to gather experience in regard of creeping and slow crack growth.



Fig. 1: Blade segment of HS

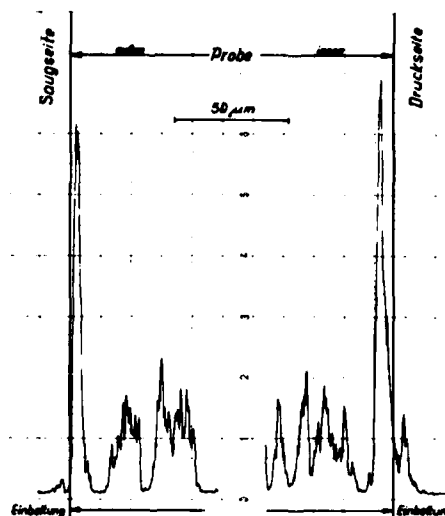


Fig. 2: Increased magnesium oxide content on blade surface
 Probe = Specimen
 Saugseite = Suction side
 Druckseite = Pressure side
 Einbettung = Embedding

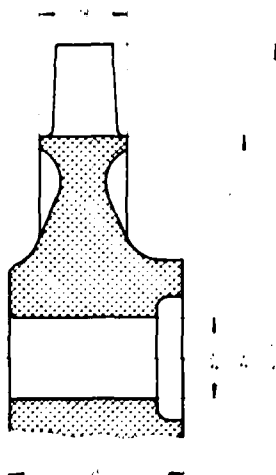


Fig. 3: Main dimensions of HS turbine wheel

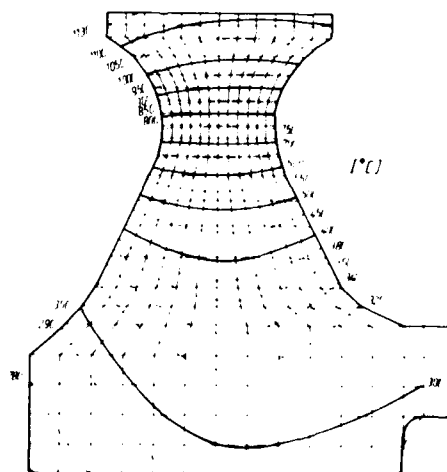


Fig. 4: Temperature distribution 50 sec after cold start

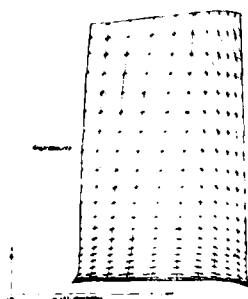


Fig. 5: Simulating structure for turbine blade

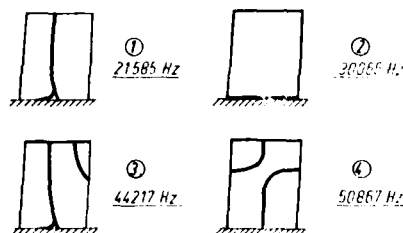
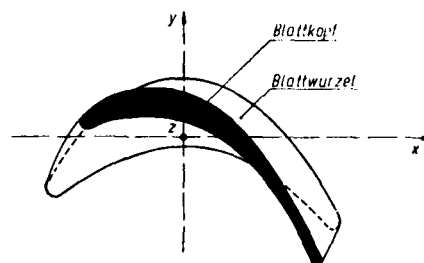


Fig. 6: Natural frequencies and nodal lines at $n = 0$ 1/min
Blattkopf = Tip
Blattwurzel = Root



Fig. 7: Mode of natural vibration (frequency 50,877 Hz).
Relative vibration amplitudes in circumferential direction
 $n = 0$ 1/min, $t = 20$ °C

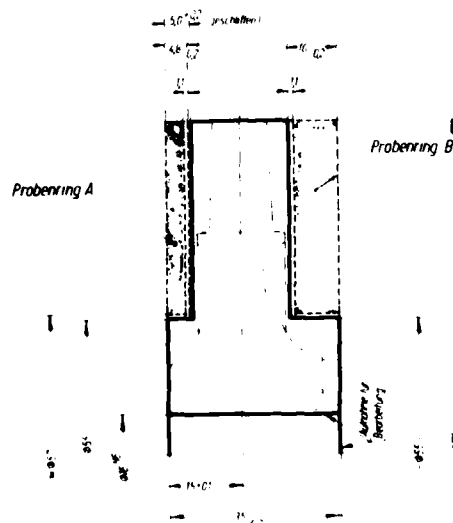


Fig. 8: HS blank
Probenring = Sample ring
geschliffen = ground
Aufnahme für Bearbeitung = Securing point for machining

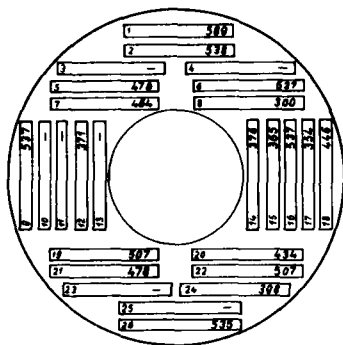


Fig. 9: Specimen plan for bending specimens (4-point) of separated side discs

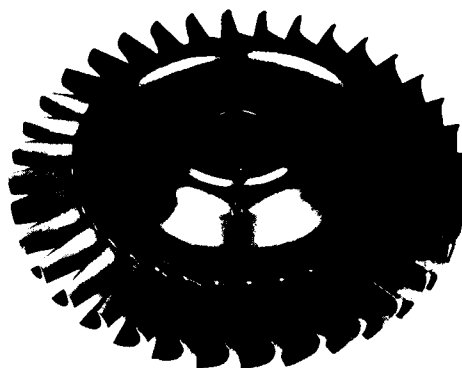


Fig. 10: Turbine wheel



Fig. 11: Thermal shock test rig

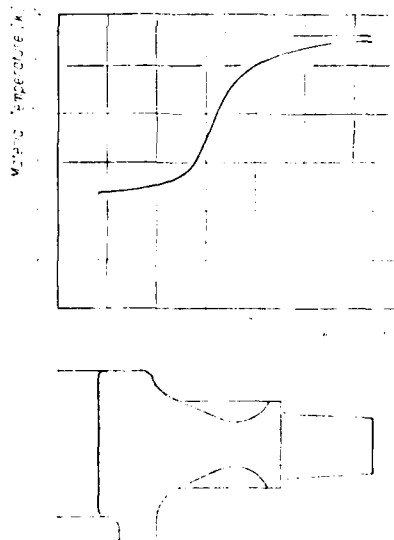


Fig. 12: Temperature profile on ceramic turbine wheel

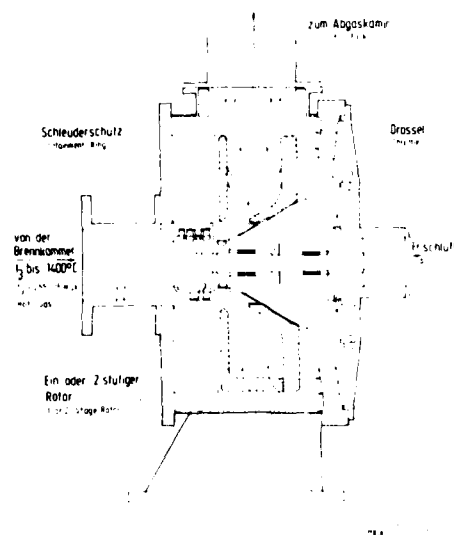


Fig. 13: Hot gas turbine test rig

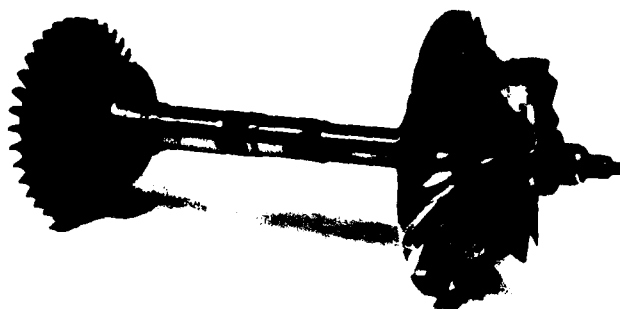


Fig. 14: Rotor

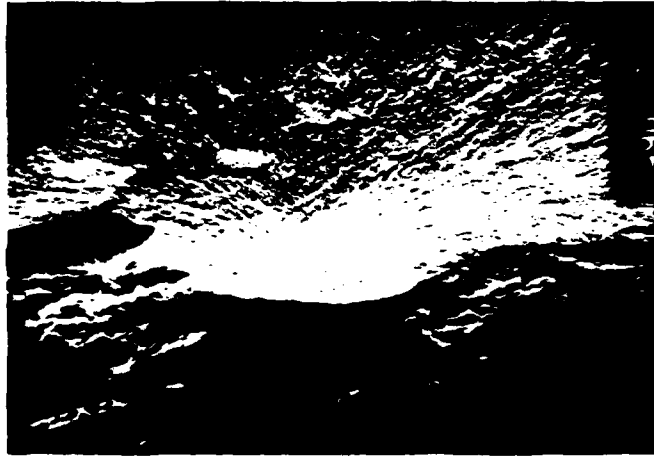


Fig. 15: Pore in the material of wheel no. 1

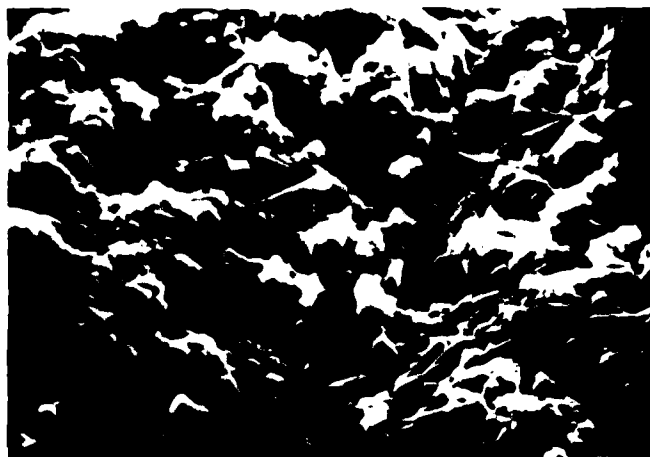


Fig. 16: Free-grown nitride needles
in the pore

	N e c k		B o r e	
	σ_r [N/mm ²]	T [K]	σ_φ [N/mm ²]	T [K]
Steady State	352	1333	348	1048
Transient	415	1033	420	563
Turbine inlet temperature $T_{3m} = 1623$ [K]				
Design speed $n = 60,000$ [1/min]				
Stressvalues calculated for $n = 66,000$ [1/min]				

Table 1: Stressvalues

Cold Spin Testing	75,000 [rpm]	300 [K]
Typ. Hot Runs	50,000 [rpm]	1475 [K]
Max. Running Time of one Rotor	22 [hrs]	
Sum of Running Time of all Rotors	47 [hrs]	

Table 2: Achieved speeds and temperatures

Ceramics in Rolling Element Bearings

Charles F. Bersch
Acting Head
Materials and Processes Branch
Naval Air Systems Command
Washington, D. C. 20361

SUMMARY

The feasibility of using hot pressed silicon nitride (HPSN) for rolling elements and for races in ball bearings and roller bearings is being explored. HPSN offers opportunities to alleviate many current bearing problems including DN and fatigue life limitations, lubricant and cooling system deficiencies and extreme environment demands. The history of ceramic bearings and the results of various element tests, bearing tests in rigs and bearing tests in a turbine engine are reviewed. The advantages and problems associated with the use of HPSN in rolling element bearings are discussed.

Introduction

The feasibility of using hot pressed silicon nitride in rolling element bearings (ball bearings and roller bearings) is being explored. Efforts during the 1960's by Zaretsky,^{1,2} Sibley³ and Godfrey⁴ had demonstrated that the concept of using ceramics in rolling element bearings probably had merit if sufficiently strong ceramics became available. The advent of hot pressed silicon nitride in the early 1970's with new levels of strength and very good uniformity appeared to overcome the earlier deficiencies.

The first phase of the current effort was a study of how hot pressed silicon nitride performed in the various functions demanded of a bearing material. This included studies of when it failed, how it failed and why it failed so that failures due to material or process deficiencies could be identified and corrected. It was determined that fully dense hot pressed silicon nitride, without inclusions, with a surface finish of 1 μ inch (0.0254 μ m) AA or better, and free of subsurface machining damage, is an unusually promising candidate material for a variety of critical bearing applications.

The second phase of the current effort has two objectives. The first involves an attempt to assure that adequate quality, properly machined components are available on a reproducible basis. The second involves an exploration of the dimensions of the performance envelope for silicon nitride bearings. The latter includes an effort to develop a limited data base.

Selected Results - General

From the beginning the ceramic bearing program has included both element tests and bearing tests in test rigs. Recently bearing tests in engines have been added. The element tests provide relatively inexpensive qualitative and quantitative information about specific functional capabilities such as rolling contact fatigue resistance, coefficients of friction and wear, elastohydrodynamic lubrication, failure modes, etc. The bearing tests are appreciably more expensive and those conducted on test rigs are generally of an accelerated nature, that is, the bearings are typically grossly overloaded to provide for failures within a timeframe that is manageable. The advantages of testing actual bearings include:

- a. The fabrication of the bearings demands production of material in appropriate sizes and highlights production requirements and cost drivers.
- b. The fabrication of the bearings demands demonstration of machining capabilities. The need to machine actual bearings has exposed various problems.
- c. Designers and fabricators are confronted by the need to recognize and provide for material differences such as higher modulus, lower density, lower thermal conductivity and lower thermal expansion. For example, new concepts are needed to mount ceramic bearings or to attach them to metal shafts.
- d. Testing of actual bearings provides information unavailable from element tests, both because it simultaneously combines the features of all the element tests and because it includes factors not addressed by element tests. Where element test data contradicts bearing test experience, one must go with the latter.

Selected Results - Element Tests

A quick summary and evaluation of the element tests indicates:

- a. Hot pressed silicon nitride is the only currently credible ceramic candidate for rolling element bearings.
- b. Silicon nitride of adequate quality and with satisfactory surface quality (surface smoothness better than 1μ inch ($0.0254\mu\text{m}$) AA and no subsurface damage) may never experience fatigue failures. In rolling contact fatigue (RCF) tests there have been no failures at 600,000 psi (4137 MPa) Hertzian stress, few failures at 700,000 psi (4826 MPa) and many instances of suspended tests after over 100 million cycles at 800,000 psi (5516 MPa). Typical Hertzian stresses in ball and roller bearings are less than half these values.
- c. Silicon nitride and conventional lubricants provide essentially the same lubrication and elastohydrodynamic lubrication characteristics as do bearing steels with the same lubricants.
- d. The coefficient of friction of unlubricated silicon nitride against itself is about the same as that of lubricated steel on steel. However, there are indications that as the temperature rises, the friction of silicon nitride against itself rises. The prospects for very high temperature unlubricated bearings of silicon nitride are being investigated.
- e. Silicon nitride appears to wear much more rapidly than most ceramics, both against itself and steel. Current evidence suggests that wear is a function of surface finish and that wear may be eliminated when surface smoothness is measured at less than 1μ inch ($0.0254\mu\text{m}$) AA.
- f. Silicon nitride usually fails by spalling, as do bearing steels. Some failures have been caused by inclusions in the materials and some have been attributed to slow crack growth of subsurface machining damage, possibly with an assist from the high Hertzian stresses used in our RCF tests.
- g. Silicon nitride has failed quite rapidly after lubricant shutoff during RCF tests. On the other hand, roller bearings have run as much as 120 hours without damage after lubricant shutoff in the test rig and for several hours in an engine without damage. It is uncertain whether the very high stress of the RCF test (800,000 psi (5516 MPa) Hertzian stress) versus the more normal stress in the actual bearings can account for the different behaviors.

Selected Results - Bearing Tests in Rigs

The initial objective was the fabrication, assembly, test and evaluation of a turbine engine main shaft roller bearing. This particular bearing was chosen for two reasons: (1) the rotating velocity of turbine engines is limited by the ability of the outer races of the bearings to cope with the centrifugal forces of the rollers as well as the loads they are intended to carry, and the lower specific gravity of silicon nitride versus bearing steels (3.2 vs 6) promised to ease that problem; and (2) roller bearings experience essentially only rolling contact forces whereas ball bearings also encounter slipping and sliding, which introduces a somewhat uncontrollable unknown. It was thus planned to conduct a simple substitution of ceramic rollers for metal rollers, with no changes in lubrication or any other factor except to redesign the crown on the roller to compensate for the difference in Young's modulus.

Six 55mm bore bearings were fabricated, three hybrid bearings having silicon nitride rollers and M50 steel races and three all ceramic bearings having silicon nitride rollers and races. Each bearing had twenty ceramic rollers 0.345 inch (8.76mm) in diameter and length. The races had a 2.25 inch (57.1mm) bore and 3.74 inch (95mm) outer diameter. The design operating conditions were for speeds up to 6500 rpm and radial loads up to 400 pounds (1.78kN). The available test rig was limited to 10000 rpm so that high DN capability could not be tested directly. Instead, two bearings of each type were tested under overload conditions to simulate the heavy outer race loading that would be sustained in high speed operation. The bulk of the testing was performed at a speed of 10000 rpm and 2500 pounds (11.1kN) load). (Under these conditions, the calculated L_{10} life of a similar, all steel bearing is 120 hours.) The tests were highly successful. Testing of the two hybrid bearings was suspended after 221 and 641 hours, respectively, of total test time. Testing of the all ceramic bearings was suspended after 62 and 331 hours. The tests were suspended because the programmed funding had been expended and the test equipment was scheduled for other work. All of the bearings were in excellent condition when the tests were suspended.

Since prediction of bearing performance is based on statistical parameters, the next objective was to make ten hybrid bearings and test them to failure, to learn how they fail and to get a feel for the distribution of their lives. The shaft speed was 5400 rpm and the radial load was 5050 pounds (22.46kN) (408,000 psi (2813 MPa) Hertzian stress). Overall the results summarized in Table 1 were encouraging.

- a. The L_{10} life was 45 hours, in comparison with an AFHMA calculated L_{10} life of 21.6 hours for a similar all steel bearing.

- b. Bearings 2, 5 and 6 used the same ceramic rollers in three sets of steel races.
- c. After 365 hours of full load testing, bearing 9 was run at a 2000 lb (8.89kN) radial load for an additional 117 hours with the lubricant shutoff without sustaining damage.
- d. Both steel race and ceramic roller failures occurred. All the ceramic roller failures except one could be traced to the combination of high loading, full roller contact and unblended roller corner radii -- an unfortunate combination of circumstances that undoubtedly reduced the L_{10} life.
- e. The one "bad" result, bearing 10, was a massive failure of several rollers, subsequently attributed to an isolated, irregular surface finishing procedure during the preparation of the roller blanks. This failure was useful in two ways. It illustrated what would happen in the event of a massive failure, thereby serving to inhibit unchecked speculation, and it reaffirmed the critical importance of the surface quality of ceramics to their performance in bearings.

There have been several subsequent bearing rig test projects. Most notable are two in which ceramic elements (balls and rollers) were tested side by side with steel elements in a high speed test rig. Test speeds went up to 71500 rpm (2.5 million DN).

General observations and conclusions from a review of bearing rig test results include:

- a. There appears to be considerable potential for silicon nitride ball bearings and for silicon nitride roller bearings, both with steel races and with ceramic races. But the future of all-ceramic bearings versus hybrid bearings has not been sorted out.
- b. Silicon nitride rolling element bearings may be attractive for some applications solely because of the excellent fatigue life of silicon nitride.
- c. The low specific gravity of silicon nitride in rolling elements proffers higher DN numbers, and it also offers higher fatigue life (quite apart from the excellent prospective fatigue life of ceramic components) by virtue of the lower loading on the outer race and the opportunity to reduce the preload.
- d. Hybrid bearings with silicon nitride rolling elements seem to run cooler than steel bearings. So far ball bearings seem to do better than roller bearings. There is no data available for bearings with ceramic races, but conceivably they might run even cooler. This feature might lead to smaller lubrication systems because of reduced coolant requirements.
- e. Hybrid and all ceramic bearings have performed outstandingly in lubricant-starved situations. Hybrid bearings perform better than steel bearings but appreciably poorer than all ceramic bearings when completely devoid of lubricant.
- f. Silicon nitride rolling element bearings run noticeably more quietly than comparable all steel bearings. The reasons, and any potential benefits, all unclear.

Selected Results - Bearing Tests in Engines

As the ceramic bearings program progressed and modest successes accumulated, interest in testing bearings in actual engines increased. Throw-away engines used to power cruise missiles and non man-rated engines used to power target drones seemed to be candidates both for tests and for early applications of ceramic bearings. Both types of engines were attractive for tests because their relatively low costs reduced the financial risk in the event of bearing failure. They were also attractive for early applications because they were not man-rated and because it seemed likely that ceramics might satisfy their unusually severe environmental and operational requirements better than metals.

The Teledyne J402 family of engines fitted these criteria excellently. The J402-CA-40C engine is used in the Harpoon missile and the J402-CA-700 engine is used for the VSTT target drone. In both cases the rear bearing is contained essentially within the burner can and does not have recirculating lubrication. The Harpoon bearing is fitted with a grease cup containing 15cc of Krytox grease while the VSTT rear bearing is lubricated by a 60 cc/min fuel flow through the bearing.

Six all-ceramic bearings were made to be tested in the VSTT engine. The intention was to demonstrate the utility of a ceramic bearing in an engine and to explore the

possibility of operating the engine without lubrication for the bearings.

Table II summarizes the results obtained. Test 4 was a complete success, with 48 minutes total time without lubrication. Tests 1 and 2 were qualified successes in that bearing failure followed failure of some other component. Tests 3, 5 and 6 were partial successes; the failure in number 5 has been attributed to poor surface quality on the bearing surface of the inner race. The cause of failure in numbers 3 and 6 (and maybe 5) is believed to be due to design deficiencies in mounting the inner race to the main shaft. It was reassuring to note, in all cases, that bearing failure did not result in freeze-up and subsequent engine damage; rather, in the most extreme cases, the failed component was pulverized and the shaft continued to rotate till shutdown.

This test program is continuing, to expand experience with ceramic bearings in engines and to pursue further the prospect for a successful bearing that would operate without the need for lubricant or coolant after indefinite storage. The design simplicity, cost savings and system reliability are very attractive.

At least two other projects are underway to explore the use of ceramic bearings in engines. The Army is exploring the prospects of hybrid bearings and maybe all-ceramic bearings in the 10KW Gemini turboalternator.⁵ Recently two 12mm bore hybrid bearings were run at 93500 rpm for over 800 hours. The Air Force recently initiated a Manufacturing Technology program to produce hybrid and all-ceramic bearings for the Williams Research Company F107 engine.⁶

Limiting Areas

The first requirement for a viable ceramic bearing technology is the availability of a bearing quality material. At present, good quality hot pressed silicon nitride material is available only in pilot-plant quantities, not production scale quantities. Also, it is available only in hot pressed billets that necessitate extensive diamond grinding to be converted to bearing components. (There is some current effort addressing pressing to shape--that is, pressing rough balls and cylinders but it has had only limited success so far.) Lastly, Norton's NC 132, the material used almost exclusively so far, is not necessarily the optimum bearing material.

The second requirement for a viable ceramic bearing technology is the ability to machine silicon nitride into bearing components with acceptable surface quality (surface finish and subsurface damage) at acceptable cost. Excellent progress was made recently with balls but much remains to be done with rollers and races. Computer controlled machining is helpful in eliminating operator introduced variability.

The third requirement for a viable ceramic bearing technology is the ability to measure and control the quality of the material and its surface. Substantial improvements in NDT/I techniques are required, especially to assess the presence and extent of low atomic weight inclusions and subsurface damage.

The fourth requirement for a viable ceramic bearing technology is a design capability to accommodate ceramic-metal interfaces, especially when mounting ceramic races on metal shafts.

The fifth requirement for a viable ceramic bearing technology is a large data base including information on load-life relationships; material characterization; design modifications necessitated by differences in modulus, toughness, specific gravity, thermal expansion, thermal conductivity, etc.; and information on performance limits in extreme environments caused by unusual thermal or lubrication requirements, etc.

Attractive Features and Prospective Applications

Sprinkled throughout the foregoing are many attractive features of silicon nitride as a rolling element bearing material such as low specific gravity, outstanding fatigue life, attractive lubrication (and non-lubrication) characteristics, low thermal conductivity, low heat generation and low noise generation. To those can be added electrical nonconductivity, wide thermal stability range and excellent corrosion resistance.

Many or all of the above features offer prospective solutions to high DN requirements, lubrication problem areas, corrosion prone applications, stray current problem areas, extreme thermal environments, prolonged storage and minimum coolant requirements.

References

1. Zaretsky, E. V. and Anderson, W. J., "Rolling Contact Fatigue Studies with Four Tool Steels and Crystallized Glass Ceramics", J. Basic Engineering, TRANS ASME, Series D, 83, 60? (1961).
2. Parker, R. J., Grisafee, S. G. and Zaretsky, E. V., "Rolling Contact Studies with Four Refractory Materials to 2000°F, ASLE Trans., 8, 208 (1965).
3. Taylor, K. M., Sibley, L. B. and Lawrence, J. C., "Development of a Ceramic Rolling Contact Bearing for High Temperature Use", Wear 6, 266 (1963).
4. Godfrey, D. J. and Taylor, P. G., "Inorganic Non-Metallic Bearings, with Special Reference to Silicon Nitride", Special Ceramics 4, p. 265 ed. by P. Pepper, British

Ceramic Research Association 1967.

5. Contract DAAG53-76-C-0228 from U. S. Army Mobility Equipment Research and Development Command, Electromechanical Division, Fort Belvoir, VA 22060 to Solar Group of International Harvester Company, San Diego, CA 92138 with subcontract to SKF Industries, Inc., King of Prussia, PA 19406.
6. Contract F33615-78-C-5110 from Air Force Systems Command, Aeronautical Systems Division, Wright-Patterson AFB, OH 45433 to SKF Industries, Inc., King of Prussia, PA 19406.

TABLE I

SUMMARY OF RESULTS OF 10 ROLLER BEARINGS RUN IN TEST RIG

<u>Bearing No.</u>	<u>Endurance Test Hrs*</u>	<u>Comments</u>
1	846	Test suspended. Good condition.
2	164	Outer race failure.
3	461	Roller spalls (2) and outer race spall.
4	146	Roller spall and damaged races.
5	83	Inner race failure. Rollers were reclaimed from #2 test bearing.
6	26	Outer race failure. Reclaimed rollers from test #2 & #5 still in good condition.
7	185	Roller spall and damaged races. Assembly contained slightly deviate rollers.
8	222	Roller spall and inner race spall.
9	365	Endurance test suspended after 365 hours. Bearing tested additional 117 hours under lube shutoff conditions**. Final condition good.
10	21	Previously run 117 hours as lubricated companion bearing in lube shutoff test for #9. Failure with severe race and roller damage.

*Endurance test conditions: 5400 rpm. - 200°F (93.3°C). Load 5050 lb. (22.46kN).
 (408.5 Ksi (2813 MPa) Hertz).
 AFEMA L₁₀ for M50 steel = 21.6 hours.
 L₁₀ for Si₃N₄ = 45 hours.

**Lube shutoff conditions: 5400 rpm ~210°F (98.9°C). Load 2000 lb (8.9kN).

TABLE II
SUMMARY OF RESULTS OF 6 ROLLER BEARINGS RUN IN VSTT ENGINE

<u>Test No.</u>	<u>Date</u>	<u>Lube Flow</u>	<u>Test Time</u>	<u>Results</u>
1	08-19-77	60cc/min	17 min	Bearing failed @ 34,000 RPM (Retaining ring failure)
2	11-11-77	60cc/min	5.1 hrs	Visual inspection after 1 hr: Bearing in excellent condition. Continued testing - turbine rotor failed after 4 hrs of scheduled 5 hr run.
3	03-09-78	60cc to Zero	2 hrs	Shaft @ 39,000 RPM - 15 min - Zero lube. Shaft @ 41,000 RPM - 3 min - 10cc lube. Attempted 41,200 RPM with Zero lube; Bearing temp climbed steadily - Test aborted - Outer race failed on rundown.
4	03-31-78	60cc to Zero	1 hr. 41 min.	Shaft @ 41,200 RPM - 22 min - 10cc lube Bearing temp 620°F (330°C) Shaft @ 41,200 RPM - 4 min - 0-10cc lube. Bearing temp 670°F (354°C) Shaft @ 39,000 RPM - 33 min - Zero lube. Bearing temp 573°F (298°C) Bearing in excellent condition.
5	05-11-78	60cc to Zero	35 min	Shaft @ 39,000 RPM - 3 min - Zero lube Bearing temp climbed steadily. Test aborted - Inner race disintegrated. Remaining new bearing returned to manufacturer for race surface analysis.
6	10-20-78	60cc to Zero	45 min	Shaft @ 39,000 RPM - Lube @ 10cc/min reducing to Zero. Bearing temp climbed steadily. Test aborted - Inner race disintegrated.

THE FABRICATION AND PROPERTIES OF REFEL SILICON CARBIDE IN RELATION TO GAS TURBINE COMPONENTS

by

P Kennedy

United Kingdom Atomic Energy Authority
Springfields Nuclear Power Development Laboratories
Salwick
Preston
Lancashire
PR4 0RR

SUMMARY

REFEL silicon carbide was originally developed as a cladding material for high temperature nuclear reactor fuel, because of its high temperature stability, its oxidation resistance and its thermal stress and thermal shock resistance, and the reliability of the manufacturing process and the consistency of the product were established at an early stage in the development. The gas turbine engine is analogous to the nuclear reactor in that the same material characteristics are required and fabrication processes have now been developed which enable most gas turbine components to be formed from REFEL silicon carbide effectively and with a minimum of machining. The material has been shown to perform satisfactorily in most stator applications and to be superior to other available ceramic materials for combustors. It has also given encouraging results in the turbocharger tests. In this paper the properties of REFEL silicon carbide are discussed, the fabrication processes are outlined and some of the published test data is reviewed.

1. INTRODUCTION

REFEL silicon carbide, was developed by the UKAEA in the early 1960's as a cladding for nuclear fuel for use in a high temperature gas-cooled reactor. Silicon carbide was chosen because it was one of the few materials with low neutron absorption which could be used in carbon dioxide at temperatures above 1000°C. In addition the projected fuel rating was such that it was anticipated that thermal stress would be the key factor governing fuel performance. Thus, it was concluded that if polycrystalline silicon carbide could be made strong enough it would have excellent resistance to thermal stress because of its intrinsic high thermal conductivity and low expansivity.

To ensure low permeability for the containment of fission products and for ease of manufacture a reaction-bonding process was chosen for development. The first phase of material development was to examine the self-bonding process in some detail and the raw materials, extrusion process and firing cycle were optimised to give a fine grain, high strength product.⁽¹⁾ In the second phase of development a pilot plant was established to provide silicon carbide tubes in production quantities so that large scale in-reactor tests could be made. In the production facility some 1500 tubes were manufactured over a period of six months. During this phase rigorous process controls were enforced and the quality of each tube was assessed by visual, radiographic and ultrasonic examination.⁽²⁾ In addition each tube was proof tested using internal hydraulic pressure, to a maximum fibre stress of about twice that anticipated in the irradiation test. The majority of tubes passing non-destructive testing also survived the proof test - a small fraction failing at very low pressures. Thus, the consistency and reliability of REFEL silicon carbide was established at a relatively early date.

In the third and final phase of the work it was demonstrated that REFEL silicon carbide fuel cans were completely retentive to fission products at temperatures from 1000 to 1100°C in carbon dioxide and at a fuel burn up of 5,000 MWd/tell. A detailed assessment of the effects of fast neutron dose, up to 2×10^{21} n/cm², on material properties confirmed that an overall probability of can failure of 1×10^{-6} could be achieved at a peak fuel rating of 40 W/cm². At this rating the radial temperature gradient in the can wall was about 400°C/mm. It was also shown that at lower temperatures the thermal conductivity decreased under irradiation by as much as a factor of five, and the corresponding increase in thermal stress had to be compensated by using thinner cans.

Despite the encouraging performance of REFEL silicon carbide in the nuclear application, an alternative high temperature reactor concept, based on a graphite matrix fuel with helium coolant, superseded it and eventually the entire development of high temperature reactors in the UK came to an end. It was appreciated however that REFEL silicon carbide was a ceramic with great engineering potential and development was continued in the non-nuclear field with support from the Department of Industry. The new objective was to identify potential applications and to produce components to a size/shape specification and with properties designed to meet these applications. This work has been performed through the UKAEA but the material is now produced by its licensee, British Nuclear Fuels Ltd., who have recently completed the construction and commissioning of a new manufacturing plant for this purpose.

The biggest volume of business is in the wear-resistant field, REFEL silicon carbide is widely used for mechanical seal faces. However, it was its high temperature properties that led to the original development of REFEL silicon carbide. The analysis of requirements of the nuclear reactor and the advanced engine, with respect to high temperature stability, oxidation resistance, thermal stress resistance, creep resistance and impermeability, have made the material a prime contender for advanced engine components.

In this paper the more important properties of REFEL silicon carbide are presented and, moreover, the fabrication techniques available are described and the results of some of the published tests on REFEL silicon carbide for turbine components are reviewed.

2. THE SELF-BONDING PROCESS

In the self-bonding process, first described by Popper⁽³⁾, a body containing graphite and silicon carbide is heated in contact with molten silicon. The silicon moves through the body under the influence of capillary forces, reacting with the graphite and converting it to silicon carbide. It is this silicon carbide, formed in situ, which bonds the original grains together. The process has several important features:

- (a) Provided that sufficient porosity is present in the 'green' body to accommodate the molar volume change on reaction, little or no dimensional change occurs and a 'green' component can be formed closely to the final desired shape.
- (b) There is little or no grain growth in the process and so if a fine grain feed material is used a fine grain product is formed.
- (c) No grain-boundary phase is observed in the final product.

In theory a fully dense silicon carbide could be formed in this process, by a careful control of the 'green' porosity. In practice it is necessary to have additional porosity in the green body to allow free transit of the silicon and completion of the silicon-graphite reaction. Thus, the resulting material, in the case of REFEL silicon carbide, is a fully dense body but about 90% dense with respect to silicon carbide and containing about 10% free silicon as a finely dispersed but continuous network. The microstructure of this material is shown in Figure 1.

3. PROPERTIES

Most of the outstanding properties of REFEL silicon carbide stem from its fully dense, self-bonded fine-grain microstructure. Some of the properties are shown in Table 1 and the corresponding properties of other engineering materials are shown for comparison.

Strength

Perhaps the most important property of any ceramic is its strength and extensive measurements have been made on REFEL silicon carbide. The results of these measurements are presented in detail elsewhere⁽⁴⁾ but in summary it may be stated that the observed mean strength is a function of surface finish, stressed volume and the degree of biaxiality in the applied stress system, whilst the probability of failure at a given stress is a function of the flaw distribution. A Weibull modulus of 10 has been observed and the variation of mean bend strength with temperature, shown in Figure 2, is invariant with temperature up to 1400°C when the free silicon melts. It should be noted however that the residual strength above 1400°C is still appreciable and that the free silicon could be removed for applications where it would prove embarrassing. The variation of Young's modulus with temperature is also shown in Figure 2.⁽⁵⁾

Time dependence of strength

Early work by Rumsey and Roberts⁽⁶⁾ and Marshall⁽⁷⁾ established a logarithmic relationship between component life and applied stress and using these workers' results it was deduced that failure would not occur within 10 years at a sustained load equal to 75% of the instantaneous fracture stress.

More recently Davidge et al.⁽⁸⁾ have constructed a Strength-Probability-Time diagram for REFEL silicon carbide based on measurements made at 20°C and this is shown in Figure 3. From the diagram it may be seen that there is an approximate degradation in strength of 2% for each order of magnitude increase in time under stress. Thus for example if it is assumed that the time to failure in a short term test is 1 sec, the component life would be about 77 years at 82% of the instantaneous fracture stress at the given failure probability. Although certain assumptions were made in the construction of the diagram, and the time to failure in a short term test is not accurately known, it is clear that the delayed fracture effect at room temperature is extremely small.

In the same paper⁽⁸⁾ data on the performance of REFEL silicon carbide at 1400°C is presented and although it is somewhat limited, the mean strength of the material was found to increase when held at a stress level below the instantaneous fracture stress. The authors attributed this increase to the increase in plasticity of the silicon phase at higher temperatures and they inferred that the delayed fracture behavior at 1400°C would not be worse than at room temperature and would probably be better.

Creep resistance

By far the most important mechanism for creep in a ceramic, in the absence of a low melting point grain boundary phase, is diffusion and because the process is activated, and because the activation energies for the diffusion of vacancies and atomic species through most ceramics are high, little creep might be expected below 1200°C. Farnsworth and Noble⁽⁹⁾ were the first to show that a diffusion-controlled mechanism could be applied to dense polycrystalline silicon carbide, but their measurements were made only in the temperature range 1400-2200°C.

The creep of REFEL silicon carbide was first examined by Bestall and Patel⁽¹⁰⁾ who showed that at 1200°C and 77 MN/m² the total observed creep strain after 10⁵ h was 0.2%, and at 1400°C and 110 MN/m², 0.17% in the same time interval. Subsequently Urbane⁽¹¹⁾ confirmed the 1200°C measurement and showed that even at 1400°C and 77 MN/m² the observed creep in 10⁵ h was only 0.05%, a value slightly higher than that for hot pressed silicon carbide but considerably lower than the values for reaction bonded silicon carbide, hot pressed silicon nitride and sialons.

Thermal stress and thermal shock resistance

The most important parameters affecting thermal stress and thermal shock resistance are linear expansion ' α ' and thermal conductivity ' k '. The variations of linear expansion and thermal conductivity with temperature are shown in Figure 4 and it may be seen that ' α ' is small and varies little with temperature between 20-1000°C, whilst ' k ' is high even at 1000°C. Consequently the calculated value of ' $\frac{\alpha}{k}$ ', a "figure of merit" for thermal stress resistance⁽¹¹⁾, shown in Table 1, is higher than the corresponding figures for the other materials cited.

A number of thermal shock tests on REFEL silicon carbide have been carried out in various laboratories but one example of customer appraisal is offered by the work of Saunders and Probst⁽¹²⁾ at NASA Lewis Research Centre. Their results show the excellent endurance of the material in a thermal fatigue programme consisting of 100 thermal cycle in air from room temperature to 1200°C with a 1 h exposure to temperature per cycle and a cooling time of 30 sec to black heat and 300 sec further to room temperature. These authors support the view that the good endurance of REFEL silicon carbide derives from its fine grain, uniform microstructure.

Oxidation resistance

Bennett and Chaffey⁽¹³⁾ have examined the oxidation of REFEL SiC at 950°C and have shown that the rate decreases with time according to a parabolic rate law with a rate constant of $2.3 \times 10^{-11} \text{ cm}^2/\text{h}$. After the initial reaction, for all practical purposes no further oxidation occurs and as the rate is governed by diffusion through the silica layer, the SiC and silicon behave similarly.

At low-oxidant pressure, volatile silicon monoxide is formed, the SiC surface is no longer protected by a silica layer and a greatly enhanced corrosion rate is observed. However this only occurs below 10^{-6} atmos at 1000°C⁽¹⁴⁾ and most oxidation is protective.

Hardness and wear resistance

Microhardness measurements have been made in two laboratories at loads of 50 and 100 g. Good agreement has been obtained between measurements, the average value being about 3000 kg/mm². Early measurements of wear resistance related to the use of REFEL silicon carbide as a fuel tube material. Buttons of silicon carbide were rubbed on silicon carbide plates at 650°C in CO₂ and no wear was observed. Other tests have been made under different sets of conditions and similar results have been observed, but wear rate is such a subjective property, depending on geometry, surface finish, environment etc. that it is practically impossible to generalise. Suffice it to say that applications requiring high wear resistance are the ones that have proved most successful to date, and in certain mechanical seals REFEL silicon carbide has been shown to last up to thirty times longer than tungsten carbide.⁽¹⁵⁾

Electrical resistivity

Both silicon and silicon carbide are Group IV semiconductors and in the pure form they are practically insulators at room temperature, the electrical resistivity decreasing exponentially with increasing temperature to a constant value at about 1000°C. In practice the small amounts of impurity, mainly nitrogen, present in standard REFEL silicon carbide leads to a room temperature resistivity of about 1 ohm-cm which decreases to about 0.5 ohm-cm at 1000°C. However, North and Gilchrist⁽¹⁶⁾ have shown that by doping with certain Group III and Group V elements such as Boron and Antimony the room temperature resistivity may be varied by three orders of magnitude as shown in Figure 5. These results are particularly relevant to heater applications but have some relevance to the manufacture of gas turbine components because the higher conductivity materials may be machined by spark erosion at an economic rate.

1. FABRICATION

A number of processes are now available for forming 'green' REFEL silicon carbide bodies. Historically, because small diameter tube was needed for the nuclear project, extrusion was the first route developed.⁽¹⁷⁾ However, as more diverse applications arose the extrusion process was extended to form finned tube, spline, and slab; die pressing was introduced for the mass production of smaller items such as cups and balls, and static pressing in conjunction with green machining was developed for producing large components and those with some degree of asymmetry.⁽¹⁷⁾ It is worth noting that most of the large static components which have been made for gas turbine evaluation to date, were produced by this latter route.

As the requirements for more complex components increased, transfer moulding and slip casting techniques were also developed. With these processes have been used for making stator and rotor vanes although slip casting is more economic than transfer moulding for small batch production, and is potentially a better method than static pressing for forming combustors.

Finally the thin film process developed by AMEK Barwell for making silicon nitride heat exchangers can also be used for forming 'green' REFEL silicon carbide and honeycomb matrices have been made with a mean hydraulic diameter of 1 mm and a throughway ratio of 0.6%.

Any one of these methods may be used for forming a green body and this factor combined with the small dimensional change on firing makes the manufacturing route very versatile. However it is important that REFEL silicon carbide should be made to the same target specification whichever route is chosen. The same basic raw materials and sintering conditions are used in every case but probably the most important factor which must be controlled, if uniformity is to be achieved, is 'green density' and in the development of the fabrication processes most of the work has centred on this parameter. Thus, for example, in the extrusion process the 'green density' is controlled by the binder content whilst in slip casting it is critically dependent upon the properties of the slip and the mould. Provided that the target green density is reached, differences in microstructure and consequently in properties are minimised.

5. APPLICATIONS

The key properties of REFEL silicon carbide which place it in the field of engineering ceramics are its hardness and wear resistance, its high resistance to thermal stress and shock and its exceptional corrosion resistance in high temperature oxidising atmospheres. Thus the applications may be grouped into two general areas, namely components operating at high temperatures in oxidising environments with varying degrees of thermal stress and components operating in abrasive environments. In addition there is the well established use of silicon carbide in heaters and a singular application which exploits the brittle nature of the material - namely body armour.

In this paper only the gas turbine applications, which have been exploited to date, are considered but it is worth noting a related application in the field of rocketry where REFEL silicon carbide nozzles have been used most successfully at temperatures up to 2500°C when low erosion rates and long firing times are required.

Compressor-turbine nozzle shroud

One of the first gas turbine components to be made and tested was a compressor turbine nozzle shroud which was being considered for use in the British Leyland 25/350R engine, before the demise of their gas turbine programme.⁽¹⁸⁾ The shroud which had an inside diameter of 200 mm is shown in Figure 6. The test was carried out in a blowing rig at a gas flow of about 1.5 lb/sec and the only temperature gradient through the shroud wall arose from differential heat transfer due to different gas velocities at the inner and outer surfaces.

This component withstood 19.5 h at 1050°C and 14.5 h at 1150°C with 68 cycles from $800-1050^{\circ}\text{C}$, 44 cycles from $650-1150^{\circ}\text{C}$ and 35 starts, and eventually failed due to mechanical rather than thermal damage. Silicon nitride shrouds were also tested but with less success and it was concluded that REFEL silicon carbide might be a better proposition above 1050°C .

Combustors

REFEL silicon carbide combustors were also made for the BLMC gas turbine programme but these were never run, and since then a variety of flame cans and combustors have been made for many different engine manufacturers and some of these are shown in Figure 7.

The first REFEL silicon carbide combustor tests were carried out by Ford (USA) as part of the AFMA/MTA FORD programme.⁽¹⁹⁾ A wide variety of materials were evaluated on a combustor test rig and REFEL silicon carbide proved to be the most successful. Subsequently one combustor was run and survived 201 h of rig testing made up of 174 h at 1050°C and 275 h at 1322°C , with a large number of cycles to room temperature. However three other REFEL silicon carbide combustors, made to the same design, failed the 10 h qualification test. Because it was appreciated that the thermal stress levels in the combustor were high, the component was redesigned with a thinner wall, to effect a 40% reduction in steady state thermal stress. Combustors made to the new design all passed the 10 h qualification test. The initial and redesigned combustors are shown in Figure 8.

Flame cans and combustors have been tested more recently by MTU and again the material has proved superior to the other materials tested.⁽²⁰⁾ In the early work two-piece parallel-sided flame cans were used and these operated successfully for a total 150 h without failure, during which period there were 460 cycles between room temperature and $1300-1400^{\circ}\text{C}$. At a later stage in the programme a conical combustor was introduced which, by virtue of the reduced primary cone volume ensured more homogeneous combustion and consequently a more uniform wall and gas outlet temperature distribution. At the time the work was reported these combustors had operated for a total 250 h under the most varied conditions, involving 21 starting operations, without a failure. During the tests also, conditions had been made artificially more severe and gas temperatures up to 1400°C were measured.

One REFEL silicon carbide combustor test which did give rise to failure was carried out at Lucas Aerospace and the results are reported by Sedwick.⁽²¹⁾ In this case excessive temperature gradients were measured adjacent to the primary air inlet holes and the cracks occurred in the same region. However, it is worth noting that the combustor did not fail catastrophically but remained in one piece and continued to run.

Nose cones

Turbine inlet nose cone assemblies consisting of conical inner members bolted and centred in outer annular members by ceramic bolts have been made in REFEL silicon carbide and one is shown in Figure 9. These components were tested at MTU⁽²²⁾ in conjunction with and under the same conditions as the combustors. Again no failure had occurred at the time the work was reported and the nose cones had operated for a total 150 h with 600 thermocycles.

Stator vanes

Some REFEL silicon carbide stator vanes have run satisfactorily in tests, but no results have been published. A number of different designs of vane have been made and some of these are shown in Figure 10.

Rotors

Blades for composite metal/ceramic axial rotors have been made but none has yet been tested. However some radial rotors have been made and tested⁽²²⁾ and one of these is shown in Figure 11. Ideally these rotors would be transfer moulded and some have now been fabricated by this route, but initially the components were copymilled from statically pressed billets, fired and finish-machined to remove excess material, left for support during the milling.

The rotors were submitted to Ricardo & Co. Ltd., a consultant and design organisation, for testing. After balancing these were run in a turbine test rig consisting basically of a turbocharger, converted into a single shaft gas turbine, which could be run at increasing temperatures and rotational speeds until failure occurred.

Three rotors were tested in all. The first would not self sustain because the shaft was too rough but the other two became self sustaining at about 63,000 rpm and as this represents a measure of aerodynamic efficiency, such results were encouraging. The tests were continued and one rotor failed at 80,000 rpm and 661°C and the other at 83,000 rpm and 624°C. Although these results are good, the potential strength of the material was not achieved and it is thought that failure was initiated by flaws introduced on 'green' machining. Thus transfer moulded or slip-cast rotors should perform better.

6. FUTURE DEVELOPMENT

The main aim of the REFEL silicon carbide development programme in recent years has been to increase the repertoire of fabrication processes without loss of quality and consistency in the final product. To a great extent the programme has been successful as evidenced by the performance of a wide range of REFEL silicon carbide components in engine trials.

However, if ceramic components are to be used in commercial engines then cheapness, ease of fabrication and guaranteed life are all important. Thus, the present REFEL silicon carbide development programme has three major objectives. The first is to reduce production costs by development of mass production techniques which are appropriate both for the compaction and firing processes. The second objective is to increase the versatility of all the recently established fabrication routes so that the more complex shapes may be made by simpler and cheaper techniques. To this end basic studies are being made on injection moulding and slip casting. Finally, the third objective is to improve the performance range of REFEL silicon carbide components. The present target is a significant improvement in strength and strength distribution. Again, the current programme is concerned with a basic study of the factors controlling strength with particular reference to grain size and the effect of surface condition. At the same time the effect of using sub-micron feed materials on the developed fabrication technology is being assessed.

7. CONCLUSIONS

REFEL silicon carbide was developed to operate in the extremely hostile environment of a nuclear reactor, at temperatures in excess of 1000°C, in an oxidising atmosphere and at relatively high levels of thermal stress.

The properties of REFEL silicon carbide which suited it to the nuclear application viz. high temperature stability in an oxidising environment under conditions of thermal stress are the same as those needed for the analogous Gas Turbine application.

The manufacturing route for REFEL silicon carbide is well established and the product is consistent.

A wide range of fabrication techniques may be used to form components in the 'green' state and because little or no dimensional change occurs on firing, final machining is minimised.

Gas turbine tests to date have shown REFEL silicon carbide to be a suitable material for most stator applications, and superior to other materials for the combustor. In addition turbocharger rotor tests have been encouraging.

The aim of future work is to increase the versatility of the fabrication process, to make component manufacture cheaper and easier and to produce a stronger material.

8. REFERENCES

1. Fabrication and properties of self-bonded silicon carbide bodies. C W Forrest, P Kennedy, J V Shennan. Special Ceramics 5. (BCRA) p99 1972.
2. Non-destructive testing of silicon carbide tubes. J Rooney. Non-destructive testing, June 1973.
3. P Popper ed. Special Ceramics, London, Heywood P209, 1960.
4. An assessment of the performance of REFEL Silicon Carbide under conditions of thermal stress. P Kennedy, J V Shennan, P Braiden, J McLaren and R Davidge. Proc. Brit. Ceram. Soc. Vol. 22, 1973.
5. Ceramics with potential for gas turbine applications. C R Gostelow, J E Restall. Proc. Brit. Ceram. Soc. Vol. 22, 1973.
6. Delayed fracture and creep in silicon carbide. J Rumsey, A L Roberts. Proc. Brit. Ceram. Soc. Vol. 7, 1967.
7. The relationship between delayed fracture, creep and texture in silicon carbide. P Marshall. Special Ceramics 4 (BCRA) 1968.
8. Strength parameters relevant to engineering applications for reaction bonded silicon nitride and REFEL silicon carbide. R W Davidge, G Tappin, J R McLaren. Powder Metallurgy International Vol. 8, No. 3, p110, 1976.
9. Deformation behaviour of dense polycrystalline SiC. P L Farnsworth, R L Coble. J. Am. Ceram. Soc. Vol. 49, no. 5, p264, 1966.
10. Creep testing of high temperature engineering ceramics. N J Osborne. Proc. Brit. Ceram. Soc. Vol. 25, 1975.
11. Figures-of-Merit for the Thermal Stress Resistance of High-Temperature Brittle Materials: a Review. D P H Hasselman. Ceramurgia International, Vol. 4, no. 4, p147, 1978.
12. High gas velocity burner tests on silicon carbide and silicon nitride at 1200°C. W A Saunders, H B Probst, NASA Technical Memorandum X-714 79.
13. The effect of fission fragment irradiation upon the oxidation resistance of silicon carbide by oxygen at 950°C. M J Bennett, G H Chaffey. J. Nucl. Mat. Vol. 39, p253, 1971.
14. Active to passive transition in the oxidation of silicon carbide. J Antill. Corrosion Science Vol. 11, p337, 1971.
15. The impact of high technology on mechanical seals for industrial applications. R A W Green. Indian Pump Manufacturers Association - Silver Jubilee International Technical Seminar, November 1976.
16. The effect of impurity doping on some physical properties of REFEL silicon carbide. B North, K E Gilchrist. J. Am. Ceram. Soc. (to be published).
17. Fabrication of REFEL silicon carbide components by isostatic pressing. C W Forrest, P Kennedy. Special Ceramics 6 (BCRA) 1975.
18. Nozzle guide vane systems for automotive engines. J S O'Neill - private communication.
19. ARPA/ERDA/FORD ceramic turbine programme. A F McLean. Ceramics for High Performance Applications II. - Proc. 5th Army Materials Technology Conference, 1977.
20. Development of ceramic parts for a truck gas turbine at MTU. W H Peschel, W Siebmann, E Trappmann. Ceramics for High Performance Applications II. - Proc. 5th Army Materials Technology Conference, 1977.
21. Some experience in the design and evaluation of ceramic combustion chambers for small gas turbine engines - G Sedgwick. This meeting.
22. Development and testing of REFEL silicon carbide radial turbine rotors. R W Oldfield, P Kennedy. Proceedings of Science of Ceramics No. 10, 1979. (To be published).

TABLE 1

Comparative values for REFEL self-bonded silicon carbide and other materials

Material	Density g/cc	Hardness kg/mm ²	Rupture modulus 'σ' MN/m ²	Young's modulus 'E' GN/m ²	Poissons ratio	Thermal expansion coefficient 'α' x 10 ⁻⁶ /°C 0-1000°C	Thermal conductivity 'k' W/m°C		Thermal shock parameter kσ/Eα at 500°C W/m
							500°C	1200°C	
REFEL SiC	3.10	3000	525	413	0.24	4.3	83.6	38.9	25000
Hot pressed Silicon Nitride	3.20	2500-3500	689	310	0.27	3.2	17.5	14	12000
Reaction Bonded Silicon Nitride	2.60	900-1000	241	220	0.27	3.2	15	14.2	5500
Sialon	3.2	2500-3500	550	304	0.27	3.2	15.3	11.5	8500
Hot pressed Beryllia	3.03	-	207	400	0.34	8.5	62.7	16.7	4000
Hot pressed Alumina	3.90	2500	480	365	0.27	9.0	8.4	5.0	1000
Tungsten Carbide (6% CO)	15.0	1500	1412	606	0.26	4.9	86.0	-	-

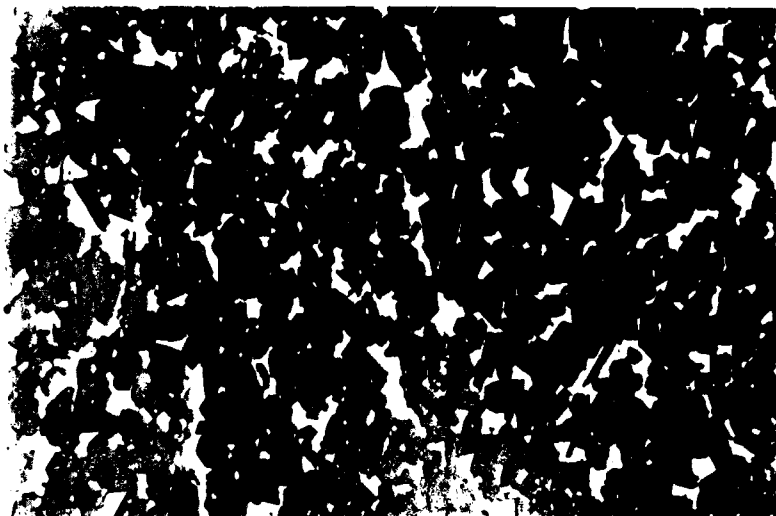


Fig. 1 Photograph showing the microstructure of REFEL silicon carbide

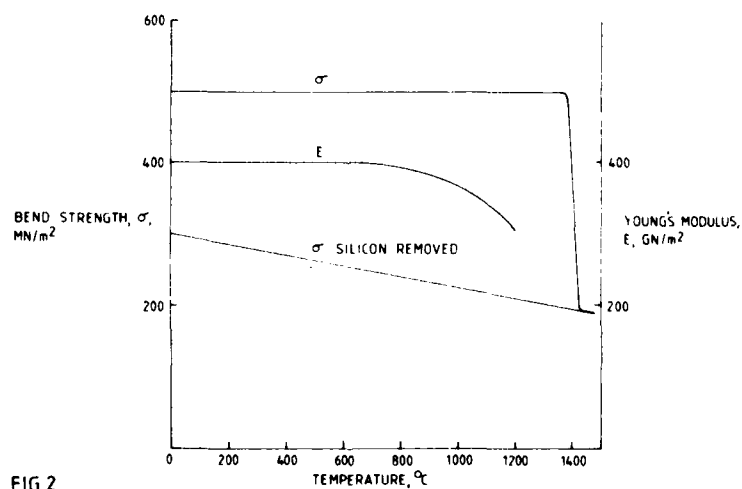
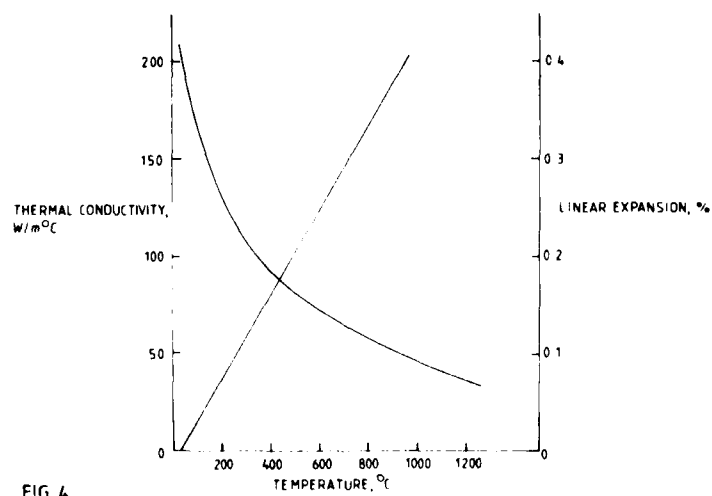
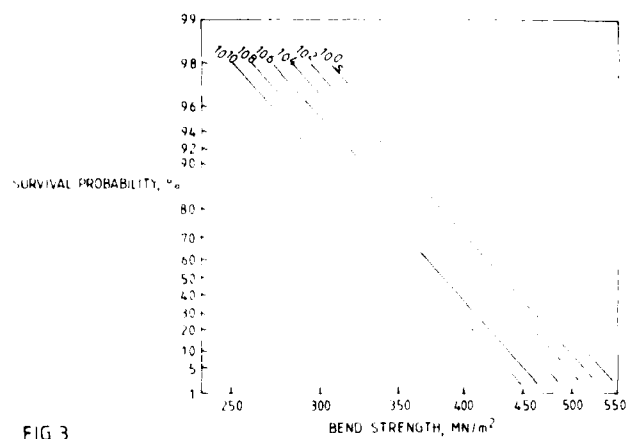


FIG 2
VARIATION OF THE STRENGTH AND YOUNG'S MODULUS OF REFEL SILICON CARBIDE WITH TEMPERATURE



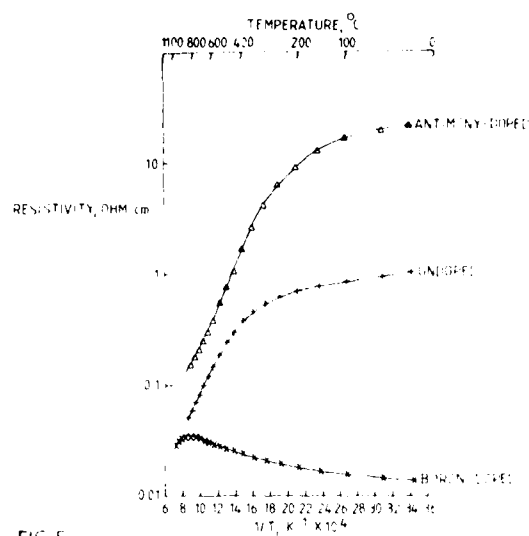


FIG 5
VARIATION OF ELECTRICAL RESISTIVITY WITH
TEMPERATURE FOR DOPED AND UNDOPED REFEL
SILICON CARBIDE



Fig. 6 Photograph showing a British Leyland shroud

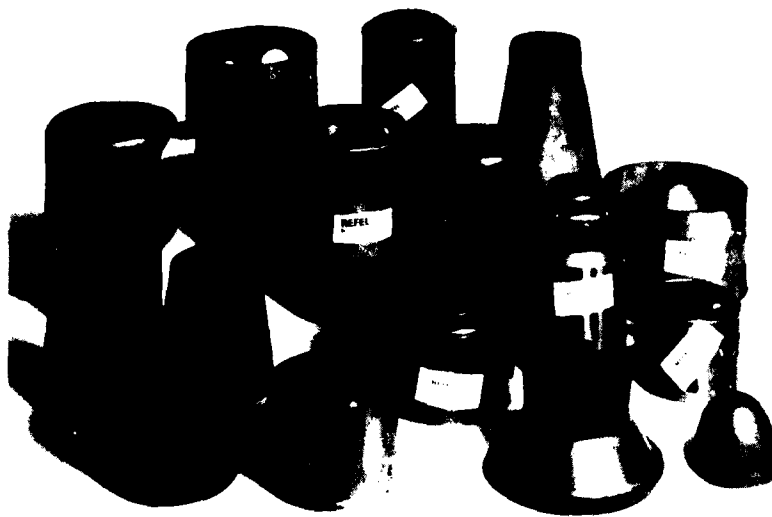


Fig. 7 Photograph showing assorted combustors

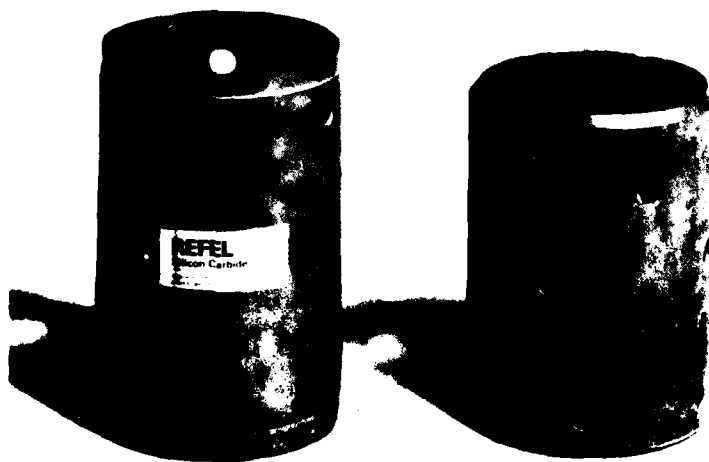


Fig. 8 Photograph showing Ref combustors



Fig. 1. Mechanical part with "M" marking on the side.



Fig. 2. Mechanical part with "M" marking on the side.

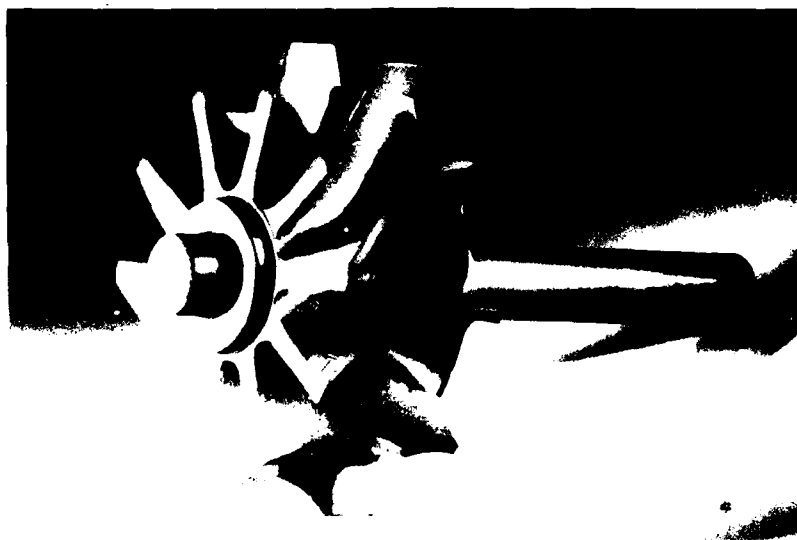


Fig. 11 Photograph of turbocharger rotor

DISCUSSION SUMMARY

SESSION II - ROTATING CERAMIC COMPONENTS

by

A.F. McLean
Engineering and Research Staff
Ford Motor Company
Dearborn, Michigan 48121

Chairman Acurio opened the session by welcoming attendees. He suggested to those in doubt about the potential use of ceramics to tour the local Roman Museum to find out how many ceramic pieces have withstood the test of the ages.

During the session, Chairman Acurio thanked authors for what he called pioneering efforts on ceramic turbine blades and rotors. He cited two urgent problems: (1) to assure ourselves that we can process materials as we wish, and (2) to put innovative designers to work to solve problems of ceramic adaptation such as ceramic-to-metal couplings. He felt that the successes in the area of ceramic rolling element bearings should provide stimulus to explore more applications.

Chairman Acurio closed the session and, on behalf of Professor Pucci and Propulsion and Energetics Panel, thanked Professor W. Bunk and DFVLR for joining the SEMP Meeting and thanked authors and interpreters for their fine efforts.

An edited record of the session discussions follows:

SILICON NITRIDE TURBINE BLADE DEVELOPMENT

by F.B. Wallace, J.E. Harper, C.R. Dins, D.W. Richerson and H.L. Kington

W.H. Brown, US

You mentioned a significant amount of power increase and fuel consumption reduction. How much did you demonstrate?

Author's Reply

We approached testing conservatively with large tip clearances on the order 0.050"; however, even with that we demonstrated an increase of about 30% in horsepower and a reduction of about 7% in SFC.

E.C. van Rueth, US

Would you say a word about two things in the program: (1) the chipping rig that your people have developed, and (2) the problems that you have had with the static components?

Author's Reply

Both of these areas relate to the static hardware, and it is clear that the problem of contact stresses needs further technical effort. We feel that this is a problem that we do not readily understand. For example, how are the stresses tied in with friction, and how is it to be handled in ceramics - we are not entirely sure at this time. Some of the difficulties in the static structure are possible due to relatively high loads taken through the outside flowpath where we have loads accumulating from the first and second-stage stators. Those loads have been shown to be high enough to cause chips. In order to resolve the problem, we would like to better understand the chipping contact stress phenomena. Does that answer your question?

E.C. van Rueth, US

Yes, but would you say a little more about the chipping experiments you are doing?

Author's Reply

AiResearch is now engaged in some preliminary chipping tests; we are just now getting a direction and are going through some matrix experiments to sort out some of the contact stress problems. With respect to silicon nitride chipping, we are finding problems with reaction bonded material - not hot pressed material. With the reaction

bonded material, there can be sticking at higher temperatures and coefficients of friction can increase to .5 and even up to 1.0. When operating in the 2000°F range, compliant layers don't necessarily help and, in some cases, can aggravate sticking to further contribute to chipping. Again, we really don't understand the phenomena adequately at this time but are gathering experimental data.

A.F. McLean, US

Are your attachment problems primarily ceramic-to-ceramic problems or ceramic-to-metal problems?

Author's Reply

It's primarily between the ceramic components. In some locations in our design, we have ceramic-to-ceramic attachments where we have to be concerned about friction because it can get higher at higher temperatures. We have used compliant layers or metal strips between ceramic components but, despite this, we have seen sticking in some cases, which contributes to chipping problems. Again, we are still learning in this area.

H.M. Burte, US

In light of the continuing problem of ceramic attachments of which the contact stress problem is one specific part, would you say that the state-of-the-art at present does not allow us to analytically treat the contact in a satisfactory way, and that we still have to proceed using an iterative empirical approach to the problem?

Author's Reply

Relative to the blade, we have had excellent correlation with our analysis and test. We have not seen any problems in the contact area with the blades. The chipping and sticking problems that we have seen have been primarily with the static reaction bonded materials.

H.M. Burte, US

But I heard you talk about the blade in one case where you had to empirically change the nature of your compliant layer because you didn't adequately analyze the situation.

Author's Reply

The problem there was irregularities in the contact area; the harder layer did not provide for complete seating. Once we'd lapped the slot, the blade frequencies were as predicted; using the platinum compliant layer was an additional seating aid which did not change the frequency but, we felt, would help reduce risks.

Question: (questioner unidentified)

You mentioned the strength improvement of the oxidation treatment over ground specimens. Did you do any thermal cycling to see how the strength level was retained after cycling?

Author's Reply

We did some preliminary cyclic tests in our materials characterization program as a survey to check temperatures in the hot pressed materials. Most of this testing involved 50-hour, 25-cycle testing. We did not get into very long times and very many cycles.

N.L. Parr, UK

I wonder if you've given any consideration in your future work for developing an overspeed proof test as a means of correlating your ordinary NDE techniques with real life situations? It seems to me if you're going to use ceramics at all with confidence, you must adopt a proof test philosophy. For instance, in examining your chip work or compliant layer work, if you could increase the severity by proof load testing up to 150% to 170% load—that sort of thing—you might get a very good NDT technique which would give you confidence in use.

Author's Reply

Again, the chipping problem is primarily related to the reaction bonded static structures, hot pressed silicon nitride blades have not really given any problems. Both NDE and proof testing appear to be satisfactory for the current demonstration program.

N.L. Parr, UK

Well, that's not my point. It seems to me the proof test route with ceramic materials is a good *research area* to pursue and I'd like to see that as one of your future objectives.

Author's Reply

Yes, the proof testing of the blade is straight forward and does lend itself very well. Some of the problems in our static structure are not quite so easily resolved with proof testing, but you're right; this is an area for research.

K.Trappmann, Ge

In one of your slides you said that you didn't have primary blade failures. Did you have secondary failures and what sort of secondary failures did you have?

Author's Reply

The primary failures were related to the static hardware either from thermal shock or other problems such as attachments. For example, a crack might propagate through an airfoil causing a large chunk to come out and generate further secondary damage. It's difficult to tell but when debris comes through the rotor, the rotor blades are smashed and the secondary damage usually entails losing the airfoils of the turbine blades.

K.Trappman, Ge
Completely?**Author's Reply**

Yes.

R.Kochendorfer, Ge

You mentioned a number of six rejects out of 205. That was after non-destructive testing. Can you give us the number selected related to the total number of plates manufactured?

Author's Reply

The bulk of the blades that were rejected other than by proof testing exhibited chips or cracks from machining; they maybe would account for another 10% as a very rough estimate; I don't have the exact number. These defects are usually very obvious and usually a problem in manufacturing such as dropping or bumping or abuse in machining. We seldom had blades rejected in x-ray, because of prior control of the billet material. As a result, the material in blades was very sound and the failure rate in proof test was quite low.

E.M.Lenoe, US

You did your engine and rig tests with vintage 1977 materials. Would you comment on what you would choose now, or if you would change your material selections?

Author's Reply

We feel that the hardware we have has a good chance of making the goals. Obviously, there have been many material improvements and we have incorporated some of those as we went along such as flash oxidation. As far as investigating other ceramics such as silicon carbide, we really haven't looked into that. We have been concentrating on our design as it is, and we feel that minor improvements such as flash oxidation will get us through our demonstration program.

DUO-DENSITY CERAMIC TURBINE ROTOR CONCEPTS, MATERIALS, PROCESSES AND TEST RESULTS

by R.R.Baker and A.F.McLean

E.Tiefenbacher, Ge

I have two questions. The first question is: Have you ever measured the aerodynamic efficiency of your rotor in a cold flow rig?

Author's Reply

No, we haven't. However, we have taken the dimensional inspection charts from actual ceramic turbine rotors that we've made and found that dimensions fell within the tolerance band of the aerodynamic design. So if the aerodynamist did a good job, the rotor should perform.

E.Tiefenbacher, Ge

The second question is: In your hot spin rig it seems to me that the tip clearance is about as big as half of the blade height. Is that correct?

Author's Reply

Yes, the tip clearance in the hot spin rig is very big

E.Tiefenbacher, Ge

Do you think you get realistic conditions with such a clearance? I would say that the heat transfer to the blade is much less than in an engine so the temperature in the rotor is less than it should be.

Author's Reply

Well, to the contrary, one of the things that I didn't particularly like about the hot spin rig is that it's more severe on the blades temperaturewise because we heat up the blades with jets of natural gas until we get a correct temperature on the rim of the rotor. Under this condition for a given rim temperature, the blades get hotter in the test rig. When we run in the engine, we control the average turbine inlet temperature and have tip clearances in the order of 0.010".

R.Kochendorfer, Ge

Just to get a feeling about the number of rotor fabrication trials you have made, did you start with serial number 1?

Author's Reply

The serial number relates to a hot pressing trial and includes the pressing of billets as well as rotors. If you divided the serial number by 2, that would probably be a reasonable estimate of the number of rotor trials.

R.Kochendorfer, Ge

Well, you mentioned a serial number rotor of about 2000, so it is quite a big number isn't it?

Author's Reply

Yes, however, the simplified two-piece hot press bonding concept that ran in the engine for 37 hours was only the second or third rotor made with that particular concept. The major problem before that breakthrough was that of damaging the blade ring during hot pressing often to the extent of fracturing complete blades, so a test wasn't needed to assess quality.

H.M.Burte, US

I have two questions: (1) Your numbers seem to indicate that, from a distribution function point of view, the Weibull function is an adequate approximation. Do you have any reason to think, based upon scaling experiences, that the Weibull function isn't adequate, and (2) Do you feel that for actual use of ceramic rotors, some proof testing approach will be needed or do you think you can avoid that?

Author's Reply

Let me answer your second question first. I believe proof testing is mandatory if you can do it without severely overstressing the component. For instance, proof testing the blades on an all ceramic rotor or a metal ceramic hybrid makes sense because you can spin it up to speed without overstressing, for example, the center of the metal or ceramic rotor. However, if you tried to cold spin an all-ceramic rotor to a speed where you would stress the center of the rotor disk to the same stress experienced in engine operation, you would lose nearly all the blades because you have to centrifugally generate a stress equivalent to a combined centrifugal and thermal stress. Certainly we like the idea of proof testing, but sometimes don't see how you can do it.

On your first question regarding the adequacy of Weibull for scaling, we have looked at both surface and volume effects but have based our predictions to date on volume and that seems to be adequate.

A.F.McLean, US (Co-author)

Can I make an additional comment on the question "Is it adequate to assume we could extrapolate Weibull now for scaling up to production?" I think the answer at this time is probably, "no" because we have not yet tested the large number of samples needed to confirm the high reliability, say 99.9+%, that would be required in production. Data used to date to represent the 99.9+% condition, are really estimates based on extrapolation from lower tested reliabilities. Clearly to apply ceramics to say automobiles, we must do more testing to verify extrapolations.

E.M.Lenoe, US

I wanted to suggest to Mr Baker that it would be useful to the audience to very briefly indicate the number of concepts that Ford had actually gone through as a number of people here are unaware of the magnitude of the effort.

Author's Reply

In the duo-density rotor concept alone, we went through about a dozen totally different changes in the graphite tooling concept to bond the blade ring to the hub, for each of these, we made several rotor fabrication trials. In addition, prior to the duo-density rotor concept, we investigated other ways of making all-ceramic rotors, such as

CVD* silicon carbide rotors; machined rotors from hot pressed silicon nitride and hot pressed silicon carbide using ultrasonic machining, electric discharge machining and diamond grinding; and pseudo iso-pressing of rotor pre-forms of reaction bonded silicon nitride.

**DEVELOPMENT OF AN INTEGRAL CERAMIC BLADE-METAL DISK WITH
CIRCUMFERENTIAL BLADE ATTACHMENT**
by S.A.McLeod, B.H.Walker and M.I.Mendelson

G.Wirth, Ge

Did you apply any heat treatment after bonding of the super plastically deformed rim to increase grain size?

Author's Reply

Yes, we applied two types of heat treatment. One was for the disk to develop the correct microstructure and provide improved creep and stress rupture characteristics. The other was for the blades and was basically an oxidation heat treatment to form a thin SiO_2 layer similar to that mentioned in the first paper in this session.

G.H.Sines, US

I wonder if you would like to make some more comments about using a metal compliant layer. In the compression testing of ceramics, it seems as if a compliant metal layer is not very good; in fact, it's liable to drop your strength at the interface by a factor of three sometimes. Perhaps, in your case, the compressive stresses between the two surfaces are quite low but have you given thought to other materials? Are you satisfied with platinum, and how much platinum do you normally carry with you on these meetings?

Author's Reply

The last question is the easiest really, none that I know of! From our experience to date, the main feeling about platinum as a compliant layer is that it works. Certainly, we don't think it's an ideal material, but its compliancy has given satisfactory results. Now, it's not perfect because sometimes it becomes extruded out of the disc attachment area; sometimes it thins down and other times it tends to overlap, so there have been some small problems connected with the use of platinum as a compliant layer. To solve these, we have modified the details of our fabrication procedures and since then have had improved results, and haven't looked at any other materials.

G.H.Sines, US

I believe that the compliant metal layer has several disadvantages. One is the extrusion transversity would give you a shear flow that would give you transverse tensile stresses. Its transverse elastic compliance is much lower than the specimen which is bad and also gives you transverse tensile stresses. Further, there is always a possibility that the compliant layer might intrude into surface flaws and pry them open to split your specimen. Perhaps, you're in a low enough stress range to avoid these problems, but I believe these three things could lead to difficulty.

Author's Reply

I'd be extremely pleased if you would suggest any other materials, and I don't say that facetiously, but you know we haven't discovered any.

G.H.Sines, US

At room temperature, paper works very nicely, but I'm trying to think of a high temperature paper for you.

P.Popper, UK

To a ceramist, your description of forging brings up an image of hammer blows, but I have a suspicion that your process involves a squeeze rather than hammer blow which I would call hot pressing. Could you say which it is?

Author's Reply

Yes, as a ceramist myself, you're correct. This is an iso-thermal hot pressing operation where the advantage of the superalloy is its super plasticity. We apply the pressure at temperature and squeeze it down to size keeping the grain size very fine; that's very important in the whole process.

K.Trappmann, Ge

Does the forging process have any detrimental effect on the material properties of your blades? I got the impression that the failure speeds of your blades are relatively low.

* Chemical Vapor Deposited

Author's Reply

We haven't seen any although that doesn't mean we don't have any. One of the problems in assessing this is the fact that the blades can twist about their radial axis and have to be supported very well on the sides, or else they pick up extra stresses. We don't believe there is any material degradation and would expect that, if failure speeds are low, it could be due to this mechanical attachment stress.

INVESTIGATIONS OF A HOT-PRESSED SILICON NITRIDE TURBINE ROTOR

by E. Tiefenbacher

F. Blake Wallace, US

Could you tell me the source of your hot press silicon nitride billets?

Author's Reply

Yes, we got our billets from Norton Company and from Annawerk. Today we prefer billets from Annawerk because they guarantee us a certain strength, and, if one of the billets fails in proof testing, we can get a replacement without any cost.

H.M. Burte, US

I take it from what you have said and from your paper that, despite all of the progress in analyzing temperature and stress distributions, you still find it necessary to experimentally test and modify. In other words, the analysis is not yet adequate. Is that true in your experience?

Author's Reply

Yes, though one of our problems is accurately assessing the environmental conditions of a high temperature ceramic wheel. We are working daily to better assess temperatures in the neighborhood of the wheel as a basis for establishing heat transfer coefficients, etc. Of course we have done quite a lot of calculations, but I didn't mention them here because this maybe would be tedious. We try to combine experimental procedure with theoretical calculations; and, at this time, we are convinced that we have to do quite a lot of experimental work.

G.C. Deutsch, US

What do you see as the fabrication or production method to get the cost down from the present obviously very expensive way you're doing it?

Author's Reply

Today we make it by a laboratory procedure using a single machining spool. The most simple scale up would be to make multi-spool equipment to machine several blades at a time; then you could divide the time by 5 or 10. However, we have to learn so much at this time not only on the rotor, that we believe we should continue using the laboratory machining procedure to make rotors. Once we reach our goals with the engine, then we will think about other manufacturing methods; and, of course, there are quite a number of material and process developments underway which we will continue to monitor.

P. Popper, UK

If I understood you correctly, you started by doing thermal shock testing using hot and cold gas; later you made a very interesting remark that if you have a ceramic heat exchanger the temperature cannot change very rapidly. Could you give an idea what sort of rates of temperature change you might expect with a ceramic heat exchanger, for instance, if fuel was suddenly cut off?

Author's Reply

Well, there is no question that the temperature goes down during deceleration more slowly with the the heat exchanger. I think maybe from 1200°C to 600°C in about one second. Now, without a heat exchanger, temperatures would come down about twice as fast or more.

I. Kvernes, No

Are you considering use of ceramic coatings instead of solid ceramics for some parts?

Author's Reply

With respect to thermal barrier coatings on superalloys, we have not done any work in this area but are following the literature. However, I think it's very difficult to achieve a thermal barrier on small blades.

I.Kvernes, No

Ceramic coatings have been used as a thermal barrier in some diesel engine experiments and have worked very well.

CERAMICS IN ROLLING ELEMENT BEARINGS

by C.F.Bersch

H.T.Larker, Sweden

Did you experience any adverse effects from the directionality of hot pressed silicon nitride, that is, different strengths in different directions?

Author's Reply

I can only say no, predicated on our experience with ceramic balls which is at least as extensive as that with rollers. Obviously, balls would show directional problems if there were any, and we haven't had any when the balls were of proper quality.

THE FABRICATION AND PROPERTIES OF REFEL SILICON CARBIDE IN RELATION TO GAS TURBINE COMPONENTS

by P.Kennedy

E.M.Lenoe, US

This is not a question but an expression of gratitude to Peter Kennedy for pointing out a deficiency in the graphs regarding Refel that were presented in Session I. The data was very early data and of questionable quality, for instance, it was obtained from oversized specimens with a much larger span than most organizations now use. I am sure that the material of the qualification test combustor that you illustrated had a significantly higher flexural stress.

J.Mowill, No

I have two questions: (1) I would like to know which is the largest part you have made of a scroll type, for example, a transition duct? and (2) What is the longest life of any given part at a temperature of about, say 1200°C?

Author's Reply

In answer to the first question, we haven't actually made a scroll yet; although, I feel it could be made. A component which was rather similar from a fabrication point of view to a scroll is a combustor with a side tube which is illustrated in the paper; this part is about 7" diameter. With a more squat component like a scroll, I think we could increase the diameter to perhaps 10" or maybe 11" at the moment. With respect to longest life, I would rather quote from my own experience which involved a piece of silicon carbide running in a nuclear reactor; it ran for up to about a year under conditions of fairly severe thermal stress especially since the thermal conductivity dropped by a factor of 5 to 10 under irradiation conditions, so that the temperature gradients and hence thermal stresses increased accordingly.

STATIONARY CERAMIC COMPONENT CONSIDERATIONS FOR LARGE INDUSTRIAL COMBUSTION TURBINES

R. J. Bratton
Westinghouse Research and Development Center
Pittsburgh, Pennsylvania 15235 USA
and
K. L. Rieke
Westinghouse Combustion Turbine Systems Division
Concordville, Pennsylvania 19331 USA

SUMMARY

There are major R&D efforts underway in the United States to improve the performance of industrial combustion turbines. The major goals are improved system reliability, capability for fuel flexibility and reduced emissions. Other goals desired are improved efficiency and decreased equipment cost. Design studies have shown that significant performance advantages can be achieved if ceramics can be made to perform reliably. Since stationary ceramic components are likely to find first application in industrial turbine systems, initial efforts will be directed to their development. For the near term, the development of a low emission combustion system that meets regulations for industrial turbines burning heavy fuels has a high priority. This paper reviews work that has considered hot-wall combustion systems to help meet the desired performance goals.

INTRODUCTION

Industry and government in the United States are working together to achieve several specific goals to improve the industrial combustion turbine technology. The major goals are improved system reliability, increased fuel flexibility, reduced emission, higher operating efficiencies, and decreased equipment cost. Achievement of these goals will provide the opportunity for wide-scale use of combustion turbine engines in combined cycle power generating systems operating on coal-derived fuels (gaseous and liquid). These highly efficient combined cycle plants can be advantageously applied to base load or intermediate load duty. In addition, the combustion turbine systems alone can continue to serve peak load duty in the simple cycle mode.

The concept of utilizing ceramic components in advanced turbine systems has been continuously studied in recent years (see References 1-7) as one of several concepts to improve operating performance. These studies have shown that when ceramics are used in engines, reliable performance can be predicted along with significant performance improvements. However, it has been shown also (3-7) that: a) much work remains in order to achieve ceramic turbine technology readiness, and b) stationary components are likely to find first application in industrial combustion turbines. Stationary components in this case include ceramic parts for the combustion system (combustor/transition piece) and those for the combustion turbine (vanes and shrouding).

Improved combustors are needed, in the near term, to meet exhaust emissions regulations for combustion turbines. Of particular concern is the low nitrogen oxide emission limitations imposed by U.S. and local Environmental Protection Agencies. The combustion problems are further compounded with the current trend toward use of heavy petroleum fuels and the use of coal-derived liquid and gaseous fuels. Thus, the industrial combustion turbine manufacturer must be forward looking regarding combustor systems development which addresses fuel flexibility.

The present paper reviews the cycle performance benefits that can be obtained by the use of ceramics in industrial combustion turbines while pointing to specific benefits of the stationary ceramic components, and then focuses on advanced combustor concepts that utilize stationary ceramic components.

COMBINED CYCLE PERFORMANCE OF TURBINE SYSTEMS

A combined cycle plant performance improvement realized over advanced air-cooled turbines provides incentive to develop a coal-derived fuel fired engine with turbine ceramic components operating at high turbine inlet temperature (TIT) (2300 to 2600°F). A potential thermal efficiency of above 51% is attainable on coal-derived liquid fuel delivered-on-site and with a 2600°F TIT (technology development goal) as shown in Figure 1. The coalpile-to-bus bar efficiency potential is about 13% less on low Btu coal gas fuel generated on-site.

The application of ceramics to utility size engines can provide the following benefits:

- Combined cycle plant efficiency approximately 2.8 percentage points greater than that of air-cooled engines at 2600°F TIT (see Figure 1, Ref. 1, 2, 3, 6 and 7).
- Same combined cycle efficiency at 2300°F as at 2600°F TIT air-cooled high temperature turbine (HTT) (see Figure 1).
- Improved corrosion/erosion resistance.

Figure 2 shows the contribution to efficiency when adding ceramics to the turbine stationary vanes and rotating blades (combined forming a stage) or to the stationary vanes only.

- 1st Stage, 51% of total improvement or approximately 2.5% in cycle performance.
- 1st and 2nd Stages, 82% of total improvement or approximately 4% in cycle performance.
- 1st and 2nd Vanes, about 57% of total improvement or approximately 2.9% in combined cycle thermal efficiency.

This allocation of improvement in combined cycle thermal efficiency becomes a major factor in planning the cost effective development and implementation of structural ceramics to commercial engines for utility power generation systems. The benefits of stationary ceramic vane components in the turbine stages are noteworthy.

ADVANCED COMBUSTION SYSTEM

The combustion system (i.e., combustor and transition components functionally and mechanically integrated as a system) is a major and important element of any heat power engine, be it an internal or external combustion engine. The function of the combustor is to convert chemical energy bound in the fuels to thermal energy which is readily extracted as mechanical energy by the turbine element. The transition component of the combustion system functionally contains the hot gas product and ducts it to the turbine inlet under specified flow, temperature, combustor outlet environment, and imposed design constraints.

The primary objective of an advanced combustion system is to meet the following engine design requirements:

- The design high temperature exit gas temperature (technology development goal up to 2600°F).
- A pattern factor (PF) goal = 0.05, where

$$PF = \frac{(T_{max} - T_{avg})}{(T_{avg} - T_{combustor\ inlet})}$$
- Ability to operate on coal-derived fuels (fuel flexibility).
- Ability to meet federal and local EPA emission regulations.

Presently, no known combustion systems exist that provide these high temperature performance goals.

In the case of the combustion turbine system, maximum temperature (i.e., hot spot as defined by T_{max} in the pattern factor (PF) equation above) at the combustor exit is important. At the turbine inlet temperature goal of 2600°F, even a modest local temperature above average may exceed the temperature limit of present "state-of-the-art" structural ceramic materials applied to the combustion system and the turbine inlet vane components. Thus, the need for establishing a PF goal is evident.

Additional key development issues associated with the combustion system designs are summarized as:

- Structural integrity against vibrational forces.
- Structural configuration to minimize thermal stress and interstitial leakage.
- Attachment interfaces designed to accommodate differential expansions and allow for temperature differences between "hot wall" ceramic and outer metal support system.
- Capability to reliably maintain component integrity under engine transient operation conditions, including severe emergency shutdown conditions.

COMBUSTION SYSTEM CONCEPT DEVELOPMENT

As previously noted, the combustion system function is to burn fuel efficiently (whether it be gaseous or liquid) with the combustion air. The combustor is also required to provide a near uniform turbine inlet temperature distribution to limit the value of the local hot spot temperature. Two areas of technology development needed to advance the state-of-the-art application of ceramics to utility sized engine combustion systems are:

1. Combustion process
2. Hot wall combustion system structures

Combustion Process

The following design requirements and system constraints must be factored into the complete combustion process, i.e., chemical energy release process within the containment structure:

- Steady state performance parameters such as pressure drop, turn down, reference velocity, efficiency, maximum wall temperature, heat release rate, etc.
- Positive ignition and flame stability that meet start-up.
- Steady state and shutdown operation requirements of the engine system.
- A 0.05 pattern factor (PF) goal at the combustion system exit (i.e., 94°F hot spot temperature above 2600°F TIT goal).
- Exhaust emissions that meet EPA regulations.

Combustion process designs in general have the following three regions (zones) of commonality to functionally meet design requirements for the combustion "process" (see Figure 3).

- Primary Combustion Zone - Involves fuel preparation, ignition and chemical reactions. This zone also provides means of flame stabilization.
- Secondary Combustion Zone - Completes chemical reactions and provides diluent to the hot gases.
- Mixing - Completes mixing of diluent and products of combustion for turbine entry.

The engine operational requirements and integrated engine and combined cycle performance design constraints influence the high temperature combustion process. As an example, the total pressure drop of the combustion system in today's turbine engine is limited to about 4% in order to maintain high performance; furthermore, combustor efficiency greater than 99% is required by its direct relationship with engine fuel economy and exhaust pollutants.

The combustion process design must be integrated with the mechanical configuration in order to assure that positive and reliable ignition occurs. The combustion process must meet transient fuel/air ratio scheduling requirements of the engine for both normal and predictable malfunction operational modes. The combustion process must remain stable, provide thermal energy to the engine system and meet performance goals and emission limits imposed upon it during the steady state and transient modes of operation.

The pattern factor goal of 0.05 is the most stringent single requirement imposed to date on any combustion system. A critical assessment which weights a development goal of up to 2600°F average turbine inlet temperature against the current available ceramic material strength capability provides the incentive to impose this pattern factor goal on the combustion system.

The EPA emission requirements must be factored into the combustion process development plan from the beginning. The pollutants included in the EPA regulatory requirements are sulfur oxide, unburned hydrocarbons, smoke, particulate matter, carbon monoxide, and nitrogen oxides. With the exception of nitrogen oxides (NO_x) the above pollutants can be controlled by careful attention to combustion system design and fuel clean up. However, NO_x control at high temperatures and high pressures requires fundamental changes in the combustion design approach and requires development.

The thermal NO_x reaction occurs at high temperatures for all combustion processes involving air (i.e., $\text{N}_2 + \text{O}_2$) as an oxidant, and is essentially independent of the fuel. In contrast, fuel bound nitrogen found in many coal-derived liquid fuels forms NO -type compounds during the combustion process. The relative appearance of the two types of NO_x (thermal vs. fuel-bound) is dependent on time and temperature. The NO_x formation can be limited to two processes:

- Low temperature combustion (i.e., lean burn catalytic combustion and others).
- Rich combustion (i.e., a deficiency of oxygen). (The relatively inactive nitrogen doesn't compete with carbon and hydrogen for oxygen.)

The use of either approach means moving through the air/fuel vs. temperature plane of Figure 4. The low NO_x window lies within ABCD, where AB represents the lean limit of combustion without a catalyst. Segments AD & CB represent thermodynamic equilibrium conditions. Segment CD connects maximum acceptable NO_x values on the rich and lean side. If a catalyst is used, the operable NO_x window can be extended to ADCBEF. The rich limit for catalytic combustion has not yet been defined; it is assumed to be at least equal to normal combustion at point A. Point G is assumed to define a reasonable shape of the line connecting A and F.

Hot Wall Combustion System Structures

The potential application of hot wall structures in combustion system component designs include the following concepts:

- Catalytic combustor
- Conventional combustor
- Transition section

An assessment of the application of ceramics in hot wall combustion systems results in the following benefits:

- Hot walls provide high probability of attaining 0.05 pattern factor goal (i.e., low turbine inlet local maximum temperature).
- Hot walls increase flexibility in fuel usage (i.e., coal, gas, coal derived liquids, residuals, etc.).
- Hot wall designs (including catalytic) permit burning over wider air/fuel ratios.
- Hot wall designs reduce coolant requirements when operation at high exit temperatures (especially important when operating with low Btu gas).
- Hot wall designs provide flexibility in rich/lean staged combustor concepts to meet NO_x emissions with high bound N_2 fuels.
- Hot wall designs assist in meeting emissions with other combustion process concepts (such as lean burn).

- Hot walls potentially increase life and reliability over cooled metals by providing improved oxidation/corrosion/erosion resistance with coal-derived fuels and reducing structural distortions (thermally induced stress).
- Ceramic hot walls reduce the need for high cost, strategic materials.

The application of ceramic hot wall structures to combustor conceptual designs is shown in Figures 3 and 5 for the conventional combustor and catalytic combustor, respectively. Figure 5 also shows a reference engine used for design concept studies on ceramics in turbine hot section components (9).

The transition section is common to all the combustion systems concepts. This component directs the combustion products to the turbine and maintains or improves the pattern factor developed in the combustor. The shape of the transition is more complicated than the cylindrical combustor regions (see Figure 6). Its complex shape causes additional structural design considerations when applying ceramics to the hot wall concepts. The structures have about the same thermal design objectives with high temperature products of combustion as those expressed for hot wall combustors; i.e., operation at high inner surface wall temperatures, with low heat flux. The concept shown in Figure 7 makes use of a segmented ceramic tile liner concept. The common design elements of such hot wall structures are:

- Inner structural ceramic material.
- Insulation capability to control the hot wall temperature and heat loss to ambient surroundings.
- Cooled attachment layer between the ceramic and outer support layer.
- Outer metal support system.

SEGMENTED APPROACHES TO HOT WALL STRUCTURES

The various combustor and transition concepts are expected to require structural segment designs. The key development issues identified for such structures are:

- Configurations that minimize thermal stress and interstitial leakage.
- Attachment schemes that provide the necessary flexibility to accommodate differential expansions.
- Interface schemes that accommodate thermal gradients within ceramic and metal components, and high temperature differences between them.
- Structural designs that endure high temperature product of combustion without compromising the objective of the 0.05 pattern factor design goal or attainment of the emissions regulatory requirements.
- Structural designs that withstand start-up and shutdown transients and the steady state engine operation.

Examples of a segmented wall structure are shown in Figure 8a and 8b. In Figure 8a, a layered hot wall concept is used. It illustrates ceramic-to-ceramic edge treatments, and use of compliant layers between metal and ceramic. Figure 8b shows a potential hot wall design approach that has been employed in experimental MHD work at Westinghouse. The concept shows a design which features an offset at ceramic edges, a stainless steel plate about the spring clip, and a sealer between clips. This experimental design has successfully contained combustion products approaching 4000°F in the MHD application. The preceding examples display a multi-concept basis from which ceramic hot wall combustion systems may be evolved through development and test programs.

CONCLUSIONS

Recent studies have reaffirmed that significant cycle performance improvements, engine durability and reliability may be achieved through the use of high performance structural ceramics in combustion turbine systems. Reliable stationary ceramic components are needed in the near term, in particular for advanced combustor concepts, that must be developed for the purpose of meeting emission regulations, while providing the user with the capability of using fuels ranging to heavy petroleum fuels and coal-derived fuels. Ceramic hot wall structures are feasible in the near term for the conventional combustor, catalytic combustor and the combustion transition section.

REFERENCES

1. D. T. Beecher et al, "Energy Conversion Alternative Study - ECAS-Westinghouse Phase I Final Report," NASA CR 134941, February 1976.
2. D. T. Beecher et al, "Energy Conversion Alternative Study - ECAS-Westinghouse Phase II Final Report," NASA CR 134941, March 1977.
3. "Final Report, Concept Feasibility Study of Ceramics for Use in Electric Utility Gas Turbines Fired with Coal Derived Fuels," by Committee on the Use of Ceramics in Industrial Gas Turbines, University of Pittsburgh, Pittsburgh, PA 15235, Report SETEC DO 76-10, October, 1976.
4. Bratton, D. G. Miller, "Brittle Material Design, High Temperature Gas Turbine, Final Report on Contract DAAG-46-71-C-0162, AMMRC CTR 76-32, December, 1976.
5. Bratton, "Ceramic Turbine Components Research and Development," Final Report EPRI Contract RP 421-1, March, 1979.
6. "Ceramic Technology Readiness Development Program, Phase I - Conceptual Materials Screening, Interim Report," DOE Contract EF-77-C-01-2786, July,

7. K. L. Rieke, "Ceramic Technology Readiness Development Program, Phase I - Conceptual Designs and Materials Screening, Final Report," DOE Contract EF-77-C-01-2786, March, 1979 (draft not yet released).

ACKNOWLEDGEMENTS

The authors acknowledge the Electric Power Research Institute and the U.S. Department of Energy for their recent sponsored work in the areas reviewed in the present paper.

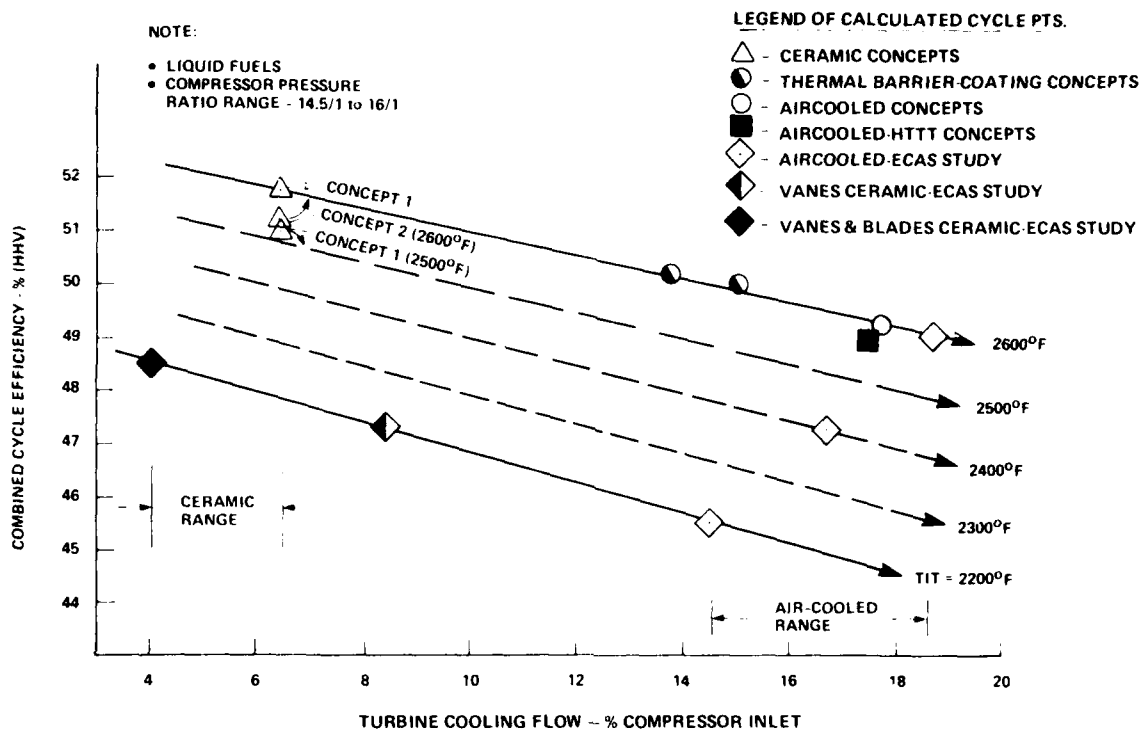


Figure 1 - Combined Cycle Efficiency vs. Cooling Flow

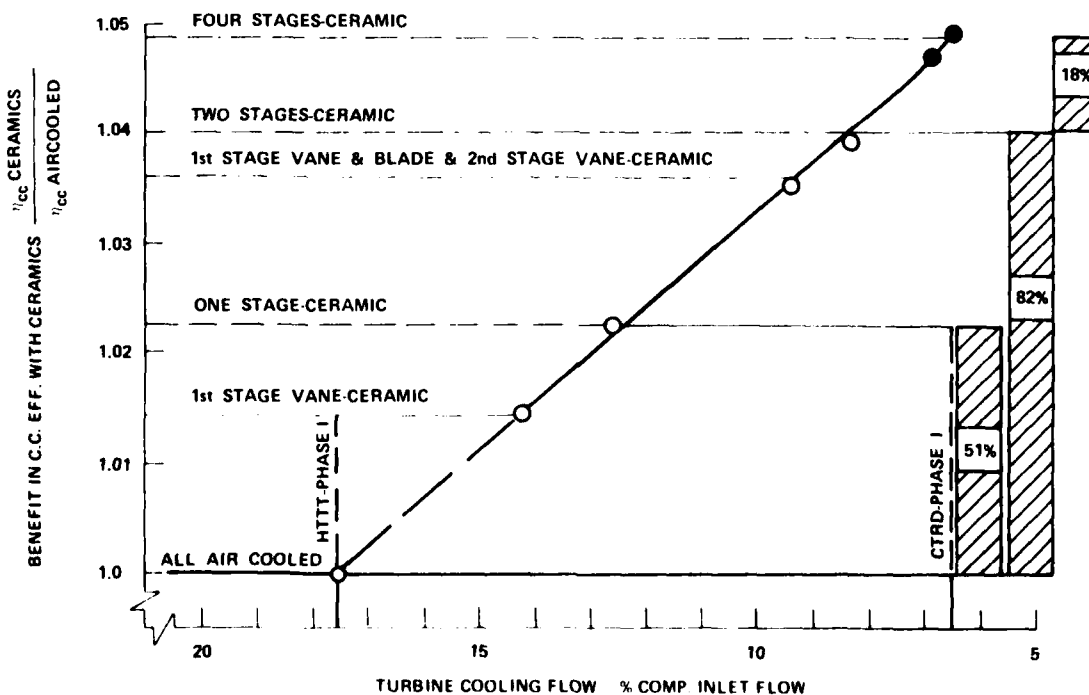


Figure 2 - Benefits in Combined Cycle Efficiency

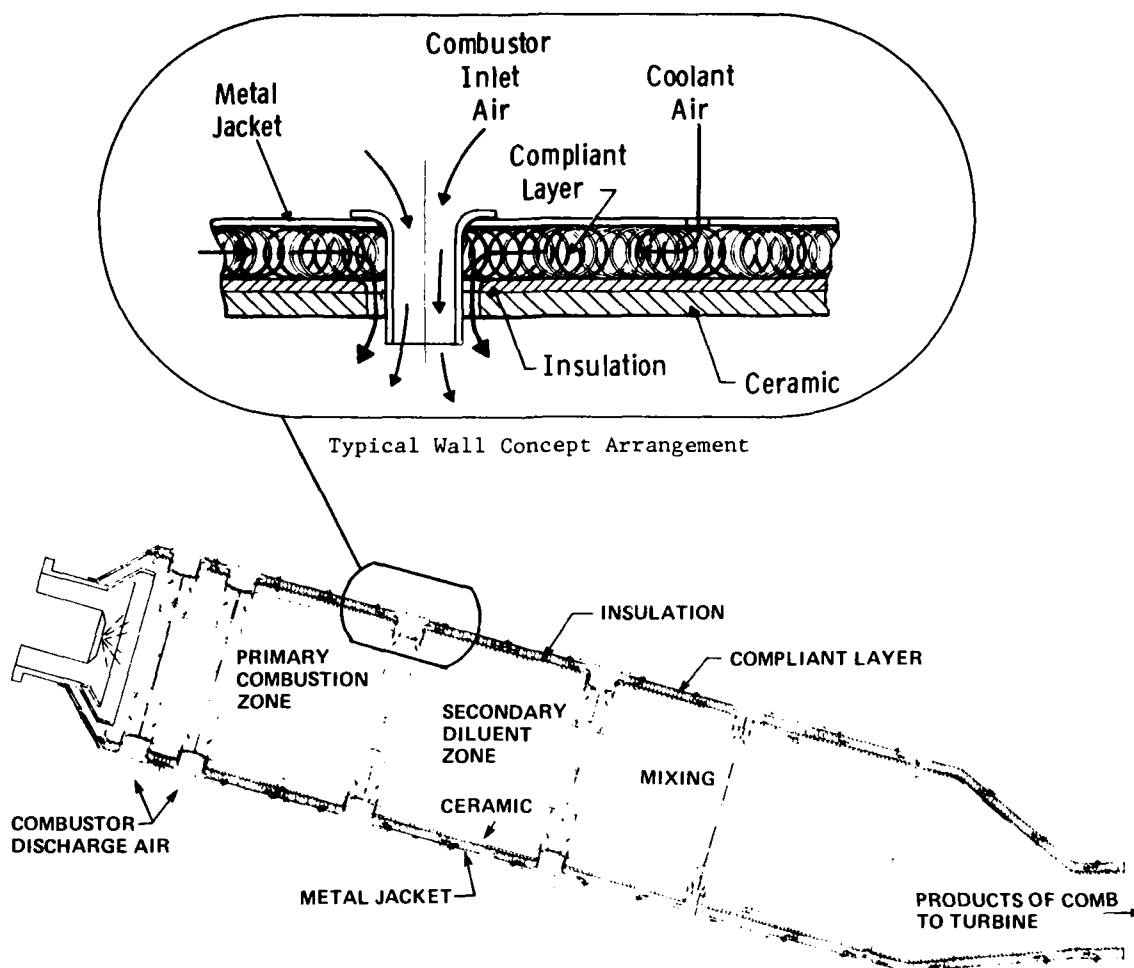
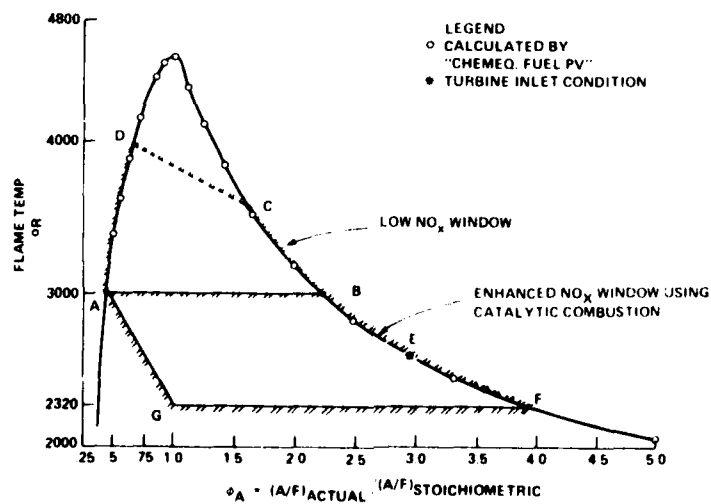


Figure 3 - Combustion Process Zone Allocations

Figure 4 - Low NO_x Window in Temperature-Equivalence Ratio Plane

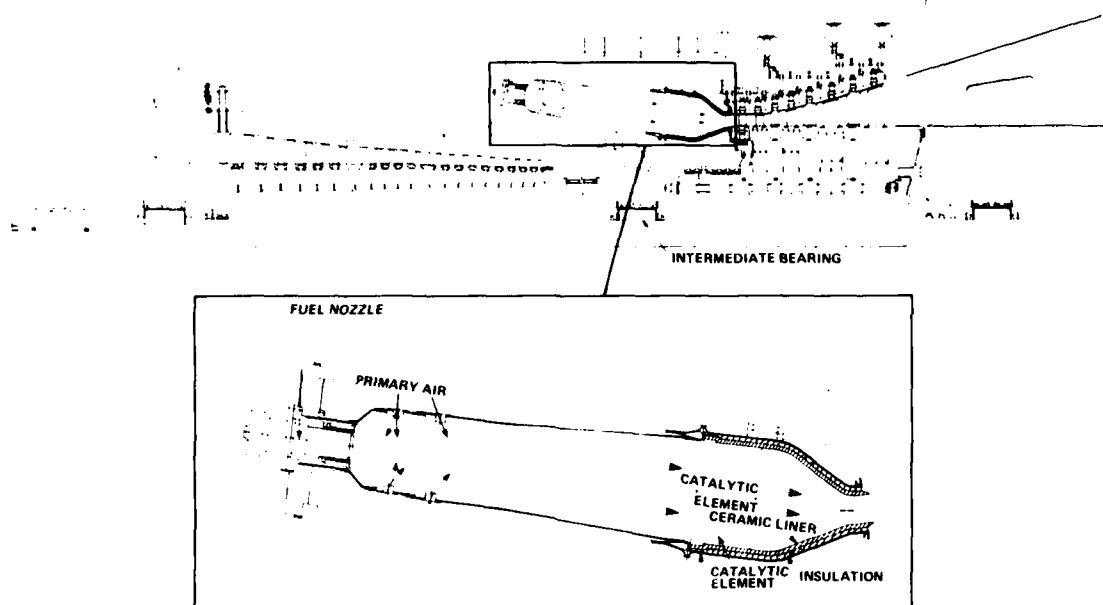


Figure 5 - Arrangement Drawing Showing Catalytic Element in Hot Wall Combustion System

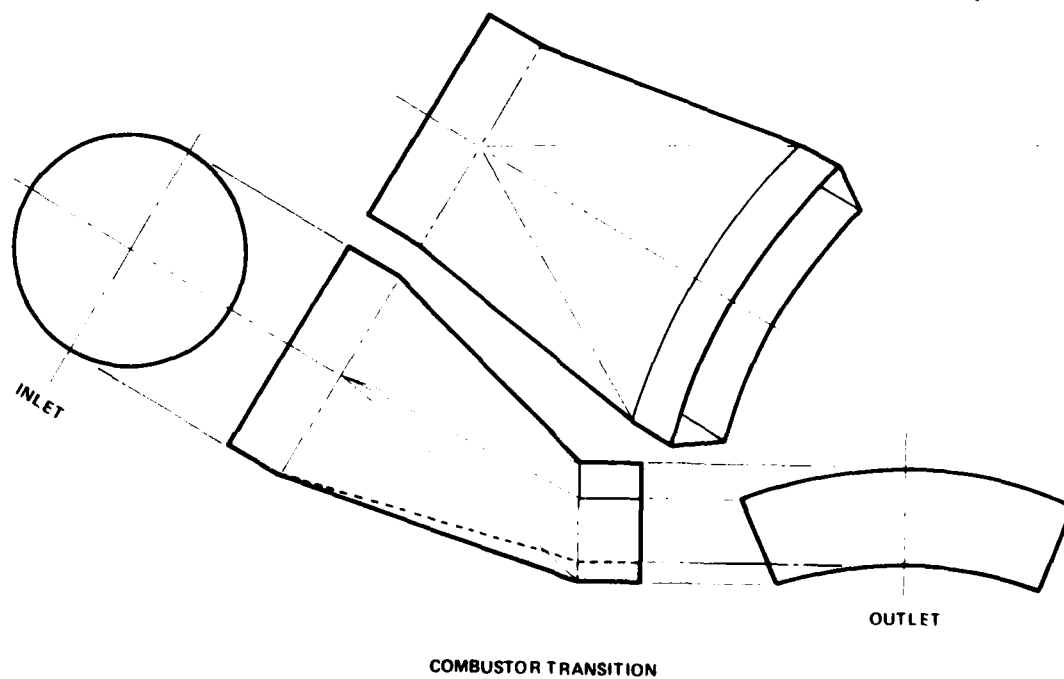


Figure 6 - Typical Transition Configuration

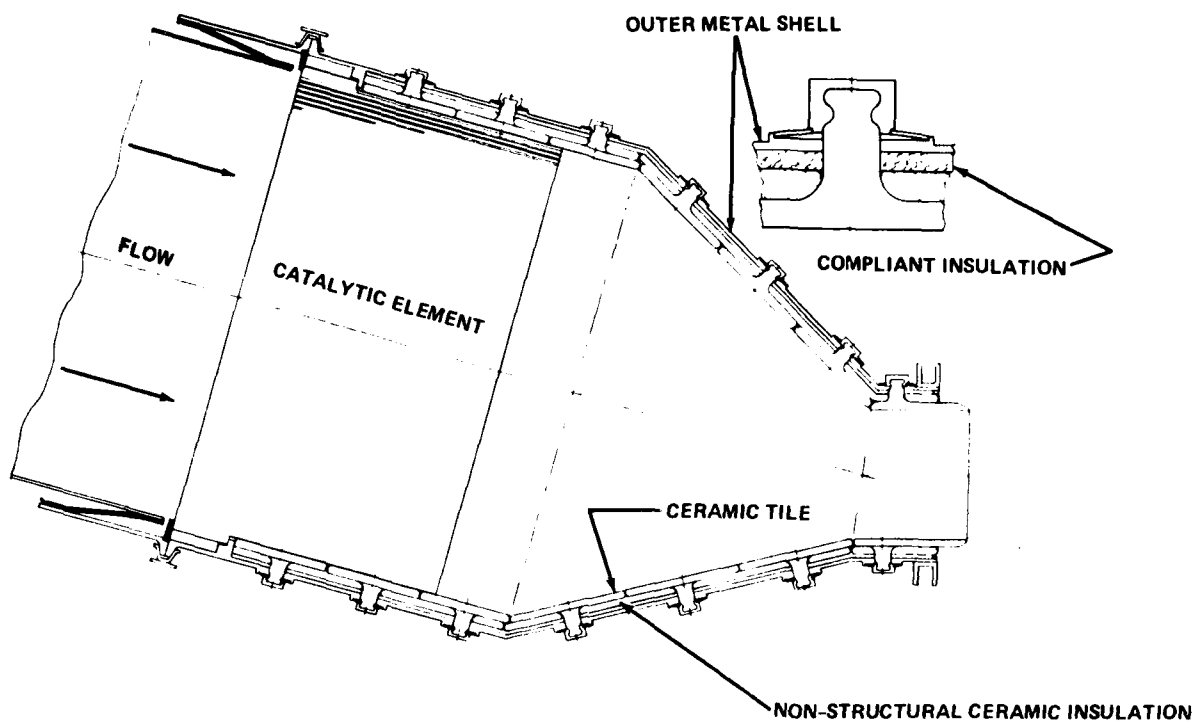
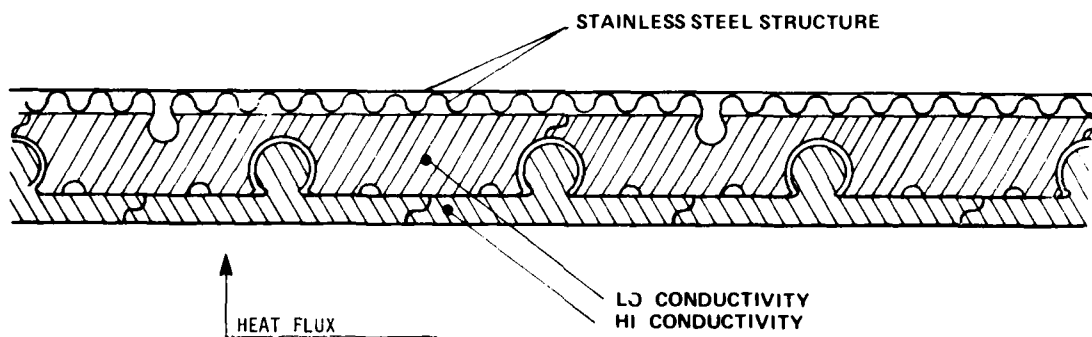


Figure 7 - Multi-Piece Ceramic Tile Liner Transition Concept

(A) CERAMIC LINER WITH KEYED PLATES AND COMPLIANT LAYERS



(B) A HOT WALL DESIGN APPROACH

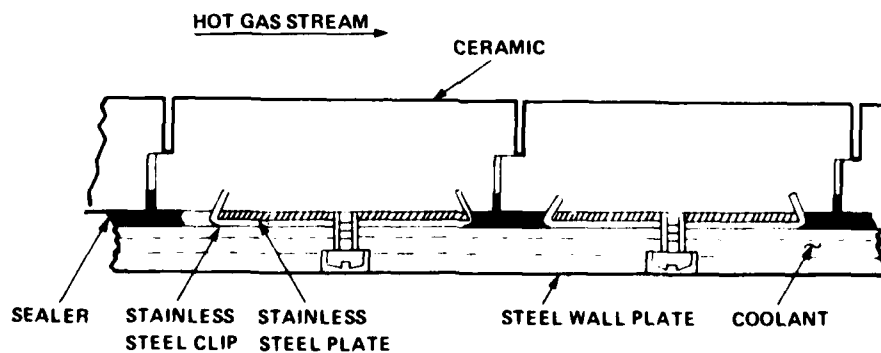


Figure 8 - Segmented Wall Structures Concepts

DEVELOPMENT OF CERAMIC NOZZLE SECTION FOR SMALL RADIAL GAS TURBINE

by

J. C. Napier
 Solar Turbines International
 2200 Pacific Highway
 San Diego, California 92138 - USA
 and

J. P. Arnold
 U.S. Army Mobility Equipment Research & Development Command
 Fort Belvoir, Virginia 22060

ABSTRACT

Ceramics not only offer improved gas turbine performance through higher turbine inlet temperature but can increase engine life because of improved hot end erosion resistance. Development work leading to engine test of both erosion-resistant and high-temperature ceramic nozzle concepts is described here. The first nozzle concept employs ceramic vane sections and had demonstrated a ten to one-hundred fold hot end life improvement under erosive conditions in engine tests. The second concept has been engine demonstrated and offers high erosion resistance as well as the capability of operating at elevated turbine inlet temperatures.

Work on ceramics manufacturing methods for cost reduction with the goal of providing economic incentives for ceramics in production turbines is described.

INTRODUCTION

Recent emphasis on the development of silicon based ceramics for use in the severe environment of gas turbine engines has provided the incentive to consider ceramic materials for engines used in military application to obtain the benefit of improved erosion and corrosion resistance. The Gemini engine shown in Figure 1 has been developed as a simple cycle radial gas turbine engine to provide 10 kW continuous electrical power for various military needs. The engine has been designed for long life (6000 hours minimum before overhaul) with low maintenance requirements. Its multipurpose uses may frequently include operation in dusty or corrosive environments on a variety of fuels which can be detrimental to performance, increase maintenance and shorten life of the engine. Research and development has been initiated to consider the optimum use of ceramic materials throughout the engine to increase power output, improve thermal efficiency, extend life, and decrease dependence on strategic metals.

Promising near term uses of ceramic materials appear to exist in engine applications for wear and corrosion resistance where thermal and mechanical stresses are moderate in comparison to ultimate usage objectives for these materials. Near term cost premiums for ceramic components may be offset by decreases in life cycle costs if significant improvements can be realized in reliability, life and maintenance. Use of ceramic materials in a conservatively loaded mode will contribute to the technology of materials fabrication, quality control and engineering design so that more advanced highly loaded applications may be realized in the future. This paper deals with the rationale for selecting the turbine nozzle as the component for the initial utilization of ceramic materials and the research, design and testing to achieve operational success.

BACKGROUND

Experience in field operation has shown that nozzle vanes in the Gemini radial turbine engine are the most vulnerable portion of the engine to degradation in extended service. Nozzle vane deterioration, particularly in the form of erosion, can severely reduce performance as shown in Figure 2. There appears to be two principal sources of this degradation. The first results from the ingestion of dust particles when high loading conditions do not allow practical removal of all particles with filters or other air cleaning devices at the engine compressor inlet. (Figure 3 shows severe nozzle section



Figure 1. 10 kW Turboalternator Set

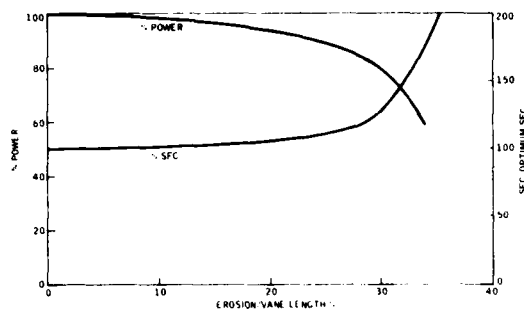


Figure 2. Relative Performance Loss With Nozzle Vane Erosion in a Small Radial Gas Turbine (Ref. 1 and 2)

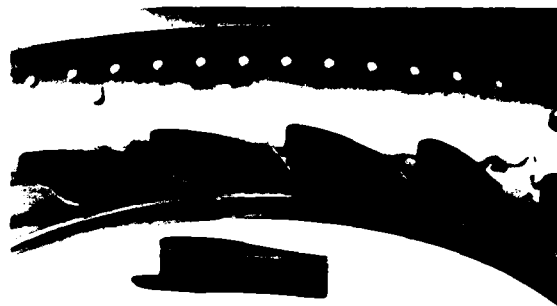


Figure 3. Typical Turbine Nozzle Vanes After 68 Hours of Vietnam Dust Erosion

erosion in a radial turbine similar to the Gemini after only 68 hours operation in a high dust loading environment.) The second source of degradation relates to the uniquely small size of the engine and multifuel capability. The use of heavy fuels (e.g., Diesel #2) over long periods of operation can result in carbon particle buildup in the small scale Gemini combustor. These carbon particles eventually break off and can result in highly erosive conditions downstream at the nozzle. In affected engines, teardown experience has shown nozzle vane trailing edges to suffer damage in the form of erosion and/or sulfidation (due to high sulfur in Diesel #2) before other hot components of the engine, including the turbine wheel. (This is due to particle trajectory mechanics in a radial turbine to be discussed later.) In addition, warm ambient environments, which necessitate higher TIT, are more severe on vane trailing edges than most other hot turbine parts because of inherent thermal isolation from cool sections, susceptibility to pattern factor and fast thermal response.

Operation of the 10 kW with heavy fuels in a hot, dusty, desert environment is not uncommon and, as a result of the above factors, imposes severe requirements on vane materials.

Certain ceramics offer properties which meet all of the above needs for a vane material, i.e., high erosion resistance, stable to corrosive/sulfidizing environments and temperature capability well in excess of requirements cited here. Ceramics show the promise of meeting the material needs of this application which includes a specified engine TBO interval of 6000 to 10,000 hours regardless of severity of operating environment or fuels to be used during this period. Additional incentive for use of ceramic materials in this turbine, or any turbine, is the non-criticality of ceramic material supply which has become an increasingly important problem recently for superalloys, especially those containing cobalt.

The high-temperature potential of ceramics has also led to the consideration of uprating turbine inlet temperature of this engine through application of ceramics for improved specific fuel consumption and specific power. An all ceramic nozzle along with other select ceramic components, not necessarily to include the turbine wheel, would allow this engine uprating.

All of the benefits given here for ceramics translate into incentives for ceramics application because of improved total life cycle costs, which include costs of maintenance, component replacement, fuel, fuel logistics, and secondary costs of unscheduled shut-downs.

COST CONSIDERATIONS

A life cycle cost model has been developed to compare the sensitivity of cost factors based on a typical military mission involving electrical power generating equipment. Total cost for operating a specific generator set, based on an estimated ten year life cycle, is divided into three major cost categories as indicated in Figure 4. This cost division must be qualified since it is composed of many assumed variables; however it does suggest that the major cost is in operation and support. Operation and support may be further divided approximately equally into consumables and maintenance. Substantial savings may be attained through research and development if significant improvements can be gained either in fuel consumption or in maintenance.

For cost comparison analysis it has been assumed that with sufficient development a ceramic turbine inlet nozzle can be produced at a near term cost of 1-1/2 times that of superalloy metal nozzles. The metal nozzle assembly represents 2.3 percent of the total generator set. If this production cost is achievable it would add slightly greater than one percent to the acquisition cost of the generator set. This degree of cost increase in investment costs are insignificant in the total life cycle and are quickly recoverable if maintenance and overhaul intervals can be extended even by conservatively estimated amounts. As erosion tests have indicated there may be 10 to 100 times increase in erosion resistance in ceramic materials over superalloy metals. Assuming as little as 10 percent increase in overhaul intervals and increased total life of the

equipment, cost savings can be shown even when considering relatively small production quantities. Further savings may also be accrued as a result of decreased nozzle wear rate if engine thermal efficiency can be maintained at peak levels over longer periods of operating life. Fuel cost and associated logistic burden are major factors in the total cost of power generation and even minor reductions represent significant cost savings.

PROGRAM FOR DEVELOPMENT OF CERAMIC NOZZLE

Turbine nozzle erosion in the 10 kW radial engine characteristically occurs at vane trailing edges and gradually shortens the vane length until overhaul is necessary because of performance loss. Erosion is concentrated on this surface because of particle trajectories as they pass through the nozzle and turbine sections. Vane leading edges suffer no measurable erosion because gas and particle velocities are low at the nozzle inlet. Gas velocity and particle velocity increase through the nozzle throat. However, it is estimated that particle velocity reaches only a fraction of gas stream velocity at the nozzle exit and particles continue to accelerate as they travel downstream. Depending on their size, particles will either continue radially inward and exit with the gas stream (small particles) or be forced outward by centrifugal forces (larger particles). The larger particles are overtaken by the turbine wheel and slung outward since they have not attained the full gas stream velocity by the time they enter the turbine wheel section. It is estimated that these larger particles bounce between the turbine wheel and the downstream segment of nozzle vanes until they are pulverized to a smaller size and can follow the gas stream and exit inward through the turbine section (Ref. 2).

Studies have shown that erosion due to dust or particle ingestion can be controlled for most engine components (compressor, diffuser, air inlet housing) by use of coatings (Ref. 1). Unfortunately, the nozzle section of the 10 kW engine is not amenable to erosion resistant coatings due to the high temperatures involved. This is also true for the turbine wheel. However, engine operating experience shows erosive attack of the turbine wheel to be minor in relation to that of the nozzle. Therefore, the limiting component for erosion deterioration of an engine of this type is the turbine nozzle.

Silicon nitride and silicon carbide ceramics exhibit the physical properties required of a material to prevent severe erosion of the nozzle. They also have improved strength, corrosion properties and thermal shock resistance over other ceramics. Figure 5 illustrates the relative erosion of three ceramic materials and 713LC superalloy, the 10 kW nozzle material. Hot pressed silicon nitride (HPSi₃N₄) shows more than 50 times the erosion resistance of 713LC superalloy in this ambient temperature test. The NC-430 silicon carbide material shows 13 times the erosion resistance of 713LC in this test. (NC-430 is a silicon filled recrystallized silicon carbide and has the advantage of better economics of fabrication over not pressed silicon nitride.)

Early experiments were initiated at Solar to study the erosion behavior of HPSi₃N₄ in a radial flow turbine. Figure 6 compares the erosion of a HPSi₃N₄ vane and a N-155 superalloy vane after a 10 hour engine run in a 60 kW radial turbine, where 2×10^{-5} kg (4.4×10^{-5} pounds) of -140 mesh silica dust per pound of air was introduced into the engine inlet. The N-155 vane has receded by approximately 1.27 cm (1/2 inch) due to erosion, while the ceramic vane did not erode to any measurable extent. This test verified that the general erosion relationship observed in the laboratory ambient temperature tests cited above hold for materials in the turbine nozzle environment.

DESIGN OF EROSION RESISTANT CERAMIC VANE NOZZLE

Figure 7 shows the design of a ceramic vane nozzle selected for rig and engine test evaluation. This configuration addresses the major ceramic turbine design obstacles which are:

1. Transition between ceramic and metal members.

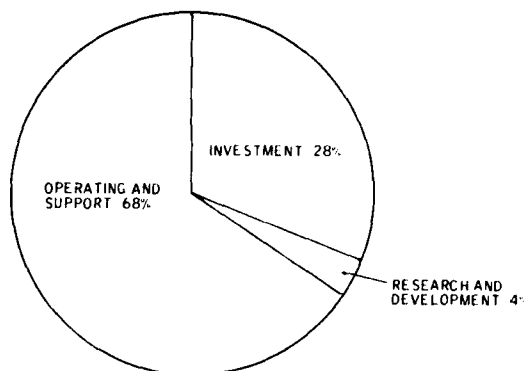


Figure 4. Major Life Cycle Cost Categories for Military Electric Power Generator

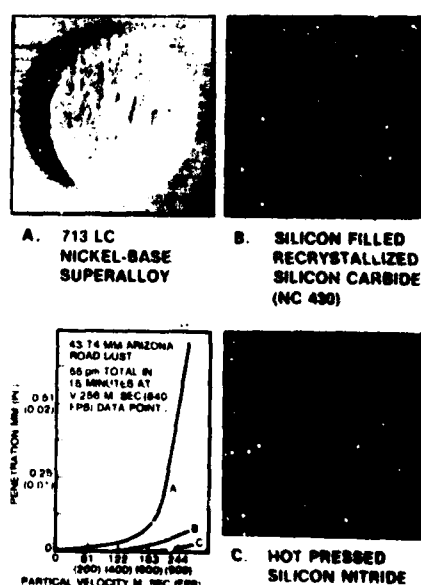


Figure 5. Relative Erosion Between Ceramics and 713LC Superalloy Nozzle Material at Ambient Temperature

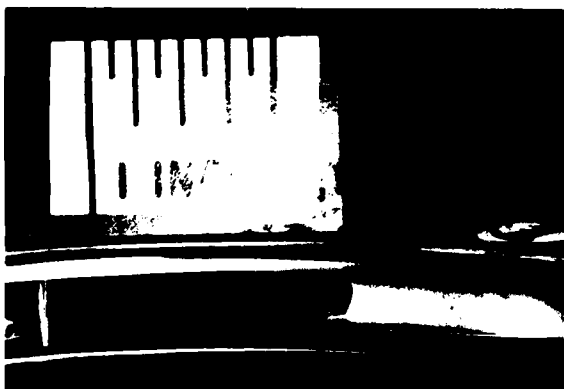


Figure 6. Silicon Nitride (Left) and N-155 (Right) in Solar 60 kW Radial Turbine Engine After Testing

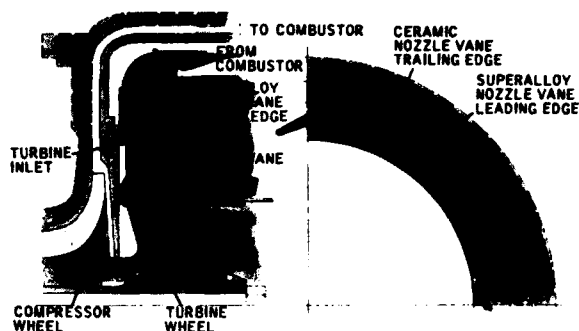


Figure 7. Nozzle Design With HPSi_3N_4 Vane Sections

2. Thermal expansion coefficient mismatch between ceramics and superalloys.
3. Localized contact stresses in ceramics due to normal surface irregularities.
4. Manufacturing misfit contact stresses resulting from normal machining tolerances.
5. Stresses induced into the assembly due to static and transient thermal distributions.
6. Statistical nature of failure in ceramics.

The ceramic vanes (HPSi_3N_4) shown in Figure 7 are captured in recesses in 713LC forward and rear shrouds. The recesses are slightly oversized to avoid stresses due to thermal expansion differences and thermal distributions in the nozzle. Accurate nozzle throat size is maintained in this assembly despite oversize recesses because static aerodynamic forces locate each ceramic vane at its furthest inboard downstream position. A specially developed relaxing glass adhesive is applied at ceramic-vane metal-shroud interfaces to alleviate localized contact stresses due to surface irregularities and assembly mismatches. The glass adhesive is in a high viscosity state at operating temperatures to allow differential growths while providing interface cushion to prevent contact stress failures in the ceramic vanes. The assembly of vanes in the nozzle section imposes no direct physical restraints on vanes and therefore essentially zero assembly stresses on the ceramic.

EVALUATION OF CERAMIC VANE NOZZLE

Nozzle evaluation included engine simulator rig tests which exposed the ceramic vane nozzle and a reference all superalloy (713LC) nozzle to thermal shock, dust erosion, and sea salt corrosion. This was followed by two 24 hour plus 50 stop/start cycle engine tests.

Thermal Shock. The thermal shock test was designed to duplicate the most severe thermal transient condition observed in engine operation. Figure 8 shows vanes as they progress through one thermal cycle. The temperature indicated in this figure is the local temperature of the vane trailing edge as measured by an optical pyrometer. Five hundred cycles were run and all vanes survived with the exception of one (Fig. 9) which chipped at the trailing edge. This failure was determined to be the result of a lower temperature glass used at that location which generated a longitudinal contact stress on cooldown.

Dust Erosion. The nozzle was eroded in the simulator by means of a special particle impinger with 43-74 μm Arizona road dust with vane temperatures monitored optically to 927°C (1700°F) for a 10 hour period. Figures 10 and 11 compare erosion of a superalloy vane (713LC) and hot pressed silicon nitride vane (NC 132) in the engine simulator rig. The ceramic vanes offer substantial improvement in erosion in this elevated temperature test.

Sea Salt Corrosion. A 70 hour 927°C (1700°F), 3ppm simulated sea salt test was made with the ceramic vane nozzle and reference 713LC nozzle. Figure 12 shows that the relative surface attack of 713 LC superalloy is much higher than that of the HPSi_3N_4 ceramic.

Engine Test. An engine test of the ceramic vane nozzle consisting of 24 hours of steady-state running at various loads (see Table 1) and 50 start/stop cycles showed the ceramic vane nozzle to perform well with the exception that six vanes had suffered trailing edge fractures. Figure 13 shows typical fractures (Ref. 3).

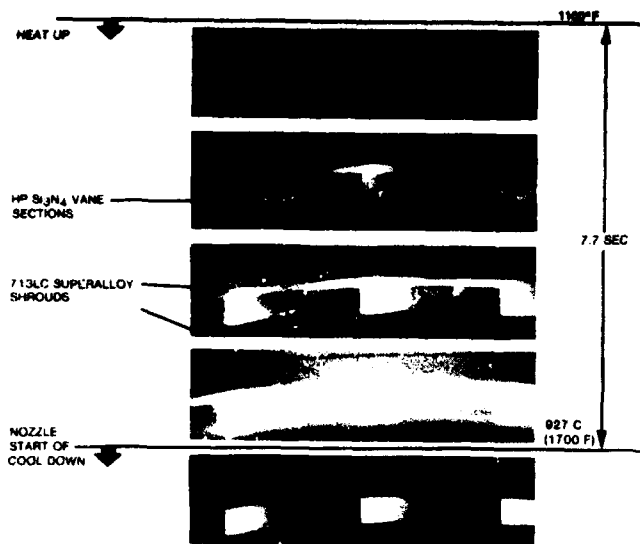


Figure 8. Thermal Shock Test Cycle for Ceramic Vane Nozzle (HPSi₃N₄ Vanes and 713LC Shrouds)

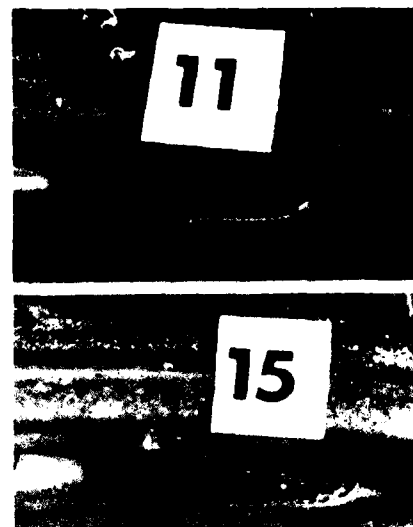


Figure 9. HPSi₃N₄ Vanes After 500 Thermal Shocks (Note Single Failure out of 15 Vanes Tested at Vane No. 15 Trailing Edge)

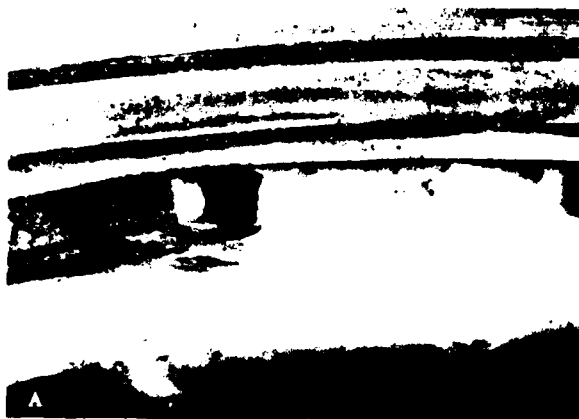


Figure 10. Comparison of A - Superalloy and B - HPSi₃N₄ Vane Erosion in 10 kW 927°C (1700°F) Engine Simulator Test

Analysis showed the failures to be a direct result of deformation of the inner diameter lip of the forward shroud due to nozzle assembly loads.

A redesign of the assembly was made (Fig. 14) and a re-run of the engine test gave positive results. The nozzle is shown after test in Figure 15.

Current work on the ceramic vane nozzle for hardening the hot end section to highly corrosive conditions has moved to a cost reduction program to show life cycle cost advantages of this concept. A manufacturing methods and technology study for cost reduction of ceramic vane inserts and overall net cost of this nozzle is in progress at Solar under the sponsorship of MERADCOM.

The hot pressed silicon nitride used in the first engine test is known to be more than adequate in solving this problem and as a result other ceramics more amenable to low cost fabrication are being considered along with HPSi₃N₄ in a trade-off study to find the optimum ceramic material for this application. Figure 16 shows relative erosion resistance of some alternate materials that are being considered in this project

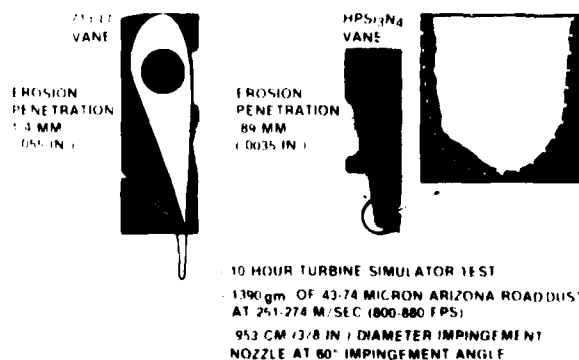


Figure 11. Comparison of Erosion of Nozzle Vanes From 713LC Superalloy and HPSi₃N₄ (NC-112) at 1700°F in an Engine Simulator

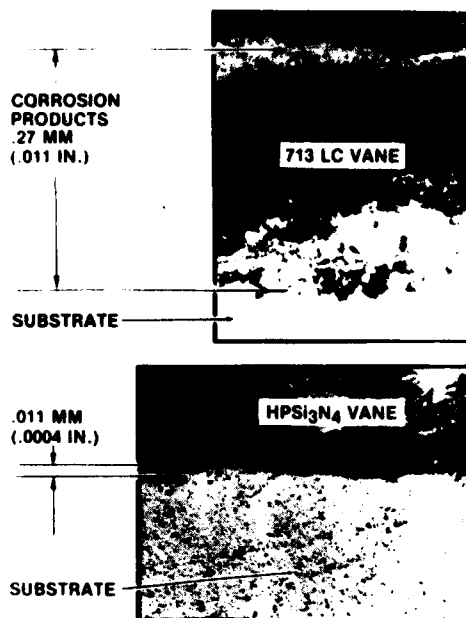


Figure 12. Comparison of Corrosion in 713LC Superalloy and HPSi₃N₄ Vanes After a 70 Hour, 972°C (1700°F) Engine Simulator Test With 3 ppm Simulated Sea Salt

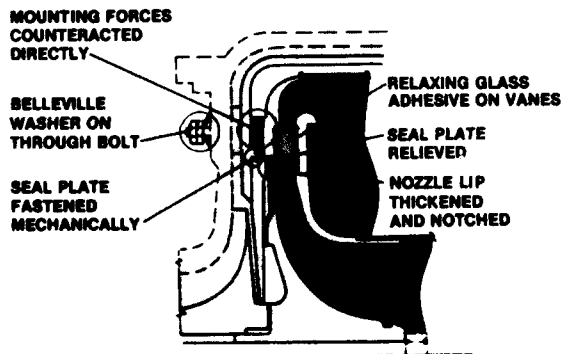


Figure 14. Design Change to Ceramic Vane Nozzle Prior to Second Engine Test

Table 1
Engine Test Sequence for Ceramic Vane Nozzle

Load (%)	Time at Load (hrs)
75	6
0	1
50	6
25	6
75	6



Figure 13. Typical Vane Fracture (6 Fractures out of 15 Vanes) After First Engine Test

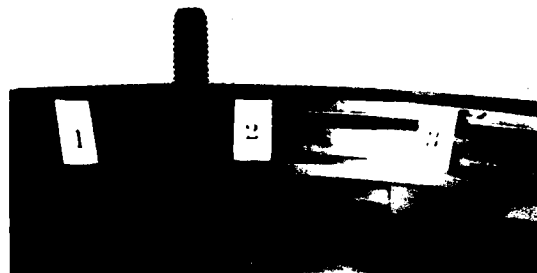


Figure 15. Hot Pressed Silicon Nitride Vanes Nos. 1, 2 and 3 After Second Engine Test

Vendors of ceramic materials have been contracted to fabricate and assess costs for vanes made from the following materials:

HPSi₃N₄ - Hot pressed to 2-D bar, sliced and final machined
 Sintered Si₃N₄ - Injection molded to shape and fired
 Silicon filled SiC - Slip cast to 2-D bar, fired, sliced and final machined
 Alpha Sintered SiC - cold pressed to shape and fired

These materials will be evaluated in as-fabricated form for modulus of rupture, dimensional and surface control as well as other relevant property tests. As-fabricated vanes will be subjected to thermal shock engine simulator tests and finally engine test.

All-Ceramic Nozzle Design

An all-ceramic nozzle must overcome the same design difficulties iterated above.

Three alternate design concepts shown in Figures 17-19 were chosen for engine simulator evaluation which lead to selection of Design Concept No. 1 for engine test.

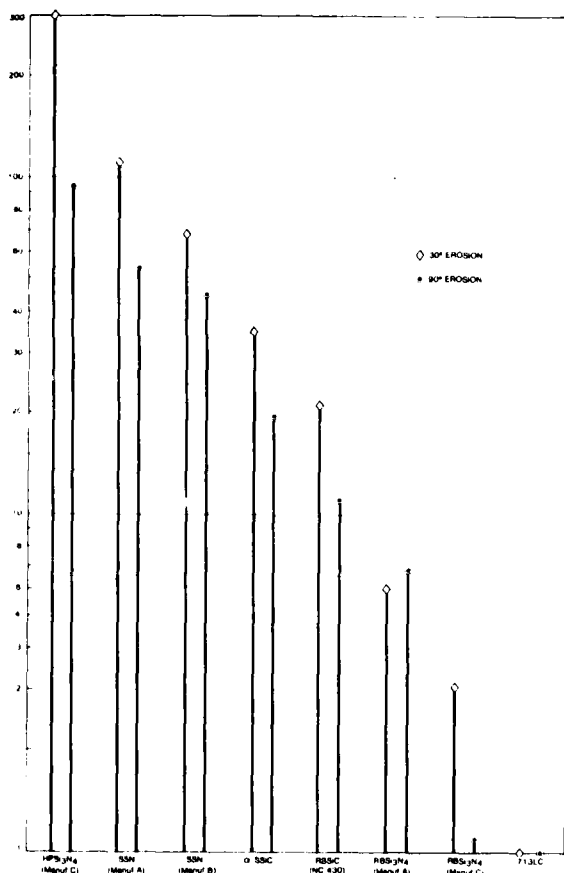


Figure 16. Room Temperature Erosion of Ceramics and 713LC Superalloy; 43-74 Micron Arizona Road Dust - 155 gms Total - 15 Minutes; Gas Velocity 305 m/sec (1000 fps), Mean Particle Velocity 256 m/sec (840 fps), 0.95 cm (3/8 in.) Diameter Impingement Tube

Design Concept No. 1 (Figure 17) uses RBSi₃N₄ shrouds and cooled 718 superalloy support bolts. (RBSiC was used for the forward shroud in the engine test.) The bolts are piloted at the compressor diffuser housing such that they will accurately locate the rear (inner) shroud which must closely match the turbine wheel contour. The bolts are spring loaded in the axial direction to accommodate relative thermal growth. The rear shroud has radial slots at the bolt penetration points to allow for relative thermal growths, which are substantial. The forward (outer) shroud has clearance holes at the penetration point and is located by the seal plate which is made from INCO 903 (Ref. 4), a low expansion, high temperature alloy. The net diametrical growth at this junction is well matched to the ceramic shroud because of the lower operating temperature of the seal plate and the low thermal expansion coefficient of the 903 alloy.

Design Concept No. 2 (Fig. 18) is similar to No. 1 except HPSi₃N₄ bolts are used in place of the cooled 718 bolts. They are also sprung in the axial position and have spring loaded colllets at the external cool position in lieu of nuts. A 0.10 mm (0.004 inch) pure platinum interface layer was used successfully at the collet bolt interface to avoid contact stress imposed fracture.

Design Concept No. 3 (Fig. 19) uses silicon filled reaction bonded silicon carbide shrouds and hot pressed silicon carbide vanes. The shrouds and vanes are bonded with a relaxing glass adhesive for contact stress reduction at vanes and ease of assembly. Aerodynamic forces and a spring loaded exhaust scroll also hold the nozzle in position against the seal plate.

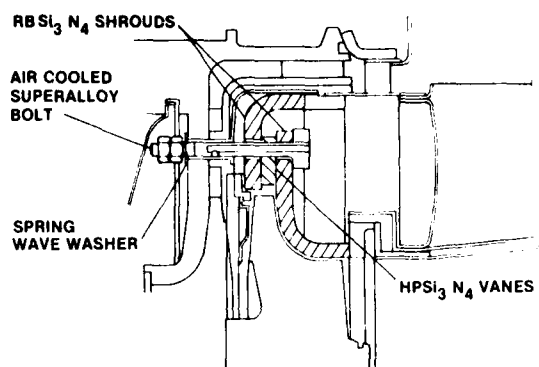


Figure 17. All-Ceramic Nozzle Design Concept No. 1, RBSi₃N₄ Shrouds, HPSi₃N₄ Vanes and Cooled 718 Bolts

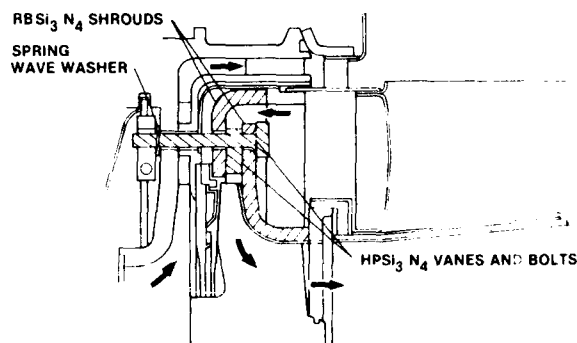


Figure 18. All-Ceramic Nozzle Design Concept No. 2, RBSi₃N₄ Shrouds, HPSi₃N₄ Vanes and HPSi₃N₄ Bolts

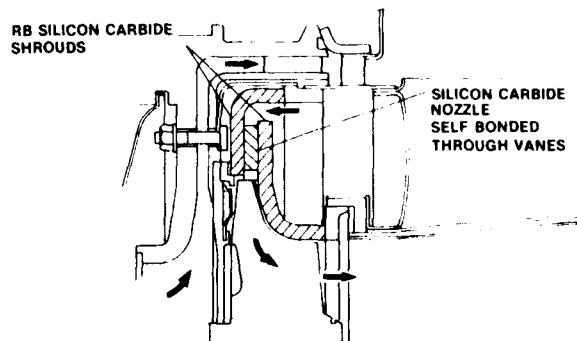


Figure 19. All-Ceramic Nozzle Design Concept No. 3, RBSiC Shrouds, HPSiC Vanes and Vanes Bonded to Shrouds

In all designs the forward shroud is held in place with a René 41 leaf spring attached to the diffuser housing which pulls the nozzle to the left against the seal plate by attachment to the nozzle retainer ring. Also, the rear shroud has a face seal load applied at its gas exit point by a pressure actuated bellows spring system at the right section of the exhaust scroll (not shown in Figs. 17-19).

Figure 20 shows nozzle assembly components which make up each of the three designs.

Evaluation of All-Ceramic Nozzle.
Each of the design concepts was exposed to various engine simulation experiments to evaluate factors such as leakage at seal interfaces and turbine tip clearances under full rated engine operating conditions. Results have shown that face seal interfaces at ceramic section inlet and exit positions function well without special materials applied. The design provisions which allow compatibility of large differential expansions between ceramics and metal alloys have been proven to function well. Accurate rear shroud centering critical to turbine tip clearance has been demonstrated with each of the concepts in the engine simulator (shown in Fig. 21) at 927°C (1700°F) and 640 m/sec (2100 fps) nozzle throat velocity.

Engine simulator testing, which included 500 thermal shock cycles (similar to that shown in Figure 8 but to 1093°C (2000°F) peak temperature), and some steady state testing in which turbine tip clearances were checked, consistently showed the reaction bonded silicon nitride forward shroud to fail despite design measures taken to avoid failure. The silicon filled reaction bonded silicon carbide forward shroud of design concept #2 had no difficulty in surviving the same test sequence.

From this result it was concluded that reaction bonded silicon carbide should be used for the forward shroud in the engine test of the nozzle. Design Concept 1 was selected over the others because it offered the most conservative design of the three considered. The use of a silicon carbide forward shroud and silicon nitride rear shroud was found to be a thermally coordinated design since the higher expansion coefficient SiC at the cooler forward shroud position would match thermal growth of the Si₃N₄ rear shroud.

No features specific to design concepts 2 or 3 were found to be a problem in engine simulator tests. The ceramic bolts of Concept No. 2 survived steady state testing in the simulator and both silicon carbide shrouds of Concept No. 3 were found to be in perfect condition after 500 thermal shocks. However, the concept No. 2 ceramic bolts had not been proven through the entire engine performance sequence and location of the rear shroud in Concept No. 3 remained an uncertain issue.

A direct substitution of the silicon carbide forward shroud of Concept No. 3, which does not include penetration for support bolts required in Concept No. 1, was possible without going through a re-fabrication cycle with the ceramic supplier since the free silicon content of this material allows it to be electro discharge machined.

Engine Test of All-Ceramic Nozzle

A 50 hour engine test of the all-ceramic nozzle described above with a load sequence given in Table 2 was completed at the conclusion of simulator testing. Figures 22 through 25 show the ceramic nozzle after the test. The silicon carbide forward shroud survived the test and showed no flaws or cracks in NDE examination after the test. The rear shroud sustained one fracture at a support bolt location at 33 hours of testing (see Fig. 25) and incurred a more substantial fracture between 33 and 50 hours due to metal exhaust scroll collapse. Since the rear shroud face seal is static loaded during engine operation by a PCD pressure actuated loading system, this collapse of the exhaust scroll viewed in Figures 26 and 27 resulted in



Figure 20. All-Ceramic Nozzle Assembly Components (Shown With RBSi₃N₄ Shrouds)

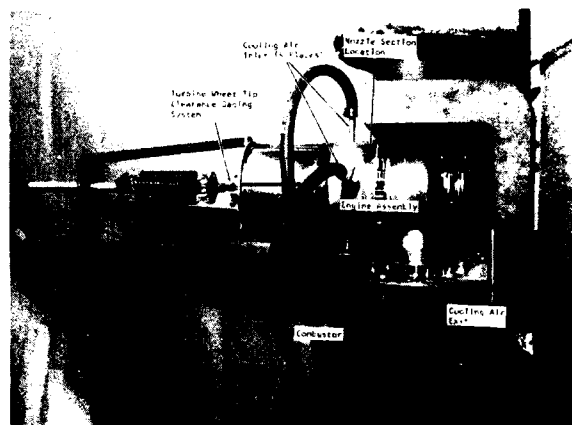


Figure 21. Engine Simulator Used in All-Ceramic Nozzle Testing

Table 2

Engine Test Sequence for All-Ceramic Nozzle

<u>Operating Condition</u>	<u>Time at Load</u>
Calibration	5 hours
50% load	24 hours
0	4 hours
100	10.5 hours
75	6.5 hours
	50 hours total



Figure 22. All-Ceramic Nozzle After 50 Hour Engine Run

Figure 23. HPSi_3N_4 Vanes and RBSiC Forward Shroud After 50 Hour Engine TestFigure 25. Crack in RBSi_3N_4 Rear Shroud After 33 Hours Engine Running

Figure 24. RBSiC Forward Shroud After 50 Hours Engine Test

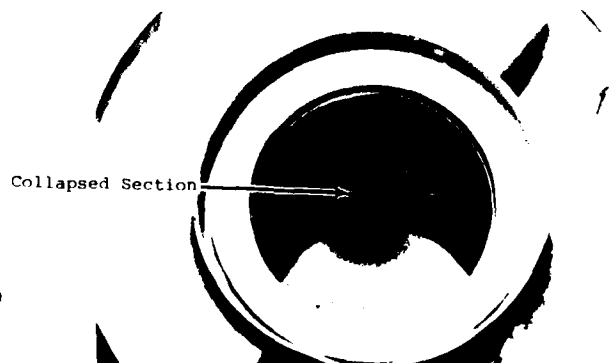
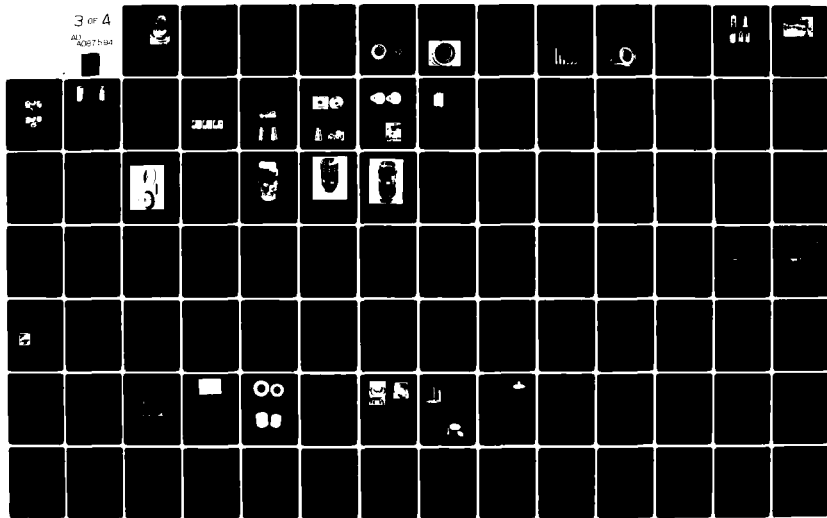


Figure 26. Collapsed Exhaust Section

CERAMICS FOR TURBINE ENGINE APPLICATIONS
MAR 80 H M BURTE, J ACURIO, W HANSEN
AGARD-CP-276

NL

ALJ
8/10/75 4:45



thermal binding and overload of the silicon nitride rear shroud. The resultant fracture is shown in Figure 28.

An engine retest is currently in the process of preparation. Appropriate changes in design of metal elements of the exhaust scroll will be made for this test, and due to the unexplained rear shroud failure at 33 hours (Fig. 25) the rear shroud will also be from RB silicon carbide.

CONCLUSIONS

Laboratory, engine simulator and engine tests have shown the feasibility of using ceramic vanes in a radial gas turbine nozzle section for substantial increases in hot end durability. Current work in manufacturing technology for cost reduction of this ceramic vane nozzle is pointing towards economic incentives in using this concept over standard superalloy hardware due to increased hardening to severe service conditions. Reduced projected maintenance costs and improved reliability have been shown to be the direct result of high performance turbine ceramics.

A 50 hour engine test of an all-ceramic radial turbine nozzle has shown promise in proving workability of this idea which is the key element in additional uprating this engine for improved specific fuel consumption and specific power through an increase in turbine inlet temperature. As was shown in the eventual development of the ceramic vane nozzle, the iterative method of turbine ceramic component development including engine testing and progressive design refinement is expected to prove successful in developing an all-ceramic radial 10kW turbine nozzle.

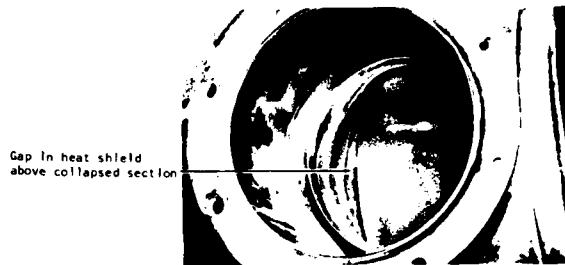


Figure 27. Gap in Exhaust Scroll Heat Shield Below Side Can Combustor Above Exhaust Scroll Collapsed Section

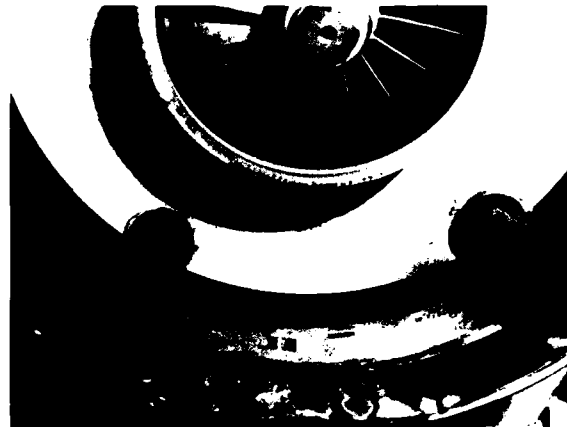


Figure 28. All-Ceramic Nozzle After 50 Hour Engine Run (Note Fracture at Bottom Section of RBSi₃N₄ Rear Shroud)

REFERENCES

1. H. E. Shoemaker, "Techniques for Reducing Sand and Dust Erosion in Small Gas Turbine Engines", Final Report, Army Aviation Systems Command, August 1970, Contract No. DAAF01-67-C-2155(G).
2. "Army Product Improvement Program", Solar Engineering Report T-4287, June 1970.
3. Jordan, F. D., Napier, J. C., Metcalfe, A. G., and Duffy, T. E., "Application of Ceramics to a Radial Inflow Gas Turbine," SAE 770342, Society of Automotive Engineers, 1977.
4. International Nickel Company, Inc.

DEVELOPMENT OF A CERAMIC TURBINE NOZZLE RING

by

H. Burfeindt and M. Langer
Research and Development Division
Volkswagenwerk AG, Wolfsburg

West Germany

P.M. Stuart

PMS Analysis AG

Zentralstrasse 2A, CH-8160 Uster Zurich
Switzerland

SUMMARY

This paper describes the way in which experimental testing and finite element design analysis have contributed to the understanding of the special problems associated with the use of ceramic materials in a turbine nozzle. During the design analysis two problem areas, the shrouds and the trailing edge, were immediately revealed. The design of an optimized nozzle ring resulted in a reduction of the high stresses in these two areas down to a level acceptable for ceramic materials currently available such as silicon nitride or silicon carbide.

INTRODUCTION

At Volkswagen several ceramic components for small gas turbine application have been developed over the last few years (1). One of the most critical of these has been the turbine nozzle ring. While mechanical loads on the ring are small, thermal loads are severe and demand considerable design effort to reduce resulting stresses to acceptable levels. In this case the nozzle is required to withstand gas temperatures up to 1623 K and thermal shocks of about 500 K/s.

The ceramic material chosen must withstand the stresses generated by these thermal gradients and also the attack by combustion gases without loss of strength over many hours of running. It must also be suitable for the production of complex shapes with the limitation of trailing edge thickness specifications down to 0.5 mm.

During the development program, parts must be designed to be made by a process which, without modification, could later be used for quantity production. This is because of the strong manufacturing process dependence of the structural behaviour of such parts.

DEVELOPMENT PROGRAM

A preliminary series of tests was performed by Volkswagen on test bars provided by the ceramics manufacturers to determine whether the material characteristics were suitable for application in gas turbine parts. To obtain correlation of parallel results from both design analysis and experimental test, a first design was created for the production of hardware for test purposes. The geometry chosen followed the pattern already established for metallic parts in the same application. Further test bars of the selected material were also produced for long time tests under combinations of thermal, mechanical and corrosive loads. Results from test and design analysis have led to the production of an optimized design which is currently under test.

MATERIAL SELECTION

A review of the materials and processes made available by the ceramics industry for such applications suggested silicon nitride and silicon carbide in various types as the most likely candidates. The cost and production difficulties associated with hot pressing together with the expected low stress requirement of the nozzle reduced the choice to the materials:

- reaction bonded silicon nitride (RBSN)
- infiltrated silicon carbide (ISC)
- sintered silicon nitride (SSN)
- sintered silicon carbide (SSC)

using injection moulding or slip casting production processes. These materials offered the potential of low cost production of complex shaped, high density parts with a low degree of open porosity and not requiring rework.

Efforts by the ceramics manufacturers during the period of Volkswagen's development program have yielded much improved material quality. For example, RBSN can now be obtained with a density up to 2.8 g/cm³ and a 4-point bending strength of 300 MN/m². The material chosen after review at the start of the program was RBSN with open porosity of approx. 20 % and a 4-point bending strength of about 200 MN/m². Some early parts were also made from SSC with a silicon content of 15 - 20 % and a 4-point bending strength of roughly 300 MN/m².

INITIAL DESIGN

The first designs assumed the assembly of individual vanes into a nozzle ring. This permitted a variety of connection possibilities between vanes and to support rings of simple design. The minimized tooling costs involved in this approach for production of the small quantities required during development supported the decision. Simplified 2-D analysis was performed to estimate stress values under load prior to manufacture.

A monolithic nozzle ring was investigated because the power plant manufacturer requires a stator which permits simple mounting in the power plant, minimum gas leakage and close control on throttle cross-section dimensions.

The shroud rings of the assembled versions were pressed isostatically, the guide vanes being produced using the injection moulding method. In one version the guide vanes were bonded together with the outer shroud ring, the inner shroud ring not being provided. After reaction sintering the stator can be viewed as a one-piece component. The guide vanes of another version were loosely supported between the inner and outer shroud rings. In this configuration the inner shroud is complete, while the outer shroud is in two pieces. Fig. 1 shows these initial design concepts.

EXPERIMENTAL TESTING

The nozzle ring is exposed to the highest thermal gradients during cold starts. The air in the otherwise cold power plant is immediately heated up to approx. 1500 K in the combustor. The circumferential temperature profile at the combustor outlet at start-up is particularly non-uniform. Changes in gas temperature of 500 K/s occur during acceleration. There are also severe temperature gradients when the power plant is shut down, although they are not so pronounced as during cold start.

The nozzle is subjected in operation to average gas temperatures of over 1600 K. In addition, thermal loads from the non-uniform temperature distribution around the ring and mechanical loads as reaction forces due to pressure reduction and flow direction changes must be withstood.

The test equipment used at Volkswagen was designed to permit the application of programmed temperature variations in the hot gas supply to the nozzle. This permitted the simulation of functions including thermal shock, cyclic thermal loading, disconnection of the fuel supply and steady state operation. Typical test programs are shown in Fig. 2.

Test results following the application of different cyclic loading to the nozzle ring showed a consistent recurrence of failure patterns after total test times of up to several hours. In nozzles where the vanes were bonded to the inner, outer or both shrouds, cracks or complete breaks occurred in the rings generally between vanes, see Fig. 3. In nozzles where the individual vanes were contained by rings but loosely without any bond, cracks or complete breaks occurred in the vane trailing edges at about midspan. The variation of temperature around the nozzle was not insignificant and two cases are shown in Fig. 4 clearly indicating non-axisymmetric loading on the rings. It was also observed that these temperature distributions varied with time in orientation and amplitude.

Such complicated effects and other local vane stress concentrations were not conceived or detected by the original simplified 2-D calculations. 3-D analysis was seen to be essential for proper understanding and support of the next design iteration.

FINITE ELEMENT ANALYSIS

It was necessary to obtain realistic thermal loading boundary conditions during the design transients and the thermal and mechanical properties of the materials including their temperature dependence in order to perform a complete transient thermal stress analysis. The thermal load was described as a variation of gas temperature and heat transfer coefficient with time as shown in Fig. 5. The heat transfer coefficient was also allowed to vary across the airfoil and shroud surfaces.

Reference Analysis

The reference model was considered to be one in which a one piece integral nozzle ring was represented. The 3-D FE model shown in Fig. 6 shows the reference configuration of a one vane sector. The two principal problem regions were immediately revealed as tensile principal stresses in the shrouds in the throat region and in the trailing edge at midspan during heat-up and in the fillet radius during cool-down. These corresponded well with test findings. Interestingly the airfoil/shroud fillets, although regions of higher than average stress, did not show up as problem areas as expected. The two problem areas were considered separately as follows.

Shroud Problem

The maximum tensile stress in the shroud was tangential and had a value of 650 MN/m^2 . The traditional engineering practice of providing a free surface where high stress is found was adopted here. In the case of the nozzle assembly it took the form of disconnecting adjacent vanes in regions of high stress. Connection variations considered included cases where vanes were totally separated from each other and where slots (regions of no bond) were represented. Fig. 7 shows how strongly stresses could be affected in the configuration chosen as a satisfactory optimum.

Trailing Edge Problem

The dominant component of the tensile stress in the trailing edge was noted to be radial. The maximum trailing edge value during heat-up was 190 MN/m^2 and in the fillet during cool-down was 200 MN/m^2 . During heat-up the temperatures at the airfoil midspan were significantly higher than those near the shrouds. The consequence of this was that the thermal expansion of the chord at midspan was greater than that near the shrouds causing the leading and trailing edges to bow outwards at midspan. This resulted in these edges being stretched to an extent greater than that caused by the thermal expansion of the edges along their own lengths. During the cool-down cycle the temperature gradient was reversed, resulting in compressive stresses in the trailing edges and tensile stresses in the fillet radii.

A reduction in the stress would therefore be achieved by a reduction in the thermal gradient between midspan and shrouds. A solution to the problem using materials with higher conductivity, such as SSC, was unsuccessful because of a conflict with elastic modulus and expansion coefficient values which are also high.

An alternative was to restrict the cross-section of the heat flow path leaving the airfoil. The airfoil temperature would then rise more rapidly during the critical heat-up period but the gradient between midspan and shrouds would be smaller.

Optimized Designs

Based on the experimental and analytical results and their correlation, the causes of fracture in the nozzle are thought to be understood. Solution possibilities resulting from analysis trials have resulted in the construction of two further experimental models. Both incorporate slots between the vanes but the two designs, while both incorporating heat flow control, have differing shroud configurations, one using existing tooling as far as possible, the other requiring new tooling.

These optimized design concepts are shown in Fig. 8 and Fig. 9. The design in Fig. 8 shows that the vanes are only bonded at the shrouds in the leading and trailing edge areas. This will cause the restriction of the heat flow from the vanes to the shrouds which results in the trailing edge problem. Between the vanes there is a region of no contact to overcome the shroud problem.

The concept shown in Fig. 9 consists of single vanes bonded to each other to form a continuous nozzle ring so that additional shrouds are not necessary. For both design concepts the thermal gradient in the vanes could be reduced to an extent which yields a maximum tensile stress of only 90 MN/m^2 in the trailing edge and a shroud stress of 55 MN/m^2 , see Fig. 7.

CONCLUSIONS

The failure of the components can be attributed to the following causes:

- unsuitable component design
- irreproducible material quality
- progressive inner oxidation of the RBSN materials

In certain RBSN materials the inner oxidation results in a rapid decline in strength as a result of structural fatigue cracking, so thermal stresses occurring in the thermal shock test can no longer be withstood by the component. Production of components with reproducible material quality is one of the most important problems to be solved. Only then it will be possible to evaluate components of statistically identical behaviour.

Using finite element calculations it is possible to arrive at favourable component shapes in terms of stress. However, the extent to which these shapes can then be produced economically may compromise the aerodynamic design prerequisites.

As a result design changes have been evaluated which show a great reduction of peak stresses compared with the original design concept. With improved bonding techniques developed in parallel with this work, the current plan is to proceed with nozzles assembled from individual vane mouldings rather than to switch to the integral ring approach (2).

ACKNOWLEDGEMENTS

This work was partially sponsored by the German Ministry of Science and Technology. The authors would like to acknowledge this support and to express their appreciation to Volkswagenwerk AG for the permission to present this paper.

REFERENCES

1. H. Burfeindt, M. Langer and P.M. Stuart "Ceramic Turbine Nozzle Ring Development by Finite Element Analysis". Ceramics for High Performance Applications III Reliability, Sixth AMMRC Materials Technology Conference, Orcas Island, Washington, July 10 - 13, 1979
2. P.H. Havstad and E.A. Fisher "The Development Iteration Process". Ceramics for High Performance Applications - II. Proceedings of the Fifth Army Materials Technology Conference. Newport, Rhode Island, March 21 - 25, 1977

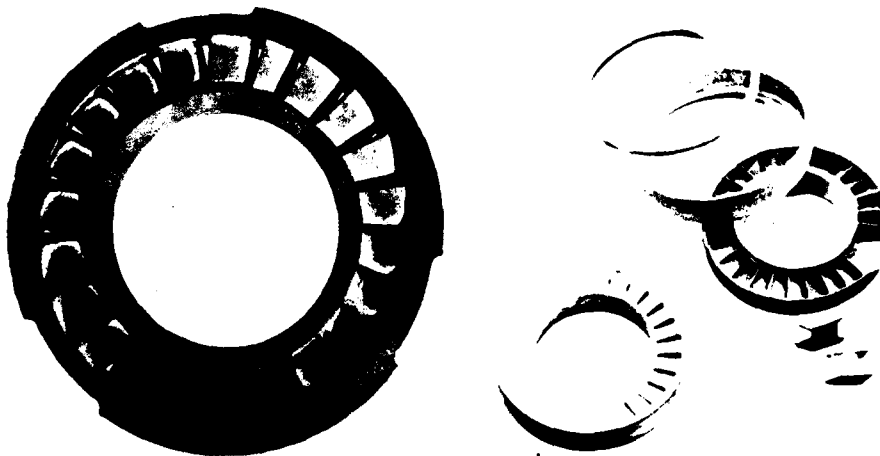


Fig. 1 Initial Design Configurations

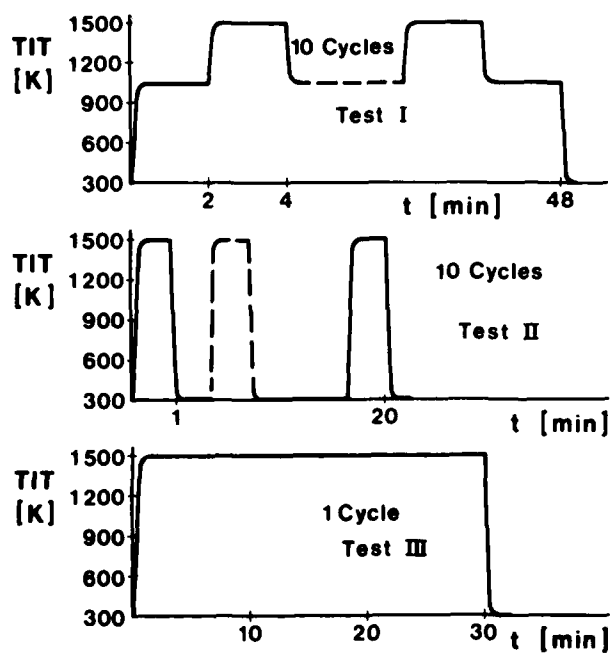


Fig. 2 Thermal Load Test Programs

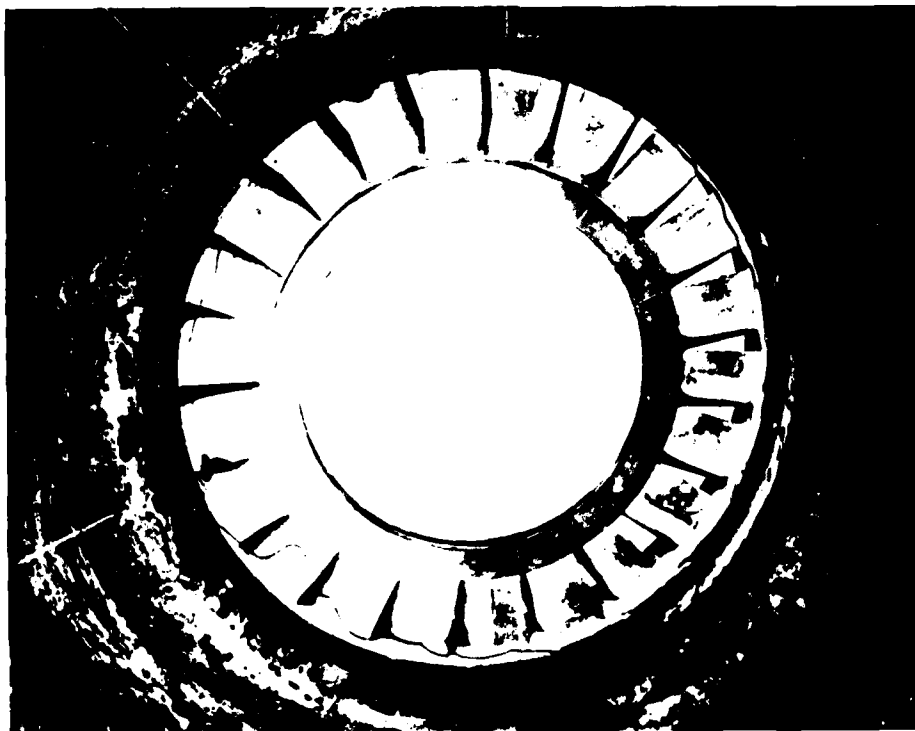


Fig. 3 Monolithic Nozzle Ring Thermal Stress Failure

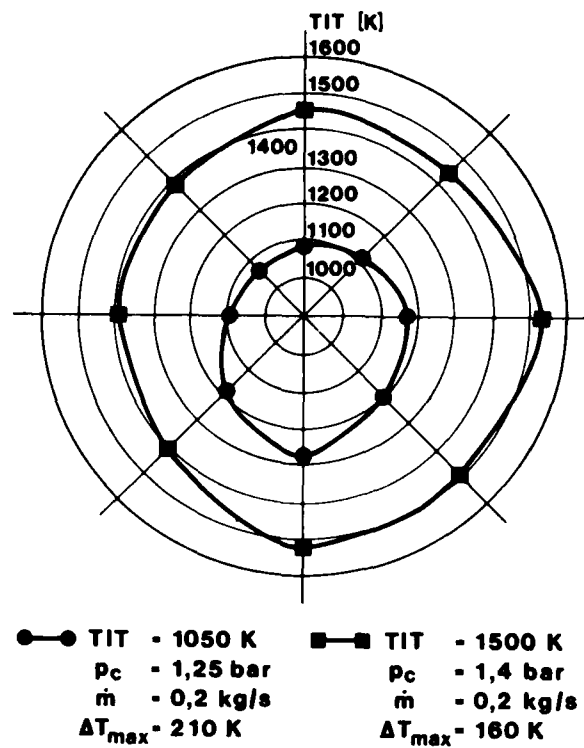


Fig. 4 Nozzle Inlet Temperature Profiles

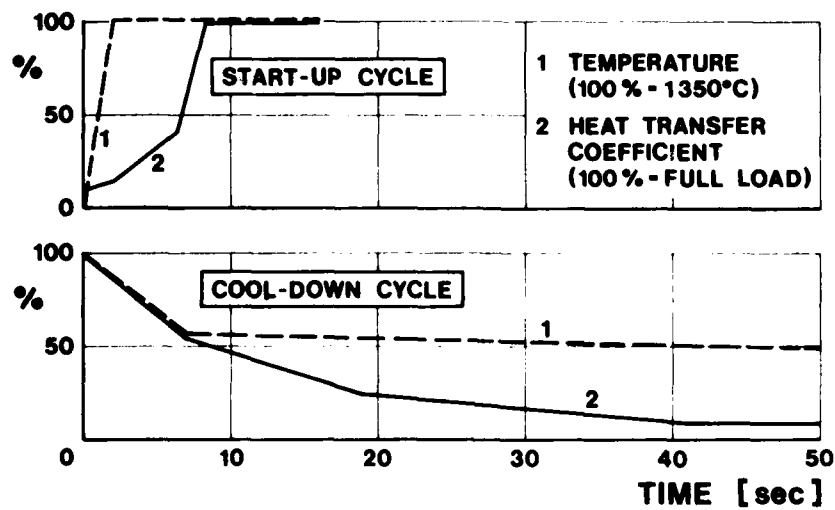


Fig. 5 Analysis Load Cycles

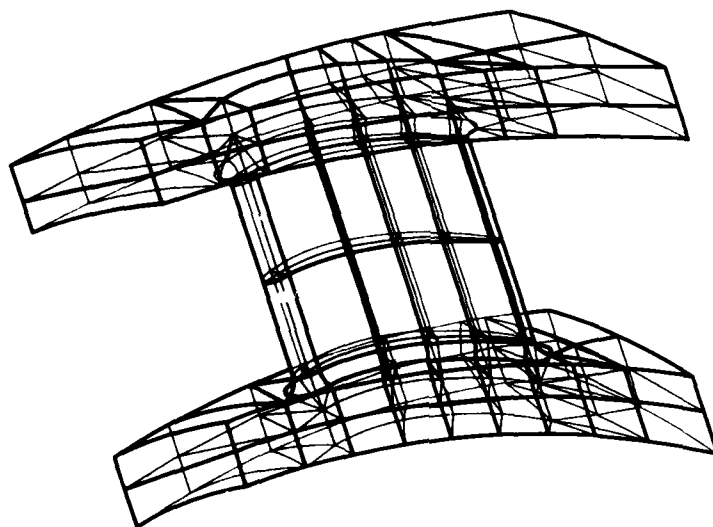


Fig. 6 3-D Finite Element Model

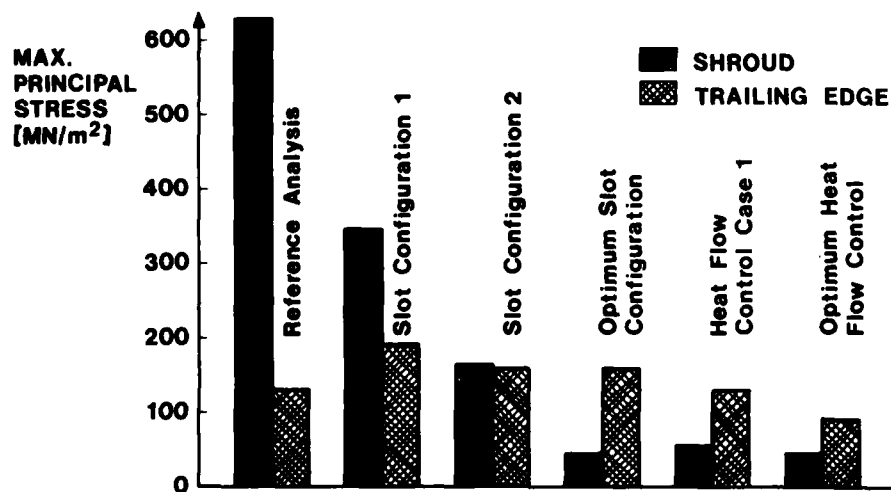


Fig. 7 Stress Reduction during Iterative Design Improvement

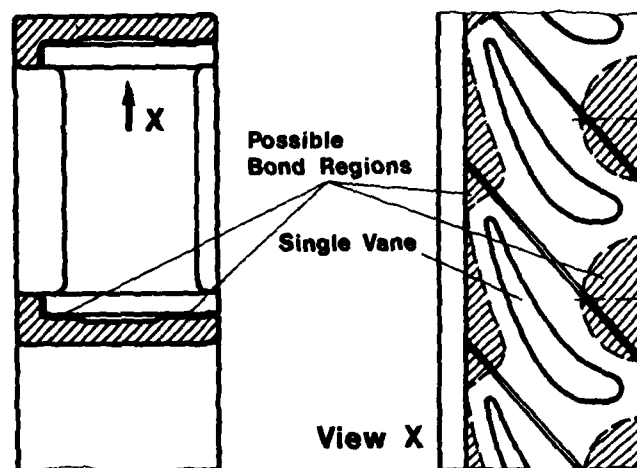


Fig. 8 Design Concept based on Analytical Optimization with Shroud Rings

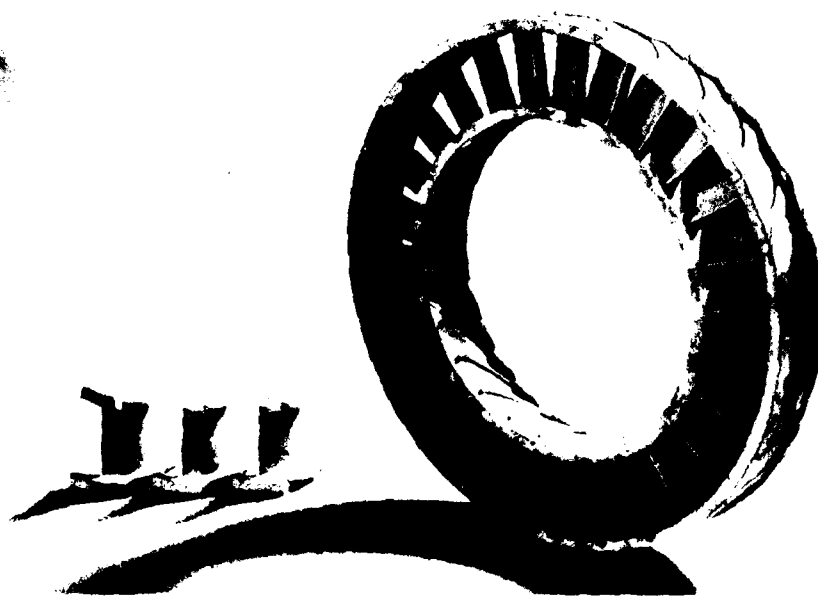


Fig. 9 Optimized Design not Requiring Shroud Rings

DEVELOPMENT OF COMBUSTORS OF CERAMIC MATERIALS

G. Kappler, G. Langel, L. Schindhelm
 MTU Motoren- und Turbinen-Union GmbH
 8000 München 50, Dachauer Str. 665
 West-Germany

1. Summary

Following early feasibility tests of various ceramic materials in hot environments, a research program was initiated to develop ceramic combustors for gas turbine applications. The design of the first ceramic combustors was based on experience with metallic flame tubes. Since test results, which are described in the paper, showed that conventionally designed cylindrical combustors fracture during steady operating conditions at combustor exit temperatures above 1000 K, conical flame tubes were developed.

Conical combustors which are more suited to ceramic material requirements were manufactured from Si_3N_4 and siliconized SiC and subjected to cyclic tests. The test results and their evaluation are reviewed in the paper. Combustors made from hot pressed silicon carbide (Refel) have completed long duration cyclic tests at chamber pressures of 4.9 bar, the cyclic temperature variation adjusted at the combustor outlet being 1065 K to 1355 K. To improve the technology of ceramic combustor design and to gain experience with ceramic combustor behaviour, a combustor flame tube was installed in a vehicular gas turbine engine operating at 1250 K turbine inlet temperature.

2. Introduction

The development of gas turbine with high turbine inlet temperatures and minimized cooling flows will lead to major fuel savings. Engine components fabricated from ceramic materials have the potential to operate at the required high gas temperatures. In order to overcome their inherent brittleness, research programs have been initiated to link improvements in ceramic material properties and fabrication methods with specific ceramic design technologies.

The design of a ceramic combustor¹ has to satisfy two main requirements: - high temperature gradients along the flame tube walls, caused by the temperature reduction from the primary combustion zone to the turbine inlet, and thermoshock loads during ignition events or fast changes in operating conditions. Furthermore, the combustors have to be operational over the full load spectra of vehicular gas turbine engines² and their gas and particulate emissions must comply with government-imposed regulations.

3. Design considerations and selection of ceramic combustors

The design of first ceramic combustors was based on technical experience gained with metallic flame tubes. The combustion chambers fabricated from ceramic materials thus had conventional cylindrical shapes. The main difference to metallic combustors was the omission of cooling rings.

In order to acquire a thorough understanding of the surface temperature distribution, identical cylindrical metallic combustors were fabricated and used for thermopaint tests. From the analysis of temperature distribution along the combustion chamber liner and flame expansion through the combustor volume a conical combustor shape emanated. Through the conical shape the combustor walls were brought closer to the hot flame zone, thus better suiting the ceramic material requirements which suppose high temperature levels but low temperature gradients along the liner.

Some typical cylindrical and conical ceramic combustors investigated during the program are shown in Fig. 1 together with their metallic counterpart. The ceramic materials used for fabrication of combustor liners were Si_3N_4 and siliconized SiC . The fabrication processes were isostatic pressing for Si_3N_4 and slip casting as well as isostatic pressing for SiC . By procuring the ceramic combustors from different manufacturers the selection of specific fabrication methods was possible.

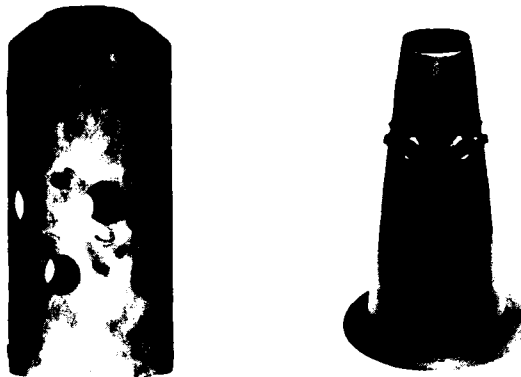
4. Test equipment

The ceramic combustor tests were carried out on a combustion test rig which permitted the simulation of steady and transient operating conditions of gas turbines for truck utilization. The rig set up is shown schematically in Fig. 2.

Together with the nose cone, the ceramic combustor was installed in a casing equipped with a viewing window. Air was fed through two adjacent ducts into the casing and uniformly distributed along the combustor. According to the required operating condition, the air mass flow was adjustable between 0.17 and 0.83 kg/s and the air inlet temperature (T_{IN}) between 300 K and 1050 K. The fuel was injected through a commercial spray nozzle

at pressures up to 20 bar and ignited by an open spark ignition torch with an electrical energy of 6 Joule at 24 V and a frequency of 2 pulses per second. The maximum fuel mass flow, which corresponds to full power engine operation, amounted to 11.5 grams per second. The additional air fed into the combustor head cooled the nozzle and improved the fuel droplet preparation. A traverse gear was mounted on the nose cone exit permitting full annular exit temperature distribution measurements.

METALLIC COMBUSTORS



CERAMIC COMBUSTORS

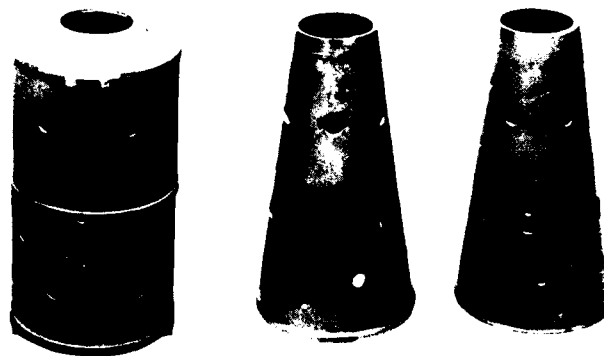


Fig. 1 Combustion Chambers

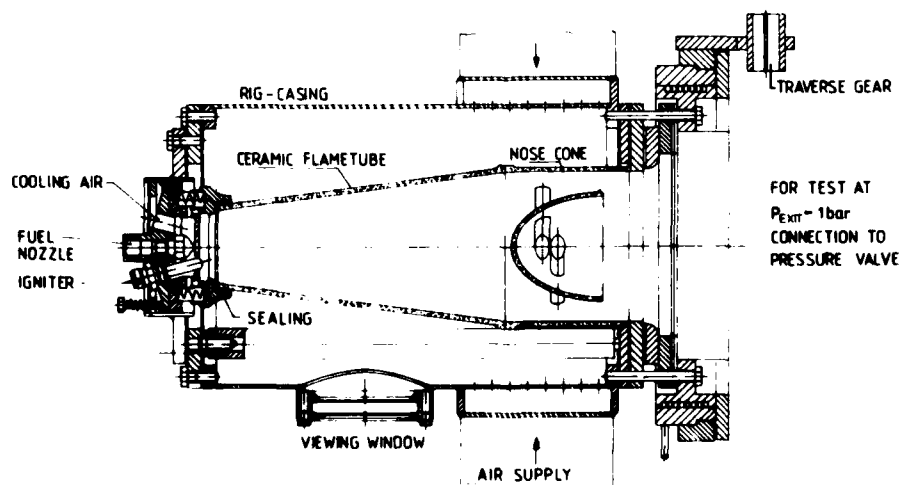


Fig. 2 Schematic of Test Rig

For increased pressure tests above 1 bar, a water-cooled nozzle was installed just behind the nose cone. Fig. 3 shows a photograph of the rig set-up during a test at a combustion chamber pressure of 4.9 bar. One can see the water-cooled nozzle and the shiny viewing window. A pyrometer was placed in front of the window for combustor surface temperature measurements.

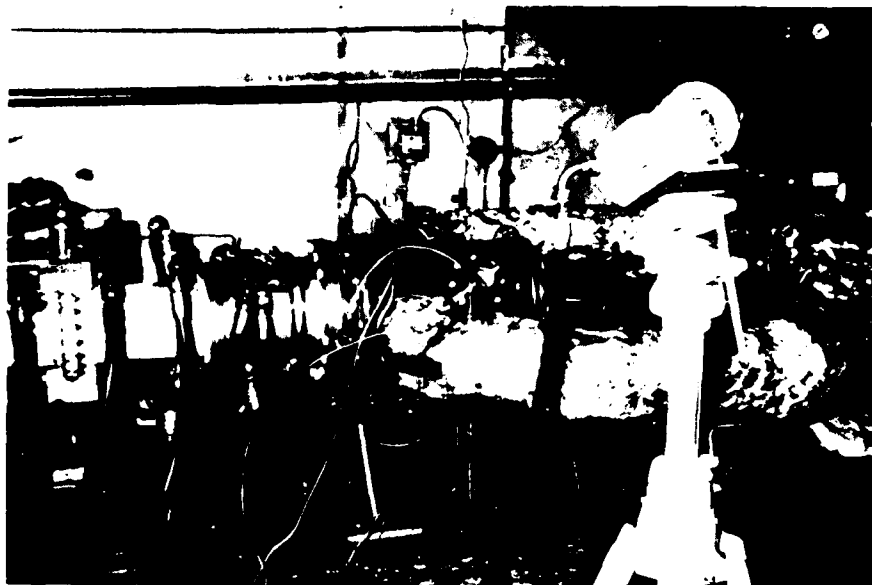


Fig. 3 Rig set up for Pressure Tests up to 5 bar

5. Investigations under steady test conditions including cold start trials

The series of ceramic combustor tests commenced under steady operating conditions, with flame ignition initiated only after a preheating sequence. The main goal was to determine which of the selected ceramic materials and combustor shapes withstands the steep gas temperature drop from the primary zone towards the combustor outlet.

The sequence of steady operating conditions is listed in Fig. 4. During the warm-up phase the temperature was slowly reised from ambient conditions to ignition in steps of

PHASE	DURATION Min	T _{IN} K	T _{EXIT} K	MASS FLOW kg/s	PRESSURE bar
WARM UP (NO THERMOSHOCK)	105	100 DEGREES / 15 Min		0.3	1.0
IGNITION (WEAK LIMIT)	—	700	≈1000	0.3	1.0
EXIT TEMPERATURE INCREASE	60	700	1270	0.3	1.0
BURNING (STATIONARY)	200	700	1270	0.3	1.0
END	SLOW REDUCTION IN TEST CONDITIONS				

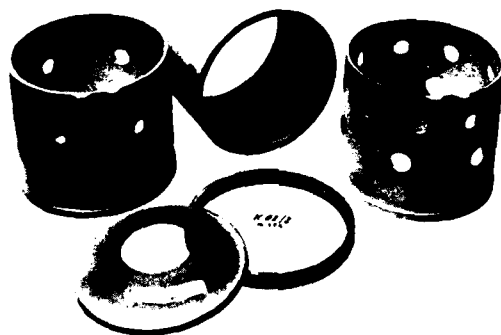
Fig. 4 Steady Test Conditions

100 degrees every 15 minutes. At ignition the combustor air entry temperature amounted to 700 K and the pressure to 1.02 bar. The air fuel ratio was 125. After ignition the temperature was slowly increased to 1270 K and then kept constant for 200 minutes. The test sequence was ended by slowly reducing the state parameters.

The test results showed that cylindrical combustors made from Si_3N_4 fracture during the high temperature burning sequence whereas combustors made from SiC withstand hot steady conditions. However, the cylindrical combustors made from SiC revealed fracture lines around the primary zone air ports and along the transition line from the cylindrical to the concave shape of the combustor head.

The ceramic combustors were exposed to higher loads by including cold starts in the steady test conditions, because of the extreme temperature shock. The temperature increases in fractions of a second from the ambient temperature to the combustion temperature level. After these tests, the cylindrical combustors made of isostatically pressed SiC , which had already revealed cracks, fractured completely. The fractured ceramic parts are shown in Fig. 5.

BEFORE TESTING



AFTER STEADY TEST



Fig. 5 Cylindrical Ceramic Combustor

In order to determine the surface temperature distribution along the combustor liner a cylindrical combustor was duplicated from metal, sprayed with thermopaint and processed at steady burning conditions. A typical result of such thermopaint tests is shown in Fig. 6. For the cylindrical combustor pictured on the left, the highest surface temperatures and the highest temperature gradients as well occurred in the sudden transition region of the combustor head from conical to cylindrical shape and around the air ports. The aim to reduce such high surface temperature gradients led to the design of conical combustors. As the thermopaints of the conical combustor pictured on the right of Fig. 6 reveal, a reduction of the high temperature peak in the primary zone was obtained. Furthermore, the temperature gradients are no longer locally concentrated in narrow zones but rather uniformly spread along the surface. Another important design feature of the conical combustor was the balance of the air injection along the liner in such a way to obtain uniform flame expansion throughout the combustor volume.

Considering the disappointing experience with Si_3N_4 , the conical ceramic combustors were fabricated from siliconized SiC only. They underwent the same steady burning conditions and cold ignition tests as the cylindrical combustors. The analysis of the tests showed that conical combustors made of siliconized SiC withstood hot exit temperature conditions and thermoshocks.

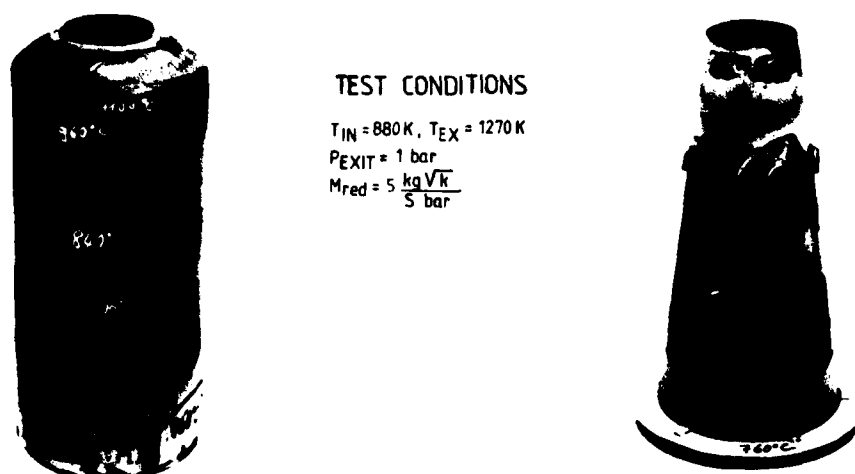


Fig. 6 Temperature Distribution on Metallic Combustors

After the cold ignition tests, the ceramic combustors were investigated under conditions corresponding to engine operating loads, such as idle and full power. The combustor surface temperature (T_{SR}) was measured during the test sequences. The measured temperature distribution along the ceramic surface of a conical combustor is shown in Fig. 7, in comparison with a cylindrical combustor described in Ref. 1. The surface temperature along the conical ceramic combustor, which was measured with the aid of an optical pyrometer, reveals a continuous distribution with no temperature peaks. In contrast, the cylindrical combustor shows a temperature peak at the combustor enlargement region which becomes more pronounced with increased loading.

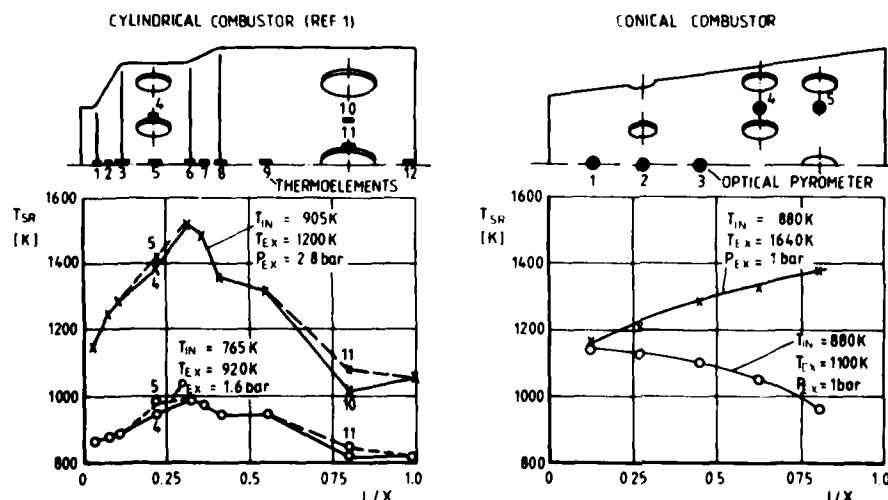


Fig. 7 Surface Temperatures under Steady Test Conditions

At low exit temperatures, the continuous surface temperature distribution of the conical combustor follows the familiar drop from the primary zone towards the combustor outlet. At higher exit temperatures, the surface temperature distribution is still continuous but shows a slight increase along the combustion chamber liner. The immediate primary zone temperature, however, remains unchanged for both operating conditions. This important

result is attributable to the intended combustion expansion throughout the whole combustor volume. At higher exit temperatures, the additional fuel flow leads to a continuous flame stretch downstream of the primary zone producing the slight surface temperature increase. Although the nose cone may also cause an increased outlet surface temperature by improving heat transfer conditions, the main contribution stems from the expansion of the combustion zone beyond the primary zone. The conical combustor in essence permits continuous adaptation of the combustion volume to the operating conditions, thus avoiding high local gas temperature peaks.

The ceramic combustor exit temperature distribution measured with a water cooled probe with three radially spaced thermocouple beads is shown in Fig. 8. The annular as well as the radial temperature distribution is rather uniform, the highest and the lowest gas temperatures differing only by a ratio of 1.09.

LEGEND	OPERATION CONDITIONS	TEST RESULTS
\times 1425	$T_{IN} = 880\text{ K}$	$T_{MAX} = 1445\text{ K}$
$+$ 1400	$P_{EXIT} = 1\text{ bar}$	$T_{MIN} = 1321\text{ K}$
Δ 1375	$AFR = 71$	$\frac{T_{MAX}}{T_{MIN}} = 1.09$
\circ 1350	$\dot{M}_{AIR} = 0.174\text{ kg/s}$	$OTDF = 14.6\%$
\square 1325	$\dot{M}_{RED} = 5 \frac{\text{kg}}{\text{s}} \frac{\text{VK}}{\text{bar}}$	$RTDF = 1.3\%$

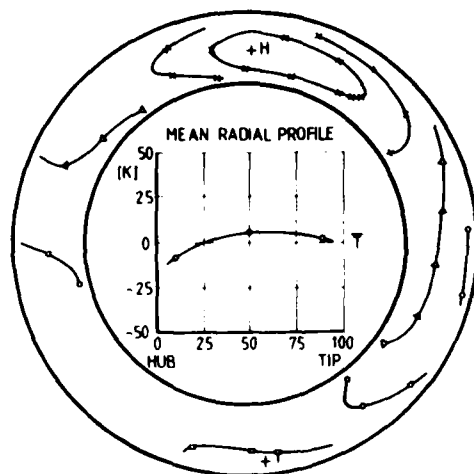


Fig. 8 Temperature Distribution at Nose Cone Exit

6. Cyclic Tests at ambient high plenum pressure

After having successfully undergone the investigations under steady conditions including cold starts, the conical combustors made from siliconized SiC were cyclic tested.

The tests began with temperature cycles applied at ambient pressure. The cycle depicted in Fig. 9 is made up of an acceleration and deceleration phase which were applied more than 50 times. The highest and the lowest temperatures of the cycle (T_H and T_L), measured at the combustor outlet, the corresponding air fuel ratios (AFR) and the time intervals are listed in the table. The air temperature at the combustion chamber entry was 800 K.

The surface temperatures of the liner were monitored at certain locations during the cyclic tests. Together with the variation in the gas exit temperature, they are plotted in Fig. 7. Since with increasing fuel flow the flame spreads downstream of the first row of air ports, the surface temperature decreases at location 1 and increases at location 4 whereas it remains nearly constant between the primary air ports at location 2. The marked increase in the exit surface temperature at location 4 proves the previously explained mechanism of continuous combustion expansion along the conical combustor with increasing fuel flow. During the deceleration phase, the surface temperatures drop steadily towards their starting values without sudden gradients.

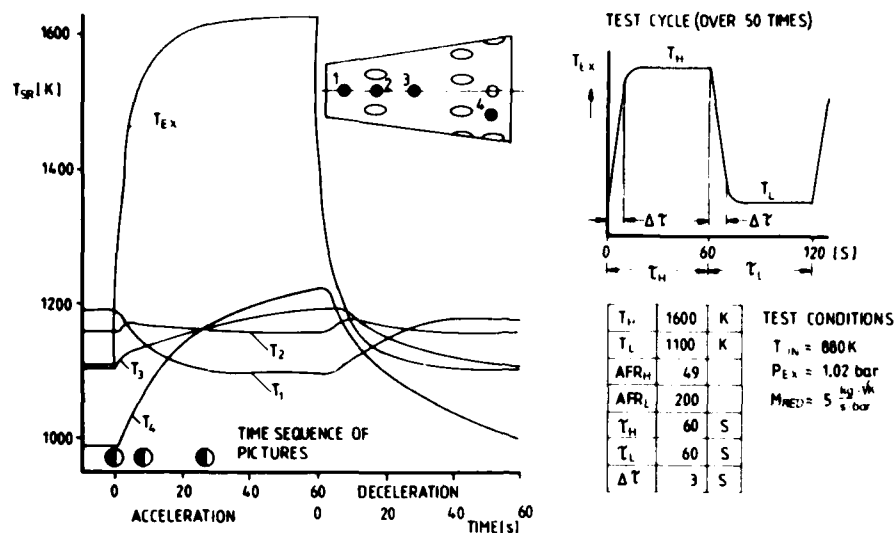


Fig. 9 Cyclic Testing of Ceramic Combustor

The photographs of the glowing surface taken through the viewing window at the beginning of the acceleration phase and at 9 and 27 seconds later are represented in Fig. 10. The downstream expansion of the combustion zone is quite evident. With increasing fuel flow, after 9 seconds the combustion zone has reached the region of the second row of air injection holes making the previously dark ports shine brightly. One can also see the continuous increase in the downstream surface temperature as indicated by the brighter red color, which became nearly uniform after 27 seconds.

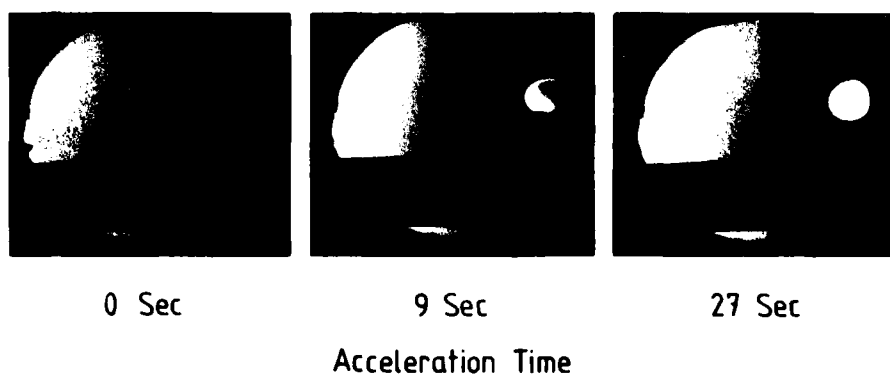


Fig. 10 Pictures of glowing Combustor Surface

Combustor tests at higher plenum chamber pressures were commenced by increasing the pressure in stages as depicted in Fig. 11, and by keeping the air entry and the gas exit temperature nearly constant. The test data apply to steady conditions. The surface temperature measured at a location just in front of the second row of air ports revealed a pressure-related increase. At the point of measurement in question the surface temperature was higher than the gas exit temperature at pressures over 2 bar.

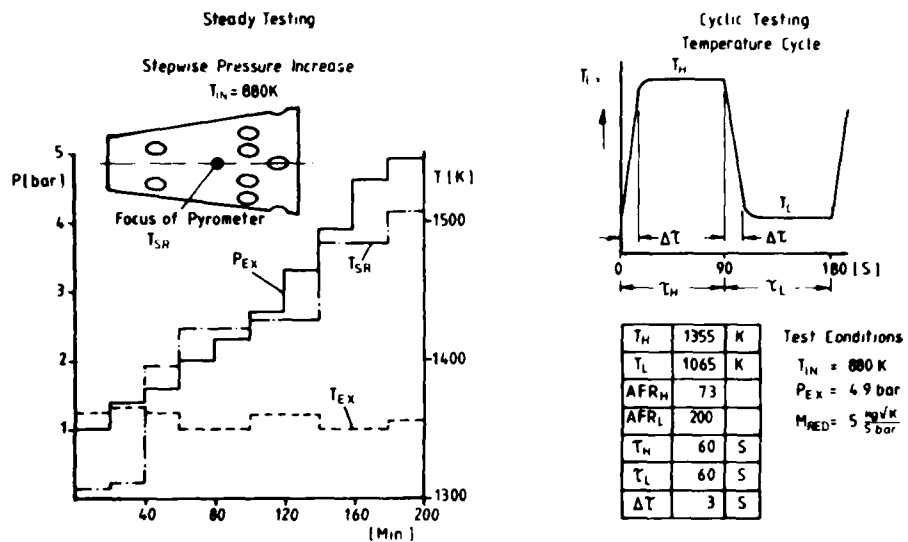


Fig. 11 Ceramic Combustor Tests at Elevated Pressures

After the tests, only small silicon secretions were found in the siliconized SiC (Retel) combustors manufactured by BNFL, and the combustors remained undamaged. Similar conical combustors, also made of siliconized SiC but slip casted and manufactured by NORTON, fractured during the tests. As shown in Fig. 12 the cracks run along the first and second row of air ports, where the material is inherently weakened. The inner surface became wavy and

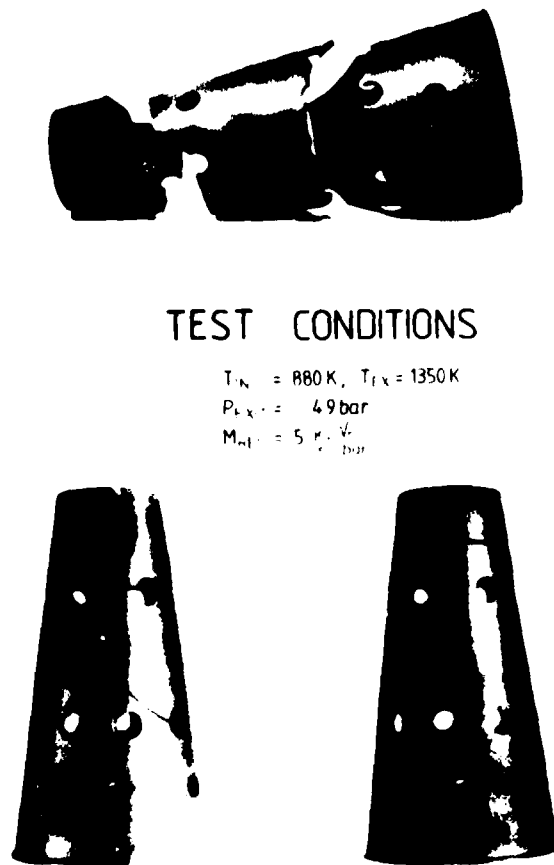


Fig. 12 Fractured Combustor at BNFL by Norton

exhibited a change in color with silicon secretions. Since details of the manufacturing methods of the two companies are not available, the lower resistance of the NORTON combustor can be only superficially related to the slip casting process.

Various nose cones were also investigated during the tests at elevated pressures. In Fig. 13 two nose cones are shown after having undergone high pressure tests. In general the results were similar to those of combustor tests; nose cones of Si_3N_4 as well as integrally molded SiC nose cones fractured.

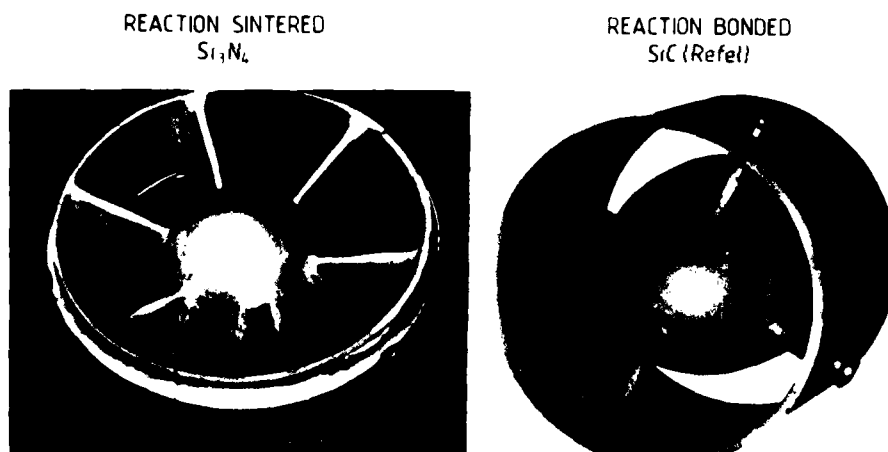


Fig. 13 Ceramic Nose Cones after Cyclic Tests at Elevated Pressures

Therefore, for the continuation of the program with cyclic tests at elevated pressures, only combustors and nose cones of Refel were considered further. The temperature cycle applied to the ceramic combustors at full power pressure of 4.9 bar is also shown in Fig. 11. The characteristic values of the cycle are listed in the table. The combustors were subjected to 200 cycles, i.e. to temperature leaps of 290 degrees, with an inspection being carried out at the half-way stage after 100 cycles. The ceramic combustors made of Refel investigated so far showed no signs of major damage after the cyclic tests. A two-part combustor having successfully gone through the full cycle is pictured in Fig. 14.



Fig. 14 Ceramic Combustor after Cyclic Tests at Elevated Pressures

The combustor revealed a thin fracture line on the outer surface between two air ports (marked in white) and strong silicon secretion with some fracture lines in the region of high surface roughness on the inner surface. Two unsplit combustors made of Refel with wall thicknesses of 4 mm and 2 mm respectively are shown in Fig. 15 after the cyclic tests.

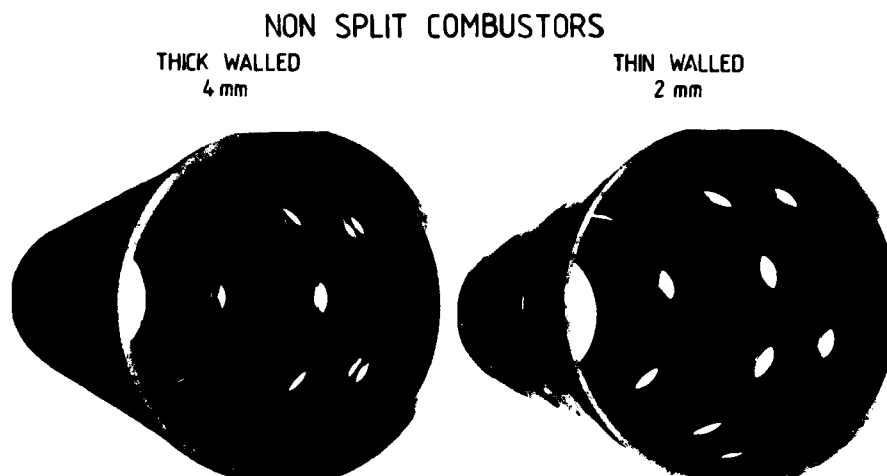


Fig. 15 Ceramic Combustors after Cyclic Tests at Elevated Pressures

Neither combustor has fracture lines and both exhibit fewer secretion bubbles. It was concluded, therefore, that some air enters the two-part combustor between the division plane, disturbing uniform combustion and thus producing temperature gradients. This again stresses the requirement for avoiding temperature gradients along ceramic combustion liners.

7. Operation of a hybrid ceramic-metal combustor in a vehicular gas turbine

In order to investigate the behaviour of ceramic materials under full engine operating conditions a hybrid ceramic-metal combustor was installed in a vehicular gas turbine. A design scheme of the combustor and the installation in the engine is shown in Fig. 16.

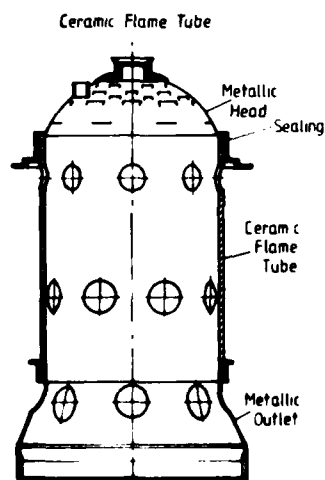


Fig. 16 Ceramic Flame Tube for Vehicular Engine Test

The combustor consists of an air-cooled metal head end, a ceramic cylinder made of siliconized SiC (Refel) and a metallic transition section. The ceramic cylinder was connected to the metallic parts by a seal and the mechanical loads were transmitted across it through adjustable staves. Such hybrid combustors have accumulated over 20 hours of testing in a vehicular gas turbine. After test inspections some of the ceramic cylinders revealed cracks originating from the adjoining regions. A typical fracture line, which starts at the head end seal and crosses the ceramic liner up to the second row of air ports, can be seen in Fig. 17. The transition area from metal to ceramic parts, in general, presents a

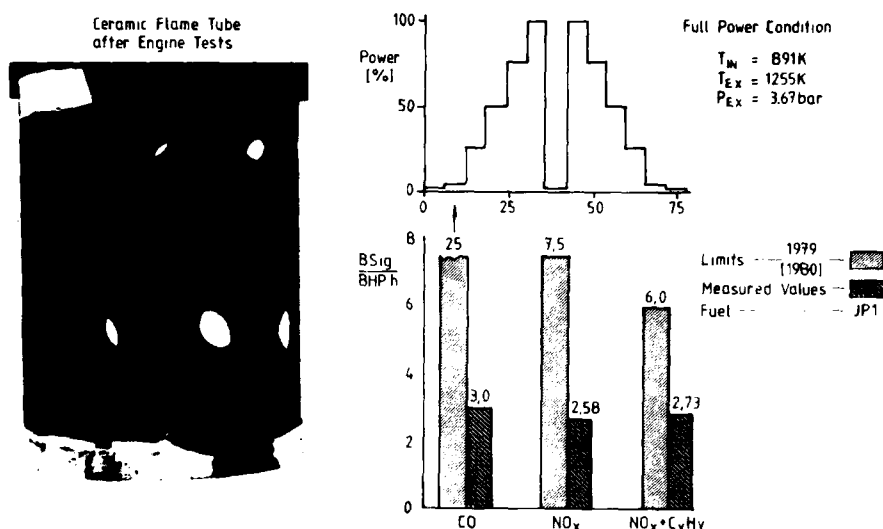


Fig. 17 Results of Ceramic Flame Tube Tests in Vehicular Engine

very demanding design problem because of the diversity in thermal expansion. A new design approach, to be investigated next, omits the insulation, allowing each part to move without direct restrictions. The ceramic cylinder has not yet failed as a result of thermal fatigue and thin mechanical cracks have not hampered engine operation.

The hybrid combustor was subjected to a 13-point California test cycle and the exhaust emissions were measured. Under full power the combustor air entry temperature was 891 K, the plenum pressure was 3.67 bar and the exhaust temperature 1255 K. The emissions, plotted in Fig. 17 as brake specific emission factors, in comparison with the emission limits set or to be set for diesel engines in 1979 and 1980, highlight the environmental advantages of the gas turbine. Although the vehicular gas turbine was run on JP1 fuel, because the sulfur in diesel fuel affects the heat-exchanger material, the consequently high NO_x values were still well below the emission limits for truck engines.

8. Conclusions

The results of development as it stands show that ceramic combustors can withstand thermoshocks during cold starts and steady operating conditions with high gas temperatures. Conical ceramic combustors designed to avoid high surface temperature gradients have proved their ability to withstand cyclic temperature tests at full power pressure conditions, and investigations with a hybrid ceramic-metal combustor confirmed the potential of ceramic materials to satisfy full engine operating conditions. The technical knowledge gained so far, however, is not sufficient to enable a ceramic combustor to be designed, built and used for complete vehicular gas turbine applications.

Cooperation with the producers of ceramic materials in order to develop better ceramic-oriented design concepts is necessary before the demands of vehicular gas turbine operation can be met. Testing will have to continue with regard to sharper high temperature test cycles and durability. The iterative experience gained will promote the development of a ceramic technology. To reach the objective, an all-ceramic demonstrator is being set up to demonstrate the low cost and high reliability of ceramic components and the low fuel consumption predictions.

9. Acknowledgements

The authors acknowledge the German State Department for Research and Technology (Bundesministerium für Forschung und Technologie) for support of these programs.

10. References

1. G. Kappler, K. Giesen, "Stand der Entwicklung von Brennkammern aus keramischen Werkstoffen," Keramische Komponenten für Fahrzeug-Gasturbinen; Springer-Verlag Berlin-Heidelberg-New York 1978.
2. P. Walzer, "Keramische Bauteile für Fahrzeug-Gasturbinen," MTZ Motortechnische Zeitschrift Nr. 10/1978.
3. K. Trappmann, "Development of Ceramic Components at MTU-München," Overview of German Ceramic Gas Turbine Program, ASME Gas Turbine Conference, San Diego, California, March 12-15, 1979.

SOME EXPERIENCE IN THE DESIGN AND EVALUATION OF CERAMIC COMBUSTION CHAMBERS

By

G Sedgwick - Project Designer
Lucas Aerospace Limited, Fabrications
Lucas Laboratories, Burnley
England

SUMMARY

The paper reviews the design, component evaluation and combustion testing of a small reverse flow annular combustion chamber constructed in silicon nitride. Initially heat transfer assessments were made of the temperature levels which components would reach during combustion testing, and a thermal test programme was formulated which enabled loadings well in excess of those estimated for the actual flame tube environment to be imposed upon specimen components. From calculated thermal stresses, values for the probabilities of survival were obtained using a brittle failure analysis based on a Weibull distribution and a volume flaw weakest link hypothesis. A subsequent programme of combustion tests carried out on a pressure rig culminated in operation at a chamber exit temperature of 1762K.

A pipe combustion chamber programme is also described using a monolithic construction in silicon carbide, in which failure modes are presented and analysed.

1. INTRODUCTION

The Ministry of Defence has sponsored work programmes at the Lucas Aerospace Limited, Lucas Laboratories Burnley, England, to evaluate ceramic combustion chambers for small gas turbine engines.

Two work programmes have been undertaken:-

- (i) The demonstration of the suitability of silicon nitride for potential use in small gas turbine engines as an aid to increasing specific power, using a small annular combustion chamber.
- and (ii) A programme with the two-fold objectives of studying the effect on exhaust emissions of operating a ceramic combustion chamber without any wall cooling, and to assess the limitations of a monolithic ceramic flame tube construction.

2. GENERAL CONSIDERATION - SMALL ANNULAR COMBUSTION CHAMBER

A reverse flow annular combustion chamber was chosen as a test vehicle for this investigation, such a configuration being consistent with the general requirements of a small main or auxiliary power unit.

It was initially considered impracticable and unduly expensive to use unconventional flame tube arrangements since these would require combustion development to obtain a basic performance. Such designs were therefore eliminated in favour of configurations on which experience existed on developed metallic designs.

The strength of reaction bonded silicon nitride was thought to be insufficient to withstand the thermal stresses which would be imposed on a monolithic construction and consequently, of a number of alternatives considered, two main concepts were pursued.

- (i) A tile concept which would minimise both axial and circumferential stresses.
- (ii) A stacked ring construction which would minimise axial stresses.

Following stress analysis, typical components were manufactured in hot pressed silicon nitride (HPSN) and others in reaction bonded silicon nitride (RBSN), both types being subjected to bench thermal stress testing.

3. THERMAL STRESS TESTS

Heat transfer assessments were made of the temperature levels which components would reach during combustion testing to a chamber exit temperature of 1700K (2600°F). Primary zone mean wall temperatures estimated by use of Lucas computer programmes are given in Table 1, together with the radial gradients through the material. Also given are the assumed peak temperatures associated with local hot spots.

Stress distributions, based on the temperature conditions in Table 1, were established which showed peak tensile stresses in inner and outer elemental rings to be 113 MPa (16380 lbf/in²) and 161 MPa (23350 lbf/in²) respectively (1).

To give an increased severity factor for the component tests, however, a radial gradient of 150°C (300°F) was adopted and the superimposition of local hot spots, such as would occur in a practical combustion chamber, imposed additional thermal stress on the test specimens up to a level of 240 MPa (34800 lbf/in²) on an inner ring.

In the series of proving tests, inner faces of components were heated by a ring burner using an oxygen enriched air/gas mixture, whilst the outer faces were cooled by cold air jets from a ring manifold. A hot

spot was applied by means of an oxy-hydrogen flame at a single point on each specimen.

TABLE I
PRIMARY ZONE WALL TEMPERATURES

	Mean Temperatures		Local Hot Spot Temperatures	
	Wall Temp.	Gradient	Wall Temp.	Gradient
Outer F/T	870°C (1598°F)	68°C (154°F)	1115°C (2039°F)	104°C (219°F)
Inner F/T	820°C (1508°F)	77°C (171°F)	1055°C (1931°F)	115°C (239°F)

3.1 Reaction Bonded Silicon Nitride (RBSN) Rings

A statistical approach to brittle failure analysis based on the "weakest link" hypothesis (2) was applied to the flame sprayed RBSN rings, a volume critical flaw distribution being used to predict the probability of failure under the applied loading. Values of material strength and Weibull modulus were obtained from test bars produced at the same time as the test components.

Six rings of inside diameter 200 mm (7.9 in), length 32 mm (1.26 in), and of 5.08 mm (0.2 in) and 7.62 mm (0.3 in) thicknesses were tested, failure occurring at stress levels between 61.2 MPa (8875 lbf/in²) and 127 MPa (18415 lbf/in²).

Measurements of Material Strength and Weibull modulus taken from the above components fell short of those expected and the failures were attributed to shortcomings in the material (3).

3.2 Hot Pressed Silicon Nitride (HPSN) Rings

Initial trials were carried out using a ring which contained castellations along one edge to permit ingress of air into the annular chamber for combustion purposes. Failure occurred when mean temperatures of 860°C (1580°F) and 760°C (1400°F) were imposed on the inside and outside faces respectively, and when the superimposed peak temperature had reached 1200°C (2192°F). Fracture originated at the root of a castellation within the hot streak. A further castellated ring, with a small radius introduced at the edges, and plain rings were tested to mean temperatures of 790°C (1454°F) and 640°C (1184°F). A hot streak was superimposed on each specimen, the temperature being increased incrementally from 1050°C to 1250°C (1922°F to 2282°F). X-ray examination showed no cracks in any of these specimens which had been subjected to conditions giving peak tensile stresses of the order of 240 MPa (34800 lbf/in²).

3.3 Hot Pressed Silicon Nitride (HPSN) Tiles

The plain inner faces of each of six specimens were heated to a mean temperature of 870°C (1598°F) whilst the outer faces were cooled generally to 800°C (1472°F). Hot streaks were superimposed in steps from 900°C to 1350°C (1652°F to 2462°F). No failures were induced in any component. Gradients through the tile thickness were quite severe since, when the inner face was at 1350°C (2462°F), the outer face was at 1050°C (1922°F) i.e. 300°C (572°F) over 7.6 mm (0.3 in).

4. DESIGN STANDARD - GENERAL

Whilst proving tests on both rings and tiles in HPSN showed both to be capable of withstanding thermal conditions more severe than those anticipated in service, the stacked ring concept was selected for combustion testing for the following reasons:-

- (a) The potentially lower manufacturing cost.
- (b) The elimination of the sealing problems inherent with the tile construction.
- (c) The simpler mounting to the engine pressure casing.
- (d) The elimination of the flame tube annulus blockage present in the tile design.

Subsequent finite element analysis has shown this approach to be a viable design concept, provided consistent material properties can be achieved.

The stacked ring annular flame tube design lends itself to the basically iterative programme undertaken which can be categorized into four phases, viz:-

- Phase I - The use of HPSN complete rings with sloping interface.
- Phase II - Evaluation of alternative ring constructions and RBSN material forms.
- Phase III - Consideration of larger monolithic ceramic components.

Phase IV - Evaluation of ring constructions using fail safe features, with and without re-designed head ring and rear disc components.

5. PHASE I

5.1. Design Standard

A prototype stacked ring type annular flame tube was constructed for combustion testing on a pressure rig (Figure 1).

Concentric stacks of HPSN rings formed the inner and outer walls of the flame tube. The head ring and rear disc components were tested in both RBSN and a "low calcium" form of HPSN.

5.2. Operating Conditions

The selected full load operating conditions, corresponding to sea level static ISA conditions included a turbine entry temperature of 1473K (2192°F) with an inlet pressure of 4 bar, and a nominal air mass flow of 0.91 kg/s (2.00 lb/s).

5.3. Description of Tests and Results

A full description of the testing in this phase of the programme is reported in Reference 1. For completeness however, the test operating conditions are included in Table II.

6. PHASE II

6.1. Design Standard

The HPSN outer flame tube, and metallic head ring and rear disc components were used in the second phase of the programme in advance of re-designed ceramic components becoming available. The inner flame tube assembly was used as the vehicle for testing alternatives in RBSN. Full inner rings were first tested, followed by split and segmental rings, which were intended to eliminate the hoop stress induced in full rings by the thermal gradient through the material thickness.

6.2. Description of Tests and Results

A total of 15 hours 40 minutes testing was carried out during this phase, over 11 hours of which were at turbine entry temperatures in excess of 1500K (2240°F).

Inner flame tube component failures were experienced attributable to a reduction in the end mounting load resulting from differential expansion between the metallic head ring and the ceramic flame tube stack. Split and segmental rings survived the testing but displacement of one of the segments occurred. Component temperatures in the region of 1200°C (2192°F) were identified.

7. PHASE III

7.1. Design Standard

A monolithic inner flame tube in silicon carbide was now introduced replacing the complete silicon nitride inner ring stack. The material is produced by British Nuclear Fuel Limited, under the trade name REFEL.

7.2. Description of Test and Results

The silicon carbide inner flame tube was tested for 2 hours 30 minutes, 2 hours of which were at a turbine entry temperature of 1530K (2295°F). The component suffered two longitudinal cracks without impairing the integrity of the assembly. Temperature assessments, based on colour-change thermal paints, suggest that failure initiated as a result of the axial thermal gradient which is accommodated in the stacked ring design.

8. PHASE IV

8.1. Design Standard

Following break-down of the inner stacked ring assembly during Phase II, in which components incorporating the angled interface principle were used, attention was directed towards providing features which would ensure assembly viability in the event of one or more component failures.

Of a number considered a vee-block principle was selected as being worthy of testing. Figure 2b) shows this concept together with the sloping face version used in earlier testing (Figure 2a).

Temperature measurements made during earlier testing using temperature sensitive paints showed that the central section of the inner flame tube subjected to the highest thermal gradients. Consequently, this area was chosen for the design iteration comparison testing. The ring stack was re-arranged to allow components to be introduced which accommodated the transition from the angled interface to the vee-lock concept (Figure 2a and 2b). Vee-lock iterations tested, in RBSN, included full rings, split rings and three-part segmental rings.

In addition, during this phase, RBSN head rings and rear discs were tested, each being slotted from the outer circumference radially inwards.

TABLE II
TEST OPERATING CONDITIONS

Phase	Test No.	Air Mass Flow kg/s (lb/s)	Fuel Flow kg/s (lb/s)	Air/Fuel Ratio	Inlet Pressure kPa (lbf/in ² abs)	Chamber Exit Temp. K (°F)	Duration Mins.
I	1	0,904 (1.99)	0,01 (0,02)	90,4:1	393 (56.9)	950 (1250)	30
	2	0,703 (1.55)	0,008 (0.017)	87,9:1	241 (34.9)	800 (980)	25
	3	0,590 (1.30)	0,008 (0.017)	73,7:1	207 (30.0)	-	30
	4	0,987 (2.17)	0,019 (0.04)	51,9:1	395 (57.3)	1143 (1598)	55
	5	1,02 (2.25)	0,025 (0.055)	40,8:1	397 (57.6)	1273 (1832)	60
	6	1,01 (2.22)	0,027 (0.059)	37,4:1	396 (57.4)	1200 (1700)	30
	7	0,997 (2.20)	0,033 (0.073)	30,4:1	397 (57.6)	1515 (2267)	90
II	8	0,92 (2.01)	0,0303 (0.067)	30:1	407 (59.1)	1618 (2453)	150
	9	0,935 (2.06)	0,031 (0.069)	30,2:1	403 (58.5)	1616 (2449)	90
	10	0,949 (2.09)	0,029 (0.064)	33:1	403 (58.5)	1533 (2300)	90
	11	0,932 (2.06)	0,029 (0.064)	31,8:1	407 (59.1)	1568 (2363)	80
	12	0,925 (2.04)	0,028 (0.062)	33,3:1	406 (58.9)	1523 (2282)	45
	13	0,949 (2.09)	0,036 (0.080)	26,13:1	409 (59.3)	1762 (2712)	150
	14	0,963 (2.12)	0,029 (0.064)	33,7:1	407 (59.1)	1516 (2269)	105
	15	0,969 (2.14)	0,028 (0.062)	34:2	403 (53.5)	1506 (2251)	135
III	16	0,952 (2.10)	0,028 (0.062)	33,5:1	402 (58.3)	1522 (2280)	80
	17	0,94 (2.07)	0,028 (0.062)	33:1	404 (58.6)	1530 (2295)	150
IV	18	0,935 (2.06)	0,028 (0.062)	33,7:1	403 (58.4)	1516 (2269)	150
	19	0,93 (2.05)	0,028 (0.062)	33:1	402 (58.3)	1535 (2304)	135
	20	0,955 (2.1)	0,028 (0.062)	34,4:1	404 (58.6)	1494 (2230)	170
	21	0,909 (2.00)	0,028 (0.062)	33:1	402 (58.3)	1552 (2304)	120
	22	0,939 (2.07)	0,028 (0.062)	33,4:1	401 (58.1)	1523 (2282)	120
	23	0,935 (2.06)	0,029 (0.064)	32:1	404 (58.6)	1543 (2318)	160
	24	0,960 (2.11)	0,028 (0.062)	34,8:1	409 (59.3)	1473 (2162)	155

8.2 Description of Tests and Results

Seven combustion tests were carried out during this phase using components incorporating the vee-lock principle. A total running time of 16 hours 15 minutes was accumulated including 12 hours at a turbine entry temperature in the order of 1500K (2240°F) or higher. Breakages of the inner ring components occurred, in particular the first transition (Item 3, Figure 26), but at all times the inner flame tube ring assembly remained viable.

9. SUMMARY OF TEST RESULTS

A total of 41 hours 25 minutes combustion testing has been carried out on a pressure rig to date in a programme of twenty-four tests, 25 hours 40 minutes of which have been at turbine entry temperatures in excess of 1500K (2240°F) (Table II).

10. CONCLUSIONS - SMALL ANNULAR CHAMBER PROGRAMME

- 10.1 A silicon nitride flame tube has been designed, and combustion tested to turbine entry temperatures up to 1700K (2600°F), six of the 12 components making up the flame tube assembly surviving a total of twenty-four combustion tests of 41 hours 25 minutes duration. These components were all in HPSN produced by Lucas Research Centre.
- 10.2 The greatest number of failures occurred on the two most complex components, namely the head ring (four failures) and the rear disc (five failures). Subsequent re-design reduced the stress levels in these components to trivial levels but failures again occurred which were directly attributable to material inhomogeneity.
- 10.3 Simulated structural bench tests undertaken in this programme were useful in highlighting local design features acting as stress raisers and these were largely eliminated in the design which was combustion tested.
- 10.4 The programme revealed the requirement for manufacturing development of all but the simplest type of components. However, providing consistent material properties and manufacturing techniques for silicon nitride can be developed, this programme demonstrates that the design of a specific ceramic combustion chamber for a typical present generation small gas turbine is a practical possibility.

11. GENERAL CONSIDERATIONS - MONOLITHIC PIPE CHAMBER

This work programme was initiated with the two-fold objectives of studying the effect on exhaust emissions of operating a ceramic combustion chamber without any wall cooling, and to assess the limitations of a monolithic ceramic flame tube construction. A metallic pipe chamber flame tube, conventionally skin cooled, which had been used in previous combustion research programmes was taken as a datum test vehicle and comparisons were made against an uncooled similar diameter flame tube construction in 'Refel' silicon carbide supplied by British Nuclear Fuels Limited, shown in Figure 3.

During this series of tests, cracking of the silicon carbide chamber was observed at a condition typical of full load at a mean exhaust gas temperature (T_3) of 1473K (2192°F). A second flame tube also suffered damage at this condition.

An analysis was initiated to investigate the cause of these failures and it is this aspect of the programme which is described.

12. TESTING

A total of three flame tubes were used during the testing. All three withstood conditions equivalent to normal idling and a higher load condition having a T_3 of 1273K (1832°F) without any visible damage. At higher exhaust temperature, 1473K (2192°F), at full load conditions all flame tubes exhibited extensive cracking typically as shown on Figure 4.

The flame tubes did not fragment but remained substantially in one piece thus enabling emissions testing to be completed without premature shutdown. The full load conditions for this combustion chamber were inlet pressure 700 kPa (101 lbf/in² abs), inlet temperature 700K (800°F), exhaust temperature 1473K (2192°F), air mass flow 1.41 kg/s (3.1 lb/s), fuel flow 0.026 kg/s (0.058 lb/s). The longest running time at this condition before failure occurred was approximately two hours. The total test time achieved on all three flame tubes was of the order of fifteen hours. Temperature sensitive paints were employed during the programme to determine the temperature distributions, see Figures 5 and 6.

13. STRESS ANALYSIS

From the paint test results it was concluded that the most severe gradients occurred in the axial direction with local gradients of lower magnitude occurring in the region of the air admission holes. Some asymmetric distributions were also observed in the circumferential direction particularly at the higher gas temperature condition. It will be noted that the axial temperature distributions for the two loading conditions differ and this will be referred to at a later stage.

The analysis undertaken used the Lucas 'FELSET' suite of programmes which uses the 'REFSAFE' finite element programme, developed by the Central Electricity Generating Board (U.K.).

Although it is obviously preferable to carry out a 3-D analysis, the lack of symmetry would have required a large segment of the circumference of the flame tube to be considered which would result in mesh requirements outside the capabilities of the Lucas (FELSET) system at the time, this feature having now been incorporated into the programme. It was therefore decided to consider axial and radial temperature gradients only, limiting the assessment of 2-D axisymmetric analysis.

The temperature distributions used in the analysis are as shown in Figure 7.

The corresponding stress distributions resulting from the temperature distributions are shown in Figures 8 and 9. The air admission holes are indicated on the section for reference purposes only.

At the 1273K (1832°F) running condition shown in Figure 8 both the axial and hoop stresses are considerably less than those occurring at the higher temperature conditions, and tend to be approximately equal in magnitude.

It is clear from Figure 8 that the air admission holes are in a regions of high axial stress at the higher 1473K (2192°F) condition. The hoop stress is in general at a much lower level and never exceeds 80% of the maximum axial stress.

The shape of the hoop and axial stress distributions at the higher exhaust temperature are interesting. On the inner surface the two curves follow each other closely whereas on the outer surface the hoop and axial stresses are out of phase. This is explained by reference to Figure 7 where it can be seen that the axial position at which the temperature is a maximum is between two areas of relatively lower temperature. Thus although there are induced axial bending stresses, which are tensile on the outer surface and compressive on the inner surface, there will also be a net compressive hoop stress at the plane of maximum temperature due to the restraining effect of the colder masses on either side.

The finite element output stresses may now be analysed statistically using the 'FELBRIT' brittle failure analysis programme, originally developed by Sivill (2), to estimate failure probabilities and mean failure stresses.

The brittle failure analysis, based on a volume flaw weakest link hypothesis and a Weibull distribution, correlates probability data in terms of the Weibull modulus 'm'.

Figure 10 shows the mean failure stress plotted against 'm' for the exhaust temperature conditions (T_3) of 1273K (1832°F) and 1473K (2192°F). Superimposed on this graph is the actual calculated maximum stress and clearly, for the 1473K (2192°F) condition, the computed stress falls in the critical area where a failure is likely.

An alternative presentation to Figure 9 is to compute a failure stress ratio, $\frac{\text{mean failure stress}}{\text{applied maximum stress}}$, and to plot against 'm', as shown in Figure 11. The failure stress ratio defined in this manner may be considered analogous to a reserve factor in conventional stress analysis i.e. a failure stress ratio greater than 1.0 indicates an acceptable design whereas a value less than 1.0 indicates an expectancy of failure.

14. DISCUSSION OF RESULTS

14.1 Temperature Distributions

The shape of the two temperature distributions were based on a combination of experimental values and a theoretical analysis. Figures 5 and 6 show the two paint tests carried out at 1273K and 1473K respectively. Interpretation of the results together with a theoretical prediction of the radial gradients form the basis of the stress analysis. Figure 7 shows the axial temperature distribution along the flame tube wall, and in particular the somewhat surprising distribution in the region of the dilution holes for the 1473K exhaust condition. In considering this condition it must be remembered that the optimum redistribution of skin cooling air in the ceramic flame tube may not have been achieved and as a consequence the combustion process may not have been completed at the plane of the dilution holes.

14.2 Pressure Loading

The flame tube overall pressure loss is approximately 5% of the inlet pressure of 700 kPa (101 lbf/in²) resulting in a compressive hoop stress on the flame tube of 0.45 MPa (65 lbf/in²). The end loading due to pressure results in a compressive axial stress of 0.09 MPa (13 lbf/in²). Both these stresses may be ignored in comparison with the thermally induced stresses. Stresses due to pressure loading have therefore been neglected.

14.3 Mechanical Loading

The failures that have occurred during testing have not been in areas where the ceramic flame tube is in direct contact with the metallic parts of the test rig and there was no indication, either visually or audibly, of any particular resonance effects from the combustion process. Contributory failure stresses due to mechanical loading, vibration, etc., have therefore been ignored.

14.4 Unit Strength

A unit strength value for silicon carbide was abstracted from published data in order to carry out the analysis. This value will be confirmed when the flame tubes are finally cut up and test bars obtained.

15. ANALYSIS OF TESTS

In analysing the results major emphasis is placed on the higher temperature condition at which all three flame tubes suffered cracking. An examination of the three flame tubes showed that several of the cracks ran in a circumferential direction and appeared to initiate at the dilution and intermediate air admission holes. This pattern is consistent with high axial tensile stresses in the region of the holes as indicated on Figure 9. Hoop stresses are also high, however, in the region of the holes and therefore the direction of crack propagation is likely to be more uncertain away from the highest stress areas. Evidence of cracks running in the form of a helix around the flame tube could be seen on all three flame tubes and would indicate a combination of high axial and hoop stresses. At the lower temperature

conditions, no cracking was observed after testing. The stress distribution indicates a fairly low nominal stress level and would infer that a failure at this condition is unlikely.

A factor which has not been included in the present 2D analysis is the stress concentration which will occur due to the geometric arrangement of the holes and due to any surface finish effects on the hole edges; clearly in a full 3D stress analysis these effects would be automatically included. As the material is brittle, notch sensitivity is likely to be high and therefore the stress concentration factor (S.C.F.) can be assumed to be fully effective. The geometric S.C.F. estimated using Peterson (5), is 1.5. Surface condition of the holes was fair with a radius machined at the hole edges. Occasional flaws were observed on the edges of holes, within the thickness of the flame tube wall - hence not subjected to the highest stress levels. It has not been possible to quantify the S.C.F. due to surface effects but this is taken at least partly into account during the statistical analysis and indicates that the high temperature condition is more arduous than the present analysis shows.

16. CONCLUSIONS - MONOLITHIC PIPE CHAMBER

- 16.1 The stress analysis based on thermal paint tests have confirmed that unacceptably high stresses are induced at the 1473K (2192°F) mean exhaust gas temperature condition consistent with the failures obtained during testing.
- 16.2 The lower 1273K (1832°F) mean exhaust gas temperature condition does not induce thermal gradients as severe as the 1473K (2192°F) condition and consequently the stresses are much reduced and are such that a significant amount of combustion running should be possible at this lower level.
- 16.3 The high thermal gradients experienced at the 1473K (2192°F) condition suggests that a combustion development programme would be required to minimise these effects.

17. REFERENCES

- 1. Sedgwick G Evaluation of a Ceramic Combustion Chamber for a Small Gas Turbine Engine. Proceedings of AGARD Conference on High Temperature Problems in Gas Turbine Engines, No. 229, 1977, pp. 27.1 - 27.10.
- 2. Sivill A D Thermodynamic Stress Analysis of Silicon Nitride Components. PhD Thesis 1974, University of Nottingham.
- 3. Sedgwick G Annular Combustion Chamber Studies, Autumn Meeting TTCP, P2 Panel, 1975.
- 4. Godfrey D J Ceramics for Gas Turbines: Engineering Philosophy and Material Property Considerations, Proceedings 3rd US/UK Conference-Gas Turbine Materials in a Marine Environment, 1976, pp.7.
- 5. Peterson R E Stress Concentration Design Factors, Wiley, New York, pp. 21-51.

ACKNOWLEDGEMENTS

Thanks are due to the Directors of Lucas Industries Limited for permission to publish the paper, and also to the Ministry of Defence (U.K.) on whose behalf the described programmes were carried out.

The author also wishes to thank colleagues for their support during the design and test programmes and in the preparation of the paper.

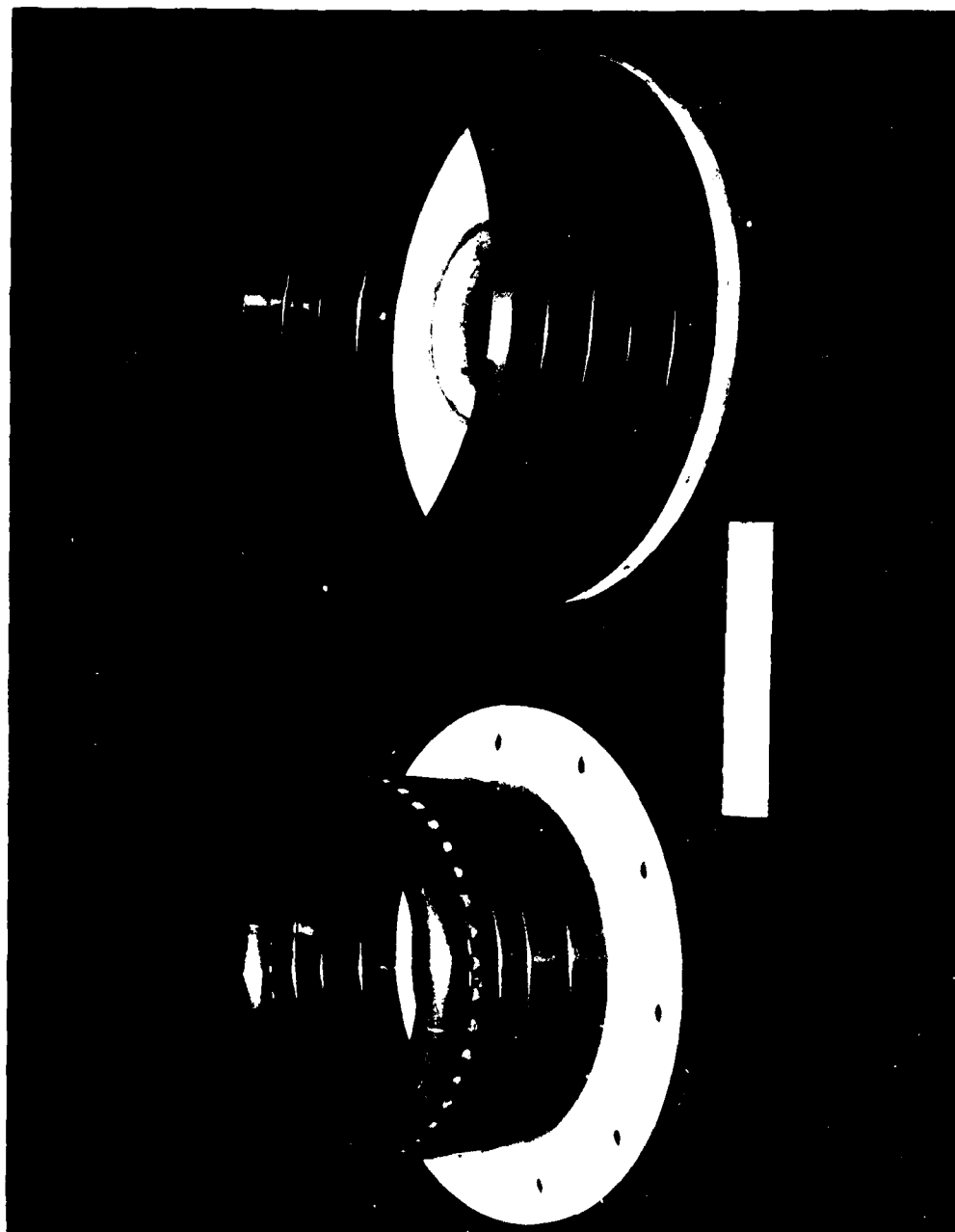


FIG.1 PROTOTYPE FLAME TUBE COMPONENTS

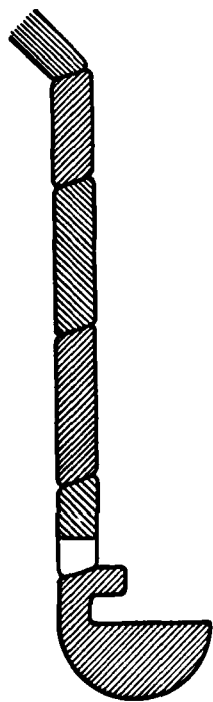


FIG.2a ANGLED INTERFACE CONCEPT

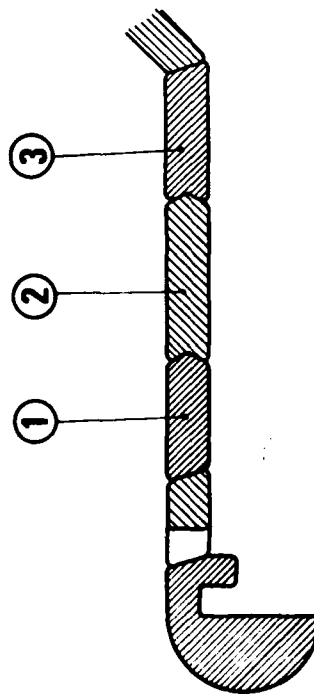
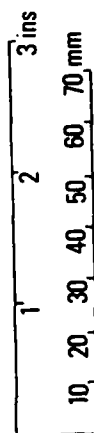
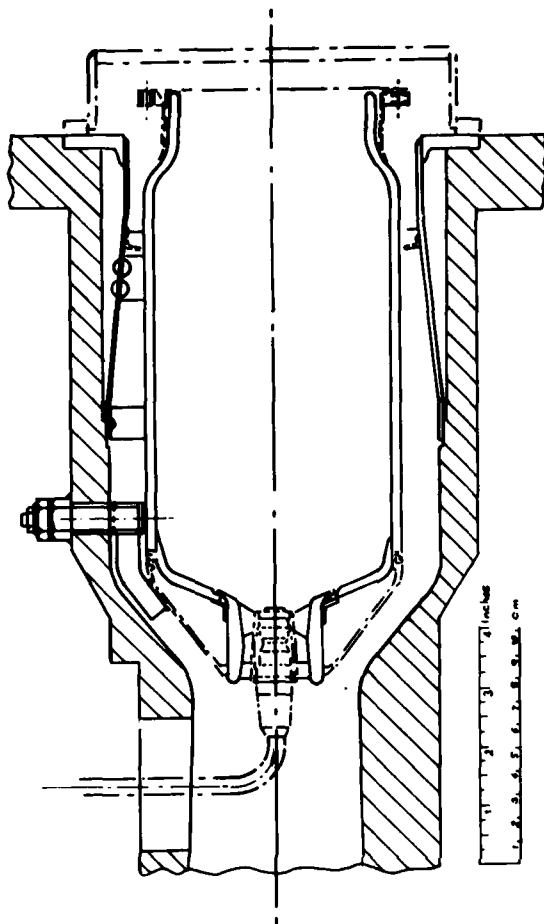


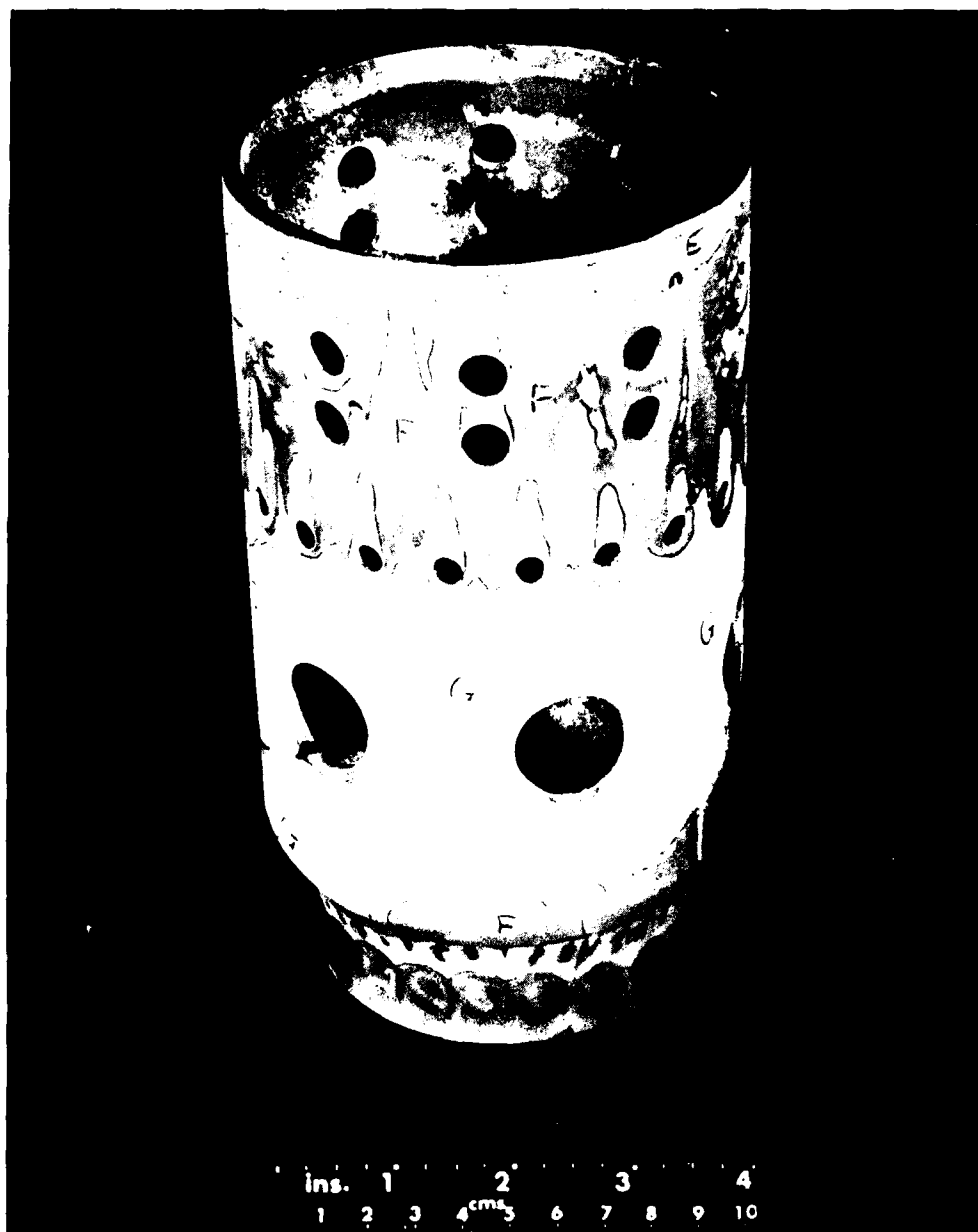
FIG.2b VEE LOCK CONCEPT



**FIG.3 ARRANGEMENT OF COMBUSTION CHAMBER
IN TEST RIG**



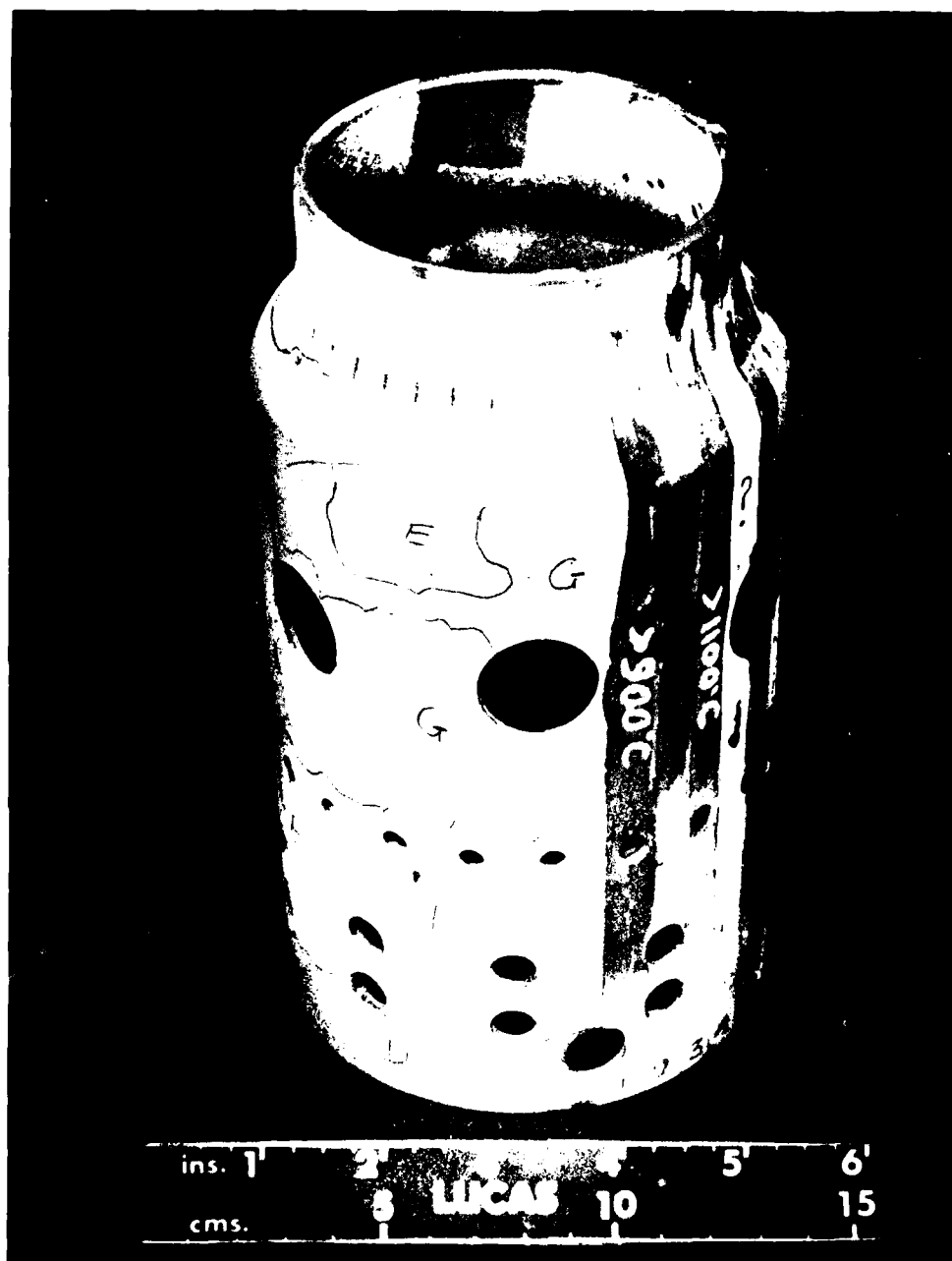
**FIG.4 SILICON CARBIDE FLAME TUBE AFTER TESTING
AT 1473K (2192°F) EXHAUST TEMPERATURE**



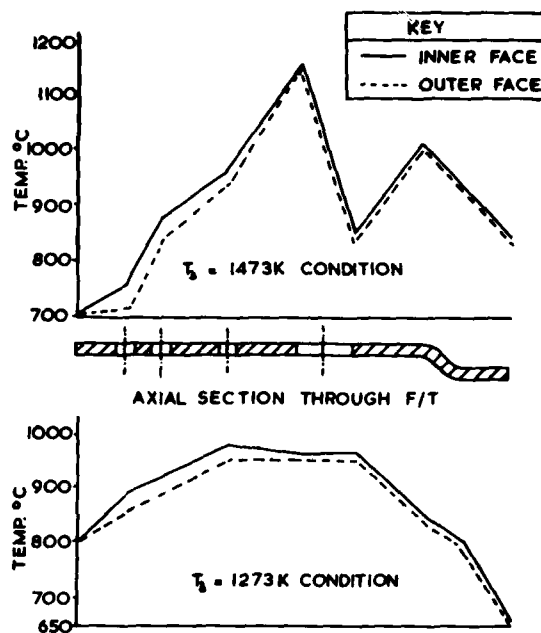
COLOUR CHANGE KEY

D - 580°C (1076°F)
E - 730°C (1346°F)
F - 844°C (1551°F)
G - 890°C (1634°F)

**FIG.5 PAINT TEST AT 1273 K (1832°F)
MEAN EXHAUST TEMPERATURE**



**FIG.6 PAINT TEST AT 1473 K (2192°F)
MEAN EXHAUST TEMPERATURE**

**FIG.7 TEMPERATURE DISTRIBUTIONS**

HOOP AND AXIAL STRESS DISTRIBUTIONS

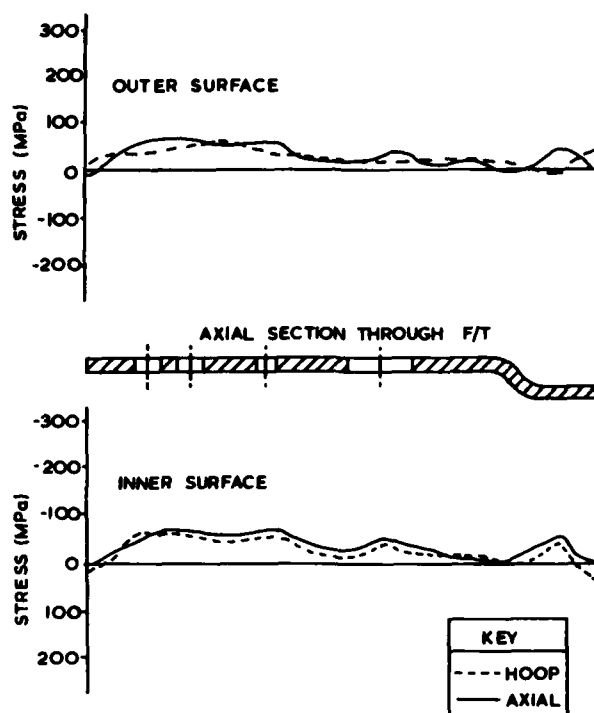


FIG. 8 FOR 1273K EXHAUST TEMPERATURE

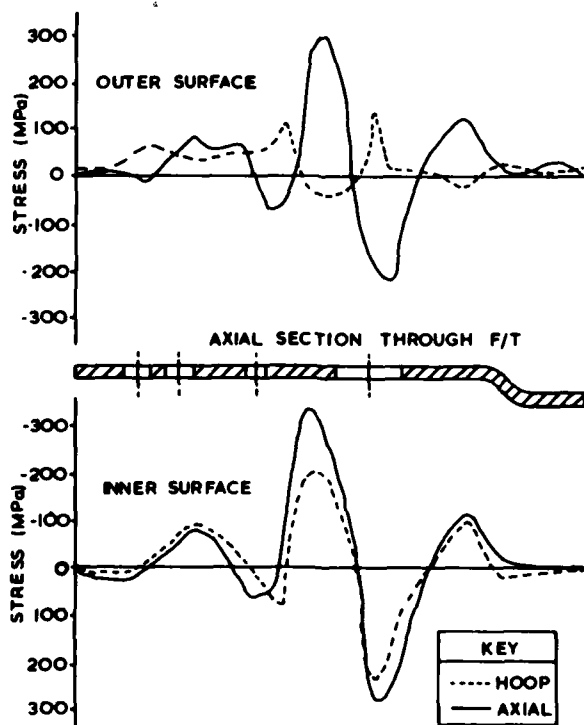


FIG. 9 FOR 1473K EXHAUST TEMPERATURE

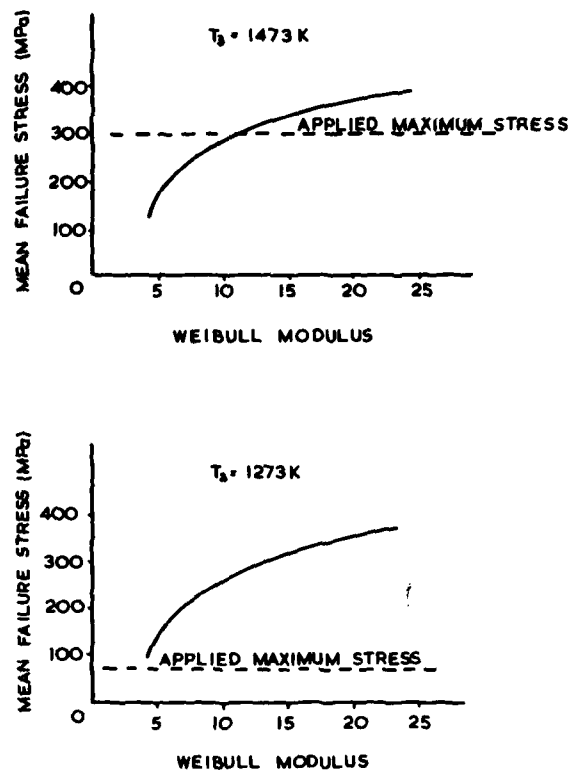


FIG.10 EFFECT OF WEIBULL MODULUS ON MEAN FAILURE STRESS

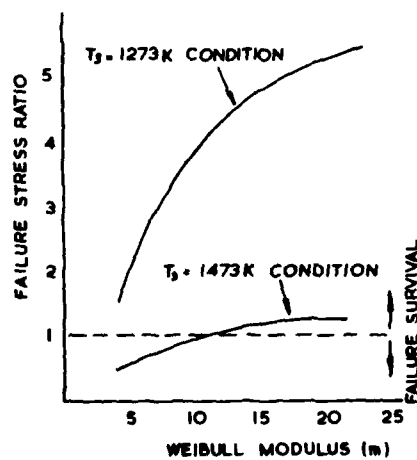


FIG.11 FAILURE STRESS RATIO vs WEIBULL MODULUS

DISCUSSION SUMMARY

SESSION III - NON-ROTATING CERAMIC COMPONENTS

by

K. Trappman
Motoren- und Turbinen-Union
München GmbH
Dachauer Str. 665
8000 Munich 50
W. Germany

The lectures given in Session III represented what may be described as a typical cross-section of worldwide endeavours to use ceramics instead of high-temperature alloys for stationary components in the hot section of gas turbines, i.e. flame tubes, gas ducts and turbine nozzles. The present state of the art is characterized by successful demonstrations of the survival of ceramic components under near-to-actual engine operating conditions, as well as by experimental results that are still not satisfactory and by the effort to learn from initial mistakes and to attain a sufficient probability of survival thanks to optimal component configuration on the basis of precise calculation of the component stresses in operation.

In any case, successes to date cannot be regarded as a breakthrough. The use of ceramic components in production gas turbines, when looked at in detail, is still not conceivable for two reasons:

1. In many cases, the methods of manufacture used so far either have led to components of insufficient strength, or are too wasteful, thus precluding their use for economic series production.

The manufacture of complex-geometrie components of sufficient precision accompanied by acceptable expenditure has until now only been possible when reaction-bonded silicon nitride or silicon carbide have been used. However, reaction-bonded material has only moderate strength, which in many cases has shown a tendency to decrease sharply with time. For this reason, highly-stressed components have until now been made from hot-pressed materials associated with machining with diamond-tipped tools, which can be very elaborate.

2. In view of the present shortage of experience based on relatively short usage periods, the risks involved in the use of ceramics in production turbines are still too great.

Imprecise knowledge of the stresses actually occurring in ceramic components as well as of the actual material properties, which depend on the geometry and time, has led and continues to lead to failures. Whilst it is true that there are sufficiently accurate processes and programmes for calculating component stresses available today, these are often not applied on account of the not inconsiderable expenditure involved. Even determination of the material properties is confronted by high expenditure, and this is all the more so as long as these properties are constantly changing in the wake of material development.

Further intensive development work is necessary in order to overcome the obstacles in the path leading towards a "ceramic" gas turbine, namely:

- The strength properties, especially long-term stability of reaction-bonded materials, must be further improved.
- New processes (sintering, hot isostatic pressing) are being developed for the profitable manufacture of mechanically highly stressed components of complex geometry, and these must be pursued ever more intensively.
- There is still room for considerable improvement in some areas of component design. VW have shown very impressively how stresses in a turbine nozzle can be reduced by a multiple by optimization of the design, based on a conventional model derived from metallic prototypes, provided that manufacturers are prepared to invest in appropriate computer systems (three-dimensional finite element method).

- Materials which come into consideration for use in gas turbines and whose development has reached a satisfactory level should be subjected to comprehensive testing of their properties under all conceivable service conditions. This should include the manufacture and testing under near-to-actual conditions of components, as testing material samples of simple geometry alone does not provide indicators as to how far the strength properties of a material at critical areas of a complex-shape part, bearing an economically acceptable production process in mind, correspond to the strength values measured on simple specimens.

Not least, however, success will also depend on realistic objectives being set for the development work. Here for example the path pioneered by Solar - the stepwise introduction of ceramic components into gas turbine in keeping with the state of the art - would appear to offer the best chances of success.

STATIONARY CERAMIC COMPONENT CONSIDERATIONS
FOR LARGE INDUSTRIAL COMBUSTION TURBINES
by R.J. Bratton and K.L. Rieke

DISCUSSION

A.F. McLean, USA

What particular ceramics are you thinking of for application in the combustion system and do you visualize any corrosion-types problems using coal-derived fuels?

Author's Reply

Ceramic parts in the combustion system are mainly loaded by steady and cyclic thermal stresses, they are not heavily mechanically loaded. We therefore believe that sintered or reaction-bonded material will be used, hot-pressed material should not be needed. We do not believe that we have to limit ourselves to silicon carbide or silicon nitride, other materials in the oxides area should also be investigated for this application. Since contaminants in coal-derived fuels should generally be much lower in concentration than in residual oils - as an example - we would not expect many difficulties concerning corrosion/erosion by burning coal-derived fuels.

Dr. H.M. Burte, USA

What is your experience with respect to reliability of the segmented construction in the MHD-System - time of operation, ability to withstand start and stop conditions?

Author's Reply

The information I got relative to the reliability of the segmented construction was that, using a low-strength ceramic, pieces not larger than 2" x 2" are needed to withstand the thermal stresses, induced by a temperature difference of approx. 2000 °F between the inner and outer flame tube surface.

W.H. Brown, USA

Since the utility industry have been lining their furnaces with fire-bricks for years is there any reason you haven't applied a hot-wall technique to reduce pollution today?

Author's Reply

Up to approx. 5 - 7 years ago pollution was a secondary consideration. Since then it has become more and more an environmental factor and tighter EPA - regulations have to be met, especially in California. It is up to us to find the technical solutions to improve our environment, yet we must have time.

DEVELOPMENT OF CERAMIC NOZZLE SECTION FOR SMALL RADIAL GAS TURBINE
by J.C. Napier and J.P. Arnold

DISCUSSION

Dr. E.M. Leno, USA

1. You showed 3 approaches to reduce the cost of the nozzle vanes for the simple insert concept. What factor of cost reduction are you after?
2. What are your cost estimations for the upgraded concepts?

Author's Reply

1. Our goal for cost reduction is a factor of 10. In actual numbers: We are currently paying \$ 100 per vane and expect - in agreement with four vendors we are working with - to have the cost down to around \$ 10 per vane. Depending on quantity one could expect costs even lower than \$ 10 per vane, for instance for injection-molded and sintered silicon nitride vanes in quantities of 10000.
2. A cost estimate for quantity production of the ceramic parts needed for the upgraded concepts hasn't yet been provided by the vendors.

E.Tiefenbacher, GERMANY

To what extent were surface roughness and strength of the ceramic nozzle material influenced by erosion?

Author's Reply

As could be seen, hot-pressed material did not visually change under the influence of erosion, other materials showed only a minor increase in surface roughness. The effect on material strength has not yet been evaluated.

Jan Mowill, NORWAY

Because of it's poor sulfidation resistance Inco 713 is not considered to be a representative metal alloy for a comparison with ceramics. Did you compare the sulfidation resistance of ceramics with other metals than Inco 713?

Author's Reply

I agree that there are alloys with much better sulfidation resistance than Inco 713. The reason for choosing 713 was that, at the time the comparison was made, the nozzle material actually had been 713. We haven't done any other experiments since then.

A.F.McLean, USA

1. Do you think that the bonded stator shroud arrangement - where the support bolt doesn't go through all three pieces - is a feasible design?
2. Was your mounting scheme the same for RBSC as for RBSN shrouds?
3. Have the vane recesses in the SiC-shrouds been machined by EDM (electro discharge machining)?

Author's Reply

The answer to the 2nd and 3rd questions is "yes". A definite answer to the first question cannot be given because that particular design hasn't been run in an engine yet. We pursue that design especially for economical reasons; it minimizes the number of parts and avoids complications of assembly. Centering of the rear shroud against the turbine wheel will not be a problem; the shroud could either be centered by the vanes, which proved to be accurate enough in our rig experiments, or by radial slots meshing with corresponding studs in the metal casing.

Dr. F.Blake Wallace, USA

You are to be congratulated on the very excellent and encouraging work.

1. What is the maximum-size particle you think you can ingest without an impact fracture?
2. Do you feel that you have an efficiency loss due to stator vane end leakage with the multi-piece configuration?

Author's Reply

1. We haven't put any large particles into the engine; we also didn't have engine-generated particles, such as carbon particles, so we really don't know.
2. We did a performance calibration on the ceramic engine but couldn't find a distinct difference to the all metallic engine which has a brazed, that means end leakage-proof, nozzle assembly. Therefore one might assume that there wasn't any measurable leakage.

DEVELOPMENT OF A CERAMIC TURBINE NOZZLE RING
by H. Burfeindt, M. Langer and P.M. Stuart

DISCUSSION

Dr. E.M.Lenoe, USA

I would like to compliment you and your colleagues on the fine paper. A 6-fold reduction in shroud stresses and approximately 2-fold reduction in trailing edge stresses as a result of stress analysis clearly shows the importance of structural analysis for progress in ceramic engine developments, especially, if compared with the much smaller potential of improvements in materials strength.

To capitalize further on your structural analysis it would be interesting to display the stressed volumes and the locations of the stressed volumes, so that the manufacturer could try to improve the quality, particularly in the highly stressed areas. It would also be interesting to put some confidence limits on calculated stress values by doing a sensitivity analysis on the impact of uncertainties with regard to boundary conditions and materials properties. Those confidence limits could lead to higher survivability levels.

Author's Reply

We don't manufacture ceramic parts, we therefore don't have the opportunity to directly push materials development. Stress calculations as accurate as possible - that means using 3D finite element models for complex shapes - are our contribution to the progress in the ceramic area. Moreover the results of our stress analysis should help the ceramic parts manufacturer to understand what is really needed in terms of material strength in actual ceramic parts, formed to fulfil the operational requirements in a gas-turbine engine. Testing of those parts in an engine-like environment - thereby evaluating their material qualities - is the complementary task to the structural analysis. Material development using just simple probes is not sufficient since many problems connected with the actual shape of a part would not be recognized. We expect to have the first nozzle in the optimized configuration on test at the end of this year.

M. Zippel, GERMANY

Did you calculate the actual local values of the heat-transfer coefficient on the airfoil surface?

Author's Reply

Yes, that has been done.

Dr. H.M. Burte, USA

Have you considered the use of proof testing and if so, how should those tests be carried out?

Author's Reply

We feel that all components should be proof tested prior to engine tests but we haven't fixed the procedure yet.

M. Zippel, GERMANY

Did you vary the divisions of the finite element model or have you used just one division in your calculations?

Author's Reply

(given by Mr. P.M. Stuart)

Yes, we looked at different divisions. The division chosen for the first model and shown in Fig. 6 turned out to be of sufficient refinement. More refined models showed the same trends but in more detail.

DEVELOPMENT OF COMBUSTORS OF CERAMIC MATERIAL by G. Kappler, G. Langel and L. Schindhelm

DISCUSSION

Dr. H.M. Burte, USA

Did you make a conical combustor from silicon nitride in order to get a comparison between silicon nitride and silicon carbide as flame tube materials?

Author's Reply

No, we had conical combustors only made from silicon carbide.

A.F. McLean, USA

What are the influences of the conical combustor design on combustion stability, weak and rich extinction limits, and also on emissions?

Author's Reply

Combustion stability could be improved by the conical shape. The combustor is very easy to start; we don't have any thermal shock problems which usually arise in cylindrical flame tubes because of the large primary zone volume and which can easily lead to failures due to high temperature gradients in the flame tube wall. Combustion efficiency was also better compared with the cylindrical combustor, especially at idle condition, where we had an efficiency as high as 97 % compared with 86 % for the cylindrical combustor. CO-emission at idle was correspondingly low, the difference between idle and full power CO-emission being much smaller than usual. NO_x-emission, however, didn't change very much.

P. Popper, UK

I was surprised about the discontinuity in wall temperature exhibited by the combustor made in two parts. How were those parts joined?

Author's Reply

In first tests with a metallic combustor of the same shape we had found high gradients in flame tube wall temperatures between the primary and secondary zones. So we designed a combustor built from two separate pieces, the idea being that by free expansion of each of the two zones high thermal stresses in the flame tube walls could be avoided. However, we learned from tests that cold air which leaked through the sliding interface evidently caused high thermal gradients in each of the adjacent parts, thereby generating cracks.

So, since the aim of the two-piece design was not attained, we went to the one-piece design which, as I have shown, proved to be satisfactory.

Dr. J. Zech, GERMANY

Did you find differences in temperature and stress distribution between the metallic and the ceramic version of a specific combustor design?

Author's Reply

Yes, there are differences; the wall temperature pattern of the ceramic combustor is more even. We have just started stress analysis for the conical combustor on the basis of measured wall temperatures. We expect the stress distribution to be as uniform as the temperature distribution.

SOME EXPERIENCE IN THE DESIGN AND EVALUATION OF CERAMIC COMBUSTION CHAMBERS

by G. Sedgwick

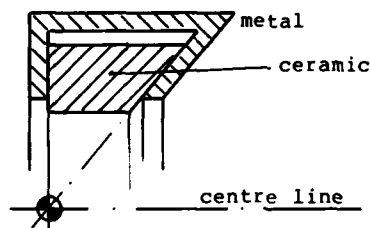
DISCUSSION

Prof. J. Odgers, Canada

How did you take into account the differential expansion between metal and ceramic in your small annular combustion chamber design?

Author's Reply

The principle used for the small annular flame tube was evolved during earlier work at Lucas and is shown in the following sketch.



Under the influence of thermal expansion all points of a rotationally symmetric structure move away from a datum point on the centre line on straight trajectories which run through the datum point. So, if a ceramic ring is encompassed by a metal ring as shown in the sketch contact between ceramic and metal at the sliding interfaces is maintained at all temperatures.

Dr. E.M. Lenoe, USA

Did you calculate the temperatures on the interior flame tube surface from exterior wall temperature measurements by thermal paints and did you use a linear elastic analysis for stress calculation?

Author's Reply

Yes, that is correct.

Dr. E.M. Lenoe, USA

Did you use mean or characteristic strength values for your calculation of failure stress ratio versus Weibull modulus and is it a two-parameter Weibull?

Author's Reply

I apologize for not being able to answer that question in the moment because I haven't done that calculation myself.

Dr. K. Goebels, GERMANY

We have seen a lot of broken parts in this session, but not one of the authors has mentioned a need for non-destructive evaluation (NDE) of parts before they go to tests to keep costs down. Have you done NDE before rig tests.

Author's Reply

Yes, we do NDE on all components before they are rig tested. We use X-rays to identify the porosity and thermal proof tests.

Dr. H.M. Burte, USA

Did you look at the fracture surfaces of broken parts to inquire, whether any discrepancies in the material may have contributed to the failures?

Author's Reply

Fracture analysis of the broken parts has been done by Dr. Godfrey in his laboratory. Therefore I would like to ask Dr. Godfrey to comment on that.

Dr. D.G. Godfrey, UK

We found that the thermal proof test introduces oxidative degradation of the exterior strength of the material which can be seen in the fracture origins. Microstructural analysis has also been done in this work. We sometimes found a remarkable difference between large and small components, even if they were nitrided together.

STATE-OF-THE-ART OF SiAlON MATERIALS

by
 Sunil Dutta
 NASA-Lewis Research Center
 21000 Brookpark Road
 Cleveland, Ohio 44135

SUMMARY

Concurrent with the recent engineering efforts in developing advanced ceramics such as Si_3N_4 and SiC for structural components of high temperature heat engines, "SiAlON" ceramics have also become candidates for consideration. The acronym "SiAlON" was originally given to new compositions derived from silicon nitrides and oxynitrides by simultaneous replacement of silicon and nitrogen by aluminum and oxygen. Other metal atoms M such as Be, Mg, Li, and Ga can be incorporated, and the term has become a generic one applied to Si_3N_4 based materials. In this review, the state-of-the-art of "SiAlONS" is examined. The review includes work on phase relations, crystal structure, synthesis, fabrication, and properties of various SiAlONS. The essential features of compositions, fabrication methods, and microstructure are reviewed. High temperature flexure strength, creep, fracture toughness, oxidation, and thermal shock resistance are discussed. These data are compared to those for some currently produced silicon nitride ceramics to assess the potential of SiAlON materials for use in advanced gas turbine engines.

INTRODUCTION

Materials currently being evaluated for structural components of high temperature heat engines include Si_3N_4 , SiC , and a class of materials called SiAlONS. The term "SiAlON" was adopted to designate any composition containing the elements Si-Al-O-N as major constituents e.g. β' -SiAlON (ref. 1,2,3), O' -SiAlON (ref. 4), 15R -SiAlON (ref. 4) etc. However most frequently, the term SiAlON refers to β - Si_3N_4 solid solution called β' -SiAlON. SiAlON compounds can be made by a high temperature reaction between silicon nitride or oxynitride and alumina in which simultaneous replacement of silicon and nitrogen by aluminum and oxygen occurs. Other metal atoms M such as Be, Mg, Li (ref. 5) and Ga (ref. 6) can also be incorporated and the term has thus become a generic one applied to Si-M-O-N based materials. Among various SiAlON materials, β -SiAlON has been of great interest because it was claimed to have a low thermal expansion (ref. 2,6), good high temperature modulus of rupture and good oxidation resistance (ref. 7). It was also reported that the β' -SiAlON could be fabricated to high density by conventional sintering techniques (ref. 2). These reported properties indicate that β' -SiAlON ceramics might be candidates for high temperature applications, and therefore, have generated considerable interest. In this paper, the state-of-the-art of SiAlON is examined. The paper reviews work on phase equilibria, structure, fabrication and properties. Based on this review, the potential of SiAlON materials for use in advanced gas turbines will be examined.

PHASE EQUILIBRIA AND STRUCTURE

The existence of β' -SiAlON in the system Si_3N_4 - Al_2O_3 was first reported by Oyama and Kamigaito (ref. 1) in Japan and by Jack and Wilson (ref. 2) in England. Subsequent studies by the same workers reported a solid solution (β' -SiAlON) forming region in the systems Si_3N_4 - SiO_2 - Al_2O_3 (ref. 5) and Si_3N_4 - AlN - Al_2O_3 (ref. 3). Detailed compatibility and phase equilibria studies were reported by Gauckler et. al (ref. 8) and Jack (ref. 4) in the system Si_3N_4 - AlN - SiO_2 - Al_2O_3 and their diagrams are shown in Figs. 1 and 2. Jack (ref. 4) refers to his diagram (Fig. 2) as an "Idealized Behavior Diagram" rather than an equilibrium diagram since it combines data obtained from specimens hot pressed at temperatures ranging from 1550 to 2000 C. Most of the data, however, were obtained at 1775 C. On the other hand, the diagram by Gauckler et. al (ref. 8) is an isothermal section at 1760 C (Fig. 1). According to both Jack and Gauckler, the β' -SiAlON region extends from the Si_3N_4 corner in the direction of $\text{AlN}.\text{Al}_2\text{O}_3$ along a line representing a constant metal/non-metal (M/X) ratio of 3:4 and can therefore, be described by the empirical formula $\text{Si}_{6-x}\text{Al}_x\text{O}_x\text{N}_{8-x}$ with $x=0$ to 4.2. In the oxygen rich part of the diagram, mullite and X-phase SiAlON (formula $\text{Si}_4\text{Al}_4\text{O}_{11}\text{N}_2$) were observed. In the AlN-rich part of the system, five new phases were identified (ref. 8) in the region between β' -SiAlON and AlN. The phases called X2, X4, X5, X6, and X7 are shown in Fig. 1 and are located along lines of constant metal: non-metal ratios. These were later identified by Jack (Fig. 2) as AlN polytypes (ref.4). The diagrams proposed by Jack and Gauckler et. al. are quite similar except that the locations of AlN polytypes are slightly different. Work by Layden (ref. 9) established the liquidus isotherms (Fig. 3) in part of the system lying between SiO_2 -rich corner of the diagram and X-phase.

β' -SiAlON has a β -silicon nitride structure which extends along the 3M/4X line but the sizes of the tetrahedra and hence also the unit-cell dimensions, increase as aluminum and oxygen replace silicon and nitrogen (ref. 8). Silicon oxynitride O' -SiAlON

(ref. 4) extends along the 2M/3X (metal/non-metal) line with the $\text{Si}_2\text{N}_2\text{O}$ -type structure and larger unit-cell dimensions. The structure of X-phase, also designated as "Oyama-Phase" (ref. 4) and "J-phase" (ref. 4) has been interpreted in terms of several different unit cells. Drew and Lewis (ref. 10) proposed a triclinic structure, while Gugel (ref. 11) proposed and orthorhombic lattice. Most recently, the unit cell has been determined to be monoclinic (ref. 4).

Single phase β' -SiAlON forming regions in other systems such as Si_3N_4 - Al_2O_3 - Be_2SiO_4 , Si_3N_4 - Al_2O_3 - Li_2O and Si_3N_4 - Al_2O_3 - MgO were reported by Jack (ref. 5), while Oyama (ref. 6) reported a β' -forming region in the system Si_3N_4 - Al_2O_3 - Ga_2O_3 . Extensive ternary solid solutions were found to exist in all of these systems. Detailed phase equilibria in the system Si_3N_4 - SiO_2 - Be_3N_2 - BeO were reported by Huseby et. al (ref. 12) and are shown in Fig. 4. A large solubility of Be_2SiO_4 in β - Si_3N_4 and of BeO in BeSiN_2 was found to occur in this system. The solid solubility of Be_2SiO_4 in β - Si_3N_4 decreases with increasing temperature from 19 mol% at 1770 C to 11.5 mol% Be_2SiO_4 at 1880 C. There are other single-phase materials in this system and all have moderate solubilities along lines of definite metal:non-metal (M/X) ratios and small solubilities perpendicular to these lines.

In the system Si_3N_4 - SiO_2 - AlN - Al_2O_3 - Be_3N_2 - BeO , Gauckler (ref. 13) found that the single-phase solid solution with β - Si_3N_4 structure was restricted to the plane connecting the points Si_3N_4 , Be_2SiO_4 , BeAl_2O_4 and $\text{AlN}:\text{Al}_2\text{O}_3$. This is shown in Fig. 5a. These four points are co-planar in the quaternary diagram. All composition points on this plane have a constant metal to non-metal ratio of 3:4. The plane of 3:4 is shown in Fig. 5b. A large area of single phase region with the β - Si_3N_4 structure is located on this plane. No single-phase solid solution was found either above or below this plane.

In the quasiternary system Si_3N_4 - AlN - Be_3N_2 shown in Fig. 6, Gauckler et. al (ref. 13) found a complete solid solubility exists from AlN to BeSiN_2 . The lattice parameters in this solid solution with a wurtzite structure increase linearly with increasing Al concentration.

FABRICATION

A. Hot Pressing

Hot pressing has been found to be the easiest technique for fabricating theoretically dense, fine-grained bodies with high strength in covalent materials such as Si_3N_4 and SiC . Consequently, most early work on phase equilibria, structure, and property evaluation was conducted on β' -SiAlONs fabricated by hot pressing. Table I lists starting materials for various β' -SiAlON formulations and their hot pressing parameters. In most of the investigations, various material combinations listed in Table I were hot pressed at temperatures where simultaneous chemical reaction and densification were taking place under applied pressure. MgO was commonly used as an additive to promote densification. The most effective hot pressing temperature range was 1650-1750 C. Time at temperature varied in these investigations, but generally ranged from approximately 30 minutes to 2 hours. Heating the compacts was accomplished by induction or resistance heating of graphite or SiC . The reaction of carbon with the compact was minimized by using a BN liner or container.

The experimental studies shown in Table I illustrate the varied nature of investigations in hot pressed β' -SiAlONs. Characterization of the hot pressed materials has included phase equilibria, structure, and chemistry which have been discussed in the preceding sections. Strength, creep, thermal and oxidation behavior will be discussed in following sections.

B. Pressureless Sintering

Pressureless sintering when compared to hot pressing has the advantage of shape capability and high volume production of small as well as large components. The expense of machining prevents hot pressing from being a cost effective process for many applications. As a result, much effort has been devoted to fabrication by pressureless sintering. Table II shows a list of pressureless sintering studies conducted with various material combinations with and without additives. Sintering was conducted at about one atmosphere of nitrogen to produce bodies with densities as high as 98% theoretical. The most effective sintering temperature regime and time period were 1700-1760 C for 2 - 4 hours respectively, although a much broader range of temperature and time was used by different investigators.

Jack (ref. 2) reported that a Si_3N_4 and Al_2O_3 mixture could be fabricated to dense single phase β' -SiAlON bodies by pressureless sintering. However, other work (ref. 11) indicated that the resulting SiAlON contained other phases. Morgan (ref. 24) predicted in a presentation cited by Layden (ref. 9) that single phase β' -SiAlON compositions having stoichiometries given by the formula $\text{Si}_{3-x}\text{Al}_x\text{O}_x\text{N}_{4-x}$ would not sinter. Layden (ref. 9) also reported that as a pure phase β' -SiAlON could not be sintered to high final density. However, β' bodies formulated from starting materials that form some liquid at the sintering temperatures could be sintered to high density. For example, Layden introduced the term "transient liquid phase sintering" or TLP. In

this process, SiAlON bodies of composition $\text{Si}_{1.4}\text{Al}_{1.6}\text{O}_{1.6}\text{N}_{2.4}$ were formulated from two prereacted compositions, one of which was X phase which melts in the neighborhood of 1700 C. The second composition was calculated from the lever rule to yield single phase β' -SiAlON when reacted with a predetermined amount of the X-phase at temperatures above 1700 C. The "transient liquid phase sintering" was confirmed by Gauckler et. al (ref. 25) during sintering of β' -SiAlON compositions utilizing as starting materials only AlN and SiO_2 and no additives. Gauckler et. al concluded that different sintering kinetics would be expected for different sets of starting materials e.g. Si_3N_4 , AlN, SiO_2 powders or Si_3N_4 , AlN, Al_2O_3 powders or SiO_2 and AlN powders because of different reaction mechanisms (ref. 25). The formation of liquid facilitates densification and chemical reaction. Drew and Lewis (ref. 10) also observed the formation of liquid phase during sintering of Si_3N_4 and Al_2O_3 mixtures.

Recently, Arias (ref. 26) determined the effect of oxygen to nitrogen ratio (O/N) on the pressureless sinterability of SiAlONs of formula $\text{Si}_{2.55}\text{Al}_{0.6}\text{O}_y\text{N}_{4-0.667y}$ (where y varied from 0.57 to 1.92). Utilizing starting materials Si_3N_4 , AlN, and SiO_2 plus a small amount of Al_2O_3 from the grinding media but no additive, a maximum density of about 98% of theoretical occurred in the O/N ratio range between 0.2 and 0.3. It is very likely, that liquid formed in various phase fields according to the behavior diagram shown in Fig. 2 and promoted densification in all compositions as y varied from 0.57 to 1.92.

In contrast to sintering by forming liquid within the system itself, additives which provide a liquid phase at the sintering temperatures are commonly used for densifying Si_3N_4 based ceramics. For example, Fig. 7 shows typical densification behavior of β' -SiAlON ($\text{Si}_{2.4}\text{Al}_{0.8}\text{O}_{0.6}\text{N}_{3.6}$) as a function of temperature (ref. 31). The starting materials used were Si_3N_4 , AlN, and Al_2O_3 with 6 and 3 mol% of additives (Y_2O_3 - SiO_2). The Y_2O_3 to SiO_2 molar ratio was constant at 1:2. Sintering was promoted by a liquid formed by an initial reaction between Y_2O_3 , SiO_2 and Al_2O_3 . In any case whether a liquid formed by the foreign additives or during sintering of bodies formulated with major constituents such that some liquid is formed at the sintering temperature, a grain boundary glassy phase is retained in the sintered body. It will be seen later that this glassy phase has a controlling influence on the high temperature properties of the sintered body (ref.9).

DENSITY AND MICROSTRUCTURE

β' -SiAlON compositions have been fabricated to essentially theoretical density by hot pressing, while pressureless sintering has resulted in maximum densities close to 98% of theoretical, (ref. 30, 31). The density values of hot pressed β' -SiAlONs have varied from 3.09 to 3.16 g/cc (ref. 17) depending on the location along the β' -homogeneity line (Fig. 2,3). The density of other phases has been found to be 3.05 g/cc for X-phase (ref. 18) and 3.08 g/cc for 15R polytype phase (ref. 18).

In general, the microstructures of both hot pressed and sintered materials consisted of β' -SiAlON as the predominant phase with some isolated porosity and metallic looking phase in a uniform β' matrix. In some cases isolated grains of X-phase and 15R polytype phases were also identified (ref. 10). Typical grain sizes of the hot pressed compositions were found to vary between 0.2 - 2 μm (ref. 10) while the grain size range 0.15 - 5.0 μm was observed in pressureless sintered compositions (ref. 31). The grain morphology in both sintered and hot pressed materials was characteristic of the presence of a liquid phase during densification. This liquid phase was retained in inter-crystalline spaces during cooling from the hot pressing (ref. 19) or sintering temperature (ref. 31) and formed a glassy phase at the grain boundaries.

PROPERTIES

Most of the mechanical properties reported in the literature are for β' -SiAlON in the system Si - Al - O - N, while other systems e.g. Si, Be/N, O; Si, Al Be/N, O etc., have been examined primarily with respect to solid solubility, phase relationships, and structure. Because of their similar structures, the physical and mechanical properties of β' -SiAlON and β' - Si_3N_4 are also similar. In this review, the properties of various β' -SiAlON compositions in the system Si-Al-O-N are discussed.

Modulus of Rupture

Arrol (ref. 7) reported the room temperature modulus of rupture (3-point MOR) of a hot pressed β' -SiAlON to be as high as 825 MPa. He also reported the strength of sintered β' -SiAlON to be 330 MPa. The compositions or formulations of neither material were defined. Other workers have reported the MOR of hot pressed and sintered β' -SiAlONs where the formulations or compositions are defined to varying degrees. These are summarized in Table III. In Table III, average values at room temperature and at 1370 C are given for various β' -SiAlONs made from different starting materials. The highest room temperature strength of hot pressed β' -SiAlON bodies was found to be 648 MPa (ref. 17), while the highest strength obtained in pressureless sintered bodies was 483 MPa (ref. 31). At 1370 C, the highest MOR for sintered materials was 375 MPa (ref. 29). Only one value 240 (ref. 18) MPa is listed for a hot pressed β' -SiAlON at 1370 C.

Where data are available over a range of temperatures, the strength of sintered β' -SiAlONs is compared with the strength of silicon nitride currently produced in USA. This is shown in Fig. 8. As can be seen, the room temperature strength of sintered β' -SiAlON compares favorably with room temperature strength of sintered Si_3N_4 . On the other hand, the room temperature strengths of sintered β' -SiAlON are considerably lower than the room temperature strength of hot pressed Si_3N_4 (NC-132).

At high temperature (1370 C), the strength of sintered β' -SiAlON is equivalent to or higher than the strength of sintered Si_3N_4 but lower than the strength of hot pressed Si_3N_4 (NC-132).

The room temperature strength is controlled by residual porosity, surface flaws, foreign inclusions etc., in the body, while the high temperature strength is controlled by the grain boundary phases retained in the body during cooling from the sintering temperature. The grain boundary phase softens at high temperatures thus leading to slow crack growth and subsequent loss in strength. Fig. 9 shows an example of such typical slow crack growth failure (V-shaped area) in the fracture surfaces of a 1380 C MOR bar of β' -SiAlON sintered with 6 mol% ($\text{Y}_2\text{O}_3 - \text{SiO}_2$) additive. Since the intended use of SiAlON has largely been for high temperature, high performance applications similar to those being attempted with Si_3N_4 and SiC, improvement in strength at high temperature is desirable.

Creep

Limited creep data are available on β' -SiAlONs as compared with modulus of rupture data. Arrol (ref. 7) determined the creep behavior of several hot pressed SiAlONs, and compared the data with hot pressed Si_3N_4 (HS-110) and (HS-130), hot pressed SiC and reaction bonded Si_3N_4 . These are shown in Fig. 10. As can be seen, creep in the SiAlONs can vary depending on composition from a high value similar to that of HS-110 to a value as low as that of hot pressed SiC. Lumby et. al (ref. 33) compared the creep data of a pressureless sintered SiAlON with the data for various silicon based ceramics which are shown in Fig. 11. The sintered SiAlON has a creep rate lower than that of hot pressed Si_3N_4 (HS-130), reaction bonded Si_3N_4 or Refel SiC but slightly higher than that of hot pressed SiC. Lumby further observed a strong dependence of creep behavior on AlN concentration. Creep after 20 hours at 1227 C and 77 MN/m² decreased from 0.275% strain for a β' -SiAlON composition contained 7.75 wt% AlN down to 0.06% strain for a composition which contained 11.25% AlN (ref. 17).

According to Layden (ref. 9), three point flexural creep tests in argon of TLP sintered SiAlON gave a steady state creep rate of $3.1 \times 10^{-4} \text{ hr}^{-1}$ at a stress level of 82 MN/m² at 1400 C. This value was below the compressional creep rate of hot pressed Si_3N_4 under these conditions which has been reported (ref. 36) to be $5.4 \times 10^{-4} \text{ hr}^{-1}$. Layden also determined that the creep rate of the Y_2O_3 containing β' -SiAlON bodies was about $6 \times 10^{-5} \text{ hr}^{-1}$ at 1370 C and a stress level of 69 MN/m² which was comparable to that of commercial hot pressed Si_3N_4 (HS-130) at the same stress and temperature. He observed that creep behavior was controlled by the properties of the grain boundary phases. For example, β' -SiAlON compositions containing ZrO_2 additives exhibited slow crack growth during testing due to rapid flow of the grain boundary phases at stresses as low as 69 MN/m² at 1370 C. On the other hand, β' -SiAlON containing Y_2O_3 exhibited higher refractoriness of the grain boundary phases. Therefore, no slow crack growth occurred during testing to 345 MN/m² at 1370 C and the specimens failed by fast fracture.

Fracture Toughness

Fracture toughness (K_{IC}) values reported in the literature for various SiAlON compositions are listed in Table IV. Generally, the values are lower than those of hot pressed Si_3N_4 . For example, Wills et. al (ref. 37) found the fracture toughness values varying between 1.32 and 2.65 MN/m^{-3/2} as compared with 6 MN/m^{-3/2} for (HS-130) hot pressed Si_3N_4 . Wills also suggested that the presence of X - phase should be kept at very low levels and preferably be eliminated completely to improve the fracture toughness in SiAlONs. Similarly, Gauckler et. al (ref. 18) reported lower fracture toughness values (Table IV). However, Lumby et. al (ref. 33) observed a high fracture toughness value (6.0 MN/m^{-3/2}) for a pressureless sintered SiAlON similar to (HS-130) hot pressed Si_3N_4 as well as hot pressed SiAlON, measured by the same technique (ref. 33). He also determined the variation of fracture toughness with temperature for both hot pressed and sintered SiAlONs which is shown in Fig. 12. Lumby suggested that the increase in fracture toughness at higher temperatures was associated with the viscous deformation of the grain boundary phase. The variation in K_{IC} values shown in Table IV could probably be attributed to variation with SiAlON composition and fabrication techniques as well as variation with the fracture toughness measuring technique.

Oxidation

Oxidation resistance is one of the key properties that must be satisfied by a material in order to be candidate for high temperature applications. Jack (ref. 2) and Arrol (ref. 7) reported that the oxidation resistance of β' -SiAlONs is better than that of hot pressed Si_3N_4 (HS-130). Layden (ref. 9) later confirmed this in his evaluation of oxidation behavior of TLP sintered SiAlON compositions. He observed that the oxidation rate of TLP $\text{Si}_{1.4}\text{Al}_{1.6}\text{O}_{1.6}\text{N}_{2.4}$ was an order of magnitude less than that of (HS-130) hot pressed Si_3N_4 at 1400 C (ref. 38). Layden (ref. 29) also made an ex-

tensive study on the oxidation behavior of β' -SiAlON compositions pressureless sintered with various additives such as CeO_2 , Y_2O_3 , ZrO_2 , Y_2O_3 - ZrO_2 . These are shown in parabolic plots in Fig. 13 (ref. 29, 39). CeO_2 doped material had the highest weight gain while TLP material (without any additive) had the lowest weight gain followed by ZrO_2 doped SiAlON (Fig. 13). Both TLP and ZrO_2 doped SiAlONS had much higher oxidation resistance than that of hot pressed Si_3N_4 (HS-130). Similarly, Dutta (ref. 31) and Arias (ref. 30) reported a higher oxidation resistance in β' -SiAlONS doped with Y_2O_3 - SiO_2 and Y_2O_3 respectively, as compared with HS-130. Very recently, Arias (ref. 32) determined the oxidation resistance of SiAlON-C ($\text{Si}_{2.55}\text{Al}_{0.60}\text{O}_{0.72}\text{N}_{3.52}$) to be even higher than that of TLP and ZrO_2 doped SiAlONS. This is shown in Fig. 14. The oxidation behavior of several SiAlONS is compared with those of hot pressed silicon nitride (HS-130) produced commercially. All the sintered SiAlONS showed better oxidation resistance than hot pressed HS-130. This hot pressed Si_3N_4 had the highest weight gain, while SiAlON - C (ref. 32) had the lowest weight gain followed by TLP SiAlON (ref. 9). The oxidation rate constant for SiAlON - C is $2.5 \times 10^{-10} \text{ g}^2/\text{cm}^4 \text{ hr}^{-1}$ as compared with $2.67 \times 10^{-8} \text{ g}^2/\text{cm}^4 \text{ hr}^{-1}$ for hot pressed Si_3N_4 and $1.96 \times 10^{-9} \text{ g}^2/\text{cm}^4 \text{ hr}^{-1}$ for TLP SiAlON, indicating that SiAlON compositions can be produced with excellent oxidation resistance as compared with this hot pressed Si_3N_4 . However, these sintered SiAlONS such as SiAlON - C and TLP SiAlON have poor room temperature strength as compared with hot pressed Si_3N_4 . For these materials to be accepted for turbine applications, further composition development is necessary to combine good oxidation behavior and good mechanical properties.

Thermal Expansion

Jack (ref. 2) reported the linear thermal coefficient of expansion of β' -SiAlON ($\text{Si}_3\text{Al}_{2.67}\text{O}_4\text{N}_4$) to be $2.7 \times 10^{-6} \text{ C}^{-1}$ which was less than that of β - Si_3N_4 ($3.5 \times 10^{-6} \text{ C}^{-1}$). On the other hand, Gauckler et. al (ref. 18) reported an average value of $3.4 \times 10^{-6} \text{ C}^{-1}$ which was in good agreement with the value for pure β - Si_3N_4 . Gauckler observed an almost linear decrease of the thermal expansion coefficient with increasing Al concentration for the $\text{Si}_{6-x}\text{Al}_x\text{O}_x\text{N}_{8-x}$ SiAlON which is shown in Fig. 15.

Wills et. al (ref. 37) reported linear thermal expansion of three sintered SiAlON compositions. The expansion of the two compositions $\text{Si}_{4.94}\text{Al}_{1.06}\text{O}_{1.06}\text{N}_{6.94}$ and $\text{Si}_4\text{Al}_2\text{O}_2\text{N}_6$ was identical ($3 \times 10^{-6} \text{ C}^{-1}$) but the third composition $\beta' + \text{X}$ showed greater expansion ($3.3 \times 10^{-6} \text{ C}^{-1}$) because of X - phase (ref. 37). However, collective data clearly indicated that the thermal expansion coefficients of β' -SiAlON compositions and of β - Si_3N_4 are quite similar.

Thermal Shock

Water quench thermal shock resistance (ΔT_C^*) of several SiAlONS determined by various investigators are listed in Table V along with data for other silicon based ceramics for comparison. The collective ΔT_C values for β' -SiAlONS are comparable to those of various silicon carbide ceramics and reaction bonded silicon nitride. However, the values are considerably lower than that of hot pressed silicon nitride (Table V). Gauckler suggested that the poor thermal shock behavior of the β' -SiAlON despite its lower coefficient of thermal expansion was caused by the low thermal conductivity and poor fracture toughness of the material.

CONCLUDING REMARKS

The present review has shown that since the discovery of SiAlONS, a number of investigations have been made of their phase equilibria, structure, fabrication and properties. SiAlONS can be prepared by several chemical routes. Fully dense bodies can be produced by hot pressing, while a final density ~98% of theoretical can be achieved by pressureless sintering. Both room temperature and high temperature strengths of sintered β' -SiAlONS are equivalent to or higher than the strengths of sintered silicon nitrides but lower than the strength of hot pressed silicon nitride (NC-132). On the other hand, many SiAlON compositions have higher oxidation resistance than those of hot pressed silicon nitrides, and therefore, have a better chance of longer survival in an oxidizing environment. However, the most significant lack in the current state of the art of SiAlON is that no SiAlON composition has yet been developed which exhibits good low temperature strength as well as good oxidation resistance. Indeed some of the SiAlONS that have exhibited the best oxidation resistance have also had low strength at high temperature. Only a few of the SiAlONS identified to date hold promise for high temperature use in gas turbines. Because of their low strength at lower temperature, it is not likely that sintered SiAlONS nor sintered silicon nitride will be used for integrally bladed turbine wheels. Such wheels are highly stressed in the lower temperature region of the hub. To date hot pressed Si_3N_4 has been the favored material. However, SiAlON materials have the advantage of pressureless sintering to high density and thereby have the potential for providing low cost net shape components to intricate geometry without expensive machining.

* ΔT_C - critical quenching-temperature difference required to initiate thermal stress fracture (see ref. 41 for more detailed explanation).

At present, a more likely use for sintered SiAlONs in the turbine is for stator vanes which run hotter, and at lower stresses than turbine blades or disks. For those SiAlONs that have potential for use in gas turbines, much work remains to be done to characterize them in the depth required for such an application.

It is to be hoped that improvement in mechanical properties can be achieved in combination with good oxidation resistance by choosing proper chemical formulations. Work to date indicates that such a combination can be best achieved at low Al_2O_3 concentrations. However, to select an optimum composition, a clear understanding of the phase equilibria of the particular system is essential.

REFERENCES

1. Y. Oyama and O. Kamigaito, "Solid Solubility of Some Oxides in Si_3N_4 ," Jap. J. Appl. Phys., 10, 1971, p. 1637.
2. K. H. Jack and W. I. Wilson, "Ceramics Based on the Si-Al-O-N Related Systems," Nature Phys. Sci., 238, 1972, pp. 28-29.
3. Y. Oyama, Solid Solution in the Ternary System, Si_3N_4 -AlN- Al_2O_3 ," Jap. J. Appl. Phys., 11, 1972, pp. 750-751.
4. K. H. Jack, "SiAlONs and Related Nitrogen Ceramics," J. Mat. Sci., 11, 1976, pp. 1135-1158.
5. K. H. Jack, "Nitrogen Ceramics," Trans. J. Brit. Ceram. Soc., 72, 1973, pp. 376-384.
6. Y. Oyama, "Solid Solution in the System Si_3N_4 - Ga_2O_3 - Al_2O_3 ," Jap. J. Appl. Phys., 12, 1973, pp. 500-508.
7. W. J. Arrol, "The SiAlONs - Properties and Fabrication," Ceramics for High Performance Applications, Edited by J. J. Burke, A. E. Gorum, and R. N. Katz, Chestnut Hill, Mass., Brook Hill Publishing Co., 1974, pp. 729-738.
8. L. J. Gauckler, H. L. Lukas, and G. Petzow, "Contribution to the Phase Diagram Si_3N_4 -AlN- Al_2O_3 - SiO_2 ," J. Amer. Cer. Soc., 58, 1975, pp. 346-347.
9. G. K. Layden, "Pressureless Sintering of SiAlON Gas Turbine Components," East Hartford, Conn., United Technologies Research Center, 1977. Warminster, Pa., Naval Air Development Center, NADC-75207-30, 1979.
10. P. Drew and M. H. Lewis, "The Microstructures of Silicon Nitride/Alumina Ceramics," J. Mat. Sci., 9, 1974, pp. 1833-1838.
11. E. Gugel, I. Petzenhauser, and A. Fickel, "X-Ray Investigation of the System Si_3N_4 - Al_2O_3 ," Powder Metall. Int., 7, 1975, pp. 66-67.
12. I. C. Huseby, H. L. Lukas, and G. Petzow, "Phase Equilibria in the System Si_3N_4 - SiO_2 -BeO- Be_3N_2 ," J. Amer. Cer. Soc., 58, 1975, pp. 377-380. (1975)
13. L. J. Gauckler and G. Petzow, "Representation of Multicomponent Silicon Nitride Based Systems," Nitrogen Ceramics, Edited by F. L. Riley, NATO Advanced Study Institute, Noordhoff, Leyden, The Netherlands, 1976, pp. 41-62.
14. Y. Oyama and O. Kamigaito, "Hot Pressing of Si_3N_4 - Al_2O_3 ," Yogyo-Kyokai-Shi, 80, 1972, pp. 327-336.
15. F. F. Lange, Fabrication and Properties of Silicon Compounds, Task 1, Fabrication, Microstructure and Selected Properties of SiAlON Compositions, Pittsburgh, Pa., Westinghouse Research Labs., 1974, pp. 1-23.
16. W. B. Crandall, A. Z. Hed, L. E. Shipley, "Preparation and Evaluation of SiAlON," Wright-Patterson AFB, Ohio, Aerospace Research Labs., ARL-TR-74-99, 1973.
17. R. J. Lumby, B. North and A. J. Taylor, "Chemistry and Creep of SiAlONs," Special Ceramics, Vol 6, Edited by P. Popper, Manchester, England, British Ceramic Research Assoc., 1975, pp. 283-298.
18. L. J. Gauckler, S. Prietzel, G. Bodemer, and G. Petzow, "Some Properties of $(\text{Si}_{16-x}\text{Al}_x\text{O}_x\text{N}_{8-x})$," Nitrogen Ceramics, Edited by F. L. Riley, NATO Advanced Study Institute, Noordhoff, Leyden, The Netherlands, 1977, pp. 529-538.
19. M. H. Lewis, B. D. Powell, P. Drew, R. J. Lumby, B. North, and A. J. Taylor, "The Formation of Single-Phase Si-Al-O-N Ceramics," J. Mat. Sci., 12, 1977, pp. 61-74.
20. H. C. Yeh and W. J. Waters, "Effects of Pressure and Temperature on Hot Pressing a SiAlON," NASA TM-78945, 1977.

21. P. L. Land and S. Holmquist, "Evaluation of β -SiAlON for Radome Application," Wright-Patterson AFB, Ohio, Air Force Materials Lab., AFML-TR-78-79, 1978.
22. W. M. Phillips and Y. S. Kuo, "SiAlONs as High Temperature Insulators," Pasadena, Calif., Jet Propulsion Lab., MPL-Publ-78-103, 1978.
23. H. C. Yeh, W. A. Sanders and J. L. Fiyalko-Liettnner, "Pressure Sintering of Si_3N_4 - Al_2O_3 (SiAlON)," Amer. Ceram. Soc. Bull., 56, 1977, pp. 189-193.
24. P. E. D. Morgan, "Amorphous Silicon Nitride and a Classification of SiAlON," Amer. Ceram. Soc. Bull. 53, 1974, Abstract 4-S2-74, p. 392.
25. L. J. Gauckler, S. Boskovic, I. K. Naik, and T. Y. Tien, "Liquid Phase Sintering of β - Si_3N_4 Solid Solutions Containing Alumina," Ceramics for High Performance Applications-II, Edited by J. J. Burke, E. N. Lenoe, R. N. Katz, Chestnut Hill, Mass., Brook Hill Publ. Co., 1978, pp. 559-571.
26. A. Arias, "Effect of Oxygen to Nitrogen Ratio on the Sinterability of SiAlONs," NASA TP-1382, 1979.
27. A. Gatti and M. J. Noone, "Methods of Fabricating Materials," Wright-Patterson AFB, Ohio, Air Force Materials Lab., AFML-TR-77-135, 1977.
28. R. R. Wills, R. W. Stewart and J. M. Wimmer, "Fabrication of Reaction-Sintered SiAlON," J. Am. Ceram. Soc., 60, 1977, pp. 64-67.
29. G. K. Layden, "Development of SiAlON Materials," NASA CR-135290, 1977, East Hartford, CT, United Technologies Research Center, R77-912184-21, 1977. NASA CR-135290, 1977.
30. A. Arias, "Pressureless Sintered SiAlONs with Low Amounts of Sintering Aid," NASA TP-1246, 1978.
31. S. Dutta, "Pressureless Sintered β - Si_3N_4 Solid Solution: Fabrication, Microstructure and Strength, NASA TM-78950, 1977.
32. A. Arias, "Modulus of Rupture and Oxidation Resistance of a $\text{Si}_{2.55}\text{Al}_{0.6}\text{O}_{0.72}\text{N}_{3.52}$ SiAlON," NASA TP-1490 1979.
33. R. J. Lumby, B. North and A. J. Taylor, "Properties of Sintered SiAlONs and Some Applications in Metal Handling and Cutting," Ceramics for High Performance Applications-II, Edited by J. J. Burke, E. N. Lenoe, and R. N. Katz, Chestnut Hill, Mass., Book Hill Publishing Company, 1978, pp. 893-906.
34. D. C. Larsen and G. C. Walther, "Property Screening and Evaluation of Ceramic Turbine Engine Materials," Chicago, Ill., IIT Research Inst., IITRI-D6114-ITR-36, (Interim Tech. Report No. 6), July 1978.
35. S. Dutta, "Microstructure and Property Characterization of Sintered Si_3N_4 , SiC and SiAlON," Ceram. Soc. Bull. 58, 1979, Abstract 102-B-79, p. 348.
36. M. S. Seltzer, "High Temperature Creep of Ceramics", Wright-Patterson AFB, Ohio, Air Force Materials Lab., AFML-TR-76-97, 1976. (AD-A031766)
37. R. R. Wills, R. W. Stewart, and J. M. Wimmer, "Effect of Composition and X-phase on the Intrinsic Properties of Reaction-Sintered SiAlON," Am. Ceram. Soc. Bull. 56, 1977, pp. 194-198.
38. W. C. Tripp and H. C. Graham, "Oxidation of Si_3N_4 in the Range 1300 to 1500 C," J. Am. Ceram. Soc., 59, 1976, pp. 399-403.
39. R. L. Ashbrook, "Improved Performance of Silicon Nitride-Based High Temperature Ceramics," NASA TM 73719, 1977.
40. C. C. Seaton, "Thermal and Acoustic Fatigue of Ceramics and Their Evaluation," Watertown, Mass., Army Materials and Mechanics Research Center, AMMKC-MS-74-7, 1974. (AD-785547)
41. D. P. H. Hasselman, "Unified Theory of Thermal Shock Fracture Initiation and Crack Propagation in Brittle Ceramics," J. Am. Ceram. Soc. 52, 1969, pp. 600-604.

Acknowledgments

The author would like to thank Dr. Richard L. Ashbrook for many helpful discussions and suggestions in preparing this manuscript.

TABLE I. - FABRICATION OF SIALONS BY HOT PRESSING

Starting materials	Additives	Temperature, C	Time, min	Pressure, MN/m ²	Nature of investigation	Reference
Si ₃ N ₄ , Al ₂ O ₃ , Li ₂ CO ₃	(a)	1750	20	29	Solid solubility	1
Si ₃ N ₄ , Al ₂ O ₃		1700	60	(a)	Formation, structure and thermal expansion	2
Si ₃ N ₄ , AlN, Al ₂ O ₃		1730	30	25	Solid solubility	3
Si ₃ N ₄ , Ga ₂ O ₃ , Al ₂ O ₃		1730-1800	20-180	25	Solid solubility and thermal expansion	5
Si ₃ N ₄ , Al ₂ O ₃ , AlN, SiO ₂		1760	60-300	30	Phase equilibria and compatibility relation	7
Si ₃ N ₄ , AlN, Al ₂ O ₃ , SiO ₂ , Si ₂ N ₂ O		1500-2000	(a)	(a)	Phase equilibria, compatibility and structure	8
Si ₃ N ₄ , Al ₂ O ₃		1700	60	15	Microstructure and phase analysis	10
Si ₃ N ₄ , Al ₂ O ₃		1700	30	(a)	Phase analysis	11
Si ₃ N ₄ , Be ₃ N ₂ , BeO, SiO ₂		1765-1880	60-120	28	Phase equilibria	12
Si ₃ N ₄ , Al ₂ O ₃		1650-1850	6-60	25	Sintering, grain growth and phase equilibria	14
Si ₃ N ₄ , Al ₂ O ₃	MgO	1750-1850	30-240	28	Fabrication, modulus of rupture and thermal properties	15
Si ₃ N ₄ , Al ₂ O ₃	Si, Al, MgO, AlN, SiO ₂ , Kaolin	1500-2000	1-1440	28	Processing and properties	16
Si ₃ N ₄ , AlN, SiO ₂	MgO	1750	60	20	Fabrication, chemistry and creep	17
Si ₃ N ₄ , Al ₂ O ₃ , AlN, SiO ₂	MgO	1760	(a)	(a)	Physical, mechanical and thermal properties	18
Si ₃ N ₄ , AlN, SiO ₂	MgO	1800	60	15	Formation, microstructure characterization	19
Si ₃ N ₄ , Al ₂ O ₃	(a)	1500-1700	120	5.5-27.5	Effects of pressure and temperature on sintering	20
Si ₃ N ₄ , AlN, Al ₂ O ₃	(a)	1600-1800	5-60	3.5-22	Modulus of rupture, dielectric properties and rain erosion	21
Si ₃ N ₄ , AlN, Al ₂ O ₃	MgO	1700-1870	30-120	13.8-34.5	Electrical resistivity and compatibility with W and Mo	22
Si ₃ N ₄ , Al ₂ O ₃	(a)	1200-1700	120	27.6	Hot pressing and microstructure characterization	23

*Not reported.

TABLE II. - FABRICATION OF SIALONS BY PRESSURELESS SINTERING

Starting materials	Additives	Temperature, C	Time, min	Nature of investigation	Reference
$\text{Si}_3\text{N}_4, \text{Al}_2\text{O}_3$	(a)	1700	60	Fabrication (slip casting) and sintering	2
$\text{Si}_3\text{N}_4, \text{Al}_2\text{O}_3$		1600-1850	15-720	Fabrication, modulus of rupture, creep, impact oxidation	9
$\text{Si}_3\text{N}_4, \text{Al}_2\text{O}_3$		1400-1800	60	Microstructure analysis	10
$\text{Si}_3\text{N}_4, \text{Al}_2\text{O}_3$		(a)	(a)	Phase analysis	11
$\text{Si}_3\text{N}_4, \text{AlN}, \text{Al}_2\text{O}_3$		1400-2000	0-180	Liquid phase sintering	25
$\text{Si}_3\text{N}_4, \text{AlN}, \text{SiO}_2$		1670-1830	240	Effect of oxygen to nitrogen ratio on densification	26
$\text{Si}_3\text{N}_4, \text{Al}_2\text{O}_3, \text{AlN}$		1775-1800	60	Fabrication and modulus of rupture	27
$\text{Si}_3\text{N}_4, \text{AlN}, \text{Al}_2\text{O}_3$		1740	60	Fabrication and modulus of rupture	28
β -SIALON	$\text{CeO}_2, \text{Y}_2\text{O}_3, \text{ZrO}_2, \text{AlPO}_4, \text{GaPO}_4, \text{ZrC}, \text{La}_2\text{O}_3, \text{Er}_2\text{O}_3, \text{Nd}_2\text{O}_3, (\text{Sm}, \text{Gd})\text{O}_3$	1700-1600	60-180	Fabrication, modulus of rupture, creep and oxidation	29
$\text{Si}_3\text{N}_4, \text{SiO}_2, \text{AlN}$	Y_2O_3	1760	240	Fabrication, modulus of rupture and oxidation	30
$\text{Si}_3\text{N}_4, \text{AlN}, \text{Al}_2\text{O}_3$	$\text{Y}_2\text{O}_3\text{-SiO}_2$	1450-1750	60-120	Fabrication, modulus of rupture and oxidation	31
$\text{Si}_3\text{N}_4, \text{AlN}, \text{Al}_2\text{O}_3$	$\text{Y}_2\text{O}_3, \text{MgO-Y}_2\text{O}_3, \text{MgAl}_2\text{O}_4$	1750	240	Fabrication, modulus of rupture and oxidation	Current work by the author

*Not reported.

TABLE III. - MODULUS OF RUPTURE OF HOT-PRESSED AND SINTERED SIALONS

Starting materials ^b	Basic formula	Fabrication method	Average 4-point modulus of rupture, MPa		Reference
			25° C	1370° C	
$\text{Si}_3\text{N}_4, \text{Al}_2\text{O}_3$	$\text{Si}_{1.3}\text{Al}_{2.67}\text{O}_4\text{N}_4$	Hot-pressed	310	a	4
$\text{Si}_3\text{N}_4, \text{Al}_2\text{O}_3$	a		420	a	15
$\text{Si}_3\text{N}_4, \text{AlN}, \text{Al}_2\text{O}_3, \text{SiO}_2$ (MgO)	$\text{Si}_{2.67}\text{Al}_{0.30}\text{O}_{0.43}\text{N}_{3.57}$		c648	a	17
$\text{Si}_3\text{N}_4, \text{AlN}, \text{Al}_2\text{O}_3$	$\text{Si}_{2.25}\text{Al}_{0.75}\text{O}_{0.75}\text{N}_{3.25}$		c510	c240	18
$\text{Si}_3\text{N}_4, \text{Al}_2\text{O}_3$	a	Sintered	250	a	15
$\text{Si}_3\text{N}_4, \text{AlN}, \text{SiO}_2$	$\text{Si}_{1.4}\text{Al}_{1.6}\text{O}_{1.6}\text{N}_{2.4}$		208	180	9
$\text{Si}_3\text{N}_4, \text{AlN}, \text{Al}_2\text{O}_3$	$\text{Si}_4\text{Al}_2\text{O}_6\text{N}_6$		352	135	26
Basic (Y ₂ O ₃)	$\text{Si}_{2.45}\text{Al}_{0.55}\text{O}_{0.55}\text{N}_{3.45}$		450	335	29
(Y ₂ O ₃)	$\text{Si}_{2.7}\text{Al}_{0.3}\text{O}_{0.3}\text{N}_{3.7}$		460	375	
(CeO ₂)	$\text{Si}_{2.45}\text{Al}_{0.55}\text{O}_{0.55}\text{N}_{3.45}$		400	a	
(ZrO ₂)	$\text{Si}_{2.45}\text{Al}_{0.55}\text{O}_{0.55}\text{N}_{3.45}$		430	235	
$\text{Si}_3\text{N}_4, \text{AlN}, \text{SiO}_2$ (Y ₂ O ₃)	$\text{Si}_{2.6}\text{Al}_{0.39}\text{O}_{0.4}\text{N}_{3.6}$		460	175	30
$\text{Si}_3\text{N}_4, \text{AlN}, \text{Al}_2\text{O}_3$ (Y ₂ O ₃ -SiO ₂)	$\text{Si}_{2.4}\text{Al}_{0.8}\text{O}_{0.6}\text{N}_{3.6}$		483	228	31
$\text{Si}_3\text{N}_4, \text{AlN}, \text{SiO}_2$	$\text{Si}_{2.55}\text{Al}_{0.6}\text{O}_{0.72}\text{N}_{3.52}$		404	260	32
$\text{Si}_3\text{N}_4, \text{AlN}, \text{SiO}_2$ (MgO)	a		410	310	33
$\text{Si}_3\text{N}_4, \text{AlN}, \text{Al}_2\text{O}_3$ (Y ₂ O ₃)	$\text{Si}_{1.8}\text{Al}_{1.6}\text{O}_{1.5}\text{N}_{3.0}$		404	65	Current work by the author
	$\text{Si}_{2.07}\text{Al}_{1.24}\text{O}_{1.2}\text{N}_{3.2}$		305	69	
	$\text{Si}_{2.4}\text{Al}_{0.8}\text{O}_{0.9}\text{N}_{3.4}$		295	95	
	$\text{Si}_{2.2}\text{Al}_{1.08}\text{O}_{1.08}\text{N}_{3.28}$		195	135	

*Not reported.

^bThe additive or sintering aid is enclosed in parentheses.^c3-point MOR.

TABLE IV. - FRACTURE TOUGHNESS (K_{Ic}) OF SIALON MATERIALS

Starting materials	Basic formula	Fabrication method	Fracture toughness (25° C) $\text{MN/m}^{-3/2}$	Reference
$\text{Si}_3\text{N}_4, \text{Al}_2\text{O}_3$	^a	Hot-pressed	1-2	15
$\text{Si}_3\text{N}_4, \text{AlN}, \text{SiO}_2$	$\text{Si}_{2.25}\text{Al}_{0.75}\text{O}_{0.75}\text{N}_{3.25}$	Hot-pressed	4	18
$\text{Si}_3\text{N}_4, \text{MgO}$	Si_3N_4 (HS-130)	Hot-pressed	6.0	33
$\text{Si}_3\text{N}_4, \text{AlN}, \text{SiO}_2$ (MgO)	^a	Sintered	6.0	33
$\text{Si}_3\text{N}_4, \text{AlN}, \text{Al}_2\text{O}_3$	$\text{Si}_6\text{Al}_2\text{O}_2\text{N}_6$	Sintered	2.2-2.7	37
$\text{Si}_3\text{N}_4, \text{X}$	^a	Sintered	1.32	37

^aNot reported.TABLE V. - WATER QUENCH THERMAL SHOCK RESISTANCES (T_c) OF
SIALON, Si_3N_4 and SiC CERAMICS

Material	Basic formula	T_c	Reference
Hot-pressed SIALON	$\text{Si}_{2.25}\text{Al}_{0.75}\text{O}_{0.75}\text{N}_{3.25}$	320	18
Sintered SIALON	$\text{Si}_{2.4}\text{Al}_{0.8}\text{O}_{0.6}\text{N}_{3.6}$	460-480	31
Sintered SIALON	^a	510	33
Reaction sintered SiC	SiC	305	40
Hot pressed SiC	SiC	415	40
Reaction sintered Si_3N_4	Si_3N_4	460	40
Hot pressed Si_3N_4	Si_3N_4	750	18

^aNot reported.

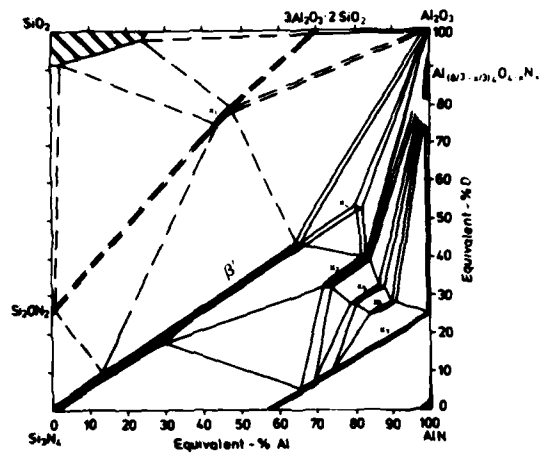


Figure 1. - Isothermal section Si_3N_4 - AlN - Al_2O_3 - SiO_2 of the system Si-Al-O-N at 1760°C (ref. 8).

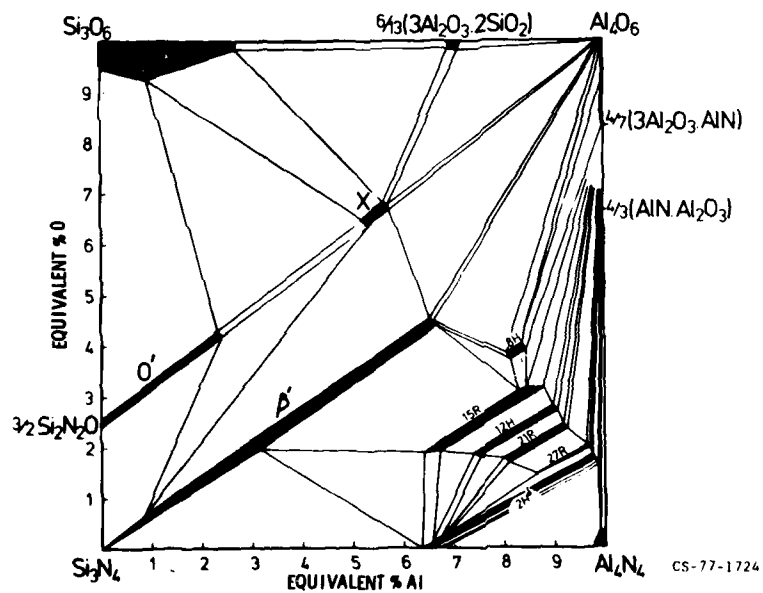


Figure 2. - The Si_3N_4 - AlN - Al_2O_3 - SiO_2 system (ref. 4).

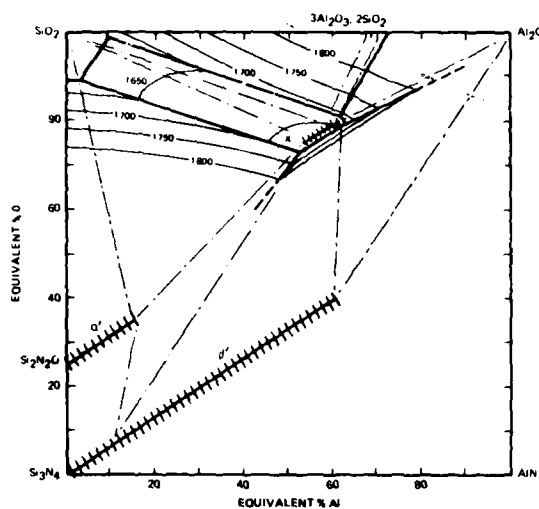


Figure 3. - The Si_3N_4 -AlN- Al_2O_3 - SiO_2 system showing liquidus isotherms (1650° - 1800° C) between the SiO_2 corner and X-phase (ref. 9).

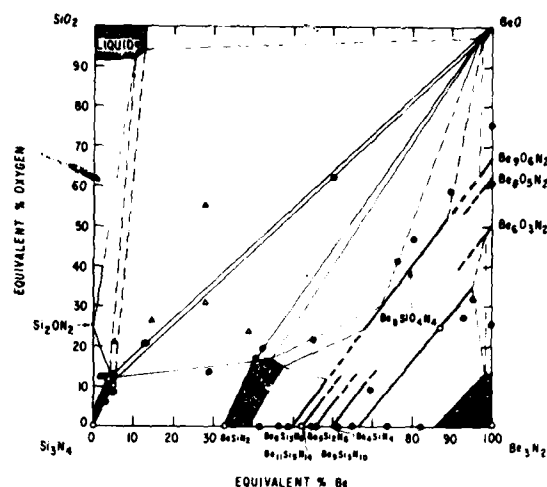


Figure 4. - Isothermal section of the system Si_3N_4 - SiO_2 -BeO- Be_3N_2 at 1780° C (ref. 12).

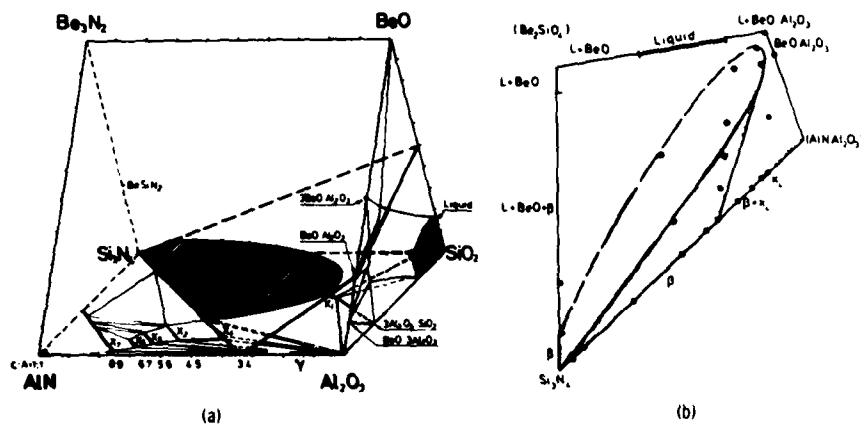


Figure 5. - Phase diagram of the quaternary system Si_3N_4 -AlN- Al_2O_3 - Be_3N_2 -BeO at 1760° C (ref. 13).

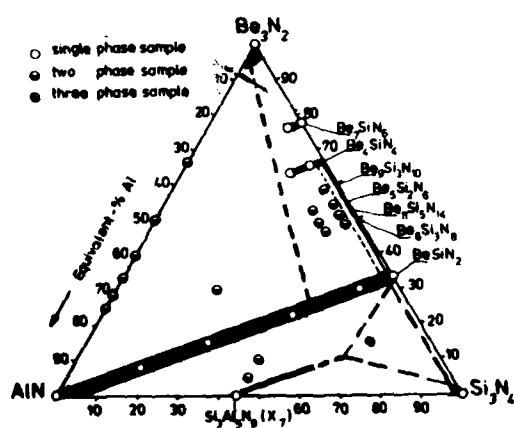


Figure 6. - The systems Si-Al-Be-N at 1780° C (ref. 13).

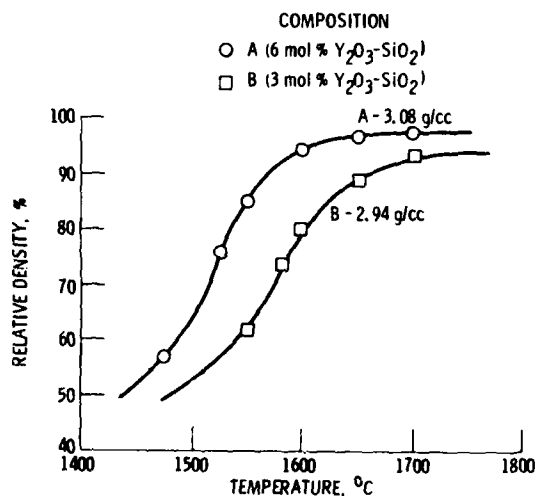


Figure 7. - Density of sintered β' - SiAlON for 1 hour at different temperatures (ref. 31).

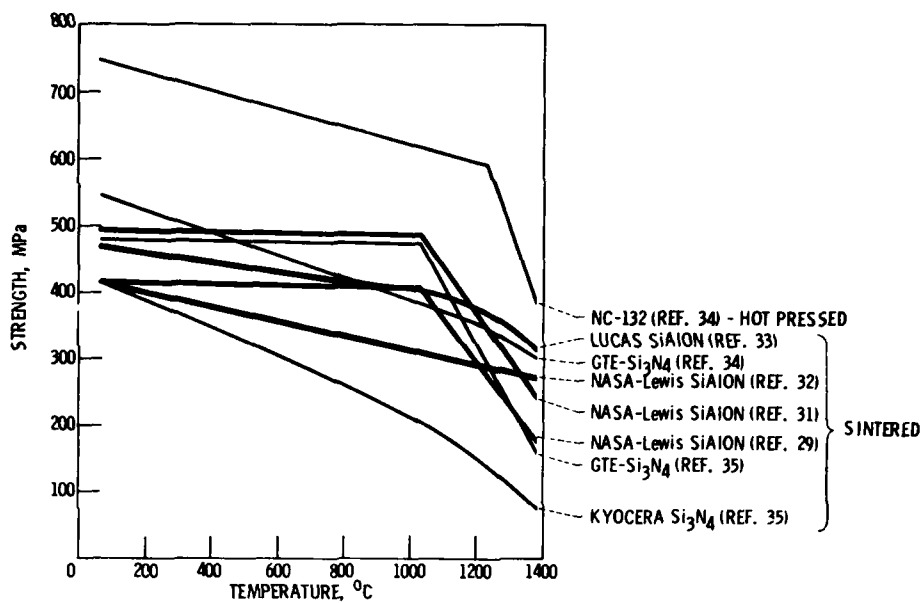


Figure 8. - Comparison of strength behavior of β' SiAlON and Si₃N₄ materials.



A - 6 mol% Y₂O₃-SiO₂

Figure 9. - Fracture surface (1380°C) of sintered β' -SiAlON (Si_{2.4}Al_{0.8}O_{0.6}N_{3.6}) bend bar. V-shaped area indicates slow crack growth (ref. 31).

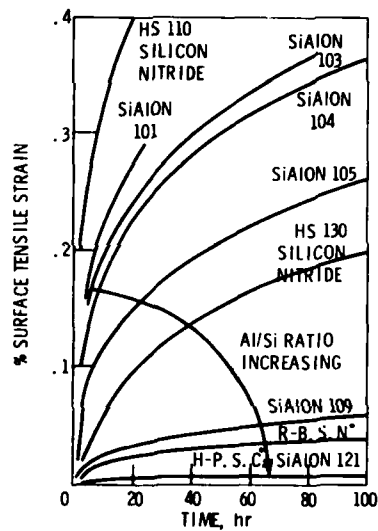


Figure 10. - Creep of various ceramic materials. 1227°C, 77 MN/m². (After Arrol⁷).

* Composition not defined.

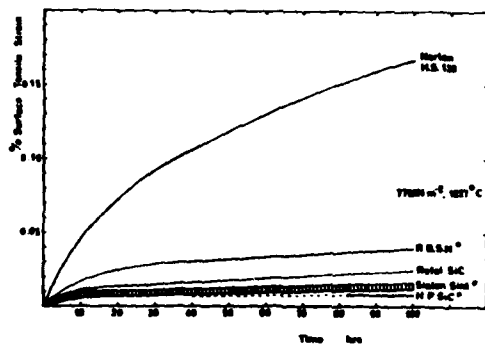


Figure 11. - Comparison of creep (4-pt. bend) behavior of Si_3N_4 , SiC , and SiAlON (ref. 33).

* Composition not defined.

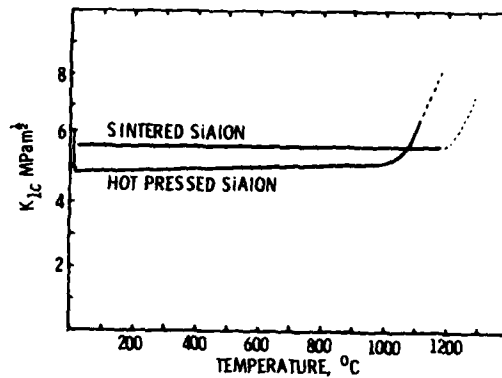


Figure 12. - Variation of fracture toughness with temperature for hot-pressed and sintered SiAlONs (ref. 33).

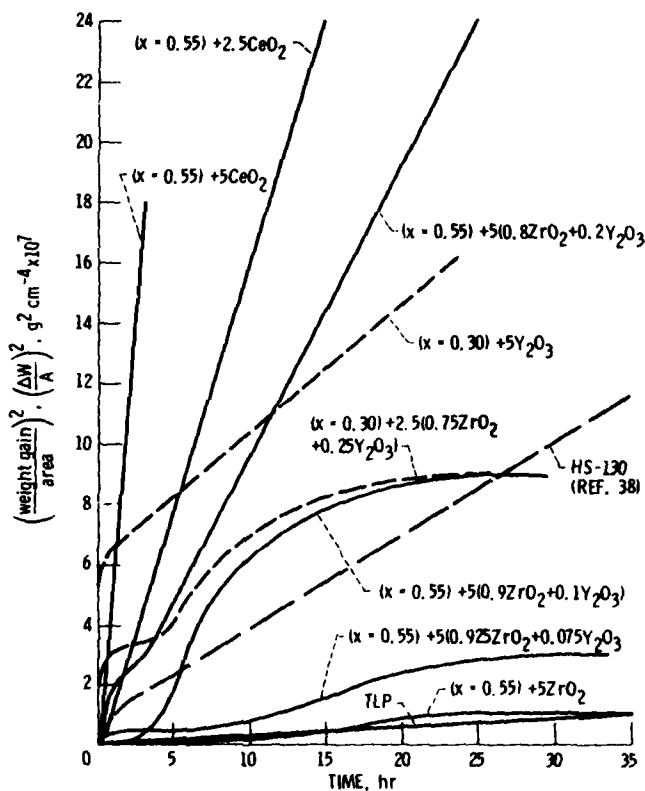


Figure 13. - Weight gain in air at 1400°C (2550°F) of various SiAlON compositions ($\text{Si}_{3-x}\text{Al}_x\text{O}_x\text{N}_{4-x}$) after Layden (ref. 29) and Ashbrook (ref. 39).

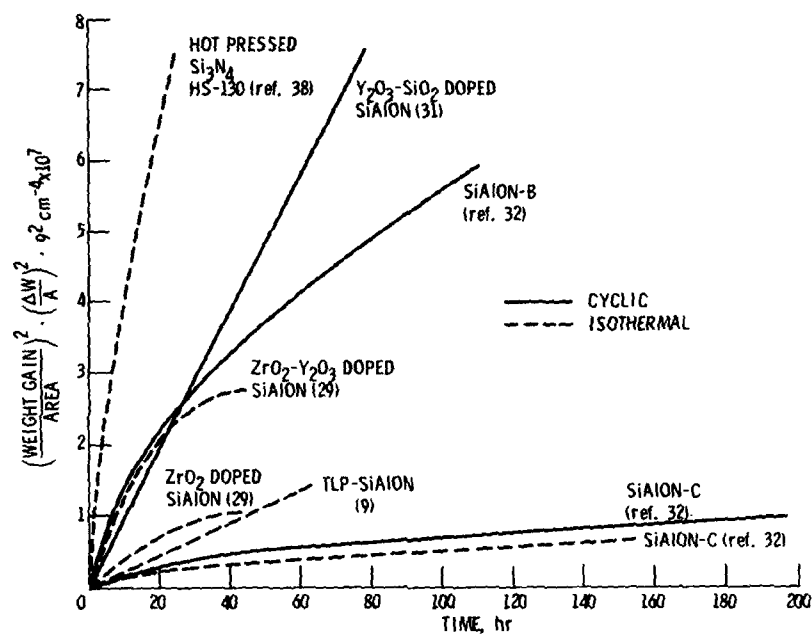


Figure 14. - Parabolic plots of the oxidation of various Si_3N_4 ceramics at 1370° to 1400° C.

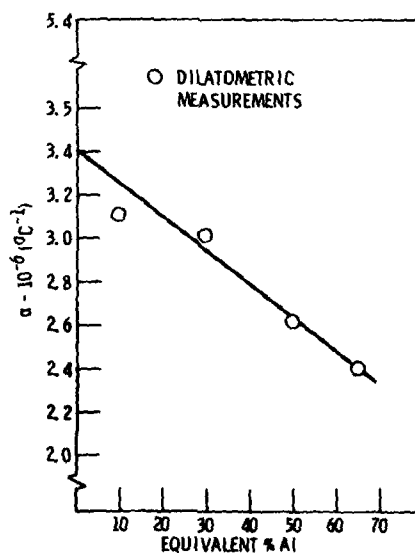


Figure 15. - Linear coefficient of thermal expansion between 25° and 1000° C for β' - $\text{Si}_{6-x}\text{Al}_x\text{O}_{8-x}\text{N}_{8-x}$ SiAlON (after Gauckler, ref. 18).

PRESSURELESS SINTERING OF SILICON CARBIDE

by

Prof. Dr. Ernst Gugel and Dr. Gerhard Leimer
Annawerk Keramische Betriebe GmbH
Ceranox Division
D-8633 Rodental

SUMMARY

In the past few years, the number of candidate ceramic materials for application in automotive engineering was supplemented by one, namely silicon carbide sintered without pressure. In 1973, U.S. scientists for the first time succeeded in sintering the mainly homopolar compound silicon carbide to almost the retical density, without pressure and by adding only small quantities of sintering aids. The stage of development of this material is reported with respect to the parameters influencing the sintering process, the properties achieved and the forming possibilities for gas turbine components. A comprehensive literature survey is attached.

INTRODUCTION

Silicon carbide has been used for technological purposes since the turn of the century, with an annual production rate of approx. 700,000 tons at present. In most fields of application, the silicon carbide grain is formed to components by applying different kinds of bonding materials, so that the properties particular to the nature of silicon carbide cannot, or can only partially be used. This is due to the fact that in spite of most intensive efforts it has not been possible up to now to sinter silicon carbide in a "normal" way. However, other methods have been developed, which result in the production of self-bonded silicon carbide. A porous material can be produced by recrystallization, a porous or dense silicon containing material by reaction sintering, and a dense pure silicon carbide by hot pressing. Among these materials, the dense, silicon-containing and the hot-pressed silicon carbide offer excellent properties, which make their use as an engineering material appear promising and advantageous, especially under high thermal and mechanical loads even under corrosive and abrasive conditions.

Consequently, silicon carbide, in addition to silicon nitride, is considered a promising candidate for the manufacturing of components to be used at high temperatures and under extreme corrosive and erosive environments. The non-oxide ceramic materials include the mainly covalently bonded refractory compounds of the light elements boron, silicon, carbon and nitrogen. These elements are generally regarded as either not sinterable or only suitable for sintering under great difficulties.

With silicon carbide, however, normal sintering has now proved possible, i.e., a powder compact can be densified without pressure using only small quantities of additives. While in the beginning this seemed to be possible only with β -silicon carbide, it soon appeared possible with α -silicon carbide too, which can be manufactured much more economically on a proven, large technical scale.

Thus, silicon carbide materials can be supplemented by a new material made via sintering, which from the quality point of view matches hot-pressed material, yet offers the advantage of being more economic in manufacturing.

This, of course, is a most interesting feature for the fabrication of high-strength components, especially for use in high-temperature engineering, and intensive development activities have made very good progress.

Components fabricated in accordance with various shaping methods were made and subjected to applicability tests.

Below, the present stage of this development is reported, both with regards to our own work and from published literature.

STARTING POWDER

The SiC starting powder used plays a most decisive role in obtaining high sintered densities. Essential characteristics are, besides phase composition (polytypes, α -, β -SiC), the type and quantity of impurities and of additives, and grain shape and grain size and consequently the specific surface area. Grain distribution substantially determines the obtainable green density, which for its part has an influence on the sintering result. SiC production, processing and cleaning have to meet the requirements set.

At first, the possibility of sintering silicon carbide without pressure was limited to β -SiC (1), involving the disadvantages of an expensive starting raw material. Further developments have shown that equivalent or improved material can be produced (2,3) by use of α -SiC of suitable powder quality and produced by an economic method.

A powder suitable for sintering, however, is not yet available in the general market place. Usually it is proprietary to the companies developing the material, the most important being Carborundum Company and General Electric in U.S.A., Annawerk and H.C. Starch in Germany, and recently Kyoto Ceramics in Japan.

MANUFACTURING OF β -SILICON CARBIDE POWDER

Taking into account the sinterability of the powder, manufacture by chemical vapor deposition is the most advantageous way. Carbon and silicon-containing organic substances, e.g., polycarbosilanes, are used, which have been synthesized by polymerisation of silicon-organic compounds followed by decomposition using plasma techniques. Numerous possibilities have been tested here, but most of them did not get beyond a laboratory scale (2, 4, 5, 55, 57, 58, 61, 65, 66, 69). Depending on the type of the starting material and the decomposition conditions, α -SiC or amorphous powder may also result.

A β -SiC powder with good sintering properties and small crystallite size, large specific surface area, high purity and low oxygen content is obtained by chemical vapor deposition from methylsilane in a flow reactor (6,61).

Another way to manufacture β -SiC suitable for sintering and perhaps also α -SiC powder is the vaporizing of metallic silicon in an electric arc and reaction with methane or vaporous carbon (7). The advantage of this method, if optimized, is that a finer, more uniform, purer and less agglomerated powder will result as compared to powders obtained from chemical processes.

With present-day's state of the art, the manufacturing of β -SiC via all these processes is uneconomical as a mass produced product for further processing to sintered silicon carbide, but efforts are being taken to improve economic efficiency (8).

Synthesis from the elements or by reduction of SiO_2 (4, 8, 9, 16, 55, 57, 58, 60, 77) is another way. This method is cheaper than the plasma approach, but does not yield as favourable a powder.

MANUFACTURING OF α -SILICON CARBIDE POWDER

Sinterable α -SiC is manufactured by processing Acheson SiC (2, 9, 57, 62, 76) obtained from highly pure silica and high-quality coke. Here the economic advantages as compared to β -SiC powder should be mentioned, besides the other advantages resulting in sintering.

PROCESSING

Processing of the synthesized SiC powders is done in ball mills, colloid mills and similar processing equipments (1, 10, 62, 76).

The powders can be cleaned by annealing in air and subsequent hydrofluoric acid treatment (11-15), in order to remove any adherent carbon, and silica which originates in the annealing process.

GRAIN SIZE

The patent literature (55, 57, 62, 64, 68, 76) indicates that grain sizes required for sintering with sufficient densification vary widely, between 0 and 20 μm . Yet good sintering results can only be achieved using a powder which, if possible, is in the sub-micron range. In this range, the grain size distribution which is decisive for densification, cannot be given. For characterizing the raw material, it is customary to measure the specific surface area; the result serves to calculate an average grain size diameter, assuming a ball shaped grain.

For β -SiC (1, 10) as well as for α -SiC (76), specific surface areas between 5 and 15 m^2/g are considered favourable. Indications in the literature range between 1 and 100 m^2/g (2, 4, 11, 12, 13, 17, 55, 57, 62, 64, 74, 76).

PURITY

No general standard can be indicated for the purity required, or rather for the nature and quantities of impurities allowable.

Many investigations trying to clarify the influence of impurities in SiC suitable for sintering have been made (1, 4, 11-13, 55, 62, 64, 74). The influence on the sintering result is significant at any rate. It may well be assumed that oxygen plays the most decisive part. A maximum oxygen content in β -SiC of 0.2% is considered tolerable, also a content of metallic impurities in the form of oxides <1000 ppm is required to obtain high densities. It is not so critical, if there are impurities in the form of some metals, since no negative influence could be found with the presence of 1% aluminum, tungsten or tungsten carbide (1). With an oxygen content of 0.7% resulting from the addition of silica, only a negligent shrinkage could be obtained. An unfavourable effect is reported to result from Fe, Ca, Na and K, as elements or compounds, and from silica (66).

SINTERING AIDS

The break-through to sintered silicon carbide was made, when the effect of the simultaneous presence of boron and carbon in powder with acceptable fineness for sintering was realized.

In 1973 (1, 55) the possibility for pressureless sintering of β -silicon carbide using a boron compound (boron or boron-carbide) and carbon as sintering aids was first mentioned. The sintering aids may already be added during the synthesis of the silicon carbide powder, or later to the finished powder. The sintering of α -silicon carbide using additions

of boron and carbon or their compounds was first reported in 1975 (56,76). Use of this cheaper starting powder offers substantial economic savings.

The efforts to create optimum sintering conditions were considerable and were first taken by General Electric in U.S.A., where the method was also introduced (1, 4, 10-13, 19, 20), later by Carborundum Company (2, 23, 27) and in Germany by Annawerk (3, 18) and by the Technological University of Berlin (6, 14, 15, 21, 22) and recently also the Elektroschmelzwerk Kempten (16, 29). Where as at first a solid state sintering mechanism was supposed, it later appeared that liquid phase sintering was involved (17, 18).

Such efforts showed quite clearly that only the joint presence of boron and carbon in comparatively small quantities offers the best sintering effect. This can be seen from the results obtained by high temperature dilatometer investigations shown in Fig. 1 (18). Carbon alone practically renders no densification at all. Boron causes moderate shrinkage, which does not increase beyond an addition of 0.4% of boron. This corresponds to the solubility limit of boron in silicon carbide (81-85). With boron additions exceeding 0.4%, areas rich in boron can be found in the microstructure.

A uniform distribution of the additions is essential, the distribution of the carbon having to be done more critically and therefore more carefully than that of boron, because of the much smaller diffusion coefficient (12). In case of careless distribution, the microstructure will show carbon agglomerates which do not react. It is recommended therefore to add carbon in the form of a solution of organic decomposable substances; many suggestions have been made to this approach (55, 57, 58, 68, 76).

Boron has its best effect when added in elemental form. Fig. 2 shows the shrinkage effect of boron as compared to boron carbide and boron silicide in the high-temperature dilatometer (18). Not only the extent of shrinkage is most favourable with elemental boron, but the maximum sintering rate is found at lower temperatures (fig. 3) (18).

Boron compounds, too, can be added via solid or liquid organic substances, which later in the thermal treatment transform into boron carbide of finest distribution. This ultra-fine boron carbide, added in a quantity of at least 10% to the β -SiC, has an additional advantageous effect: it impedes exaggerated grain growth and regulates in this way the structure (58).

Other boron compounds such as boron nitride, boron phosphide, aluminum diboride or mixtures thereof were examined and proved to affect sintering (12, 28, 64, 68, 78-80).

Instead of boron, beryllium or compounds thereof, e.g., Be_2C alone or together with boron were used as sintering aids in the presence of carbon (62, 64). Furthermore, besides boron Al, Fe, Ti, W and Mg as elements or in the form of compounds were also named as preferred sintering aids, and other sintering aids (Ca, Ga, Ni, Cr, Mn, Zr, In, Sc) were pointed out, with hot-pressing being included (66).

Additions of low quantities of SiO_2 , Fe, Ca, Na and K however, show a considerable negative influence on sintering behavior, according to (62).

Effectiveness of aluminum was confirmed recently (22, 29): 1.1 to 1.4% of aluminum together with approx. 2% C rendered a similarly good densification of α -silicon carbide as with boron and carbon. Different aluminum compounds were also examined; yet their effect is not so favourable as that of aluminum in elemental form.

When making use in practice of these results mostly obtained in laboratories, i.e., when larger components in larger number of pieces are to be manufactured, it is essential to have a mass, which with regard to microstructure development - and consequently the properties - is insensitive to temperature differences which cannot be avoided in the technological kiln. This emphasizes the significance of uniform distribution of the required additions used, as well as of the use of α -SiC, which allows equiaxed microstructure development also with higher temperature differences.

SINTERING

SINTERING ATMOSPHERE

Sintering is done under nitrogen, hydrogen, helium, argon or in vacuum (2, 4, 12-15, 17, 18, 21, 55, 57, 58, 62, 64, 66, 68, 76). The latter method, however, is not recommended because of the silicon vapour pressure. This can be recognized by carbon forming during decomposition and separating on the surface (1, 10). A boron-containing atmosphere will have positive influence on the sintering behaviour, if boron is used as a sintering additive (30, 63, 74). The loss of boron during sintering, which is usually observed, is stopped, and a more homogeneous, less porous structure will form. The boron-containing atmosphere is created by adding e.g., boron trichloride or boron compounds offering a sufficiently high vapour pressure at sintering temperature. With conditions being otherwise unchanged, bulk densities of e.g., 2.57 and 3.08 g/cm^3 were achieved without and with a boron-containing sintering atmosphere (74).

The use of nitrogen during sintering of β -SiC (55) can delay the undesired transformation of β -SiC into α -SiC and so prevent exaggerated grain growth. This is a result of the effect of nitrogen stabilizing the β -SiC phase (9, 86). Nitrogen, however, will reduce sintering rate, so that now higher sintering temperatures will be necessary. Another effect of nitrogen is its influence on electric conductivity, with the specific electric

resistance of the SiC sintering product being substantially reduced (55).

SINTERING TEMPERATURE AND SINTERING TIME

Both are dependent on the powder to a certain degree. In general, it may be stated that the interval with regard to temperature is very narrow and that the sintering densities optimum for a powder are obtained after a relatively short period.

For β -SiC, a sintering temperature ranging between 1900 and 2000°C and maintained for 15 minutes will be sufficient. The sintering temperature here should be observed with particular care, since excessive temperatures will impede shrinkage as a result of a β - to α -SiC phase transformation producing very coarse grains.

Sintering of α -SiC is less sensitive to temperatures, so that the most advantageous temperature range is extended up to 2200°C upwards. Detailed indications of sintering temperature and time for certain masses are given in (2-4, 12-15, 17, 18, 21, 55, 58, 62, 64, 66, 68, 76).

SINTERING GAS PRESSURE

Besides occasional tests to sinter under vacuum, pressureless sintering of β - as well as of α -SiC in a protective atmosphere normally takes place under normal pressure, at the most with a slightly increased pressure (57, 58, 72).

SINTERING MECHANISM

For decades, intensive, but at first unsuccessful efforts were taken to sinter nonoxide ceramic substances without a second phase under shrinkage. The strongly covalent bonding of these materials with their short interatomic distances impedes the volume diffusion required for material transportation whilst shrinkage takes place. According to Pauling (87), silicon carbide has a covalent bonding share of 88%. Furthermore suitable thermodynamic and kinetic data were not available.

According to more recent observations (4, 31) sintering in the sense of neck growth and densification is principally possible for thermodynamic reasons.

Measurements of self-diffusion in silicon carbide within the temperature range of 1800 to 2300°C (88, 89), which in (32) are listed, very clearly do point out, however, that at least in relation to silicon nitride, some sintering capability should be possible via volume diffusion. Here, the mobility of carbon in the SiC lattice is two or three orders of magnitude higher than that of silicon. This was also confirmed by creep measurements (33).

The possibility of transporting material via surface diffusion and via vaporizing/condensation processes was realized at an earlier date. This leads to a recrystallization with some strengthening, but without densification. Recrystallized silicon carbide is already used on a large technical scale (34).

In 1956 (35) it became possible to densify silicon carbide under hot-pressing conditions with comparatively little additions of aluminum or iron and later boron carbide (36), achieving practically theoretical density.

Thus it is proved that silicon carbide can be sintered. While the question of the sintering mechanism was being worked on, experimental work on pressureless sintering of silicon carbide was continued intensively at the same time.

In 1973 Prochazka (1) succeeded in sintering β -silicon carbide of finest grain size to almost theoretical density by adding boron and carbon at the same time. With the know-how and experiences available, efforts were taken to clarify the sintering process with known sintering mechanisms and to bring them into accordance. These concepts were based on the fact that the sintering mechanism takes place via a solid state diffusion, which, however, can only happen to a sufficient extent if a certain ratio of grain boundary energy to surface energy is not exceeded. So the term used for the driving force in the equation for diffusion sintering according to Coble (90) must be modified by introducing grain boundary energy. These energy levels are modified by additives.

Consequently, sintering becomes possible by corresponding influencing of the surface and/or grain boundary energies in the following way: The addition of carbon causes the adherent oxygen (SiO_2) to disappear, at the same time setting free the SiC surface provided with high surface energy, and the addition of boron is intended to reduce the grain boundary energy via diffusion in the boundary surfaces. Thus the conditions for the boundary surfaces to grow are created, meaning that the volume and grain boundary diffusion can take place in accordance with the values of the diffusion coefficients.

The effect of boron is explained by the possibility of ternary solid solution formation. Furthermore, it is supposed that this ternary solid solution also accelerates grain boundary diffusion (91).

Also the densifying effect of pressure applied from outside is consistent with the sintering mechanism suggested.

By presenting some models for various grain circuits, it was shown that with the given

energy ratio for obtaining a material transport into the pore, i.e., to make sintering possible, the individual grains must enclose the pores in a dihedral angle as large as possible. The minimum angle required is dependent on the grain circuit, and its minimum (3-grain circuit) is 60° . Packing, and consequently green density in the unfired pre-shape are of decisive significance under these aspects (92).

With continuing sintering, or with the decreasing porosity, concentration of the remaining oxygen on the grain surface is increased. This can cause densification to stop because of the shifting of the energy ratio as a result of the increasing oxygen content. As a consequence, in extreme cases with very long sintering periods, pore formation may again result.

Continuing the work of Prochazka, Greskowsch (4) has engaged very intensely in the sintering of covalent compounds, taking into consideration thermodynamic and kinetic principles. He pointed out the fact that for sintering with shrinkage it is a prerequisite that there are no changes in structure as a result of surface diffusion and vapour phase transportation and that no formation of grain shapes differing in size in the length to width ratio will occur. Furthermore, he indicated the necessity of using submicron powder.

In contrast to a densification mechanism by volume or grain boundary diffusion in the solid state, Lange (17) assumes a reaction sintering and liquid phase sintering mechanism. This is confirmed by the discovery of a second phase rich in boron, which doubtlessly was in the liquid condition during sintering, as could be seen from micrographs.

Furthermore, a loss in weight was often found, which can only be due to the decomposition of silicon carbide into silicon and carbon. A part of the silicon evaporates in the process, but might also react with B_4C to yield SiC and SiB_6 (93). Thus, in the equilibrium range $SiC-SiB_6-Si$ of the system $Si-B-C$, liquidus temperatures within the SiC -sintering temperature level are obtained. The lowest-melting eutectic composition in the silicon-boron system is $1360^\circ C$. This, together with the fact that the addition of more boron will lead to worse sintering results - as a consequence of the distance from the lowest-melting composition, also confirm the sintering mechanism assumed here.

The formation of a liquid phase, when boron is added to SiC , and its possible effect as a vehicle for the sintering process may also be considered as the possible cause for the exaggerated grain growth under certain conditions (9).

Since the quantity of the liquid phase present is very low, it may be assumed that both sintering mechanisms take place and complement each other in the sense of good densification. A dense SiC grain structure is obtained under conditions, where an $Si-B-C$ melt can serve as a vehicle for dissolution and precipitation of SiC , at the same time bringing about a closed arrangement with a certain volume and grain boundary diffusion. In order to initiate these processes, a favourable ratio of the grain boundary to the surface energy is required as a driving force. The crystal modification of SiC or a β/α -transformation do not play a role, only grain fineness. The fact that originally only β - SiC was considered suitable for sintering is due to its inherent finer grain size. As soon as it was found that α - SiC prepared as finely can also be sintered, it was used with advantage.

MICROSTRUCTURE

Already in the first reports on the suitability of β - SiC for sintering it was found (1, 10), that under certain conditions exaggerated grain growth will occur during sintering of β - SiC . Of considerable importance in this respect are temperature and sintering time, but also impurities in SiC as well as the sintering atmosphere and the additives in so far as they influence the originating of possible polytypes in the α - SiC during the phase transformation of β - to α - SiC . Perhaps nucleation-controlled exaggerated grain growth occurs mostly with the formation of the polytypes 6 H and 4 H (12, 19). When boron is added, phase transformation is accelerated and besides 6 H additionally leads to 4 H. With the simultaneous presence of nitrogen, the 6 H polytype is stabilized (9). This growth, for which an explanation was unsuccessfully sought (19), takes place very rapidly, within minutes, with pore inclusions being involved, which cannot be removed anymore, so that no highly dense materials can be obtained. Also the inclusion of second phases (carbon, B_4C) is possible in the process. The collision of the grains of exaggerated size even while the densification process is going on leads to a rigid, not mobile structure, which cannot be sintered and again has a densification-impeding effect. The low bulk densities are responsible for bad mechanical properties. However, with almost dense materials also, where grains get coarser only after densification, mechanical properties will worsen substantially.

With differences in bulk density in the green compact, the coarser crystals form in the more porous parts, also with decisive influences on the mechanical properties, so that the forming process too, has some influence.

Sintered silicon carbide has no, or only very unimportant, content of a glassy phase. This is a result of the removing of oxygen, which is necessary for complete densification. Micrographs do not show the presence of any glassy phase. This is significant for the mechanothermal properties compared to hot-pressed silicon carbide which may have an amount of glassy phase (33, 37).

The grain size of the carbon added must be within the sub-micron range and be distributed equally. When larger agglomerates form, they remain unchanged during sintering, and pores filled with carbon show in the structure.

The uncontrolled grain growth is also the reason for the fact that it was first believed that highly dense and strong materials can only be obtained by means of β -SiC, when sintering conditions are observed which do not lead to any phase transformations. With α -SiC, negligent sintering shrinkage was recognized at that time, but the limitation of a more extensive densification was attributed to the 6 H-polytype always present in α -SiC, or rather to the exaggerated grain growth in connection with it.

Figures 4 and 5 show etched micrographs of sintered β -silicon carbide, with an evenly fine-grain structure after sintering under optimum conditions as well as with long-stretched plates and exaggerated grains, as they may appear with unfavourable conditions during phase transformation. Easy to recognize here is the inclusion of pores, which obstructs further densification.

Strong grain growth can be avoided by adding larger quantities of B_4C (10-30%) during sintering of β -SiC, and an evenly fine-grained structure is also obtained when the β is transformed into the α -phase. The transformed α -SiC shows the same morphology as β -SiC and cannot be distinguished from it.

Fine grained B_4C is also observed as a second phase, because, as is known, only a small percentage can be dissolved in silicon carbide (58).

By the addition of α -SiC to β -SiC, exaggerated grain growth can also be better controlled (57). It is assumed, that the evenly distributed fine-grained SiC in quantities of 0.5 to 5% act as nuclei for a simultaneous and rapid transformation of β - into α -SiC. The α -crystals grow and collide very early, when they are still of small grain size, and then stop growing. A uniform comparatively fine-grained structure will form, with more columnar grains as compared to a faultless β -structure. As an advantage, a greater sintering range and better mechanical properties result.

Sintered α -SiC has a very uniform microstructure (2, 23; fig. 6). As a result of the missing phase transformation and the danger of formation of large columnar α -crystals in connection with it, a more extensive range with regard to sintering temperatures and period is possible with only a more coarse, but still equiaxed and homogeneous microstructure resulting from higher sintering temperatures.

PROPERTIES

Although extensive property measurements on sintered silicon carbide have not been made as yet, since it is still in the development stage, it is possible to give a comparatively good characterization. In general, properties are very familiar to those of hot-pressed silicon carbide, as far as it is not influenced by too high a flux content. The data are listed in Table 1, arranged under sintered α -silicon carbide and sintered β -silicon carbide. Listed separately is another sintered silicon carbide whose nature is not known, but which is probably α -silicon carbide.

The theoretical density is normally not reached, but the highest value given for α -silicon carbide, which is 3.18 (99% of theoretical density) must be considered as quite an excellent result.

Strength at room temperature does not appear to be sufficiently developed, as compared to the strength of a hot-pressed material. Yet further developments in this field are likely. Worth mentioning is the constant or even increasing strength at a temperature of up to 1650°C (measured), which clearly distinguishes this material from the other non-oxide ceramics.

The factors determining strength are defects such as inclusions or pores (23) as well as surface flaws caused by preparation. Careful improvement of the surface made it possible to obtain peak values of as much as 630 N/mm² (2). On specimens with as fired surfaces, bending strength values of 500 N/mm² were measured, which are higher values than those of machined specimens (20).

A common feature of all dense ceramics is that the grinding direction has a clearly visible effect on strength. On qualities of low strength as compared to other data, the following bending strength values were determined: Unworked 340 N/mm², specimens ground lengthwise 290 (320) N/mm² and specimens ground in transverse direction 250 (280) N/mm² (38). The Weibull parameters were ranging between 8 and 10 in all cases.

By annealing components, ground only superficially and therefore showing flaws, to 1400 to 2100°C in vacuum, the initially sharp-edged grinding traces are rounded, the effect of grooves thus being reduced. As a result, an improvement of strength by 10 to 30% could be found (72).

The Weibull parameters not exceeding 10 in most cases, which are found for bending strength, can be explained by a multi-modal strength distribution, which is a result of fracture statistics analyses (23). It is therefore useless to indicate the Weibull modulus calculated from unselected data. Pores with an extensive size distribution are assumed to be responsible for this fact, together with inclusions with a narrow size distribution as well as surface flaws.

Up to 1400°C, no influence of load rate on fracture stress is apparent, meaning that up to this temperature any slow crack growth is unlikely. The first hints for slow crack growth appear at 1500°C. As a consequence of the multimodal strength distribution, which

changes in addition to load rate, it is rather not safe, to determine the crack growth parameter (23).

The Young's modulus of sintered silicon carbide is given as a function of density in accordance with the relation $E = 480 \times 10^3 \times e^{-3.21(1-\rho/\rho_{th})}$ (39) and $E = 491 \times 10^3 \times e^{-3.21(1-\rho/\rho_{th})}$ (20). Accordingly, silicon carbide of 100% density has a Young's modulus of 480 to 490 $\times 10^3$ N/mm², a value rather high as compared to the measurements taken on single crystals.

Poisson's ratio was calculated out of Young's modulus and shear modulus, which, ranging between 0.14 and 0.16, is extremely low, when compared to other ceramics.

Coarse equiaxed chemical vapor deposited SiC grains and fibrous SiC is added in order to increase toughness, but the suitability for sintering is reduced (40).

The small number of creep measurements (20, 41) taken as yet have already shown that even at temperatures of 1500°C in oxidizing atmosphere, creep behavior is better than that of any other non-oxide ceramic material.

Steady-state creep rate was measured to be $7 \times 10^{-6} K^{-1}$ at a load of 180 N/mm², with exponent of 1.1 to 1.2.

Oxidation resistance of this material has also proved to be excellent. Sintered silicon carbide here corresponds to CVD silicon carbide. After one week in air at 1600°C, weight gain is only 0.2 to 0.7 mg/m² (20).

Thus, good behaviour can be expected in a pending 3500 hour test at 1370°C (42), which simulates the combustor discharge environment encountered by hot flow path components.

Because of the high thermal conductivity and relatively high strength, resistance to thermal shock also proves to be most favourable in spite of the very high Young's modulus and the fair thermal expansion. The strength drop as a result of quenching occurs at a temperature of 400°C (43).

Doubtlessly, abrasive behaviour of sintered silicon carbide is excellent. Comparative test results are not yet available.

Just like silicon carbide, sintered silicon carbide is chemically almost completely resistant to numerous substances. Hydrochloric acid, nitric acid, sulphuric acid, phosphoric acid and fluoric acid as well as mixtures of these acids (with the exception of nitric acid/fluoric acid mixtures) in all concentrations and up to boiling temperatures practically do not affect the material.

SHAPING

Sintered silicon carbide is a ceramic material like all the others; therefore shaping, which takes place before the firing process, requires the real technological development work, as soon as the material itself has been developed.

Shaping means the manufacturing of components of more or less complex type, in low or very high piece rates to as close a final shape as possible. This means that net shaping processes (94) should be preferred. In the case of sintered silicon carbide, however, it must be observed that the formed component suffers a linear shrinkage of > 15% during firing. This has to be considered in forming. This high change of volume also allows reaching a dimensional accuracy after firing not below 1%.

Shaping further means distributing the mass in the individual component so homogeneously that no cracks, density inhomogeneities or stress can appear which make the material worse than possible for the material quality. This - and also the uniformity of all pieces - is a main problem with any brittle ceramic.

In general, it may be stated that in spite of the relatively short development period in which this material was available, progress has been excellent. Of course a great deal of further work is necessary to make forming processes suitable for greater complexity, especially with regard to components with different wall thicknesses, as well as to insure the reliability of series production.

It shows that principally all known conventional ceramic forming processes can be used for sintered silicon carbide (fig. 7). By 1974 dry-pressed, slip-cast and extruded components, at that time consisting of β -silicon-carbide, were presented (10); injection molded turbine blades were presented as early as 1975 (20).

For the manufacturing of first specimens and also first components, axial and isostatic dry-pressing is used. A small quantity of a pressing lubricant or plasticizer can be added to the powder, so as to densify and strengthen the raw piece in a better way, so that it can also be machined. Machining is possible, even after an initial firing process at 1600 to 1800°C (20).

The next step towards a degree of series production is the step towards slip casting (10, 18, 20, 44-46, 55, 76). It is most advantageous especially within the scope of development for engineering purposes, since at comparatively low tool costs a sufficient number of components can be produced, so that to some extent application tests can also be made. Any design modifications required are not very expensive, so that conditions for application

tests are ideal.

To make the mold, a master model is needed whose dimensions in case of sintered silicon carbide must be exceeded to a considerable degree because of the high shrinkage.

Naturally water is preferred as a dispersion agent, even if organic liquids may bring certain advantages. Substantial know-how of slip-casting includes the deflocculents used, to keep the silicon carbide solid content of the slip, which may even exceed 80%, as high as possible.

The mold material mainly used is plaster of paris. Complicated components (fig.8) can be made using composed molds. A further basic problem for the development of the casting method is the construction of molds. The material must flow out evenly inside without leaving remaining pores.

With complex parts any shrinkage of the mass in the mold must lead to destruction. Therefore it has been necessary to develop a method which avoids shrinkage of the thickening mass completely or almost completely (46).

Fig. 8 shows a stator vane, on the left hand side in green, on the right-hand side in fired condition. Density reached in this case did not exceed 90%, porosity, however, consisting almost completely of closed pores. Fig. 9 shows a burning chamber as a further study, also before and after sintering.

A substantial problem of slip-casting is the keeping under control of the pores, especially with more complex components. The pores are the result of bubbles which were caused during preparation of the slip, or which can be introduced during casting. Because of their round shape they are more harmless flaws, but still lead to a weakening of loaded parts of the components.

For manufacturing a large number of similar components, the possibility of injection molding or also or transfer molding, should be considered (94). Injection molding has also met with much attention in the early stage of development of sintered silicon carbide (20), and has now reached a rather high standard (45, 47, 55, 70, 76).

Silicon carbide powder is mixed with thermoplastic resins with or without wax and heated up in conventional plastic forming equipment, injected into a mold and cooled there and set. For removing the organic substances, the component must be baked very carefully.

The intention here is also to keep the SiC content as high as possible and to exclude deformation during the baking process. A further problem is the development of stress in the mold as a consequence of the mass flow, which may cause layers and voids. To avoid this, exact temperature control in the entire machine area encountered by the mass as well as a design adapted to the component, e.g., optimum arrangement of the fan gates (47) are of utmost significance.

Suitable plasticization also allows extrusion with sinterable silicon carbide (10, 20, 76), but this is significant only for tube-shaped components.

APPLICATION

Sintered silicon carbide is still in the initial phase of realization for application. Because of its combination of favourable properties - especially strength, mechanical and chemical wear resistance, thermal properties, resistance even to high temperatures -, it is of course a candidate material for application under severe environments, where the question of the material is decisive for the realization of the entire technical system. In some cases, the low specific weight plays a role, which therefore may be the reason for some interest.

Table II shows a survey of all basic types of second-phase and self-bonded silicon carbide materials, characterized by their density, SiC content and strength. Capability of sintered silicon carbide can be realized clearly here.

As compared to reaction-sintered non-oxide ceramics, sintered silicon carbide offers the advantage of being suitable for dense-sintering, without a second phase, as is usual with reaction-sintered silicon nitride. The possibility of pressureless sintering to high densities means, that now a material exists which formerly could only be manufactured by the expensive hot-pressing method. The advantage is obvious, but must be paid for by high firing shrinkage, which limits shape stability, i.e., tolerance limit must be set to $\pm 1\%$ at least.

As to properties, sintered silicon carbide is distinguished from the other non-oxide ceramics by its strength at temperatures beyond 1000°C. If moreover a material with high thermal conductivity is needed, e.g., for heat exchangers, sintered silicon carbide is particularly preferable.

It must be observed that care is needed during handling because the very high Young's modulus of silicon carbide renders it tremendously sensitive to impacts. Edge splitting occurs very frequently and of course ruins the component before it has been used. Silicon nitride offers clear advantages here.

Naturally gas turbine components are in the focus of interest at present (2, 3, 10, 44, 46). Reports are available on the first very promising results obtained with stator blades (38, 48, 49). Other sectors discussed are those of the reciprocating piston type engine (50), especially the rotor of the exhaust turbocharger, the sector for high temperature testing (23) as well as the entire field of wear technology, e.g., supports for paper industry, as well as bearings, sealing rings and nozzles.

CONCLUSION

The development of sintered silicon carbide may well be considered the most remarkable achievement in the field of high-performance ceramics in the past few years. Although only some years ago nobody believed it possible, scientists from the U.S.A. succeeded in proving that there is a way to sinter this homopolar bonded material under certain conditions. Thus, the foundations were laid for an intensive development work aimed at producing this interesting material for practical applications.

This development is still proceeding: it deals with the material as well as with the technological aspects.

Of course it is the intention to come as close as possible to theoretical density, in order to fully utilize the favourable mechanical properties of silicon carbide in the component. But it is generally known that sintering becomes more difficult, the closer the theoretical density is approached. A theoretical density of 98-99% is quite certain, and further improvement is possible with certainty, if starting grain mixture, doping and thermal treatments are suitably selected.

Apart from the forming of complex components, which requires developments specific to the component, the essential problem, from the technological point of view, is the realization of a high density in the components, which is homogeneous in the piece and from piece to piece. Much work is left to be done in this field, since this is the absolutely necessary prerequisite for any practical use.

The introduction of sintered silicon carbide as a gas turbine material - or, more generally as a potent additional material under the engineering ceramics - means that a material has become available whose properties are very similar to hot-pressed silicon carbide, the production of which is much more expensive and its forming possibilities more limited, yet which offers as many forming potentialities as e.g., oxide ceramics.

Its disadvantage is the high linear shrinkage involved which results in a lower dimensional accuracy than can be obtained with components fabricated by a reaction-sintering process.

Furthermore, it should be emphasized that silicon carbide as compared to silicon nitride is obviously more brittle, so that it may be less favoured when used for engineering applications.

If these disadvantages can be overcome - and this can be expected to a certain degree - there is at our disposal in sintered silicon carbide a prime candidate for use in gas turbine, Diesel and Sterling engines, turbochargers, heat exchangers and other automotive components, as well as for applications in the more traditional technical ceramic fields, where its extraordinary strength, abrasion and corrosion resistance are needed and can be utilized.

REFERENCES

Literature on Silicon Carbide Powder Preparation and Sintering

- (1) S. Prochazka: Sintering of Silicon Carbide, General Electric Report 73CRD325 (1973)
- (2) J. A. Coppola, C. H. McMurtry: Substitution of Ceramics for Ductile Materials in Design, National Symposium on "Ceramics in the Service of Man", Carnegie Institution, Washington, D.C. (1976)
- (3) E. Gugel, G. Leimer: Entwicklung von Werkstoffen hoher Festigkeit auf der Basis von Siliziumcarbid für den Einsatz in der Gasturbine, BMFT 01ZA055-Z13NTS1003, Final Report (1978)
- (4) C. Greskovich, J. H. Rosolowski: Sintering of Covalent Solids, J. Amer. Ceram. Soc. 59 (1976) 336-433
- (5) O. De Pous: Production of ultrafine β -Silicon Carbide Powder by Plasma Synthesis, Ceram. Inf. (143), 283; 291 (1978)
- (6) W. Böcker, H. Hausner: Verfahren zur Herstellung von Siliziumcarbid-Pulvern aus der Gasphase, Ber. Dt. Keram. Ges. 55 (1978) 233-237
- (7) P. F. Becher, R. P. Ingel, R. W. Rice: Vapour Productions of SiC and Si_3N_4 Powders, MCIC-Report 78-36
- (8) B. Krismer, W. D. Glaeser: Entwicklung und Herstellung eines optimal verdichtbaren Siliziumcarbid-Pulvers, BMFT 01ZA045-Z13NTS1003, Final Report (1978)
- (9) G. G. Gnesin, A. V. Kurdunov, G. S. Oleinik: Effect of Temperature and Topants on Polytropic Transitions in SiC, Inorganic Materials 9 (1973) 1036-1038
- (10) S. Prochazka: Sintering of dense SiC, "Ceramics for High Performance Applications", Hyannis, Nov. 1973; GE Report No. 74CRD067, March 1974
- (11) S. Prochazka, R. M. Scanlan: The Effect of Boron and Carbon on Sintering of SiC, GE Report No. 74CRD226, 1974
- (12) S. Prochazka: The Role of Boron and Carbon in the Sintering of Silicon Carbide, Special Ceramics 6 (1974) 171-181; "Mass Transport Phenomena in Ceramics", Mat. Sci. Res. 9, S. 421-431, Plenum Press New York (1975)
- (13) S. Prochazka, R. M. Scanlan: Effect of Boron and Carbon on Sintering of SiC, J. Amer. Ceram. Soc. 58 (1975) 72
- (14) W. Böcker, H. Landfermann, H. Hausner: Sintering of Alpha Silicon Carbide with Additions of Aluminum Powder Met. Intern. 11 (1979) 2, 83-85
- (15) W. Böcker, H. Hausner: The Influence of Boron and Carbon Additions on the Microstructure of Sintered Alpha Silicon Carbide, Powder Met. Intern. 10 (1978) 87-89
- (16) K. A. Schwetz, A. Lipp: Herstellung und Eigenschaften ultrafeiner β -SiC-Sinterpulver, Radex-Rundschau 2 (1978) 489-498
- (17) F. F. Lange, T. K. Gupta: Sintering of SiC with Boron Compounds, J. Amer. Ceram. Soc. 59 (1976) 537-538; Contr. Nr. N00014-74-C-0284, 1976
- (18) G. Leimer, E. Gugel, A. Novotny, H. Hausner, W. Böcker: Sintern von Siliziumcarbid, BMFT-Statusseminar, Bad Neuenahr, 1978, 251-281
- (19) S. Prochazka: Abnormal Grain Growth in Polycrystalline SiC, Intern. Conference on SiC, Miami, Florida, 1973
- (20) R. A. Giddings, C. A. Johnson, S. Prochazka, R. J. Charles: Fabrication and Properties of Sintered Silicon Carbide, GE Report No. 75CRD060, 1975
- (21) W. Böcker, H. Hausner: Observations on the Sintering Characteristics of Submicron Silicon Carbide Powders, Science of Ceramics 9 (1977) 168-175
- (22) H. Hausner: Pressureless sintering of non-oxide ceramics, 4th CIMTEC, Energy and Ceramics, St. Vincent, Italy, 1979
- (23) E. H. Kraft, J. A. Coppola: Thermo-Mechanical Properties of Sintered Alpha Silicon Carbide, "Ceramics for High Performance Applications II", Newport, Rhode Island, 1977
- (24) E. H. Kraft, R. H. Smoak: Crack Propagation in Sintered Alpha Silicon Carbide, Fall Meeting Amer. Ceram. Soc., Hyannis, Mass. 1977
- (25) E. H. Kraft, G. J. Doohar: Mechanical Response of High Performance Silicon Carbides, Second Intern. Conference of Mechanical Behavior of Materials, Boston, Mass. 1976
- (26) R. H. Smoak, E. H. Kraft: Sintered Alpha Silicon Carbide: Some Aspects of the Microstructure-Strength Relationship, Fall Meeting Amer. Ceram. Soc., Hyannis, Mass. 1977
- (27) R. H. Smoak, R. S. Storm: Iterative Development on Injection Molded Sintered Alpha SiC Turbine Material, ASME, San Diego 79-GT-77 (1979)
- (28) Y. Murata, R. H. Smoak: Densification of Silicon Carbide by the Addition of BN and B_4C and Correlation of their Solid Solubilities, Intern. Symposium of Factors in Densification and Sintering of Oxides and Non-Oxide Ceramics, Hakone, Japan, 1978
- (29) K. A. Schwetz, A. Lipp: The effect of boron and aluminium sintering additives on the properties of dense sintered alpha silicon carbide, Science of Ceramics 10, Berchtesgaden, 1979
- (30) H. Hausner, W. Böcker: Herstellung von sinteraktiven SiC-Pulvern, BMFT 01ZC026-ZA/NT/NTS1005 4. Sachbericht, 1978
- (31) C. D. Greskovich, S. Prochazka, J. H. Rosolowski: The Sintering Behaviour of Covalent Bonded Materials, GE Report 76CRD216 (1976) and Nitrogen Ceramics (ed. F.L. Riley), Nordhoff Leyden, (1977) 351-357
- (32) F. Thummler: Sintering and High Temperature Properties of Si_3N_4 and SiC, "Sintering and Related Phenomena", Notre Dame, In. 1979
- (33) S. Prochazka: Investigation of Ceramics for High Temperature Turbine Vanes, Final Report, General Electric Co. SRD-72-171 (1972)
- (34) E. Gugel: SiC als feuerfester Hochleistungswerkstoff, Vortrag Dt. Keram. Ges. Bezirksgruppe Bayern, Rödental 1978
- (35) R. A. Alliegro, L. B. Coffin, J. R. Tinklepaugh: Pressure-Sintered Silicon Carbide, J. Amer. Ceram. Soc. 59 (1976), 386-389
- (36) J. M. Bind, J. K. Biggers: Hot-Pressing of Silicon Carbide with 1 % Boron Carbide Addition, J. Amer. Ceram. Soc. 58 (1975) 304-306
- (37) F. F. Lange: Fabrication and Properties of Silicon Compounds, Westinghouse Res. Lab. Final Report 73-904-SERAM-R1, 1973

- (38) H. E. Helms: Ceramics for Truck and Bus Gas Turbine Engines, 6. AMMRC Conference "Ceramics for High Performance Applications III Reliability", Orcas Island 1979
- (39) W. S. Coblenz: Elastic Moduli of Boron-Doped Silicon Carbide, Amer. Ceram. Soc. J. 58 (1975) S. 530-531
- (40) H. Abe, R. C. Bradd: Effect of Additions of Coarse Grains and Fibers on the Densification of a Sinterable SiC, Amer. Ceram. Soc. J. 58 (1975) S. 525
- (41) D. C. Larsen, G. C. Walther: Property Screening and Evaluation of Ceramic Turbine Engine Materials, IIT Research Institute Chicago, Ill. 1978, Semiannual Interim Technical Report No. 6 Contract F33615-75-C-5196
- (42) W. D. Carruthers: 3500 hour durability testing of commercial ceramic materials, Proc. of Highway Vehicle Systems, Dearborn (1978) 267-277
- (43) Y. Hamano: Sintered Silicon Carbide, 6. AMMRC Conference "Ceramics for High Performance Applications II Reliability" Orcas Island 1979
- (44) J. A. Coppola: Processing of Silicon Carbide Components, 6. AMMRC Conference "Ceramics for High Performance Applications III Reliability" Orcas Island 1979
- (45) E. H. Kraft: Silicon Carbide for DOE/NASA Sponsored Vehicular Gas Turbine Programs, Proc. Highway Vehicle Systems 1978, 236-247
- (46) A. Novotny, E. Gugel, G. Leimer: Schlickergegossene Gasturbinenbauteile aus Siliziumnitrid und Siliziumkarbid, BMFT-Statusseminar, Bad Neuenahr, 1978, 161-181
- (47) R. H. Smoak, R. S. Storm: Iterative Development of Injection Molded Sintered Alpha SiC Turbine Material, ASME, San Diego 79-GT-77 (1979)
- (48) P. Khandelwal, P. W. Heitmann: Characterization of Ceramic Component Materials, 6. AMMRC Conference "Ceramics for High Performance Applications III Reliability" Orcas Island 1979
- (49) H. E. Helms: Ceramic Applications in Turbine Engines, ASME, San Diego 79-GT-75 (1979)
- (50) R. C. Phoenix: Design and Performance Experience of Silicon Carbide Piston Engine Components, 6. AMMRC Conference "Ceramics for High Performance Applications III Reliability" Orcas Island 1979
- (51) R. M. Cannon, U. Chowdhry, D. C. Cranmer: Microstructure Control in SiC, Proc. Workshop on Ceramics for Advanced Engines, Orlando, Fla. 1977, 175-181
- (52) D. M. Kotchick: High-Temperature Mechanical Properties of Sintered Alpha Silicon Carbide, Contract N00014-76-C-0249, 1978
- (53) A. G. Evans, F. F. Lange: Crack propagation and fracture in silicon carbide, Journal of Mat. Science 10 (1975) 1659-1664

German Patent Applications

- (54) OS 23 57 217, 1973, General Electric, USA
- (55) OS 24 49 662, 1974, General Electric, USA
- (56) OS 26 24 641, 1976, Carborundum Company, USA
- (57) OS 26 27 856, 1976, General Electric, USA
- (58) OS 27 34 425, 1977, General Electric, USA
- (59) OS 27 36 073, 1977, Kyoto Ceramic K. K., Japan
- (60) OS 27 37 521, 1977, Nippon Crucible Co. Ltd., Japan
- (61) OS 27 44 636, 1977, W. Böcker, Berlin
- (62) OS 27 51 769, 1977, Carborundum Company, USA
- (63) OS 27 51 827, 1977, Carborundum Company, USA
- (64) OS 27 51 851, 1978, Carborundum Company, USA
- (65) OS 27 56 168, 1978, PPG Industries, Inc., USA
- (66) OS 28 03 658, 1978, Kyoto Ceramic K. K., Japan
- (67) OS 28 13 665, 1978, Carborundum Company, USA
- (68) OS 28 13 666, 1978, Carborundum Company, USA
- (69) OS 28 48 452, 1978, NGK Insulators Ltd., Japan
- (70) OS 28 54 612, 1977, Carborundum Company, USA

US Patent Applications

- (71) US Patent 39 93 602, 1976, General Electric, USA
- (72) US Patent 40 31 178, 1976, General Electric, USA
- (73) US Patent 40 41 117, 1976, General Electric, USA
- (74) US Patent 40 80 415, 1976, Carborundum Company, USA
- (75) US Patent 41 23 286, 1976, Carborundum Company, USA
- (76) US Patent 41 24 667, 1977, Carborundum Company, USA
- (77) US Patent 30 85 863, 1960, General Electric, USA
- (78) US Patent 38 52 099, 1972, General Electric, USA
- (79) US Patent 39 54 483, 1974, General Electric, USA
- (80) US Patent 39 68 194, 1975, General Electric, USA

Other Literature on Silicon Carbide

- (81) P. T. B. Shaffer: The Phases in the System SiC-B₄C-C, Mat. Res. Bull. 4 (1969), 213
- (82) Y. A. Vodakohov, K. N. Mokhov: Diffusion and Solubility of Impurities in SiC, Proc. of the Third International Conference on Silicon Carbide, Miami, Fla. 1973
- (83) A. B. Kalinina, M. I. Sokhor, F. I. Shamrai: Silicon-Boron-Carbon System Compositions, Izv. Akad. Nauk SSSR, Neorg. Mater., 7 (1971) 5, 778-785
- (84) V. P. Novikov, V. I. Vigdorovich, A. I. Krestovnikov, Izv. Akad. Nauk SSSR, Neorg. Mater., 4 (1968) 502
- (85) G. A. Meerson, L. A. Nisel'son, Chou Chu-ming, Izv. Akad. Nauk. SSSR, Metallurgiyai Gornoe Delo, No 1 (1964) 67
- (86) R. Kieffer, P. Ettmayer, E. Gugel, A. Schmidt: Phase Stability of Silicon Carbide in the Ternary System Si-C-N, Met. Res. Bull. 4 (1969) SiC Issue, 153-166
- (87) L. Pauling: The Nature of Chemical Bond, 3rd. ed. (Cornell, 1960)
- (88) R. N. Ghoshtagore, R. L. Coble: Self Diffusion in Silicon Carbide, Phys. Rev. 143 (1966)

- (89) J. D. Hong, M. H. Hon, R. F. Davis: Self diffusion in α - and β -silicon Carbide, 4th CIMTEC, Energy and Ceramics, St. Vincent, Italy, 1979
- (90) R. L. Coble, T. K. Gupta: Intermediate Stages of Sintering, in Sintering and Related Phenomena, G. C. Kuczinski ed. Gordon and Breach (1967)
- (91) W. F. Knippenberg: Growth Phenomena in SiC, Philipp Res. Repts. 18 (1963) 161
- (92) C. E. Hoge, J. A. Pask: Thermodynamics of Solid State Sintering, III. Intern. Meeting on Sintering, Herceg Novy, 1973
- (93) R. Kieffer, E. Gugel, G. Leimer, P. Ettmayer: Investigations on the System Boron-Carbon-Silicon, Ber. Dt. Keram. Ges. 49 (1972) 41-46
- (94) E. Gugel: Net-Shape Processing of Non-oxide Ceramics, AGARD-CP-256, 1978

Literature	20, 29, 41, 53	2, 23, 24, 25, 41	43
Phase	β	α	(α)
Bulk density (Theor. density = 3.20) [g/cm ³]	3.04 - 3.08	3.14 - 3.18	3.1
Hardness	-	2600 Hnoop	941 HKA
Flexural strength [N/mm ²]	(3 pt) - (4 pt)	(3 pt) - (4 pt)	(7 pt)
20°C	560 - 440	410 - 330 - 460	500
1000°C	560 - 530	470 - 385 - 440	500
1400°C	540 -	540 - 430	500
1500°C	520 - 440	- 405	-
(Ar) 1650°C	- -	560 - 495	-
Weibull modulus m	9 - 10	8 - 14	-
K_{IC} [MPa/m ^{1/2}]	20°C	3.6 - 4.6	3.5
1000°C	3.2	4.0 - 6.8	3.5
1400°C	3.4	-	4.8
1600°C	-	8.8	-
Young's modulus [N/mm ²] $\cdot 10^{-3}$	20°C	417	385 - 416
1000°C	389	378 - 390	-
1400°C	382	382	-
Shear modulus [N/mm ²] $\cdot 10^{-3}$	20°C	-	178 - 182
1000°C	-	-	169
Poisson's ratio	20°C	0.165	0.14
1000°C	-	-	0.12
Thermal expansion on 20 - 700°C [$\mu\text{m/m} \cdot 10^{-3}$]	4.8	4.02	3.5
40 - 800°C	-	-	-
700 - 2000°C	5.3	4.8 - 5.32	-
Thermal conductivity [cal/cm sec °C]	20°C	2.08 - 0.217	0.145
400°C	-	0.117	0.105
600°C	-	0.118 - 0.120	0.095
800°C	-	-	0.110
Specific heat [cal/g °C]	20°C	-	0.160
200°C	-	-	0.220
600°C	-	-	0.252
1500°C	-	-	0.334

Table I:

Properties of sintered SiC

Table II:

SiC-materials with different binders

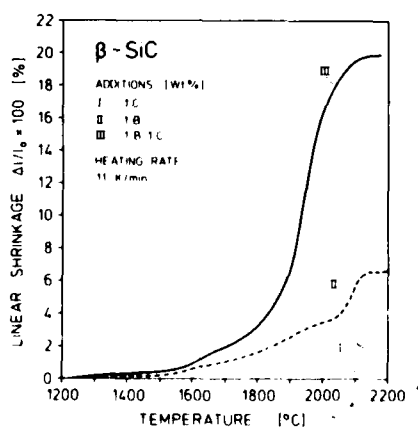
Binder		SiC-content [%]	Bulk density [g/cm ³]	Flexural strength [N/mm ²]	
Additive	in the produkt			20°C	1400°C
Clay, silicates	Silicates, minerals, glass	≤ 95	≤ 2.6	30	15
Oxides	" "	≤ 95	≤ 2.6	30	20
Silicon	Si_3N_4 , Si_2ON_2	≤ 90	≤ 2.6	40	30
Self-bonding	Recrystallized	100	2.5 - 2.6	100	100
	Reaction bonded	100	2.5 - 2.7	250	250
	Recrystallized Reaction bonded } + Si	80 - 90	3.0 - 3.1	400	200
	Sintered	> 99	3.1 - 3.2	450	450
	Hot pressed	> 99	3.2	600	550

Annawerk
CERANOX

SiC-materials with different binders

Dr. G. V. 79
J. 7934.4

Fig. 1:

Densification of β -SiC
Influence of boron and carbon

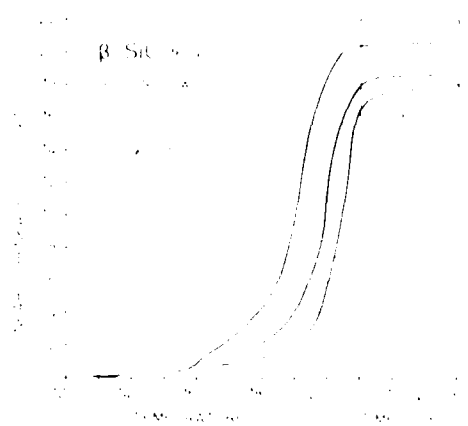


Fig. 23
Densification of B-SiC
Influence of various boron compounds



Fig. 24
Densification of B-SiC
Linear shrinkage rate and influence of
various boron compounds



Fig. 25
Microstructure of fine grained sintered B-SiC, 1900°C, length 1.00 per



Fig. 26
Microstructure of fine grained sintered B-SiC, 1900°C, length 1.00 per



Fig. 6:
Microstructure of sintered α -SiC, 2050 °C, length 220 μ m

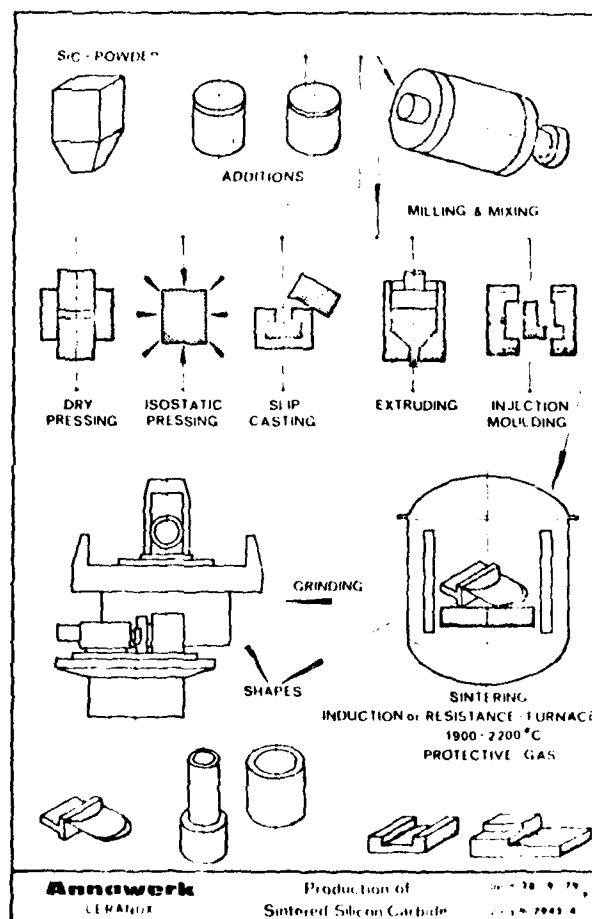


Fig. 7:
Production of sintered SiC

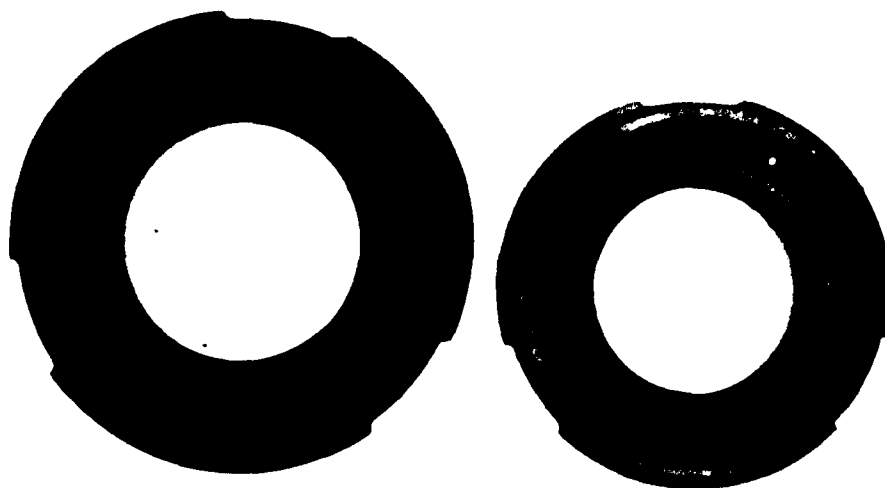


Fig. 8:
Stator vane of sintered SiC

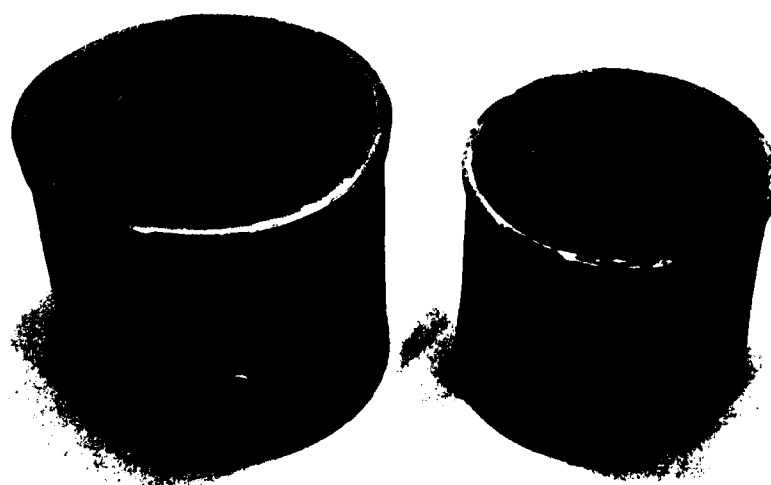


Fig. 9:
Burning chamber of sintered SiC

HIP SILICON NITRIDE

by

Hans T. Larker

Manager, High Pressure Laboratory

ASEA AB

S-915 00 Robertsfors

Sweden

SUMMARY

Hot isostatic pressing (HIP) is being developed as a manufacturing process for intricately shaped fully dense silicon nitride parts e.g. integrated turbine wheels. The process promises to combine the most attractive features of both the reaction bonding (the easy shaping possibilities and good creep strength) and the hot pressing processes (the high strength and low specific surface area). An encapsulation system compatible with silicon nitride under the HIP conditions has been developed. Hubs with protruding blades and airfoils with trailing edges as thin as 0.3 mm have been made. It is considered feasible to develop the process to high production and to attractive processing costs.

INTRODUCTION

Hot Isostatic Pressing (HIP) is a pressure assisted sintering process. It could be considered as a combination of two older concepts in powder technology, uniaxial hot pressing and cold isostatic pressing. The former is a well known method to make high density and strong silicon nitride material and the latter is often used for making shaped preforms of silicon powder for subsequent nitriding to reaction bonded silicon nitride parts.

ASEA has applied HIP to silicon nitride powder and a new process principle gives accurately shaped products of virtually pore free material. The process is adaptable for mechanized high volume production.

HOT ISOSTATIC PRESSING

In hot isostatic pressing a gas at a pressure of typically 100-300 MPa, acts via a gas impermeable membrane on a mass of powder during its sintering. As the pressure acts three-dimensionally die friction problems in conventional hot pressing are eliminated as well as directionality in the properties of the pressed product. The powder mass is hermetically enclosed throughout the pressing process and atmospheric contamination, as well as loss of volatile components of the powder mass, is avoided. The only limitation of shape is in principle that all surfaces must be accessible to the high pressure gas. The size of the parts to be made are limited only by the size of the high pressure equipment. Typically up to an order of magnitude higher pressure, than typical for uniaxial hot pressing in graphite tools, can readily be used in HIP. The equipment used, a so called hot isostatic press, has a pressure vessel which is kept at low temperature at all times. The temperature of the work zone is controlled by an electrically heated furnace with temperature control placed inside the pressure vessel. The furnace thus operates in the high pressure medium usually argon gas and the insulation is of a special design to control the very strong tendency to self convection in this gas, due to its very high density but low viscosity under operating conditions.

HIP equipments are since the beginning of this decade being used industrially on a larger scale for e.g. cemented carbide products, high speed tool steels and super alloys. Figure 1 shows the interior of a large bottom loaded hot isostatic press for manufacture of gas turbine parts of super alloys. Internal diameter for the work piece is 1.2 m, the height 1.5 m, max pressure 140 MPa and max temperature 1260°C. Preheating furnaces of bell type are in this case used for preheating of the charge which is then transferred to the hot isostatic press, resting on the furnace bottom insulation.

A large number of parts can be pressed simultaneously as figure 2 demonstrates. In this case cemented carbide parts are lowered into a top loaded hot isostatic press with 1400°C temperature capability.

NEW ASEA PROCESS FOR PRECISION PARTS

The ASEA process differs from what is common in other techniques for hot isostatic pressing of shaped parts. Usually a shaped container of metal or glass is filled with powder. The internal shape of the container is initially directing the shape of the pressed body. Distortion of the shape is however a problem because the container wall, which is of dense material from the beginning, must be plastically deformed in such a way that its surface decreases and its thickness increases. The resistance of the container wall to this defor-

mation results in distortion such that the total surface of the part pressed from powder will be larger than if no distortion took place.

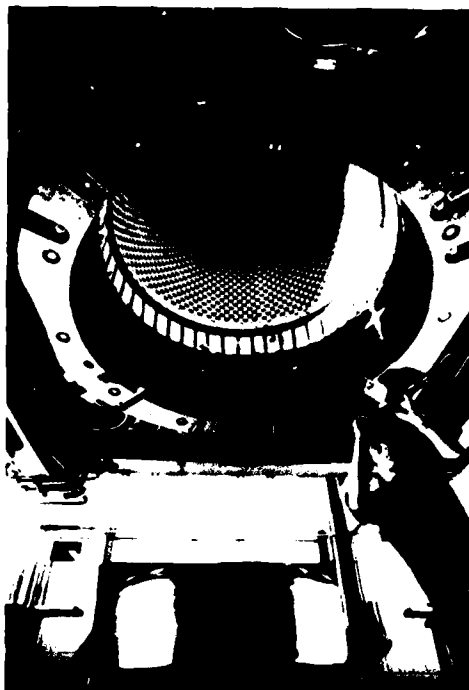


Fig. 1. Interior of large bottom loaded hot isostatic press with hot charging and decharging capability.



Fig. 2. Number of cemented carbide parts on a charging fixture being lowered into a top loaded hot isostatic press.

In the new process, particularly developed for silicon nitride, the shape and precision of the finished part is determined by a green body of silicon nitride powder, not by a container, figure 3. Such a shaped green body is surrounded by an envelope of glass which is evacuated and sealed before pressure is applied. As this envelope has no shaping function, it can be made very resilient.

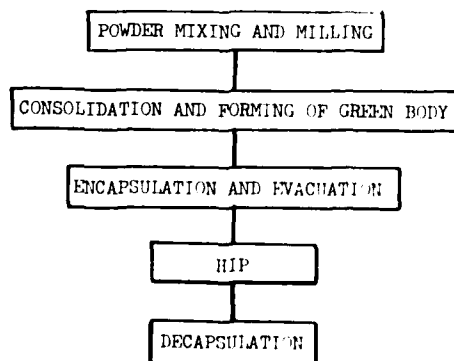


Fig. 3. The generic ASHA process for shaped silicon nitride parts.

One way of utilizing this principle is enclosing a cold isostatically pressed and machined body of silicon nitride powder in an ampoule of high silica glass (1). The ampoule is heated to a soft state before applying the pressure. It then folds over and conforms to the shape of the green powder body, figure 4. After HIP processing at predetermined temperature and pressure the part is cooled down and the glass which is not removed during the process is taken off by sand blasting. Accurately shaped parts with good surface finish can be made with this simple technique but the process is not really suited for mass production purposes.

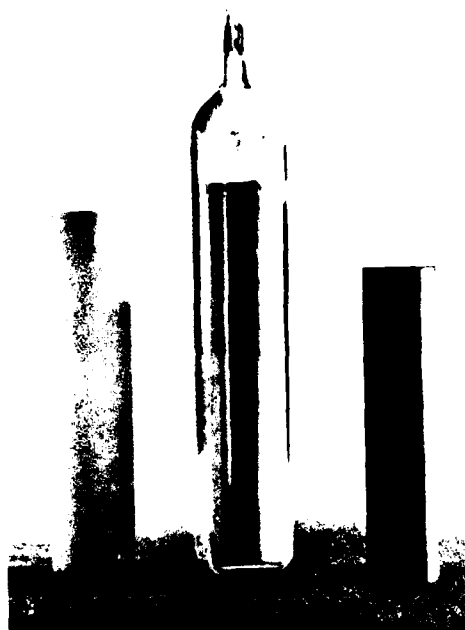


Fig. 4. Realization of the ASEA process using a glass ampoule for encapsulation. Machined green body, encapsulated green body, final dense HIP silicon nitride (left to right).

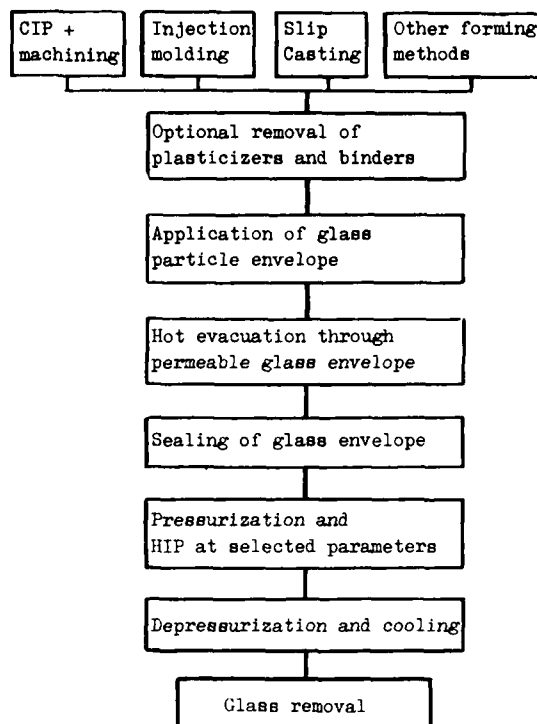


Fig. 5. Principle of improved realization of the ASEA process.

That is however a further development and figure 5 shows the principle for this improved HIP process for accurately shaped and dense silicon nitride. The forming in the green state can be made by any appropriate method and the technique will be depending on the requirements of the product and in what quantities it will be made. The accuracy of the shape of the green body as well as the reproducibility of the density distribution through the body will be important for the precision of the finished part. The requirements of mechanical strength of the green body are modest and determined by what is needed for transfer of the products. A glass particle envelope is applied and the part then passes through a hot evacuation step which is carried out through the still porous and permeable glass envelope. After this the temperature is raised further to seal the glass envelope. Gas pressure and temperature are then increased to the selected pressure and temperature. After a hold time needed for full densification the pressure and temperature are decreased. A special processing during the cooling down helps removing the glass envelope but sand blasting is used for the final cleaning of the products.

Figure 6 shows as-HIPed and cleaned hubs with blades and an airfoil.

The surface finish of the produced parts is dependent on powder grain size and green forming methods but a surface finish of $Ra\ 1\ \mu m$ is readily obtained. The tolerances of the finished product are highly dependent on the reproducibility of the green forming method. With cold isostatic pressing and machining a reproducibility of better than $.1\ mm$ in $100\ mm$ diameter has been obtained. It should be pointed out that it is not a requirement for good shape precision that the green body density must be exactly the same throughout the green body. The requirement is rather that it should be the same from part to part. Experience from injection molding indicates that adequate precision might be obtained for most purposes also with this technique.

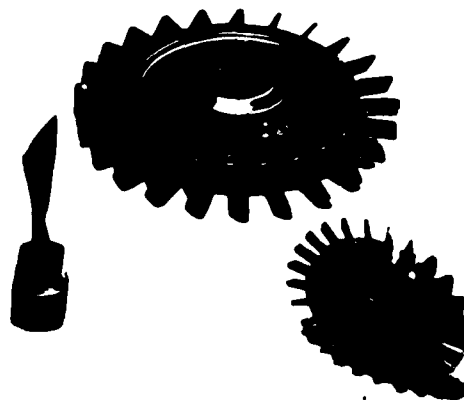


Fig. 6. Dense as-HIPed and cleaned silicon nitride parts made by the process shown in fig. 5. One of the hubs with blades is $\varnothing\ 104$ and $\varnothing\ 52\ mm$.

The glass particle technique allows for sharp edges and corners to be made and small air foils with trailing edges as thin as .3 mm has not presented any problems. Figure 7 shows a hub with airfoils in as-HIPed and cleaned condition. The mechanical properties of the surface of the as-HIPed material appears to be at least comparable to the bulk material. The strength when in transverse bending tests with the tensile stress in the HIPed surface in many cases gives a higher strength level than obtained with normally diamond cut and ground test bars.



Fig. 7. As-HIPed and cleaned hub with airfoils (ϕ 112 mm).

MATERIAL PROPERTIES

The material properties of as-HIPed products are of course highly dependent on the properties of the starting material. In parallel tests on the same powder preparation the same strength was obtained with HIP as the strength in the strong direction of uniaxially hot pressed material. HIP however produces material with fully isotropic mechanical properties. With good starting powders high values of the Weibull modulus, m , are obtained and this has a large effect on the design stress allowable.

The pressure level which is used, roughly one order of magnitude higher than in uniaxial hot pressing, as well as the three-dimensional way of application of pressure which minimizes internal friction, makes it possible to keep the quantity of additives to a minimum. As is reported in studies on very pure silicon nitride (2) the intrinsic properties of silicon nitride are regarding high temperature strength and creep as well as oxidation resistance very much higher than is common for to-days hot pressed material. The HIP process facilitates the development towards materials with low content of foreign material.

PROCESSING COSTS

The process is adaptable for large scale production. After the green forming process, e.g. injection molding, and placing the objects on a support structure, a line production with a minimum of manual handling can be utilized. Production cost estimates indicate that an acceptable level can be achieved for parts like integrated turbine wheels with blades for passenger car gas turbines.

CONCLUDING REMARKS

The ASEA hot isostatic pressing process for silicon nitride has now been developed to a level where good green powder bodies of complicated shape in a reproduceable manner can be processed to dense, accurately shaped parts. The process offers good possibilities for an improvement of material properties by reduction of the amount of foreign elements. It is judged feasible to develop the process to high production and to attractive processing costs.

REFERENCES

1. H. Larker, J. Adlerborn and H. Bohman, "Fabricating of Dense Silicon Nitride Parts by Hot Isostatic Pressing", SAE Technical Paper No 770335 (1977).
2. C. Greskovich, J. H. Rosolowski, S. Prochazka, 1975 "Ceramic sintering" Final Report SRD-75-064, General Electric Corp. R and D.

NONDESTRUCTIVE FAILURE PREDICTION IN CERAMICS

by

A. G. Evans

Materials Science and Mineral Engineering
University of California
Hearst Mining Building
Berkeley, CA 94720

SUMMARY

The prediction of failure of a ceramic component can be made using non-destructive methods for detecting and characterizing the fracture critical defects. The accept, reject decision based on the non-destructive measurement requires a probabilistic analysis of both the measurement and fracture processes. The fundamental probabilistic approach and several specific NDE methods are described in this paper.

INTRODUCTION

Several unique properties of ceramics are presently being exploited in structural applications. Specifically, their good high temperature strength and oxidation (corrosion) resistance has engendered considerable interest in ceramic energy conversion systems (turbines, heat exchangers), while their high hardness renders them uniquely applicable to bearings, valves, etc. One of the primary problems associated with the structural application of such brittle materials is their wide fracture strength variability. In consequence, effective failure prediction techniques are a prerequisite to the reliable use of ceramics in structural applications.

The prediction of failure in structural ceramics can, in principle, be achieved using a number of independent techniques. The most extensively developed are the direct defect detection techniques (x-radiography, penetrants, and ultrasonics) and the flaw strength characterization techniques (overload proof testing and statistical analysis). Many other methods are available as possible (but less likely) failure prediction candidates; some of these are based on quite independent physical phenomena, e.g., acoustic emission, exoelectron emission, while others are alternate methods of visualizing similar physical effects, e.g., acoustic holography. All of the available techniques have limitations when applied to ceramic systems, and one method is unlikely to merge as the universal failure prediction approach. The pertinent method will probably depend on the component geometry, the in-service stress state, and the material microstructure. Also, several independent techniques may be required to assure the structural integrity of a given component, without the excessive rejection of satisfactory parts.

In this review, an approach for nondestructive failure prediction in ceramic systems is developed, to provide a basis for assessing the capabilities of the potential failure prediction approaches. Then, the merits and limitations of the principal available techniques for failure prediction are reviewed.

ACCEPT/REJECT CRITERIA

The fracture of ceramics generally occurs by the direct extension of small cracks in the vicinity of pre-existing defects; these defects include large pores, inclusions and large grains (frequently as sites for machining flaws). The fracture condition is not, in general, related uniquely to the defect dimensions. A probability of fracture $\phi(\sigma/a, b, c)$ must, therefore, be assigned to a defect of given size (with three principal dimensions, a, b, c) for a specific level of applied stress σ in the volume element containing the defect.

The nondestructive capability for determining the dimensions of a defect depends on the inspection method; invariably, an error is associated with the estimate of these dimensions. The magnitude of the error and its specific form are sensitively dependent on the method of inspection. In general, there will be a specific probability, e.g., $\phi(a_{es}/a)$, for each technique that the estimated defect dimensions (a_{es}, b_{es}, c_{es}) will be in a certain size range, given the actual defect dimensions (a, b, c).

We have thus far identified two probabilities: one concerning the fracture probability for a defect of given dimensions, the other concerning the nondestructive estimate of the defect dimensions. However, a third probability is also needed to complete the reliability analysis; namely, the probability that a defect in a given size range will exist in the volume of the component being inspected, $\phi(a)$. This probability is estimated by metallographic studies on samples taken from each batch of material.

The product of these three probabilities can be integrated to various inspection levels, a_{es} , to obtain two interrelated probabilities: the false-accept probability ϕ_A and the false-reject probability ϕ_R (Fig. 1a):

$$\phi_A = \int_0^{\sigma_A} \int_0^{a_{es}^*} \int_0^{\infty} \left[\phi(\sigma_{\infty}^C/a) d\sigma_{\infty} \right] \left[\phi(a_{es}/a) da_{es} \right] \left[\phi(a) da \right] \quad (1)$$

$$\phi_R = \int_{\sigma_A}^{\infty} \int_{a_{es}^*}^{\infty} \int_0^{\infty} \left[\phi(\sigma_{\infty}^C/a) d\sigma_{\infty} \right] \left[\phi(a_{es}/a) da_{es} \right] \left[\phi(a) da \right]$$

where σ_A is the level of the applied tension in the volume element containing the defect. The inspection level a_{es}^* refers to the defect dimension(s), as estimated by the inspection technique, that is selected for the rejection or acceptance of the component, e.g., all components with an estimated maximum dimension less than a_{es}^* are accepted and all components with an estimated dimension greater than a_{es}^* are rejected. The false-accept probability ϕ_A is thus the probability that components that have been accepted, in accord with the specified inspection level, will contain defects more severe than indicated by the estimate, and will actually fail in service, i.e., related to the failure probability this probability decreases, of course, as the inspection level decreases (Fig. 1a). The false-reject probability ϕ_R is the (related) probability that rejected components would, in fact, have performed satisfactorily in service, because the defect severity has been overestimated by the selected inspection level. This probability increases as a_{es}^* decreases (Fig. 1a). However, it is crucial to recognize that these probabilities are interrelated, i.e., they merely represent different ranges of integration of the same combination of probability functions (Eq. 1). This interdependence is exemplified in Fig. 1b, which is a typical plot relating the false-accept and false-reject probabilities - once one of these probabilities has been selected, the other probability as well as the associated inspection level are necessarily defined. It is now apparent from Fig. 1b that the inspection technique, or combination of techniques, that would be preferred is that which yields a curve as close as possible to the probability axes. For example, in Fig. 1b, technique B is preferred over technique A, because the rejection of satisfactory components required to satisfy the failure probability requirements is much lower. Such curves thus represent a quantitative method for characterizing the failure prediction capabilities of various inspection techniques, for a given material and service condition. However, the generation of these curves represents a major experimental effort, and the information presently available is limited. The present status and imminent developments are examined in subsequent sections. It is hoped that all future studies will be directed toward the development of false-accept, false-reject curves, to enable a quantitative framework for failure prediction in structural ceramics to be constructed.

FAILURE MODELS

The fracture process in a ceramic depends specifically on the material and the defect responsible for fracture. In most materials, surface cracks introduced by machining are a consistent source of failure. This failure mechanism is particularly prevalent in dense, coarse grained materials. Inclusions introduced during fabrication are another prominent origin of failure, particularly in dense, fine grained materials (for which failure from surface cracks is less dominant). Individual large pores, or a concentrated array of fine pores, are another frequently observed source of failure, particularly in sintered materials. Finally, surface cracks introduced by post fabrication, environmental interaction phenomena can be important, i.e., cracks introduced by projectile impact, contact stresses, etc., or cracks formed by oxidation.

Probabilistic information concerning these failure processes is limited. The most extensive information is available for hot pressed silicon nitride. This material is thus used as an example of the probabilistic treatment of failure. However, it is re-emphasized that the failure model can be highly specific, both to the host material and the defect type. Therefore, the models described should only be extended to other materials/defects with considerable caution.

Surface Cracks

The surface crack has been the subject of extensive recent analysis. In consequence, the stress intensity factor distribution is now relatively well comprehended for semi-circular cracks normal to the surface (Fig. 2) and reasonably well-characterized for normal semi-elliptical cracks. The equivalent solutions for cracks at other inclinations to the surface are not known in detail; although reasonable estimates can be based on results for contained elliptical cracks.

One possible model of fracture from surface cracks considers that fracture occurs when the peak value of the stress intensity factor reaches the local toughness of the material, K_C , yielding;

$$\sigma_f = Z(a/c, \theta) K_c a^{-1/2} \quad (2)$$

where σ_f is the fracture stress measured in the absence of slow crack growth, a and c are the two principal dimensions of the crack, θ is its inclination to the surface, and Z is the analytically determined stress intensity function. For this model, the variability in the fracture stress is attributed exclusively to variations in the local toughness: distributions in σ_f ($\phi(\sigma_f | a, c, \theta)$) pertinent to such variability are likely to be Gaussian. However, sub-critical extension of the crack in a region of high local stress intensity factor (Fig. 2) may precede final fracture. Then, there may be systematic trends in the fracture stress with a/c and θ . Probability functions that neglect these possible trends will exhibit a wider and less characteristic distribution than those that take these effects into account. The details of the fracture model thus constitutes an important part of the reliability analysis.

Specific probability functions for surface cracks have not yet been obtained, largely because of the difficulty in distinguishing the profile of the fracture initiating crack on the fracture surface. A viable solution to this difficulty has not yet been identified. Some useful information can be obtained by introducing well-defined cracks using the Knoop indentation technique (Fig. 3). However, this method samples only the variability in the fracture toughness. Much additional work is needed in this area.

Voids

Fracture from isolated voids in ceramics has been analyzed using several models. The model which accounts most effectively for the observed trends with void size is a statistical model, which considers that fracture occurs by the activation of a distribution of flaws that pre-exist in the vicinity of the void (Fig. 1). The most likely fracture initiating flaws are microcracks associated with grain boundary cusps on the void surface (small inclusions near the void are an alternate possibility). Analyses of both surface and volume distributed flaws have been conducted by considering a flaw strength distribution of the type

$$g(S) = \lambda (S/S_0)^k \quad (3)$$

where $g(s)ds$ is the number of flaws in the unit area (volume) with a strength (i.e., extension stress in uniaxial tension) between S and $S+ds$, and λ , S_0 and k are distribution parameters to be determined from the test data. For the surface flaw problem, the analysis encompasses all possible flaw sizes, and yields the general result that the probability of fracture $\phi(\sigma_\infty^C)$ at an applied stress σ_∞^C is given by:

$$\phi(\sigma_\infty^C) = 1 - \exp \left[-8\lambda r^2 \left(\frac{\sigma_\infty^C}{S_0} \right)^k D^k(\alpha) \exp(0.52k - 0.14) \right] \quad (4)$$

where r is the void radius, $\alpha = (1/r)(K_c/S_0)^2$ and $D(\alpha)$ is the function plotted in Fig. 4. For the volume flaw problem, the analysis has only been conducted for flaws very much smaller than the void radius, and is thus restricted in utility. Additional work is needed to extend the analysis into the large flaw regime.

A considerable quantity of fracture data are required to determine the detailed applicability of the surface model vis-a-vis the volume model for a particular material. Sufficient data for this purpose are not presently available. However, the general pertinence of a statistically based model seems to be substantiated by the available data, particularly by the size dependence of the fracture stress at constant probability: other models predict either no size dependence (stress concentration model) or on inverse square root size dependence (crack equivalence models). Values of the distribution parameters can be obtained from the data.

Inclusions

The pertinent inclusion fracture model depends on the specific inclusion. Three types of inclusions in silicon nitride are considered, to illustrate the range of possibilities: silicon, tungsten carbide, and iron silicide. The trends with inclusion size obtained for these inclusions are depicted in Fig. 5. The silicon inclusion has a strong influence on the strength; whereas the effect of the tungsten carbide inclusion is minimal. The need to nondestructively identify the defect type is thus dramatically demonstrated.

Post-fracture inspection of the silicon inclusions indicates that they are dense, i.e., contain little porosity, and exhibit transgranular fracture. These observations, coupled with the low toughness of silicon (0.6 MPa \sqrt{m}), suggest that the silicon inclusions fracture

sub-critically, i.e., without propagating into the much tougher ($5 \text{ MPa}\sqrt{\text{m}}$) silicon nitride matrix. This expectation is verified by acoustic emission studies on stressed samples containing silicon inclusions. Hence, since the elastic properties of silicon are similar to those of silicon nitride, a plausible model of ultimate fracture considers the inclusions as cracks of equivalent dimensions (Fig. 6). Then, the fracture stress is governed by an equation similar to Eq. (2) that contains the appropriate $Z(a/c)$ for an internal crack. A comparison of measured strengths with strengths predicted by the crack equivalence model for an assumed toughness K_{IC} of $5 \text{ MPa}\sqrt{\text{m}}$ is presented in Fig. 6. The variability in the measured fracture stress might be attributed either to a toughness variability or to a combined toughness, sub-critical extension effect. The data are not comprehensive enough to unequivocally separate these possibilities, but it is noted that the ratio of the measured to the predicted strength exhibits a close conformance to a normal distribution. This type of distribution would be anticipated for the toughness when, as in the present case, the crack front samples a large number of silicon nitride grains. The center of this distribution at 0.8 indicates either that the average local toughness is less than the assumed value (4 compared with $5 \text{ MPa}\sqrt{\text{m}}$), or that the crack dimensions at criticality are consistently larger than the inclusion dimensions, because of sub-critical extension phenomena. Finally, note that the important inclusion dimensions are the two dimensions (a,c) normal to the applied tension.

Inspection of the fractured iron silicide inclusions indicates extensive porosity and an irregular fracture surface. A different fracture mechanism might thus pertain. This is verified when the above fracture model is applied to test data; the measured strengths greatly exceed the predicted values and exhibit a diminished dependence on the inclusion size. An alternative model suggested by the fracture morphology is that fracture initiates from the pores within the inclusions, i.e., the inclusion is treated as a porous body subjected to the stress field imposed through the silicon nitride matrix. This stress field is the result of thermal expansion mismatch and the applied stress. For ellipsoidal inclusions, both of these stresses are hydrostatic (equal in all three directions), and the analysis of fracture then becomes a simple statistical problem. Analyzing the porous inclusion using statistical flaw distributions, in the manner described above for fracture from voids, the probability of fracture becomes

$$\phi = 1 - \exp \left[-V \left(\frac{\beta \sigma_{\infty} + \sigma_a}{S_0} \right)^k \right] \quad (5)$$

where V is the volume of the inclusion, σ_a is the thermal mismatch stress and β is the ratio of the applied stress to the stress in the inclusion. Test data analyzed according to this model are plotted in Fig. 7. Reasonable values of the parameters are obtained, indicating that the model has merit. Note, therefore, that the inclusion parameter of interest in this instance is its total volume, V .

The minor effect of tungsten carbide inclusions on the strength derives from both their high toughness and large elastic modulus. The high toughness prevents premature inclusion fracture, while the large modulus confines the zone of tension in the matrix to a small region around the poles of the inclusion. In consequence, the statistical analysis of fracture from this small zone of tension indicates low fracture probabilities at appreciable levels of the applied stress. In qualitative confirmation of these expectations, the fracture of samples containing tungsten carbide inclusions usually occurs from small matrix voids in the vicinity of the poles. There are not yet sufficient fracture data to identify the distribution parameters pertinent to this fracture process; but, tentatively, the fracture probability for these inclusions can be equated to zero, for the stress levels of practical interest, $\leq 300 \text{ MPa}$ (Fig. 5).

DEFECT SIZE ESTIMATION

It is apparent from the fracture models that greatly reduced false-reject probabilities will result if the defect type, as well as its pertinent dimension(s), can be elucidated by the inspection method. This requirement is a vital consideration in the comparison of the various methods of defect determination. This particular problem is not a concern for the indirect failure prediction method, which estimates the defect 'strength'; but other problems are introduced. The indirect methods are thus considered first, followed by a discussion of the direct defect detection methods.

INDIRECT METHODS

Statistical Analysis

The statistical prediction of failure relies on an ability to directly characterize the flaw strength distribution function. The strength distribution function $q(S)dS$ is defined as the number of flaws per unit volume (or unit area for surface flaws) with a strength between S and $S+dS$. For non-interacting flaws, this function is related to the fracture probability $\phi(S)$ by

$$\phi(S) = 1 - \exp \left[- \int_{V_0} dV_0 \int_0^S g(S) dS \right] \quad (6)$$

where V_0 is the sample volume. Recently, a method for obtaining $g(S)$ from fracture data has been devised. A typical example, which applies to tensile tests is

$$g(S) = \xi' / \pi r^2 l \quad (7)$$

where r is the specimen radius, l is the gauge length, and $\xi = -\ln(1-\phi(S))$. Once $g(S)$ has been obtained in this way, within the stress range that exists in the test component, Eq. (6) can be evaluated numerically for any specimen geometry and stress distribution. The constraint that the test data pertinent to low failure probabilities be obtained in the stress range of concern (because extrapolation to low stresses cannot be performed with appreciable confidence) means, for most applications, that extensive tensile data on relatively large samples are required. (By contrast, the low failure probabilities for the direct methods relate primarily to the probability, $\phi(a)da$ (see Eq. 1), which can be determined metallographically.)

The method in its present form has an additional weakness - notably, the requirement that the flaw population be invariant from component to component. Such an invariance is quite unlikely for typical ceramic fabrication processes and hence, high confidence in the predicted fracture probability cannot be achieved. Some independent method for identifying variations in the flaw population is thus required before statistical methods can be realistically applied. Such a possibility has recently been proposed, based on the ultrasonic attenuation α of the component.

Ultrasonic attenuation affords a measure of the large extreme of the microstructure, or of the surface crack population;

$$\alpha(f) = \frac{1}{2} \int_0^\infty \Omega(r, f) g(r) dr \quad (8)$$

where f is the frequency, Ω is the cross section of the scatterer, and $g(r)dr$ is the number of large grains (pores, inclusions, surface cracks) per unit volume (area) in the size range r to $r+dr$. Hence for materials in which fracture is determined by the large extreme of the microstructure (e.g., large pores in reaction bonded silicon nitride and large grains in relatively coarse grained materials), or by surface cracks, $g(r)dr$ is related to the flaw strength distribution $g(S)dS$ through the usual relation

$$S = \frac{K_c}{Y\sqrt{r}} \quad (9)$$

where Y is a parameter that depends on the flaw shape. Hence, an attenuation measurement could define $g(S)dS$ and thereby the fracture probability $\phi(S)$. Variation in the flaw population from component might thus be directly incorporated into the failure prediction. This intriguing possibility is presently being explored.

Overload Proof Testing

The theory of proof testing has been established for several years, but the pertinent experimental evaluation is only now in progress. The present status is as follows. The utility of overload proof testing to eliminate those components that would normally fail during service has been established theoretically and experimentally for proof tests conducted in an ambience that excludes significant slow crack growth during the test. For such conditions the minimum time to failure, t_{min} , is

$$t_{min} = \frac{2}{(n-2)v_0} \left(\frac{K_c}{\sigma_a Y} \right)^2 \left(\frac{K_0}{K_c} \right)^n \left[R^{n-2} - 1 \right] \quad (10)$$

where R is the proof ratio and n , v_0 and K_0 are slow crack growth parameters ($v = v_0(K/K_0)^n$). There is also a well-defined variance of the failure time that depends on the variances in the slow crack growth parameters and the proof ratio. This minimum failure time is realized whenever the stress in each element of the component during the proof test exceeds the service stress (in the equivalent element) by an amount greater than R ; provided that ex-

transverse interface stresses are not developed during unloading and that additional defects are not produced (e.g., by projectile impact and oxidation) during service.

When it is not possible to exclude slow crack growth during the proof test, theory indicates that a minimum unloading time is needed to assure a finite survival time after proof testing. However, even if this minimum is impractical, the theory predicts that the failure probability after proof testing can be many orders of magnitude less than the failure probability without proof testing. This latter effect has been observed, but the failure probability is often larger than the predicted value. This disparity is probably associated with the presence of crack growth instabilities that occur during unloading at stress intensities close to the critical value.

Another restriction of proof testing concerns the practicality of reproducing the in-service stress distribution in the proof test. Except for simple geometries or service environments, a substantial fraction of volume elements in the proof test will experience stress ratios that differ from the ideal value specified by Eq. (10). Those elements for which R is smaller than ideal introduce a false-accept probability, and those for which R is greater than ideal introduces a false-reject probability. Hence, each proof test can be expressed as a false-accept, false-reject curve for comparison with the curves derived for the direct methods. This quantification of proof tests has not yet been implemented, but it is urged that this method of gauging the relative efficacy of a particular proof test design, vis-a-vis the direct nondestructive methods, be adopted as a future requirement.

Direct Methods

A wide range of methods for direct defect detection has been devised (Table I). However, only the ultrasonic and x-ray methods have been sufficiently developed that some of the important issues concerning defect distinction and size characterization can be adequately discussed. The detailed discussion is restricted to these two methods, but this should not be construed to indicate that the other methods, as they develop, will not ultimately play an important role in the overall failure prediction scheme. For example, the ability of microwave methods to detect silicon inclusions might be of great significance in failure prediction in silicon nitride; also, improved penetrant techniques (e.g., dye enhanced x-ray methods) may perhaps find an important niche in surface crack characterization schemes.

X-Radiography

X-radiography is a well-developed technique, and the principles involved in the generation of images from defects are largely understood. A brief statement of these principles allows judgments to be made about the role of X-radiography in ceramic failure prediction. The two image variables are the resolution and the image contrast. The resolution χ is related to the focal spot diameter f , and the distances d_1 , between the focal point and the defect and d_2 , between the defect and film by

$$\chi = f \left(\frac{d_2}{d_1 + d_2} \right) \quad (11)$$

Conventional x-ray equipment utilizes focal spot tubes $> 500\mu\text{m}$ in diameter and hence, for typical dispositions of the source, component and film (as realized for nonsimple component geometries) the maximum resolution ($> 100\mu\text{m}$) is inadequate for most structural ceramic applications. However, refined x-ray systems are capable of achieving much smaller focal spot sizes; in fact, the Cosslett-Nixon type projection instrument (which utilizes electron focussing tubes) is capable of producing spot sizes as small as $\sim 1\mu\text{m}$. Hence, resolution is not a limitation per se to the application of X-radiography to structural ceramics.

The image contrast represents a more serious limitation. The contrast, ΔI , on the film is given by

$$\Delta I = 0.86 \Delta\mu \text{ ay } \rho / \beta \quad (12)$$

where $\Delta\mu$ is the difference in linear absorption coefficient between the defect and the matrix, $2a$ is the defect thickness (in the direction of the beam), γ_D is the x-ray "gamma" of the film and β is a numerical build-up factor. The linear absorption coefficient is primarily determined by the atomic number and density of the material and varies with the energy of the incident x-ray photons. The atomic number/density relation for the elements of the matrix and defect are often very similar; hence, large x-ray absorption differences and vice versa. Certain types of defects will thus be capable of generating significant image contrast in a given matrix material; these defect types can often be predicted from available data. The absorption differential, $\Delta\mu$, for a given defect increases quite rapidly with the x-ray photo energy decreases and hence, to maximize detectability, the minimum energy consistent with a practicable exposure time should be selected. The build-up

factor, β , increases as the sample thickness increases and thus, the component thickness is a variable effecting defect detectability. Finally, since ΔI is directly proportional to the defect thickness a , there will exist a lower limit to the defect size that yields detectable image contrast.

The quantities γ_p and β cannot be effectively predetermined; hence, empirical guidelines on defect detectability must firstly be obtained for typical defect/matrix systems, and then approximate scaling effects can be predicted using Eqn. (12). Preliminary studies on inclusions in silicon nitride indicate that inclusions containing high atomic number elements (e.g., W, Fe) are readily detected using microfocus systems, at the smallest sizes of interest ($\sim 25\mu\text{m}$). The detectability of inclusions with comparable atomic numbers to the matrix, such as Si and SiC, voids and cracks is less satisfactory; although, the detection limits that can be achieved with image enhancement capabilities has yet to be ascertained. Similarly, the ability to distinguish different defect types has yet to be evaluated. Some information is clearly available in the contrast ΔI (Eq. 12), but the extent to which this provides a satisfactory classification remains to be determined. Another difficulty that must be surmounted concerns the ability to obtain the defect dimension normal to the surface. This dimension influences the contrast (Eq. 12), but it is not likely to be separable from the effect of the defect type. Tomographic techniques are a more plausible probability; but again, their efficacy in components of complex shape has yet to be determined.

The nature of the probability function $\phi(a_{\text{es}}|a)$ pertinent to the x-ray method deserves brief mention. Since the method creates an image of the defect, the error is concerned both with the measurement of the dimensions from the image, and the ability to obtain a three-dimensional image. The former represents a random error, and is probably Gaussian; while the latter is a systematic error related to the component geometry and its effect on accessibility of the x-ray beam to the defect. The magnitudes of these errors are presently being evaluated.

Finally, it is instructive to cursorily explore the utility of the x-ray method for failure prediction in hot pressed silicon nitride. If Si inclusions $\geq 800\mu\text{m}$ cannot be discerned, (as the available information suggests) then, since Si inclusions $\geq 150\mu\text{m}$ in diameter are potential critical defects (Fig. 5), it may be concluded that the x-ray method is incapable of estimating the dimensions of certain types of critical defects. The false-accept (or failure) probability for the x-ray method is thus identical to the probability of occurrence of Si inclusions, in the size range ~ 150 to $800\mu\text{m}$. The method has not, therefore, effected a substantial reduction in the false-accept probability, vis-a-vis its value without inspection. This result suggests that future x-ray development pertinent to silicon nitride should be devoted to enhancing the detectability of inclusions of this type.

Ultrasonics

The advances in ultrasonic defect characterization have been appreciable in recent years. It is now apparent that all of the bulk defects and most of the surface defects of concern in ceramics can be detected with the appropriate ultrasonic technique. However, much additional study is needed to determine how well the pertinent defect dimensions and the defect type can be characterized. The requisite defect detectability has been achieved by noting that the amplitude of the ultrasonic wave scattered by the defect increases rapidly as the wavelength λ decreases, to $\sim 2\pi a/\lambda$. Detectability is thus enhanced by selecting frequencies (up to 200 MHz) in excess of those conventionally used for defect detection (up to ~ 20 MHz). It also appears that the acoustic impedance mismatch between the defect and the matrix is sufficient for most defects of interest (especially when the defect contains porosity which reduces its effective impedance) to permit the required detectability.

The background scattering (which often imposes a lower limit on defect detectability) is not a concern for bulk defects of critical size ($\sim 25\mu\text{m}$) in fine-grained polycrystalline ceramics (hot pressed Si_3N_4 , hot pressed and sintered SiC); because the grain boundary scattering is minimal up to 400 MHz. The background is a concern, however, for surface defect detectability. The background in this case is associated with the scattering from arrays of surface cracks introduced by surface grinding. Typical detectability limits are indicated in Fig. 8. On polished surfaces, the smallest cracks that can be introduced ($60\mu\text{m}$ diameter) are easily detected (Fig. 8a); for surfaces ground with $30\mu\text{m}$ diamond particles, the smallest cracks that can be detected are $\sim 80\mu\text{m}$ in diameter; while, for rough ground surfaces, cracks smaller than $\sim 120\mu\text{m}$ cannot be detected.

The specific ultrasonic methods for bulk and surface defects are different, but the principles are the same. Bulk defects are characterized using longitudinal and/or shear waves propagated directly into the component; preferably using a transducer array that permits rapid electronic scanning of components, through a ceramic buffer contoured to match the component. Alternatively, a traversable transducer focused through a liquid metal medium may be employed. Surface cracks are characterized using surface waves, which can be excited on the component using ceramic waveguides and a fluid or polymeric couplant. Additional studies are needed, however, to design optimum transducer configurations.

The ultimate approach for ultrasonic defect characterization in ceramics remains to be developed. However, present knowledge suggests the following sequence. Following an initial rapid scan to determine the location of defects, the defect type will be identified from the characteristics of the scattered signal at high frequencies (100-400 MHz). The signal in the time domain has very characteristic features, as indicated by comparing the

void signal (Fig. 9a) with the signal from a WC inclusion (Fig. 9b). Additionally, the frequency domain (obtained using a fast Fourier transform) contains information characteristic of the defect type. Note, however, that the pertinent information can only be obtained experimentally if the transducer response is subtracted, e.g., using an inverse filter. Finally, the frequency dependence of the scattered amplitude in the long wavelength limit ($\lambda \gg 10a$), i.e., at between approximately 5 and 50 MHz, can be used to provide a unique measure of the volume of the defect (Fig. 10). The scattering model used to obtain this information has been well-substantiated experimentally, at least for defects of regular shape, (viz. generalized ellipsoids, surface cracks). The model indicates that the scattered amplitude A at low frequencies is given by;

$$A = V \eta^2 \omega^2 \quad (13)$$

where ω is the frequency, and η is a parameter that depends on the defect type and shape: for example, η for a spherical void is,

$$\eta = \left[1 + \frac{1+\nu}{7-2\nu} + \frac{10(1-2\nu)}{7-5\nu} \right] \left(\frac{1}{4\pi c_L^2} \right) \quad (14)$$

where ν is Poisson's ratio and c_L is the longitudinal wave velocity in the matrix. Individual defect dimensions (a,b,c) and orientations can also be obtained from long wavelength data, if information is available for the same defect as several (up to 5) scattering angles. The viability of obtaining the quantity of information required to determine individual dimensions has yet to be demonstrated for a practical system.

The error associated with the estimate of the defect volume required for the reliability analysis has not been evaluated in detail for real defects; although the appropriate experiments are now underway. The errors are expected to be: a random error in the amplitude associated with the level of the background (probably Gaussian), a systematic error if the defect type is incorrectly assigned from the high frequency analysis, and an error (probably random in most cases) associated with the unknown orientation of the axes of the defect. These errors combine to yield the required function, $\phi(v_{es}|V)$.

SUMMARY

The general approach for quantitative failure prediction in ceramics using nondestructive methods of defect characterization has been described. The current state of knowledge as it impinges on the quantitative failure prediction issue, has been reviewed. The knowledge is incomplete, but considerable progress has been realized in the last two years toward attaining the requisite information. The next two years should see progress at an equal or more rapid rate, and the emergence of the first quantitative nondestructive failure prediction scheme for ceramics. At that juncture, it will be possible to select the best possible technique, or combination of techniques, pertinent to a specific material and component geometry. Substantial scope for the improvement of existing inspection techniques, and for the introduction of new techniques, will exist at that stage; such advances are to be encouraged, using the quantitative basis for technique comparison developed in this review.

REFERENCES

1. Interdisciplinary Program for Quantitative Flaw Definition, ARPA/AFML Contract F33615-74-C-5180. D.O. Thompson et al.
2. Ultrasonic Attenuation in Ceramics, A. G. Evans, B. R. Tittmann, L. Ahlberg, B. T. Khuri-Yakub and G. S. Kino, J. Appl. Phys. 49 (1978).
3. Failure Prediction in Structural Ceramics, A. G. Evans, G. S. Kino, B. T. Khuri-Yakub and B. R. Tittmann, Materials Eval., April 1977, p. 85.
4. Ultrasonic Detection of Surface Cracks in Ceramics, B. T. Khuri-Yakub, A. G. Evans, G. S. Kino and B. R. Tittmann, Science Center Report SC5064.3TR on ONR program N00014-76-C-0624.
5. Development of Nondestructive Testing Techniques for High Performance Ceramics, M. R. Baumgartner, R. H. Brockelman and P. M. Hanson, AMMRC Report, AMMRC Tr78-11.
6. Error Analysis of Failure Prediction, S. M. Wiederhorn, E. R. Fuller, J. Mandel and A. G. Evans, J. Amer. Cer. Soc. 59, (1976).

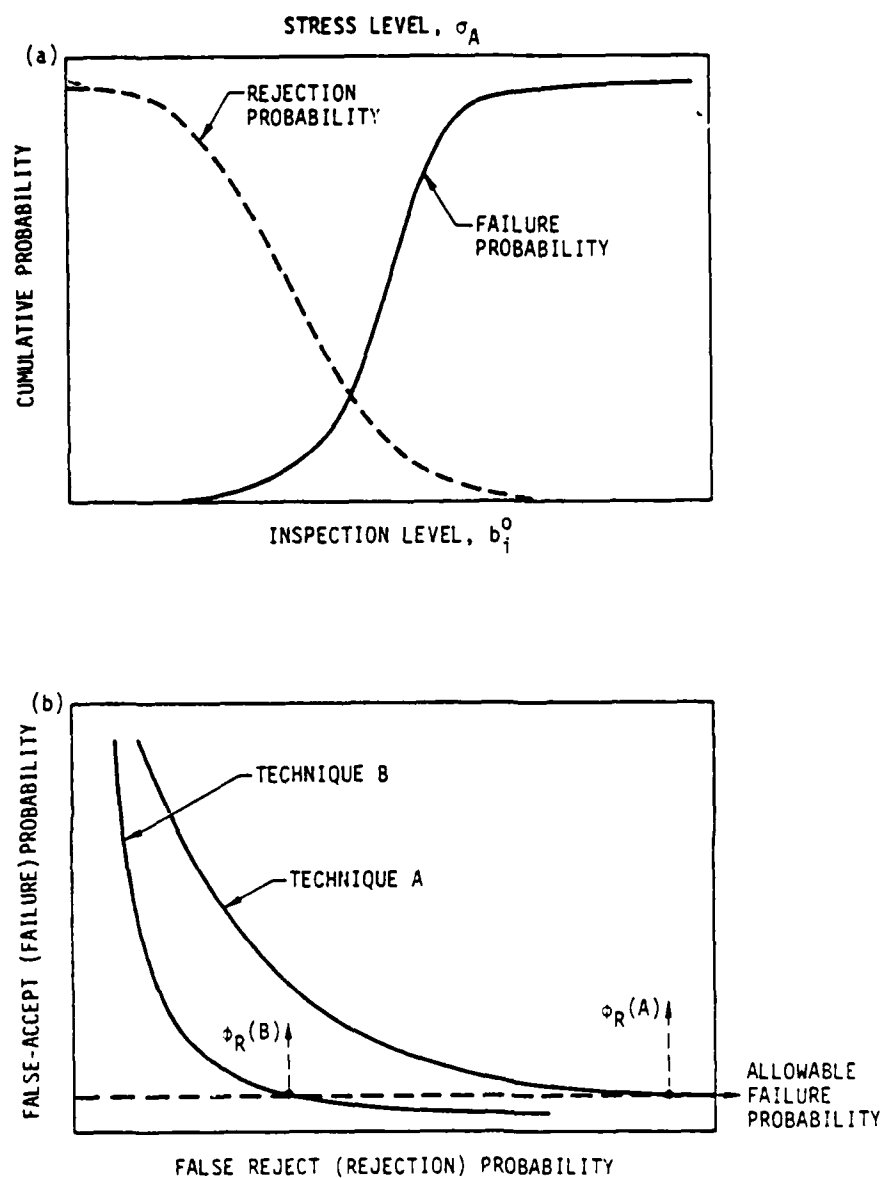
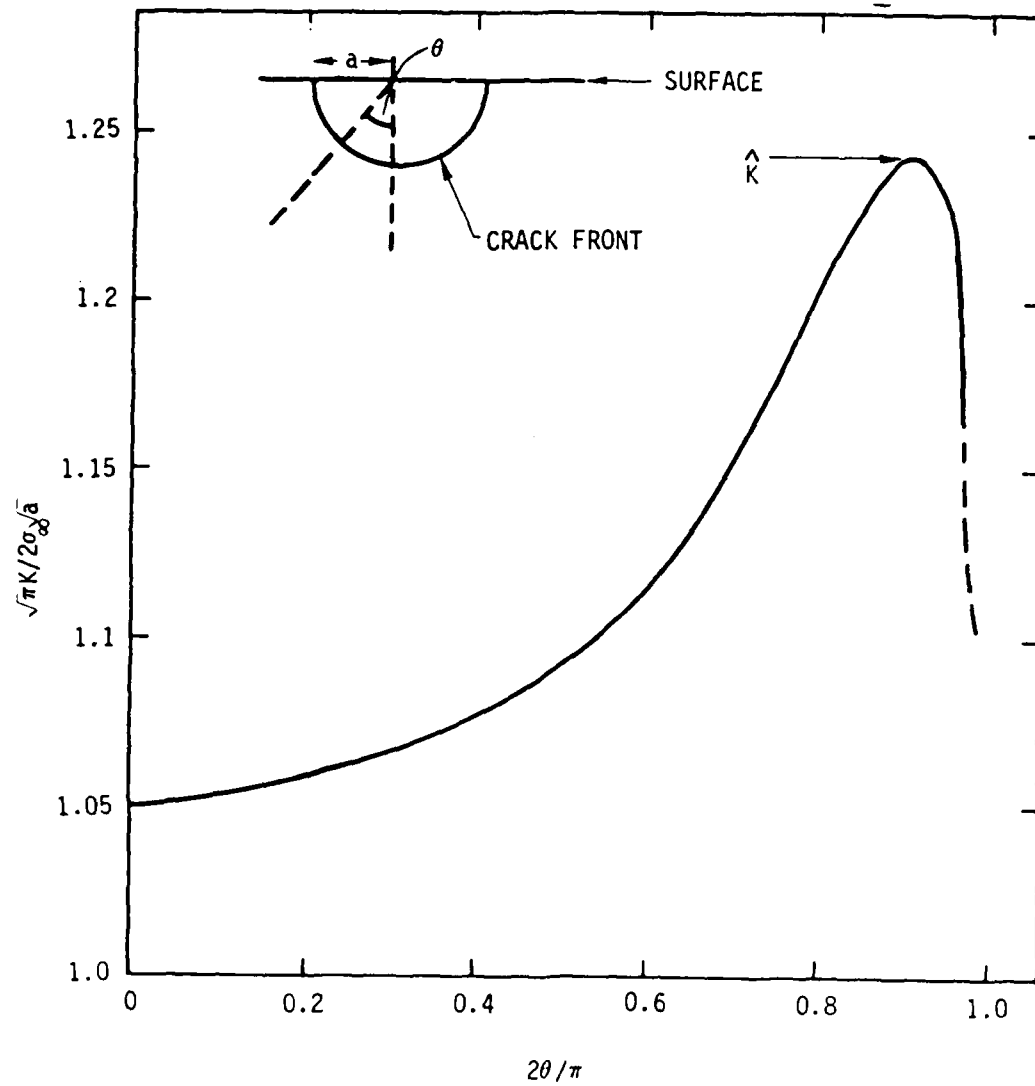


Figure 1

False-accept and false-reject probabilities

XBL 797-10502



XBL 794-9416

Figure 2

Stress intensity factor distribution
around a semi-circular surface crack.

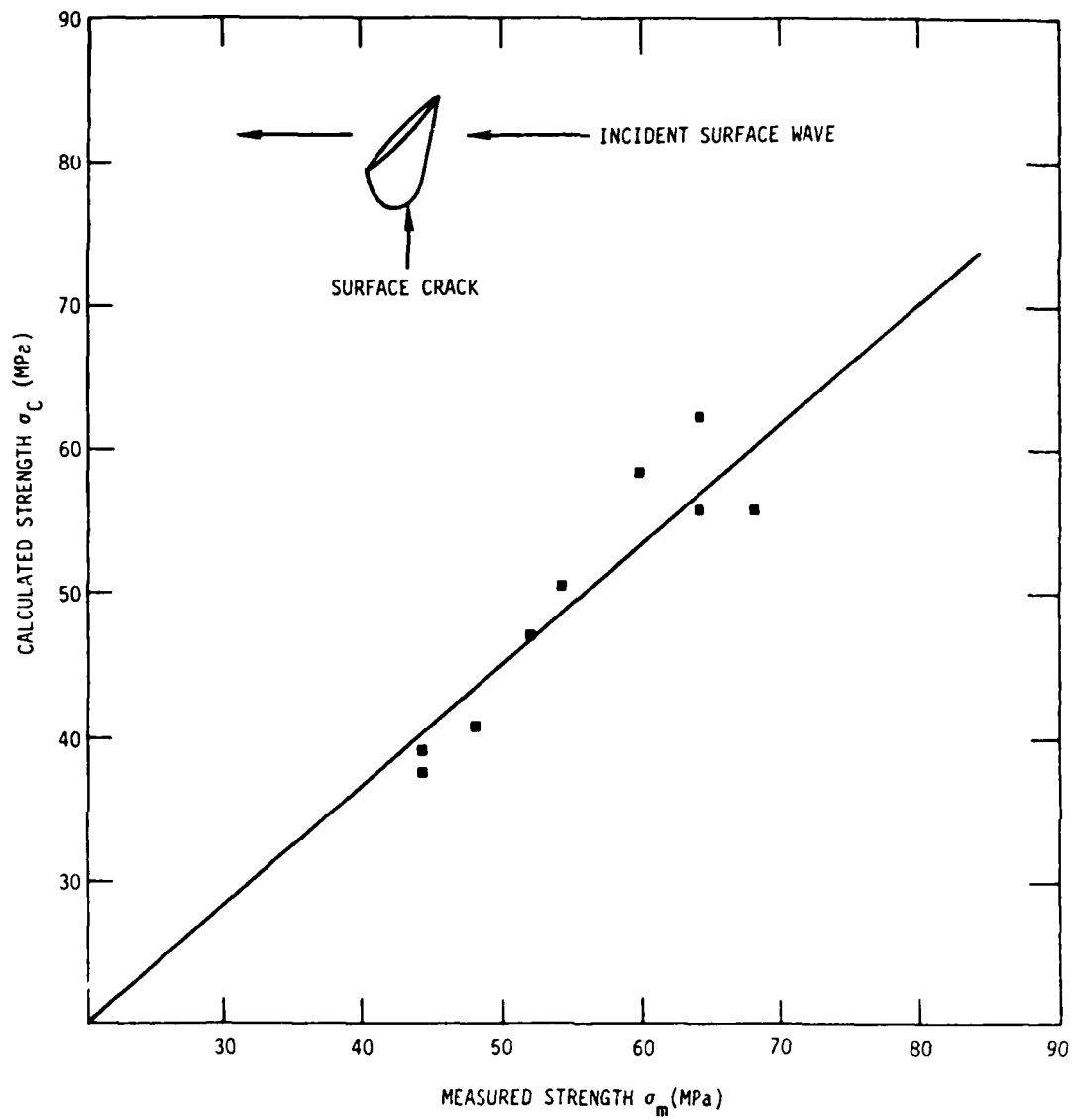
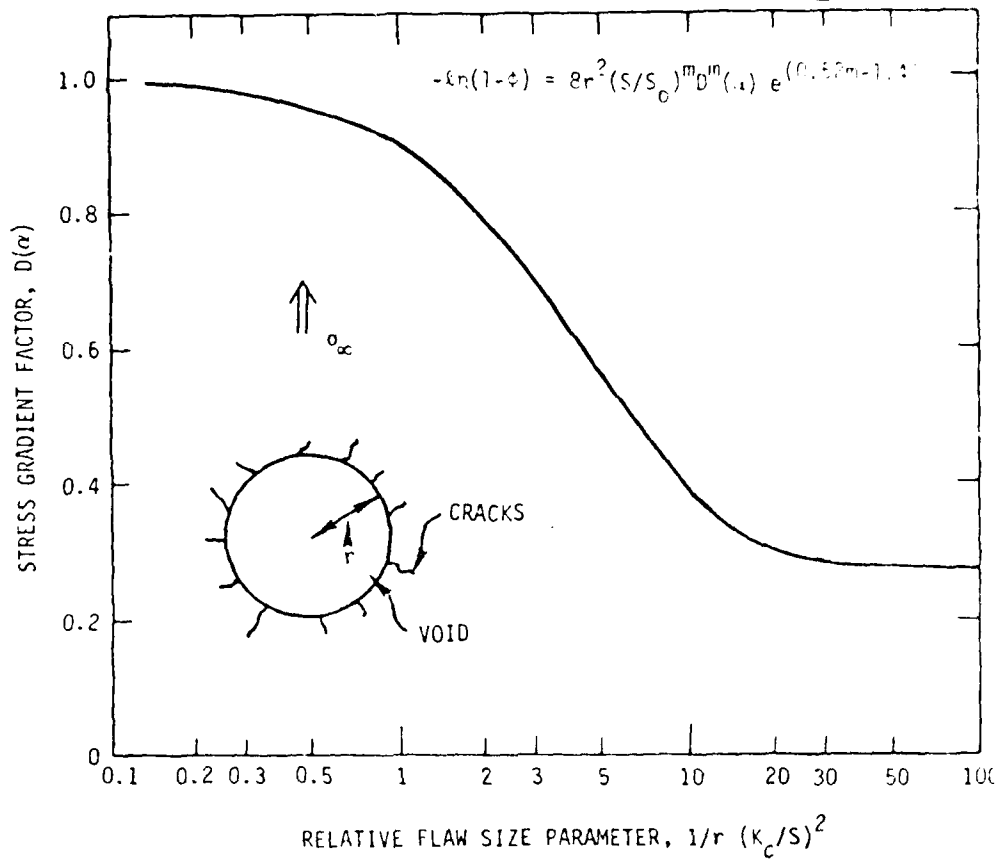


Figure 3

Fracture prediction data for surface cracks in glass.

XBL 797-10503

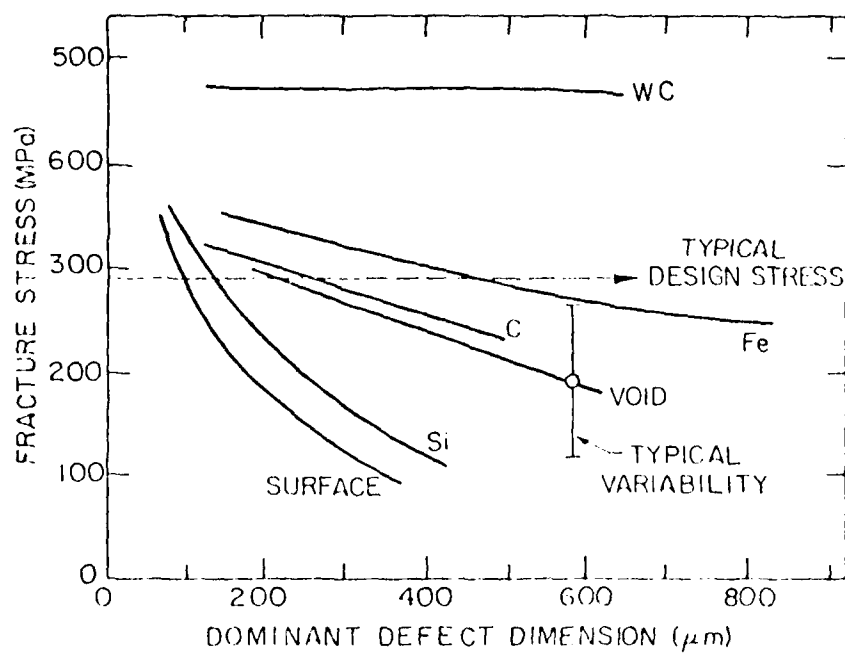
SC7b-14b7



YSL 194-9419

Figure 4

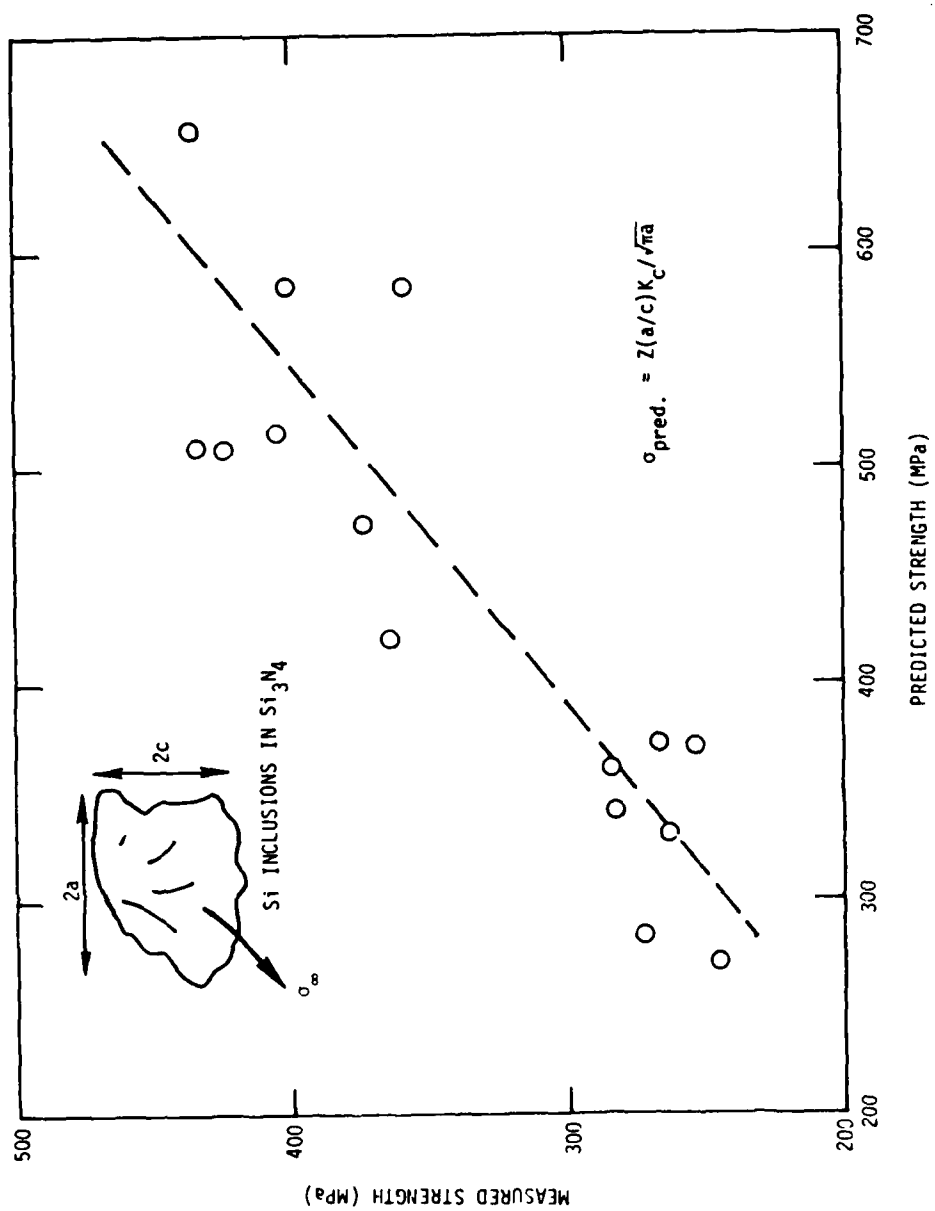
Fracture from voids in brittle materials: the distribution parameter, $D(\alpha)$.



X86 797-10634

Figure 5.

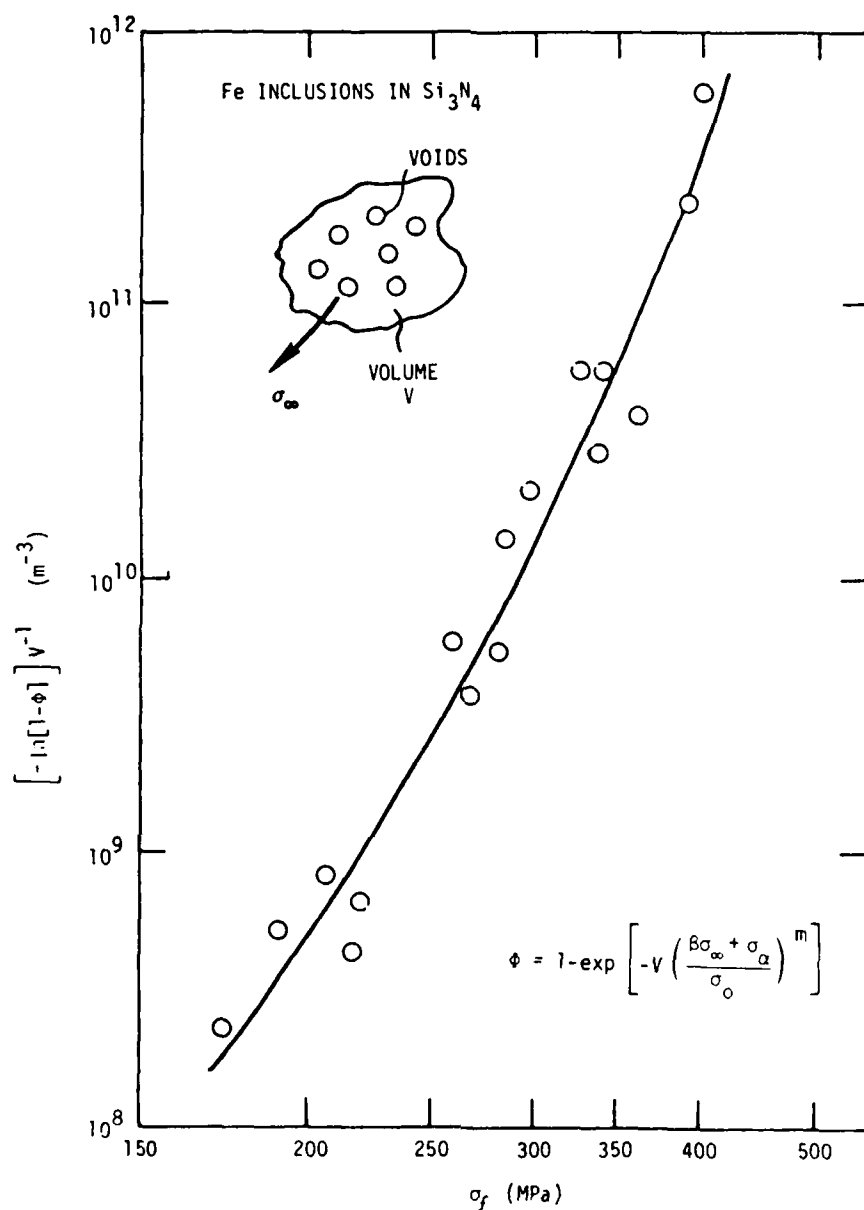
The dependence of the fracture strength
of silicon nitride on the inclusion size.



XBL 797-10505

Figure 6

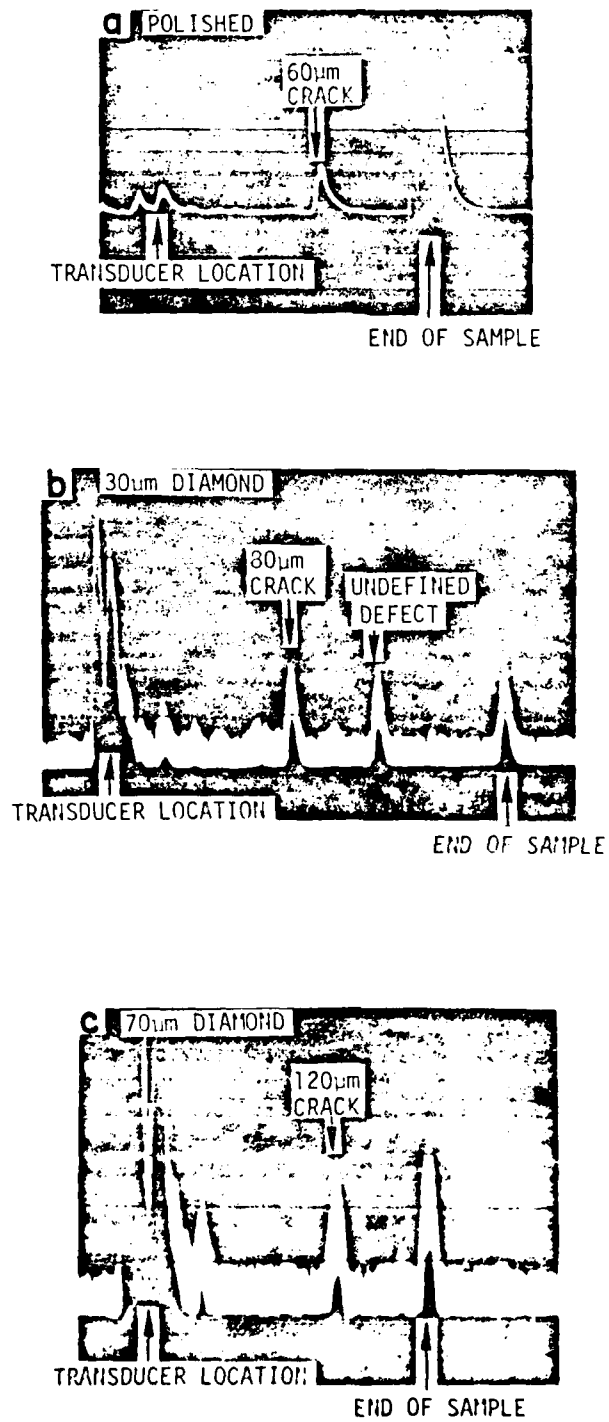
The correlation of the fracture data for Si inclusions with the fracture model.



XBL 794-9421

Figure 7

The correlation of the fracture data for Fe inclusions with the fracture model.



XBB 797-8936

Figure 8

The detectability of surface cracks in silicon nitride using ultrasonic surface waves.

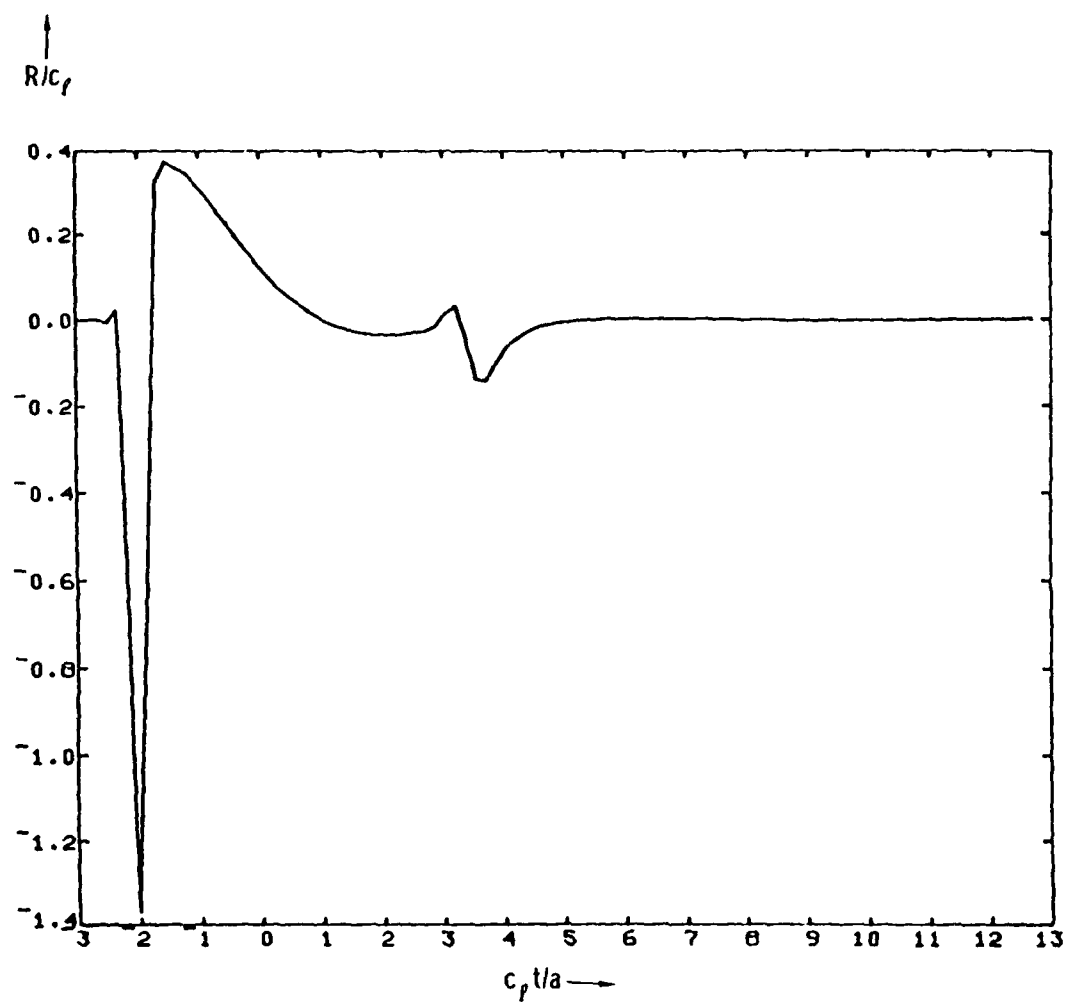


Figure 9a

The calculated scattering characteristics in the time domain spherical void.

XBL 797-10506

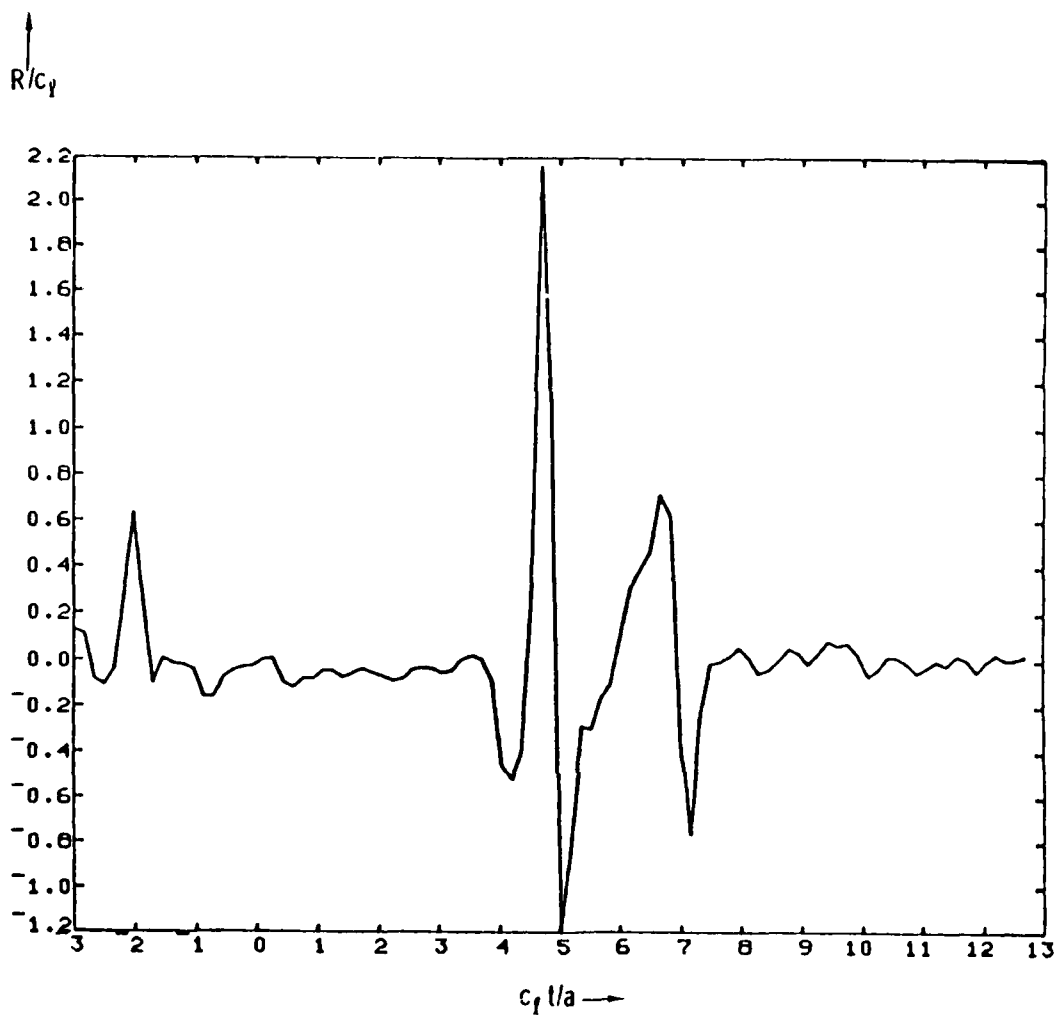
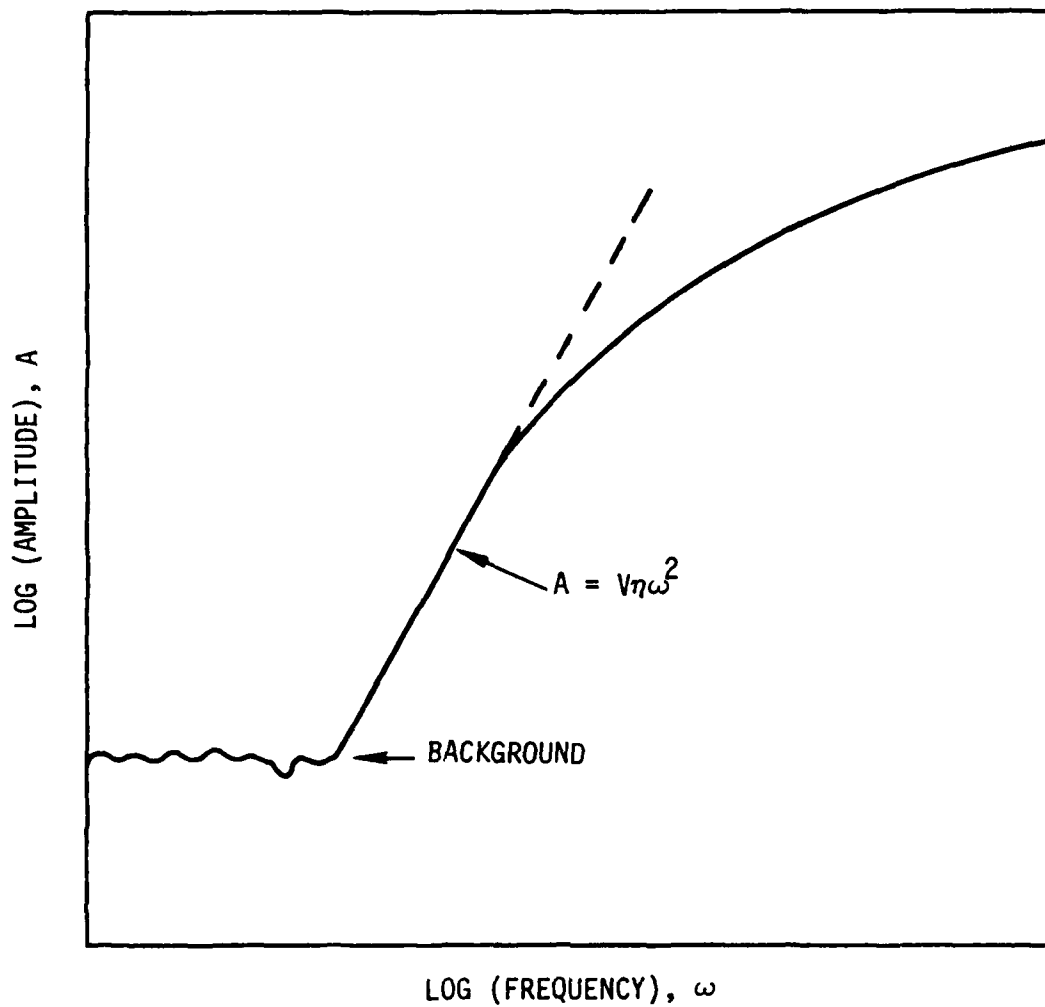


Figure 9b

The calculated scattering characteristics in the time domain spherical WC inclusion.

XBL 797-10507



XBL 794-9424

Figure 10

A schematic indicating the long wavelength method for estimating the defect volume.

AD-A087 594 ADVISORY GROUP FOR AEROSPACE RESEARCH AND DEVELOPMENT--ETC F/6 11/2
CERAMICS FOR TURBINE ENGINE APPLICATIONS.(U)
MAR 80 H M BURTE, J ACURIO, W HANSEN

UNCLASSIFIED AGARD-CP-276

NL

4 OF 4

2025 5 24

END

DATE _____
 FOR MR. _____

9-80

DTIC

TABLE I

<u>INSPECTION METHODS</u>		<u>PRIMARY SENSITIVITY</u>
	<u>Bulk Defects</u>	
1. X-Radiography (Microfocus)		Density (Atomic Number)
2. Ultrasonics		Acoustic Impedence
	<u>Near Surface Defects</u>	
1. Ultrasonics (Surface Waves)		Acoustic Impedence
2. Microwaves		Dielectric Constant
3. Acoustic Microscopy		Acoustic Impedence
	<u>Novel Approaches</u>	
	Photo-Acoustic Spectroscopy (Optical Absorption)	
	Eddy Currents (Space Charge Interaction)	
	Exo-Electron Emission	

FRACTURE STATISTICS IN DESIGN AND APPLICATION

C. A. Johnson
Ceramics Branch
Physical Chemistry Laboratory

General Electric Company
Corporate Research and Development
Box 8
Schenectady, New York 12301

SUMMARY

The use of ceramics for load-bearing structural components requires a detailed understanding of the variability in flaw size and the resulting scatter and size dependence of fracture strength. The quantitative description of these effects is known as fracture statistics. Distribution functions approximating the fracture behavior of brittle materials are discussed with emphasis on the Weibull distribution. In the application of fracture statistics as an aid for design of structural components, several factors may introduce errors in the resulting failure analysis. One such source of error, the presence of multiple flaw distributions, is discussed and illustrated.

INTRODUCTION

The ability to properly design stressed components of structural ceramics requires a detailed understanding of the statistical nature of fracture in brittle materials. Unlike most metals, ceramics require this additional knowledge to account for the large variability in strength which is commonly observed and to account for the size dependence of strength which is a natural consequence of the variability. The variability or scatter in strength arises from the large range of flaw sizes and severities present in most brittle materials. The size dependence then arises from sampling statistics. As the specimen size is increased, the total number of flaws per specimen increases in proportion to the specimen size. The more defects of a given distribution, the greater the probability of sampling a very severe defect. Fracture strength, therefore, tends to decrease with increasing specimen size.

The majority of the mathematical descriptions of fracture statistics presently available are based on the weakest link concept which simply states that the entire body will fail when the stress at any defect is sufficient for unstable crack propagation of that defect. Examples of weakest link distribution functions are the Weibull distribution(1,2), the three extreme value distributions(3,4), and flaw density distributions(5,6). No distribution function has been identified which is universally acceptable. The Weibull distribution has become very popular, however, due to the mathematical simplicity and the relatively good success of the distribution in describing most fracture data.

In very simple terms, the application of fracture statistics involves the measurement of fracture strength of a moderate to large number of specimens of the material of interest. This data base is combined with a distribution function and the appropriate service stress distribution to calculate an estimated probability of failure of the structural component of interest. The design of the component and/or the characteristics of the service environment are then modified in an iterative fashion until an acceptable probability of failure is reached. The probability of failure calculated for the component is only an estimate of the real failure probability. Many possible sources of error exist, both experimental and analytical, that may lead to false conclusions concerning the reliability of a component. Some of these sources of error include:

1. The test specimens may not properly characterize the flaw population in the component. The origin of most defects can be traced to the fabrication process. Conversely, different fabrication processes yield different flaw populations. Valid test specimens must contain the flaw population of the component of interest, therefore, the test specimens and the component should be fabricated by the same technique.
2. The flaw population may be modified during service. Oxidation, corrosion or subcritical crack growth in the service environment can initiate new defects and enlarge existing ones. The nature of the new or modified flaw population may bear little resemblance to the flaw population characterized in test specimens(7).
3. The assumed distribution function may be incorrect. If the assumed distribution does not describe the fracture behavior, then estimates of probability of failure may be incorrect. The magnitude of the error generally increases as the distribution function is extrapolated to component sizes significantly larger or smaller than the test specimens.
4. Too few test specimens may have been fractured. For a given distribution function, the smaller the number of test specimens, the smaller the statistical confidence in the adjustable parameters of the distribution. Accordingly, as the number of test specimens decreases, the probability of calculating incorrect parameters of the distribution increases(8,9).
5. Multiaxial stresses may be incorrectly incorporated in the analysis. Most test specimens contain either uniaxial or well defined biaxial stress states. Most structural components in service, however, contain biaxial or triaxial stress states. A correct statistical analysis must account for differences in stress state between the test specimen and the component of interest(10).

6. Multiple flaw distributions may be present but not recognized. Test data on materials with multiple flaw distributions can be forced to fit a distribution function meant for a single flaw distribution, but the resulting predictions of failure probability are subject to errors which generally increase as the distribution function is extrapolated beyond the test specimen data base.

Most of the potential sources of error included above are either covered adequately in the literature or avoidable by good experimental practice. An exception, however, is the last item concerning multiple flaw distributions. Much of the remainder of this paper will be devoted to the effects of multiple flaw distributions on the fracture statistics of brittle materials. In order to quantitatively illustrate some consequences of multiple flaw distributions, the Weibull distribution function will be used. Other distribution functions lead to analogous effects.

Before discussing multiple flaw distributions, the Weibull distribution function will be reviewed.

REVIEW OF THE WEIBULL DISTRIBUTION

The Weibull distribution function(1) relates the cumulative probability of failure (P) to the volume (V) under tensile stress (σ) with two parameters--the Weibull modulus (m) and a normalizing constant (σ_0) as follows:

$$P = 1 - \exp - \int_V \left(\frac{\sigma}{\sigma_0} \right)^m dV \quad (1)$$

This form of the function has two adjustable parameters and integrates over the volume of the specimen. Thus it is generally referred to as two-parameter, volume Weibull statistics. Other variations of the Weibull distribution function can include a third adjustable parameter and may integrate over the surface of the body rather than the volume (if all flaws are expected to be surface flaws). The Weibull modulus, m, is a measure of the scatter or dispersion of the distribution (similar to the standard deviation of the normal distribution) where a small m represents a large degree of scatter. Most ceramics are reported to have m's in the range of 5 to 15, whereas metals which fail in a ductile manner are estimated to have m's in the range of 30 to 50. The normalizing constant σ_0 , is an indirect measure of the average strength. For instance, if the Weibull modulus, the specimen size and the loading configuration are held constant, the average strength is directly proportional to σ_0 .

For bodies under uniform tension, the integration of Eq.(1) is trivial, but for the general case where the stress in a body is a function of position, the integration must be carried out either analytically or numerically. As an example, the stress in a rectangular beam in three-point bending can be described analytically as:

$$\sigma = \frac{6 P x y}{w h^3} \quad (2)$$

where P is the load applied at the center load point, x is the distance from the nearest outer load point, y is the distance from the neutral axis, w is the specimen width and h is the specimen height. Substituting this into Eq.(1), expanding the volume integral into a triple integral and rearranging results in:

$$P = 1 - \exp \left[-2 \left(\frac{\sigma_M}{\sigma_0} \right) \frac{4}{hL} \right] \int_0^w \int_0^{h/2} \int_0^{L/2} (xy)^m dx dy dz \quad (3)$$

where σ_M is the maximum tensile stress in the beam. Integration of this expression yields:

$$P = 1 - \exp \left[- \frac{1}{2(m+1)^2} V \left(\frac{\sigma_M}{\sigma_0} \right)^m \right] \quad (4)$$

or

$$P = 1 - \exp \left[-K_V V \left(\frac{\sigma_M}{\sigma_0} \right)^m \right] \quad (5)$$

where K_V is a "load factor":

$$K_V = \frac{1}{2(m+1)^2} \quad (6)$$

The load factor for four-point bending with volume flaws can be derived from Eq.(1) in a similar manner and results in:

$$K_V = \frac{\left(\frac{a}{b} \right) m + 1}{2(m+1)^2} \quad (7)$$

where a is the inner span and b is the outer span. Equation (7) correctly reduces to Eq.(6) for three-point bending where the inner span, a, is zero. In those cases where failure is controlled by surface flaws, Eq.(1) should be integrated over all elements of surface rather than volume. The resulting load factor for four-point bending can be related to Eq.(7) as follows:

$$K_A = K_V \left(\frac{mw}{w+h} + 1 \right) \quad (8)$$

where w and h are the specimen width and height respectively.

The product of K_V times V is often referred to as the "effective volume" under tension and, as the term implies, can be pictured as the volume of material which is effectively being tested under uniform tension.

Accordingly, K_A times surface area is the effective area under uniform tension. Eq.(1) can be integrated either analytically or numerically to the form of Eq.(5) for a stressed body of any geometry and loading configuration. Except for the case of uniform tension, the resulting load factors will always be numerically less than one and will always be a function of m .

The Weibull modulus and σ_0 can be estimated from fracture data by a number of methods, but most of the common ones use order or ranking statistics. Fracture strengths are measured on a number of specimens of identical geometry. The strengths are ordered from weakest to strongest, and each is assigned a probability of failure based on its ranking, n , as follows:

$$P = \frac{n}{N+1} \text{ or } P = \frac{n-0.5}{N} \quad (9)$$

where N is the total number of data points. The second estimate of failure probability is preferred(9). A regression analysis can then be performed using Eq.(5) to find the best values for m and σ_0 to describe all N data points (each data point consists of a measured fracture strength and an estimated probability of failure).

Variations of this method arise from different weightings of the errors in the regression analysis. One popular method is very convenient because it allows a simple linear regression analysis of the data. Equation (5) can be manipulated and rearranged to:

$$\ln \ln \left(\frac{1}{1-P} \right) = m \ln \sigma_m + \ln \left(\frac{KV}{\sigma_m} \right) \quad (10)$$

This is an equation of a straight line and is therefore easily subjected to linear regression. Equation(10) also allows a convenient graphical representation of the data as shown schematically in Fig.(1) by plotting $\ln \ln (1/1-P)$ vs $\ln \sigma_m$. The slope of the linear regression line through the transformed data is m and the position of the line defines σ_0 .

It should be noted that the maximum stress of each specimen is used in all of this discussion despite the fact that fracture in three-point bend specimens, for example, virtually never originates exactly at the line of maximum tensile stress.

Graphical representation of data plotted as Fig.(1) also allows judgements concerning the quality of the distribution function in describing the data. If the data points are clearly non-linear on such a plot, then the distribution function probably does not adequately describe the behavior, regardless of the choice of statistical parameters m and σ_0 .

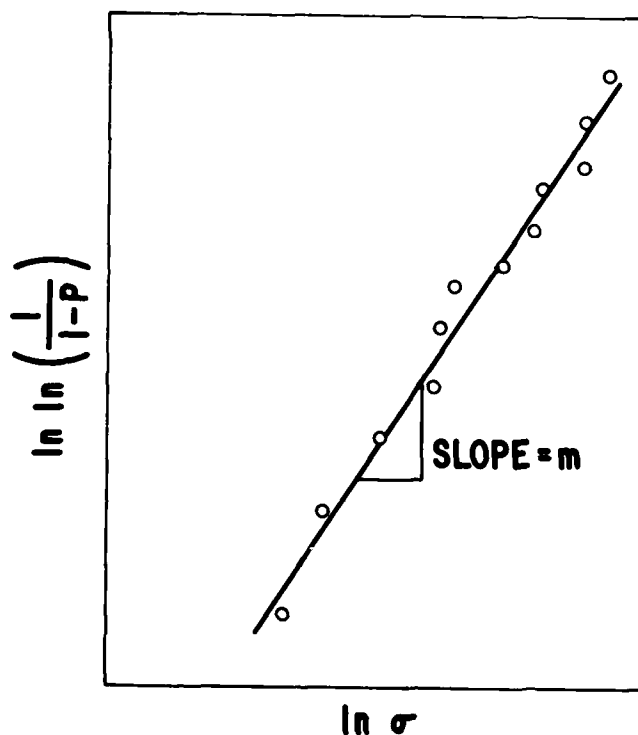


Fig.(1). Schematic illustrating linear transformation of variables for the Weibull distribution.

EFFECTS OF MULTIPLE FLAW DISTRIBUTIONS

Most treatments of fracture statistics assume that a single distribution of flaws is present uniformly throughout the material and that multiple pieces of the same material contain the same flaw distribution. Real ceramic components, however, generally contain two or more types of defects each with its own characteristic flaw size distribution, and multiple pieces of presumably the same material may have been manufactured from different lots of powder, fired in different furnaces or even purchased from different manufacturers. By relaxing the assumptions of a single flaw distribution and of uniformity from specimen to specimen, relationships can be derived which more accurately describe the fracture of many ceramics.

Careful fractography of most ceramic materials reveal more than one type of fracture initiating flaw within a group of specimens. The nature and origin of the defects, of course, is a function of the powder handling and consolidation techniques. Many different types of flaws are observed in ceramics including voids or void clusters, inclusions, machining damage, etc. Each type of flaw, when present, is contained as a distribution of flaw sizes and densities which, in general, is totally independent of all other flaw distributions. For instance, the size and severity of machining flaws can be varied independently of the size and severity of inclusions.

There are two methods of experimentally identifying the presence of multiple flaw distributions. The first and more convincing method is fractography. Multiple active flaw distributions in a group of test specimens will yield more than one type of fracture initiating defect. The second method involves discrepancies between measured fracture data and expected distribution functions. For instance, if the two-parameter Weibull distribution is expected to describe a given material, then the fracture data should fall along a reasonably straight line when plotted as Fig.(1). If the data fall on a clearly non-linear relationship, then the discrepancy may be due to the presence of multiple flaw distributions. Unfortunately, a non-linear relationship on Fig.(1) may be due instead to a single distribution of flaws that conform to some distribution function other than the two-parameter Weibull distribution. Thus, discrepancies between observed and expected relationships are not usually sufficient to conclude the presence of multiple flaw distributions.

The most positive confirmation and characterization of multiple flaw distributions involves both fractographic identification of more than one type of fracture initiating defect and simultaneous deviation of the data from the expected distribution function. Very few characterizations of fracture strength included in the literature satisfactorily study both aspects. Those investigators primarily interested in characterization of fracture initiating defects generally test only a small number of specimens, while those investigators who fracture a moderate to large number of specimens for derivation of statistical parameters are generally overwhelmed by the task of properly identifying the associated defects.

The literature contains many references to multiple flaw distributions based on discrepancies from expected distribution functions. When plotted as Fig.(1), for instance, the data may fall on two apparently intersecting straight lines, thus generating a "knee" in the curve, sometimes with positive and sometimes with negative curvature. The manner in which multiple flaw distributions generate such knees is seldom questioned. As will be described below, details of any deviations from linearity can be used to deduce information concerning the nature of the flaw distributions present.

Consider a group of components or test specimens that, when failed, are found to have two distinctly different types of fracture origins. Some specimens fail from flaw type "A" while the remainder fail from flaw type "B". There are at least three ways in which the specimens can contain flaw distributions A and B to yield this result:

1. Both flaw distributions may be present in each and every specimen. The most severe defect in some specimens will be one of type A, while in other specimens the most severe defect will be one from flaw distribution B. Since both distributions are present concurrently in every specimen, this case will be referred to as "concurrent" flaw distributions. An example of concurrent distributions is a group of specimens machined from a billet of ceramic which contains strength degrading inclusions. Each specimen then contains both machining flaws on the surface and inclusions throughout the volume.
2. Within a group of specimens, any given specimen may contain flaws either from distribution A or from distribution B but not from both. When several specimens are fractured, those that contain only flaw distribution A will obviously fail from a flaw of type A, while those that contain only distribution B will fail at a flaw of type B. Since the two flaw distributions are mutually exclusive within a single specimen, this case will be referred to as "exclusive" flaw distributions. An example of exclusive flaw distributions is a group of specimens comprised of two sub-groups purchased from two different manufacturers. It is inconceivable that the two manufacturers fabricated the specimens with identical flaw distributions, even if the chemical compositions were nominally identical. If the two sub-groups were mixed together without identification before testing, the combined group of specimens would contain exclusive flaw distributions.
3. Within a group of specimens, flaw distribution A may be present in all specimens, while flaw distribution B may be present in only some. When several specimens are fractured, those that do not contain flaws from distribution B will fail at a flaw of type A, while the remainder which contain both distributions may fail at a flaw of either type. In those specimens which contain both types of flaws, the distributions are present concurrently, therefore this case will be referred to as "partially concurrent" flaw distributions. An example of partially concurrent distributions is a group of die-pressed and sintered test specimens which were all sintered in the same furnace, but could not all be sintered in a single furnace cycle. All the test specimens contained strength degrading inclusions which could be traced to foreign material introduced during powder preparation. One of the furnace cycles underwent an unscheduled and unrecorded temperature excursion to a much higher maximum temperature than the other furnace cycles. The test specimens from the overfiring underwent exaggerated grain growth such that the largest grains acted as quite severe defects. When tested, all of the properly fired specimens failed at

Accordingly, K_A times surface area is the effective area under uniform tension. Eq.(1) can be integrated either analytically or numerically to the form of Eq.(5) for a stressed body of any geometry and loading configuration. Except for the case of uniform tension, the resulting load factors will always be numerically less than one and will always be a function of m .

The Weibull modulus and σ_0 can be estimated from fracture data by a number of methods, but most of the common ones use order or ranking statistics. Fracture strengths are measured on a number of specimens of identical geometry. The strengths are ordered from weakest to strongest, and each is assigned a probability of failure based on its ranking, n , as follows:

$$P = \frac{n}{N+1} \text{ or } P = \frac{n-0.5}{N} \quad (9)$$

where N is the total number of data points. The second estimate of failure probability is preferred(9). A regression analysis can then be performed using Eq.(5) to find the best values for m and σ_0 to describe all N data points (each data point consists of a measured fracture strength and an estimated probability of failure).

Variations of this method arise from different weightings of the errors in the regression analysis. One popular method is very convenient because it allows a simple linear regression analysis of the data. Equation (5) can be manipulated and rearranged to:

$$\ln \ln \left(\frac{1}{1-P} \right) = m \ln \sigma_m + \ln \left(\frac{KV}{\sigma_m^m} \right) \quad (10)$$

This is an equation of a straight line and is therefore easily subjected to linear regression. Equation(10) also allows a convenient graphical representation of the data as shown schematically in Fig.(1) by plotting $\ln \ln (1/1-P)$ vs $\ln \sigma_m$. The slope of the linear regression line through the transformed data is m and the position of the line defines σ_0 .

It should be noted that the maximum stress of each specimen is used in all of this discussion despite the fact that fracture in three-point bend specimens, for example, virtually never originates exactly at the line of maximum tensile stress.

Graphical representation of data plotted as Fig.(1) also allows judgements concerning the quality of the distribution function in describing the data. If the data points are clearly non-linear on such a plot, then the distribution function probably does not adequately describe the behavior, regardless of the choice of statistical parameters m and σ_0 .

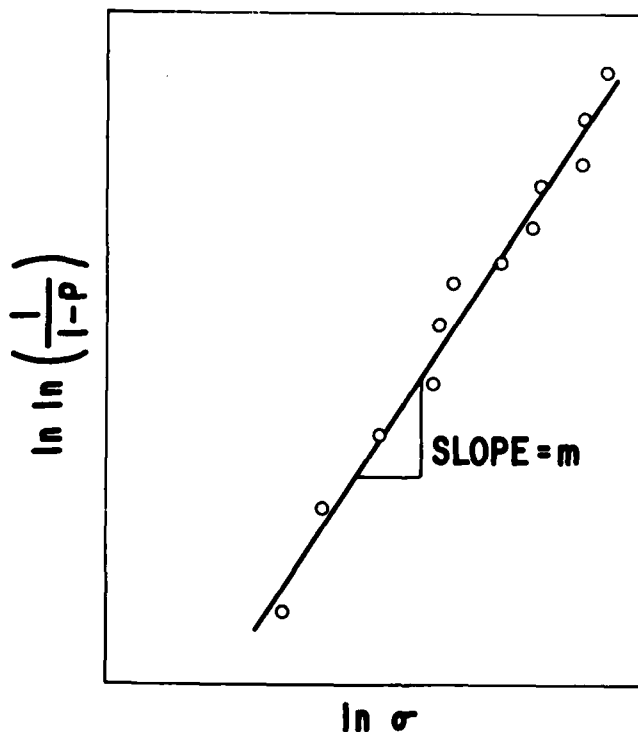


Fig.(1). Schematic illustrating linear transformation of variables for the Weibull distribution.

EFFECTS OF MULTIPLE FLAW DISTRIBUTIONS

Most treatments of fracture statistics assume that a single distribution of flaws is present uniformly throughout the material and that multiple pieces of the same material contain the same flaw distribution. Real ceramic components, however, generally contain two or more types of defects each with its own characteristic flaw size distribution, and multiple pieces of presumably the same material may have been manufactured from different lots of powder, fired in different furnaces or even purchased from different manufacturers. By relaxing the assumptions of a single flaw distribution and of uniformity from specimen to specimen, relationships can be derived which more accurately describe the fracture of many ceramics.

Careful fractography of most ceramic materials reveal more than one type of fracture initiating flaw within a group of specimens. The nature and origin of the defects, of course, is a function of the powder handling and consolidation techniques. Many different types of flaws are observed in ceramics including voids or void clusters, inclusions, machining damage, etc. Each type of flaw, when present, is contained as a distribution of flaw sizes and densities which, in general, is totally independent of all other flaw distributions. For instance, the size and severity of machining flaws can be varied independently of the size and severity of inclusions.

There are two methods of experimentally identifying the presence of multiple flaw distributions. The first and more convincing method is fractography. Multiple active flaw distributions in a group of test specimens will yield more than one type of fracture initiating defect. The second method involves discrepancies between measured fracture data and expected distribution functions. For instance, if the two-parameter Weibull distribution is expected to describe a given material, then the fracture data should fall along a reasonably straight line when plotted as Fig.(1). If the data fall on a clearly non-linear relationship, then the discrepancy may be due to the presence of multiple flaw distributions. Unfortunately, a non-linear relationship on Fig.(1) may be due instead to a single distribution of flaws that conform to some distribution function other than the two-parameter Weibull distribution. Thus, discrepancies between observed and expected relationships are not usually sufficient to conclude the presence of multiple flaw distributions.

The most positive confirmation and characterization of multiple flaw distributions involves both fractographic identification of more than one type of fracture initiating defect and simultaneous deviation of the data from the expected distribution function. Very few characterizations of fracture strength included in the literature satisfactorily study both aspects. Those investigators primarily interested in characterization of fracture initiating defects generally test only a small number of specimens, while those investigators who fracture a moderate to large number of specimens for derivation of statistical parameters are generally overwhelmed by the task of properly identifying the associated defects.

The literature contains many references to multiple flaw distributions based on discrepancies from expected distribution functions. When plotted as Fig.(1), for instance, the data may fall on two apparently intersecting straight lines, thus generating a "knee" in the curve, sometimes with positive and sometimes with negative curvature. The manner in which multiple flaw distributions generate such knees is seldom questioned. As will be described below, details of any deviations from linearity can be used to deduce information concerning the nature of the flaw distributions present.

Consider a group of components or test specimens that, when failed, are found to have two distinctly different types of fracture origins. Some specimens fail from flaw type "A" while the remainder fail from flaw type "B". There are at least three ways in which the specimens can contain flaw distributions A and B to yield this result:

1. Both flaw distributions may be present in each and every specimen. The most severe defect in some specimens will be one of type A, while in other specimens the most severe defect will be one from flaw distribution B. Since both distributions are present concurrently in every specimen, this case will be referred to as "concurrent" flaw distributions. An example of concurrent distributions is a group of specimens machined from a billet of ceramic which contains strength degrading inclusions. Each specimen then contains both machining flaws on the surface and inclusions throughout the volume.
2. Within a group of specimens, any given specimen may contain flaws either from distribution A or from distribution B but not from both. When several specimens are fractured, those that contain only flaw distribution A will obviously fail from a flaw of type A, while those that contain only distribution B will fail at a flaw of type B. Since the two flaw distributions are mutually exclusive within a single specimen, this case will be referred to as "exclusive" flaw distributions. An example of exclusive flaw distributions is a group of specimens comprised of two sub-groups purchased from two different manufacturers. It is inconceivable that the two manufacturers fabricated the specimens with identical flaw distributions, even if the chemical compositions were nominally identical. If the two sub-groups were mixed together without identification before testing, the combined group of specimens would contain exclusive flaw distributions.
3. Within a group of specimens, flaw distribution A may be present in all specimens, while flaw distribution B may be present in only some. When several specimens are fractured, those that do not contain flaws from distribution B will fail at a flaw of type A, while the remainder which contain both distributions may fail at a flaw of either type. In those specimens which contain both types of flaws, the distributions are present concurrently, therefore this case will be referred to as "partially concurrent" flaw distributions. An example of partially concurrent distributions is a group of die-pressed and sintered test specimens which were all sintered in the same furnace, but could not all be sintered in a single furnace cycle. All the test specimens contained strength degrading inclusions which could be traced to foreign material introduced during powder preparation. One of the furnace cycles underwent an unscheduled and unrecorded temperature excursion to a much higher maximum temperature than the other furnace cycles. The test specimens from the overfiring underwent exaggerated grain growth such that the largest grains acted as quite severe defects. When tested, all of the properly fired specimens failed at

inclusions, while the overfired specimens were mixed with some failures at inclusions and some at exaggerated grains.

A large number of cases analogous to the three above are generated when more than two flaw distributions are contained in a group of specimens. It should be noted that, unlike the preceding examples, one does not generally know a priori the number of active flaw distributions nor the manner in which flaw types are distributed among specimens.

The following three sections will discuss concurrent, exclusive and partially concurrent flaw distributions in more detail including mathematical descriptions of the probabilities of failure, examples from the literature, similarities and contrasts, etc.

A. Concurrent Flaw Distributions

Consider a component which has two independent means of failure, A and B, with associated probabilities of failure, P_A and P_B . The probability of non-failure of the component is then the product of the two individual probabilities of non-failure.

$$1 - P_T = (1 - P_A) (1 - P_B) \quad (11)$$

Solving for the total probability of failure, P_T , yields:

$$P_T = 1 - (1 - P_A) (1 - P_B) \quad (12)$$

Equation (12) as applied to fracture statistics was first proposed by Weibull(11). Ceramic components containing two concurrent flaw distributions conform to Eq.(12) where P_A is the probability of failure should distribution A be present alone and P_B is the probability should distribution B be present alone. Equation(12) is valid regardless of the form of the distribution functions describing P_A and P_B . If the two-parameter volume Weibull distribution is valid for both flaw populations, then Eq.(5) and Eq.(12) yield:

$$P_T = 1 - \exp \left[-K_V V \left(\frac{\sigma_M}{\sigma_{OA}} \right)^{m_A} - K_V V \left(\frac{\sigma_M}{\sigma_{OB}} \right)^{m_B} \right] \quad (13)$$

This failure probability function contains four adjustable parameters, m_A , σ_{OA} , m_B , and σ_{OB} . Each additional concurrent flaw distribution adds another term in the exponential and an additional two adjustable parameters. Since the load factor, K , is generally a function of the Weibull modulus, the effective volume, $K_V V$, is different for the two distributions and cannot be factored out of the terms in the exponential.

Equation(13) is plotted on Fig.(2) for somewhat arbitrary values of the four adjustable parameters. For simplicity, uniform tensile loading was imposed, thus $K = 1 \neq f(m)$ and $K_V V = V$. The units of σ_0 are MPa. The units of volume shown on Fig.(2) are cm^3 , but for input into Eq.(13), the volume must be converted to m^3 to maintain consistent units with MPa. The meaning of π_A and π_B listed on Fig.(2) will be explained in subsequent sections, but values of unity for both imply concurrent flaw distributions.

The solid line on Fig.(2) is the total probability of failure where both distributions are present concurrently. The dashed lines illustrate the individual failure probabilities when the distributions are present one at a time. As illustrated, two concurrent distributions result in a single knee in the curve with positive curvature. Knees with negative curvature cannot be generated with concurrent flaw distributions. At high fracture stresses, the combined behavior asymptotically approaches the behavior of the distribution with the larger Weibull modulus (smaller variability). At low stresses, the combined behavior asymptotically approaches that of the distribution with the smaller modulus.

An extraordinarily large range was chosen for the ordinate of Fig.(2) in order to illustrate the overall behavior of Eq.(13). Failure probabilities for 20,000 test specimens could be plotted on Fig.(2). A range of experimentally realistic failure probabilities is included on Fig.(3) with curves similar to Fig.(2) generated from the same four adjustable parameters. In this case, however, the figure includes data from 50 "measurements" of fracture strength generated by computer. The computer chose 50 specimens containing two concurrent Weibull flaw distributions with the parameters shown on Fig.(3). The fracture strength for each specimen was calculated by choosing a pair of random fracture strengths, one from distribution A and one from B. If the fracture strength from A was less than that from B, the specimen was designated as failing from flaw type A at that fracture strength. Conversely, if fracture strength B was less than A, the specimen was designated as failing at a flaw of type B. The type of fracture origin in each specimen is identified on Fig.(3) by its associated symbol. Although it is not overwhelming in this example, there is a tendency for fracture origins from flaw type A to predominate at lower stresses (where the combined behavior approaches the behavior of flaw distribution A) and for origins of type B to predominate at higher stresses.

The 50 data points of Fig.(3) were chosen from a population of specimens containing flaw distributions described perfectly by the two-parameter Weibull distribution. Nevertheless, sampling errors in this moderate number of specimens result in less than perfect fit of the data to the relationship which generated them. Many other random choices of 50 specimens will result in considerably greater discrepancies. Thus, caution should be exercised in interpretation of minor "kinks" and "knees" in real experimental data.

Extrapolation of empirical functions are always subject to error, but extrapolation of fracture probability functions are particularly dangerous if multiple flaw distributions may be present. For instance,

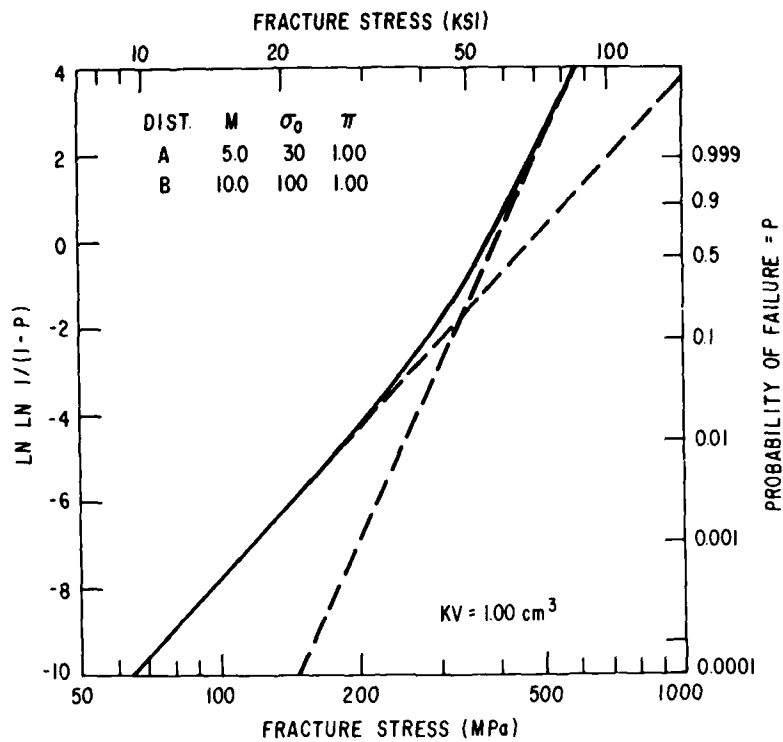


Fig.(2). Example of two concurrent flaw distributions.

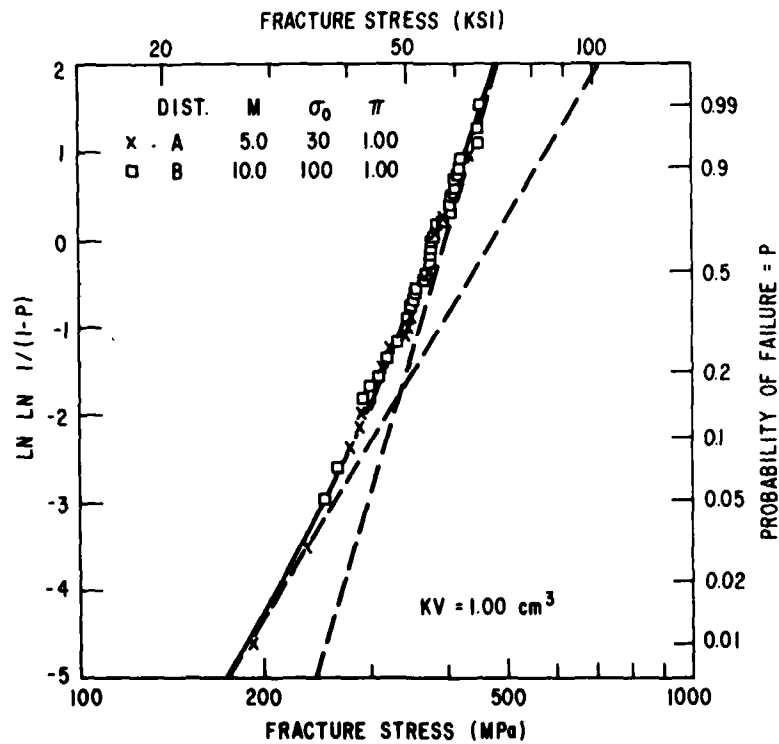


Fig.(3). Concurrent flaw distributions of Fig.(2) with 50 computer-generated fracture strengths.

if the flaw distributions illustrated in Figs.(2) and (3) were contained in test specimens with effective volumes of 0.01 cm^3 , the fracture behavior would correspond to the solid line on Fig.(4). An effective volume of 0.01 cm^3 is not uncommon in bend specimens. Also included on Fig.(4) are 50 computer-generated fracture strengths. Although each test specimen contained both distributions, distribution B with the larger Weibull modulus was heavily favored due to the smaller effective volume. Of the 50 specimens illustrated on Fig.(4), only one failed from a flaw of distribution A. If this data alone were used to predict the failure probability of a large component, one would have to assume that the apparently linear relationship of the data would continue uninterrupted over all ranges of strength and failure probability. Assuming a single distribution of flaws, linear regression would yield an estimated m and σ_0 very similar to those of distribution B.

If a large component of interest has an effective volume of 100 cm^3 , the same two flaw distributions result in the relationships plotted on Fig. 5. Again, 50 computer-generated fracture strengths are included, illustrating that the fracture behavior is predominated by distribution A with the smaller Weibull modulus. The solid line of Fig.(5) shows that the weakest of 50 components should fail at approximately 75 MPa. If the data of Fig.(4) were used to predict that value, the best estimate would be approximately 160 MPa as shown by the dashed line for distribution B. At a stress of 160 MPa, nearly 40 percent of the large components would fail instead of 2 percent as predicted from Fig.(4).

Several additional comments should be included concerning concurrent flaw distributions:

1. Unobserved concurrent distributions outside the experimental data base cannot be ruled out. Extrapolation to larger specimen sizes or lower probabilities of failure are therefore subject to non-conservative errors as illustrated in Figs.(4) and (5).
2. When several concurrent flaw distribution are present, the distribution with the lowest Weibull modulus (largest variability) will predominate at the largest specimen sizes and the smallest probabilities of failure.
3. In general, the removal of a distribution of concurrent flaws which had been responsible for the majority of failures will result in an increase in the average strength and a decrease in the apparent Weibull modulus. Such an improvement will not increase the strength of large components if their strength is controlled by a lower modulus distribution.
4. Changes in processing and fabrication procedures may introduce a concurrent flaw distribution which will decrease the useful strength of a large structure, but the change in flaw population may not be evident in small test specimens.
5. The knee in the curve resulting from concurrent flaw distributions is near the intersection of the two straight line relationships for the individual flaw distributions (near the intersection of the dashed lines on Figs.(2)-(5)). If both distributions are composed of volume flaws or both surface flaws, the fracture strength at the intersection is independent of the specimen size and loading configuration. If one distribution is volume and the other is surface, however, the strength at the intersection will vary with different load factors.

Confirmed examples of concurrent flaw distributions in real materials are rare, but one probable example is a commercial Al_2O_3 tested in three and four-point bending by Bansal, Duckworth and Niesz(12,13). In this example, the fracture origins were identified, thus helping to substantiate the presence of multiple flaw distributions. The authors kindly provided more detailed results than those available in the literature. A total of 76 bend specimens of Alsimag 614[®] were tested in six variations of specimen size, loading configuration and environment. Specimens were prepared in two sizes: $2.5 \times 5.0 \times 38 \text{ mm}$ and $13 \times 25 \times 190 \text{ mm}$. The smaller specimens were tested in both three-point bending on a 32 mm span and four-point bending with a 32 mm outer span and 19 mm inner span. The larger specimens were all tested in four-point bending with 159 mm outerspan and a 95 mm inner span. The above specimen configurations were tested both in dry nitrogen at high loading rates (100 MPa/s) to minimize subcritical crack growth, and in distilled water at slower loading rates (4 MPa/s) to enhance the rate of crack growth. The results of the six variations, as included in Ref.(13), are plotted on Fig.(6) as $\ln \ln (1/1-P)$ vs. \ln strength. As expected, the specimens tested in water had lower strengths than those tested dry. Also, the larger specimens consistently yielded lower strengths than small specimens. The Weibull moduli of the three groups tested in water were constant at a value of 34, but the moduli of the specimens tested dry varied from 34 for the small three-point specimens to 11 for the large four-point specimens.

Fractography as reported by Bansal et al. revealed that all specimens tested in water failed from flaws extending from the tensile surface. No voids or inclusions were associated with the surface flaws. Of the small specimens tested in dry nitrogen approximately 80 percent failed from origins extending from the tensile surface, 10 percent were located at large, subsurface pores, and the remaining 10 percent were not clearly identified. All of the large specimens tested in dry nitrogen failed from large, irregular, subsurface pores. Bansal et al. concluded from the decrease in Weibull modulus and the two types of fracture origins that two active flaw distributions were present. They also concluded that Weibull statistics could not describe the observed behavior. No attempts were made to determine if the data were consistent with relationships such as Eq.(13). The following re-analysis illustrates that two-parameter Weibull statistics describe the data exceptionally well if the specimens are assumed to contain two concurrent flaw distributions.

In order to visually and mathematically judge the agreement between a distribution function and data from multiple specimen sizes and loading configurations, one must normalize all data to a single specimen size and loading configuration(14). Each original piece of fracture data consists of a fracture strength and an estimated probability of failure. Normalizing to a different specimen size can be accomplished in two

[®]3M Co., Technical Ceramic Products Division, Chattanooga, Tenn.

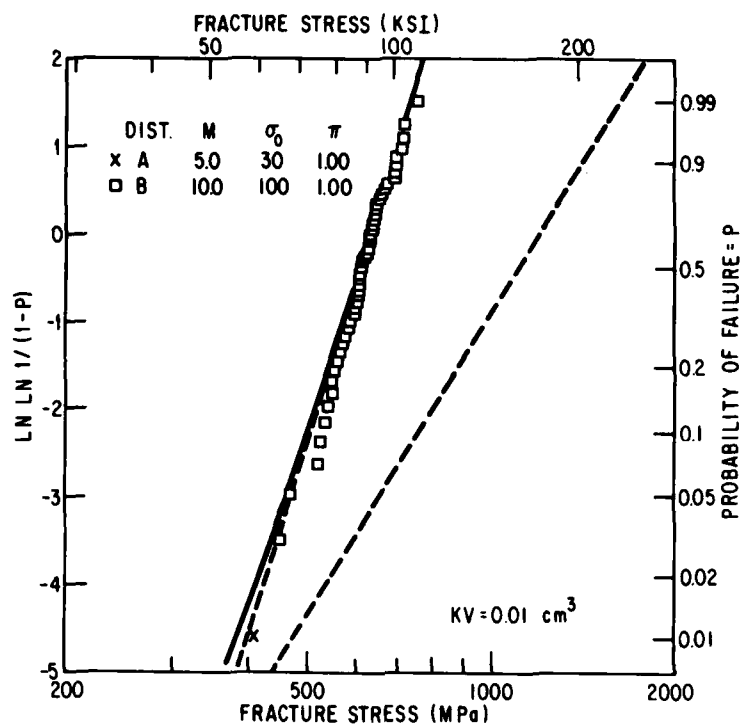


Fig.(4). Concurrent flaw distributions when present in specimens with 1/100th the volume of those in Fig.(3).

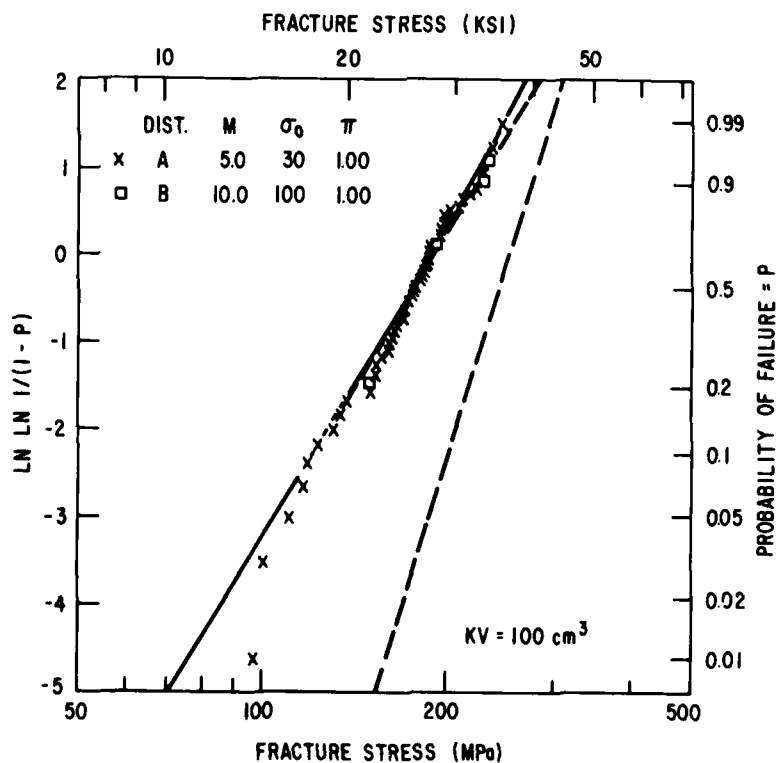


Fig.(5). Concurrent flaw distributions when present in specimens with 100 times the volume of those in Fig.(3).

ways: the strength can be shifted by an appropriate amount with no change in probability of failure, or the probability of failure can be shifted with no change in the strength. The latter is the only practical choice for multiple flaw distributions.

Consider a material such as that tested by Bansal et al. which may contain two concurrent flaw distributions, one consisting of surface flaws and the other consisting of volume flaws. Equations of the form of Eq.(13) can be written for each of two specimen sizes and loading configurations designated by subscripts α and β .

$$P_{\alpha} = 1 - \exp \left[- K_{\alpha} A_{\alpha} \left(\frac{\sigma_M}{\sigma_{OA}} \right)^{m_A} - K_{\alpha} V_{\alpha} \left(\frac{\sigma_M}{\sigma_{OB}} \right)^{m_B} \right] \quad (14)$$

$$P_{\beta} = 1 - \exp \left[- K_{\beta} A_{\beta} \left(\frac{\sigma_M}{\sigma_{OA}} \right)^{m_A} - K_{\beta} V_{\beta} \left(\frac{\sigma_M}{\sigma_{OB}} \right)^{m_B} \right] \quad (15)$$

These two equations can be combined and rearranged to yield:

$$P_{\beta} = 1 - (1 - P_{\alpha})^{\gamma} \quad (16a)$$

$$\gamma = \frac{K_{\beta} A_{\beta} \left(\frac{\sigma_M}{\sigma_{OA}} \right)^{m_A} + K_{\beta} V_{\beta} \left(\frac{\sigma_M}{\sigma_{OB}} \right)^{m_B}}{K_{\alpha} A_{\alpha} \left(\frac{\sigma_M}{\sigma_{OA}} \right)^{m_A} + K_{\alpha} V_{\alpha} \left(\frac{\sigma_M}{\sigma_{OB}} \right)^{m_B}} \quad (16b)$$

Equation(16) can be used to normalize the probability of failure from any specimen size and geometry to any other. It should be noted, however, that m and σ_0 must be known or estimated for each distribution before data can be normalized.

Using Eq.(16), all of the fracture data of Fig.(6) were normalized to probabilities of failure for small three-point bend specimens and were re-plotted on Fig.(7). Using the hypothesis that both area and volume flaws were active in dry nitrogen, the four Weibull parameters of the bimodal flaw distribution were varied iteratively to find the combination with the least scatter between measured and predicted behaviors. For the specimens tested in dry nitrogen, these parameters were $m_A = 29.1$, $\sigma_{OA} = 5.76$ MPa, $m_B = 8.2$, $\sigma_{OB} = 1.33$ MPa. The first two parameters describe the distribution of surface flaws, while the second two describe the volume flaws. The solid curve drawn through the dry nitrogen data of Fig.(7) represents the predicted behavior of the combined distribution according to the above parameters. The fracture origins below the knee are predominated by volume flaws while those above are predominated by surface flaws.

The same two distributions of flaws were present in specimens tested in water. If a mechanism of subcritical crack growth became active due to the environment, however, the effects would be seen only on surface flaws since the internal flaws were isolated from the aqueous environment. The fracture origins of specimens tested in water were reported to be exclusively surface flaws with no failures observed at internal voids. All of the fracture data of specimens tested in water are consistent with a single distribution of surface flaws. Presumably, these flaws are of the same distribution as the surface flaws observed in dry nitrogen, but in the aqueous environment the flaws are significantly extended by subcritical crack growth prior to failure. The curve drawn through the solid data points of Fig.(7) was calculated by assuming that the volume flaws observed in dry nitrogen were also present in the specimens tested in water and that they were not affected by the aqueous environment. The two parameters for the volume distribution were therefore assumed to be identical to those listed above for dry nitrogen. The remaining two parameters for the modified surface distribution were varied iteratively to find those which best described the data. The resulting four parameters were: $m_A = 36.3$, $\sigma_{OA} = 4.49$ MPa, $m_B = 8.2$ and $\sigma_{OB} = 1.33$ MPa. As seen on Fig.(7), the volume distribution should not become active within the range of probabilities of failure of the data. If more data had been collected on the large four-point specimens tested in water or if even larger specimens had been tested, then one would expect some failures to originate from the volume flaws.

B. Exclusive Flaw Distributions

As described earlier, a group of specimens or components contain exclusive flaw distributions if those specimens containing flaw distribution A contain no flaws of distribution B and vice versa. The fraction of specimens containing only flaws from distribution A will be designated as π_A and that fraction containing only distribution B will be designated π_B . Since every specimen is contained in one of the two subgroups:

$$\pi_A + \pi_B = 1 \quad (17)$$

If the subgroups are mixed without identification and one specimen is chosen randomly from the mixture, the probability of failure is:

$$P_T = \pi_A P_A + \pi_B P_B \quad (18)$$

A relationship similar to Eq.(18) was first suggested by Weibull(11) and has since been used by others(15,16). Eq.(18) is valid for exclusive flaw populations regardless of the form of the distribution functions describing P_A and P_B . If the two-parameter volume Weibull distribution is valid for both flaw

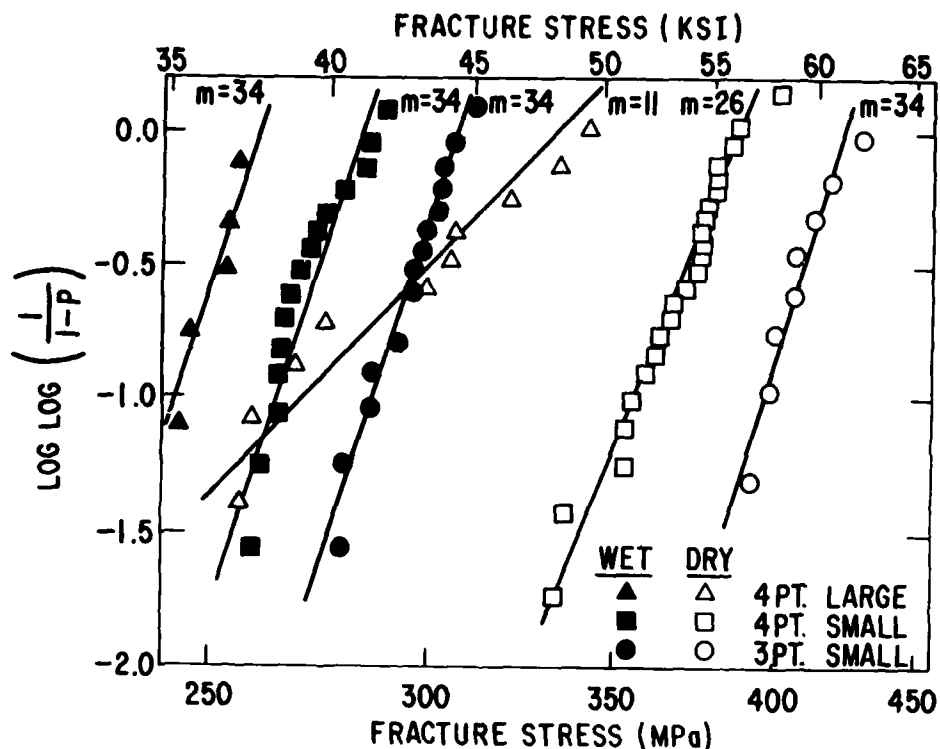


Fig.(6). Effects of specimen size, testing configuration and environment on the strength of Al_2O_3 (12,13).

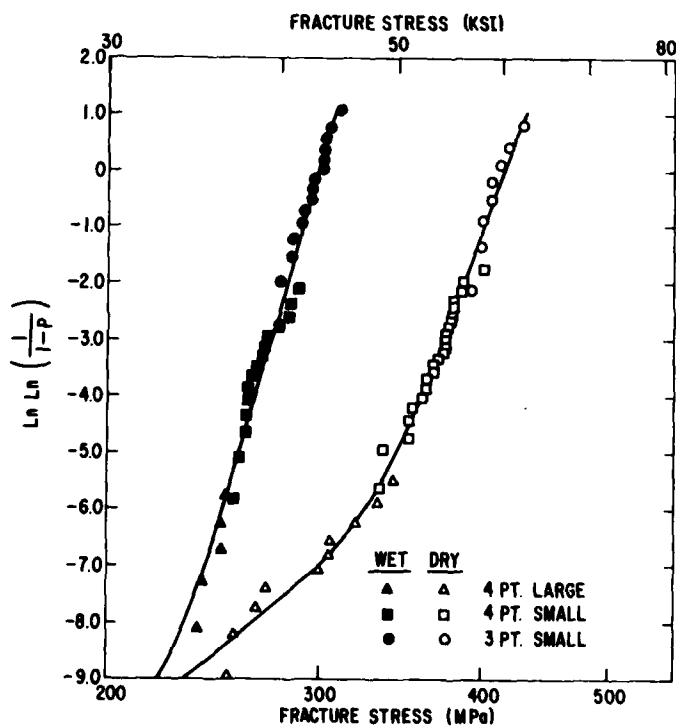


Fig.(7). Data of Fig.(6) normalized to equivalent probabilities of failure for the small three-point bend specimens.

populations, then Eq.(5) and Eq.(18) yield:

$$P_T = 1 - \pi_A \exp \left[-K_V V \left(\frac{\sigma_M}{\sigma_{OA}} \right)^{m_A} \right] - \pi_B \exp \left[-K_V V \left(\frac{\sigma_M}{\sigma_{OB}} \right)^{m_B} \right] \quad (19)$$

Equation(19) is plotted on Fig.(8) with the same four adjustable parameters as those in Figs.(2)-(5), with $\pi_A = \pi_B = 0.5$ and with an effective volume of 0.01 cm^3 . Again, the solid line represents the combined distribution function while the dashed lines represent the individual distributions. As illustrated in Fig.(8), the combined behavior asymptotically approaches the behavior of the distribution with the smaller Weibull modulus at very high stresses and probabilities of failure. At very low stresses and probabilities of failure, the combined behavior asymptotically approaches a straight line parallel to the low modulus distribution but displaced downward by a factor of π_L (where π_L is the value of π for the lower modulus distribution). The solid line and the two dashed lines intersect at a common point. This is the case for all exclusive distributions as can be easily proven from Eq.(18).

Again, an extremely large range of probabilities is included on Fig.(8) to illustrate the overall behavior of exclusive flaw distributions. The same relationship is plotted on Fig.(9) with an experimentally realistic range of failure probabilities. Also included are 50 computer-generated data points. The computer chooses random specimens from an infinite number of possible specimens all of which are consistent with Eq.(19). Thus, the number of failures from distribution A will not generally equal the exact expected number which is π_A times the total number of specimens.

The shape of the combined distribution function is sufficiently complex that details of the shape cannot be deduced from the fracture of only 50 specimens. The data points of Fig.(9) could be easily interpreted as falling on two intersecting straight lines producing a knee with negative curvature. Extrapolation of such an assumed relationship would obviously lead to large errors. Knowledge that exclusive distributions cannot produce a single knee with negative curvature should help to avoid such errors.

Additional comments concerning exclusive flaw distributions include:

1. As illustrated on Fig.(9), the apparent slope of data points with common fracture origins is not necessarily an accurate estimate of the Weibull modulus of that distribution.
2. Since the low modulus distribution controls the combined distribution at both very high and very low stresses, fracture origins from the low modulus distribution should predominate in both extremes of fracture stress. The range of experimental data, however, may not be sufficient to reveal such a predominance at both extremes.
3. Variations of the values for m , σ_0 and π can yield a variety of appearances for the combined behavior of two exclusive distributions. Space limits the number of graphical examples, but over limited ranges of probability, the combined distribution function can appear to have a straight line behavior with both types of origins mixed quite uniformly; it can have a knee with positive curvature similar to concurrent distributions; or it can have multiple knees proceeding from positive to negative curvature with increasing stress or from negative to positive curvature such as Fig.(9).
4. If exclusive distributions are assumed, then a reasonable estimate for π_A is the number of fracture origins from flaw type A divided by the total number of specimens tested.
5. Unlike concurrent distributions, the frequency of occurrence of particular fracture origins is independent of specimens size, loading configuration, etc.

C. Partially Concurrent Flaw Distributions

A group of specimens or components contains partially concurrent flaw distributions if all specimens contain one flaw distribution but only a fraction contain the other. The distribution contained in all specimens will be designated as distribution A, while the other will be designated as distribution B. By the terminology of the previous section, $\pi_A = 1$ and $\pi_B < 1$. In the limit of $\pi_B = 1$, all specimens contain both distributions and the behavior is that of concurrent flaw distributions. The mathematics of partially concurrent distributions are best described by considering two mutually exclusive states. A specimen either contains distribution A alone or it contains both distributions in a concurrent manner. The fraction of specimens in the second state is π_B , therefore the fraction in the first state must be $1 - \pi_B$. Combining Eq.(12) and Eq.(18) yields:

$$P_T = (1 - \pi_B) P_A + \pi_B (1 - (1 - P_A)(1 - P_B)) \quad (20)$$

If $\pi_B = 1$, Eq.(20) properly reduces to Eq.(12) for concurrent distributions. If $\pi_B = 0$, then $P_T = P_A$ as expected. Equation (20) is valid for partially concurrent flaw populations regardless of the type of distribution function describing P_A and P_B . If the two-parameter volume Weibull distribution is valid for both flaw populations, then Eqs.(5) and (20) yield:

$$P_T = 1 - (1 - \pi_B) \exp \left[-K_V V \left(\frac{\sigma_M}{\sigma_{OA}} \right)^{m_A} \right] - \pi_B \exp \left[-K_V V \left(\frac{\sigma_M}{\sigma_{OA}} \right)^{m_A} - K_V V \left(\frac{\sigma_M}{\sigma_{OB}} \right)^{m_B} \right] \quad (21)$$

Eq.(21) is plotted on Figs.(10) and (11) using the same four adjustable parameters as used earlier. In Fig.(10), the lower Weibull modulus distribution is chosen as distribution A (contained in all specimens). In Fig.(11), the higher modulus distribution is distribution A. This seemingly minor variation leads to significant differences in the shapes of the curves describing the combined behaviors. In all cases of partially concurrent distributions, the combined behavior asymptotically approaches the behavior of distribution A at high stresses and probabilities of failure. Similar to exclusive distributions, at low stresses

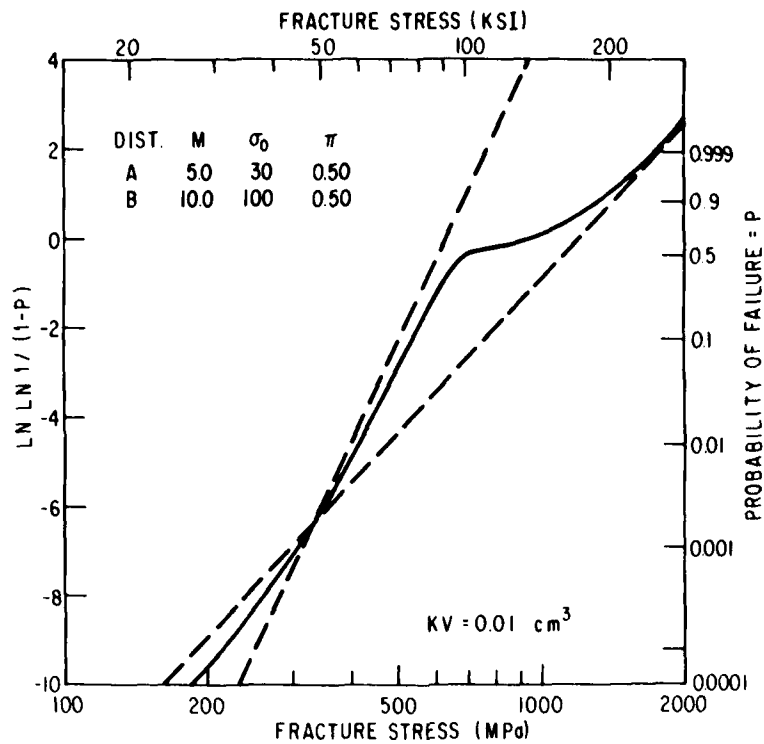


Fig.(8). Example of two exclusive flaw distributions.

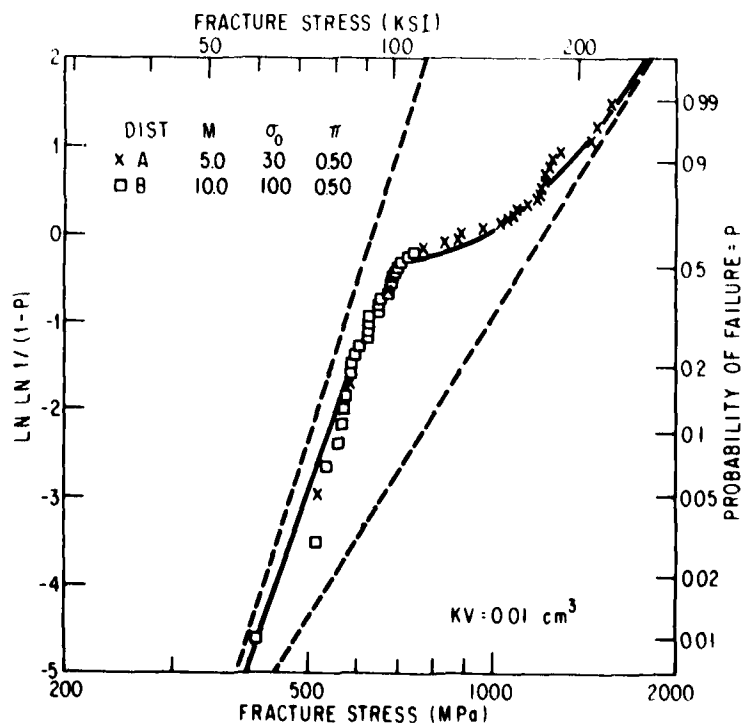


Fig.(9). Exclusive flaw distributions of Fig.(8) with 50 computer-generated fracture strengths.

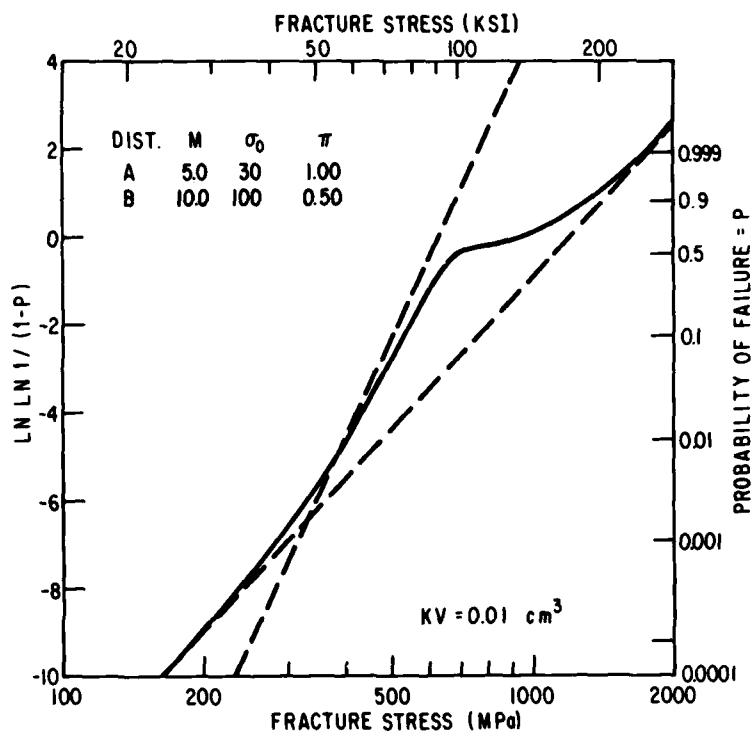


Fig.(10). Example of two partially concurrent flaw distributions with the smaller Weibull modulus distribution present in all specimens.

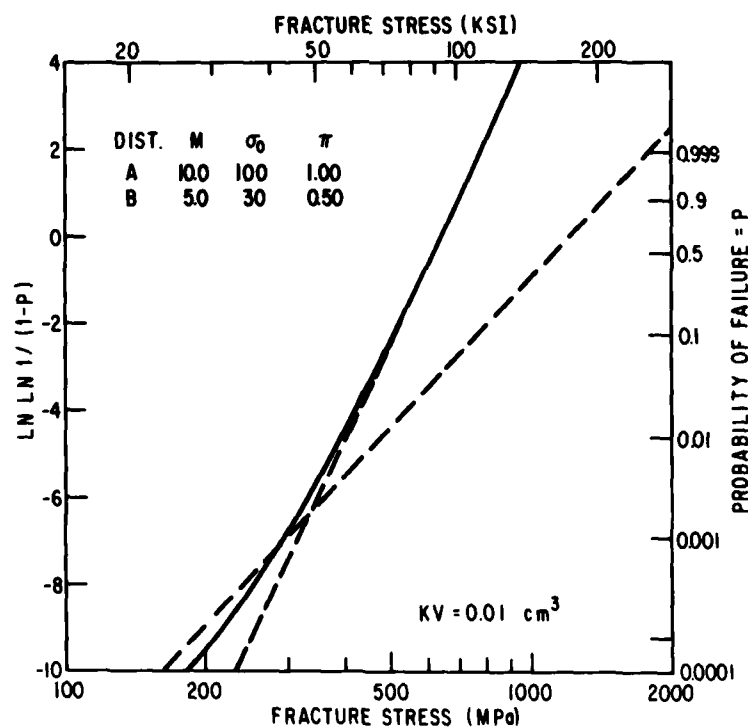


Fig.(11). Example of two partially concurrent flaw distributions with the larger Weibull modulus distribution present in all specimens.

and probabilities of failure, the combined behavior asymptotically approaches a straight line parallel to the low modulus distribution but displaced downward in probability of failure by a factor of σ_L .

Note that the shape of the combined behavior in Fig.(10) is nearly indistinguishable from that on Fig.(8) for exclusive distributions and the shape of the combined behavior on Fig.(11) is nearly indistinguishable from Fig.(2) for concurrent distributions. The partially concurrent distributions of Figs.(10) and (11) are plotted on Figs.(12) and (13) with a smaller range of probability of failure and with 50 computer-generated fracture strengths for each. The trends of predominate fracture origins are remarkably similar on Figs.(12) and (9) and on Figs.(13) and (4). Due to such similarities, given the fracture strengths and fracture origins of Fig.(12), one cannot differentiate between exclusive and partially concurrent distributions. In a similar manner, given the data of Fig.(3), one cannot differentiate between concurrent and partially concurrent distributions. The ability to differentiate does not improve significantly even with 500-1000 specimens.

On the other hand, if the behaviors cannot be distinguished from each other, the error involved in assuming the incorrect behavior must be very small. Thus, from a practical point of view, one can assume that all multiple flaw distributions are adequately described as either concurrent or exclusive flaw distributions.

DISCUSSION

None of the three types of multiple flaw distributions discussed above is capable of yielding a single knee with negative curvature when plotted as Fig.(1). A mathematical description exists for such behavior, but the physical analog seems unlikely in real materials. Such a material would contain both distributions in each specimen similar to concurrent distributions. Failure would not occur, however, until the critical stress had been reached for a flaw from each distribution. For example, if the most severe flaw in a specimen were one of type A, failure would not occur until the stress was sufficient to propagate the most severe flaw of type B. The total probability of failure of a material with two such distributions is:

$$P_T = P_A P_B \quad (22)$$

When plotted as Fig.(2), the combined behavior would asymptotically approach the high modulus behavior at low stresses and asymptotically approach the low modulus behavior at high stresses. This behavior contradicts the weakest link concept and is therefore considered unlikely, even in composite materials.

Previous discussions and examples have used the two-parameter Weibull distribution in order to graphically demonstrate the behaviors of different types of multiple flaw distributions. Most of the conclusions, however, can be applied equally well to other distribution functions. In order to plot the two-parameter Weibull function as a straight line (for a single flaw population), the two variables, P and σ , were transformed to $\ln \ln (1/1-P)$ and $\ln \sigma$. When the variables were so transformed, a single flaw population resulted in a straight line. An analogous transformation of variables exists for every possible distribution function. The transformation of variables for other distributions may be considerably more complex than that illustrated for the Weibull distribution and may even require numerical methods. Nevertheless, every distribution can be transformed to linear variables. When plotted as the appropriate transformed variables for the distribution function of interest, the deviations from linearity, the asymptotic trends, etc. described earlier for Weibull distributions are equally valid for multiple flaw populations conforming to other distribution functions.

As discussed earlier, problems often arise in distinguishing concurrent distributions from some types of partially concurrent distributions and in distinguishing exclusive distributions from other types of partially concurrent distributions. Testing programs can sometimes be planned to help identify the manner in which the multiple flaw populations are contained. As an example, consider a group of 100 bend specimens which fail from two types of flaws. The specimens were purchased from a vendor, not as test specimens, but as 25 components. Four test specimens were machined from each component and records of position and originating component were kept for each specimen. After testing and fractography, if specimens from common components always have a common type of fracture origin, then the distributions are probably exclusive. If specimens from common components generally contain mixed fracture origins, then the distributions are probably concurrent. If several sub-groups are found to have common origins of one flaw type while most of the remaining sub-groups have mixed origins, then the distributions are probably partially concurrent. If the specimens from the "center" of the components tend to fail from flaws of a different type than those from near the component surface, then the components are probably inhomogeneous in properties through the thickness. In any case, none of this additional information would be available without proper records for each specimen.

REFERENCES

1. W. Weibull, "A Statistical Theory of the Strength of Materials", Royal Swedish Academy of Eng. Sci. Proc., 151, 1-45 (1939).
2. W. Weibull, "A Statistical Distribution Function of Wide Applicability", J. App. Mech., 18, 293-297 (1951).
3. E. J. Gumbel, Statistics of Extremes, Columbia Univ. Press (1958).
4. A. G. Evans and T. G. Langdon, "Structural Ceramics", Prog. Mater. Sci., 21, (3-4) 171-441 (1976).
5. J. R. Matthews, F. A. McClintock and W. J. Shack, "Statistical Determination of Surface Flaw Density in Brittle Materials", J. Am. Ceram. Soc., 59 (7-8) 304-308 (1976).
6. A. G. Evans and R. L. Jones, "Evaluation of a Fundamental Approach for the Statistical Analysis of Fracture", J. Am. Ceram. Soc., 61 (3-4) 156-160 (1978).

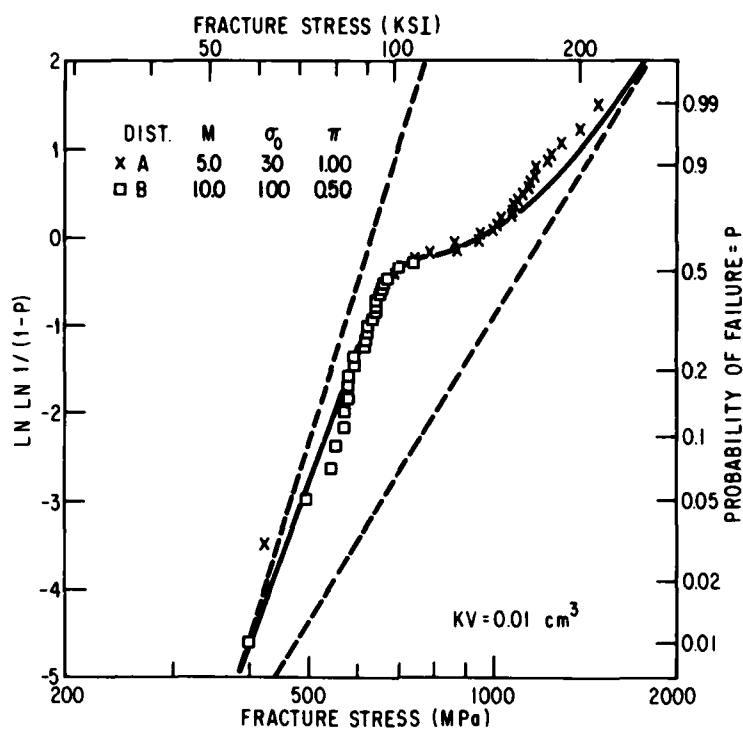


Fig.(12). Partially concurrent flaw distributions of Fig.(10) with 50 computer-generated fracture strengths.

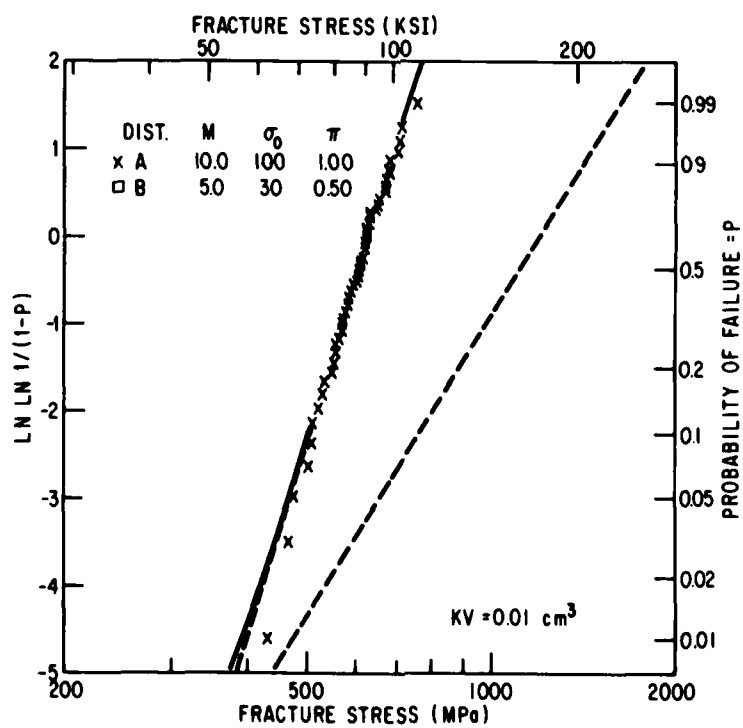


Fig.(13). Partially concurrent flaw distributions of Fig.(11) with 50 computer-generated fracture strength.

7. S. M. Wiederhorn and N. J. Tighe, "Proof-Testing of Hot-Pressed Silicon Nitride", J. Mater. Sci., 13 (8) 1781-1793 (1978).
8. N. R. Mann, "Estimators and Exact Confidence Bounds for Weibull Parameters Based on a Few Ordered Observations", Technometrics 12 (2) 345-361 (1970).
9. C. A. Johnson, "Confidence Bounds on Parameters of the Weibull Distribution", to be published.
10. S. B. Batdorf, "Some Approximate Treatments of Fracture Statistics for Polyaxial Tension", Int. J. of Fracture, 12(1), 5-11 (1977).
11. W. Weibull, "The Phenomenon of Rupture in Solids", Royal Swedish Academy of Eng. Sci. Proc., 153, 1-55 (1939).
12. G. K. Bansal, W. H. Duckworth and D. E. Niesz, "Strength-Size Relationships in Ceramic Materials", Final Report, Contract N00014-73-C-0408, NR 032-541, Oct. 1975.
13. G. K. Bansal, W. H. Duckworth, D. E. Niesz, "Strength-Size Relations in Ceramic Materials: Investigation of an Alumina Ceramic", J. Am. Ceram. Soc., 59 (11-12) 472-478 (1976).
14. C. A. Johnson and S. Prochazka, "Investigation of Ceramics for High Temperature Turbine Components", Final Report, Contract N62269-76-C-0243, June 1977.
15. W. D. Scott and A. Gaddipati, "Weibull Parameters and the Strength of Long Glass Fibers", in Fracture Mechanics of Ceramics 3, 125-142 (1978) Plenum Press.
16. D. Kalish, B. K. Tariyal and R. O. Pickwick, "Strength Distributions and Gage Length Extrapolations in Optical Fibers", Am. Ceram. Soc. Bull. 56 (5) 491-503 (1977).

REACTION-BONDED, SIALON AND CVD Si_3N_4 CERAMICS FOR ENGINEERING APPLICATIONS

D J Godfrey
Admiralty Marine Technology Establishment (Holton Heath)
Holton Heath, Poole, Dorset BH16 6JU

SUMMARY

Recent developments in the development of reaction-bonded, chemical-vapour deposited, and sialon and related silicon nitride ceramics in the UK are reviewed in relation to their possible application in engines. Factors which affect the strength of RBSN include nitriding conditions (flow, temperature schedule, furnace sealing), powder size and reaction-promoting impurities. Significant variations in thermal conductivity have been observed. Oxidative degradation of strength can be serious, and oxide impregnation can reduce it. CVD Si_3N_4 materials have so far had disappointing strengths and have been difficult to apply thickly over large areas, although recently progress has been made. Basic scientific research on Sialon and related materials has continued to elucidate their often complex nature, but recent UK activity has concentrated successfully on the metal cutting and processing applications of sintered sialons, rather than optimizing them for engine applications.

INTRODUCTION

Silicon nitride ceramics can be divided into four categories:

- (1) reaction-bonded ("reaction-sintered") materials produced by the nitridation of silicon powder compacts (RBSN).
 - (2) hot-pressed ("pressure sintered") materials made by the effect heat and pressure on silicon nitride powder to which additions have been made (HPSN).
 - (3) sintered ("pressureless-sintered") materials, usually made from Si_3N_4 powder with an addition of other materials.
- and (4) chemically formed materials, by methods such as chemical vapour deposition ('CVD or pyrolytic') or, recently, by decomposition of inorganic polymers.

Both RBSN and HPSN have been developed during the last two decades. RBSN typically is relatively easy to fabricate in large, complex or precise shapes, but has only a moderate strength (up to about 300 MPa) but this is however relatively unaffected by temperature. HPSN is much stronger but large, complex or precise components are difficult and expensive to fabricate, and strength shows a progressive deterioration with temperature above about 1000°C, although considerable progress has been made in ameliorating this problem. Both materials can show considerable falls in strength after oxidation (up to 40%), although again some progress has been made in mitigating this.

Silicon carbide has a better thermal stability at very high temperatures ($\geq 1600^\circ\text{C}$), has a thermal conductivity 4 to 2 times greater (depending on temperature) than silicon nitride, it has however a thermal expansivity about 50% greater than silicon nitride; and also its stiffness is also about 50% greater than a Si_3N_4 material of comparable texture. Although its good thermal conductivity make it a powerful candidate amongst the ceramic materials options for engines, and it has been extensively developed in the UK to yield a material with mechanical properties falling in between RBSN and HPSN by the UKAEA (Refel), it falls outside the specific scope of this review.

The materials situation was further complicated when it was discovered by Jack et al and also by Oyama that alumina Al_2O_3 was very soluble in beta Si_3N_4 , and a new family of materials existed in which nitrogen was substituted by oxygen, and silicon by aluminium (or even another cation), now generally known as Sialons (Si-Al-O-N).

Silicon nitride materials typically do not easily show the phenomenon of consolidation by sintering, this being a term generally used in ceramic science to denote densification by solid state diffusion or liquid surface tension and solution/precipitation effects, unless pressure was applied after suitable liquid-forming oxide had been added, such as MgO in the case of HPSN. This absence of such diffusional or liquid phase effects is responsible for the good creep performance possible from some silicon nitride ceramics.

Recently, methods of using liquid phase sintering mechanisms at very high temperatures have been evolved to yield sintered high density materials without the application of pressure, through the use of appropriate additives and an understanding of the complex solid-solution and crystalline phase equilibria involved.

Chemical vapour deposition with silicon halides or with silane have also been used to produce materials which have high density, but which are free of other phases which impair their high temperature mechanical properties, phase stability and corrosion resistance.

These areas will now be examined in greater detail, with special reference to the current state of the art in the UK, where most of the material approaches in this field originated, although it is currently not heavily supported, and their relevance to current experimentation with the use of ceramics in engines will be discussed.

REACTION BONDED SILICON NITRIDE

Most recent UK work has been concerned with the processes involved in the reaction of silicon powder with nitrogen and how these affect the development of mechanical properties of the silicon nitride ceramic. Silicon monoxide volatilization has been shown, by an approach which utilizes a strength/nitrided density plot with Si compacts nitrided to various degrees of completion, to play an important role in the primary nitridation process¹. Conditions such as a flowing instead of a static nitrogen gas atmosphere remove Si as SiO and increase the spacing between silicon particles, and reduce the strength of the final product. The reaction has two stages; in the first SiO volatilizes and reacts with N₂ to form Si₃N₄ and with Si to form SiO₂, which may then form more SiO by reaction with Si; nitrogen also reacts with the silicon uncovered by the initial volatilization of the original SiO₂ skin on the silicon particles; in the second stage which is the major part of the reaction, nitrogen reacts with liquid silicon alloy eutectic or with liquid silicon. As the melting point of pure silicon is 1414°C, this mechanism does not at first appear probable as the majority of the nitridation of 'commercial purity' silicon appears to take place around 1350°C. It is found however that pure silicon does not react appreciably until it is very near to its melting point, but that commercial-purity material reacts at an appreciably lower temperature². Further work has shown that only a very small amount of impurity is needed to give sufficient molten material as the eutectic is not itself turned into silicon nitride and impurity metal. Effective impurities in this respect are those in or near the first Periodic Table transition eg Mn, Fe, Co, Ni and Cu; all have oxides which are easily reducible at low oxygen potentials, and the temperatures at which the peak reaction occurs have been determined and correlate well with eutectic melting in the metal/silicon binary equilibrium diagrams. As the formation of liquid is therefore apparently virtually essential for the majority of the silicon powder to be reacted, it is difficult to avoid the production of some voids as silicon particles are lost to join the melt micropools, leaving empty the space which they occupied. If unreacted silicon particles are large, their melting does not take place until 1414°C is approached; the large particle is then mobilized, mostly probably by a "wetting" mechanism into a porous Si₃N₄ area, leaving a void which is a large strength-controlling defect. Wetting becomes favourable when oxide on the Si₃N₄ surface is reduced, as is shown by the ability of a vacuum environment to promote wetting of Si₃N₄ by Si. Thus it is necessary to produce a molten material to obtain substantially complete reaction, but melting tends to form defects such as voids, void-silicon associations, or large unnitrided inclusions of silicon. Sometimes silicon globules may be seen on the surface of the body which has been reaction-bonded; such translocation of silicon occurs by melting, especially if the reaction becomes too vigorous, as can occur if the temperature rise rate of the nitridation furnace is too great just below the maximum of the first or second reaction stage. This effect must increase the void content of the ceramic, but usually a void commensurate with the size of the globule of surface silicon cannot be found if the RBSN is microsectioned, showing that these globules are formed by the melting of widely dispersed silicon particles.

In the presence of carbon, or silicon carbides, serious reductions in the strength of the RBSN can occur, due to formation of appreciable quantities of silicon carbide and even silicon oxynitride. This effect was maximized experimentally in an impervious alumina reaction tube, by nitriding silicon powder compacts very close to (but not in contact with) graphite or silicon carbide powder. In several experiments the presence of graphite caused low strengths in the range 13 - 41 MPa for specimens within either a loose-lidded Al₂O₃ or RBSN box containing graphite powder; outside the box RBSN was produced with strengths which ranged between 21 and 65 MPa. Static nitrogen with a carbon rod adjacent to the specimen gave 112 MPa. Nitridation in the box which had been used for the graphite powder experiments but with deposits removed gave RBSN with strength ~205 MPa. Silicon carbide powder caused less severe strength reductions below the normal 200-230 MPa, and a silicon carbide heater rod beside two Si bars gave nearly normal RBSN strengths of 206 and 217 MPa. It is apparent that gaseous transport of carbon occurred, most probably via CO gas formed from trace impurities, inward diffusion of O₂ and H₂O through the refractory tube, and possibly the reaction of SiO with C, which is thermodynamically possible. This investigation was prompted by the experience that material 'nitrided' commercially could occasionally contain larger amounts of silicon carbide and silicon oxynitride than of silicon nitride; such material had very poor strength and the composition of the experimentally-produced low strength RBSN was similarly abnormal.

In the experimental 'carburizing' investigation referred to above already-nitrided RBSN exposed within the Si₃N₄ or Al₂O₃ boxes did not lose strength, although it gained just over 1% in weight, and SiC was formed in its surface.

Production of components for gas turbine experimentation, especially when quite large and complex shapes are required, is therefore a complex undertaking, and UK experience has shown that sometimes difficulties can be encountered with the commercial nitridation facilities, for experimental prototype production. In some of the commercial applications of RBSN the highest mechanical strength may not be of paramount importance, and also temperature schedules which suit the production of large numbers of small components are not always suitable for large components. Such difficulties are not inevitable. The shaping and nitridation of RBSN diesel pistons for experimental research on their engineering feasibility has however been successful in producing material with adequate strength and thermal conductivity, although this research project was not primarily concerned with optimisation of processing and nitridation to maximise thermomechanical properties³. Nevertheless, the funding of engineering programmes is often not very cognisant of the need for processing research on component fabrication, looking upon this as simply a purchasing operation; but there is need for research on the fabrication of large or complex components. At AMTE a 33 cm diameter 33 cm long nitridation facility is being constructed for this purpose.

It is now realized that material quality may vary, and the best way to monitor this has been found to be the 'control bar' approach, in which bars of silicon powder compact are placed adjacent to the component, and their strength measured afterwards. It is also easy to measure the weight gain due to reaction with nitrogen, although with commercial purity silicon the theoretical value of 67.6% is never achieved due to impurities, volatilization and unnitrided silicon. Experience has shown that weight gain is not a sensitive indicator of the mechanical strength of components.

For instance, relatively small variations in end-seal effectiveness on an experimental 10 mm diameter refractory-tube nitridation facility produced the following weight gain and strength data:

Strength MPa	Standard deviation	No. of tests	Weight % gain	Standard deviation	No. of bars
230	10	42	63.63	0.55	14
262	32	42	62.52	0.25	14
268	25	36	62.78	0.25	12
252	40	27	62.60	0.59	9
217	14	24	62.13	0.65	8

Deliberate attempts to contaminate the nitridation gas with oxygen do not produce a significant fall in quality,⁴ and it is possible that the leakage produces turbulence in the gas: as nitrogen 'flow' conditions have been shown to produce lower strength RBSN than a 'static' nitrogen nitridation environment,¹ it is possible that seal leakage effects are due to kinetic rather than impurity mechanisms.

The effects of oxidation are very important, especially their influence on strength. RBSN, because of its ca 12-14% accessible porosity (eg for a relative density of about 80%), has an appreciable surface area. Although the actual amount of oxidation is not great, nor very progressive, its effect on strength can be serious, with a deterioration in room temperature strength of up to 40% after a single exposure to 1250°C. It appears that some materials are worst affected at around 1029°C (1900°F), when the silicon dioxide protective film is less protective because it has considerable 'amorphous' character, whereas at higher temperature crystalline cristobalite tends to be formed. The loss in strength is due to the alpha-beta crystallographic phase change volumetric contraction undergone by cristobalite at around 270°C; when tested above this temperature strength is found to have been less seriously affected by high temperature oxidation: probably because a significant proportion of the strength deterioration is due to elastic strain, as well as actual cracking of the silica caused by the phase transformation contraction. Some workers have not experienced the serious degradation that has been studied in the UK with two different RBSN materials; if density can be improved giving a reduction in open void content it is probable that such disadvantageous behaviour can be made less severe. Another approach has been to impregnate with materials which react with silica, such as metal oxides, as these produce protective surface layers which diminish oxidation, and also do not show such severe degradation of room temperature strength, presumably because cristobalite formation is either reduced or virtually prevented. The most efficacious materials proved to be calcium oxide, strontium oxide, and magnesium aluminate. Their effects on creep performance were also assessed; calcium oxide produce the most significant increase, but the effect was not catastrophic. With an essentially non-porous material like HPSN it might be thought that oxidative degradation of strength would not occur, but strength deterioration of up to 40% has been observed with 5% MgO material, due to surface pitting. However close attention to stating material purity and the amount of hot pressing additives, and preoxidation treatments such as those developed at AiResearch can reduce such degradation significantly.

Corrosion of silicon nitride and silicon carbide can occur in liquid melts containing basic sodium; Riley has shown that at 1300°C Na₂SO₄ vapour converts the parabolic oxidation behaviour of RBSN into a linear process controlled by the availability of soda (as Na₂SO₄), which reacts to give non-protective liquid Na₂SiO₃ until the solubility of SiO₂ reaches that corresponding with the liquidus in the Na₂O-SiO₂ system. It would be interesting to see if those oxides which are effective in reducing RBSN oxidation and oxidative strength degradation would be helpful in improving soda corrosion resistance if this problem proves to be serious in the engine environment. Tests in the AMTE sea-salt sulphidation test rig for 200 hours at 750° and 830°C showed no detectable corrosion or significant strength deterioration of RBSN, although in such tests some unprotected superalloys are severely attacked. It is clear that the silicon ceramics have some advantages over superalloys at such temperatures, and it is not apparent how severe the sodium attack problem will prove; since the presence of appreciable molten corrodent on Si₃N₄ or SiC components would be a necessary factor. Singhal reported that HPSN and SiC exposed at 1100°C and 3 atmosphere pressure for 250 hours with diesel fuel to which 5 ppm sodium, 2 pp vanadium and 0.5 % sulphur had been added, performed as well as when tested with clean fuel. Presumably, the physical conditions for liquid melt residence on the test samples were not favourable in the high velocity environment. Schlichting has shown that Sialon has a better resistance than HPSN to attack when cycled in burner gas, and exposed to Na₂CO₃ solution during the cool part of the cycle. Sialon materials can form a mullite protective surface oxide which is more resistant to corrosion than silica. A further consideration is that engine environment is acidic and at high pressure, giving high values of pSO₂ which will tend to diminish the reaction: $\text{SiO}_2 + \text{Na}_2\text{SO}_4 \rightarrow \text{Na}_2\text{SiO}_3 + \text{SO}_3$.

SIALON MATERIALS

The discovery that silicon and nitrogen in Si₃N₄ can be replaced by aluminium and oxygen to form solid solutions in beta silicon nitride (β') called Sialons has led to a large amount of work on elucidation of the relevant phase equilibria and crystal chemistry, and on development of materials with enhanced performance. Hot pressed Sialon materials have been produced, and the absence of a silicon carbide surface layer after hot pressing is a useful advantage over HPSN. However it has proved possible to produce materials with good engineering properties, by sintering (eg at 1830°C), whereas attempts to produce dense silicon nitride by pressureless sintering without additives, have been rather unproductive, often involving high pressure environments or very fine powders, and have not proved very practicable.

The outstanding work at University of Newcastle-upon-Tyne on the understanding of the crystal structures, phase equilibria and properties of Sialons and related materials has continued, as has the technological development of materials by Lucas Industries Ltd, where the basic Si₆₋₇Al₂O₂N₈₋₇ formula for Sialons was established by Lumby.

Be-Si-Al-O-N materials prepared by the Lawrence Livermore Laboratories have been characterized at Newcastle⁶, and an extensive range of solid solutions has been shown to exist at high temperatures; up to 2 or 3 phases can coexist, probably due to the occurrence of a miscibility gap, and it appears that at least some compositions can be melted and cooled without decomposition. This is a conclusion of considerable technological importance, since decomposition and gas evolution during high temperature firing is a serious

problem with Sialon-type materials, since it can hinder the development of optimum mechanical properties. The early promise of improved mechanical properties at elevated temperatures (as compared with magnesia-containing HPSN) offered by the use of yttrium oxide as a hot-pressing additive has been complicated by the tendency of quaternary crystalline phases such as Nitrogen-melilite $Y_2Si(Si_2O_3N_4)_2$, N-apatite $Y_{10}(SiO_4)_6N_2 - Y_9.7(SiO_4)_6ON$, N-yttrium aluminate $Y_4Si_2O_7N_2$ and N- α -Wollastonite $Y_2O_3Si_2N_2O$ to oxidize catastrophically at around 1000°C. These phases have been studied at Newcastle and further research on the Y-Si-O-N system has confirmed that, as discovered by Lange, compositions within the $Si_3N_4 - Si_3N_2O - Y_2Si_2O_7$ compatibility triangle, ie without quaternary crystalline phases, do not show a catastrophic oxidation behaviour, and in fact give ceramics with excellent promise. Since crystalline phases are not present to absorb impurity oxides (eg CaO) which are compatible with their crystalline structures, such materials are more susceptible to impurities which can increase the proportion of glass and lower its softening temperature. Addition of aluminium oxide to the Y-Si-O-N system slightly reduces its high temperature strength, although the highest-ever room temperature strength reported for silicon nitride (1330 MPa at RT - Venables⁷) was obtained with a Sialon containing an yttrium aluminosilicate glass. The Ce-Si-O-N system has been studied. It has the advantage that the molar content of Ce_2O_3 to form unwanted easily-oxidized N-apatite phase is three times the level at which this phase is formed in the Y-Si-O-N system, and it is easier to stay in the quaternary phase-free $Si_3N_4 - Si_3N_2O - Ce$ silicate compatibility triangle (this is often somewhat difficult to arrange as the amount of silica on the surface of silicon nitride may vary). Although there is little surface degradation with a 2 w/o CeO_2 material at 1400°C, serious attack occurs with greater concentrations, and generally the oxide film tends to crack. At appreciable oxygen potentials the Ce^{3+} state oxidizes and oxynitrides decompose to CeO_2 with gas evolution disrupting the surface layer.

The possibility of forming high strength silicon nitride ceramics by hot pressing and sintering has been the subject of much research and development at Lucas Industries. More details on the sintering of Sialon materials containing moderate amounts of AlO (eg typically $x = 0.5$, ranging up to 1.1, in the formula $Si_{6-2x}Al_2O_2N_{3-2}$), have been published (US Pat No 4,127,416), and some of the more interesting are given in Table 1. Pressureless-sintered materials with good strength at room temperature in the range 700-800 MPa, and strengths >600 MPa at 1225°C and even 1370°C have been achieved, as have significant improvements in creep resistance eg 0.01% strain in 43 hours with a load of 77 MPa at 1227°C. Creep resistance is improved by a heat treatment at 1400°C which transforms most of the vitreous phase to yttrium aluminium garnet ($Y_3Al_5O_{12}$). There is great interest in these materials for metal handling and cutting applications and optimisation for this application appears to have been emphasised recently, so that their potential for engine applications has not been explored. Data quoted by Lumby suggest that their thermal conductivity may not be as low as other data for sintered Sialons eg thermal diffusivity at 200°C of 4 mm²/s, quoted in comparison with a value of 3 for HPSN, (such comparison are difficult: other UK work has indicated a value of 13.0 mm²/s for HPSN at 211°C). However good resistance to thermal stress is claimed.

Before such materials can be used easily and effectively in engines more complete data should be obtained on thermal transport properties, in view of the wide range of published data. Such research could enable thermal conductivities to be optimized; it is noteworthy that mechanical properties are frequently used to monitor technological development work whilst this is in progress, and thermal properties determined after the materials have been developed, almost as an afterthought.

Two new interesting areas of research deserve further consideration. Jack et al and Mitomo have begun to explore a new family of materials related to alpha Si_3N_4 , but no information is yet available on their technological potential for engineering applications. Some pure materials in the M-Si-Al-O-N system where M is Li, Ca or Y have been prepared and a start made on their characterisation. Another development of even greater novelty is the concurrent discovery at the Universities of Utah and Newcastle-upon-Tyne of a continuous series of solid solutions between silicon carbide and aluminium nitride. These two materials do not form mutual solutions easily however, although such materials can be prepared from carbon, silica and alumina, or from $CaSi_3Al_3ON_{15}$ with carbon in flowing N_2 at 1300°C. The compound Al_2OC is also soluble. At present there is no indication of their engineering potential.

CVD SILICON NITRIDE

The ability to form dense deposits of pure alpha silicon nitride, in appreciable thicknesses by chemical vapour deposition has led to the hope that such materials might have superior resistance to oxidation and corrosion at high temperatures, and being free from vitreous phases it is expected that their mechanical properties will be less affected by high temperature than hot pressed or sintered silicon nitrides.

However the mechanical properties which have been measured are very modest although there is no doubt that CVD Si_3N_4 is substantially harder than HPSN, and that it can be formed in thickness of over 1 mm on graphite substrates or on RPSN materials.

Strength data of 199 - 305 MPa for ground bars have previously been reported⁸. Niihara and Hirai⁹ have shown that deposition rates of over 0.7 mm/h could be achieved over relatively small areas (~ 2 cm²), and recent work at the Fulmer Research Institute with a large scale deposition facility has shown that areas as large as 150 cm² can be covered with deposits of a mean thickness of about 0.75 mm in 6.5 hours¹⁰. Unground strips cut from this deposit were tested in bend with the smoothest face in tension, but only gave a strength of 172 ± 42 MPa. These low strengths appear to be a consequence of inter-columnar defects, and it is possible that better strength might be obtainable if the growth morphology could be changed. At present the material is not very suitable for most applications in free-standing form, but the recent substantial improvement in ability to coat large areas make its use more feasible as a protective layer for RBSN where gas sealing, corrosion and oxidation resistance or extreme hardness and wear properties are required.

CONCLUSIONS

The incompletely-dense silicon nitride ceramics are readily fabricable materials, especially suitable for moderately-stressed components or prototype optimisation research when component failure is informative and an acceptable part of the design reiteration process.

Improvements are still being made in their strength, but these are likely to be modest. Their mechanical properties can be quite severely affected by fabrication procedures, especially the high temperature nitridation process, and large complex components require especial care because the atmosphere and temperature within large furnaces are more difficult to control adequately.

RBSN does not have sufficient vitreous phase content to impair mechanical properties above 1000°C significantly, but strength below 270°C can be quite severely affected by prior oxidation, although the addition of some oxides which form silicates easily may reduce this strength degradation appreciably. Both hot pressed and sintered fully dense materials can be very strong, especially so below 1000°C, and the vitreous phase effects which may impair strength and creep behaviour at higher temperatures can be reduced considerably, especially with yttrium oxide additions. Oxidation problems also can be difficult, and oxidative degradation of strength of HPSN of similar magnitude to that with RBSN has been reported, but with both materials it is possible to use preoxidation procedures to mitigate these effects. With yttrium and some other 'Sialons' quaternary crystalline phases may be responsible for catastrophic oxidation effects, but if these phases are avoided, as for instance with materials whose composition falls in the $\text{Si}_3\text{N}_4 - \text{Si}_2\text{O}_2\text{N} - \text{Y}_2\text{Si}_2\text{O}_7$ phase equilibrium diagram compatibility triangle, oxidation effects become non-catastrophic.

There appears to have been little exploration of the engineering potential of pressureless-sintered Sialons especially with heat treatments which convert their minor vitreous phases content to yttrium aluminium garnet and thus improve their high temperature mechanical properties. More detailed information is needed about the thermal properties of these complex materials. The potential of pure dense Si_3N_4 material produced by chemical vapour deposition for obtaining mechanical properties which are relatively insensitive to temperature has not yet been realized, as strengths at best are comparable only to RBSN, due to the unsatisfactory microstructure of the material as currently produced. However, progress has been made in making large area deposits with useful thicknesses, which may be useful for sealing RBSN, and protecting it against aggressive melts (eg containing sodium oxide) and oxidation, and in very onerous tribological conditions.

It is apparent that a case for continuing research on all three types of silicon nitride material exists, with the following principal objectives:

Reaction-bonded silicon nitride: improved strength

Sintered silicon nitrides (hot-pressure and pressureless sintered): improved high temperature properties and easier processing

CVD silicon nitride: better strength and easier processing.

REFERENCES

1. B F Jones, K C Pitman and M W Lindley, 'The Development of Strength in Reaction Sintered Silicon Nitride', *J. Materials Sci.*, **12**, 1977, 563-576.
2. D J Godfrey, 'The Effects of Impurities, Additions and Surface Preparation on the Strength of Silicon Nitride', *Proc. Brit. Ceram. Soc.*, **25**, 1975, 325-337.
3. D A Parker and R F Smart, 'An Evaluation of Silicon Nitride Diesel Pistons', *Proc. Brit. Ceram. Soc.*, **26**, 1978, 167-181.
4. D J Godfrey and M W Lindley, 'The Strength of Reaction-bonded Silicon Nitride Ceramics', *Proc. Brit. Ceram. Soc.*, **22**, 1973, 229-252.
5. D J Godfrey, 'The Effect of Added Oxides on the Strength of Reaction-bonded Silicon Nitride After Oxidation', *Proc. Brit. Ceram. Soc.*, **26**, 1978, 265-279.
6. K H Jack. Private communication.
7. J D Venables, D K McNamara and R G Lye in F L Riley (ed.), 'Nitrogen Ceramics', Noordhoff, Leyden, Noordhoff Internat. Publ., 1977, 391-392.
8. K C Pitman and D J Godfrey, 'Pyrolytically-deposited Silicon Nitride', *Proc. Brit. Ceram. Soc.*, **26**, 1978, 225-236.
9. K Niihara and K Hirai, 'Chemical Vapour-deposited Silicon Nitride', *J. Materials Sci.*, **11**, 1976, 593-611 and 1233-1252.
10. C Hayman and R Archer. Private communication.

TABLE 1

Some Pressureless-Sintered Sialons

Composition SN = Si_3N_4 parts AN = AlN by AO = Al_2O_3 wt. YO = Y_2O_3	Processing Method (See US Pat No. 4,127,416)	Heat Treatment	Density Mg/m^3	Strength at RT (Weibull m subscript)	Strength at 1225°C	Creep Behaviour time to 0.05% strain	X-ray Phase Analysis %		
							β'	'YSiON'	'YAG'
92 SN } 5 AN } 3 AO } 6 YO }	PS 60 min 1880°C " " cool to RT " then to 1400°	- reheat 5h 1400°C 5h 1400°	3.152	750 14 705 11 615 13	379	1 h 11 h	90 ~0.5	-	- ~5 ~5
92 SN } 6 AN } 2 AO } 6 YO }	" " cool to RT " then to 1400°	- reheat 5h 1400°	3.175	564 16 709 8 555 14		32 h 40 h	>90 ~0.5	6 2	
92 SN } 7 AN } 1 AO } 6 YO }	" " cool to RT " cool to 1400°	- reheat 5h 1400° 5h 1400°	3.141	520 15 618 11 535 9	608 620 622 (605 at 1370°C)	8.5 h 70 h 120 h	>90 (2 ^v /Ox-Wollastonite) >90 ~0.5		4 8
92 SN } 4 AN } 4 AO } 6 YO }	"	-		733 14	274	0.7	>90 ~0.5	rest glass	
42 Al } 14 Si } 44 AO } 12 of '15R' 88 SN 6 YO	nitrided in $\text{N}_2/\text{H}_2\text{Ar}$, powdered, fired at 1800°C to yield '15R' polytype material. PS 60 min 1880°C		3.201	767 13			>90 ~0.5	+	
As above but 7 YO 14.25 '15R' 85.75 SN 7 YO	PS 60 min 1840°C " then to 1400°		3.197 3.208 3.230	815 13 810 577			>90 ~0.6 >90 ~0.8	10	
18.75 '15R' 81.25 SN 7 YO	"	"	3.188 3.179	520 543		0.1% in 48 h	>90 ~0.9 >90	4	7
20.25 '15R' 78.25 SN 7 YO	"	"	3.224	500		0.023% in 48 h	>90 ~1.0		8
21.75 '15R' 78.25 SN 7 YO	"	"	3.198	501		0.01% in 48 h	>90 ~1.1		8.5

COMPRESSION LOADED CERAMIC TURBINE ROTOR

R. Kochendörfer

Institut für Bauweisen- und
 Konstruktionsforschung/ DFVLR
 Forschungszentrum Stuttgart
 7000 Stuttgart-80 (Vaihingen)
 Pfaffenwaldring 38/40
 Germany

Summary

Ceramic materials offer a great potential for high temperature application. This, however, means it is necessary to live - even in future - with a brittle material with small critical crack length and high crack growth velocity. Thus it will not be easy to ensure reliability for highly loaded ceramic components, keeping in mind that for reaction bonded ceramics the material inherent porosity is in the same order of magnitude as the critical crack length. A solution to increase the reliability of ceramic turbines may be a compression loaded rotor design with fiber reinforced hooping.

The most attractive properties of fiber reinforced materials - high strength to density ratio σ/ρ combined with high stiffness to density ratio E/ρ can be utilized with maximum benefit. However, this group of materials does not allow high temperature application. Therefore, in the proposed design the center core of the turbine wheel which is exposed to the hot gas flow is surrounded by a concentric cooling ring, both kept under compression up to the design speed by a composite ring combination. Cold spin test results of fiber reinforced rings made of carbon epoxy, boron aluminum and carbon/carbon are presented as well as cold spin test results of a possible wheel/shaft connection and of compression loaded rotors.

Introduction

The application of ceramic materials for highly loaded components in the hot gas flow of a turbine engine is in a developmental stage since a few years. Especially for small engines, powering cars and trucks, the high-technology cooling systems known from jet engines are too costly. Thus, the turbine inlet temperature is limited to about 1300 K which leads to thermodynamic efficiencies lower than those for gas or Diesel engines. It would be a big step forward if a ceramic turbine could be realized with turbine inlet temperatures up to 1700 K:

- The specific fuel consumption would be as low as for good Diesel engines
- The material fabrication costs would be about 10% of complex steel
- Almost no raw material procurement problems will arise in future as are expected for alloy metals
- The vibration level as well as the emission values of a turbine are lower than for piston engines.

However, this ceramic turbine should offer at least today's standard of reliability.

Present situation / state of the art

For hardware application silicon nitride and silicon carbide are favored candidates, both as reaction sintered materials as well as in hot pressed condition. Published test results indicate that stationary hot-flow-path ceramic components like combustion chamber, nose cone, and stators were the first parts which have been successfully tested / 1 /. The realization of ceramic recuperators is more difficult /2,3/. The hardest problem still is a low cost ceramic rotor with high reliability, although ceramic turbines were tested at Ford Motor-Company in 1977 and at Garrett Corporation in 1979, operating at desired turbine inlet temperatures of 1645 K and 1485 K with blade tip speeds of 407 m/sec and 437 m/sec, respectively /4,5/.

There are known three concepts to realize a ceramic rotor,

(1) Duo-density design

High strength hot pressed silicon nitride (HPSN) is used for the hub, where stresses are high but temperatures moderate. The blading material is injection molded or slip cast reaction sintered silicon nitride (RBSN).

This material combination is advantageous for more than one reason;

- To guarantee a consistent material quality the fabrication of HPSN is limited to simple billet shapes. The shape of a hub is simple whereas the realization of complex blade shapes needs a time consuming and costly machining procedure as a grinding or ultrasonic process.
- To achieve a HPSN-material with an almost theoretical density a densification aid is used. Thus, at high temperatures a certain plastic behavior occurs. On one hand this is positive because it reduces stress concentration and impact failure, on the other hand this leads to creep effects. However, the temperature of the hub is moderate compared to that of the blades.
- The complex shape and the high operating temperature combined with relatively low stress levels due to centrifugal forces require a different material for the blades. RBSN matches these requirements.

However, the duo-density design offers a weak point, too. The joint between these two materials is not easy to realize - and is tension and shear loaded in operating condition. Both facts render it more difficult to guarantee reliability. Presumed the problems are solved by improved materials as well as processing and nondestructive testing methods this concept offers the potential of a low cost rotor in series production. Ford Motor Comp. as well as Volkswagen are testing this concept since 1971 and 1974, respectively, Fig. 1.

(2) Metal-hub/ceramic blading-concept

The advantages of this design are based on the fact that the connection of hub and shaft is today's standard and that in case of a defect single blades can be replaced. But exactly from this single blade attachment the problems arise;

- Stress concentration due to the small contact area
- Compliance layer between hub and blade to increase the contact area and to reduce effects caused by elastic hub deformation.
- possible deviation of an aerodynamically optimized blade spacing due to the attachment volume requirement especially in realizing a small rotor size.

The results published up to now indicate that low-cost RBSN-blades are hardly able to fulfil the requirements because of the low strength potential. HPSN-blades will sustain the applied stresses but they are costly to fabricate and limited in temperature application. Thus, and because of metal hub cooling requirements, the operating temperature is lower than for the duo-density design. However, it is a time saving and cost effective solution to realize a ceramic turbine and to test stationary hot-flow-path ceramic components under real engine conditions. Garrett Corp., Volkswagen, and MTU-Munich are testing this concept, Fig. 1.

(3) All-HPSN-rotor design

A more exotic design - exotic with respect to costs - is the all-HPSN-rotor, where hub and blades are machined from one billet. Of course, this can't be cheap, but apart from the hub/shaft connection no problems with joints and attachments and no insurmountable problems with stress levels will arise. Thus, with today's machining technology an all-ceramic rotor can be realized within a short period, at least for the purpose of testing an all-ceramic turbine. If it would be possible in future to fabricate a homogeneous HPSN material also in complex shapes, this design will be competitive with other solutions. Mercedes Benz is testing this rotor concept.

Design philosophy

The design philosophy for all these concepts did not change by changing from metal to ceramic materials. They are still based on tension loaded blades and disks. However, we assume this is not the strongest base for a ceramic rotor design. Recent publications indicate similar considerations /6, 7/. No doubt, the properties of ceramic material were improved in the last few years and will be improved in future, Fig. 2. But even then we will have to deal with a brittle material if we intend to take advantage of the full potential of high temperature applicability. A small critical crack length combined with a high crack growth velocity at all those loading conditions which tend to open a crack will lower tension strength and increase scatter. Accepting this as a ceramic inherent peculiarity, we were urged to look for design concepts which avoid this weak point and guarantee reliability not only by nondestructive testing methods and proof tests. Looking at the past we recognize breathtaking and almost unbelievable architecture and dome constructions offering a design concept for brittle materials like bricks and stones which is obviously adequate to their properties. Those monuments, which endured for centuries, are based on a simple design concept: compression-loaded and form-locked under their own weight. To realize this concept in a rotating structure the brittle material must be combined with a structural member which offers an extremely high potential of specific strength and stiffness. Fiber reinforced materials with low density are the only candidates to accomplish this demand. The stress level resulting from their own rotating mass is low enough to offer additionally a high tension load capacity.

Compression-loaded ceramics and tension-loaded composites form a fascinating combination with an inherent imperfection - difference in temperature stability. To overcome this mismatch for a turbine rotor application, a low cost cooling system separating the composite material and the hot gas flow is the only solution. It depends on the rotor design, whether this concept can be competitive in cost, efficiency, and reliability to already existing designs.

Design concept

These considerations lead to a rotor design shown in Fig. 3, using ceramic materials of the reaction bonded type only / 8 /. The turbine blades, exposed to the hot gas flow, build up the inner section of the rotor. They are concentrically surrounded by a cooling section where the blades are arranged to guarantee a compression load path from rim to hub. The hot and the cold gas flows are separated by a ceramic ring. Two further ceramic rings border the blading area inside and outside. The inserted hub is divided into a number of sections to avoid tensile loading. The hub function is reduced to a centering disk which is capable to transfer torque to the shaft. The whole ceramic structure should be constricted by a composite ring or a ring combination in such a way, that the essential parts are compression-loaded up to the design speed. To realize this goal two extreme solutions are suggestable: the "completely sliced wheel" and the "completely closed wheel". In case of the "sliced wheel" the single slices are pressed against the composite hoop due to centrifugal forces - the more the higher the speed. At zero speed only a small prestress is necessary to clamp together the single slices. In case of the "closed wheel", the prestress at zero speed has to be high to obtain a high compression level within the ceramic structure, which will be reduced with increasing speed due to centrifugal stresses. Between these two extremes a variety of design parameters is possible.

Program tasks

There are two main topics to be investigated.

(1) Thermodynamic efficiency

The cooling effort which is necessary to realize the compression loaded rotor design is adequate to a reduction in thermodynamic efficiency. A high service temperature of the hooping material coincides with a small drop in efficiency. Thus, the objective of this investigation is on one hand to improve the technology to achieve high-temperature-stable, low-density composite rings, which offer high weight related strength and stiffness values. On the other hand, the cooling effort should be integrated advantageously into the thermal circle to minimize the efficiency drop. The aim is an overall thermodynamic efficiency which is substantially above the values of uncooled metal turbines and close to the values which can be achieved with the duo-density ceramic rotor.

(2) Hardware demonstration

If this seems to be possible, the feasibility of this compression rotor design should be demonstrated in hardware tests with emphasis on a low cost test program, qualifying the reliability on principle. The test schedule comprises spin tests of rotor components like hooping rings and hub as well as completed rotors under room temperature and elevated temperatures.

Thermodynamic efficiency

Our specific interest is mainly directed towards structural design concepts. A competent partner in thermodynamic calculations was found in the Institute for Aircraft Propulsion at the University of Stuttgart. A large variety of parameter studies by means of already existing or modified computer programs were made assuming the cooling ring:

- as a compressor, a cold gas turbine, or a neutral stage
- operating at low, medium, or high pressure level
- with no, partial, or total feedback to the thermal circle.

The results are described in detail in reference / 2 /. As this paper is not dealing with thermodynamics, only the main results are summarized with respect to the rotor design.

- o As shown in Fig. 4, the cooling ring is assumed to be a cold gas turbine stage at low pressure level with no feedback to the thermal circle. Thus, the blade length in the cooling ring is not too short and the inlet temperature low enough to offer a high cooling potential of the air flow.
- o This thermal circle is used as a base to compare different rotor systems, characterized by the turbine inlet temperature and the percentage of additional cooling effort related to the condition at the outlet of the compressor. As shown in Fig. 4, the prospects for the compression loaded ceramic rotor are not looking too bad. If it will be possible to realize this concept with a cooling effort of 5%, the thermodynamic efficiency is in the same order as for the duo-density ceramic rotor. Thus, thermal isolation of the hot gas flow and a minimized cross section of the cooling blades are of essential interest, as well as radiation reflecting coatings to reduce heat flow toward the lower temperature areas of the rotor.

Rotor definition (First generation)

Several decisions were made to achieve the program tasks with a minimum of manpower, time and money:

- (1) Only reaction bonded ceramic material should be applied.

This is advantageous for several reasons:

- It is a low cost material which can be slip casted or injection molded to complicated shapes
- It is a low density material, thus loads due to centrifugal forces are low
- It is a low modulus material, thus lowering the required prestress level of the hooping material
- It is a material with a low thermal conductivity, thus reducing thermal flux and cooling effort
- It is a material with a good thermoshock stability, which is essential especially in the area between the hot and cold gas flows.

- (2) As far as possible already existing molds should be used.

At the beginning the rotor should be built up by an assembling method rather than in an one-shot-processing technique to cut costs. An arrangement with MTU-Munich was made to employ its stator vanes to build up the hot gas blading of the compression loaded rotor design. These stator vanes were injection molded piece by piece at Rosenthal Engineering GmbH. The completed RBSN-rotor was ordered from this company.

- (3) The results should be comparable to other rotor concepts.

In consequence to the decision to use the identical hot gas flow geometry MTU uses, also the same design speed was determined. The tip speed of the turbine blade is 372 m/sec, corresponding to 56 000 rpm.

- (4) The test results should be available as fast as possible.

To demonstrate the feasibility and reliability of the compression-loaded rotor concept, a composite ring with high weight-related strength and stiffness values was an absolute premise of the program. Due to the fact that for higher-temperature-stable systems like boron/aluminum, carbon/carbon or carbon/glass the processing technology is not as sophisticated as for carbon/epoxy, the latter material was selected for demonstration purposes at least up to cold spin tests. At the same time the processing technique to fabricate high quality B/Al- and C/C-rings should be developed to a higher standard.

By these decisions the number of parameter variations was reduced, however, there is still a large design variability between the already mentioned two extreme solutions "completely sliced wheel" and "completely closed wheel".

To run parametric studies on a computer, two mathematical models were developed. One is based on a spoked wheel where the blades are simulated by untwisted rectangular spokes orientated parallel to the turbine axis. The other is based on a multiple ring model with anisotropic elastic behavior in radial and circumferential directions. Both are inaccurate but render a better understanding and fairly good results in attacking the target by changing the design.

Fig. 5 may be helpful to clarify some aspects of interacting effects. Rotor A is an "all sliced type" except for the outer ceramic ring Nr. 1, whereas rotor type B is "all closed" except for the hub that acts as an internal pressure loading to ceramic ring No.3 (which is valid also for type A).

The stress level of the tension ring A_{tens} is very low at zero speed. However, it is sufficient to reach a much higher compression stress in ceramic ring A_1 compared to the stress level of rings No. B_1 , B_2 and B_3 . A_{tens} increases very rapidly with increasing speed. There is no other tension member which is able to reduce its stress level because the circumferential stresses in rings No. 2 and No. 3 are zero. This is also indicated by the compression stress level of turbine spoke A_t as well as of cooling spoke A_c , which increases with increasing speed, naturally more rapidly for A_c .

Compared to that, rotor type B shows a different tendency. The "all closed" rotor type B consists of three closed ceramic rings, thus offering more rigidity or less compliance than a single ring. Therefore, the prestress level of the tension ring B_{tens}

is very high compared to A_{tens} . However, the stress increase with increasing speed is not as pronounced due to the fact, that all three ceramic rings are tension-loaded. Obviously the increase is more rapid for B_3 than for B_1 and B_2 . This is analogous to usual tension-loaded disks and corresponds with the dominating tensile effects within the turbine spokes B_t , whereas the tension and compression effects are nearly balanced within the cooling spokes B_c .

As far as the stress levels are concerned, the rotor Type A is a favorable design, however, the decision was made that the first generation of test rotors should be as easy to fabricate as possible. Under this aspect rotor type B offers the advantage that the single turbine blades can easily be positioned within two concentric rings to minimize unbalance tendencies of the completed rotor. The ceramic rotor radius became 13 mm larger than the turbine blade tip radius, by adding 8 mm insulating ring thickness between hot and cold gas flow, 2,5 mm cooling channel height, and 2,5 mm outside ceramic ring thickness. Thus the design speed at the rim increases to 448 m/sec.

Rotor hub/shaft connection

The hub/shaft connection has to fit within the concept of the compression-loaded rotor which can be realized only if the hooping acts as a support of the total ceramic structure. The enlargement of the tension ring(s) at the rim is much higher than of the hub in the rotor center at increasing rpm. If the rim is connected to the hub by rigid spoke-members, tension stresses in the spokes as well as in the hub can be prevented only if the hub is sliced, Fig. 5. As the sliced hub offers a more pronounced radial displacement with increasing speed, corresponding to the expansion of the hooping, also the hub/shaft connection has to follow this tendency and allow radial extension. This can be realized only by tolerating the fact of a relative motion between hub and shaft members. However, the centering function of the hub must be guaranteed. One possibility is separating the functions of centering and torque pickup. Out of a number of designs, one solution seems to be favorable. The mounting arrangement is demonstrated in Fig. 6,

/ 9 / .

A star of six flat, rectangular, radial orientated metal plates fits into corresponding slots in the ceramic hub to transfer the torque. For centering purposes two fingershaped sockets are inserted between these metal plates. The socket fingers will be deflected due to centrifugal forces and pressed towards the wall of the inner bore in the ceramic hub. A compromise has to be made between finger thickness and bore diameter. Thickwalled fingers will guarantee a better centering function but need a larger diameter to deflect under centrifugal forces, thus operating at higher temperatures. The inner section is covered by two closed sockets which fix the ceramic wheel at the parallel ground front faces perpendicular to the rotor axis by means of two flexible, temperature-stable rings.

Cold spin tests of hub/shaft connection

In order to prove this design, ceramic hubs were spin tested in vacuum at ambient temperature. To realize the same strain level at the rim of the hub as will occur in the case of an "all sliced rotor" type A, glassfiber reinforced epoxy was selected as hooping material. Due to the low modulus the adequate strain could be verified at moderate speed, corresponding to 45 000 rpm. The results are summarized in Fig. 7, where the enlargement of one slot is plotted versus revolutions per minute. The curves are calculated for a

"6 slot hub" and a "12 slot hub", respectively. The measurement points, gained by examination of high-speed photographs, almost coincide with the curves.

First tests were made with a "6 slot hub". Here problems arose especially at gap enlargement values exceeding 0,4 mm, mainly because the crack surfaces did not match together when they came into contact at speed reduction. Any unsteadiness in relative motion between ceramic hub sections and the composite ring became more pronounced and effective the higher the amount of relative motion increased. In most cases it became visible that the ceramic material tends to be released by additional cracks.

Therefore, the decision was made to change to a "12 slot hub" by scratching symmetrically six additional tracks into the ceramic surfaces, about 0,5 mm deep, to initiate crack growth in well defined crack tracks to avoid unbalancing effects. In fact, all twelve cracks opened, at least after several cycles, as can be seen in the enlarged lower picture in Fig. 7. With these "12 slot hubs" more than 200 cycles between zero and 45 000 rpm were conducted without any problems. Reaching that goal we stopped the test program to investigate the behaviour of a "24 slot hub". However, we did not even succeed in reaching a symmetrical 12 slot crack pattern in this configuration.

As a result of these cold spin tests the hub for the second generation test rotor was defined as a "12 slot hub" with twelve tracks for crack initiation purposes.

Cold spin tests of composite rings

When the decision was made to use CFRP-rings as tension members for demonstration purposes a program was initiated for testing a ring combination consisting of a CFRP-ring and the outer ceramic ring of the ceramic rotor. The internal ceramic rotor structure was represented by a properly dimensioned metal disk to simulate an adequate internal pressure loading at design speed to the outer ceramic ring.

To fabricate the composite rings Torray carbon fibers M 40 A ($E = 395\,000\text{ N/mm}^2$, $G_t = 2040\text{ N/mm}^2$) were impregnated with the CIBA resin system LY 556/HT 972 at a temperature of 55°C and wound onto a mandrel with a strand tension of 350 p. The mandrel was made of the same material to minimize inherent stresses due to thermal elongation during the curing process (160°C , 4 h). The cured rings were machined to the desired dimensions.

The RBSN-rings were purchased from Rosenthal Engineering GmbH. No ring selection took place because no proven nondestructive testing method was available. The outside diameter of the rings were machined with a diamond grind within a tolerance of 0,04 mm, reducing the surface roughness from $46\,\mu\text{m}$ to $6\,\mu\text{m}$.

The usual thermal shrinkage method was not practicable to fit the CFRP-ring onto the ceramic ring because RBSN material and unidirectional reinforced carbon epoxy offer only a small coefficient of thermal expansion, and allow a low shrinkage temperature. Thus, only a mechanical pressing operation was feasible. We developed a special procedure which made it possible to hold the ceramic ring under compression and at the same time enlarge the composite ring. By this mechanical shrinkage method a radius difference of 0,3 mm could be realized without visible failures in the rings.

These ring combinations with a slide-fit inserted metal disk were spin tested at ambient temperature at MTU Munich. The results are shown in Fig. 8, the small scatter within the burst speeds is obvious. The curves were calculated by assuming a linear elastic behavior up to the failure point. This was valid because the metal disk showed no plastic deformation. The failure stresses of the composite rings range from 950 N/mm² to 1080 N/mm². Increasing the fiber content above 60 V/o may further improve these good results up to 1200 N/mm².

These test results did not allow to determine whether the ceramic rings or the composite rings failed first. The ceramic rings were tension stressed at failure and a crack in the ceramic ring could initiate a local overstress in the composite ring. To separate the failure sequence, ring combinations without any prestress in the composite ring were tested, that means the ceramic ring as well as the metal disk were inserted into the CFRP-ring using a slide fit. The results are summarized in the lower portion of Fig. 8. Again the curves were calculated. The stress level for all three rings is zero at zero speed. With increasing test speed the ceramic ring failed first at about 55000rpm corresponding to 400 N/mm². Up to this speed the ceramic ring was tension loaded, thus reducing the stress level of the composite ring. As soon as the ceramic ring has cracked its stress level can be assumed in first approximation to be almost zero. The cracked ceramic ring acts as an additional internal pressure load to the composite ring, increasing its stress level. The composite rings failed at 54600 rpm and 59300 rpm which corresponds to tension stresses of 720 N/mm² and 870 N/mm², respectively. These failure stresses are low, especially for 65 V/o composite rings which offer a strength potential of about 1200 N/mm². This discrepancy may be explained by stress concentration factors which, in the area of the ceramic ring cracks, lead to peak stresses within the composite ring, exceeding the calculated stress levels, plotted in Fig. 8, by a factor of about 1,5.

As far as the rotor design is concerned, these results suggest that no cracks in the outer ceramic ring can be tolerated if the full potential of the tension loaded composite ring is to be utilized.

First results of cold spin tests with B/Al-rings are shown in Fig. 9. This type of material allows operating temperatures up to 300°C, thus reducing the cooling effort and increasing the overall efficiency. Whereas the CFRP-rings were fabricated in our own laboratory, the B/Al-rings were manufactured at Battelle Institut, Frankfurt, however, with a smaller diameter due to an already existing winding mandrel. The stress levels at burst-speed range from 1040 N/mm² to 1190 N/mm² and are comparable to those values achieved with high modulus CFRP-rings. Due to the fact that the boron fibers offer a strength potential above 3500 N/mm², it seems to be possible to increase the failure stress level of the B/Al-rings up to 1700 N/mm² by improving the fabrication technique and/or post consolidating the ring material after the filament winding process.

The first cold spin test results obtained with C/C rings, fabricated at the 'Institut für Chemische Technik' of the University at Karlsruhe, were really surprising. Although the machined rings showed a constant weight loss under centrifugal forces by a fiber unwinding effect - possibly due to the low transverse strength of the carbon/carbon material - the failure stresses ranged from 750 N/mm² to 900 N/mm². This unwinding effect may not occur if the ring surfaces are not machined and/or if the ring surfaces are protected by a coating. This coating layer may at the same time act as an oxidation barrier to allow operating temperatures exceeding 500°C.

Cold spin tests of compression loaded ceramic rotors (First generation)

Two ceramic rotors were prepared for testing. Both were of an "all closed" rotor type, having a "six slot hub", 26 injection molded turbine blades, and the same number of cooling spokes. The rotors were fitted together in an assembling method using slip cast material to connect the single pieces. The main difference between these first generation rotors was that in one case the insulation ring was "sliced", Fig. 11, 13, in the other "closed", Fig. 12, 14. However, this affects only the prestress level of the hooping material. As tension members both rotors had a ring-combination, i.e., a 4 mm steel ring and a 7 mm high modulus CFRP-ring, Fig. 14. The steel ring was selected for testing purposes, because it was easy to increase the compression stress level within the ceramic structure step by step by thermal shrinkage and unshrinkage procedures. The resulting compression strains were measured by strain gages and compared to the calculated values. We noticed that the corresponding strains in the rotor rim area were above the calculated values whereas in the rotor hub area they were lower than calculated. This can be explained by a change of the radial pressure distribution caused by the low modulus of the slip cast material between the ceramic rings. In some cases it could even be observed that the slip cast material was squeezed out of the gaps. The compliance effects of these slip cast layers may also magnify a nonuniform strain distribution in those ceramic components forming the compression load path - because of the dependence of pressure distribution on structural stiffness. This effect was particularly noticeable at the platforms of the hot gas flow blades, Fig. 12, 14. At speed levels between 20 000 rpm and 25 000 rpm triangular pieces of the platform broke off, presumably because the bending moments at the platform edges are higher when a "soft" intermediate layer is present. The compliance effects are also supposed to be the reason for radial cracks in the turbine blades, Fig. 12, a thesis which may be confirmed by the fact that an identical failure mode did not occur within the cooling spokes which had a higher compression stress level but were not embedded in a slip cast material, Fig. 13. Although both ceramic rotors showed an increasing amount of cracks and failures during the test program, it was possible to spin test them several times up to more than 20 000 rpm, when hurled-away debris terminated the test procedure by penetrating a flash synchronizing ring. In the discussion about design reliability this can be a strong argument, because the rotor did not desintegrate totally.

No doubt, failures as shown in Fig. 12 and Fig. 14 are not tolerable - and we hope to avoid this type of damage by a second generation rotor design - but these severely damaged ceramic rotors reached 32150 rpm and 28450 rpm, respectively, before they failed, not due to overstresses in the hoop ring materials but due to pronounced unbalancing effects, namely because our spin test facility is very susceptible to unbalance tendencies.

Future aspects

A number of five second-generation rotors are already ordered. They will have "two closed rings", kept under compression up to the design speed, i.e., according to Fig. 5, ring No. 1, to avoid stress concentration factors in the hoop rings, and ring No. 2 to guarantee a separation of the cold and the hot gas flow. As already mentioned the hub will be a "12 slot hub" with twelve tracks for crack initiation. The hub as well as the hot gas flow blading will not be kept under compression at zero speed. The rotors shall be fitted together in our own laboratory using an assembly method where the single pieces are clamped together only mechanically to avoid a slip cast material.

In case the compression rotor design will prove to be successful, the future applicability is not limited to vehicular gas turbines only. It can be applied in RPV's, APU's, helicopter-, or even stationary gas turbines. It even seems to be possible to utilize this system as a pumping wheel for hot and/or aggressive media by driving the rotor with the cooling blade section.

References

- /1/ "Ceramics For High Performance Application-II"
Proc. 5th Army Materials Technology Conf., March 1977, Newport, Rhode Island/
USA
- /2/ "Kleingasturbinen"
DGLR-Symposium, Universität Stuttgart, 11./12.Okt.1977,
DGLR-Bericht 78-01 (1978)
- /3/ "Keramische Komponenten für Fahrzeug-Gasturbinen"
Statusseminar im Auftrag des Bundesministeriums für Forschung und Technologie,
Bad Neuenahr, 18./19. April 1978;
Herausgeber: Projektträgerschaft "Metallurgie, Werkstoffentwicklung, Rück-
gewinnung" bei der DFVLR, Köln
Wiss. Leitung: Bunk W.; Böhmer, M.
Berlin: Springer 1978
- /4/ De Biasi, V.;
Ford runs uncooled ceramic turbine engine at 2500°F. Gas Turbine World, July 77
- /5/ "Garrett T 76 Completes Test Run"
Aviation Week and Space Technology, April 9, 1979
- /6/ Coty, P.J.;
Compression-Structured Ceramic Turbine Rotor Concept.
6th Army Materials Techn.Conf.: "Ceramics For High Performance Application -
III - Reliability", Orcas Island, Washington (U.S.A), July 10 - 13, 1979.
- /7/ Boudiques, S.; Fratacci, G.;
Technologies Conçues pour l'Utilisation des Céramiques dans les
Turboréacteurs - Application aux Missiles de Croisière.
49th AGARD-Meeting STRUCTURES AND MATERIALS PANEL, Spec.Meet. on
CERAMICS FOR TURBINE ENGINE APPLICATION, DFVLR-Köln (Germany), October 7-12, 79.
- /8/ Kochendörfer, R.; Hütter, U.;
Scheibenförmiges Laufrad für eine hochoberige Axialturbine.
Deutsches Patent DT 25 07 512, erteilt 1. Sept. 1977.
- /9/ Kochendörfer, R.;
Wellen-Scheiben-Verbindung.
Deutsche Patentanmeldung P 28 48 355. 8, angemeldet 8.Nov. 1978.

Acknowledgements

The author would like to acknowledge the help received from the colleagues of the Institut für Bauweisen- und Konstruktionsforschung with special reference to Mr. H. Vogler.

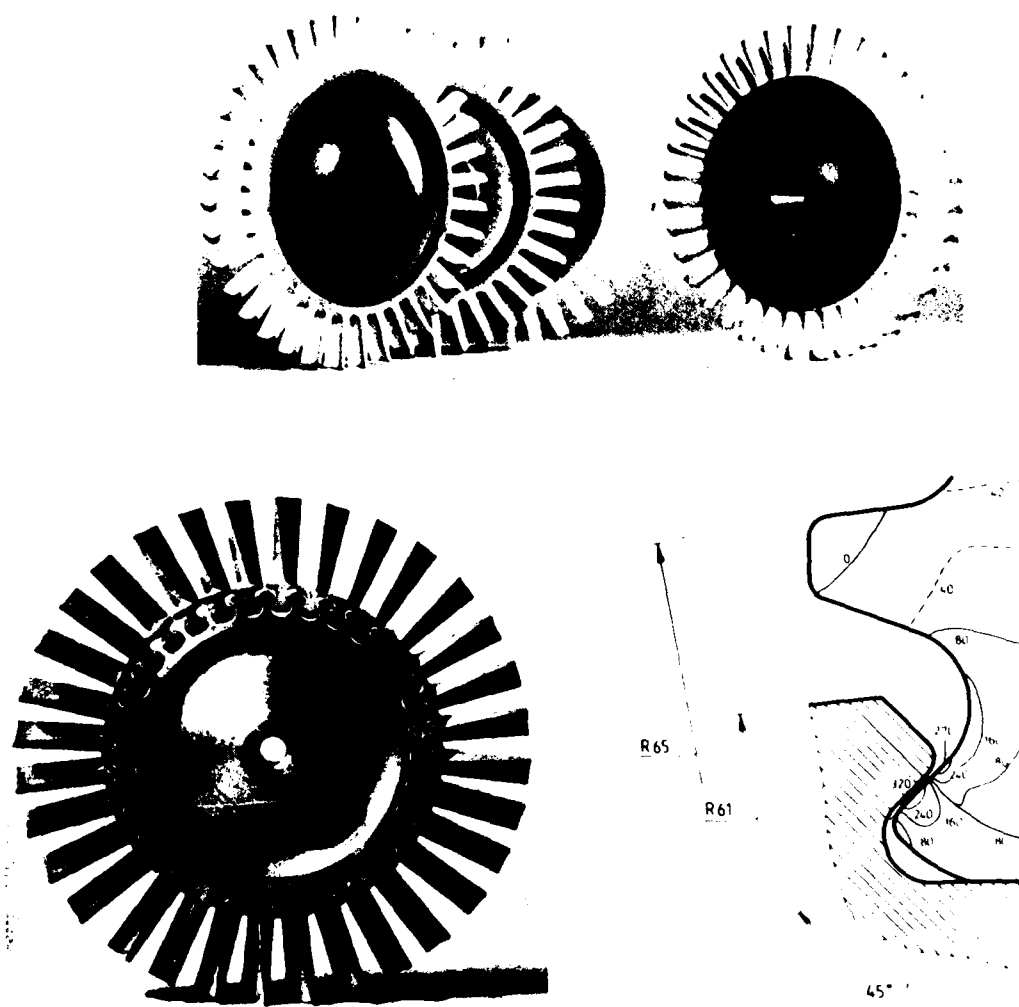


Fig.1 Duo density rotor design and metal-hub/ceramic blading concept / 2 /

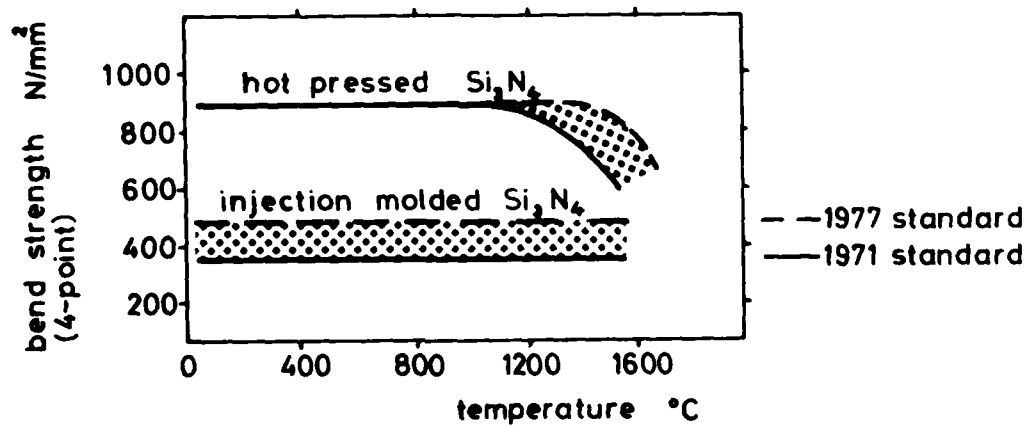


Fig.2 Improvement of Silicon Nitride materials / 4 /

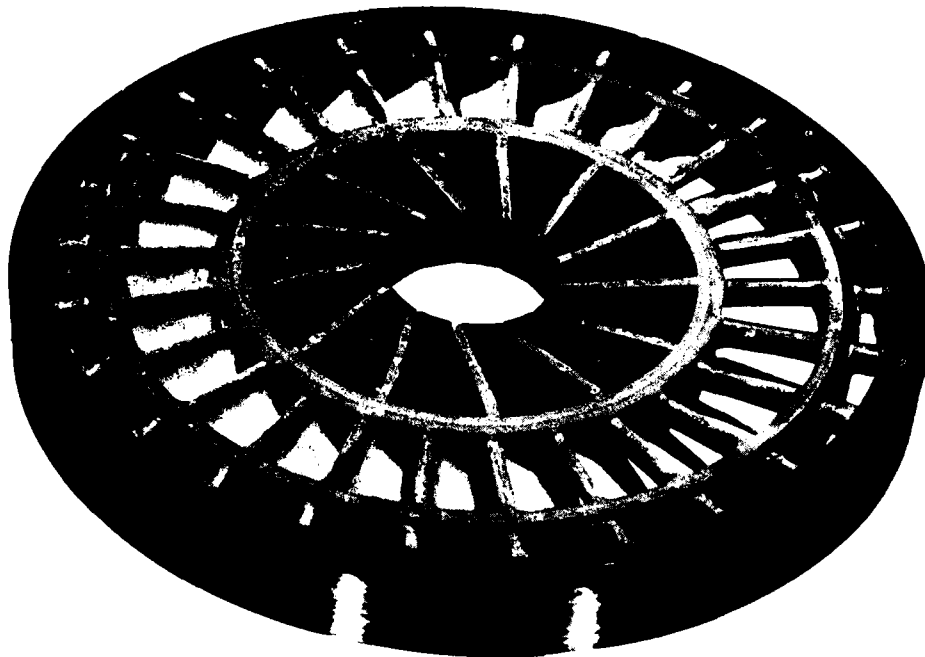


Fig.3 Compression loaded ceramic rotor design

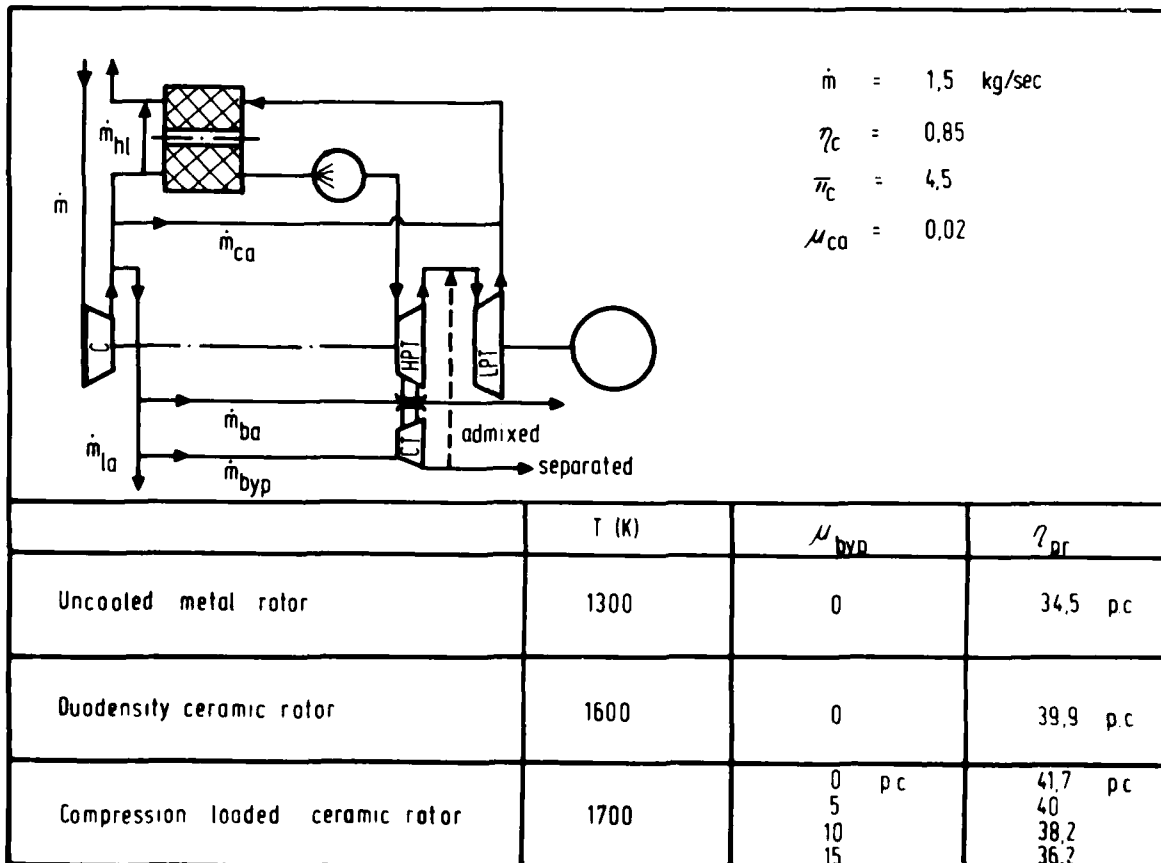


Fig.4 Comparable thermodynamic efficiency for different rotor concepts / 2 /

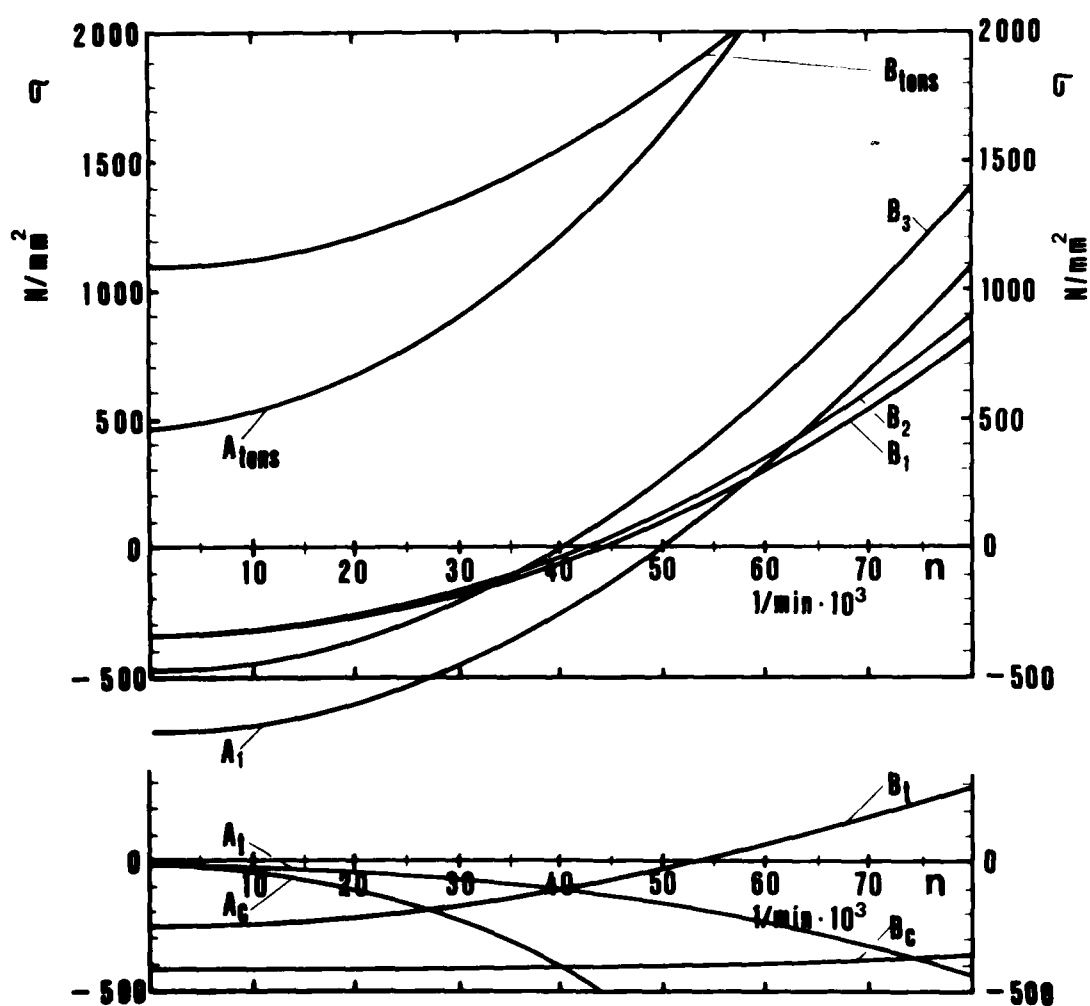
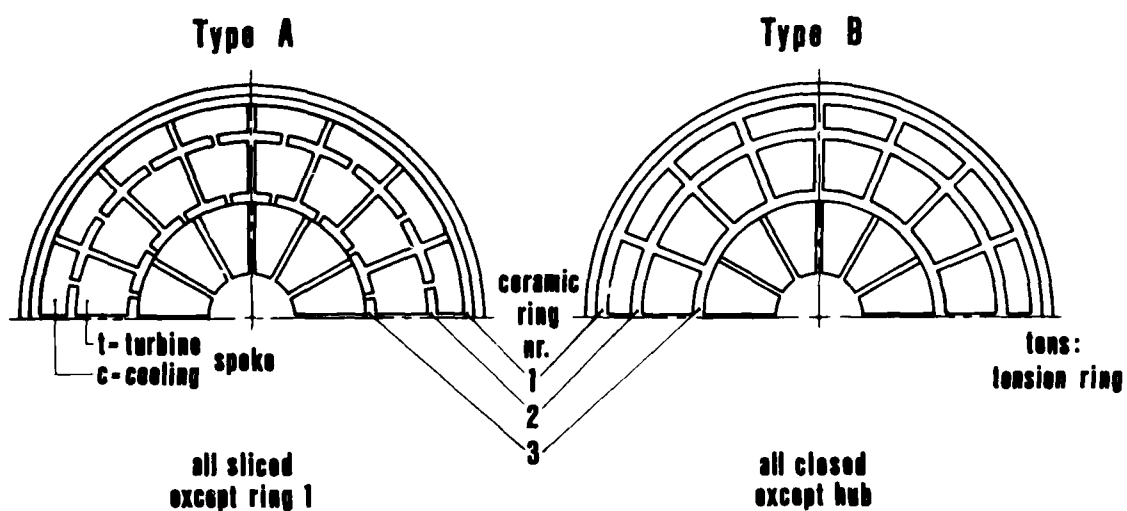


Fig.5 Comparable stress levels for an "all sliced" and an "all closed" rotor type

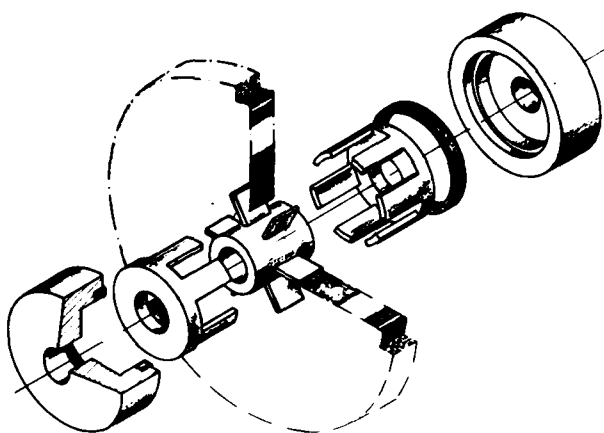


Fig.6 Explosive view of the hub/shaft connection

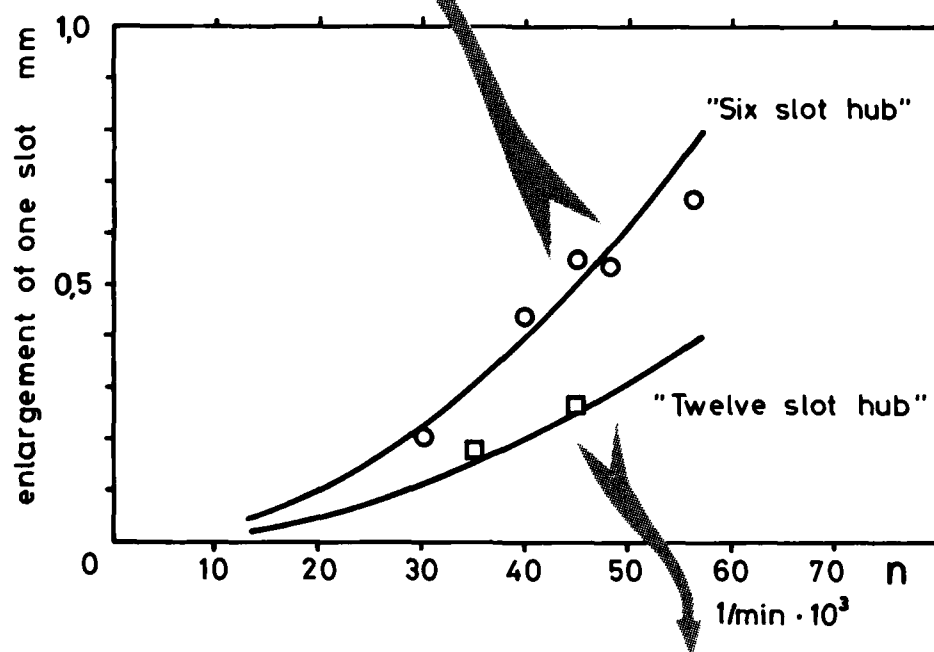


Fig.7 Cold spin test results of the ceramic hub/metal shaft connection

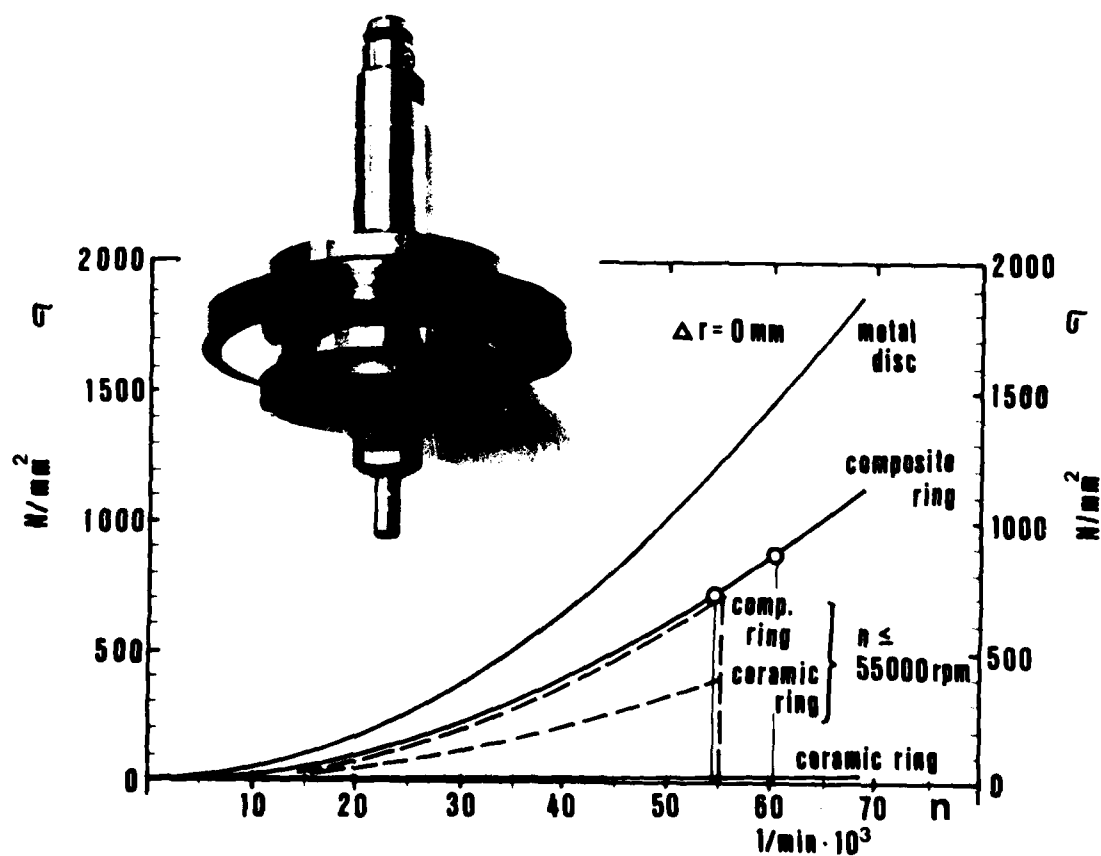
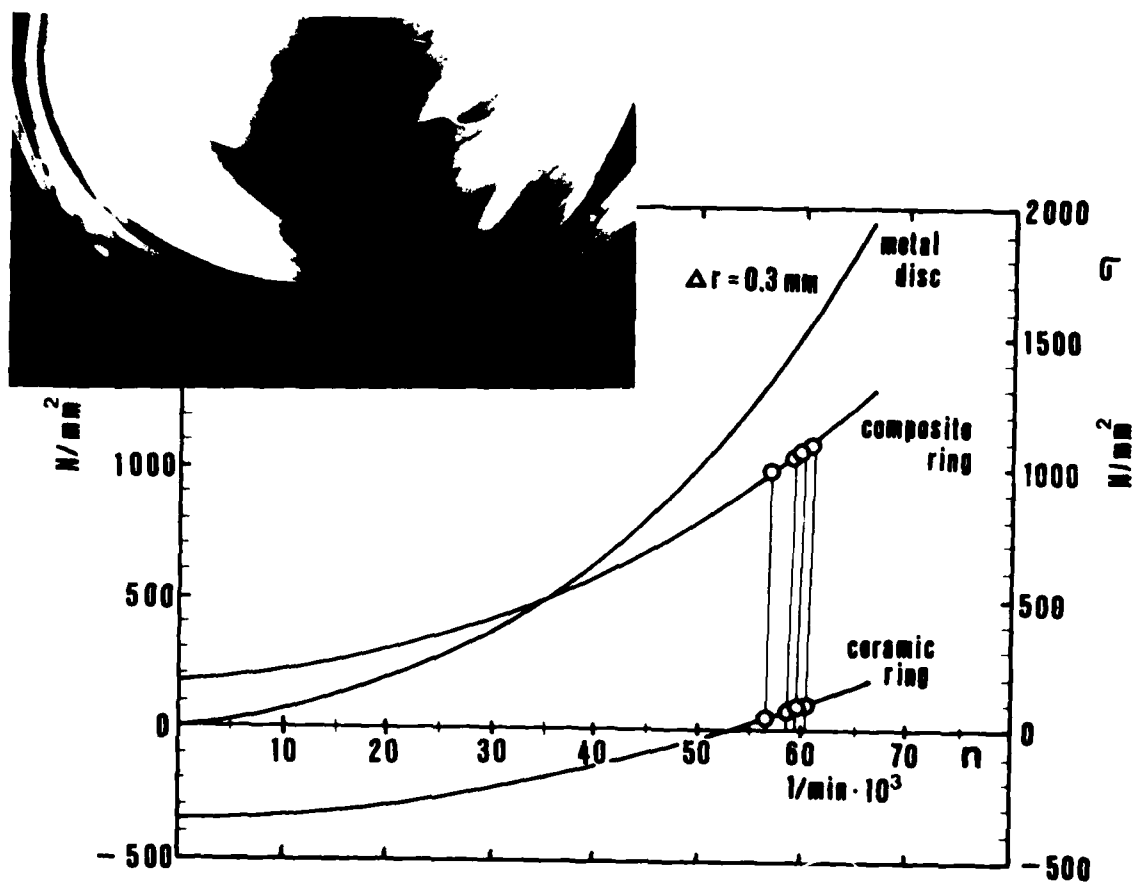


Fig. 1 Cold spin test results of CERP rings with and without prestress level

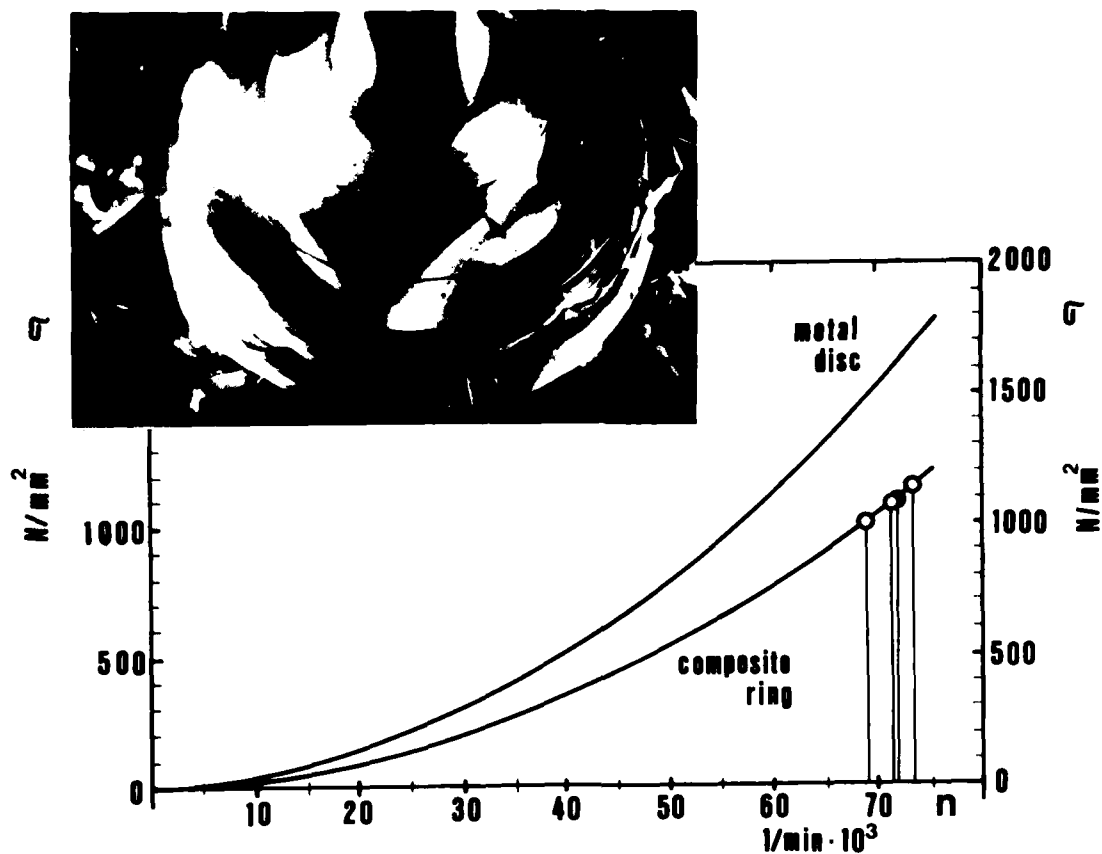


Fig. 9: Cold spin test results of B/Al rings

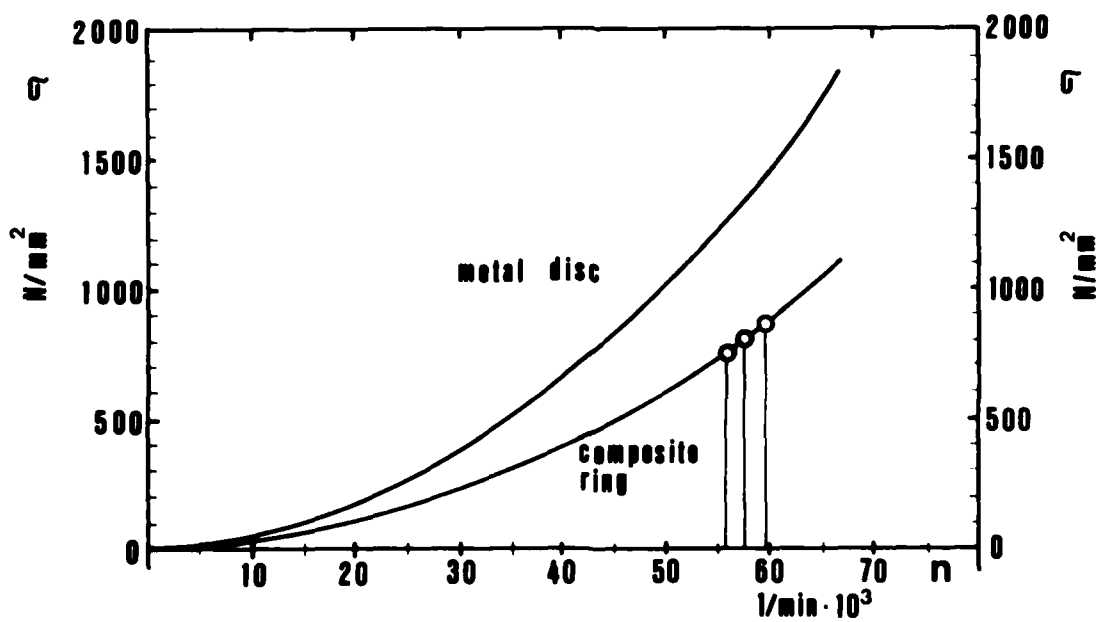


Fig. 10 Cold spin test results of C/C rings

Fig.11 Compression loaded ceramic rotor (first generation)



Fig.12 Radial oriented cracks within the turbine blades

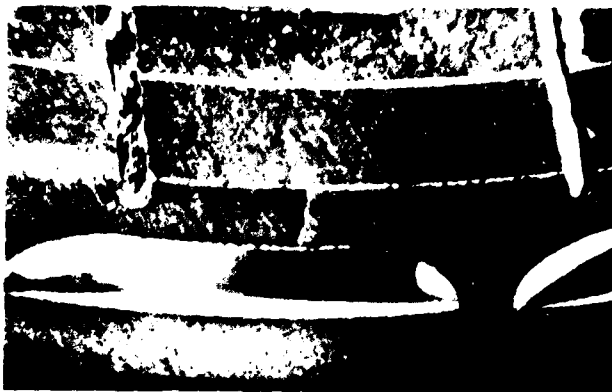


Fig.13 Close view of the cooling ring and the sliced insulation ring

Fig.14 Close view of the severely damaged area of the ceramic rotor



OXIDATION AND HOT CORROSION BEHAVIOR OF SINTERED NITROGEN CERAMICS

by

P.L.Cavallotti and U.Ducati
Politecnico di Milano
P. za L. da Vinci 32
20133 Milano
Italy

and

P.C.Martinengo
FIAT-Centro Recherche
Strada Torino 50
10043 Orbassano
Italy

ABSTRACT

We have completed a preliminary study on oxidation and corrosion of some types of nitrogen ceramics based on hot pressed (HPSN), reaction bonded (RBSN), reaction bonded and sintered (RBSSN) and pressureless sintered (PSSN) compacts.

These materials have also been tested in the presence of contaminants on the temperature range of 1170–1470 K. The gravimetric results indicate a more highly qualified resistance of RBSSN when compared with RBSN and PSSN samples; HPSN samples are corroded at somewhat lower rates possibly as a result of the very high density of the samples.

INTRODUCTION

Silicon nitride base ceramics show strong resistance to oxidation even at temperatures of 1600 K. This comes as no surprise; even burner rig tests have yielded satisfactory results at temperatures of 1570 K (Refs 1–4), and these materials have not been reported, with the possible exception of some salt dip test results^{5–6}, as suffering from catastrophic corrosion associated with superalloys.

However, we know only too well that simulation of service conditions is far from being properly mirrored by a technique of this kind. Experimental results have not been thoroughly worked out yet. All of this means:

- (1) We know that reported weight-change curves for the oxidation process reach a plateau quite rapidly and seem to substantiate the hypotheses of a "truly passive" behavior; but is it reasonable to draw up a picture of passive behavior of an oxidation process at such a high temperature?
- (2) Some experimental results confirm a low melting, sometimes glassy scale being formed during oxidation; this layer acts as an extractive solvent in respect to compaction aids (currently Mg-Y-Ca-Fe-Zr oxides); but it still remains to be seen whether all this would or would not result in an embrittlement of outer regions of unoxidized material.
- (3) We also know silicon to be apt to form both a lower oxide, that is SiO at low O_2 activities as well as normal oxide SiO_2 . The possible formation of a lower oxide in the underscale layer will produce a decrease in weight of about 8 gm per mole of reacted silicon nitride, instead of an increase of 40 gm per mole expected for the formation of SiO_2 . An appropriate combination of both reactions might lead to a balance in weight-change, so that a "passivity behavior" would be simulated in steady state oxidation conditions. On the other hand, the weight of the sample might, in some case, be a decreasing function of time! Would, moreover, possible sublimation of oxidation products be at all feasible?
- (4) Contamination with alkali metal salts may, in principle, lower the melting (or softening) point of the scale. Would this softer scale extract the above-mentioned compaction aids more efficiently?

- (5) What consequences are to be expected in connection with a given compaction procedure (i.e., with given amounts of given oxide additions)?

Research work has been started on these points, a preliminary report of which is given in this paper.

EXPERIMENTAL

Four types of silicon nitride compacts, see Table 1, have been tested under various conditions.

TABLE 1

Properties of the Tested Nitrogen Ceramics

Type	Aids %	Density (Mg/m^3)			Sintering Condition (K)	Strength at Room Temperature (MN/m^2)
		Green	Nitrided	Sintered		
HPSN	Y_2O_3 8% MgO 1%			3.26	2070 x 3 h	918
RBSN	Fe_2O_3 2% (+ 5% MgO in sint. bed)	1.52	2.35	3.05	2070 x 5 h	295
RBSSN	Y_2O_3 8% MgO 1%	1.64	2.52	3.22	2070 x 5 h	1020
PSSN	Y_2O_3 8% MgO 1%	2.0		3.25	2070 x 5 h	360

Fabrication procedure, starting materials used etc. are described elsewhere. Contaminants have been used in the amount of 20 g/m^2 and deposited by simple spray technique on samples previously polished through standard procedure. Through changing of the anion, with sodium as cation, the influence of SO_4^{2-} , Cl^- , SiO_3^{2-} , $\text{SO}_4^{2-} + 10\% \text{Cl}^-$ base contaminants has undergone thorough work study; whilst sulfates of sodium, potassium, lithium and mixed sodium-potassium 50% have been deposited to check the influence of cation.

Four types of gravimetric measurements have been obtained:

- oxidation in still air at 1470 K;
- oxidation in still air in presence of contaminants at various temperatures (1170–1270 K) with an overall weight change measurement;
- oxidation in still air, as above, in a thermobalance (Cahn R 100) or with intermediary weighings;
- oxidation as above, in the presence of an absorbing bed of catalyst grade alumina pellets, under the method schematized in Figure 1, and described elsewhere as well⁷.

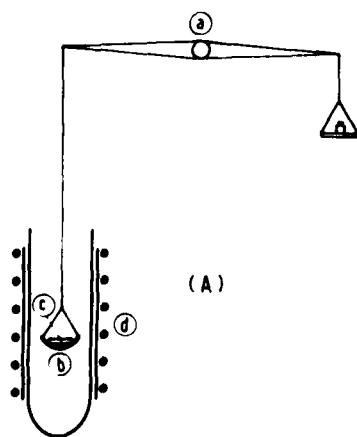


Fig. 1(A) Thermogravimetric apparatus
(a) Cahn R 100 electrobalance, (b) sintered alumina boat,
(c) sample coated by salts, (d) oven

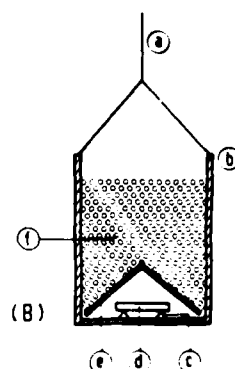


Fig. 1(B) Detail of absorber: (a) Pt wire (to electrobalance), (b) sintered alumina boat, (c) sintered alumina supports, (d) sample coated with salts, (e) sintered alumina hood, (f) catalyst grade Al_2O_3 pellets

In the last case, the sintered alumina boat, as used in conventional runs, was replaced by a porous alumina (with coarse and open porosity) crucible in which the sample was covered by a bed of alumina pellets supported by a bored alumina disc. The bed was expected to react with the volatile silicon compounds which might have escaped from the sample and to make them easily recognizable by X-ray diffraction of the pellets.

The scale has also been examined by X-ray technique. The oxidized samples were then sectioned and submitted to optical and electron microscope observation: some microhardness tests were also done.

RESULTS

Table 2 shows typical values of weight gain, as obtained on various types of material oxidized under various conditions.

TABLE 2
Gain in Weight Data for some Ceramics Tested at 1170 K

	Contaminants	Time (h)	Weight Gain (g/m ²)
HPSN	Na ₂ SO ₄	90	4.50
	NaCl	90	1.40
	Na ₂ SO ₄ + 10% NaCl	90	2.00
RBSSN	Na ₂ SO ₄	20	3.80
	Na ₂ SO ₄	60	5.80
	Na ₂ SO ₄	70	5.50
	Na ₂ SO ₄	70	1.10*
PSSN	Na ₂ SO ₄	20	5.00
	Na ₂ SO ₄	90	3.25
	NaCl	20	0.50
	NaCl	90	0
	Na ₂ SO ₄ + 10% NaCl	20	3.75
	Na ₂ SO ₄ + 10% NaCl	90	4.70
RBSN	Na ₂ SO ₄	20	38.60
	Na ₂ SO ₄	90	40.30
	NaCl	20	13.10
	NaCl	90	18.00
	Na ₂ SO ₄ + 10% NaCl	20	33.80
	Na ₂ SO ₄ + 10% NaCl	90	42.70

* The scale appeared very thin: no appreciable oxidation was found

The thermogravimetric curves in Figure 2 show the case of sulfate contaminant.

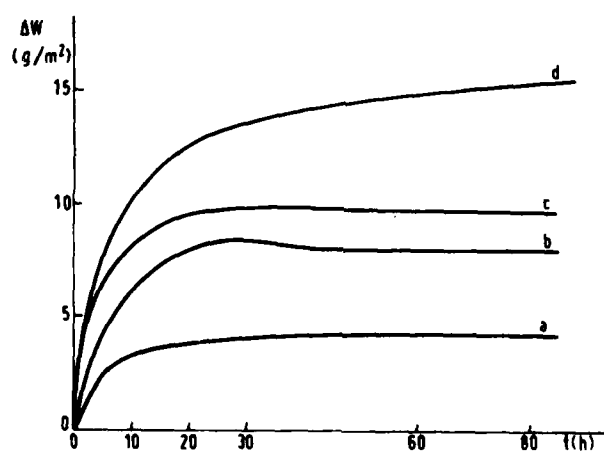


Fig. 2 Thermogravimetric curves of samples coated by different salts, 20 g/m², corroded in still air at 1170 K: (a) Na₂SO₄; (b) Li₂SO₄; (c) K₂SO₄; (d) K₂SO₄ (at 1270 K)

Figure 3 shows the comparison between sulfate and chloride contaminants. The salt loss from the surface has been accounted for when drawing up these diagrams.



Fig.3 Thermogravimetric curves of samples coated by different salts, 20 g/m², corroded in still air at 1170 K: (a) NaCl; (b) Na₂SO₄ + 50% NaCl; (c) Na₂SO₄

Figure 4 shows the X-ray pattern diffracted from the outer layer of the Al₂O₃ pellets exposed to sample oxidation products. We could identify the compound NaAlSiO₄ (Carnegieite) and this supports the hypothesis of silicon base volatile products formation during oxidation.

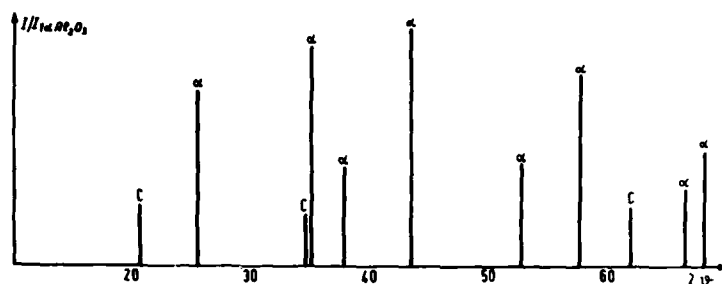


Fig.4 X-ray diffraction pattern of the outer layer of the Al₂O₃ pellets exposed to sample oxidation products
α: α-Al₂O₃; C: carnegieite (NaAlSiO₄)

Figure 5 depicts SEM image of a cross section of a pressureless sintered corroded sample.

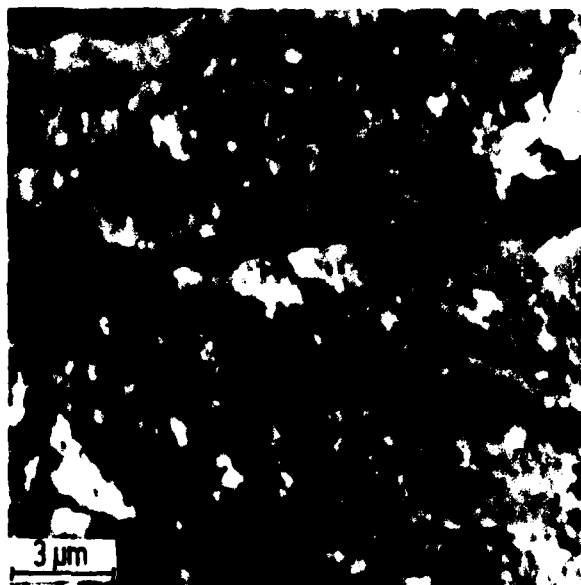


Fig.5 SEM image of a cross section of a PSSN corroded at 1170 K x 90 h
20 g/m² NaCl contaminant

In Figure 6 the Knoop microhardness prints, obtained on the same material as above, are shown.

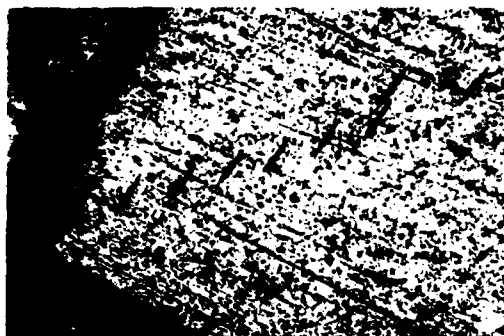


Figure 6

Figure 7 shows the glazy scale grown on an RBSSN sample oxidized in still air with sodium sulfate contaminant; the presence of trapped gas bubbles is characteristic of this type of scale.

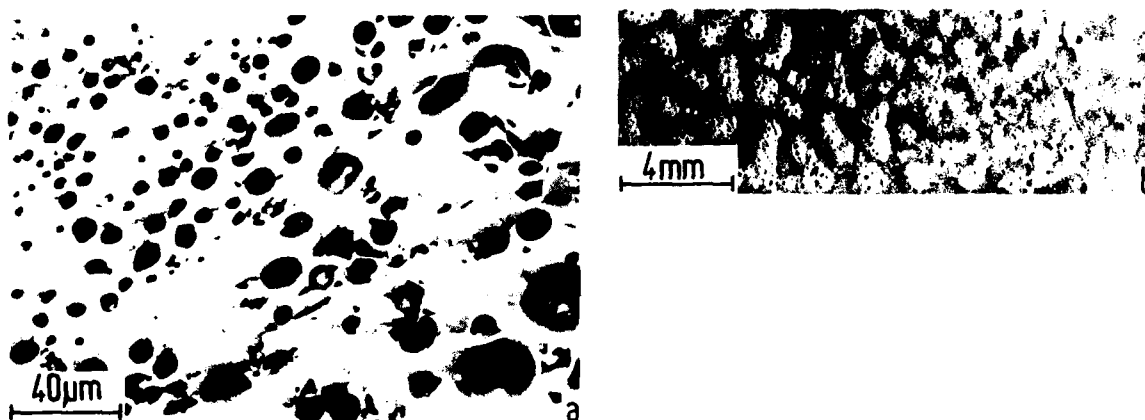


Fig.7 Images of a RBSSN sample corroded at 1170 K \times 90 h, 20 g/m² Na₂SO₄ contaminant; (a) SEM image of the cross section, (b) optical image

Figure 8 presents X-ray diffraction pattern of the scale grown on various samples.

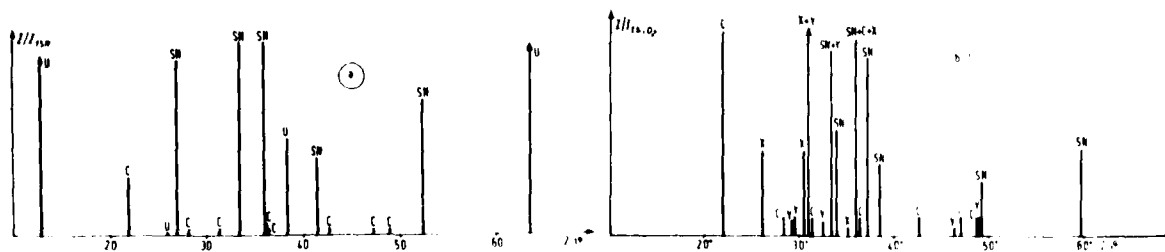


Fig.8(a) X-ray diffraction pattern of the scale grown on a PSSN, corroded at 1170 K \times 90 h, 20 g/m² Na₂SO₄ + 10% NaCl contaminants. SN: β -Si₃N₄, C: cristobalite, U: unknown substance

Fig.8(b) X-ray diffraction pattern of the scale grown on a RBSSN, oxidized in still air at 1470 K. SN: β -Si₃N₄, X: enstatite (MgSiO₃), C: cristobalite, Y: Y₂SiO₅

DISCUSSION AND RESULTS

Weight-change results as from Table 2 suggest higher resistance of RBSSN samples, compared to other pressureless compacted materials. This is probably due to the lower surface area, that is, to lower porosity produced by this compaction technique. The bend strength of the samples approaches that of HPSN. No wonder, therefore, that the corrosion behavior is practically the same, since the characteristics of the two types of material are very much alike.

The relation between corrosion behavior and the nature of the contaminant are illustrated in Figures 2 and 3.

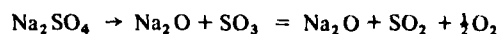
As it happens, conditions were not all equal when passing from one ion to the other, because of differences in melting point as well as vapour pressure of the compounds reported in Table 3.

TABLE 3

Melting Point and Vapour Pressure of Contaminants at 1170 K (Ref.8)

Compound	Melting point K	Vapour pressure (torr)
NaCl	1074	1.73 (9)
Na ₂ SO ₄	1157	0.03 (10, 11)
Li ₂ SO ₄	1132	
K ₂ SO ₄	1347	
Na ₂ SiO ₃	1362	
K ₂ SiO ₃	1249	
Li ₂ SiO ₃	1463	

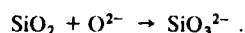
The comparison suggests, to say the best, a technical benefit: we believe that the relatively low effect of NaCl as compared to Na₂SO₄ may be related to the higher vapour pressure of the former. Besides, the latter is prone to undergoing a dissociation reaction



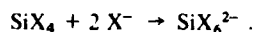
with formation of free Na₂O which can react with the silica to form low softening point glasses.

The above mentioned results, which confirm the observations of Schlichtig⁵⁻⁶, strongly suggest that a "salt fluxing" model of the corrosion process might be advisable, at least in a first order approximation approach, in order to explain the main features of the phenomena.

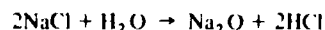
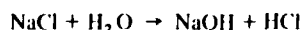
Two scale fluxing mechanism are feasible: the basic one is as follows:



The halosilicate runs like this:



Both lead to deterioration of the protective scale. All thermochemical data as collected in Table 4 have brought us to draw a conclusion based on the observation of the effect of sodium sulfate, carbonate, fluoride and chloride contaminants (presented here and in References 5 to 6). In fact the sulfate salt decomposition, may be enforced by the reaction between soda and silica, which consumes the reaction product to equilibrium: and the effect of carbonate and sulfate salts become similar, although carbonate proves more aggressive than sulfate. In addition, the two salts bias the oxidation process to the same extent as the sodium fluoride as a consequence of the activation of the halosilicate fluxing effect. On the other hand, because chlorosilicate compounds are thermodynamically unstable in oxygen containing environments, sodium chloride has little effect on oxidation behavior. Only the pyrolytic decomposition of the salt, according to the reaction equations



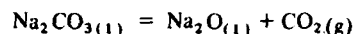
is responsible for the salt fluxing of the scale; the reaction kinetics, being diffusion controlled, is slower than the reaction kinetics for decomposition, this producing minor effects.

As for the influence of the cation, the melting points of the contaminants and of the corresponding silicates, are sufficient in themselves to explain the behavior and confirm the proposed mechanism (see Table 3).

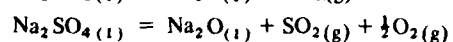
TABLE 4

Free Energy of Formation at 1170°K for Species Under Consideration

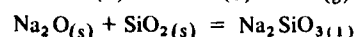
Na_2SO_4 (1)	- 918808 J/mole	Ref. (10)
Na_2CO_3 (1)	- 680718 J/mole	Ref. (8)
Na_2SO_4 (1)	- 249525 J/mole	Ref. (12)
SO_3 (g)	267803 J/mole	Ref. (9)
SO_2 (g)	- 276639 J/mole	Ref. (12)
CO_2 (g)	- 395395 J/mole	Ref. (9)



$$a_{\text{Na}_2\text{O}} P_{\text{CO}_2} = 19 \text{ mm Hg}$$



$$a_{\text{Na}_2\text{O}} P_{\text{SO}_2} = 1.7 \times 10^{-10} \text{ mm Hg}$$



$$\Delta G_r^\circ = - 239446 \text{ J/mole (9)}$$

A special feature of the work presented here is that the test temperature is much lower than that normally adopted.

With this probably lies responsibility for the result shown in Figure 5, where a subscale crack is visible. The crack is, we believe, due to effect of oxide extraction exerted by the scale on the compaction aids. This induces volume changes of the subscale layer and gives rise to tensile stresses, along with shear stresses parallel to the surface between the modified zones and the underlying unaffected material zones.

Lower microhardness values detected in the vicinity of the surface (see Figure 6) are also to be accounted for, along the same line.

Let us now consider thermogravimetric curves: our preliminary data show that in some instances a zero, or even a negative slope, characterizes the weight-change vs time curves. Reaction products evaporation might be responsible for this, as we suggested earlier on, although we believe that research on possible formation of low valence oxides ought to be carried further.

However, a scattering of experimental results has been observed in the case of materials with higher compaction aids content, undoubtedly related to lack of homogeneity.

Technical improvements of the compaction procedure will counteract much of the effect.

REFERENCES

1. Evans, A.G. J. Mater. Sci., 5, p.314, 1970.
Davidge, R.W.
2. Davidge, R.W. *Special Ceramics*, Vol.5, P.Popper ed., British Ceramic Research Ass., Stoke-on-Trent, 1972.
et al.
3. Singhal, S.C. J. Mater. Sci., 11, p.500, 1976.
4. Singhal, S.C. *Nitrogen Ceramics*, F.L.Riley ed., Noordhoff, Leyden, p.607, 1977.
5. Schlichting, J. Werk. u. Korros, 26, p.753, 1975.
6. Schlichting, J. *Nitrogen Ceramics*, F.L.Riley ed., Noordhoff, Leyden, p.627, 1977.
7. Sesini, R. Met. Ital., 71, p.10, 1979.
et al.
8. Janz, G.J. Molten Salts Handbook, Academic Press, N.Y. and London, 1967.
9. Kubaschewski, O. *Metallurgical Thermochemistry*, Pergamon Press, Oxford, 1967.
Evans, E.L.L.
Alcock, C.B.
10. Liang, W.W. J. Electrochem. Soc., 125, p.572, 1978.
Elliot, J.F.

11. De Crescente, M.A. Corrosion, 24, p.127, 1968.
 Bornstein, N.S.
12. JANAF Thermochemical Tables, 2nd ed., NBS 37, US Dept of Commerce. 1970.

DEVELOPMENT IN SINTERED SILICON NITRIDE

Authors:

E. Campo
P.C. MartinengoCENTRO RICERCHE FIAT SpA
Strada Torino 50 - ORBASSANO - ITALY

ABSTRACT

The most attractive process for Si_3N_4 production, to avoid the reaction bonding and hot pressing problems, would be one which enables high performance and complexity of shape simultaneously. At Fiat Research Centre a pressureless sintering process has been studied and developed, and various grades of Si_3N_4 have been produced. MgO and Y_2O_3 were employed as sintering aids for commercial Si_3N_4 powders and also to sinter reaction bonded silicon nitride. The present paper describes both the process and the characterization of these sintered Si_3N_4 materials particularly in respect to structure and mechanical properties.

INTRODUCTION

Silicon nitride, with silicon carbide, is one of the few numbers of ceramic materials, that for its properties is actually considered for high temperature engineering applications. The potentiality of this material for structural components operating in conditions such as might occur in a gas turbine or in a Diesel engine, are well known (1, 2), but till now the two available processes for its production, i.e. reaction sintering and hot pressing, show both some disadvantages and limitations. Reaction bonded material, which can easily shaped in complex geometry, has low density, moderate strength, corrosion and oxidation resistance; hot pressed Si_3N_4 has higher density, adequate mechanical and thermal properties, but components such as those required for the engineering applications, can be obtained only at very high production costs through complex machining process. These problems raise the question whether sintering of silicon nitride powder would not provide a suitable and cheaper alternative, and have concentrated in this field the recent research activity on the development of silicon nitride.

In this respect as silicon nitride, like other covalent powders, does not sinter readily it requires high temperature and sintering aids for its densification; some problems must be considered consequently and particularly:

- how to limit the sintering temperature
- how to limit the Si_3N_4 decomposition without applying external pressure.

As referred by Gazza (3) and Rowcliffe (4) for the first problem a possible approach is the use of very fine powders of controlled size, shape and impurities, that are more reactive than coarser one by virtue of their large surface area.

Instead of this advantage such fine powders usually present problems regarding their cold compacting and the control of the shrinkage during densification.

An alternative way is to use an adequate oxide or non oxide additive to form a liquid phase like those employed for the pressure sintering.

In any case if the densification temperature is higher than 1600°C the dissociation $\text{Si}_3\text{N}_4 \rightarrow 3\text{Si} + 2\text{N}_2$ becomes important and competitive with the sintering process (5): embedding the component to be sintered in a powder bed may be the way to solve this problem even if the chemical composition of the powder bed, because of the volatility of some of the sintering aids, has to be carefully chosen.

Interesting results have been obtained through this method (6) and this type of process has been considered for the present research.

It has been applied to sinter Si_3N_4 base compacts containing MgO and Y_2O_3 as additives but also to densify PBCN containing the same sintering aids. This last approach to the Si_3N_4 densification results from the consideration that the higher the density of the starting material for the sintering process, the greater the accuracy in the final dimension of complex shape components so obtained.

EXPERIMENTAL PROCEDURES

Three different materials were investigated during the present research: two were obtained from commercial silicon nitride powder and one from silicon. Yttria and sapphire have been used as sintering aids. The silicon nitride employed was AME Rosenthal CER8; its particle size distribution, obtained by a sedimentation balance was $1.7 \mu\text{m}$ as received and $5 \mu\text{m}$ after milling as shown by Figure 1.

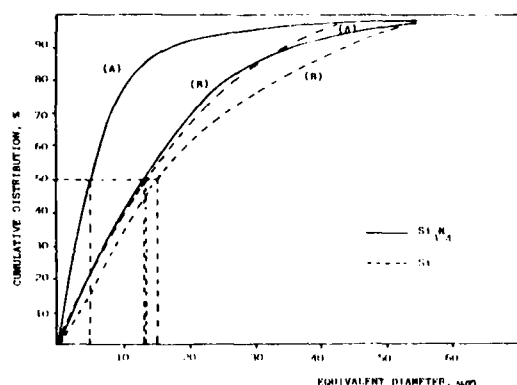


Figure 1 - Cumulative particle size distribution of Si_3N_4 and Si powders. (A) as received, (B) milled:

TYPE OF POWDER	CHEMICAL COMPOSITION, %										PHASES, %	MEAN PARTICLE SIZE, μm
	Si	Y	Al	Fe	Mg	N	O	Si ₃ N ₄	Si	BN		
Si_3N_4	93.90	0.11	0.42	0.24	0.20	0.05	0.01	96.11	0.35	0.45		15
Si	86.08	0.02	0.50	0.50	0.70	0.03	0.01	86.16				15

* DETERMINED BY LECO APPARATUS - ** DETERMINED BY SEDIMENTATION BALANCE.

Table 1 - Characteristics of the powders employed for the sintering.

The specific surface area of this powder was $4 \text{ m}^2/\text{g}$ that corresponds to a particle size of about $0.5 \mu\text{m}$. These different results indicate the presence of large amount of agglomerates which will break down in the milling/mixing operation.

The silicon powder was Baudier 4 μm type. Its particle size distribution before and after milling is reported in the previous Figure. The mean grain size was $15 \mu\text{m}$, that agrees better than in the case of Si_3N_4 with that obtained by calculation from the specific surface area ($0.6 \text{ m}^2/\text{g}$). The chemical analysis of both powders are reported in Table 1. Yttria and Magnesia powders were commercial Merck products.

The three mixtures employed were:

material M_1 - 93% Si_3N_4 + 5% MgO + 2% Fe

material M_2 - 91% Si_3N_4 + 8% Y_2O_3 + 1% MgO

material M_3 - 86% Si + 12.5 Y_2O_3 + 1.5% MgO

This mixing/milling operation, for M_2 and M_3 composition, was carried out in a porcelain jar with alumina in isopropyl alcohol for 72 h; M_1 was prepared in a steel jar, and this is the reason for its iron content. After this, the mixture was dried, pressed isostatically at 350 and 200 MPa respectively for Si_3N_4 base and Si base mixtures, into cylinders of $30 \times 40 \text{ mm}$.

Sintering experiments for the materials M_1 and M_2 were carried out on these cylinders at temperatures between 1650 and 1850°C for times in the range 0.5 and 5 h. The samples were surrounded by a powder mixture of 50% Si_3N_4 - 45% BN and 5% MgO , and the thermal treatments were performed at atmospheric pressure of nitrogen in a resistance heated vacuum furnace.

For the material M_3 , before the sintering cycle just mentioned, the samples were subjected to a conventional nitridation treatment (Figure 2) in a static nitrogen atmosphere. Conversion was about 95%; nitrided density reached 2.52, instead of 1.64 of the unnitrided material.

Samples were weighed before and after sintering; density and shrinkage were also determined.

X-ray diffractometry, optical and electron microscopy analyses have been done, and various mechanical and physical properties were determined.

Some preliminary evaluation of the influence of post thermal treatment on the mechanical resistance have been also performed.

SINTERING

Figure 3 shows the densification curves for the composition M_1 , M_2 and M_3 sintered at constant time in the temperature range 1650 - 1850°C; Figure 4 shows the influence of the sintering time on the degree of densification at 1650°C for the material M_1 and at 1800°C for the material M_2 and M_3 . As the increasing of density may be the result of changes in dimension, i.e. shrinkage, or in weight, both are recorded on Figure 5 and Figure 6.

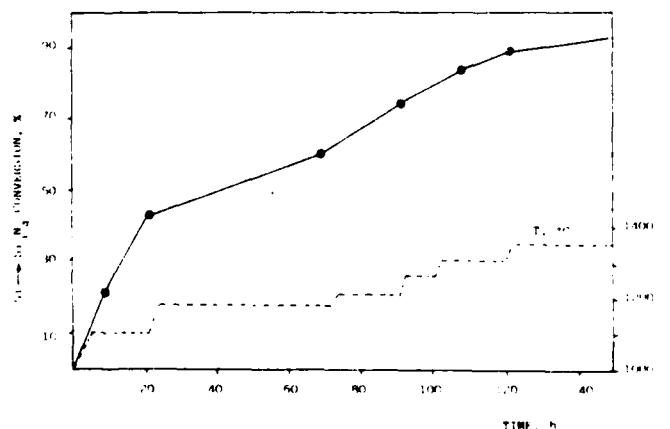


Figure 2 - Nitridation schedule in static nitrogen of the material M_3 before sintering.

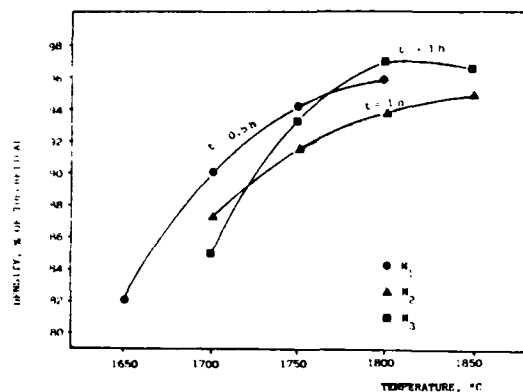


Figure 3 - Density of different sintered Si_3N_4 vs. sintering temperature.

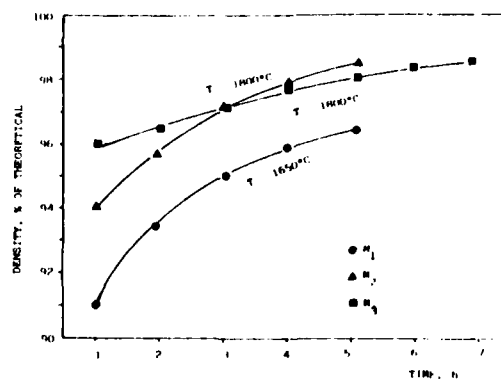


Figure 4 - Density of different sintered Si_3N_4 vs. sintering time.

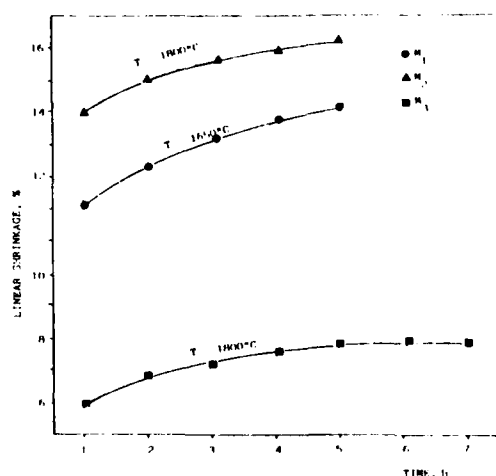


Figure 5 - Shrinkage vs. time during sintering of different Si_3N_4 grades.

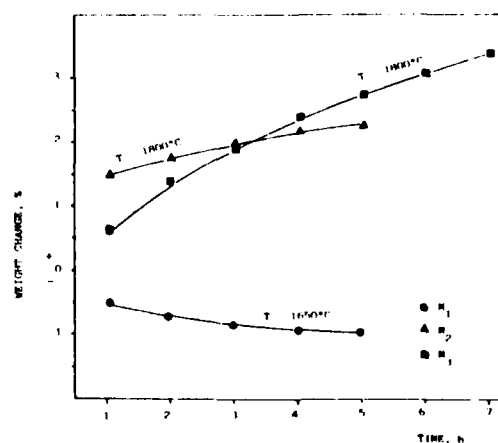


Figure 6 - Weight changes vs. time during sintering of different Si_3N_4 grades.

Looking to these results it is evident that sintering temperature of 1650°C is the best one for the M_1 composition, while for the materials containing Y_2O_3 as sintering aid, temperature of 1800°C is required for the full densification.

Sintering time of 5 hours seems necessary for all the compositions if, in order to control grain growth, lower thermal treatment is desirable.

Structure of the materials obtained with the above mentioned conditions are shown on Figure 7. The mean grain size appears of few microns with a finer texture for the M_3 composition.

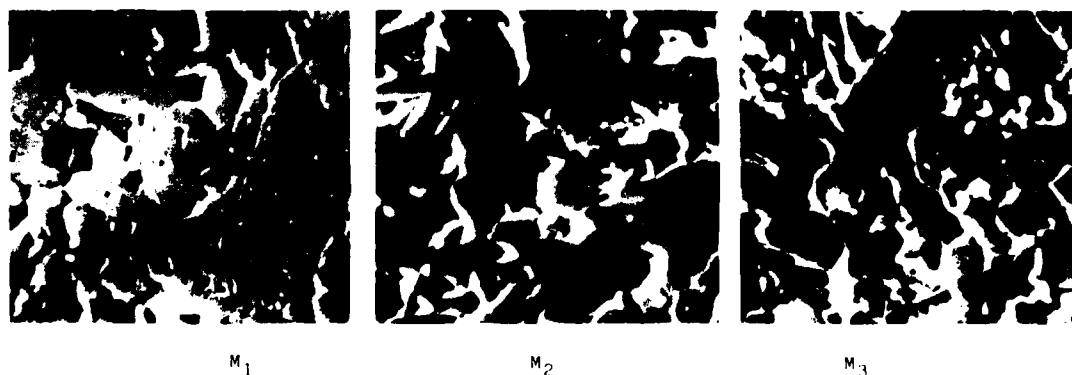


Figure 7 - Microstructure of the materials "as sintered" (5000 x)

The crystalline phases observed on the sintered materials are summarized on Table 2. On the materials M_2 and M_3 no evidence of grain boundary crystalline phases were obtained.

Devitrification of these amorphous phases was obtained by thermal treatment in nitrogen atmosphere in the temperature range 1000-1400°C. Table 2 shows also the phases developed in sintered compacts thermal treated in different conditions.

Indications of the influence of the secondary phases devitrification on the mechanical behaviour of the materials are reported below.

PHASE	Si_3N_4 M_1		Si_3N_4 M_2		Si_3N_4 M_3	
	AS SINTERED	HEAT TREATED	AS SINTERED	HEAT TREATED	AS SINTERED	HEAT TREATED
Si_3N_4	+	+	+	+	+	+
Si_2N_2O	+	+	+	+	+	+
$Si_2N_2O_2$	+	+	+	+	+	+
$Si_2N_2O_3$	+	+	+	+	+	+
$Si_2N_2O_4$	+	+	+	+	+	+
$Si_2N_2O_5$	+	+	+	+	+	+
$Si_2N_2O_6$	+	+	+	+	+	+
$Si_2N_2O_7$	+	+	+	+	+	+
$Si_2N_2O_8$	+	+	+	+	+	+
$Si_2N_2O_9$	+	+	+	+	+	+
$Si_2N_2O_{10}$	+	+	+	+	+	+
$Si_2N_2O_{11}$	+	+	+	+	+	+
$Si_2N_2O_{12}$	+	+	+	+	+	+
$Si_2N_2O_{13}$	+	+	+	+	+	+
$Si_2N_2O_{14}$	+	+	+	+	+	+
$Si_2N_2O_{15}$	+	+	+	+	+	+
$Si_2N_2O_{16}$	+	+	+	+	+	+
$Si_2N_2O_{17}$	+	+	+	+	+	+
$Si_2N_2O_{18}$	+	+	+	+	+	+
$Si_2N_2O_{19}$	+	+	+	+	+	+
$Si_2N_2O_{20}$	+	+	+	+	+	+
$Si_2N_2O_{21}$	+	+	+	+	+	+
$Si_2N_2O_{22}$	+	+	+	+	+	+
$Si_2N_2O_{23}$	+	+	+	+	+	+
$Si_2N_2O_{24}$	+	+	+	+	+	+
$Si_2N_2O_{25}$	+	+	+	+	+	+
$Si_2N_2O_{26}$	+	+	+	+	+	+
$Si_2N_2O_{27}$	+	+	+	+	+	+
$Si_2N_2O_{28}$	+	+	+	+	+	+
$Si_2N_2O_{29}$	+	+	+	+	+	+
$Si_2N_2O_{30}$	+	+	+	+	+	+
$Si_2N_2O_{31}$	+	+	+	+	+	+
$Si_2N_2O_{32}$	+	+	+	+	+	+
$Si_2N_2O_{33}$	+	+	+	+	+	+
$Si_2N_2O_{34}$	+	+	+	+	+	+
$Si_2N_2O_{35}$	+	+	+	+	+	+
$Si_2N_2O_{36}$	+	+	+	+	+	+
$Si_2N_2O_{37}$	+	+	+	+	+	+
$Si_2N_2O_{38}$	+	+	+	+	+	+
$Si_2N_2O_{39}$	+	+	+	+	+	+
$Si_2N_2O_{40}$	+	+	+	+	+	+
$Si_2N_2O_{41}$	+	+	+	+	+	+
$Si_2N_2O_{42}$	+	+	+	+	+	+
$Si_2N_2O_{43}$	+	+	+	+	+	+
$Si_2N_2O_{44}$	+	+	+	+	+	+
$Si_2N_2O_{45}$	+	+	+	+	+	+
$Si_2N_2O_{46}$	+	+	+	+	+	+
$Si_2N_2O_{47}$	+	+	+	+	+	+
$Si_2N_2O_{48}$	+	+	+	+	+	+
$Si_2N_2O_{49}$	+	+	+	+	+	+
$Si_2N_2O_{50}$	+	+	+	+	+	+
$Si_2N_2O_{51}$	+	+	+	+	+	+
$Si_2N_2O_{52}$	+	+	+	+	+	+
$Si_2N_2O_{53}$	+	+	+	+	+	+
$Si_2N_2O_{54}$	+	+	+	+	+	+
$Si_2N_2O_{55}$	+	+	+	+	+	+
$Si_2N_2O_{56}$	+	+	+	+	+	+
$Si_2N_2O_{57}$	+	+	+	+	+	+
$Si_2N_2O_{58}$	+	+	+	+	+	+
$Si_2N_2O_{59}$	+	+	+	+	+	+
$Si_2N_2O_{60}$	+	+	+	+	+	+
$Si_2N_2O_{61}$	+	+	+	+	+	+
$Si_2N_2O_{62}$	+	+	+	+	+	+
$Si_2N_2O_{63}$	+	+	+	+	+	+
$Si_2N_2O_{64}$	+	+	+	+	+	+
$Si_2N_2O_{65}$	+	+	+	+	+	+
$Si_2N_2O_{66}$	+	+	+	+	+	+
$Si_2N_2O_{67}$	+	+	+	+	+	+
$Si_2N_2O_{68}$	+	+	+	+	+	+
$Si_2N_2O_{69}$	+	+	+	+	+	+
$Si_2N_2O_{70}$	+	+	+	+	+	+
$Si_2N_2O_{71}$	+	+	+	+	+	+
$Si_2N_2O_{72}$	+	+	+	+	+	+
$Si_2N_2O_{73}$	+	+	+	+	+	+
$Si_2N_2O_{74}$	+	+	+	+	+	+
$Si_2N_2O_{75}$	+	+	+	+	+	+
$Si_2N_2O_{76}$	+	+	+	+	+	+
$Si_2N_2O_{77}$	+	+	+	+	+	+
$Si_2N_2O_{78}$	+	+	+	+	+	+
$Si_2N_2O_{79}$	+	+	+	+	+	+
$Si_2N_2O_{80}$	+	+	+	+	+	+
$Si_2N_2O_{81}$	+	+	+	+	+	+
$Si_2N_2O_{82}$	+	+	+	+	+	+
$Si_2N_2O_{83}$	+	+	+	+	+	+
$Si_2N_2O_{84}$	+	+	+	+	+	+
$Si_2N_2O_{85}$	+	+	+	+	+	+
$Si_2N_2O_{86}$	+	+	+	+	+	+
$Si_2N_2O_{87}$	+	+	+	+	+	+
$Si_2N_2O_{88}$	+	+	+	+	+	+
$Si_2N_2O_{89}$	+	+	+	+	+	+
$Si_2N_2O_{90}$	+	+	+	+	+	+
$Si_2N_2O_{91}$	+	+	+	+	+	+
$Si_2N_2O_{92}$	+	+	+	+	+	+
$Si_2N_2O_{93}$	+	+	+	+	+	+
$Si_2N_2O_{94}$	+	+	+	+	+	+
$Si_2N_2O_{95}$	+	+	+	+	+	+
$Si_2N_2O_{96}$	+	+	+	+	+	+
$Si_2N_2O_{97}$	+	+	+	+	+	+
$Si_2N_2O_{98}$	+	+	+	+	+	+
$Si_2N_2O_{99}$	+	+	+	+	+	+
$Si_2N_2O_{100}$	+	+	+	+	+	+

Table 2 - XRD Phase identification on "as sintered" and heat-treated materials.

FRACTURE STRENGTH

It is well known that the fracture strength of a brittle material depends on its characteristic structural properties and on their defects. This dependence is expressed by the critical stress factor, K_{IC} , which relates the size of the most severe crack, a , to the fracture stress σ_R , according to the relationship.

$$K_{IC} = Y \sigma_R \sqrt{a} \quad (1)$$

where the parameter Y depends on the crack geometry.

As cracks size has a random distribution, the assessment of strength requires a statistical approach. The most common method is due to Weibull (7), who gives the failure probability of a stressed element as

$$P = 1 - \exp \left\{ - \left(\frac{\sigma}{\bar{\sigma}} \right)^m \left[\Gamma \left(\frac{1}{m} + 1 \right) \right]^m \right\} \quad (2)$$

where σ is a reference stress (i.e. maximum stress), $\bar{\sigma}$ the mean value of the reference stress at failure, m the Weibull modulus, Γ the Euler function.

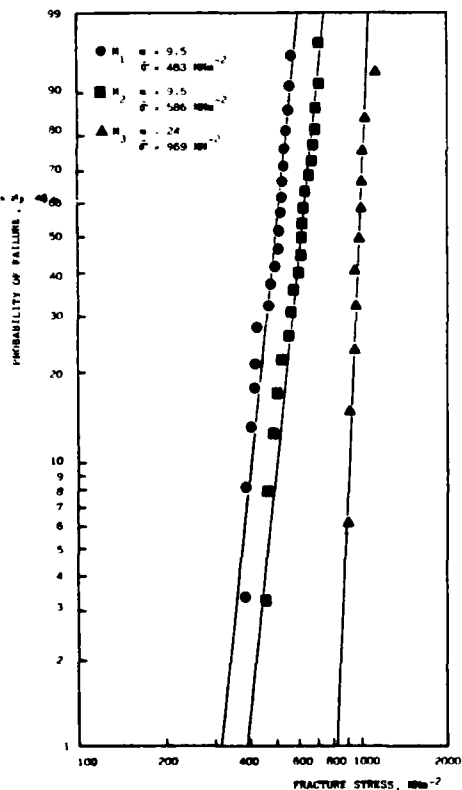


Figure 8 - Weibull distribution for fracture strength of three point bending specimens of sintered Si_3N_4 .

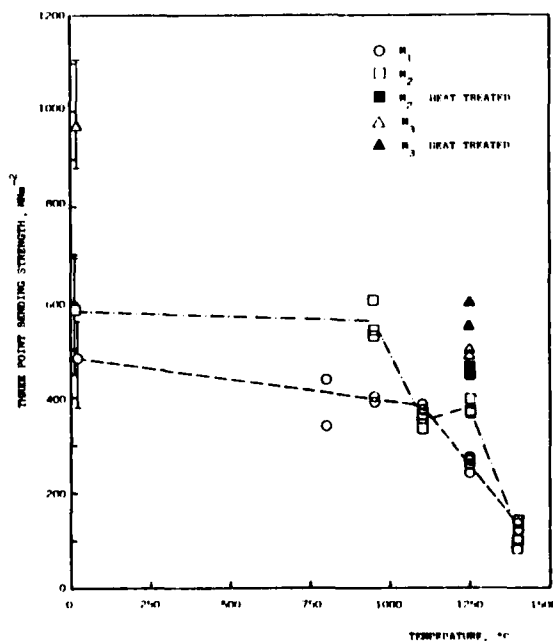


Figure 9 - Strength versus temperature, for materials M_1 , M_2 and M_3 , measured by three point bending tests.

This equation, suitable for any specimen geometry and loading arrangement, has been used for our experiments. Three point bending fracture tests were carried out at room temperature on rectangular specimens, with 4x5 mm cross section and a span between supports of 18 mm.

In order to obtain statistical strength distribution, 20 fracture experiments were carried out on material M_1 , 21 on M_2 and 11 on M_3 .

The strength values were ranked in increasing order and for each of them a probability P was assigned corresponding to the "median rank".

The distribution function of equation 2 can be approximately linearized and then the Weibull modulus m obtained by a simple graphical method.

$$\begin{aligned}\bar{\sigma} &= 483 \text{ MNm}^{-2}, \quad m = 9.5 \text{ for material } M_1 \\ \bar{\sigma} &= 586 \text{ MNm}^{-2}, \quad m = 9.5 \text{ for material } M_2 \\ \bar{\sigma} &= 696 \text{ MNm}^{-2}, \quad m = 24 \text{ for material } M_3\end{aligned}$$

High temperature fracture tests were also performed on rectangular specimens by three-points bending, but with a span of 35 mm.

Experiments were carried out in air on an Inston testing equipment with a cross head speed of 0.5 mm/min. The results are plotted in Figure 9.

In the same picture it is also shown the influence of some heat devetrification treatments on the high temperature strength of those sintered materials. More experimental analysis has to be done to optimize those treatments in respect to mechanical properties increase.

FRACTURE TOUGHNESS

The controlled surface flaw technique was used to determine the stress intensity factor (fracture toughness). In this technique a Knoop microhardness indentation is produced on the tensile side of bending specimens. It has been shown (8) that the indentation of the ceramics, produces surface cracks, which are nearly semicircular and have highly reproducible dimensions. These cracks can be assumed to have diameter equal to the length of the major diagonal of the indentation.

Specimens of the materials M_1 and M_2 , with dimensions 4x5x40 mm, were indented with a load of 2500 g, and then subjected to four-point bending tests at room temperature.

The following mean values of fracture toughness were determined:

$$K_{IC} = 4.4 \text{ MNm}^{-3/2}$$

for material M_1 , on 7 specimens, with a standard deviation of 0.4:

$$K_{IC} = 5.0 \text{ MNm}^{-3/2}$$

for material M_2 , on 4 specimens, with a standard deviation of 0.05.

Regarding case material M_1 , a controlled surface removal of about 20 μm was made before the fracture test to avoid the influence of residual stresses beneath the indentation on the strength measurement. Material M_2 specimens were not ground, because this procedure was subsequently proved to be unnecessary.

SLOW CRACK GROWTH

The strength degradation at high temperature is generally associated with the slow crack growth phenomenon which occurs above 1000°C.

The crack growth rate $\frac{da}{dt}$ has been shown to be related to the stress intensity factor by the following relationship.

$$\frac{da}{dt} = A K_I^n \quad (3)$$

where A and n are constant for a given temperature.

Experimental measurements for the evaluation of this property on our sintered Si_3N_4 have been performed by the double-torsion test method.

This technique has been described in detail by Williams and Evans (9). To a first approximate stress analysis, the double-torsion specimen gives a constant stress intensity factor K_I being independent of crack length and related only to the applied load. Since the validity of the mentioned analysis was assessed experimentally using a series of PMMA specimens, the sizes of the ceramic specimens were chosen according to calibration test results.

Double torsion tests were performed on Si_3N_4 specimens of materials M_1 and M_2 at 1200 and 1300°C. The technique was used at constant load, with crack growth rate measured by optical microscopy.

The crack front configuration was found to be curved and the growth rate was computed observing the surface where it was faster.

The obtained results are plotted in Figure 10, together with best fit according to the crack growth law. The stress intensity factor producing catastrophic fracture at high temperature was found to be greater or equal to the mean value obtained at room temperature.

FRACTOGRAPHY

For materials M_1 and M_2 a certain number of fractured specimens were examined at the scanning electron microscope.

Figure 11 shows the fractographs obtained on an M_1 specimen broken at room temperature, and on a M_2 specimen (heat-treated) tested at 1250°C.

The morphological pattern of the surface, is typical of brittle fracture with a smooth area surrounding the initiation point and radiating coarse fracture steps over the remaining rough surface.

For both materials the initiation points are large subsurface pores having a size $2a$ of about 150 μm . This value is comparable to the flaw size which can be evaluated through the fracture mechanics equation using the performed measures of strength and fracture toughness.

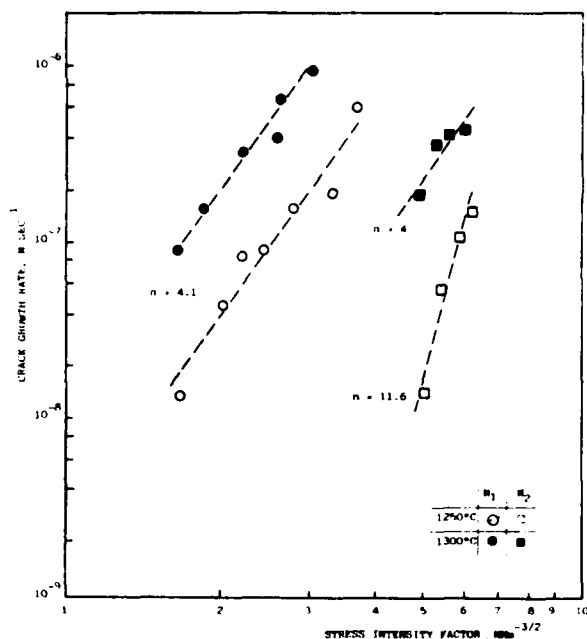
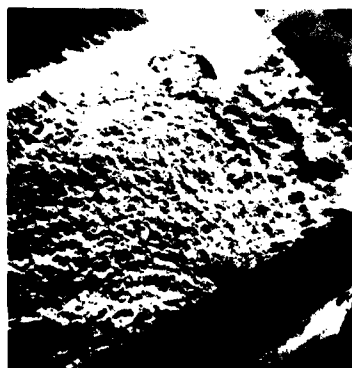
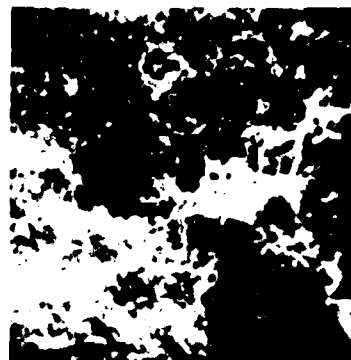


Figure 10 - Crack growth rate data for materials M_1 and M_2 tested at 1250 and 1300°C.



1 mm

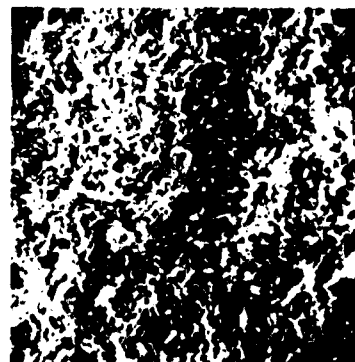


M_1

40 μm



1 mm



40 μm

Figure 11 - Scanning electron fractographs showing topography and origin of fracture in specimens of materials M_1 and M_2 .

DISCUSSION

The results of Figures 3-6 that show the dependence of densification, shrinkage and weight loss on temperature and time, allow some consideration for the three different materials.

First of all it has to be noted that M_1 sintered Si_3N_4 reached a density of 3.1 Mg m^{-3} during sintering at 1650°C for 5 h or at 1700°C for 0.5 h, with a weight loss in both cases, very limited (less than 1%). These weight losses are lower than those obtained by Terwilliger and Lange (10) during sintering experiments at atmospheric pressure of N_2 , or by Mitomo (11) with an over pressure of 10 atm of N_2 . This different behaviour, discussed in a previous work of ours (6), indicates that the weight loss occurring during sintering of $Si_3N_4 + MgO$ mixture is not only due to the dissociation of Si_3N_4 but also to the volatilization of MgO (its vapour pressure at 1600 is 0.013 Pa) which migrates from the compact to the external atmosphere. This MgO volatilization, that would be useful in a sintered material to reduce the low melting point grain boundary phase content, is critical during the sintering cycle. Thus the powder bed will have to contain the sintering aid which during sintering will achieve a suitable vapour pressure to maintain the equilibrium between the content in the sample and in the powder bed.

This is one of the most interesting observations reached during the study of the first type of material and it was the basis for the development of the subsequent sintered grades.

In fact the M_1 sintered Si_3N_4 , because of its chemical composition with particular reference to MgO and Fe content, should exhibit deterioration of its high temperature properties: it would indicate a way to produce a sintered silicon nitride by means of pressureless treatments of commercial Si_3N_4 powders.

Further materials were modified to Y_2O_3 base additives with a minimum amount of MgO , according to the previous considerations on weight loss during sintering, and on negative results of preliminary experiments on $Si_3N_4 - Y_2O_3$ mixtures.

With the composition 91% $Si_3N_4 - 8\% Y_2O_3 - 1\% MgO$ the best results have been obtained by sintering for 5 h at 1800°C (Figure 4), either starting from Si_3N_4 or from Si powders. It is noteworthy that instead of a weight loss during sintering in both materials there is a slight weight gain, that can be explained by nitridation of unnitrided silicon present in the Si_3N_4 , and transfer of MgO from the powder bed to the sample. The presence of an amorphous phase in the sintered sample (Table 3) leads to consider, according with Gazza (12) and Tsuge (13) the devitrification process of the grain boundary phases as one of the more interesting way to improve the properties of the material at high temperature.

Evidence of the beneficial effect of the recrystallization of the amorphous phases on the bend strength has been obtained (Figure 8) but the complexity of the devitrification process (14) requires a more detailed analysis of this particular aspect of the material optimization.

In respect to the densification it has to be noted that the results obtained with the M_2 type of composition are very close to the theoretical value, but looking to the linear shrinkage it can be seen that material M_1 presents, in respect to M_2 , interesting advantages; Figure 5 shows that the shrinkage of specimens with same sintered density, but obtained from silicon powder, is two time lower than that corresponding to silicon nitride starting powder.

This densification result is combined with improved mechanical properties, particularly in respect to bend strength, and indicates the possibility to have at some time, high mechanical properties of the material and complex shape feasibility.

Looking to the mechanical properties, materials M_1 and M_2 show similar mean strength value and Weibull modulus: since the strength depends on the most severe crack present in the material that indicates they have similar defect size distribution.

The small difference in σ_R is accounted only in term of toughness. Direct evidence of this fact has been obtained by fractography (Figure 11).

As the preliminary mechanical test results on M_3 show better strength data, it is reasonable to think that high values of σ_R and m are related with a significative reduction in large pore size distribution.

On the contrary of the bend strength, the fracture toughness of M_1 would be expected equal to the M_2 material because the main variable which effects toughness is the total amount of porosity.

Chemical composition of sintering aids has much influence in the high temperature behaviour of the material. In the sintered materials additive elements and impurities are located at grain boundary where a glassy phase is formed.

The reduction of viscosity, due to temperature effect, produces the phenomenon of slow crack growth, which is responsible of time degradation of strength at high temperature.

Material M_2 differs from M_1 in the amorphous phase composition and in the peculiar property of this phase to undergo to partial devitrification with formation of Yttrium compounds when heated at sufficiently high temperature.

The good crack growth resistance of material M_2 may be attributed to the high viscosity of the intergranular zones due to the presence of crystalline phases.

Other than with appropriate heat treatment, devitrification is spontaneous induced into the material by heating at a temperature above 1100°C . This explains the lack of monotonic behaviour in the strength versus temperature data, as the deleterious effect of temperature on grain boundary phase viscosity is compensated by the strengthening due to the crystalline phases formation.

CONCLUSIONS

- Uniform sintering of silicon nitride which contains MgO or MgO and Y_2O_3 as sintering aids can be achieved at atmospheric pressure of nitrogen using a powder bed containing MgO.
- The simultaneous addition of Yttria and Magnesia results in a material that can be sintered to near theoretical density.
- Reaction sintered silicon nitride containing the same sintering aids can be post sintered in a powder bed containing MgO which results in considerable improvement of strength.
- The time-independent mechanical behaviour of the pressureless sintered materials obtained from Si_3N_4 powder is similar; a noticeable improvement has been reached on the post sintered RBSN, probably due to the reduction in the critical flaw sizes.
- The devitrification of the grain boundary amorphous phase in Y_2O_3 base sintered materials produces a noticeable improvement of the crack growth resistance and in time dependent mechanical behaviour.
- The process of post-sintering of reaction sintered silicon nitride should lead to the production of complex shaped components to close dimensional tolerances and good mechanical properties.

REFERENCES

1. J.J. Burke, A.E. Gorum and R.N. Katz "Ceramic for High Temperature Applications" Proc. of the Sec. Army Mat. Tech. Conf., Nov. 1973, Brook Hill, 1974
2. F.L. Riley "Nitrogen Ceramics" Proc. NATO ASI on Nitrogen Ceramics, Aug. 1976, Noordhoff, 1977
3. G.E. Gazza "Ceramic for High Temperature Applications", II, 1978, 1001
4. D.J. Rowcliffe, P.J. Jorgensen "Proceedings of the Workshop in Ceramics for Advanced Heat Engines" Conf. 770110 UC 95a - ERDA - Rep. (1977) NTIS, US Dep. of Com.
5. G.R. Terwilliger - J. Am. Ceram. Soc. 57 (1973) 48
6. A. Giachello, P.C. Martinengo, G. Tommasini and P. Popper "Sintering of Silicon Nitride in a Powder Bed" J. Mat. Science (To be published)
7. D.G.S. Davies, Proc. British Ceram. Soc., June 1973
8. M.G. Mendiratta, J.J. Petrovic - J. Mat. Sci., 11, (1976), 973
9. D.P. Williams, A.G. Evans - J. Test. and Eval., 1 (1973) 264
10. G.R. Terwilliger, F.F. Lange - J. Am. Ceram. Soc., 57 (1974) 25
11. M. Mitomo - J. Mat. Sci., 11 (1976) 1103
12. G.E. Gazza, H. Knoch and G.D. Quinn, Am. Ceram. Bull, 57 (1978) 1059
13. A. Tsuge, K. Nishida, Am. Ceram. Bull, 57 (1978) 424
14. P.C. Martinengo, A. Giachello, A. Buri and F. Branda "Devitrification Phenomena of a Pressureless Sintered Silicon Nitride" - Proc. Int. Symp. on "Factors in Densification and Sintering of Oxide and Non-Oxide Ceramics" Hakone, Japan, Oct. 1978 (to be published)

DISCUSSION SUMMARY

SESSION IV - EMERGING DEVELOPMENTS

by

Dr W. Wallace
National Aeronautical Establishment
National Research Council of Canada
Ottawa, Ontario, Canada

A particular aim of session IV was to look at the future prospects for ceramics. To do this nine papers were presented covering a broad range of topics from the fundamentals of microstructure control, through to the design, fabrication and testing of engine components. Between them these papers touched upon most of the key problems currently affecting ceramics.

Four papers were presented describing the physical chemistry of ceramics and the problems of processing for controlled microstructure and strength. Many processes were described, but in general those which gave the better material properties were often unattractive because of their cost, or the limited range of product shapes that they could produce. Several authors emphasised that extensive machining or grinding operations must be avoided, since some of the advantages of using ceramics would be lost.

Several of the authors discussed pressureless sintering and showed that with controlled additions of what might be regarded as impurities, many of these ceramics could be sintered to high density and strength. In the case of the Si ALON family of compounds, additives such as MgO and SiO₂ were mentioned, while in the case of SiC boron was found to be effective. In all cases these additives appeared to act by promoting the formation of a liquid phase at the sintering temperature. However these practices must be used with caution, since additives which promoted sintering also caused loss of high temperature strength. In addition, at least in the case of Si ALON, the possibility of scaling up the pressureless sintering process to produce large components is in doubt.

The importance of accurate information on phase equilibria and phase compositions was mentioned in several papers, and we were fortunate to have the detailed reviews by Dutta and by Godfrey. In the case of β -Si ALON, stoichiometry seemed to be important, and it was suggested that by working with stoichiometric compositions strengths might be retained to higher temperatures, and the knee which is observed at about 1200°C in plots of strength versus temperature might be eliminated. However the situation is confounded by the fact that the closer is the compound to stoichiometry the more difficult it is to sinter.

Obviously a great deal is still to be learnt about the control of structure and chemistry. However some valuable guidelines on how to proceed were given in the paper by Campo and Martinengo. They showed that by making additions of MgO and Y₂O₃ to commercial silicon nitride powder, not only could high densities be obtained by reaction sintering, but the structure of the grain boundary amorphous phases could be modified by subsequent heat treatment. This led to significant improvements in crack growth resistance. The question arises whether similar treatments can be developed for the Si ALON compounds, and whether the fracture toughness of SiC can be improved in a similar manner. Clearly a great deal more needs to be known about the micro-mechanisms of brittle fracture in order to improve basic material properties.

A most valuable paper was presented by Cavallotti et al. which showed that not only do sintering additives affect strength and density, but they also affect oxidation and hot corrosion resistance of ceramics. It is apparent that non-oxide ceramics, such as Si₃N₄, are seriously degraded by oxidation and sulphidation in a manner analogous to that of metals. We are beginning to appreciate the damaging effects not only of oxygen, but also of elements such as sodium, potassium and lithium, and of chloride and sulphate ions. It was pointed out that these were preliminary results, but an important contribution has already been made towards understanding, and therefore controlling these degradation reactions. These results suggest that we may be on the verge of a new area of research related to the development of protective coatings, and it is well known how complex this problem has been with metals.

While many problems and failures with ceramics were described during these sessions, some promising developments did emerge. The paper from ASEA Sweden for example, described the application of hot isostatic pressing to ceramic powders, and with it a new glass canning technique that should remove many of the shape constraints associated with conventional hot pressing. While ASEA made additions of about 5% Y₂O₃ to silicon nitride powders, they also reported high rupture strengths, over 90% of the room temperature properties, at temperatures up to 1370°C. Many people will be anxious to evaluate this process more thoroughly.

The brittle nature of ceramics and the variability of their fracture behaviour present formidable problems which will not be easily overcome. However the papers presented by Evans and by Johnson have provided useful guidelines for the non-destructive evaluation of ceramic components in terms of fracture statistics. These papers call for careful study, but even without this one can appreciate the need for

a proper description of the flaw population of a material in order to design a part with an acceptable probability of failure. It was pointed out during discussion that these papers have done much to increase awareness of the existence of multiple flaw distributions in ceramics. However a great deal more needs to be done to determine the nature of these flaws, and the way they may be controlled during processing.

Finally a most imaginative study by Kochendörfer described the development of a ceramic turbine rotor loaded in compression by boron-aluminum, carbon-carbon, or carbon-fibre reinforced plastic tension rings. It is encouraging to see that new design concepts are being examined but disappointing that better performances were not observed in spin tests. However patience and further efforts are required to develop these ideas and to assess the ultimate limitations of the technique.

In conclusion it must be accepted that many problems remain unsolved. The more ambitious programmes aimed at the development of rotating engine components have been unsuccessful, and in the future a more conservative approach focussed on smaller stationary parts should be more profitable. In the past much emphasis has been placed on strength, and yet ductility, fracture toughness, and thermal shock resistance are at least as important. One might question the value of embarking on major hardware development programmes until these properties can be improved. Better materials are required that are more tolerant of the engine environment, and therefore materials scientists should expect to play a major role in the future.

SESSION V - ROUND TABLE DISCUSSION

**Prospects and Obstacles to Application --
Design and Materials Viewpoints**

Chairmen: E.C. van Reuth and W.Heilmann

Participants: F.B.Wallace
P.Walzer
H.M.Burte
B.Brown

(Discussion not reproduced)

DISCUSSION SUMMARY

SESSION V ROUND TABLE DISCUSSION

PROSPECTS AND OBSTACLES TO APPLICATION
DESIGN AND MATERIALS VIEWPOINTS

by

Dr H.B.Probst
NASA-Lewis Research Center
Cleveland, Ohio 44135, USA

This session was co-chaired by Dr. E. C. van Reuth of DARPA, USA and Dr. W. Heilmann of MTU, Federal Republic of Germany. Panel members were Dr. F. B. Wallace, AiResearch Manufacturing Company, USA, Dr. P. Walzer, Volkswagen, Federal Republic of Germany, Dr. H. M. Burte, Air Force Materials Laboratory, USA, and Mr. W. Brown, Consultant, USA. Recorders of each previous session also served as panel members; these were Dr. E. M. Leno, Army Materials and Mechanics Research Center, USA, Mr. A. F. McLean, Ford Motor Company, USA, Dr. K. Trappmann, MTU, Federal Republic of Germany, and Dr. W. Wallace, National Aeronautical Establishment, Canada.

By way of introducing the session some general observations were made. The use of ceramics in advanced gas turbine engines must be considered in terms of competing approaches. The major competition is cooling of metallic components to allow higher gas temperatures. For some specialized applications refractory metals and coated carbon/carbon composites are competing candidates. Ceramics must compete with these alternate materials in terms of both cost and performance, with cost being the more important criterion for any near term applications, and performance gains being of greater importance in the longer term. The most likely near term application in aerospace is thought to be the small, limited life, non-man-rated expendable engine such as a cruise missile engine. However, such an application does not represent a large market. Application in a large market e.g. automotive would better support and justify full scale development.

Our knowledge of ceramics can be considered and catalogued in the spectrum of Synthesis-Microstructure-Properties-Use. Our current state of knowledge should be considered at each interface within this spectrum. The synthesis-microstructure interface is currently a key pacing item; we will need a more thorough understanding of the effects of synthesis variables on microstructure in order to produce uniform and reproducible ceramic bodies. Knowledge of the microstructure-properties interface is of course necessary in order to improve properties and set values on target properties to which we might aspire. Our eventual knowledge of the property-use interface will determine our ability to design components and predict behavior.

The questions of "where we have been" in ceramic technology for gas turbines, "where we are at the present time", and "where we are going" were addressed. We have ventured into the realm of the impossible and shown it can be done. That is, ceramic components with potential for mass production have run in experimental engines several hundred degrees higher than possible for superalloys. We are presently at a hurdle; having shown that ceramics can work we must now show that, indeed, they will work. We are currently aware of many inconsistencies and have identified a host of problems. Some of these are related to powder quality and consolidation techniques and parameters. Others are related to time dependent behavior, NDE and predictive capability, attachment interfaces, and the statistics governing the behavior of components. It was suggested that we need to focus future efforts on quality processing and quantity evaluation. Although, improved materials are still desired, the concept here is to make many components by a fixed process so that these many components can be tested to failure to better understand the proper governing statistics.

The overall prospect for the use of ceramics remains high, i.e., ceramic components still offer large potential improvements to gas turbine performance. However, in spite of this favorable prospect ceramic components are not yet found in any production engine. This situation can be laid to a number of obstacles and one way to catalog these obstacles is according to their source, be it material or design.

The materials themselves present obstacles to use. Designers cannot accept materials whose characterization is as uncertain as today's ceramics. Long term behavior is particularly poorly characterized in a real engine environment which includes features such as hot corrosion, vibration, particle impact, and cyclic stresses. A major material obstacle is our inability to predict long term behavior from inspection techniques or from knowledge of the material, its composition or process history. There is a need for ma-

terials that exhibit long term stability and for reliable inspection methods that will assure components of high reliability.

Obstacles are also related to design. The design of some ceramic components in programs today represents no great departure from the design of metallic components. There appears to be little evidence that innovative designs intended to truly accommodate the specific unforgiving nature of ceramics are being pursued. More innovative unconventional design approaches are required. Also, more emphasis on modeling and truly analytical rather than empirical approaches is to be desired.

A lack of commitment was also cited as a continuing obstacle. Some organizations are playing a "wait and see" game, because they judge success to be too uncertain and too far in the future. Since commitment is motivated by the real prospect for near term profit, an alternate approach to development of totally ceramic engines could be the substitution of ceramic components for some alloy components in existing production engines. To be considered such substitutions must promise reduced life cycle costs. Successful field experience could provide the confidence needed for continuing more ambitious development and demonstration programs.

Because of the brittle nature of ceramics, their prospects for use as components (with possible exception of shrouds and bearings) are judged to be poor unless one or all of the following come to pass: a) a truly analytical solution to design; b) more reliable ceramic production materials, and/or c) NDE procedures to reject inferior components at an acceptable level of risk.

It was pointed out that historically, the introduction of new types of material has often been in response to a critical need. Indeed, ceramics may eventually be introduced into gas turbine engines as the only alternative to meet a future critical need. Current problems that could become critical needs are the cobalt/chromium shortage, fuel shortages demanding higher efficiencies and multi-fuel capabilities, and emission standards combined with future use of dirty fuels. Even though we are aware of these problems today, critical needs have a way of sneaking up. If ceramics are to be ready when a critical need arises, a faster paced program of improved focus is required.

Before ceramics can be selected for use in a full scale development engine they must be able to provide a proper balance among performance, costs, and risk. Current designs of ceramic components are not offering a significant performance increase. Improvements are needed to reduce tip clearance, improve rub tolerance, and minimize leakage paths in the static structure. Initial costs of parts must be brought down, this is particularly true of hot pressed silicon nitride. In order to minimize risks, programs that concentrate on one or two components are to be preferred over those that incorporate large numbers of differing ceramic components. In the latter type of program the consequences of component failure during engine testing is too severe. The specific problem of interfaces, both ceramic/metal and ceramic/ceramic, adds risk to any program and is a severe obstacle to which special attention should be devoted.

Opportunities exist to improve material behavior through improved basic understanding of materials and processes. Understanding of the micro-mechanisms of brittle fracture is a particular challenge. Hot isostatic pressing seems to offer hope as an improved consolidation process. The area of "alloying" both within the individual base systems Si_3N_4 and SiC as well as between these systems is as yet essentially unexplored.

In spite of the interdisciplinary intent of past and current programs, communications between designers and material developers and producers appears to remain as a major obstacle in the application of ceramics. Although both communities have made great progress within their own provinces the advancement of the total technology seems to be hampered by inadequate intercommunications between disciplines. For the short term managers in the sponsoring agencies and contract program managers as well as individual researchers must renew efforts to work together to assure adequate communication, cooperation, and cross-fertilization. In the longer term, interdisciplinary education at the graduate as well as undergraduate levels is a positive approach. The current program at the University of Washington is an example of an attempt to put students from ceramics and other disciplines into a common curriculum to foster cooperative learning and project planning and execution.

Communication problems can be manifested by conflict. On the one hand, material developers and suppliers are quick to fault the designers for unimaginative approaches and a lack of understanding the need to accommodate the unique characteristics of ceramics. On the other, designers contend they cannot successfully use materials that are not fully characterized and which show wide variances in properties from one delivery to the next. In response to the criticism of lack of characterization and wide variability, material producers feel they have been put under excessive pressure to supply hardware to large demonstration programs without receiving a proportionate amount of support for material development and characterization.

Even within the materials community we are not without conflicts. The necessity for material producers to maintain as proprietary certain processes and material formulation does not foster fruitful scientific exchange. Material producers feel there is little protection for their innovations. This position in ceramics is certainly no different from that taken in other, previous and current, developing technologies in the metals industries. However, its effect of stifling cross-fertilization among material re-

searchers is potentially acute and places another obstacle in the path of an already difficult technology.

If such conflicts as enumerated above remain unresolved, they could present major and possibly terminal obstacles to the ultimate use of ceramics.

At the current state of development of ceramics we learn more from component failures than we do from survivals. The concept of designing to failure is one to which sponsoring agencies should become more tolerant. The opposing view, of course, is that such an approach is more costly and opposed to the need to show progress and success in order to merit continued support.

Proof testing should be considered an integral part of NDE. While proof testing a rotor by spinning is fairly straightforward, the proof testing of static components is no simple matter. Development of valid proof tests which stress static components in a realistic manner could be a formidable obstacle. Further, true scientific proof testing, i.e. testing that will evaluate both material and design is an ultimate need that is currently an obstacle. As desirable as good proof testing is, it must be remembered that inherent in our present concept of proof testing is short time. Proof testing will tell us of the adequacy of the virgin properties of the material but nothing of long time effects on properties.

The use of Weibull statistics came under question since in most programs, in the interest of economy, sufficient samples are not tested to justify use of Weibull analysis. In the long run this could prove to be false economy, since sample costs and possibly even component costs are trivial compared to the cost of engine failures. Also, the wide scatter in properties that necessitates large numbers of test samples is not exclusively the fault of the material. Testing methods also contribute to scatter and require improvement. Surface characterization is also poorly understood and not properly accounted for in our evaluations and reporting of material properties. Surface variables could be the source of a great deal of current conflicting data.

Expanded efforts are required in highly focused cooperative programs to improve both materials and testing methods in order to sort out differences in test techniques and to expand the entire data base. The required cooperation and exchange of information is being started within the International Energy Association.

In summary, although many of the points brought out in this discussion appear to be negative and pessimistic let us not be discouraged. We can all take pride in the progress that has been made. Anyone who doubts that progress has been made needs only refer to the first formal symposium on the original ARPA program in the United States held at Hyannis, Massachusetts in 1973. Progress is even more apparent when compared to the earlier pioneering efforts in the United Kingdom. However, the demonstration of a high pay-off use of ceramics in gas turbines remains in the future. The prognosis for the eventual use of ceramics is good and in the aerospace field the most likely first application will be in limited life engines for unmanned vehicles. The automotive, truck, and utility gas turbines are also areas in which the long range prospects for use of ceramics is good.

Major obstacles seem to lie in four areas; the materials, the designs, communication between materials specialists and designers, and commitment on the part of Government and industry. Although many specific problems need yet to be addressed by the materials community, the questions of cost, reproducibility, durability, and effects of long term exposure on properties seem to require particular attention at this time. Designers must be imaginative and innovative and always strive to find means to accommodate the unique properties of ceramics. And, needless to say, the dialogue between the two communities must continue and be strengthened so that in the not too distant future this dialogue can lead to real results in the form of in-service ceramic components.

The high technology ceramics discussed at this AGARD meeting may well occupy a unique place in the history of technology. There are several current and developing problems which will alter many of our technologies. Some of the more obvious of these are energy sources, environmental quality, and scarcity of critical mineral resources. Ceramics can play major roles in solutions to these problems. Let us hope that our ceramic technology can meet the needs as any of these problems reach critical proportions. Of course, we must do more than hope; we must have the courage to move rapidly in the direction that our technical judgment points, i.e. to a more positive commitment to ceramics on the part of both sponsoring Government agencies and organizations in the private sector. With so many critical needs on the horizon to which ceramics could contribute solutions we can no longer afford to wait and see how ceramics will work for the other fellow.

REPORT DOCUMENTATION PAGE

1. Recipient's Reference	2. Originator's Reference	3. Further Reference	4. Security Classification of Document
	AGARD-CP-276	ISBN 92-835-0261-2	UNCLASSIFIED

5. Originator Advisory Group for Aerospace Research and Development
 North Atlantic Treaty Organization
 7 rue Ancelle, 92200 Neuilly sur Seine, France

6. Title
 CERAMICS FOR TURBINE ENGINE APPLICATIONS

7. Presented at the 49th Meeting of the AGARD Structures and Materials Panel held in
 Porz-Wahn, Köln, Germany on 8-10 October 1979.

8. Author(s)/Editor(s)

Various

9. Date

March 1980

10. Author's/Editor's Address

Various

11. Pages

364

12. Distribution Statement

This document is distributed in accordance with AGARD policies and regulations, which are outlined on the Outside Back Covers of all AGARD publications.

13. Keywords/Descriptors

Ceramics
 Turbines
 Engines

Aircraft engines
 Missile propulsion

14. Abstract

To provide a basis from which an evaluation of the "state-of-the-art" could be derived, and a forum to stimulate future progress, the Structures and Materials Panel and the Propulsion and Energetics Panel of AGARD cooperated to organize and conduct a multinational, multi-disciplinary Specialists Meeting on "Ceramics for Turbine Engine Applications" which was held in Cologne, Germany on October 8-10, 1979. Twenty three papers during two very full days presented progress in materials, design and production technologies, the results of component test programs, and analyses of potentially profitable applications for ceramics and the requirements that these generate. They were supplemented by extensive discussion and a half-day round table designed to stimulate interaction between materials scientists, materials engineers, manufacturing engineers and engine designers, and to illuminate important issues.

<p>AGARD Conference Proceedings No. 276 Advisory Group for Aerospace Research and Development, NATO CERAMICS FOR TURBINE ENGINE APPLICATIONS Published March 1980 364 pages</p> <p>To provide a basis from which an evaluation of the "state-of-the-art" could be derived, and a forum to stimulate future progress, the Structures and Materials Panel and the Propulsion and Energetics Panel of AGARD cooperated to organize and conduct a multi-national, multidisciplinary Specialists Meeting on "Ceramics for Turbine Engine Applications" which was held in Cologne, Germany on October 8-10, 1979. Twenty three papers during two very full days presented</p> <p>P.T.O.</p>	<p>AGARD CP-276</p> <p>Ceramics Turbines Engines Aircraft engines Missile propulsion</p>	<p>AGARD Conference Proceedings No. 276 Advisory Group for Aerospace Research and Development, NATO CERAMICS FOR TURBINE ENGINE APPLICATIONS Published March 1980 364 pages</p> <p>To provide a basis from which an evaluation of the "state-of-the-art" could be derived, and a forum to stimulate future progress, the Structures and Materials Panel and the Propulsion and Energetics Panel of AGARD cooperated to organize and conduct a multi-national, multidisciplinary Specialists Meeting on "Ceramics for Turbine Engine Applications" which was held in Cologne, Germany on October 8-10, 1979. Twenty three papers during two very full days presented</p> <p>P.T.O.</p>	<p>AGARD CP-276</p> <p>Ceramics Turbines Engines Aircraft engines Missile propulsion</p>
<p>AGARD Conference Proceedings No. 276 Advisory Group for Aerospace Research and Development, NATO CERAMICS FOR TURBINE ENGINE APPLICATIONS Published March 1980 364 pages</p> <p>To provide a basis from which an evaluation of the "state-of-the-art" could be derived, and a forum to stimulate future progress, the Structures and Materials Panel and the Propulsion and Energetics Panel of AGARD cooperated to organize and conduct a multi-national, multidisciplinary Specialists Meeting on "Ceramics for Turbine Engine Applications" which was held in Cologne, Germany on October 8-10, 1979. Twenty three papers during two very full days presented</p> <p>P.T.O.</p>	<p>AGARD CP-276</p> <p>Ceramics Turbines Engines Aircraft engines Missile propulsion</p>	<p>AGARD Conference Proceedings No. 276 Advisory Group for Aerospace Research and Development, NATO CERAMICS FOR TURBINE ENGINE APPLICATIONS Published March 1980 364 pages</p> <p>To provide a basis from which an evaluation of the "state-of-the-art" could be derived, and a forum to stimulate future progress, the Structures and Materials Panel and the Propulsion and Energetics Panel of AGARD cooperated to organize and conduct a multi-national, multidisciplinary Specialists Meeting on "Ceramics for Turbine Engine Applications" which was held in Cologne, Germany on October 8-10, 1979. Twenty three papers during two very full days presented</p> <p>P.T.O.</p>	<p>AGARD CP-276</p> <p>Ceramics Turbines Engines Aircraft engines Missile propulsion</p>

<p>progress in materials, design and production technologies, the results of component test programs, and analyses of potentially profitable applications for ceramics and the requirements that these generate. They were supplemented by extensive discussion and a half-day round table designed to stimulate interaction between materials scientists, materials engineers, manufacturing engineers and engine designers, and to illuminate important issues.</p>	<p>progress in materials, design and production technologies, the results of component test programs, and analyses of potentially profitable applications for ceramics and the requirements that these generate. They were supplemented by extensive discussion and a half-day round table designed to stimulate interaction between materials scientists, materials engineers, manufacturing engineers and engine designers, and to illuminate important issues.</p>
<p>ISBN 92-835-0261-2</p>	<p>ISBN 92-835-0261-2</p>
<p>progress in materials, design and production technologies, the results of component test programs, and analyses of potentially profitable applications for ceramics and the requirements that these generate. They were supplemented by extensive discussion and a half-day round table designed to stimulate interaction between materials scientists, materials engineers, manufacturing engineers and engine designers, and to illuminate important issues.</p>	<p>progress in materials, design and production technologies, the results of component test programs, and analyses of potentially profitable applications for ceramics and the requirements that these generate. They were supplemented by extensive discussion and a half-day round table designed to stimulate interaction between materials scientists, materials engineers, manufacturing engineers and engine designers, and to illuminate important issues.</p>
<p>ISBN 92-835-0261-2</p>	<p>ISBN 92-835-0261-2</p>

4
AGARD

NATO  OTAN

7 RUE ANCELLE · 92200 NEUILLY-SUR-SEINE
FRANCE

Telephone 745.08.10 · Telex 610176

**DISTRIBUTION OF UNCLASSIFIED
AGARD PUBLICATIONS**

AGARD does NOT hold stocks of AGARD publications at the above address for general distribution. Initial distribution of AGARD publications is made to AGARD Member Nations through the following National Distribution Centres. Further copies are sometimes available from these Centres, but if not may be purchased in Microfiche or Photocopy form from the Purchase Agencies listed below.

NATIONAL DISTRIBUTION CENTRES

BELGIUM

Coordonnateur AGARD VSL
Etat-Major de la Force Aérienne
Quartier Reine Elisabeth
Rue d'Evere, 1140 Bruxelles

CANADA

Defence Science Information Services
Department of National Defence
Ottawa, Ontario K1A 0K2

DENMARK

Danish Defence Research Board
Østerbrogades Kaserne
Copenhagen Ø

FRANCE

O.N.E.R.A. (Direction)
29 Avenue de la Division Leclerc
92320 Châtillon sous Bagneux

GERMANY

Zentralstelle für Luft- und Raumfahrt-
dokumentation und -information
c/o Fachinformationszentrum Energie,
Physik, Mathematik GmbH
Kernforschungszentrum
7514 Eggenstein-Leopoldshafen 2

GREECE

Hellenic Air Force General Staff
Research and Development Directorate
Holargos, Athens

ICELAND

Director of Aviation
c/o Flugrad
Reykjavik

UNITED STATES

National Aeronautics and Space Administration (NASA)
Langley Field, Virginia 23365
Attn: Report Distribution and Storage Unit

ITALY

Aeronautica Militare
Ufficio del Delegato Nazionale all'AGARD
3, Piazzale Adenauer
Roma/EUR

LUXEMBOURG

See Belgium

NETHERLANDS

Netherlands Delegation to AGARD
National Aerospace Laboratory, NLR
P.O. Box 126
2600 A.C. Delft

NORWAY

Norwegian Defence Research Establishment
Main Library
P.O. Box 25
N-2007 Kjeller

PORTUGAL

Direcção do Serviço de Material
da Força Aérea
Rua da Escola Politécnica 42
Lisboa
Attn: AGARD National Delegate

TURKEY

Department of Research and Development (ARGE)
Ministry of National Defence, Ankara

UNITED KINGDOM

Defence Research Information Centre
Station Square House
St. Mary Cray
Orpington, Kent BR5 3RF

THE UNITED STATES NATIONAL DISTRIBUTION CENTRE (NASA) DOES NOT HOLD STOCKS OF AGARD PUBLICATIONS. AND APPLICATIONS FOR COPIES SHOULD BE MADE DIRECT TO THE NATIONAL TECHNICAL INFORMATION SERVICE (NTIS) AT THE ADDRESS BELOW.

PURCHASE AGENCIES

Microfiche or Photocopy

National Technical
Information Service (NTIS)
5285 Port Royal Road
Springfield
Virginia 22161, USA

Microfiche

Space Documentation Service
European Space Agency
10, rue Mario Nikis
75015 Paris, France

Microfiche

Technology Reports
Centre (DTI)
Station Square House
St. Mary Cray
Orpington, Kent BR5 3RF
England

Requests for microfiche or photocopies of AGARD documents should include the AGARD serial number, title, author or editor, and publication date. Requests to NTIS should include the NASA accession report number. Full bibliographical references and abstracts of AGARD publications are given in the following journals:

Scientific and Technical Aerospace Reports (STAR)

published by NASA Scientific and Technical
Information Facility
Post Office Box 8757
Baltimore/Washington International Airport
Maryland 21240, USA

Government Reports Announcements (GRA)

published by the National Technical
Information Services, Springfield
Virginia 22161, USA



Printed by Technical Editing and Reproduction Ltd
Harford House, 7-9 Charlotte St, London W1P 1HD

ISBN 92-835-0261-2

CP 276

CERAMICS FOR TURBINE ENGINE APPLICATIONS



SMP